UNCOUPLED AND COUPLED SOLUTIONS OF VOLUME CHANGE PROBLEMS IN EXPANSIVE SOILS

A Thesis Submitted to the College of

Graduate Studies and Research

in Partial Fulfillment of the Requirements

for the Degree of Doctor of Philosophy

in the Department of Civil Engineering

University of Saskatchewan

Saskatoon

By

Vu Quang Hung

© Copyright Vu Quang Hung, December 2002. All rights reserved.

PERMISSION TO USE

In presenting this thesis in partial fulfillment of the requirements for a postgraduate degree from the University of Saskatchewan, I agree that the Libraries of this University may make it freely available for inspection. I further agree that permission for copying of this thesis in any manner, in whole or in part, for scholarly purposes may be granted by the professor or professors who supervised my thesis work or, in their absence, by the Head of the Department or the Dean of the College in which my thesis work was done. It is understood that any copying or publication or use of this thesis or parts thereof for financial gain shall not be allowed without my written permission. It is also understood that due recognition shall be given to me and to the University of Saskatchewan in any scholarly use which may be made of any material in my thesis.

Requests for permission to copy or to make other use of material in this thesis in whole or part should be addressed to:

Head of the Department of Civil Engineering
University of Saskatchewan
Saskatoon, Saskatchewan, Canada
57 Campus Drive
S7N 5A9

ABSTRACT

Lightly loaded structures constructed on expansive soils are often subjected to severe distress subsequent to construction, as a result of changes in the pore-water pressures in the soil. The structures most commonly damaged are roadways, airport runways, small buildings, irrigation canals, spillway structures and all near ground surface structures associated with infrastructure development. Changes in the pore-water pressure can occur as a result of variations in climate, change in depth to the water table, water uptake by vegetation, removal of vegetation or the excessive watering of a lawn.

An analytical tool for the prediction of heave is extremely valuable to geotechnical engineers. There has been little advancement in the development of such a tool for solving engineering problems. There does not appear to be a computer program that has been written and widely accepted for solving this problem. It is important that such an analytical tool be developed and that it be developed for both one- and two-dimensional problems.

The primary objective of this research study is to apply the general theory of consolidation/swelling for unsaturated soils to provide a reliable, practical technique for the prediction of one-, two- or three-dimensional volume change associated with unsaturated, expansive soils. The void ratio constitutive surface of an unsaturated, expansive soil was estimated from volume change indices obtained from conventional oedometer tests. Mathematical equations, which can be applied over a wide range of stress conditions, are proposed to describe the constitutive surfaces for both soil structure and water phase. The elastic parameter functions that are required for the volume change analysis are calculated from the constitutive surfaces with an assumed value of Poisson's ratio.

The solutions to the volume change problems associated with an unsaturated, expansive soil are obtained using both an uncoupled and a coupled approach. In the uncoupled approach, the continuity equation for the water phase and the equilibrium equations are solved independently. Uncoupled solutions are obtained using a partial differential equation solver, called FlexPDE. In the coupled approach, the continuity equation and the equilibrium equations are solved simultaneously. Coupled solutions are obtained using a finite element program, called COUPSO. The examples presented in this study represent typical volume change problems that are often encountered in engineering practice (i.e., influence of vegetation on light engineering structures, water leakage under floor slab,

and infiltration of water from ground surface). The results of the analyses appeared to be reasonable and in accordance with anticipated behaviour. The research results also showed that the answers from uncoupled solutions compared well with those from the coupled solutions. It is suggested that uncoupled solutions are adequate for the analysis of most volume change predictions for unsaturated, expansive soils.

ACKNOWLEDGEMENTS

I am indebted to my supervisor, Dr. D. G. Fredlund for his invaluable guidance, patience and kindness throughout the research program. I also wish to express my thank to him for providing me an enthusiastic interest in the subject of study. His care provided for me and my family is greatly acknowledged.

I wish to express my sincerely thank to Dr. J.H.F. Pereira for sharing his experience in coupled analysis and providing invaluable support and suggestions in the extension of the computer program used in my research study.

Special thanks go to my committee members, Dr. D. E. Pufahl, Dr. L. Wegner, and Dr. D. Bergstrom for their advice, criticism and helpful comments on my research program and the numerical results.

I am grateful to all professors, secretaries and graduate students of the Department of Civil Engineering for their helps and supports. Special thanks to Gilson Gitirana for his valuable discussions and his reading of the theory chapter. I am thankful to my Vietnamese friends, Dale Pavier and their spouses for their warm friendships and helps in different ways during my stay in Saskatoon.

I would like to express my love and gratitude to my parents, Mr. Vu Van Nham and Mrs. Tran Thi Hoe, for their endeavor to provide good education and constant encouragement throughout my life. Thank you to my wife, Mrs. Nguyen Thi Hai Hung for her love, understanding and encouragement, and my children, Huyen and Duong, for having sacrificed their affectionate attention during my study. The sentimental supports from my siblings Phuc, Long, Lan, Ha and their spouses are greatly acknowledged.

Finally, I gratefully acknowledge the financial support from the College of Graduate Studies and Research, University of Saskatchewan, the funding from the NSERC, CIDA, and Saskatchewan Department of Highways and Transportation through Dr. D. G. Fredlund for this research study.

To my family;

Father: Vũ Văn Nhậm
Mother: Trần Thị Hoè
Wife: Nguyễn Thị Hải Hưng
Daughter: Vũ Thanh Huyền
Son: Vũ Quang Dương

Many thanks for your support and patience.

Vũ Quang Hưng

TABLE OF CONTENTS

LIST OF TABLES

LIST OF FIGURES

CHAPTER 1

Introduction

1.1 General

An expansive soil is generally unsaturated due to desiccation, and contains clay minerals that swell when wetted and shrink when dried. Expansive soils are present in many parts of the world, particularly in semi-arid areas.

Lightly loaded structures constructed on expansive soils are often subjected to severe distress subsequent to construction, as a result of changes in the pore-water pressures in the soil. The structures most commonly damaged are roadways, airport runways, small buildings, irrigation canals, spillway structures and all near ground surface structures associated with infrastructure development. Changes in the pore-water pressure can occur as a result of variations in climate, change in depth to the water table, water uptake by vegetation, removal of vegetation or the excessive watering of a lawn.

Damage to light structures caused by expansive soils has been recorded in most countries in the world. In the United States, costs associated with damage to all types of structures built on expansive soils are estimated to be in the orfer of $7 billion per year (Krohn and Slosson, 1980). This amount is greater than the combined damage from natural disasters such as floods, hurricanes, earthquakes, and tornadoes (Jones and Holtz, 1973). Expansive soils have been called the hidden disaster (Snethen, 1986). While expansive soils do not cause loss of life, the economical loss in the United States makes it the most costly natural hazard. About 60 percent of all houses in the United States suffer minor damage from expansive soils. About 10 percent experience significant damage, some beyond repair. In Canada, the volume

changing clay subsoil constitutes the most costly natural hazard to buildings on shallow foundations (Hamilton, 1977).

The problems associated with expansive soils have been specially addressed in many international and regional conferences. There were three Symposiums on Expansive Clays (from 1957 to 1960), seven International Conferences on Expansive Soils (from 1965 to 1992), three International Conferences on Unsaturated Soils (from 1995 to 2002) and many other regional conferences. The research literature shows that the prediction of heave associated with the wetting of an expansive soil has received more attention than any other problem involving unsaturated soils (Fredlund, 2000).

A world-wide interest in research on expansive soils in the last four decades has resulted in numerous methods being proposed for the prediction of heave. The heave prediction methods are based either on one-dimensional oedometer test results or on direct matric suction measurements (Fredlund and Rahardjo, 1993). Although an analytical tool for the prediction of heave is extremely important, there has been little advancement in the development of such a tool for solving engineering problems. There does not appear to be a computer program that has been written and widely accepted for this problem. It is important that such an analytical tool be developed and that it be developed for both one- and two-dimensional problems.

Difficulties associated with the prediction of volume change in an unsaturated, expansive soil present several issues. These issues include the characterization of the soil properties that are required for two- or three-dimensional problems and a computing tool that can handle the highly non-linear nature of an unsaturated, expansive soil. The geotechnical community is still waiting for satisfactory analytical tools to address the expansive soil problem.

1.2 Objective and scopes

The intent of this research study is to use the general theory of unsaturated soils to provide a reliable, practical technique for the prediction of one-, two- or three-dimensional volume change associated with unsaturated, expansive soils. The objectives of this research study are as follows:

1. To summarize and further study an uncoupled model for the prediction of volume change in expansive soils (i.e., an extension of the study presented by Hung, 2000).
2. To estimate the void ratio constitutive surface from volume change indices.
3. To study the use of soil property functions that can be applied over a wide range of stress conditions for volume change and water content change prediction.
4. To develop a coupled model for the prediction of volume change in expansive soils based on the theory of swelling for an unsaturated soil.
5. To simulate typical volume change problems associated with expansive soils in engineering practice using both uncoupled and coupled approaches.

The scope of this research study is limited to a theoretical study associated with past case histories and example problems. The soil properties used in the analysis are based on results found in the literature or are predicted from other volume-mass properties measured in other studies at the University of Saskatchewan. The study considers the volume change due to changes in matric suction and applied load; effects of temperature, electric potential or osmotic suction changes in the soils are not considered.

1.3 Outline of the thesis

This thesis is organized into eight chapters. Chapter 1, "Introduction", presents the need for this research study, the objectives and scope of the research study, and the outline of the thesis.

Chapter 2, "Literature Review", contains three parts. The first part presents a brief review of stress state variables, constitutive relationships, and flow laws for an unsaturated, expansive soil. The second part reviews the solutions to one-dimensional swelling of expansive soils. The Fredlund et al. (1980) method for the prediction of heave is presented to serve as a background and the terminology is set forth for the later chapters, which deal with equations for the void ratio constitutive surface. The third part presents the development of uncoupled and coupled solutions of volume change associated with expansive soils.

Chapter 3, "Formulation Theory for the Swelling Process in an Expansive Soil", presents the physical relationships required for three-dimensional swelling formulations and the development of coupled equations for the simulation of three-dimensional swelling problems. Formulations for two-dimensional (i.e., plane strain) conditions are derived with the assumption that a continuous air phase is maintained at atmospheric pressure. Soil properties required for a swelling analysis and details related to an uncoupled analysis are presented. The finite element formulation of the coupled equations is derived for a plane strain problem.

Chapter 4, "Theory of Constitutive Surfaces", includes three parts. The first part presents estimations of void ratio surface from swelling indices. The second part contains the existing equations and proposes a new equation for the void ratio constitutive surface. Solutions to the low net normal stress and matric suction range are also presented in this part. The third part presents the soil property characterization for Regina clay. The elasticity parameters are calculated from the constitutive surfaces for soil structure and water phase using an assumed value for Poisson's ratio.

Chapter 5, "Research Program", presents the computer programs and contains an outline of the research program undertaken to illustrate the uncoupled and coupled approaches for volume change predictions associated with expansive soils. Four two-dimensional example problems are presented. The first two examples, which are associated with the problem of water uptake by trees, are analysed using the uncoupled approach. The other two examples, which are associated with the leakage of water below a floor slab and the infiltration of water from ground surface, are analysed using both uncoupled and coupled approaches. Each example problem and the soil properties used in the analysis are described. A sensitivity study with respect to the assumed value of Poisson's ratio is presented.

Chapter 6, "Presentation of the Results", contains the results of the analyses corresponding to the research program presented in Chapter 5. Uncoupled solutions of the example problems are obtained using a general-purpose partial differential equation solver, called FlexPDE. Coupled solutions of the example problems are obtained using a finite element computer program, called COUPSO.

Chapter 7, "Discussions of the Results", contains the discussions of the results presented in Chapter 6. Uncoupled and coupled solutions for the third and fourth example problems are compared.

Chapter 8, "Conclusions and Recommendations", contains a summary of the findings of this research study and proposes several recommendations related to the analysis and potential future studies.

Four Appendices are included to provide supplementary information to the thesis. Appendix A presents the comparison of the coupled solutions obtained using various finite element meshes for Examples 3 and 4. Appendix B presents additional results of the uncoupled analysis of Example 3. Appendix C presents additional results of uncoupled analysis of Example 4. Appendix D discusses the issues associated with the numerical errors of a finite element solution and presents how some of the numerical results presented in this study have been validated.

CHAPTER 2

Literature Review

2.1 General

Unsaturated soils can generally be divided into two groups with respect to volume change; namely, expansive soils and collapsible soils. Volume change is a result of a change in matric suction for both groups of soils (i.e., when the soil is wetted). Expansive soils increase in volume when wetted while collapsible soils decrease in volume when wetted. The theory of unsaturated soil behaviour is required for the study of either expansive soils or collapsible soils. The historical development of a general volume change theory for unsaturated soils has been presented by Ho, 1988; Rahardjo, 1990; Fredlund and Rahardjo, 1993; Shuai, 1996; and Pereira, 1996.

Hung (2000) presented a summary of methods for the prediction of heave and reviewed uncoupled and coupled solutions of consolidation/swelling problems in unsaturated soils. The development of methods and computer models for saturated/unsaturated seepage and stress analysis was also reviewed.

This chapter presents a brief review of stress state variables, constitutive relationships, and flow laws for unsaturated soils. Soil properties required in the constitutive relationships are examined. Relationships between the coefficients of volume change and elasticity parameters are presented and related to different loading conditions. The elasticity parameters for the soil structure constitutive surface can be calculated from conventional oedometer test results. Analytical solutions to one-dimensional heave of expansive soils are reviewed. The development of uncoupled and coupled solutions of volume change associated with expansive soils is also presented.

2.2 Stress state variables and constitutive relationships

The behaviour of unsaturated soils can be explained using the general theory of unsaturated soils, through the use of stress state variables, the constitutive relationships for soil structure and water phase and flow laws for the fluids (Fredlund and Rahardjo, 1993).

2.2.1 Stress state variables

A single stress state variable controlling the behaviour of a saturated soil is the effective stress (Terzaghi, 1936). The effective normal stresses, denoted as σ', can be written as follows:

$$\sigma' = (\sigma - u_w) \tag{2.1}$$

where:

σ = total normal stresses, and

u_w = pore-water pressure.

The use of Terzaghi's effective stress state variable has been well accepted and experimentally verified for saturated soils (Rendulic, 1936; Bishop and Eldin, 1950; Laughton, 1955; Skempton, 1961). There have been attempts to extend the effective stress equation for unsaturated soils. Bishop (1959) defined the stress state in the form of an equation by including the pore-air pressure and a soil property:

$$\sigma' = (\sigma - u_a) + \chi(u_a - u_w) \tag{2.2}$$

where:

u_a = pore-air pressure, and

χ = a parameter related to the degree of saturation of soils (called Bishop's parameter).

The magnitude of Bishop's parameter is equal to 1 for saturated soils and zero for dry soils, but depends on factors such as soil structure, drying and wetting cycles, and stress history (Bishop, 1960).

Bishop's effective equation (Eq. 2.2) has been questioned by several researchers. It was suggested that Bishop's equation did not provide an adequate relationship between volume change and effective stress for most soils, particularly those below a critical degree of saturation (Jennings and Burland, 1962). The equation could be used more accurately for shear strength behaviour than for volume change (Bishop and Blight, 1963). It was also observed that Bishop's parameter, χ, when determined for volume change behaviour differed from that when determined for shear strength (Morgenstern, 1979).

Several other effective stress equations have been proposed for unsaturated soils (Aitchison, 1961; Jennings, 1961; Richards, 1967; Aitchison, 1973). All equations incorporate a soil parameter in order to form a single-value stress variable. Experiments have demonstrated that the effective stress equation is not single-valued. Rather, there is a dependence on the stress path followed (Fredlund and Rahardjo, 1993).

Many researchers suggested that more than one stress state variable should be used to describe the behaviour of unsaturated soils (Coleman, 1962; Burland, 1965, Matyas and Radhakrishna, 1968; Barden et al., 1969; Brackley, 1971; Fredlund and Morgenstern, 1977).

Fredlund and Morgenstern (1977) proposed that the constitutive behaviour of unsaturated soils be described using two independent stress state variables; namely, net normal stress, $(\sigma - u_a)$, and matric suction, $(u_a - u_w)$. The validity of these stress state variables has been experimentally tested (Fredlund, 1973) and have now become well accepted. The use of independent stress state variables has produced a more meaningful description of unsaturated soil behaviour, and forms the basis for the formulations of shear strength and volume change problems for unsaturated soils (Fredlund and Rahardjo, 1993).

2.2.2 Constitutive relationships

Volume change constitutive relationships relate the stress state variables to the deformation variables of a continuum through the use of elasticity parameters. Several constitutive relationships have been proposed for volume change of

unsaturated soils (Terzaghi, 1936; Biot, 1941; Bishop, 1959; Coleman, 1962; Bishop and Blight, 1963; Matyas and Radhakrishna, 1968; Barden et al., 1969; Aitchison et al., 1973, Fredlund and Morgenstern, 1976; Mitchell and Avalle, 1984; Llorett and Alonso, 1985; Ho, 1988; Fredlund and Rahardjo, 1993). The proposed constitutive relationships have been presented in the form of mathematical equations and/or presented graphically. In general, two constitutive relationships are presented to describe the volume change associated with an unsaturated soil; one relationship for the soil structure (in terms of void ratio or volumetric strain) and another for the water phase (in terms of degree of saturation or water content). These relationships are expressed in terms of the total stress, σ, pore-air pressure, u_a, and pore-water pressure, u_w. The constitutive relationships for unsaturated soils should be expressed using two independent stress state variables. The constitutive relationships proposed by Fredlund and Morgenstern (1976) appeared to be satisfactory to explain the behaviour of unsaturated soils.

An unsaturated soil is considered as a four-phase mixture (Fredlund, 1979), with two phases that come to equilibrium under applied stress (i.e., soil particle and contractile skin) and two phases that flow under applied pressure (i.e., the air and the water). The total volume change of the soil element must be equal to the sum of volume changes associated with each phase. If the soil particles are assumed incompressible and the volume change of the contractile skin assumed internal to the element, the continuity requirement for an element of unsaturated soil reduces to (Fredlund and Morgenstern, 1976):

$$\frac{\Delta V_v}{V_0} = \frac{\Delta V_w}{V_0} + \frac{\Delta V_a}{V_0} \tag{2.3}$$

where:

V_0 = initial overall volume of an unsaturated soil element,

V_v = volume of soil voids,

V_w = volume of water in the element, and

V_a = volume of air in the element.

In order to describe completely the volume change in an unsaturated soil, the volume changes associated with any two of the three above variables must be measured or predicted, while the third can be computed. In practice, the overall and water volume changes are usually measured, while the air volume change is calculated.

Using Cartesian coordinate system and referencing deformation to an elemental volume, the deformation variable associated with total volume change can be written as the sum of the normal strains as follows:

$$\varepsilon_v = \frac{\Delta V_v}{V_0} = \varepsilon_x + \varepsilon_y + \varepsilon_z \tag{2.4}$$

where:

ε_v = volumetric strain, and

$\varepsilon_x, \varepsilon_y, \varepsilon_z$ = normal strain components in x-, y-, and z-directions, respectively. (Note: x- is used for the horizontal direction and y- is used for the vertical direction).

Assuming infinitesimal deformations, the same elemental volume can be used for the measurement of water volume change (Fredlund, 1973). The deformation variable associated with the water phase is defined as $\Delta V_w/V_0$.

2.2.2.1 Soil structure constitutive relationship

The constitutive relationships for an unsaturated soil can be formulated as an extension of the equations used for saturated soil, using two independent stress state variables. These relationships can be presented in various forms such as elasticity form and compressibility form.

In elasticity form, the soil structure constitutive relations associated with the normal strains in the x-, y-, and z-directions are as follows (Fredlund and Morgenstern, 1976; Fredlund, 1979):

$$\varepsilon_x = \frac{(\sigma_x - u_a)}{E} - \frac{\mu}{E}(\sigma_y + \sigma_z - 2u_a) + \frac{(u_a - u_w)}{H} \tag{2.5}$$

$$\varepsilon_y = \frac{(\sigma_y - u_a)}{E} - \frac{\mu}{E}(\sigma_x + \sigma_z - 2u_a) + \frac{(u_a - u_w)}{H} \tag{2.6}$$

$$\varepsilon_z = \frac{(\sigma_z - u_a)}{E} - \frac{\mu}{E}(\sigma_x + \sigma_y - 2u_a) + \frac{(u_a - u_w)}{H} \tag{2.7}$$

where:

E = elasticity parameter for the soil structure with respect to a change in the net normal stress, $(\sigma - u_a)$, and

H = elasticity parameter for the soil structure with respect to a change in matric suction, $(u_a - u_w)$.

The constitutive equations associated with the shear deformations are:

$$\gamma_{xy} = \frac{\tau_{xy}}{G} \tag{2.8}$$

$$\gamma_{yz} = \frac{\tau_{yz}}{G} \tag{2.9}$$

$$\gamma_{zx} = \frac{\tau_{zx}}{G} \tag{2.10}$$

where:

τ_{xy} = shear stress on the x-plane in the y-direction (i.e., $\tau_{xy} = \tau_{yx}$),

τ_{yz} = shear stress on the y-plane in the z-direction (i.e., $\tau_{yz} = \tau_{zy}$),

τ_{zx} = shear stress on the z-plane in the x-direction (i.e., $\tau_{zx} = \tau_{xz}$), and

G = shear modulus.

The constitutive equations can also be applied to situations where the stress versus strain relationships are non-linear. An incremental procedure using small increments of stress and strain can be used to apply the linear elasticity formulation to a non-linear stress versus strain curve. The non-linear stress versus strain curve is assumed to be linear within each stress and strain increment. The elasticity

parameters, E and H, may vary in magnitude from one increment to another. The soil structure constitutive relations associated with the normal strains can be written in an incremental form as follows:

$$d\varepsilon_x = \frac{d(\sigma_x - u_a)}{E} - \frac{\mu}{E} d(\sigma_y + \sigma_z - 2u_a) + \frac{d(u_a - u_w)}{H} \tag{2.11}$$

$$d\varepsilon_y = \frac{d(\sigma_y - u_a)}{E} - \frac{\mu}{E} d(\sigma_x + \sigma_z - 2u_a) + \frac{d(u_a - u_w)}{H} \tag{2.12}$$

$$d\varepsilon_z = \frac{d(\sigma_z - u_a)}{E} - \frac{\mu}{E} d(\sigma_x + \sigma_y - 2u_a) + \frac{d(u_a - u_w)}{H} \tag{2.13}$$

A change in the volumetric strain of the soil for each increment, $d\varepsilon_v$, can be obtained by summing the changes in normal strains in the x-, y-, and z-directions:

$$d\varepsilon_v = d\varepsilon_x + d\varepsilon_y + d\varepsilon_z \tag{2.14}$$

where:

$d\varepsilon_v$ = change in volumetric strain for each stress increment.

Substituting Eqs. (2.11), (2.12), and (2.13) into Eq. (2.14) gives the volumetric strain for the particular loading increment of the general three-dimensional loading conditions:

$$d\varepsilon_v = \frac{dV_v}{V_0} = 3\left(\frac{1-2\mu}{E}\right) d(\sigma_{mean} - u_a) + \frac{3}{H} d(u_a - u_w) \tag{2.15}$$

where:

σ_{mean} = mean total normal stress [i.e., $(\sigma_x+\sigma_y+\sigma_z)/3$].

Fredlund and Rahardjo (1993) presented the constitutive relationship for soil structure in a compressibility form for the general, three-dimensional loading conditions:

$$d\varepsilon_v = m_1^s d(\sigma_{mean} - u_a) + m_2^s d(u_a - u_w) \tag{2.16}$$

where:

m_1^s = $\frac{3(1-2\mu)}{E}$, coefficient of volume change with respect to a change in net normal stress, and

m_2^s = $\frac{3}{H}$, coefficient of volume change with respect to a change in matric suction.

These constitutive equations have been experimentally tested for uniqueness near a point (Fredlund and Morgenstern, 1976) and for uniqueness when larger stress increments are used (Matyas and Radhakrishna, 1968; Barden et al., 1969). The results indicate uniqueness as long as the deformation conditions are monotonic. The unloading constitutive relationship for soil structure is presented graphically in the form of constitutive surface in Fig. 2.1.a.

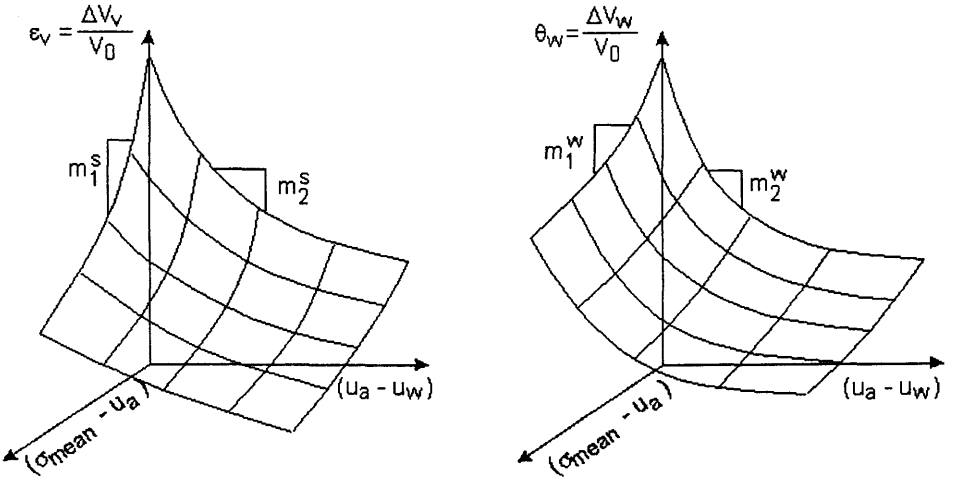

a. soil structure b. water phase

Figure 2.1 Constitutive surfaces for soil structure and water phase of an unsaturated soil

The constitutive relationship for soil structure can be plotted with respect to the logarithm of the stress state variables. The relationship of void ratio versus logarithm of effective stress is well established for saturated soils. The compression

of a saturated soil consists of two distinct stages, the recompression (or rebound) and virgin compression (Terzaghi and Peck, 1967). The virgin compression curve and rebound curve can be linearized on a semi-logarithmic scale, the rebound curves are approximately parallel to one another (Lambe and Whitman, 1969) (i.e., the slope of the rebound curves is independent of the maximum past pressure). This relationship becomes void ratio versus net normal stress when the pore-water pressure is zero. Figure 2.2 shows these linear relationships as typical results of a one-dimensional constant volume and free swell tests on Regina clay specimens. Linear relationships of vertical strain (swelling) and the logarithm of decreasing effective stress are also shown in Fig. 2.3 for Arizona clay.

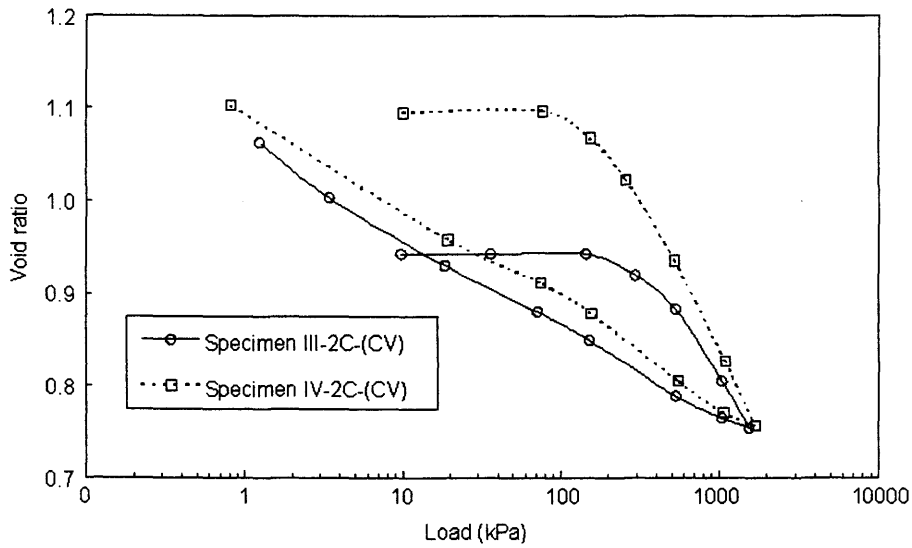

Figure 2.2 Void ratio versus pressure curve for loading and unloading portions of the curves for Regina clay (after Gilchrist, 1963)

An expansive soil is compressed due to suction increase (i.e., desiccation) and rebound due to suction decrease (i.e., wetting). The void ratio versus suction also consists of a recompression and a virgin compression portion. The virgin compression branch and the rebound curves are essentially linear on a semi-logarithmic scale (Fredlund, 1964). The semi-logarithmic plot of soil structure constitutive surface for an unsaturated soil is linear on the extreme planes over a relatively large stress range (Ho, 1988). The linear relationship of vertical strain to the

logarithm of matric suction under a constant applied total stress is presented in Fig. 2.4 for both the drying and wetting paths of Athelstone Park clay. The slope of the void ratio versus logarithm of stress state variables are called volume change indices. Fredlund and Rahardjo (1993) presented the soil structure constitutive relationship as a semi-logarithm surface. Figure 2.5 presents hypothesised unloading constitutive surface for the soil structure using a semi-logarithmic scale.

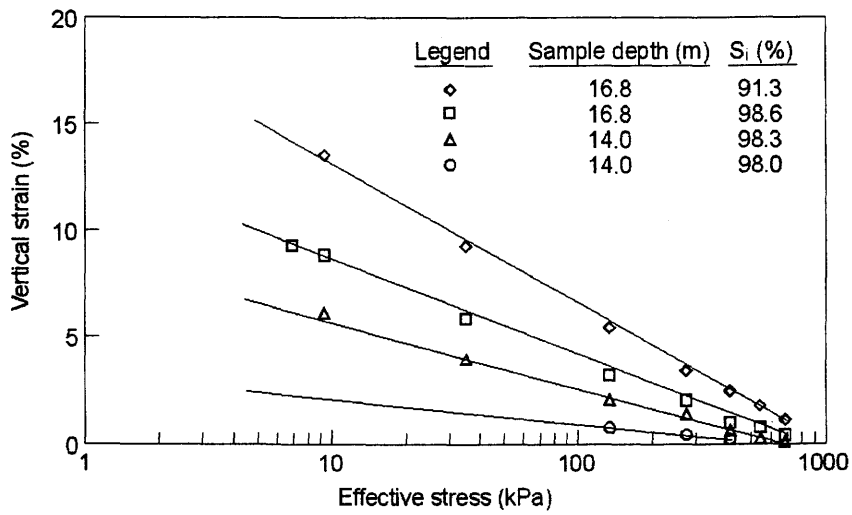

Figure 2.3 Relationship between vertical strain and logarithm of effective stress for the swelling portion for Arizona clay (Holtz and Gibbs, 1956)

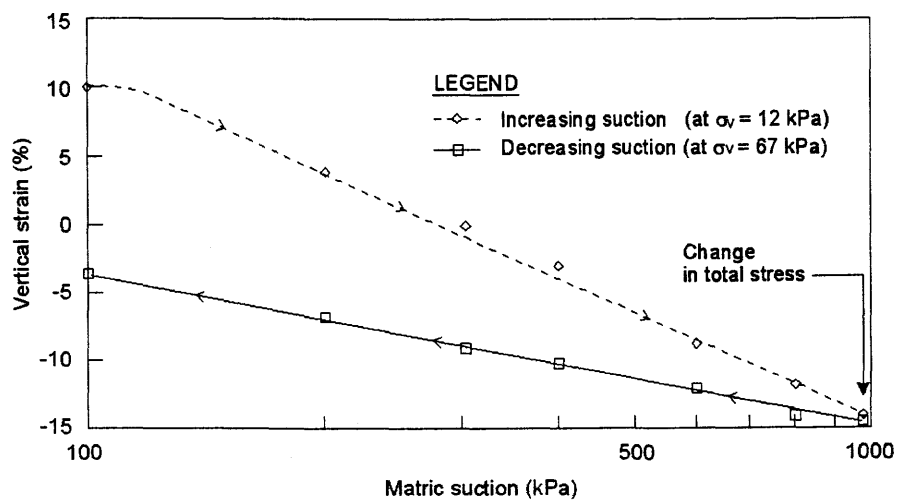

Figure 2.4 Relationship between vertical strain and logarithm of matric suction for the loading and unloading of Athelstone Park clay (Richards et al., 1984)

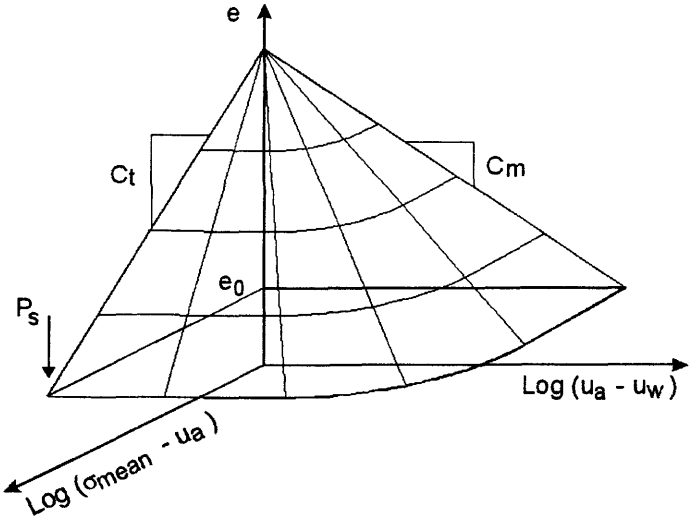

Figure 2.5 Hypothesised void ratio semi-logarithmic constitutive surface for an expansive soil (Fredlund and Rahardjo, 1993)

2.2.2.2 Water phase constitutive relationship

Fredlund and Rahardjo (1993) formulated the water phase constitutive relationship using a semi-empirical approach based on a linear combination of the stress state variables. In an elasticity form, the constitutive equation can be written as follows:

$$\frac{dV_w}{V_0} = \frac{3}{E_w} d(\sigma_{mean} - u_a) + \frac{1}{H_w} d(u_a - u_w) \tag{2.17}$$

where:

E_w = water volumetric parameter associated with a change in the net normal stress, and

H_w = water volumetric parameter associated with a change in matric suction.

Using a compressibility form, the constitutive relationship for water phase can be written as follows:

$$\frac{dV_w}{V_0} = m_1^w d(\sigma_{mean} - u_a) + m_2^w d(u_a - u_w) \tag{2.18}$$

where:

m_1^w = $\frac{3}{E_w}$, coefficient of volume change with respect to a change in net normal stress, and

m_2^w = $\frac{1}{H_w}$, coefficient of volume change with respect to a change in matric suction.

The unloading constitutive relationship for water phase is presented graphically in the form of constitutive surface in Fig. 2.1b. It should be noted that the above equations do not represent a mathematical form for the entire constitutive surface. Rather, the equations represent the mathematical form that appears near a single stress point on the constitutive surfaces. Mathematical equations to represent the entire constitutive surfaces for an unsaturated soil is still a topic of ongoing research (M. Fredlund, 2000).

2.2.2.3 Relationships of the coefficients of volume change and elasticity parameters for different loading conditions

The constitutive relationships can be written to accommodate specific loading conditions such as K_0-loading and plane strain loading (Fredlund and Rahardjo, 1993). The coefficients of volume change for any loading condition can be related to the coefficients of volume change for the general, three-dimensional loading condition and therefore to the basic elasticity parameters, E, H, and μ. Using the notation for changes in stress state variables presented in Table 2.1, and the definitions of the coefficients of volume change presented in Table 2.2, the relationship between the coefficients of volume change and elasticity parameters can be written as showed in Table 2.3.

Table 2.1 Change in stress state variables for different loading conditions

Loading	First stress state variable	Second stress state variable
Three-dimensional (3D)	$d(\sigma_{mean} - u_a)$	$d(u_a - u_w)_{3D}$
K_0-loading (1D)	$d(\sigma_y - u_a)$	$d(u_a - u_w)_{1D}$
Plane strain (2D)	$d(\sigma_{ave} - u_a)$	$d(u_a - u_w)_{2D}$

Note: $\sigma_{mean} = (\sigma_x + \sigma_y + \sigma_z)/3$; $\sigma_{ave} = (\sigma_x + \sigma_y)/2$

Table 2.2 Definition of the coefficients of volume change for different loading conditions

Loading	Soil structure	Water phase
Three-dimensional (3D)	$m_1^s = \frac{d\varepsilon_v}{d(\sigma_{mean} - u_a)}$ $m_2^s = \frac{d\varepsilon_v}{d(u_a - u_w)_{3D}}$	$m_1^w = \frac{dV_w / V_0}{d(\sigma_{mean} - u_a)}$ $m_2^w = \frac{dV_w / V_0}{d(u_a - u_w)_{3D}}$
K_0-loading (1D)	$m_{1-1D}^s = \frac{d\varepsilon_y}{d(\sigma_y - u_a)}$ $m_{2-1D}^s = \frac{d\varepsilon_y}{d(u_a - u_w)_{1D}}$	$m_{1-1D}^w = \frac{dV_w / V_0}{d(\sigma_y - u_a)}$ $m_{2-1D}^w = \frac{dV_w / V_0}{d(u_a - u_w)_{1D}}$
Plane strain (2D)	$m_{1-2D}^s = \frac{d(\varepsilon_x + \varepsilon_y)}{d(\sigma_{ave} - u_a)}$ $m_{2-2D}^s = \frac{d(\varepsilon_x + \varepsilon_y)}{d(u_a - u_w)_{2D}}$	$m_{1-2D}^w = \frac{dV_w / V_0}{d(\sigma_{ave} - u_a)}$ $m_{2-2D}^w = \frac{dV_w / V_0}{d(u_a - u_w)_{2D}}$

Note: $d\varepsilon_y = d\varepsilon_v$ for K_0-loading; $d(\varepsilon_x + \varepsilon_y) = d\varepsilon_v$ for plane strain loading

Table 2.3 provides the relationships for the coefficients of volume change and the elasticity parameters for different loading conditions. The coefficients obtained from one loading condition can be converted to other loading conditions through the use of these basic relationships (Fredlund and Rahardjo, 1993).

$$m_1^s = \frac{3(1-\mu)}{(1+\mu)} m_{1-1D}^s = \frac{3}{2(1+\mu)} m_{1-2D}^s \tag{2.19}$$

$$m_2^s = \frac{3(1-\mu)}{(1+\mu)} m_{2-1D}^s = \frac{3}{2(1+\mu)} m_{2-2D}^s \tag{2.20}$$

$$m_1^w = \frac{3(1-\mu)}{(1+\mu)} m_{1-1D}^w = \frac{3}{2(1+\mu)} m_{1-2D}^w \tag{2.21}$$

$$m_2^w = m_{2\text{-}1D}^w + \frac{2}{3}\frac{(1-2\mu)}{(1-\mu)}\frac{m_2^s}{m_1^s}m_1^w = m_{2\text{-}2D}^w + \frac{(1-2\mu)}{3}\frac{m_2^s}{m_1^s}m_1^w \tag{2.22}$$

Table 2.3 Relationship between the coefficients of volume change and the fundamental elasticity parameters (after Fredlund and Rahardjo, 1993)

Loading	Soil structure	Water phase
Three-dimensional (3D)	$m_1^s = 3\frac{(1-2\mu)}{E}$ $m_2^s = \frac{3}{H}$	$m_1^w = \frac{3}{E_w}$ $m_2^w = \frac{1}{H_w}$
K_0-loading (1D)	$m_{1\text{-}1D}^s = \frac{(1+\mu)(1-2\mu)}{E(1-\mu)}$ $m_{2\text{-}1D}^s = \frac{(1+\mu)}{H(1-\mu)}$	$m_{1\text{-}1D}^w = \frac{(1+\mu)}{E_w(1-\mu)}$ $m_{2\text{-}1D}^w = \frac{1}{H_w} - \frac{2(E/H)}{E_w(1-\mu)}$
Plane strain (2D)	$m_{1\text{-}2D}^s = \frac{2(1+\mu)(1-2\mu)}{E}$ $m_{2\text{-}2D}^s = \frac{2(1+\mu)}{H}$	$m_{1\text{-}2D}^w = \frac{2(1+\mu)}{E_w}$ $m_{2\text{-}2D}^w = \frac{1}{H_w} - \frac{(E/H)}{E_w}$

Table 2.4 presents the calculation of elasticity parameters from the coefficients of volume change with respect to different loading conditions. It is important to note that five fundamental elasticity parameters are required in the constitutive equations (i.e., E, H, E_w, H_w, and μ). However, there are only four coefficients of volume change obtained from the two constitutive surfaces (i.e., m_1^s, m_2^s, m_1^w, and m_2^w). Poisson's ratio must be measured or assumed in order to convert the coefficients of volume change for different loading conditions to the fundamental elasticity parameters.

Table 2.4 Relationship between the fundamental elasticity parameters and the coefficients of volume change

Loading	Soil structure	Water phase
Three-dimensional (3D)	$E = 3\dfrac{(1-2\mu)}{m_1^s}$ $H = \dfrac{3}{m_2^s}$	$E_w = \dfrac{3}{m_1^w}$ $H_w = \dfrac{1}{m_2^w}$
K_0-loading (1D)	$E = \dfrac{(1+\mu)(1-2\mu)}{(1-\mu)m_{1\text{-}1D}^s}$ $H = \dfrac{(1+\mu)}{(1-\mu)m_{2\text{-}1D}^s}$	$E_w = \dfrac{(1+\mu)}{(1-\mu)m_{1\text{-}1D}^w}$ $H_w = \left(m_{2\text{-}1D}^w + \dfrac{2}{3}\dfrac{(1-2\mu)}{(1-\mu)}\dfrac{m_2^s}{m_1^s}m_1^w \right)^{-1}$
Plane strain (2D)	$E = \dfrac{2(1+\mu)(1-2\mu)}{m_{1\text{-}2D}^s}$ $H = \dfrac{2(1+\mu)}{m_{2\text{-}2D}^s}$	$E_w = \dfrac{2(1+\mu)}{m_{1\text{-}2D}^w}$ $H_w = \left(m_{2\text{-}2D}^w + \dfrac{(1-2\mu)}{3}\dfrac{m_2^s}{m_1^s}m_1^w \right)^{-1}$

Table 2.5 presents the constitutive equations for the soil structure written with the use of the coefficients of volume change for three-dimensional loading (i.e., m_1^s and m_2^s).

Table 2.5 Different forms of constitutive equations for soil structure

Loading	Equations
Three-dimensional (3D)	$d\varepsilon_v = m_1^s d(\sigma_{mean} - u_a) + m_2^s d(u_a - u_w)_{3D}$
K_0-loading (1D)	$d\varepsilon_v = m_{1\text{-}1D}^s d(\sigma_y - u_a) + m_{2\text{-}1D}^s d(u_a - u_w)_{1D}$ $d\varepsilon_v = \dfrac{1}{3}\dfrac{(1+\mu)}{(1-\mu)}m_1^s d(\sigma_y - u_a) + \dfrac{1}{3}\dfrac{(1+\mu)}{(1-\mu)}m_2^s d(u_a - u_w)_{1D}$ $d\varepsilon_v = m_1^s d(\sigma_{mean} - u_a) + m_2^s d(u_a - u_w)_{3D}$
Plane strain (2D)	$d\varepsilon_v = m_{1\text{-}2D}^s d(\sigma_{ave} - u_a) + m_{2\text{-}2D}^s d(u_a - u_w)_{2D}$ $d\varepsilon_v = \dfrac{2(1+\mu)}{3}m_1^s d(\sigma_{ave} - u_a) + \dfrac{2(1+\mu)}{3}m_2^s d(u_a - u_w)_{2D}$ $d\varepsilon_v = m_1^s d(\sigma_{mean} - u_a) + m_2^s d(u_a - u_w)_{3D}$

2.2.2.4 Volume change indices for various loading conditions

Volume change indices are slopes of the void ratio versus logarithm of stress state variables. Table 2.6 defines the volume change indices for various loading paths.

Table 2.6 Definition of volume change indices

Loading	Volume change index with respect to net normal stress	Volume change index with respect to matric suction
Three-dimensional (3D)	$C_t = \frac{de}{d\log(\sigma_{mean} - u_a)}$	$C_m = \frac{de}{d\log(u_a - u_w)_{3D}}$
K_0-loading (1D)	$C_{t-1D} = \frac{de}{d\log(\sigma_y - u_a)}$	$C_{m-1D} = \frac{de}{d\log(u_a - u_w)_{1D}}$
Plane strain (2D)	$C_{t-2D} = \frac{de}{d\log(\sigma_{ave} - u_a)}$	$C_{m-2D} = \frac{de}{d\log(u_a - u_w)_{2D}}$

Based on the constitutive relations presented in Table 2.5, the following relations can be obtained along the constant matric suction plane and the constant net normal stress plane for the soil structure constitutive surface:

$$d(\sigma_{mean} - u_a) = \frac{2}{3}(1+\mu)d(\sigma_{ave} - u_a) = \frac{1}{3}\frac{(1+\mu)}{(1-\mu)}d(\sigma_y - u_a) \tag{2.23}$$

$$d(u_a - u_w)_{3D} = \frac{2}{3}(1+\mu)d(u_a - u_w)_{2D} = \frac{1}{3}\frac{(1+\mu)}{(1-\mu)}d(u_a - u_w)_{1D} \tag{2.24}$$

Equations (2.23) and (2.24) allow the following relations for the non-zero net normal stress plane and the matric suction plane with respect to different loading conditions:

$$d[\log(\sigma_{mean} - u_a)] = d[\log(\sigma_{ave} - u_a)] = d[\log(\sigma_y - u_a)] \tag{2.25}$$

$$d[\log(u_a - u_w)_{3D}] = d[\log(u_a - u_w)_{2D}] = d[\log(u_a - u_w)_{1D}] \tag{2.26}$$

Substituting Eqs. (2.25) and (2.26) into the relationships presented in Table 2.6, the following relationships can be written.

$$C_{t-1D} = C_{t-2D} = C_t \tag{2.27}$$

$$C_{m-1D} = C_{m-2D} = C_m \tag{2.28}$$

The volume change indices with respect to net normal stress, and with respect to matric suction are theoretically the same for the above mentioned loading conditions. The volume change index obtained from isotropic loading has been shown to be experimentally the same as that obtained from K_0-loading (Graham, 1997). Figure 2.6 presents the swelling versus logarithm of confining pressure from oedometer and triaxial swell tests for Al-Ghatt shale. It can be seen that the data from both the triaxial and oedometer tests are approximately fitted by a straight line. The volumetric swell curve measured from triaxal test is essentially parallel to the vertical swell curve measured from oedometer test.

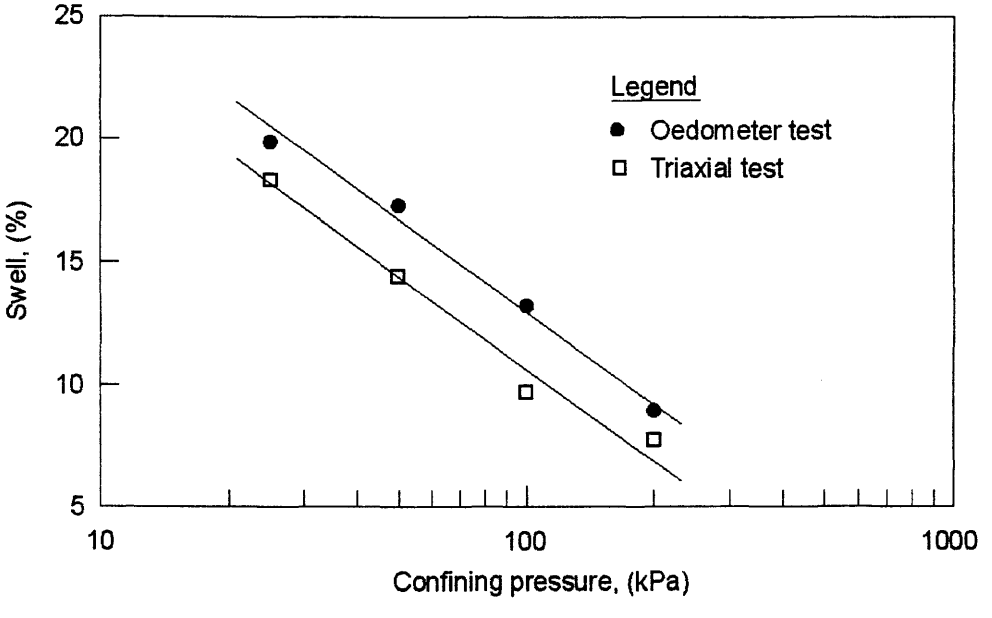

Figure 2.6 Relationship between volumetric swell and confining pressure from oedometer and triaxial swell test (Al-Shamrani and Al-Mhaidib, 2000)

2.2.2.5 Sign conventions

Fredlund and Rahardjo (1993) suggested a sign convention for the coefficients of volume change and elasticity parameters. A positive change in the state variable (i.e., deformation or stress) refers to an increase in the state variable, whereas a negative change indicates a decrease in the state variable. The signs of the fundamental elasticity parameters, E, H, E_w, and H_w, are determined by the sign of the deformation state variables and the stress state variables. For an expansive soil, all the coefficients of volume change (i.e., m_1^s, m_2^s, m_1^w, and m_2^w), volume change indices (i.e., C_t and C_m), and elasticity parameters (i.e., E, H, E_w, H_w) will have negative signs, while Poisson's ratio, μ is assumed to have a positive sign. The volume change for an expansive soil increases with decreasing net normal stress or matric suction. The values of the coefficients of volume change, elasticity parameters, and volume change indices are often presented as absolute magnitudes, without a minus sign.

2.2.2.6 Calculation of the elasticity parameters for the soil structure

The coefficients of volume change can be obtained from the constitutive surfaces (Fig. 2.1 and Table 2.2). The coefficients of volume change can then be used to calculate the elasticity parameters (Table 2.4).

Hung (2000) calculated the elasticity parameter functions, E and H, from volume change indices, C_t (from net normal stress plane) and C_m (from matric suction plane), respectively. The coefficient of volume change is first calculated by converting the volume change index from semi-logarithmic plot into the arithmetic plot. The elasticity parameters are then calculated from the coefficient of volume change as shown in Table 2.4. These elasticity parameters then are applied for the entire constitutive surface. The elasticity parameter, E, can be expressed as a function of volume change index with respect to net normal stress, C_t, initial void ratio and Poisson's ratio. The elasticity parameter, H, can be expressed as a function of the volume change index with respect to matric suction, C_m, initial void ratio and Poisson's ratio. The equations for these elasticity parameters can be written for general three-dimensional loading conditions as follows:

$$E = \frac{6.908(1-2\mu)(1+e_0)}{C_t}(\sigma_{mean} - u_a) \tag{2.29}$$

$$H = \frac{6.908(1+e_0)}{C_m}(u_a - u_w) \tag{2.30}$$

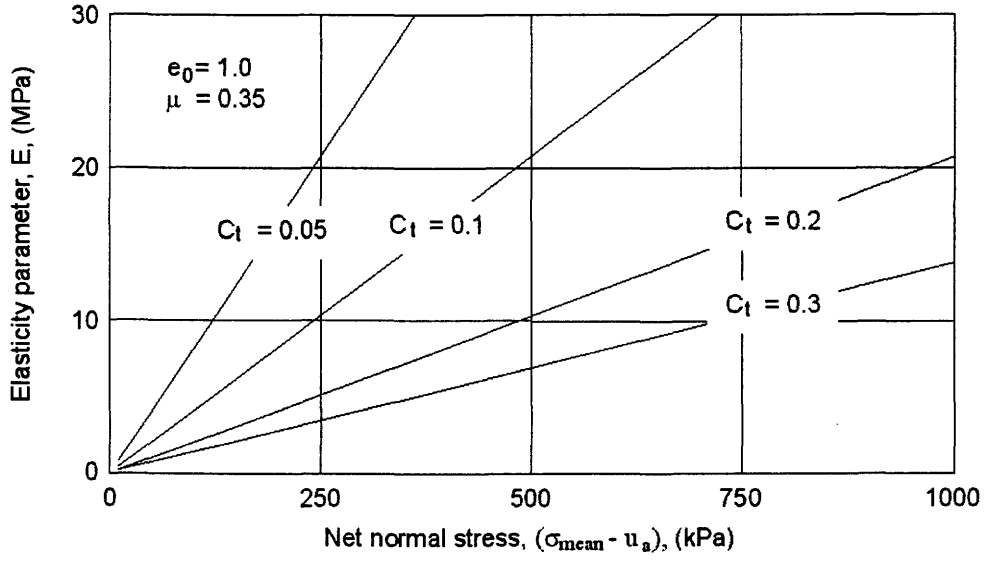

Figure 2.7 Relationship between the elasticity parameter, E and net mean stress for various values of swelling index (from Hung, 2000)

Figure 2.7 presents graphically the relationship between elasticity parameter, E and net mean stress for various values of volume change index with a constant value of Poisson's ratio. The elasticity parameter, E, increases with the increase of net mean stress and the decrease of volume change index, C_t. Figure 2.8 shows the variation of elasticity parameter, E and net mean stress for various values of Poisson's ratio with a constant value of volume change index, C_t. The elasticity parameter, E, increases with an increase in net mean stress and a decrease in Poisson's ratio. The elasticity parameter, H, increases with an increasing value of matric suction and a decreasing value of volume change index, C_m as shown in Fig. 2.9. Equations (2.29) and (2.30), and Figs. 2.7, 2.8 and 2.9 do not show the variation in elasticity parameter, E, with matric suction, and the variation of elasticity

parameter, H, with net normal stress. In addition, these equations are not valid when net normal stress and matric suction approach zero. At small values of net normal stress or matric suction, these parameters become mathematically small; resulting in an unstable computation of the volume change problem or unreasonably large deformation.

The elasticity parameters, E and H, can be related to mean net normal stress (using m_1^s); average net normal stress (using m_{1-2D}^s); or vertical net normal stress (using m_{1-1D}^s) through the use of Eqs. 2.23 and 2.24.

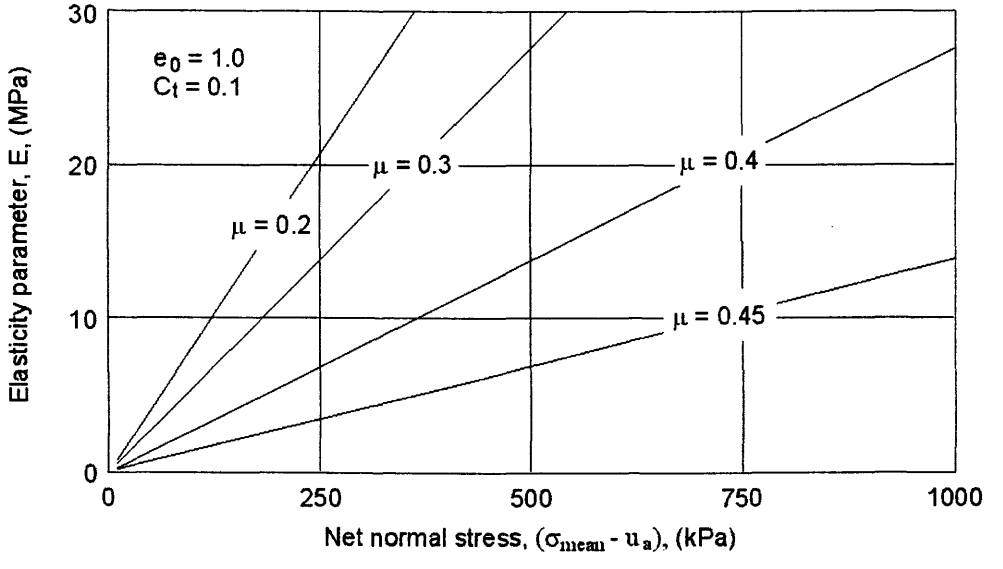

Figure 2.8 Relationship between the elasticity parameter, E and net mean stress for various values of Poisson's ratio (from Hung, 2000)

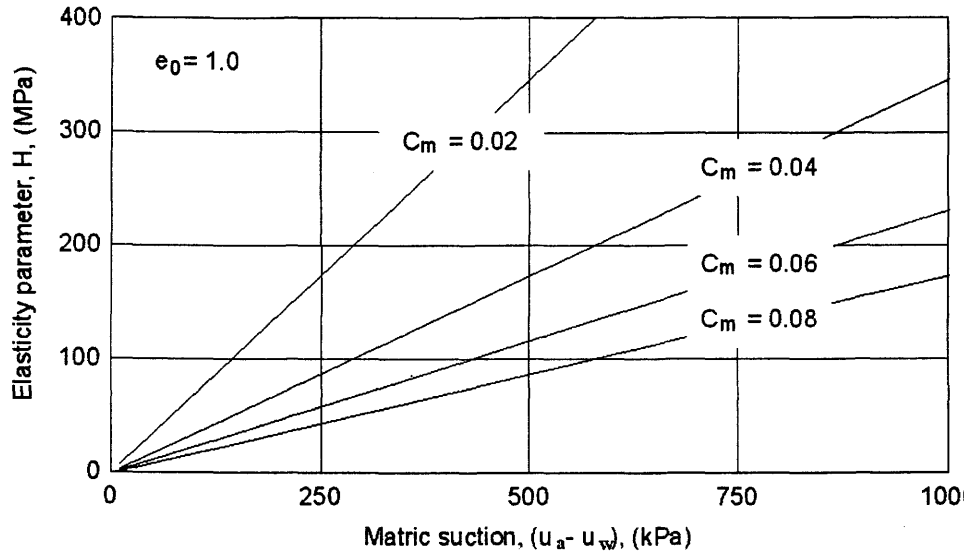

Figure 2.9 Relationship between the elasticity parameter, H and matric suction for various values of swelling index (from Hung, 2000)

2.2.3 Flow laws

In unsaturated soils, two phases are classified as fluids that can flow (i.e., water phase and air phase). Flow laws are required to relate the flow rate with driving potential using appropriate coefficients.

2.2.3.1 Flow of water

The driving potential for the flow of water is hydraulic head (or total head). The hydraulic head consists of the gravitational head and the pressure head.

$$h_w = Y + \frac{u_w}{\rho_w g} \tag{2.31}$$

where:

h_w = hydraulic head,

Y = elevation head,

$\frac{u_w}{\rho_w g}$ = pressure head,

ρ_w = density of water, and

g = gravitational acceleration.

The flow of water in a saturated/unsaturated soil system is commonly described using Darcy's law (Buckingham, 1907; Richard, 1931; Childs and Collis-George, 1950; Freeze and Cherry, 1979). Darcy (1856) stated that the rate of water flow through a soil mass was proportional to the hydraulic head gradient. Darcy's law can be written for the y-direction in the Cartesian coordinate system as follows:

$$q_w = -k_w \frac{\partial h_w}{\partial y} \tag{2.32}$$

where:

q_w = flow rate of water,

k_w = coefficient of permeability with respect to water phase, and

$\partial h_w / \partial y$ = hydraulic head gradient in the y-direction.

The coefficient of permeability with respect to water phase is a measure of space available for water to flow through the soil. The coefficient of permeability depends upon the properties of the fluid and the properties of the porous medium.

The coefficient of permeability for a given unsaturated soil is a function of degree of saturation and void ratio (Lloret and Alonso, 1980; Fredlund, 1981). For a given saturated soil, the coefficient of permeability is a function of the void ratio (Lambe and Whitman, 1969). In an unsaturated soil, the coefficient of permeability is significantly affected by combined changes in the void ratio, e, and the degree of saturation, S, of the soil (Fredlund and Rahardjo, 1993). The degree of saturation can be written as a function of matric suction, and so the coefficient of permeability is also written as function of the matric suction and void ratio. The coefficient of permeability function can be directly measured, indirectly computed or estimated by combining the soil-water characteristic curve and the saturated coefficient of permeability. Many permeability functions have been proposed in the literature to describe the coefficient of permeability of an unsaturated soil (e.g., Gardner, 1958; Phillip, 1986; van Genuchten, 1980; Fredlund and Xing, 1994; Leong and Rahardjo, 1997).

Gardner's coefficient of permeability equation (1958), as an example, is written as follows:

$$k_w = \frac{k_s}{1 + a\left(\frac{(u_a - u_w)}{\rho_w g}\right)^n} \tag{2.33}$$

where:

k_s = coefficient of permeability at saturation, which is a function of void ratio,

a = constant inversely proportional to the breaking point of the function, and

n = constant related to the slope of the function.

2.2.3.2 Flow of air

The driving potential for the flow of air in the continuous air phase is a concentration or pressure gradient. Since the elevation gradient has a negligible effect, the pressure gradient is most commonly considered as the only driving potential for the air phase (Fredlund and Rahardjo, 1993).

Flow of air through an unsaturated soil is commonly described using a modified form of Fick's law.

$$J_a = -D_a^* \frac{\partial u_a}{\partial y} \tag{2.34}$$

where:

J_a = mass rate of air flowing across a unit area of the soil,

D_a^* = $D_a \partial[\rho_a(1-S)n]/\partial u_a$, coefficient of transmission,

D_a = transmission constant for air flow through a soil,

ρ_a = air density related to the absolute air pressure,

n = porosity of the soil, and

$\partial u_a / \partial y$ = pore-air pressure head gradient in the y-direction.

Similar to the coefficient of permeability with respect to water phase, the coefficient of permeability for the air phase is a function of the fluid (i.e., air) and soil volume-mass properties. However, unlike water, air properties can no longer be considered as constants. Density and viscosity of air are functions of the absolute air pressure.

Bear (1972) and Barden and Pavlakis (1971) showed that the coefficient of permeability to air remains significantly greater (i.e., five to seven orders of magnitude) than that to water phase for almost all water contents (Fig. 2.10).

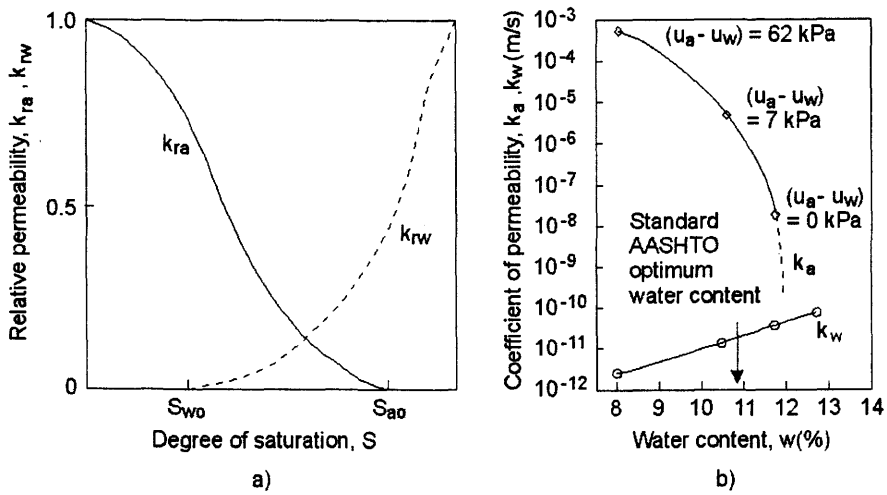

Figure 2.10 Water and air coefficients of permeability. a) Typical relative permeability curve (Bear, 1972); b) Coefficient of permeability with respect to air phase, k_a, and water phase, k_w versus water content for Westwater soil (Barden and Pavlakis, 1971)

Rahardjo and Fredlund (1995) presented an experimental verification for the theory of consolidation for unsaturated soils. The experimental study was limited to the one-dimensional case. Soil properties such as coefficient of consolidation, coefficient of permeability, and coefficients of volume change used during the simulations were assumed to be constants for a single test. The excess pore-air pressure was found to dissipate rapidly when the air-phase was continuous. This finding agreed with research results from Madedor (1967) and Barden (1974). The present study will assume that the air phase is continuous and at atmospheric

pressure; therefore, air-flow is not a relevant process and no further developments on the coefficient of permeability for the air phase are considered.

2.3 Solutions to one-dimensional heave of expansive soils

The techniques available for the prediction of heave can be divided into two main groups. The first group is associated with the heave prediction methods that are based on matric suction measurement. The second group is associated with the heave prediction methods that are based on one-dimensional oedometer test results.

2.3.1 Heave prediction methods based on matric suction measurements

The volume of an expansive soil decreases as soil suction increases and increases as soil suction decreases. Several methods of heave prediction have been proposed. In general, these methods are different in the definition of the slope of the relationship between void ratio (or vertical strain) and the logarithm of soil suction.

Richards (1967) predicted water content changes in soils from water content versus soil suction curves obtained from laboratory tests. The equilibrium suction, determined from correlation between equilibrium soil suction and climatic index, is used to estimate the final water content condition. The soil volume change is predicted on the assumption that the volume change is equal to the volume of water taken up by the soil. The soil volume change is calculated as follows:

$$\frac{\Delta V}{V} = \frac{\Delta w G_s}{100 + w_i G_s} \tag{2.35}$$

where:

Δw = change in water content,

G_s = specific gravity, and

w_i = initial water content.

The strain, $\Delta H/H$, is calculated by assuming equal volume changes in the vertical and horizontal directions as follows:

$$\frac{\Delta H}{H} = \frac{1}{3}\frac{\Delta V}{V} = \frac{1}{3}\frac{\Delta w G_s}{100 + w_i G_s} \tag{2.36}$$

where:

H = thickness of the soil layer.

Aitchison and Woodburn (1969) presented a method for prediction of heave, called the Australian method, which required the use of initial load and soil suction values and predicted final load and soil suction. The testing procedure for this approach involves the use of a modified oedometer, in which applied load and soil suction can be measured. The data are plotted to provide the strain versus soil suction relationship for various loads. Lytton (1977) defined the slope of this curve as the suction compression index or swelling index, γ_h as follows:

$$\gamma_h = \frac{\frac{\Delta V}{V}}{\log\left(\frac{h_f}{h_i}\right)} \tag{2.37}$$

where:

$\Delta V/V$ = volumetric strain, and

h_f, h_i = final and initial soil suction.

Once the suction swelling index is determined, the heave can be predicted based on initial and final conditions as follows:

$$\frac{\Delta V}{V} = \gamma_h \log\left(\frac{h_f}{h_i}\right) \tag{2.38}$$

McKeen (1976) proposed the same procedure based on the suction compression index; however, the initial conditions from suction tests are determined using the filter paper procedure.

Aitchison and Martin (1973) proposed the use of instability index, $I_p^{"}$, to relate vertical swell or shrinkage to change in soil suction:

$$I_p^{"} = \frac{\varepsilon_v}{\Delta \log h} \tag{2.39}$$

where:

ε_v = vertical strain.

Johnson (1977) suggested the calculation of the volume change index, C_τ (i.e., slope of the void ratio versus logarithm of soil suction) as follows:

$$C_\tau = \frac{\alpha G_s}{100B} \tag{2.40}$$

where:

α = compressibility factor, i.e., the fraction of applied pressure that was effective in altering the pore water pressure ($0 < \alpha < 1$), and

B = slope of the soil suction versus water content relationship.

Snethen (1980) used the soil suction versus water content relationship for the prediction of heave. The data are plotted on a pF scale and a straight-line approximation for the water content range of interest is represented as follows:

$$\log h_c^0 = A - Bw \tag{2.41}$$

where:

h_c^0 = soil suction without surcharge pressure, and

A, B = constants (i.e., y intercept and slope, respectively).

The heave of an expansive soil profile is estimated using soil suction relationship as follows:

$$\frac{\Delta H}{H} = \frac{C_\tau}{1+e_0}\left[(A - Bw_0) - \log(h_{cf} + \alpha\sigma_f)\right] \tag{2.42}$$

where:

C_τ = swelling index (i.e., $\alpha G_s/100B$),

α = compressibility factor,

h_{cf} = final soil suction,

σ_f = final applied pressure,

e_0 = initial void ratio, and

w_0 = initial water content.

Several procedures have been developed for the measurement of above volume change index and the instability index (Fargher and Stevens, 1973; Pile and McInnes, 1984; Mitchell and Avalle, 1984; Fredlund and Rahardjo, 1993; Cokca and Birand, 2000). However, for the purpose of brevity, these procedures will not be presented in this study.

McKeen (1992) included a lateral restraint factor, the effects of changes in total suction and confining stress into the equation for prediction of heave.

$$\frac{\Delta H}{H} = C_h \, \Delta h \, f \, s \tag{2.43}$$

where:

Δh = total suction change,

C_h = suction compression index,

f = lateral restraint factor ($0.5 < f < 0.8$ for clays), and

s = load effect coefficient (typically, $s = 0.9$).

The suction compression index, C_h in McKeen (1992) equation is measured using the CLOD test. McKeen (1992) presented an empirical relationship for this index as follows:

$$C_h = -0.02673\left(\frac{\Delta h}{\Delta w}\right) - 0.388704 \tag{2.44}$$

where:

Δw = change in soil water content.

Perko et al. (2000) suggested the following relationship for the McKeen's (1992) suction compression index for the Denver area:

$$C_h = -\frac{10}{3} PL^2 \left(\frac{e+F}{e+1} \right) \tag{2.45}$$

where:

PL = plastic limit (%),

F = weight percent passing the No. 200 sieve, and

e = void ratio.

2.3.2 Heave prediction methods based on one-dimensional oedometer test results

Heave prediction methods based on one-dimensional oedometer test are the most commonly used. In the oedometer methods, soil suction measurements are not required. Some of these methods are briefly reviewed in this suction.

Jennings and Knight (1957) presented the double oedometer method, which is based on the results of two oedometer tests, namely, a free-swell oedometer test and a natural water content test. The specimens are initially subjected to a token load of 1 kPa. No water is added to the oedometer pot during the natural water content test. To compute heave, the two void ratio versus logarithm of pressure curves are adjusted until the virgin compression curves matched. The change in void ratio was determined from the increased pressure caused by an increase in water content. The predicted heave was generally satisfactory since the method of analysing the data appeared to compensate for the effects of sampling disturbance (Fredlund and Rahardjo, 1993).

Sampson et al. (1965) proposed a testing procedure similar to the double oedometer method. One sample is inundated at constant volume and then allowed to swell after load removal. The second sample is loaded to in-situ overburden pressure,

inundated, and allowed to swell at this pressure. The results of the two tests account for overburden removal and increase in water content or decrease in suction.

Sullivan and McClelland (1969) presented a method, called a constant volume oedometer test. An undisturbed sample is loaded to in-situ conditions, then allowed access to water and held at constant volume. The swelling pressure is measured, the sample is then unloaded and allowed to swell by decreasing the loads in small increments to some minimum value. The change in void ratio is determined from the void ratio versus logarithm of pressure curve using the initial and final pressure condition.

Smith (1973) presented the direct model method for the prediction of heave. The method is based on a free-swell oedometer test on undisturbed samples. The specimens are subjected to the overburden pressure (or the load that would exist at the end of construction) and allowed free access to water. The predicted heave is generally significantly below the actual heave experienced in the field. The under estimation of heave appeared to be primarily due to a lack of consideration of disturbance which had been experienced by the soil during sampling (Fredlund and Rahardjo, 1993).

The Navy method (1971) involved testing of undisturbed samples under various surcharge pressures representing the overburden and structural load. These results are used to plot a depth versus percent swell curve, the area under this curve represents the total swell. The plot of total swell (i.e., the area under the above curve) versus depth was constructed to predict the heave for a given cut or depth. Komornik et al., (1969) presented a similar procedure for determining surface heave. The procedure, however, requires the estimation of the equilibrium soil suction. The samples are tested at pressures equal to overburden plus an additional surcharge equal to the equilibrium soil suction. The swell versus depth curves are plotted from these results and applied in the same manner. Wong and Yong (1973) proposed the same procedure with the exception that the additional surcharge is equal to the pore pressure at hydrostatic conditions.

Fredlund et al. (1980) presented a method for the prediction of heave that makes use of the fundamentals of volume change theory for an unsaturated soil. The details of this method are presented in the following section.

2.3.3 Fredlund et al. (1980) formulation for one-dimensional heave

The Fredlund et al. (1980) method is based on the results of constant volume oedometer tests performed on undisturbed samples. The basic data required from the laboratory test are the rebound modulus and the swelling pressure. The data should be corrected for the effects of compressibility of the apparatus prior to its interpretation. The testing procedure is presented below.

The specimens are placed in an oedometer apparatus with an initial load approximately equal to the existing overburden load (or a token load may also be used). After initial dial readings are taken, the specimen is immersed in water. As the specimen attempts to swell, an increased load is applied to the soil in order to maintain its initial volume. At some point the specimen has no further tendency to swell under the applied load; this applied load is called the (uncorrected) swelling pressure of the soil, P_s.

The specimen is then loaded (with a doubling of the applied pressure) up to approximately 1700 kPa. The specimen is subsequently rebounded in double increments to a token load. The rebound portion of the oedometer test data, plotted on a semi-logarithmic form, is essentially a straight line. The slope of this line is defined as a swelling index, C_s. The (uncorrected) swelling pressure must be corrected for sampling disturbance (Fredlund, 1983). A graphical procedure similar to Casagrande's construction for sample disturbance was also proposed (Fig. 2.11).

The test is run on samples from different layers to account for the reduction of heave with depth. The (corrected) swelling pressure obtained from the test is a measure of the *in situ* stress state of the soil. It consists of the overburden pressure plus the matric suction equivalent. The initial matric suction is represented as matric suction equivalent.

The actual stress path followed in the test can be visualized on a three-dimensional plot using the stress state variables as abscissas. An idealized

interpretation of the constant volume oedometer test results is presented in Fig. 2.12. It is assumed that sampling does not produce disturbance to the soil.

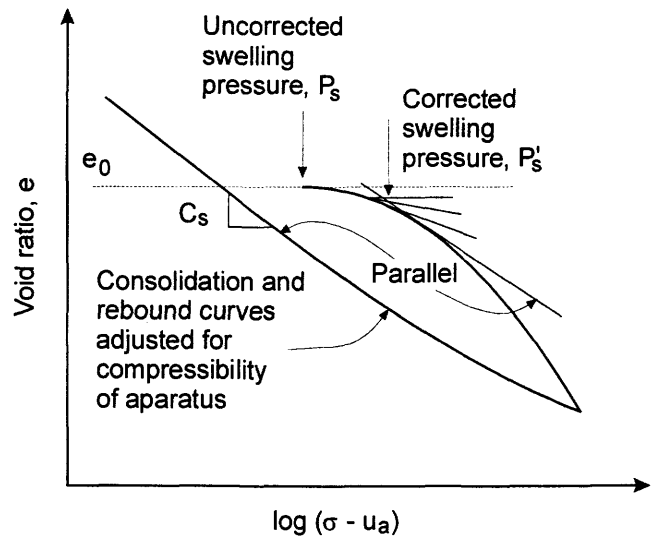

Figure 2.11 Construction procedure to correct for the effect of sampling disturbance (from Fredlund, 1987)

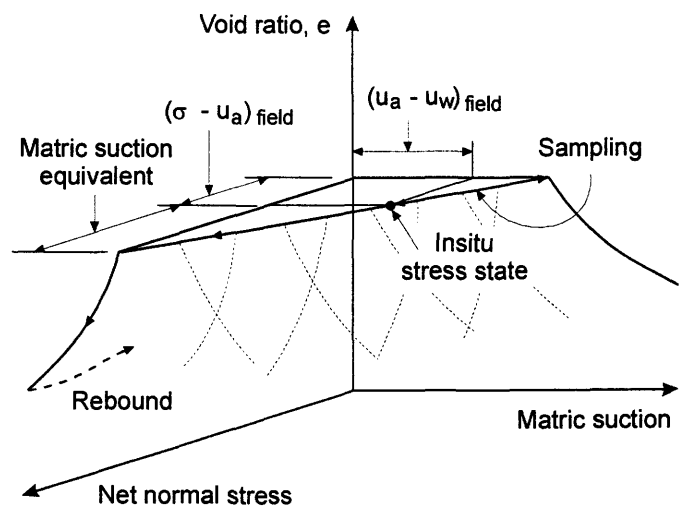

Figure 2.12 Ideal interpretation of the "constant volume" oedometer test (from Fredlund et al., 1980)

The final pore-water pressures can be assumed to be one of the following cases (Fredlund, 1979):

i) The water will rise to some elevation near or at the soil surface, which will result in a hydrostatic pore-water pressure distribution.

ii) Pore-water pressure is constant and atmospheric or zero gauge with depth. This is an unsteady state, but it might result if water is made available from the soil surface.

iii) The pore-water pressure profile is slightly negative. This type of distribution would be a function of the soil type and climatic conditions on the building placed on the ground surface.

The total heave formulation will be presented with the initial and final stress states projected onto the net normal stress plane. The results from a one-dimensional oedometer test are plotted on a semi-logarithmic scale and the slope of the plot is used in the formulation of total heave (Fig. 2.13). A measure of the *in situ* stress state is represented by the corrected vertical swelling pressure of the soil, which is determined in a one-dimensional oedometer under K_0-loading conditions. As a result, only the vertical heave is predicted.

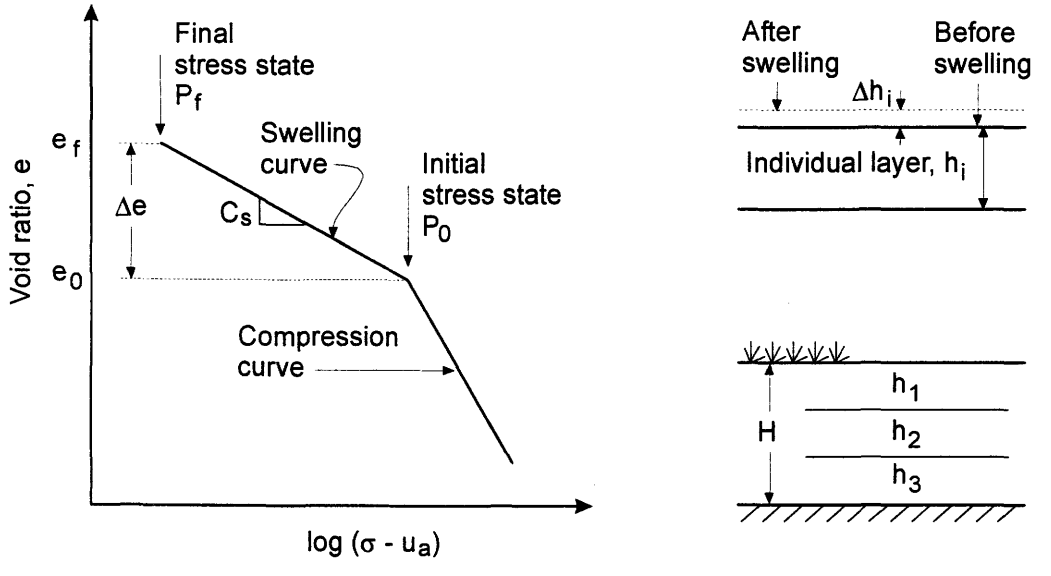

Figure 2.13 Principle of calculation for one-dimensional heave

The heave in an individual soil layer can be written in term of changes in void ratio:

$$\Delta h_i = h_i \frac{\Delta e}{1 + e_0} \tag{2.46}$$

where:

Δh_i = heave in a layer,

h_i = thickness of the layer under consideration,

Δe = change in void ratio, (i.e., $e_f - e_0$)

e_0 = initial void ratio, and

e_f = final void ratio.

The equation for the rebound portion of the oedometer test data can be written as:

$$\Delta e = C_s \log\left(\frac{P_f}{P_0}\right) \tag{2.47}$$

where:

C_s = swelling index (Note: the slope is negative but the soil property, C_s, is recorded as a positive number),

P_f = final stress state, and

P_0 = initial stress state.

The initial stress state, P_0, is the sum of the overburden pressure and the matric suction transferred to the total stress plane (i.e., matric suction equivalent). The initial stress state is always equal to the "corrected" swelling pressure.

$$P_0 = \sigma_v + (u_a - u_w)_e \tag{2.48}$$

where:

σ_v = original overburden pressure, and

$(u_a-u_w)_e$ = matric suction equivalent.

The final stress state, P_f, must account for total stress changes and the final pore-water pressure conditions.

$$P_f = \sigma_v \pm \Delta\sigma - u_{wf} \tag{2.49}$$

where:

$\Delta\sigma$ = change in total stress due to excavation or placement of fill, and

u_{wf} = estimated final pore-water pressure.

The heave in a layer in strata can be written as:

$$\Delta h_i = h_i \frac{C_s}{1+e_0} log \frac{(\sigma_v \pm \Delta\sigma - u_{wf})}{(\sigma_v + (u_a - u_w)_e)} \tag{2.50}$$

The total heave, Δh, is the sum of the heaves computed for each layer.

$$\Delta h = \sum \Delta h_i \tag{2.51}$$

2.4 Uncoupled and coupled solutions of swelling of expansive soils

Corapcioglou (1984) conducted a survey of various models used for the study of land subsidence due to the withdrawal of fluids from underlying aquifers. The models based on Terzaghi's effective stress principle (for saturated soils) were subdivided into two basic approaches. One approach stems from Biot's theory, where a simultaneous solution is sought for the pore-water pressure and for strains in the soil structure. This solution is called a "coupled" solution. In the second approach Terzaghi's theory is implemented in a two-step procedure. First, the pore-water pressure distribution is obtained either by solving a fluid flow equation in a two- or three-dimensional domain, or from field measurements. Settlement is then calculated assuming one-dimensional consolidation. The flow equation is usually derived by

assuming a constant total stress and only vertical displacement. These assumptions results in an uncoupling between the flow equation (i.e., continuity) and the equilibrium equations, and the solution obtained is called an "uncoupled" solution.

The mechanics of volume change in an unsaturated, expansive soil are complex. Several physical processes are involved, and each process depends upon other processes. These interactive processes can be listed as stress-deformation, water flow, air flow, heat flow, electrical flow and chemical flow. In addition, soil properties associated with unsaturated soils are highly non-linear. This study considers only two processes; namely, stress-deformation and water flow. The mechanical equilibrium equation governs the stress-deformation process, while water continuity equation governs the water flow process. A rigorous solution of the volume change in expansive soils requires that both the equilibrium equation and continuity equation be considered. Approximate solution can be obtained by considering the two processes independently and an uncoupled solution is obtained in this approach. This study will make use of both approaches and attempt to provide an evaluation of the merits of each approach.

Several researchers (Lloret and Alonso, 1980; Alonso et al., 1988; Alonso et al., 1999; Navarro and Alonso, 2000; Vulliet and Laloui, 2001) have been involved in the solution of coupled processes associated with unsaturated soils. In this section, only those associated with uncoupled and coupled processes between stress equilibrium and water continuity in soils for the purpose of volume change prediction will be reviewed.

2.4.1 Uncoupled approach to water flow and deformation of an unsaturated soil

Richards (1984) studied the status of computer programs which model the physical behaviour of soils, including unsaturated expansive clays. Two individual programs were developed to independently analyse the two physical processes relevant to the problem. One program analysed the load-deformation behaviour and the other program analysed the changes of soil suction due to water flow as a result of changes of load and displacements throughout the region. Non-linear behaviours of the

material properties for both water flow and deformation were modelled using incremental analyses. Application of the program to expansive soils problems was presented for the case of a suction controlled consolidation test on red clay from Griffith.

Rees and Thomas (1993) proposed an uncoupled model for the simulation of one-dimensional seasonal ground movement. It was assumed that soil was homogeneous, the soil-water characteristic curve was non-hysteretic, and pore-air pressure was atmospheric. The method required the solution of the unsaturated-seepage equation for space-time variations of pore-water pressure. Then the variations of pore-water pressure were related to the volumetric deformation. Three soil properties required for the analysis are: the coefficient of permeability; the soil-water characteristic curve; and the relationship between volumetric strain and suction.

Dinh (1996) presented a one-dimensional uncoupled formulation and solution for vertical movements in expansive soils. A finite element computer program, called CONEX1 was developed to predict soil suction distribution in a soil column. Soil suction was predicted by solving a moisture diffusion equation. Displacements were then calculated from the changes in soil suction. The result of an oedometer test on swelling soil from Darling Downs, Australia was simulated using the CONEX1 program.

Hung (2000) presented an uncoupled solution of one- and two-dimensional volume change problems associated with expansive soils. The proposed method made use of the finite element method with elasticity parameter functions (i.e., elasticity parameter of the soil structure with respect to net normal stress, E and elasticity parameter of the soil structure with respect to matric suction, H). The elasticity parameter functions were calculated from conventional oedometer test results with an assumed value of Poison's ratio. The theoretical formulation of the method was based on the general theory of volume change for an unsaturated soil. The matric suction conditions in a soil were predicted by performing a transient saturated-unsaturated seepage analysis. The deformations due to changes in net normal stress and matric suction were predicted by performing a stress-deformation analysis. Solutions of both seepage and stress-deformation problems were obtained using a general-purpose

partial differential equation solver, called PDEase2D. Several typical examples and case histories were analysed for one-dimensional heave. Five two-dimensional examples covering typical volume change problems associated with unsaturated, expansive soils were analysed and discussed. The examples represented typical conditions encountered in engineering practice such as deformation due to loading, unloading, wetting, drying, and both loading and wetting.

2.4.2 Coupled approach to seepage and deformation of an unsaturated soil

Biot (1941) proposed three-dimensional coupled equations to analyze the consolidation process for a special case of an unsaturated soil. The soil was assumed to be an isotropic and linear elastic material, and water in the pores was assumed to be incompressible. The derivations were based on the assumption that air bubbles within the pore water were occluded during the consolidation process. Two constitutive relationships were proposed in order to completely describe the deformation state of the soil. One constitutive relationship was formulated for the soil structure, and the other was for the water phase. Two stress state variables were used in the formulations. Therefore, four volumetric deformation coefficients were used to link the stress state variables and the deformation state variables.

Dakshanamurthy et al. (1984) presented a coupled, two-phase flow, three-dimensional consolidation theory for unsaturated porous media. The coupled equations were derived based on the assumption that the air phase is continuous. Two independent stress tensors are used to describe the stress state for an unsaturated soil (i.e., three-dimensional). Several other assumptions used in the derivation were similar to those proposed by Tezarghi (1943) and Biot (1941). These can be summarized as follows: i) material is isotropic, ii) reversibility of stress-strain relations, iii) linearity of stress-strain relations, iv) small strains, v) pore-water is incompressible, vi) coefficients of water and air phase are functions of the volume mass soil properties during the consolidation process, vii) the effect of air diffusing through water, air dissolving in the water phase and the movement of water vapor are ignored. The application of the consolidation theory was illustrated for a one-dimensional case. The change in pore-air and pore-water pressures was computed by

solving the continuity equations for the water phase and the air phase simultaneously, then the overall (i.e., soil structure) volume change was obtained from the equilibrium equation. Normally, the coupling of stress-deformation and continuity has no relevance for one-dimensional cases; however, the non-linearity in the formulation does not allow the coupling to "fall out" for the unsaturated soil case.

Dinh (1996) formulated coupled equations for one- and two-dimensional volume change analysis with the use of Bishop's (1959) equation for effective stress for expansive soils. A computer program, called CONEX2 was developed to analyse one- and two-dimensional swelling and shrinkage behaviour of soils. Soil suction was assumed a driving force for water flow. Several parameters such as the coefficient of water storage, the elastic modulus, E, Poisson's ratio, μ, and the coefficient of expansion were assumed constants. The multiplying factor of soil suction in Bishop's effective equation, χ, was updated for each time step of the analysis from previously calculated degree of saturation. Simulation of one-dimensional cyclic swelling-shrinkage behaviour of Darling Downs black soil in Australia was presented.

Pereira and Fredlund (1997) developed a computer program, called COUPSO, to solve the coupled equations for the consolidation of unsaturated, collapsing soils. The formulations were based on the equilibrium equation, the constitutive equations for unsaturated soils and the continuity equation for the water phase. The void ratio and degree of saturation constitutive surfaces were mathematically and experimentally defined and the elasticity parameters were obtained by differentiating the constitutive surfaces. Poisson's ratio was estimated from triaxial and oedometer test results. The program was used to simulate the behaviour of collapsing soil in an earth dam during saturation.

Shuai and Fredlund (1997) simplified the coupled equations to the one-dimensional case and developed a computer program, called SWELL to analyse volume change behaviour of an unsaturated, expansive soil during the swelling process. The formulations were based on the equilibrium equation, the constitutive equations for unsaturated soils and the continuity equation for the water phase. The program could accommodate various boundary conditions and simulate various stress

paths followed in different tests on expansive soils using oedometer apparatus. Results from free swell, constant volume, and loaded swell oedometer tests on compacted Regina clay were simulated.

Wong et al. (1998) implemented coupled equations into finite element codes, namely SEEP/W and SIGMA/W to allow two-dimensional analysis associated with the consolidation and swell of unsaturated soils. However, the programs do not allow the description of elasticity parameters, E and E_w, as functions of net normal stress. As well, the code has not been extensively verified.

The author is not aware that a comprehensive coupled solution of two and three-dimensional volume change problems in expansive soils has been published to-date.

2.5 Summary of the literature review

The general theory of consolidation (or swelling) of unsaturated soils is required to describe volume change of expansive soils. Elasticity parameters required for soil structure constitutive relationship (i.e., E and H) can be calculated from conventional oedometer test results, which are obtained from extreme planes of the constitutive surface (i.e., volume change indices) assuming a value of Poisson's ratio. Because the elasticity parameter E (or H) is calculated from one constant suction (or net normal stress) plane and then applied for entire constitutive surface, the elasticity parameter E is independent of matric suction and elasticity parameter H is independent of net normal stress. These elasticity parameters are a function of both stress state variables. In addition, the elasticity parameters presented are not be valid when net normal stress and matrix suction approaches zero. At small values of net normal stress or zero suction, these parameters become small which results in an unstable solution to volume change problems or the prediction of unreasonably large deformations. This research study suggests that the volume change indices be used to estimate the entire void ratio surface, and the elasticity parameters can be obtained by differentiating the void ratio surface with an assumption for the value of Poisson's ratio.

For volume change problems associated with expansive soils in engineering practice, the air phase can be assumed to be continuous and at atmospheric pressure.

The solution of swelling problems associated with unsaturated, expansive soils can be obtained either by using an uncoupled approach or a coupled approach. Because soil properties associated with expansive soils are non-linear, coupled solutions are difficult to obtain. Present coupled solutions are limited to one-dimensional problems and include assumptions for the simplification of the soil properties. A comprehensive coupled solution of two and three-dimensional volume change problems in expansive soils does not appear to have been published to date. A coupled, two-dimensional solution is presented in this study. The coupled solution will then be used for comparison with uncoupled solution.

CHAPTER 3

Formulation Theory for the Swelling Process in an Expansive Soil

3.1 General

A rigorous formulation of two- and three-dimensional swelling problems associated with unsaturated, expansive soils requires that the continuity equations for the water phase and air phase be coupled with the equilibrium equations. Transient flow of air and/or water changes the stress state in soils. Consequently, soil structure deforms in response to the changes in stress state and comes to a new equilibrium state. The associated deformations alter the space available for the flow of air and water, resulting in new hydraulic properties for the soil. These changes make the transient processes of air and water flow highly non-linear. The interdependence of air and water flow and the deformation process can be demonstrated through the coupling of the basic equations of physics (i.e., equilibrium equation, water continuity equation and air continuity equation) that are expressed in term of field variables (i.e., displacements and pore fluid pressures). These equations are called coupled equations (Biot, 1941; Dakshanamurthy et al., 1984; Fredlund and Rahardjo, 1993; Pereira, 1996) and can be derived as the theory of consolidation and swelling for unsaturated soils.

The development of coupled equations for the simulation of three-dimensional swelling problems are first presented in a general form where continuity conditions are considered for both continuous air and water phases. Formulations for two-dimensional (plane-strain) conditions are then derived assuming that the

continuous air phase remains at atmospheric pressure (i.e., $u_a = 0$). A finite element formulation of the coupled equations is presented in the last section.

The coupled and uncoupled formulations are derived based on the following assumptions; namely, 1) the air phase is continuous, 2) soil is isotropic, nonlinear and elastic, 3) strains are small, 4) pore-water is incompressible, and 5) the effects of air diffusing through water, air dissolving in the water, and the movement of water vapor are negligible.

Solutions to the transient swelling soil equations can be obtained either by using a coupled approach or an uncoupled approach. The assumptions used for the numerical solutions associated with each approach are presented later in this chapter. The soil properties and physical relations required to analyse the problem are presented in this chapter. The void ratio can be computed from the swelling indices associated with the swelling portion of the constitutive surface.

3.2 Physical relationships required for three-dimensional swelling soil formulations

The displacement vector, **u**, pore-air pressure, u_a, and pore-water pressure, u_w, are used as primary variables for the flow-deformation problem. For the general three-dimensional case, there are five primary variables (i.e., three variables are displacements in three directions, pore-air pressure, and pore-water pressure) that correspond to five field equations (i.e., three equilibrium equations for three directions, one equation for air continuity and one equation for water continuity).

3.2.1 Strain-displacement relations

Let us consider a three-dimensional field with x, y, and z as the rectangular Cartesian coordinates (i.e., x- for horizontal direction, y- for vertical direction) with u_i being components of the displacement vector (i.e., u, v and w for the x-, y- and z-directions, respectively). The components of strain tensor for the soil structure, ε_{ij}, are written in term of displacements as follows:

$$\varepsilon_{ij} = \frac{1}{2}(u_{i,j} + u_{j,i}) \tag{3.1}$$

The normal strains can be designated as ε_x, ε_y, and ε_z for the x-, y- and z-directions, respectively. For infinitesimal deformations, volumetric strain, ε_v, is the sum of the normal strain components.

$$\varepsilon_v = \frac{\partial u_i}{\partial x_i} = \frac{\partial u}{\partial x} + \frac{\partial v}{\partial y} + \frac{\partial w}{\partial z} = \varepsilon_x + \varepsilon_y + \varepsilon_z \tag{3.2}$$

3.2.2 Constitutive relationships and flow laws

The constitutive relations for the soil structure and water phase, and flow laws for the air and water phases required for the formulation of coupled equations associated with unsaturated, expansive soils were presented in Chapter 2. These relations are summarized using indicial notation for the formulation of the three-dimensional coupled equations for the swelling process. The stress state of an unsaturated soil can be written in terms of two independent stress tensors; namely, the net normal stress tensor, $(\sigma_{ij} - u_a\delta_{ij})$, and matric suction tensor, $(u_a - u_w)\delta_{ij}$.

3.2.2.1 Constitutive relationships for an unsaturated soil

The soil structure constitutive relationship

The constitutive relationship for the soil structure can be written in an incremental elasticity form as follows (Fredlund and Rahardjo, 1993):

$$d\varepsilon_{ij} = \frac{1+\mu}{E} d(\sigma_{ij} - \delta_{ij}u_a) - \frac{\mu}{E} d(\sigma_{kk} - 3u_a)\delta_{ij} + \frac{d(u_a - u_w)}{H}\delta_{ij} \tag{3.3}$$

where:

σ_{ij} = components of the total stress tensor for the soil structure,

δ_{ij} = the Kronecker delta,

E = elasticity parameter for the soil structure with respect to a change in the net normal stress, and

H = elasticity parameter for the soil structure with respect to a change in matric suction.

Equation (3.3) can be used to write the equation for volumetric strain in a compressibility form as follows:

$$d\varepsilon_v = m_1^s d(\sigma_{mean} - u_a) + m_2^s d(u_a - u_w) \tag{3.4}$$

where:

$\sigma_{mean} = \frac{1}{3}\sigma_{kk} = \frac{\sigma_x + \sigma_y + \sigma_z}{3}$, mean net total stress

$m_1^s = \frac{3(1-2\mu)}{E}$, coefficient of volume change with respect to a change in net normal stress, and

$m_2^s = \frac{3}{H}$, coefficient of volume change with respect to a change in matric suction.

Equation (3.3) can also be rearranged as a stress-strain equation rather than a strain-stress equation as follows:

$$d(\sigma_{ij} - \delta_{ij}u_a) = \frac{E}{1+\mu}d\varepsilon_{ij} + \frac{\mu E}{(1+\mu)(1-2\mu)}\delta_{ij}d\varepsilon_{kk} - \frac{E/H}{(1-2\mu)}\delta_{ij}d(u_a - u_w) \tag{3.5}$$

From Eq. (3.4), the mean net normal stress can be expressed as a function of volumetric strain and matric suction, as follows:

$$d(\sigma_{mean} - u_a) = \frac{E}{3(1-2\mu)}d\varepsilon_v - \beta d(u_a - u_w) \tag{3.6}$$

where:

$$\beta = \frac{m_2^s}{m_1^s} = \frac{E/H}{(1-2\mu)}$$

The water phase constitutive relationship

The water phase constitutive relationship can presented in an incremental elasticity form as follows (Fredlund and Rahardjo, 1993):

$$\frac{dV_w}{V_0} = \frac{1}{E_w} d(\sigma_{ii} - 3u_a) + \frac{1}{H_w} d(u_a - u_w) \tag{3.7}$$

where:

E_w = water volumetric modulus associated with a change in the net normal stress, and

H_w = water volumetric modulus associated with a change in matric suction.

Equation (3.7) can also be written in compressibility form as follows:

$$\frac{dV_w}{V_0} = m_1^w d(\sigma_{mean} - u_a) + m_2^w d(u_a - u_w) \tag{3.8}$$

where:

m_1^w = $\frac{3}{E_w}$, coefficient of volume change with respect to a change in net normal stress, and

m_2^w = $\frac{1}{H_w}$, coefficient of volume change with respect to a change in matric suction.

Using Eq. (3.6) for mean net normal stress, Eq. (3.8) becomes:

$$\frac{dV_w}{V_0} = \beta_{w1} d\varepsilon_v + \beta_{w2} d(u_a - u_w) \tag{3.9}$$

where:

β_{w1} = $\frac{m_1^w}{m_1^s}$, or in the elasticity form, $\frac{E}{(1-2\mu)E_w}$

$$\beta_{w2} = m_2^w - \frac{m_1^w m_2^s}{m_1^s}, \text{ or in the elasticity form, } \frac{1}{H_w} - \frac{3E}{(1-2\mu)E_w H}$$

The air phase constitutive relationship

The continuity requirement for an element of unsaturated soil [i.e., $dV_v = dV_w + dV_a$ in Eq. (2.3)] allows the volume change of air phase be computed from the volume change of soil structure and volume change of water phase. The air phase constitutive relationship can be presented in the elasticity forms as follows (Fredlund and Rahardjo, 1993):

$$\frac{dV_a}{V_0} = \frac{1}{E_a} d(\sigma_{ii} - 3u_a) + \frac{1}{H_a} d(u_a - u_w) \tag{3.10}$$

where:

E_a = air volumetric modulus associated with change in net normal stress, and

H_a = air volumetric modulus associated with change in matric suction.

Equation (3.10) is written in compressibility form as follows:

$$\frac{dV_a}{V_0} = m_1^a d(\sigma_{mean} - u_a) + m_2^a d(u_a - u_w) \tag{3.11}$$

where:

$m_1^a = \frac{3}{E_a}$, coefficient of air volume change associated with change in net normal stress, and

$m_2^a = \frac{1}{H_a}$, coefficient of air volume change associated with change in matric suction.

Using Eq. (3.6) for mean net normal stress, Eq. (3.11) becomes:

$$\frac{dV_a}{V_0} = \beta_{a1} d\varepsilon_v + \beta_{a2} d(u_a - u_w) \tag{3.12}$$

where:

$$\beta_{a1} = \frac{m_1^a}{m_1^s}, \text{ or in the elasticity form, } \frac{E}{(1-2\mu)E_a}$$

$$\beta_{a2} = m_2^a - \frac{m_1^a m_2^s}{m_1^s}, \text{ or in the elasticity form, } \frac{1}{H_a} - \frac{3E}{(1-2\mu)E_a H}$$

Because of the continuity requirement for an element of unsaturated soil (i.e., $dV_v = dV_w + dV_a$ in Eq. 2.3), the parameters β_{a1} and β_{a2} are related to β_{w1} and β_{w2} as follows:

$$\beta_{w1} + \beta_{a1} = 1 \tag{3.13}$$

$$\beta_{w2} + \beta_{a2} = 0 \tag{3.14}$$

Equation (3.12) can be written using parameters β_{w1} and β_{w2} as follows:

$$\frac{dV_a}{V_0} = (1-\beta_{w1}) d\varepsilon_v - \beta_{w2} d(u_a - u_w) \tag{3.15}$$

3.2.2.2 Flow laws

The air and water phases both require a flow law. Darcy's law can be used for the water phase and Fick's law can be used for the air phase.

Flow of water

Darcy's law relates the water flow rate to the hydraulic head (i.e., pressure head plus elevation head) as follows:

$$v_{wi} = -k_{wi} \frac{\partial}{\partial x_i} \left(\frac{u_w}{\rho_w g} + Y \right) \tag{3.16}$$

where:

v_{wi} = Darcy's flux in i-direction,

k_{wi} = hydraulic conductivity in *i*-directions,

ρ_w = density of water,

g = gravitational acceleration, and

Y = elevation.

The flow of air

Fick's law relates the mass rate of air with pore-air pressure as follows:

$$J_{ai} = -D_a^* \frac{\partial u_a}{\partial x_i} \tag{3.17}$$

where:

J_{ai} = mass rate of air in *i*-direction, and

D_a^* = coefficient of transmision for air phase.

3.2.3 Basic equation of physics

A rigorous formulation to describe the swelling behaviour of an unsaturated, expansive soil requires the coupling of the following system of equations (Fredlund and Rahardjo, 1993): i) static equilibrium of the soil medium; ii) the water phase continuity equation; and iii) the air phase continuity equation. These equations will be presented for a referential elemental volume.

3.2.3.1 Equilibrium equations

The equations of overall static equilibrium for an unsaturated soil can be written as follows:

$$\sigma_{ij,j} + b_i = 0 \tag{3.18}$$

where

σ_{ij} = components of the net total stress tensor, and

b_i = components of the body force vector.

3.2.3.2 Water continuity equation

The water continuity equation for an unsaturated soil can be written as follows (Freeze and Cherry, 1979):

$$\frac{\partial(\rho_w nS)}{\partial t} + \nabla \cdot (\rho_w \mathbf{v}_w) = 0 \tag{3.19}$$

where:

n = porosity

S = degree of saturation

ρ_w = water density

$\nabla = \frac{\partial}{\partial x}\mathbf{i} + \frac{\partial}{\partial y}\mathbf{j} + \frac{\partial}{\partial z}\mathbf{k}$, the divergence operator, and

$\mathbf{v}_w = v_w^x \mathbf{i} + v_w^y \mathbf{j} + v_w^z \mathbf{k}$, Darcy's flux.

Water is commonly considered incompressible in geotechnical engineering practice (i.e., water density is a constant) and Eq. (3.19) can be written as follows:

$$\frac{\partial(nS)}{\partial t} + \nabla \cdot (\mathbf{v}_w) = 0 \tag{3.20}$$

Or

$$\frac{\partial(\theta_w)}{\partial t} + \nabla \cdot (\mathbf{v}_w) = 0 \tag{3. 21}$$

where:

θ_w = nS, volumetric water content.

With the assumption that deformations are infinitesimal, Eq. (3.21) becomes:

$$\frac{\partial(V_w / V_0)}{\partial t} + \nabla \cdot (\mathbf{v}_w) = 0 \tag{3.22}$$

where:

V_w = current water volume in the referential element, and

V_0 = referential volume of the element.

3.2.3.3 Air continuity equation

Fredlund and Rahardjo (1993) presented the air continuity equation as follows:

$$\frac{\partial}{\partial t}[\rho_a n(1-S)] + \nabla \cdot (\mathbf{J}_a) = 0 \tag{3.23}$$

where:

ρ_a = density of air, and

$\mathbf{J}_a$ = mass flow rate of air.

With the assumption that deformations are infinitesimal, Eq. (3.23) becomes:

$$\frac{\partial (M_a / V_0)}{\partial t} + \nabla \cdot (\mathbf{J}_a) = 0 \tag{3.24}$$

where:

M_a = $\rho_a V_a$, mass of air in the soil element, and

V_a = $n(1-S)V_0$, the air volume in the soil element.

Equation (3.23) can be written in an expanded form as follows:

$$\rho_a \frac{\partial (V_a / V_0)}{\partial t} + n(1-S)\frac{\partial \rho_a}{\partial t} + \nabla \cdot (\mathbf{J}_a) = 0 \tag{3.25}$$

The air phase is a highly compressible medium and its density is a function of the air pressure. Assuming that air behaves as an ideal gas, the equation for air density can be written as follows:

$$\rho_a = \frac{\omega_a}{RT}\overline{u}_a \tag{3.26}$$

where:

ω_a = molecular mass of air,

R = universal (molar) gas constant,

T = absolute temperature,

$\overline{u}_a$ = absolute pore-air pressure (i.e., $\overline{u}_a = u_a + \overline{u}_{atm}$),

u_a = gauge-pore-air pressure, and

$\overline{u}_{atm}$ = atmospheric pressure (i.e., 101 kPa).

Equation (3.24) can be rearranged as follows:

$$\frac{\partial(V_a / V_0)}{\partial t} + \frac{n(1-S)}{\overline{u}_a}\frac{\partial u_a}{\partial t} + \frac{RT}{\omega_a \overline{u}_a}\nabla \cdot (\mathbf{J}_a) = 0 \tag{3.27}$$

3.2.4 The formulation of general three-dimensional governing partial differential equations for the swelling process

The water phase continuity equation, the air phase continuity equation, and the equilibrium equation can be expressed in terms of displacements and pore fluid pressures. These governing partial differential equations are obtained by substituting strain-displacement relations into the constitutive relationships, and then substituting constitutive relationships or flow laws into the basic equations of physics.

3.2.4.1 The governing partial differential equation for water phase

The governing equation for the water phase can be obtained by substituting the time derivative of the water phase constitutive equation [Eq. (3.9)] and Darcy's law [Eq. (3.16)] into the water phase continuity equation [Eq. (3.22)]:

$$\beta_{w1}\frac{\partial \varepsilon_v}{\partial t} + \beta_{w2}\frac{\partial(u_a - u_w)}{\partial t} - \nabla \cdot \left[\mathbf{k}_w \nabla\left(\frac{u_w}{\gamma_w} + Y\right)\right] = 0 \tag{3.28}$$

where:

$$\beta_{w1} = \frac{m_1^w}{m_1^s} = \frac{E}{(1-2\mu)E_w}$$

$$\beta_{w2} = m_2^w - \frac{m_1^w m_2^s}{m_1^s} = \frac{1}{H_w} - \frac{3E}{(1-2\mu)E_w H}$$

3.2.4.2 The governing partial differential equation for air phase

The governing equation for the air phase can be obtained from the time derivative of the air phase constitutive equation [Eq. (3.12)] and Fick's law [Eq. (3.17)] into the air phase continuity equation [Eq. (3.27)]:

$$\beta_{a1}\frac{\partial \varepsilon_v}{\partial t}+\beta_{a2}\frac{\partial (u_a-u_w)}{\partial t}+\frac{n(1-S)}{\overline{u}_a}\frac{\partial u_a}{\partial t} - \frac{RT}{\omega_a \overline{u}_a}\left[\nabla\cdot\left(D_a^*\nabla u_a\right)\right]=0 \tag{3.29}$$

where:

$$\beta_{a1}=\frac{m_1^a}{m_1^s}=\frac{E}{(1-2\mu)E_a}$$

$$\beta_{a2}=m_2^a-\frac{m_1^a m_2^s}{m_1^s}=\frac{1}{H_w}-\frac{3E}{(1-2\mu)E_a H}$$

3.2.4.3 The governing partial differential equations for soil structure equilibrium

Substituting the strain-displacement relation [Eq. (3.1)] and the stress-strain relationship [Eq. (3.5)] into the equilibrium equation [Eq. (3.18)] gives the following governing equations (i.e., three equations for x-, y- and z-directions):

$$G\nabla^2 u_i+\frac{G}{1-2\mu}\frac{\partial \varepsilon_v}{\partial x_i}-\beta\frac{\partial (u_a-u_w)}{\partial x_i}+\frac{\partial u_a}{\partial x_i}+b_i=0 \tag{3.30}$$

where:

$$\beta=\frac{m_2^s}{m_1^s}=\frac{E/H}{(1-2\mu)}$$

$\nabla^2=\dfrac{\partial^2}{\partial x^2}+\dfrac{\partial^2}{\partial y^2}+\dfrac{\partial^2}{\partial z^2}$, the Laplace operator

$$\varepsilon_v=\frac{\partial u_i}{\partial x_i}=\frac{\partial u}{\partial x}+\frac{\partial v}{\partial y}+\frac{\partial w}{\partial z}$$

$$G = \frac{E}{2(1+\mu)}$$

A rigorous solution of the three-dimensional swelling problem requires that Eqs. (3.28), (3.29) and (3.30) be solved simultaneously. It is beyond the scope of this thesis to obtain such a three-dimensional coupled solution. Rather, only coupled solutions for two-dimensional problems are presented.

3.3 Formulations for plane strain analysis of swelling

Many geotechnical problems can be simplified to a two-dimensional form using the concept of plane strain loading. Let x be the horizontal direction and y be vertical direction, strains are considered only in the xy-plane, while strain in the z-direction is assumed to be negligible (i.e., $d\varepsilon_z = 0$). The volumetric strain can be written as follow:

$$d\varepsilon_v = d\varepsilon_x + d\varepsilon_y \tag{3.31}$$

The net normal stress corresponding to zero strain in the z-direction is:

$$d(\sigma_z - u_a) = \mu d(\sigma_x + \sigma_y - 2u_a) - \frac{E}{H} d(u_a - u_w) \tag{3.32}$$

3.3.1 Strain-displacement relations

Let u and v be displacements in the x- and y-direction, respectively. The strain vector for infinitesimal deformation can be written as follows:

$$\boldsymbol{\varepsilon} = \begin{Bmatrix} \varepsilon_x \\ \varepsilon_y \\ \gamma_{xy} \end{Bmatrix} = \begin{Bmatrix} \dfrac{\partial u}{\partial x} \\ \dfrac{\partial v}{\partial y} \\ \dfrac{\partial u}{\partial y} + \dfrac{\partial v}{\partial x} \end{Bmatrix} \tag{3.33}$$

3.3.2 Constitutive relationships and flow law

The constitutive relationships for soil structure and water phase, and Darcy's law are presented for two-dimensional conditions. Assuming that air phase is continuous and atmospheric, the Fick's law for air flow is no longer required.

3.3.2.1 Constitutive relationships

The constitutive relationships for plane strain conditions can be written by substituting Eq. (3.32) into the constitutive relationships for general three-dimensional conditions [i.e., Eq. (3.3) for soil structure and Eq. (3.7) for water phase].

The soil structure constitutive relationship for plane strain conditions can be written as follows:

$$d(\boldsymbol{\sigma} - \mathbf{m}u_a) = \mathbf{D}d\boldsymbol{\varepsilon} - d(u_a - u_w)\mathbf{D}_s \tag{3.34}$$

where:

$$\boldsymbol{\sigma}^{\mathrm{T}} = [\sigma_x,\ \sigma_y,\ \tau_{xy}]$$

$$\mathbf{m}^{\mathrm{T}} = [1,\ 1,\ 0]$$

$$\mathbf{D} = \frac{E}{(1+\mu)(1-2\mu)}\begin{bmatrix} (1-\mu) & \mu & 0 \\ \mu & (1-\mu) & 0 \\ 0 & 0 & \dfrac{1-2\mu}{2} \end{bmatrix}$$

$$\mathbf{D}_s = \frac{E}{(1-2\mu)H}\begin{bmatrix} 1 \\ 1 \\ 0 \end{bmatrix}$$

The volumetric strain equation can be written as follows:

$$d\varepsilon_v = m^s_{1\text{-}2D}d(\sigma_{ave} - u_a) + m^s_{2\text{-}2D}d(u_a - u_w) \tag{3.35}$$

where:

$$\sigma_{ave} = \frac{\sigma_x + \sigma_y}{2}$$

$$m^{s}_{1-2D} = \frac{2(1+\mu)(1-2\mu)}{E}$$

$$m^{s}_{2-2D} = \frac{2(1+\mu)}{H}$$

From Eq. 3.35, the net average stress can be expressed as a function of volumetric strain and matric suction.

$$d(\sigma_{ave} - u_a) = \frac{E}{2(1+\mu)(1-2\mu)} d\varepsilon_v - \beta d(u_a - u_w) \tag{3.36}$$

where:

$$\beta = \frac{E/H}{(1-2\mu)}$$

The water phase constitutive relationship for plane strain conditions can be written as follows:

$$\frac{dV_w}{V_0} = m^{w}_{1-2D} d(\sigma_{ave} - u_a) + m^{w}_{2-2D} d(u_a - u_w) \tag{3.37}$$

where:

$$m^{w}_{1-2D} = \frac{2(1+\mu)}{E_w}$$

$$m^{w}_{2-2D} = \frac{1}{H_w} - \frac{E}{E_w H}$$

Using Eq. 3.36 for mean net normal stress, Equation 3.37 becomes:

$$\frac{dV_w}{V_0} = \beta_{w1} d\varepsilon_v + \beta_{w2} d(u_a - u_w) \tag{3.38}$$

where:

$$\beta_{w1} = \frac{E}{(1-2\mu)E_w}$$

$$\beta_{w2} = \frac{1}{H_w} - \frac{3E}{(1-2\mu)E_w H}$$

3.3.2.2 Flow law

The Darcy's law, for the case where the x- and y-coordinates are the same as the direction of the major and minor coefficients of permeability, can be written as follows:

$$\mathbf{v}_w = -\mathbf{k}_w \nabla\left(\frac{u_w}{\rho_w g} + Y\right) \tag{3.39}$$

where:

$$\mathbf{v}_w{}^{\mathrm{T}} = [v_w^x,\ v_w^y]$$

$$\mathbf{k}_w{}^{\mathrm{T}} = [k_w^x,\ k_w^y]$$

3.3.3 Basic equation of physics

The water continuity equation, Eq. (3.22), is presented below:

$$\frac{\partial(V_w / V_0)}{\partial t} + \nabla \cdot (\mathbf{v}_w) = 0 \tag{3.40}$$

The equilibrium equations, Eq. (3.18), for two-dimensional conditions can be written as follows:

$$\frac{\partial \sigma_x}{\partial x} + \frac{\partial \tau_{xy}}{\partial y} + b_x = 0 \tag{3.41a}$$

$$\frac{\partial \tau_{xy}}{\partial x} + \frac{\partial \sigma_y}{\partial y} + b_y = 0 \tag{3.41b}$$

3.3.4 Governing partial differential equations for plane strain swelling

The governing partial differential equations can be derived for plane strain loading conditions in terms of displacements (i.e., horizontal displacement, u, and vertical displacement, v), pore-water pressure, u_w and pore-air pressure, u_a as follows.

The governing equation for water phase (i.e., seepage) is as follows:

$$\beta_{w1}\frac{\partial \varepsilon_v}{\partial t}+\beta_{w2}\frac{\partial (u_a-u_w)}{\partial t}=\frac{\partial}{\partial x}\left(k_w^x\frac{\partial}{\partial x}\left(\frac{u_w}{\rho_w g}+Y\right)\right)+\frac{\partial}{\partial y}\left(k_w^y\frac{\partial}{\partial y}\left(\frac{u_w}{\rho_w g}+Y\right)\right) \quad (3.42)$$

The governing equation for stress-deformation in the x-direction is as follows:

$$\frac{\partial}{\partial x}\left(c_{11}\frac{\partial u}{\partial x}+c_{12}\frac{\partial v}{\partial y}\right)+c_{33}\frac{\partial}{\partial y}\left(\frac{\partial u}{\partial y}+\frac{\partial v}{\partial x}\right)-d_s\frac{\partial (u_a-u_w)}{\partial x}=0 \quad (3.43)$$

The governing equation for stress-deformation in the y-direction is as follows:

$$c_{33}\frac{\partial}{\partial x}\left(\frac{\partial u}{\partial y}+\frac{\partial v}{\partial x}\right)+\frac{\partial}{\partial y}\left(c_{12}\frac{\partial u}{\partial x}+c_{22}\frac{\partial v}{\partial y}\right)-d_s\frac{\partial (u_a-u_w)}{\partial y}+b_y=0 \quad (3.44)$$

where:

$$\beta_{w1}=\frac{E}{E_w(1-2\mu)}$$

$$\beta_{w2}=\frac{1}{H_w}-\frac{3E/H}{(1-2\mu)E_w}$$

$$c_{11}=c_{22}=\frac{(1-\mu)E}{(1+\mu)(1-2\mu)}$$

$$c_{12}=\frac{\mu E}{(1+\mu)(1-2\mu)}$$

$$c_{33}=\frac{E}{2(1+\mu)}$$

$$d_s=\frac{E}{(1-2\mu)H}$$

All the dependent variables are present in each of the coupled equations. The soil properties associated with unsaturated soil in the coupled equations are functions of the stress state in soils (i.e., net normal stress and the matric suction).

3.3.5 Characteristics common to coupled and uncoupled analyses

Let us assume that the air phase is continuous and at atmospheric pressure (i.e., $u_a = 0$), Eqs. (3.42), (3.43), and (3.44) can be solved for three variables, u, v, and u_w. Swelling is a time dependent problem involving non-linear soil properties and initial conditions must be specified for both coupled and uncoupled approaches. The parameters associated with plane strain coupled and uncoupled approaches are presented in Table 3.1. In the coupled approach the water phase continuity (i.e., seepage) equation and the equilibrium (i.e., stress-deformation) equations are solved simultaneously, the dynamic interdependence between the seepage and deformation problems is fully considered. There are three dependent variables (i.e., u, v, and u_w). Except for Poisson's ratio, all other soil parameters (i.e., E, H, E_w, H_w, and k_w) are considered to be functions of both net normal stress and matric suction. Boundary conditions of both the water continuity equation (i.e., pore-water pressure and water flux) and equilibrium equations (i.e., displacements and load) must be defined. The results of the analysis are displacements and pore-water pressure with time. Induced stresses and water fluxes can be obtained at any time during the transient process.

A coupled solution will be obtained through the use of the COUPSO program as part of this research study. The finite element formulation of the coupled equations [Eqs. (3.42), (3.43), and (3.44)] are implemented in the COUPSO program and presented in Section 3.6.

Table 3.1 Summary of uncoupled and coupled model for two-dimensional swelling analysis associated with expansive soils

DESCRIPTION	UNCOUPLED APPROACH		COUPLED APPROACH
	SEEPAGE MODEL	STRESS-STRAIN MODEL	
Governing PDE(s)	Water continuity equation	Stress equilibrium equations	Stress equilibrium equations Water continuity equation
Computer program	FlexPDE	FlexPDE	COUPSO
Dependent variables	Pore-water pressure, u_w	Horizontal displacement, u Vertical displacement, v	Horizontal displacement, u Vertical displacement, v Pore-water pressure, u_w
Initial conditions	$(\sigma_{mean} - u_a)_i$ $(u_a - u_w)_i$	$(\sigma_{mean} - u_a)_i$ $(u_a - u_w)_i$	$(\sigma_{mean} - u_a)_i$ $(u_a - u_w)_i$
Soil properties as constants Soil properties as functions	μ E, H at $[(\sigma_{mean} - u_a)_i ; (u_a - u_w)_i]$ $E_w = fn(u_a - u_w)$ at $(\sigma_{mean} - u_a)_i$ $H_w = fn(u_a - u_w)$ at $(\sigma_{mean} - u_a)_i$ $k_w = k_w(u_a - u_w)$ at $(\sigma_{mean} - u_a)_i$	μ $E = fn(\sigma_{mean} - u_a)$ at $(u_a - u_w)_i$ $H = fn(\sigma_{mean} - u_a)$ at $(u_a - u_w)_i$	μ $E = fn[(\sigma_{mean} - u_a), (u_a - u_w)]$ $H = fn[(\sigma_{mean} - u_a), (u_a - u_w)]$ $E_w = fn(\sigma_{mean} - u_a), (u_a - u_w)]$ $H_w = fn[(\sigma_{mean} - u_a), (u_a - u_w)]$ $k_w = fn[(\sigma_{mean} - u_a), (u_a - u_w)]$
Boundary conditions (valued) Boundary conditions (natural)	Pore-water pressure, u_w Water flux, q	Displacement, u, v Applied load	Displacement, u, v Pore-water pressure Applied load Water flux
Output	Pore-water pressure, u_w	Displacements, u, v Resulting stresses	Displacements, u, v Pore-water pressure, u_w Resulting stresses Volumetric water content
Analysis for	A change in time, Δt	A change in suction, Δu_w	A change in time, Δt

3.4 Soil properties required for swelling analysis (for both coupled and uncoupled cases)

Soil properties required for swelling analysis of an unsaturated, expansive soil are shown in Fig. 3.1.

1) Poisson's ratio, μ
2) Elasticity parameter for the soil structure with respect to net normal stress, E
3) Elasticity parameter for the soil structure with respect to matric suction, H
4) Elasticity parameter for the water phase with respect to net normal stress, E_w
5) Elasticity parameter for the water phase with respect to matric suction, H_w
6) Coefficient of permeability, k_w.

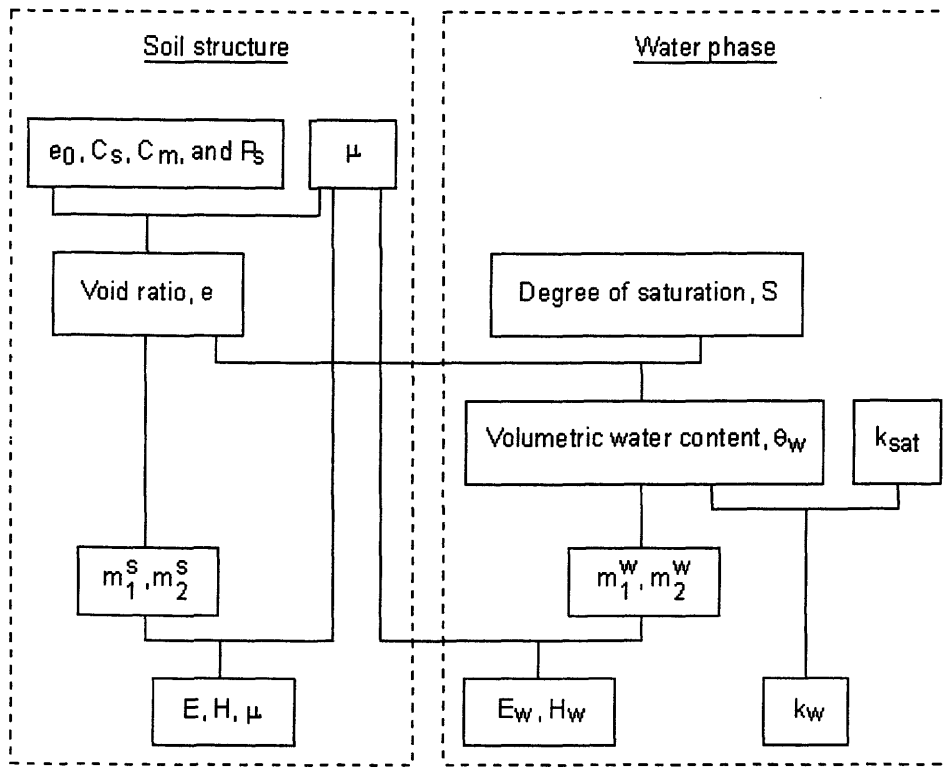

Figure 3.1 Soil property functions required for volume change analysis

All the above soil properties are known to be functions of both net normal stress and matric suction. Assuming a value of Poisson's ratio, the elasticity parameters, E, H, E_w, H_w, can be calculated from the coefficient of volume change, $m_1^s, m_2^s, m_1^w, m_2^w$, respectively from various loading conditions (Table 2.4). The coefficients of volume change, m_1^s, m_2^s, can be obtained by differentiating the constitutive surface for the soil structure. The coefficients of volume change, m_1^w, m_2^w, can be obtained by differentiating the constitutive surface for the water phase (Table 2.2).

The constitutive surfaces can be obtained directly through a laboratory program or estimated from other soil properties. Procedures for the laboratory tests were presented in Ho (1988); Fredlund and Rahardjo (1993) and Shuai (1996). Ho (1988) also presented the possible relationship among these coefficients of volume changes, and therefore the relationship among the elasticity parameters.

The constitutive surface for the soil structure can be estimated from the volume change indices, initial void ratio, swelling pressure and assumed Poisson's ratio in this study (Figure 3.1). The estimation of void ratio surface from volume change indices is presented in the next chapter.

Volumetric strain can be calculated from a change in void ratio assuming a constant referential volume as follows:

$$d\varepsilon_v = \frac{de}{1+e_0} \tag{3.45}$$

where:

e_0 = initial (i.e., referential) void ratio of the soil

de = a change in void ratio.

From Eq. (3.45) and Table 2.2, the coefficients of volume change for soil structure can be written as a function of void ratio as follows:

$$m_1^s = \frac{1}{1+e_0}\frac{de}{d(\sigma_{mean} - u_a)} \tag{3.46}$$

$$m_2^s = \frac{1}{1+e_0}\frac{de}{d(u_a - u_w)} \tag{3.47}$$

Volumetric water content can be expressed in terms of degree of saturation and void ratio as follows:

$$\theta_w = \frac{dV_w}{V_0} = \frac{Se}{1+e} \tag{3.48}$$

From Eq. (3.48), Table 2.2, and the assumption of small strain, the coefficients of volume change for water phase can be written as functions of void ratio and degree of saturation as follows:

$$m_1^w = \frac{d\theta_w}{d(\sigma_{mean} - u_a)} = \frac{S}{1+e_0}\frac{de}{d(\sigma_{mean} - u_a)} + \frac{e}{1+e_0}\frac{dS}{d(\sigma_{mean} - u_a)} \tag{3.49}$$

$$m_2^w = \frac{d\theta_w}{d(u_a - u_w)} = \frac{S}{1+e_0}\frac{de}{d(u_a - u_w)} + \frac{e}{1+e_0}\frac{dS}{d(u_a - u_w)} \tag{3.50}$$

The coefficient of permeability function, k_w, can be estimated from the saturated coefficient of permeability and the soil-water characteristic curve (i.e., from volumetric water content constitutive surface).

3.5 Details related to an uncoupled analysis

In the uncoupled approach, the water phase continuity (i.e., seepage) equation is solved separately from the equilibrium (i.e., stress-deformation) equations. The interdependence of the equations is made in an iterative manner where the flow portion of the formulation is solved for a given time period and the resultant pore-water pressure changes are used as input in a deformation analysis. In turn, volume changes and induced stresses from the deformation analysis are used in the computation of the soil properties for the next time period in the seepage analysis.

The involvement of dependent variables and a number of non-linear soil properties are separated into two analyses; namely, a seepage analysis and a stress-deformation analysis. For seepage analyses, the dependent variable is pore-water pressure (or hydraulic head). At each given time period, the elasticity parameters, E and H, for soil structure are calculated at the initial conditions of current period, and assumed to remain unchanged over the current time increment. Net normal stress is assumed to be unchanged in the seepage analysis; therefore, the elasticity parameters, E_w and H_w, for water phase and coefficient of permeability, k_w, are functions of only matric suction, rather than both matric suction and net normal stress. Boundary conditions for seepage can be either pore-water pressure (or hydraulic head) type or water flux type. The results of the seepage analysis provide the development of pore-water pressure and water flux with time in the time period considered; therefore, changes in pore-water pressure can be obtained. These changes in pore-water pressure are then used in the stress-deformation analysis.

For a stress-deformation analysis, dependent variables are horizontal displacement, u, and vertical displacement, v. In addition to Poisson's ratio, only two elasticity parameters, E and H, for soil structure need to be described as functions of matric suction at unchanged initial net normal stress. The elasticity parameters, E_w and H_w, for water phase and coefficient of permeability, k_w, are no longer needed for stress deformation analysis. Boundary conditions for the stress-deformation analyses can be of the displacement type or load type. Results of the stress-deformation analysis provide the displacements and induced stresses due to applied boundary conditions and changes in pore-water pressure.

The uncoupled solutions are obtained through the use of the general partial equation solver, FlexPDE.

Solutions using the uncoupled approach depend on the magnitude of chosen time periods for seepage analysis. Short time periods allow the stress state in the soils and the soil properties to be described more accurately with time and result in more accurate pore-water pressures and displacements.

The seepage analysis can be analysed without accounting for changes in net normal stress for the whole time considered. Pore-water pressure profiles at any

specified time during the transient process obtained from the seepage analysis are then used to estimate changes in matric suctions for the stress-deformation analysis. In this case, the seepage equation [i.e., Eq. (3.42)] has the following form:

$$m_2^w \frac{\partial(u_a - u_w)}{\partial t} = \frac{\partial}{\partial x}\left(k_w^x \frac{\partial u_w}{\partial x}\right) + \frac{\partial}{\partial y}\left(k_w^y \frac{\partial u_w}{\partial y}\right) \tag{3.51}$$

It should be noted that with the use of Eq. (3.51), soil volume change and induced stresses are assumed to be negligible. The soil water characteristic curve can be used to represent the whole water phase constitutive surface. The volume change analysis presented in Hung (2000) considered Eq. (3.51) for matric suction prediction.

3.6 Finite element formulation of the coupled equations for plane strain problem

The problem must be discretized in terms of both space and time. The spatial discretization is considered first by using the Galerkin's weighted residual method. Then the time discretization is performed using a two-level finite difference technique (Pereira, 1996).

3.6.1 Spatial discretization

The primary unknowns of the problem are time dependent displacements, u, v, pore-water pressure, u_w, and pore-air pressure, u_a. These unknowns can be approximated in the domain of the problem at any specific time as follows:

$$\mathbf{u} \cong \sum_{j=1}^{m} \overline{\mathbf{\Phi}}_j \mathbf{u}_j = \overline{\mathbf{\Phi}}\overline{\mathbf{u}} \tag{3.52}$$

$$u_w \cong \sum_{j=1}^{n} \phi_j u_{wj} = \mathbf{\Phi}\overline{\mathbf{u}}_w \tag{3.53}$$

$$u_a \cong \sum_{j=1}^{n} \phi_j u_{aj} = \mathbf{\Phi}\overline{\mathbf{u}}_a \tag{3.54}$$

where:

$$\overline{\mathbf{\Phi}} = \left[\overline{\mathbf{\Phi}}_1 \quad \overline{\mathbf{\Phi}}_2 \quad \ldots \quad \overline{\mathbf{\Phi}}_m\right]$$

$$\overline{\mathbf{\Phi}}_j = \overline{\phi}_j \begin{bmatrix} 1 & 0 \\ 0 & 1 \end{bmatrix}$$

$$\mathbf{u} = \begin{bmatrix} u & v \end{bmatrix}^T$$

$$\mathbf{\Phi} = \left[\phi_1 \quad \phi_2 \quad \ldots \quad \phi_n\right]$$

j = index for node number

m = number of nodal points for displacements

n = number of nodal points for pore-fluid pressures

$\overline{\phi}_j$ = shape function for displacements

ϕ_j = shape function for pore-fluid pressures (i.e., u_w and u_a)

$\overline{u}_j$ = nodal value of the horizontal displacement

$\overline{v}_j$ = nodal value of the vertical displacement

$\overline{u}_{wj}$ = nodal value of the pore water pressure

$\overline{u}_{aj}$ = nodal value of the pore air pressure

The strain-displacement relations can be written in matrix form as follows:

$$\boldsymbol{\varepsilon} = \mathbf{L}\mathbf{u} \tag{3.55}$$

where:

$$\boldsymbol{\varepsilon} = \begin{bmatrix} \varepsilon_x & \varepsilon_y & \gamma_{xy} \end{bmatrix}^T$$

$$\mathbf{L} = \begin{bmatrix} \dfrac{\partial}{\partial x} & 0 \\ 0 & \dfrac{\partial}{\partial y} \\ \dfrac{\partial}{\partial y} & \dfrac{\partial}{\partial x} \end{bmatrix}$$

From Eqs. (3.52) and (3.55), the strain vector can be approximated from nodal displacements as follows:

$$\boldsymbol{\varepsilon} = \sum_{j=1}^{m} \mathbf{B}_j \bar{\mathbf{u}}_j = \mathbf{B}\bar{\mathbf{u}} \tag{3.56}$$

where:

$$\mathbf{B}_j = \mathbf{L}\bar{\boldsymbol{\Phi}}_j = \begin{bmatrix} \dfrac{\partial \phi_j}{\partial x} & 0 \\ 0 & \dfrac{\partial \phi_j}{\partial y} \\ \dfrac{\partial \phi_j}{\partial y} & \dfrac{\partial \phi_j}{\partial x} \end{bmatrix}$$

3.6.1.1 Spatial discretization for the equilibrium equation

Let Ω be a domain of a problem with boundary surface S. The boundary surface S consists of two parts, S_1 and S_2. Assume that displacements, **u**, are acting on S_1, and stresses, τ_s, are acting on S_2, the equilibrium equations for any arbitrary virtual compatible displacement, $\delta \boldsymbol{u}$ ($\delta \boldsymbol{u} = 0$ on S_1), can be written as follows:

$$\int_{\Omega} \delta\boldsymbol{\varepsilon}^T \boldsymbol{\sigma} d\Omega - \int_{\Omega} \delta\mathbf{u}^T \mathbf{b} d\Omega - \int_{S_2} \delta\mathbf{u}^T \boldsymbol{\tau}_s dS = 0 \tag{3.57}$$

where:

$\mathbf{b}^T = [b_x, b_y]$, the body force vector.

Since swelling is a transient process, the equilibrium equation must be valid for any incremental deformation (i.e., time step). Equation (3.57) can be written in the incremental, time-derivative form as follows:

$$\int_{\Omega} \delta\boldsymbol{\varepsilon}^T \frac{\partial \boldsymbol{\sigma}}{\partial t} d\Omega - \int_{\Omega} \delta\mathbf{u}^T \frac{\partial \mathbf{b}}{\partial t} d\Omega - \int_{S_2} \delta\mathbf{u}^T \frac{\partial \boldsymbol{\tau}_s}{\partial t} dS = 0 \tag{3.58}$$

Equations (3.52) and (3.56) can be rewritten as follows:

$$\delta \mathbf{u}^T = \delta \overline{\mathbf{u}}^T \overline{\mathbf{\Phi}}^T \tag{3.59}$$

$$\delta \boldsymbol{\varepsilon}^T = \delta \overline{\mathbf{u}}^T \mathbf{B}^T \tag{3.60}$$

Substituting Eqs. (3.59) and (3.60) into Eq. (3.58) gives:

$$\int_{\Omega} \mathbf{B}^T \frac{\partial \boldsymbol{\sigma}}{\partial t} d\Omega - \int_{\Omega} \overline{\mathbf{\Phi}}^T \frac{\partial \mathbf{b}}{\partial t} d\Omega - \int_{S_2} \overline{\mathbf{\Phi}}^T \frac{\partial \boldsymbol{\tau}_s}{\partial t} dS = 0 \tag{3.61}$$

The first term of Eq. (3.61) can be rewritten as follows:

$$\int_{\Omega} \mathbf{B}^T \frac{\partial \boldsymbol{\sigma}}{\partial t} d\Omega = \int_{\Omega} \mathbf{B}^T \left[\frac{\partial (\boldsymbol{\sigma} - \mathbf{m} u_a)}{\partial t} + \mathbf{m} \frac{\partial u_a}{\partial t} \right] d\Omega \tag{3.62}$$

Substituting the strain-nodal displacement relationship, Eq. (3.56) into the constitutive relationship, Eq. (3.34), then substituting Eqs. (3.34), (3.62) and the approximation equations for pore-fluid pressures, Eqs. (3.53), (3.54) into Eq. (3.61) gives the following equation:

$$\begin{aligned} \int_{\Omega} \mathbf{B}^T \left[\mathbf{D}\mathbf{B} \frac{\partial \overline{\mathbf{u}}}{\partial t} - \mathbf{D}_s \mathbf{\Phi} \frac{\partial \overline{\mathbf{u}}_a}{\partial t} + \mathbf{D}_s \mathbf{\Phi} \frac{\partial \overline{\mathbf{u}}_w}{\partial t} + \mathbf{m} \mathbf{\Phi} \frac{\partial \overline{\mathbf{u}}_a}{\partial t} \right] d\Omega \\ - \int_{\Omega} \overline{\mathbf{\Phi}}^T \frac{\partial \mathbf{b}}{\partial t} d\Omega - \int_{S_2} \overline{\mathbf{\Phi}}^T \frac{\partial \boldsymbol{\tau}_s}{\partial t} dS = 0 \end{aligned} \tag{3.63}$$

The primary unknown variables, $\overline{\mathbf{u}}$, $\overline{\mathbf{u}}_a$, and $\overline{\mathbf{u}}_w$ are the vectors of nodal values at specific time. Rearranging Eq. (3.63) gives:

$$\begin{aligned} \frac{\partial \overline{\mathbf{u}}}{\partial t} \int_{\Omega} \mathbf{B}^T \mathbf{D}\mathbf{B} d\Omega + \frac{\partial \overline{\mathbf{u}}_w}{\partial t} \int_{\Omega} \mathbf{B}^T \mathbf{D}_s \mathbf{\Phi} d\Omega + \frac{\partial \overline{\mathbf{u}}_a}{\partial t} \int_{\Omega} \mathbf{B}^T (\mathbf{m} - \mathbf{D}_s) \mathbf{\Phi} d\Omega = \\ \int_{\Omega} \overline{\mathbf{\Phi}}^T \frac{\partial \mathbf{b}}{\partial t} d\Omega + \int_{S_2} \overline{\mathbf{\Phi}}^T \frac{\partial \boldsymbol{\tau}_s}{\partial t} dS \end{aligned} \tag{3.64}$$

Equation (3.64) can be written in the matrix form as follows:

$$[\mathbf{DK}]\dot{\bar{\mathbf{u}}} + [\mathbf{CW}]\dot{\bar{\mathbf{u}}}_w + [\mathbf{CA}]\dot{\bar{\mathbf{u}}}_a = \{\mathbf{F}\} \tag{3.65}$$

where:

$\dot{\bar{\mathbf{u}}}$, $\dot{\bar{\mathbf{u}}}_a$, and $\dot{\bar{\mathbf{u}}}_w$ = time derivative of the primary unknowns

$[\mathbf{DK}] = \int_{\Omega} \mathbf{B}^T \mathbf{D} \mathbf{B} d\Omega$, the soil structure stiffness matrix

$[\mathbf{CW}] = \int_{\Omega} \mathbf{B}^T \mathbf{D}_s \mathbf{\Phi} d\Omega$, the stiffness matrix related to water phase coupling

$[\mathbf{CA}] = \int_{\Omega} \mathbf{B}^T [\mathbf{m} - \mathbf{D}_s] \mathbf{\Phi} d\Omega$, the stiffness matrix related to air phase coupling

$\{\mathbf{F}\} = \int_{\Omega} \overline{\mathbf{\Phi}}^T \frac{\partial \mathbf{b}}{\partial t} d\Omega + \int_{S_2} \overline{\mathbf{\Phi}}^T \frac{\partial \boldsymbol{\tau}_s}{\partial t} dS$, the load vector related to body forces and external stresses.

For the swelling problem under consideration, pore air pressure is assumed to be at atmospheric condition (i.e., $\dot{\bar{\mathbf{u}}}_a$ equals to zero), Eq. (3.65) becomes:

$$[\mathbf{DK}]\dot{\bar{\mathbf{u}}} + [\mathbf{CW}]\dot{\bar{\mathbf{u}}}_w = \{\mathbf{F}\} \tag{3.66}$$

3.6.1.2 Spatial discretization for the water phase continuity equation

The constitutive relationship for water phase and Darcy's law for water flow in an unsaturated soil are written as follows:

$$\frac{dV_w}{V_0} = d\theta_w = \beta_{w1} d\varepsilon_v + \beta_{w2} d(u_a - u_w) \tag{3.67}$$

$$\mathbf{v}_w = -\mathbf{k}_w \nabla \left(\frac{u_w}{\rho_w g} + Y \right) \tag{3.68}$$

where:

$$\mathbf{v}_w^{\mathrm{T}} = [\, v_w^x \;\; v_w^y \,]$$

$$\mathbf{k}_w^{\mathrm{T}} = [\, k_w^x \;\; k_w^y \,]$$

The water phase continuity equation is written as follows:

$$\frac{\partial(\theta_w)}{\partial t} + \nabla \cdot (\mathbf{v}_w) = 0 \tag{3.69}$$

Let Ω be a domain of a problem with boundary surface S. Boundary surface, S consists of two parts, S_1' and S_2'. Pore water pressure and water flux are acting exclusively on the surfaces S_1' and S_2' as follows:

$$u_w = \varphi_w \text{ at surface } S_1' \tag{3.70}$$

$$\mathbf{v}_w \cdot \mathbf{n} = \lambda \text{ at surface } S_2' \tag{3.71}$$

where:

$\mathbf{n}$ = unit vector normal to the boundary

φ_w = pore water pressure acting on S_1'

Integrating the water phase continuity equation, Eq. (3.69) by using Galerkin's weighted residual method results in the following equation:

$$\int_\Omega \mathbf{\Phi}^T \frac{\partial \theta_w}{\partial t} d\Omega + \int_\Omega \mathbf{\Phi}^T (\nabla \cdot \mathbf{v}_w) d\Omega = 0 \tag{3.72}$$

Using the following identity:

$$\mathbf{\Phi}^T (\nabla \cdot \mathbf{v}_w) = \nabla \cdot (\mathbf{\Phi}^T \mathbf{v}_w) - (\nabla \mathbf{\Phi})^T \mathbf{v}_w \tag{3.73}$$

Equation (3.72) becomes:

$$\int_\Omega \mathbf{\Phi}^T \frac{\partial \theta_w}{\partial t} d\Omega + \int_\Omega \nabla \cdot (\mathbf{\Phi}^T \mathbf{v}_w) d\Omega - \int_\Omega (\nabla \mathbf{\Phi})^T \mathbf{v}_w d\Omega = 0 \tag{3.74}$$

Applying the divergence theorem to the second term of Equation (3.74) results the following equation:

$$\int_{\Omega} \mathbf{\Phi}^T \frac{\partial \theta_w}{\partial t} d\Omega - \int_{\Omega} (\nabla \mathbf{\Phi})^T \mathbf{v}_w d\Omega + \int_{S} \mathbf{\Phi}^T (\mathbf{v}_w \cdot \mathbf{n}) dS = 0 \tag{3.75}$$

Splitting the boundary term into two parts (i.e., $S_1^{'}$ and $S_2^{'}$) and applying the natural boundary condition for $S_2^{'}$ gives the following equation:

$$\int_{\Omega} \mathbf{\Phi}^T \frac{\partial \theta_w}{\partial t} d\Omega - \int_{\Omega} (\nabla \mathbf{\Phi})^T \mathbf{v}_w d\Omega + \int_{S_1^{'}} \mathbf{\Phi}^T (\mathbf{v}_w \cdot \mathbf{n}) dS + \int_{S_2^{'}} \mathbf{\Phi}^T \lambda dS = 0 \tag{3.76}$$

By choosing the Φ which gives $\phi_j(x,y)$ equal to zero on boundary $S_1^{'}$, Eq. (3.76) can be simplified as follows:

$$\int_{\Omega} \mathbf{\Phi}^T \frac{\partial \theta_w}{\partial t} d\Omega - \int_{\Omega} (\nabla \mathbf{\Phi})^T \mathbf{v}_w d\Omega + \int_{S_2^{'}} \mathbf{\Phi}^T \lambda dS = 0 \tag{3.77}$$

Applying Darcy's law to the second term of Eq. (3.77), we have

$$\int_{\Omega} \mathbf{\Phi}^T \frac{\partial \theta_w}{\partial t} d\Omega + \int_{\Omega} (\nabla \mathbf{\Phi})^T \left(\frac{1}{\rho_w g} \mathbf{k}_w \nabla u_w + \mathbf{k}_w \nabla Y\right) d\Omega + \int_{S_2^{'}} \mathbf{\Phi}^T \lambda dS = 0 \tag{3.78}$$

Using the strain-displacement relationship and approximations using the shape functions:

$$\frac{\partial \theta_w}{\partial t} = \beta_{w1} \mathbf{m}^T \mathbf{B} \frac{\partial \overline{\mathbf{u}}}{\partial t} + \beta_{w2} \mathbf{\Phi} \frac{\partial \overline{\mathbf{u}}_a}{\partial t} - \beta_{w2} \mathbf{\Phi} \frac{\partial \overline{\mathbf{u}}_w}{\partial t} \tag{3.79}$$

Substituting Eq. (3.79) into Eq. (3.78), neglecting the air phase term, gives

$$\frac{\partial \overline{\mathbf{u}}}{\partial t}\int_{\Omega}\beta_{w1}\boldsymbol{\Phi}^{T}\mathbf{m}^{T}\mathbf{B}d\Omega-\frac{\partial \overline{\mathbf{u}}_{w}}{\partial t}\int_{\Omega}\beta_{2w}\boldsymbol{\Phi}^{T}\boldsymbol{\Phi}d\Omega+$$
$$\int_{\Omega}(\nabla\boldsymbol{\Phi})^{T}(\frac{1}{\rho_{w}g}\mathbf{k}_{w}\nabla\boldsymbol{\Phi}\overline{\mathbf{u}}_{w}+\mathbf{k}_{w}\nabla Y)d\Omega+\int_{S_{2}^{'}}\boldsymbol{\Phi}^{T}\lambda dS=0 \tag{3.80}$$

Rearranging Eq. (3.80) gives

$$\overline{\mathbf{u}}_{w}\int_{\Omega}(\nabla\boldsymbol{\Phi})^{T}(\frac{1}{\rho_{w}g}\mathbf{k}_{w}\nabla\boldsymbol{\Phi})d\Omega+\frac{\partial \overline{\mathbf{u}}}{\partial t}\int_{\Omega}\beta_{w1}\boldsymbol{\Phi}^{T}\mathbf{m}^{T}\mathbf{B}d\Omega-\frac{\partial \overline{\mathbf{u}}_{w}}{\partial t}\int_{\Omega}\beta_{2w}\boldsymbol{\Phi}^{T}\boldsymbol{\Phi}d\Omega$$
$$=-\int_{\Omega}(\nabla\boldsymbol{\Phi})^{T}(\mathbf{k}_{w}\nabla Y)d\Omega-\int_{S_{2}^{'}}\boldsymbol{\Phi}^{T}\lambda dS \tag{3.81}$$

In matrix form, the water continuity equation can be written as:

$$[\mathbf{HW}]\{\overline{\mathbf{u}}_{w}\}+[\mathbf{WK}]\{\dot{\overline{\mathbf{u}}}\}-[\mathbf{TW}]\{\dot{\overline{\mathbf{u}}}_{w}\}=\{\mathbf{FW}\} \tag{3.82}$$

where:

$[\mathbf{HW}]$ = $\int_{\Omega}(\nabla\boldsymbol{\Phi})^{T}\left(\frac{1}{\rho_{w}g}\mathbf{k}_{w}\nabla\boldsymbol{\Phi}\right)d\Omega$, the coefficient of permeability matrix

$[\mathbf{WK}]$ = $\int_{\Omega}\beta_{w1}\boldsymbol{\Phi}^{T}\mathbf{m}^{T}\mathbf{B}d\Omega$, the mass matrix related to soil structure coupling

$[\mathbf{TW}]$ = $\int_{\Omega}\beta_{2w}\boldsymbol{\Phi}^{T}\boldsymbol{\Phi}d\Omega$, the mass matrix

$[\mathbf{FW}]$ = $-\int_{\Omega}(\nabla\boldsymbol{\Phi})^{T}(\mathbf{k}_{w}\nabla Y)d\Omega-\int_{S_{2}^{'}}\boldsymbol{\Phi}^{T}\lambda dS$, vector related to the gravity forces and unit flux across boundary portion $S_{2}^{'}$.

3.6.1.3 Finite element equations of the system of coupled equations

By neglecting the air phase, the system of coupled equations can be written as follows:

$$[\mathbf{DK}]\dot{\overline{\mathbf{u}}}+[\mathbf{CW}]\dot{\overline{\mathbf{u}}}_{w}=\{\mathbf{F}\} \tag{3.83}$$

$$[\mathbf{HW}]\{\bar{\mathbf{u}}_w\}+[\mathbf{WK}]\{\dot{\bar{\mathbf{u}}}\}-[\mathbf{TW}]\{\dot{\bar{\mathbf{u}}}_w\}=\{\mathbf{FW}\} \tag{3.84}$$

In a condensed form, this system can be simplified as follows:

$$[\mathbf{A}]\{\mathbf{w}\}+[\mathbf{B}]\{\dot{\mathbf{w}}\}=\{\mathbf{T}\} \tag{3.85}$$

where:

$$[\mathbf{A}]=\begin{bmatrix}0 & 0\\ 0 & \mathbf{HW}\end{bmatrix}$$

$$[\mathbf{B}]=\begin{bmatrix}\mathbf{DK} & \mathbf{CW}\\ \mathbf{WK} & -\mathbf{TW}\end{bmatrix}$$

$$\{\mathbf{w}\}=\begin{bmatrix}\bar{\mathbf{u}}\\ \bar{\mathbf{u}}_w\end{bmatrix}$$

$$\{\mathbf{T}\}=\begin{bmatrix}\mathbf{F}\\ \mathbf{FW}\end{bmatrix}$$

3.6.2 Time discretization

The transient analysis can be performed by using a finite difference discretization. For a linear problem the matrixes [A] and [B] and force vector {T} are constants with respect to time. For unsaturated soils, these matrices are nonlinear and dependent on the stress state variables and/or soil properties.

Let θ be a family of approximation that approximates a weighted average of the time derivative of the unknown variables at two consecutive time steps. The system of differential equations (3.85) can be evaluated at time ($t + \theta\Delta t$) as follows:

$$[\mathbf{A}]_{t+\theta\Delta t}\{\mathbf{w}\}_{t+\theta\Delta t}+[\mathbf{B}]_{t+\theta\Delta t}\{\dot{\mathbf{w}}\}_{t+\theta\Delta t}=\{\mathbf{T}\}_{t+\theta\Delta t} \tag{3.86}$$

A linear variation of the vector of unknown variables (i.e., w) in time increment between t and $t + \theta\Delta t$ is as follows:

$$\{\mathbf{w}\}_{t+\theta\Delta t} = (1-\theta)\{\mathbf{w}\}_t + \theta\{\mathbf{w}\}_{t+\Delta t} \tag{3.87}$$

The time derivative of the vector of unknown variables is expressed in the following form:

$$\left\{\frac{\partial \mathbf{w}}{\partial t}\right\}_{t+\theta\Delta t} = \frac{\{\mathbf{w}\}_{t+\Delta t} - \{\mathbf{w}\}_t}{\Delta t} \tag{3.88}$$

Substituting Eqs. (3.87) and (3.88) into Eq. (3.86) gives:

$$\begin{aligned}&\left(\theta[\mathbf{A}]_{t+\theta\Delta t} + \frac{1}{\Delta t}[\mathbf{B}]_{t+\theta\Delta t}\right)\{\mathbf{w}\}_{t+\theta\Delta t} = \\ &\{\mathbf{T}\}_{t+\theta\Delta t} - \left((1-\theta)[\mathbf{A}]_{t+\theta\Delta t} - \frac{1}{\Delta t}[\mathbf{B}]_{t+\theta\Delta t}\right)\{\mathbf{w}\}_t\end{aligned} \tag{3.89}$$

Rearranging Eq. (3.89) we obtain:

$$\begin{aligned}&(\Delta t\theta[\mathbf{A}]_{t+\theta\Delta t} + [\mathbf{B}]_{t+\theta\Delta t})\{\mathbf{w}\}_{t+\theta\Delta t} = \\ &\Delta t\{\mathbf{T}\}_{t+\theta\Delta t} - (\Delta t(1-\theta)[\mathbf{A}]_{t+\theta\Delta t} - [\mathbf{B}]_{t+\theta\Delta t})\{\mathbf{w}\}_t\end{aligned} \tag{3.90}$$

The matrices $[\mathbf{A}]_{t+\theta\Delta t}$, $[\mathbf{B}]_{t+\theta\Delta t}$ and the vector $\{\mathbf{T}\}_{t+\theta\Delta t}$, depend on the unknowns and must be approximated as follows:

$$[\mathbf{A}]_{t+\theta\Delta t} = [\mathbf{A}(\{\mathbf{w}\}_{t+\theta\Delta t})] = [\mathbf{A}((1-\theta)\{\mathbf{w}\}_t + \theta\{\mathbf{w}\}_{t+\Delta t})] \tag{3.91}$$

$$[\mathbf{B}]_{t+\theta\Delta t} = [\mathbf{B}(\{\mathbf{w}\}_{t+\theta\Delta t})] = [\mathbf{B}((1-\theta)\{\mathbf{w}\}_t + \theta\{\mathbf{w}\}_{t+\Delta t})] \tag{3.92}$$

$$\{\mathbf{T}\}_{t+\theta\Delta t} = \{\mathbf{T}(\{\mathbf{w}\}_{t+\theta\Delta t})\} = \{\mathbf{T}((1-\theta)\{\mathbf{w}\}_t + \theta\{\mathbf{w}\}_{t+\Delta t})\} \tag{3.93}$$

A direct iteration procedure is used for solving the nonlinear Eq. (3.90) as follows:

$$\{\mathbf{w}\}_{t+\Delta t}^{i+1} = [\mathbf{C}]^{-1}\{\mathbf{f}\} \tag{3.94}$$

where:

i = the last iteration number

$$[\mathbf{C}] = \left[\Delta t\theta[\mathbf{A}]_{t+\theta\Delta t}^{i} + [\mathbf{B}]_{t+\theta\Delta t}^{i}\right]$$

$$\{\mathbf{f}\} = \left\{\Delta t\{\mathbf{T}\}_{t+\theta\Delta t}^{i} - \left[\Delta t(1-\theta)[\mathbf{A}]_{t+\theta\Delta t}^{i} - [\mathbf{B}]_{t+\theta\Delta t}^{i}\right]\{\mathbf{w}\}_{t}\right\}$$

The iterative process stops when a previously defined accuracy is reached. The chosen time interval plays a fundamental role in the rate of convergence.

Equation (3.94) can be written in a global form as follows:

$$[\mathbf{AG}]\{\mathbf{w}\}_{t+\Delta t} = \{\mathbf{FG}\}_{t} \tag{3.95}$$

where:

$$[\mathbf{AG}] = [\Delta t\theta[\mathbf{A}]_{t+\theta\Delta t} + [\mathbf{B}]_{t+\theta\Delta t}]$$

$$\{\mathbf{FG}\} = \{\Delta t\{\mathbf{T}\}_{t+\theta\Delta t} - [\Delta t(1-\theta)[\mathbf{A}]_{t+\theta\Delta t} - [\mathbf{B}]_{t+\theta\Delta t}]\{\mathbf{w}\}_{t}\}$$

3.7 Summary of the formulation theory for the swelling process in an expansive soil

The swelling theory has been presented for an unsaturated, expansive soil. General three-dimensional coupled equations were derived for a continuous air phase and a water phase. The system of three-dimensional coupled equations includes three equilibrium equations corresponding to three directions of the Cartesian coordinate system, one continuity equation for the water phase and one continuity equation for the air phase. This system of equations can be solved for five dependent variables, three displacements correspond to three directions of the Cartesian coordinate system,

pore-water pressure and pore-air pressure. All the soil properties associated with expansive soils are dependent on the stress state of the soil (i.e., net normal stress and matric suction). Solutions to the three-dimensional case is considered to be beyond the scope of this study.

Most practical swelling problems involve a continuous atmospheric air phase, and therefore the continuity equation for air phase can be ignored. Swelling behaviour can be described through the coupling of two physical processes; seepage and stress-deformation. For the plane strain loading condition, displacement in z-direction is restricted. The dependent variables for swelling problem in two-dimensions are the displacement u in the x-direction, displacement v in the y-direction and pore-water pressure, u_w. Corresponding to three dependent variables are three governing equations, two equations are stress-deformation equations and the third equation is the seepage equation. Coupled solutions can be obtained by solving the seepage equation and the stress-deformation simultaneously. An uncoupled solution can be obtained by solving the seepage equation separately from the stress-deformation equation.

The elasticity parameters are calculated from the volume change coefficients, which are obtained by differentiating the constitutive surfaces. The void ratio surface can be estimated from swelling indices with respect to net normal stress and matric suction; however, the void ratio is represented as a set of generated data points. A mathematical equation is needed to describe the void ratio surface.

CHAPTER 4

Theory of Constitutive Surfaces

4.1 General

The research study presented in this chapter includes three parts. The first part presents the estimation of the void ratio surface from swelling indices. The second part reviews proposed equations for the void ratio constitutive surface and presents the suggested solutions for the characterization of the surface in the low net normal stress range and the low soil suction range. The proposed mathematical functions can be used to describe the constitutive relations associated with soil structure and water phase of an unsaturated, swelling soil. The third part makes use of the newly proposed functions to characterise the soil data for Regina clay. The elasticity parameters required when performing uncoupled and coupled swelling analyses in the next chapters are calculated and graphically presented in this chapter.

4.2 Estimation of void ratio constitutive surface from swelling indices

The application of the swelling theory presented in Chapter 3 requires the measurement or estimation of the elasticity parameter functions. The elasticity parameter function can be calculated from the volume change coefficients and indices. The test procedures and equipment required for the measurement of the volume change coefficients and indices were presented by Fredlund and Rahardjo (1993). Tests to define the entire constitutive surface are time consuming and involve demanding laboratory procedures. Chapter 2 presented the calculation of the elasticity parameter functions for the soil structure from volume change indices. The suggested elasticity parameter function, E, did not change with changes in matric suction and

elasticity parameter function, H, did not change with changes in net normal stress. The variation of these elasticity parameters with both stress state variables were not considered.

Research results in this study suggest that the swelling indices obtained from extreme planes (i.e., net normal stress plane and matric suction plane) can be used to estimate the void ratio surface, and then the elasticity parameters are calculated from the estimated void ratio surface. This approach allows the elasticity parameters to be described as functions of both stress state variables. For most practical problems, approximate volume change coefficients should be adequate for analysis. The procedure to approximate the coefficient of volume change will be useful in the implementation of unsaturated soil mechanics into standard geotechnical engineering practice (Fredlund, 1999).

The following soil data are required for the estimation of the void ratio constitutive surface using this approach:

1) swelling index with respect to net normal stress, C_s,
2) swelling index with respect to matric suction, C_m,
3) initial void ratio, e_0, and
4) swelling pressure, P_s.

The following assumptions associated with the void ratio constitutive surface are used:

1) a linear relationship of void ratio versus logarithm of net normal stress at an extreme net normal stress plane (suction equal to b),
2) a linear relationship of void ratio versus logarithm of matric suction at an extreme suction plane (net normal stress equal to a),
3) the void ratio versus logarithm of net normal stress and void ratio versus logarithm of matric suction converge at net normal stress equal to a and suction equal to b, and
4) a constant void ratio plane intersects the void ratio constitutive surface as a straight line.

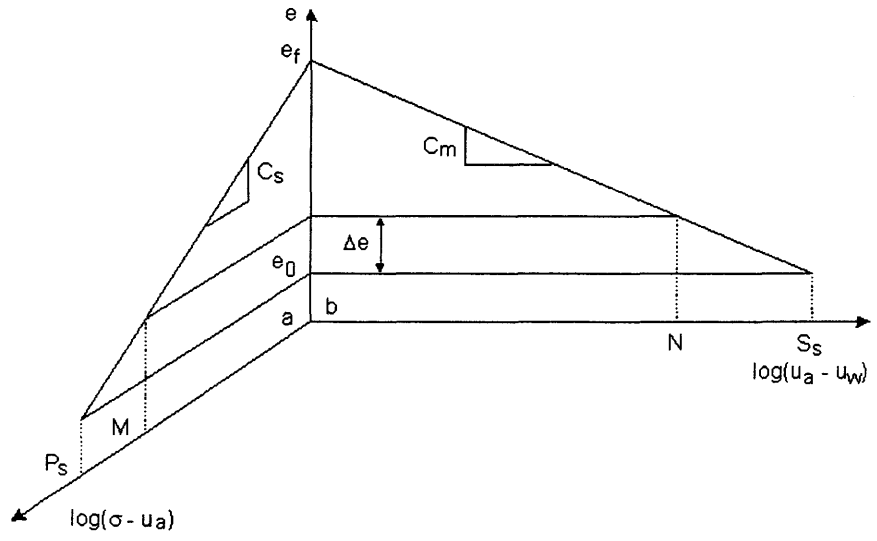

Figure 4.1 Linear relationship between void ratio and logarithm of stress state variables at extreme planes

Figure 4.1 illustrates the first, second and third assumptions. These assumptions are reasonable and well accepted (Ho, 1988; Fredlund and Rahardjo, 1993). The swelling pressures, P_s obtained at different suctions are not the same; however, at low suction, the difference is essentially negligible. The last assumption is presented in Fig. 4.2.

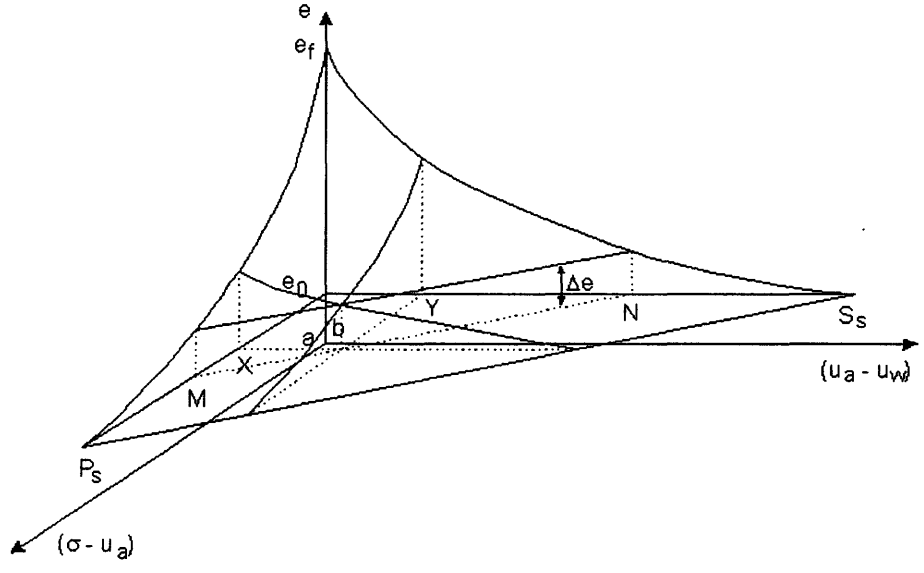

Figure 4.2 Relationship between net normal stress and matric suction at constant void ratio

The assumption of a linear relationship between net normal stress and matric suction at constant void ratio in an arithmetic scale is supported by the work of Escario (1969) (Fig. 4.3) and Matyas (1969) (Fig. 4.4). Figure 4.3 shows that the constant volume lines are essentially linear on an arithmetic scale. The same lines are asymptotic curves on a logarithmic scale. The shape of these lines suggests the form of the void ratio surface in a three-dimensional plot.

Remolded Madrid clay

Legend	γ_d (kN/m^3)	w_i (%)	w_f (%)	S_i (%)	S_f (%)	$P_{s\text{-}max}$ (kPa)
□	15.4	4.7	27.1	15.8	101.0	484
○	15.4	11.0	26.3	41.2	98.6	388
◇	15.6	16.6	27.8	63.6	106.0	244

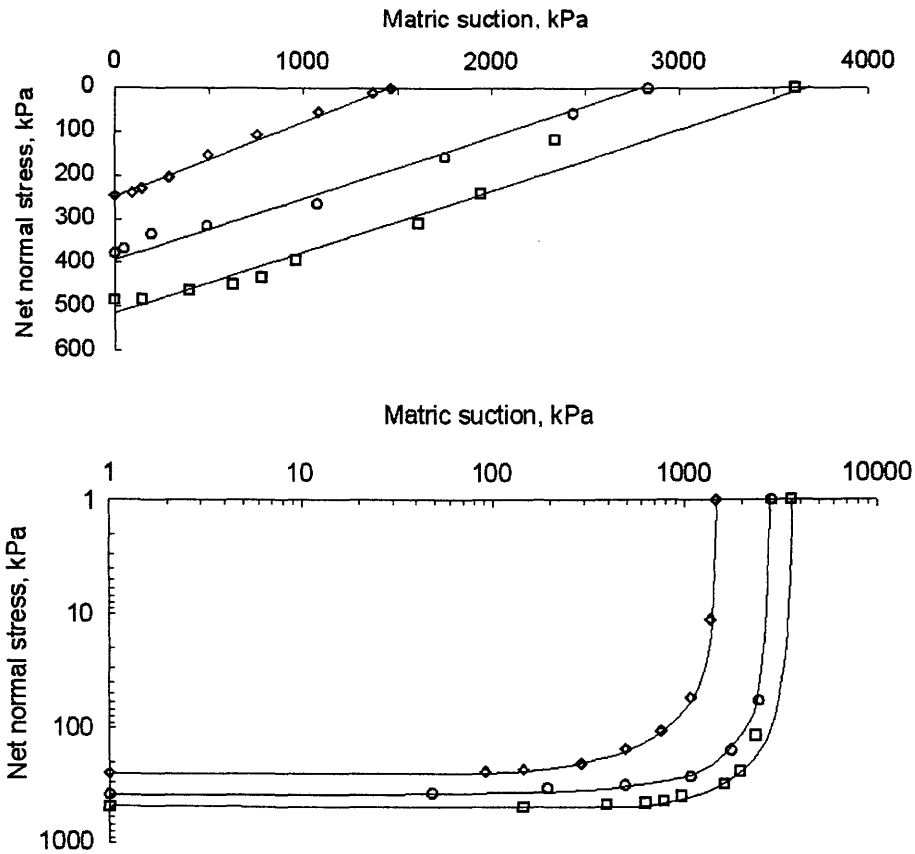

Figure 4.3 Cross sections of void ratio surfaces plotted on arithmetic scale and logarithmic scale for a remoulded Madrid clay (modified from Escario, 1969)

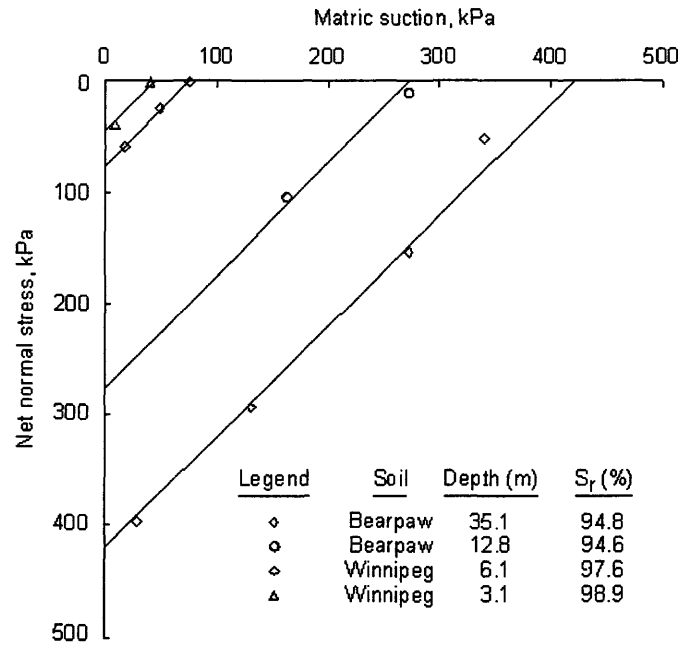

Figure 4.4 Matric suction versus isotropic net normal stress at constant void ratio (modified from Matyas, 1969)

The void ratio at a net normal stress equal to a, and a matric suction equal to b, can be calculated either from net normal stress plane or matric suction plane.

$$e(a,b) = e_0 + C_s \log \frac{a}{P_s} \tag{4.1}$$

$$e(a,b) = e_0 + C_m \log \frac{b}{S_s} \tag{4.2}$$

where:

P_s, S_s = swelling pressure and swelling suction as shown in Fig. 4.1

a, b > 0; $C_s < C_m < 0$; and $P_s < S_s$.

Equations (4.1) and (4.2) give:

$$C_s \log \frac{a}{P_s} = C_m \log \frac{b}{S_s} \tag{4.3}$$

Swelling suction can be estimated from Eq. (4.3) as follows:

$$S_s = b\left(\frac{P_s}{a}\right)^{\frac{C_s}{C_m}} \tag{4.4}$$

Let us assume that e is the void ratio at a net normal stress equal to X, and a matric suction equal to Y. The change in void ratio (Fig. 4.2) can be written as:

$$\Delta e = e - e_0 \tag{4.5}$$

From the net normal stress plane at a matric suction equal to b, the change in void ratio can be expressed as follows:

$$\Delta e = C_s \log \frac{M}{P_s} \tag{4.6}$$

Therefore:

$$M = P_s \times 10^{\frac{\Delta e}{C_s}} \tag{4.7}$$

where: $a < M < P_s$

From matric suction plane at a net normal stress equal to a, a change in void ratio can be written as follows:

$$\Delta e = C_m \log \frac{N}{S_s} \tag{4.8}$$

Therefore:

$$N = S_s \times 10^{\frac{\Delta e}{C_m}} \tag{4.9}$$

where: $b < N < S_s$

From a constant void ratio plane at a void ratio equal to e, the following relationship can be obtained:

$$\frac{N-b}{M-a}=\frac{Y-b}{M-X} \tag{4.10}$$

Rearranging Eq. (4.10) gives:

$$Y=\frac{N-b}{M-a}(M-X)+b \tag{4.11}$$

Substituting Eqs. (4.4), (4.5), (4.7), and (4.9) into Eq. (4.11) gives the relationship among net normal stress X, matric suction Y and void ratio, e:

$$Y=\frac{b\left[\left(\frac{P_s}{a}\right)^{\frac{C_s}{C_m}}\times 10^{\frac{e-e_0}{C_m}}-1\right](P_s\times 10^{\frac{e-e_0}{C_s}}-X)}{P_s\times 10^{\frac{e-e_0}{C_s}}-a}+b \tag{4.12}$$

Equation (4.12) can be rewritten as follows:

$$(u_a-u_w)=\frac{b\left[\left(\frac{P_s}{a}\right)^{\frac{C_s}{C_m}}\times 10^{\frac{e-e_0}{C_m}}-1\right]\left[P_s\times 10^{\frac{e-e_0}{C_s}}-(\sigma-u_a)\right]}{P_s\times 10^{\frac{e-e_0}{C_s}}-a}+b \tag{4.13}$$

Equation (4.13) allows the calculation of matric suction corresponding to void ratio and net normal stress, or calculation of net normal stress from void ratio and matric suction. Equation (4.13) cannot be used to estimate void ratio directly from net normal stress and matric suction.

Net normal stress and matric suction in Eqs. (4.12) and (4.13) can be determined from one-dimensional loading (i.e., $(\sigma_y - u_a)$ and $(u_a - u_w)$) or isotropic

loading (i.e., $(\sigma_{mean} - u_a)$ and $(u_a - u_w)$). While the swelling indices are essentially the same for both loading conditions, appropriate values of a and b must be used.

A set of void ratio data can be generated from Eq. (4.13). The data generated are in the range of net normal stress from a to P_s, the range of suction from b to S_s, and the range of void ratio from e_0 to $e(a,b)$. The use of this equation to estimate the void ratio surface is presented in the next part of this chapter.

A mathematical equation is needed to describe the void ratio surface. This equation will be used to fit experimental data or data generated from swelling indices [i.e., data generated from Eq. (4.13)]. Proposed equations for the void ratio surface will be presented in the next part.

4.3 Equations for the void ratio surface of an unsaturated soil

This section provides a review of the proposed equations for the constitutive surfaces of an unsaturated soil, presents a solution for low net normal stress and soil suction, and proposes a new equation for the description of the void ratio constitutive surface.

4.3.1 Review of equations for the void ratio constitutive relationship

It has become common practice in unsaturated soil mechanics to use mathematical equations to describe the variation in soil properties with respect to changes in the stress state of a soil. These mathematical equations can be divided into two groups. The first group includes those equations that are capable of representing the shape of the soil property function. These equations are determined for any specific soil under specific testing conditions by best-fitting to measured data. The equations contain fitting parameters that need to be determined. Examples of these equations include the equations proposed to best-fit the properties of soils related to the water phase such as the soil-water characteristic curve (SWCC) and the coefficient of permeability functions. These equations are flexible and can be used to describe the entire range of soil properties. The Fredlund and Xing (1994) equation, along with a correction factor, can be used for the SWCC with soil suctions varying up to a limiting value of 10^6 kPa.

The second group includes equations that use other soil properties as parameters in the equation. Examples include the equations for shear strength (i.e., using cohesion and angle of shearing resistance) and volume changes (i.e., using volume change indices). The parameters in these equations often have clearer physical meaning; however, these equations might not be suitable to describe the entire range of stress states. The equation for shear strength may not be valid at low stress conditions or high suctions. The equation commonly proposed for void ratio using volume change index cannot be used at low stress conditions and soil suctions. These equations need to be modified to provide greater flexibility in order to best-fit measured data.

Soil properties for an unsaturated soil are known to be functions of both stress state variables (i.e., net normal stress and matric suction). Often, the equations have been proposed to relate a soil property to only one stress state variable. These equations can be expanded to be functions of both stress state variables provided the properties can be evaluated. This section reviews mathematical equations that can be used to describe the constitutive surfaces associated with an unsaturated, swelling soil. Emphasis is placed on the equation representing the relationship between void ratio and stress state.

Terzaghi (1925) and Casagrande (1936) noted that the virgin compression curve of the void ratio versus logarithm of effective stress [i.e., $(\sigma - u_w)$] is essentially a straight line. The equation for the virgin compression portion of void ratio can be written as follows for a saturated soil:

$$e = e_0 - C_c \log\left(\frac{\sigma'}{\sigma'_p}\right) \tag{4.14}$$

where:

e_0 = initial void ratio,

C_c = volume change index for the virgin compression curve, and

σ'_p = preconsolidation pressure.

Similar equations can be written for the rebound curve (i.e., unloading-reloading curve). Equation (4.14) is illustrated graphically in Fig. 4.5. Equation (4.14) has the following form:

$$e = a + b\log(\sigma) \tag{4.15}$$

where:

σ = designation of the stress state, and

a, b = constants (i.e., fitting parameters).

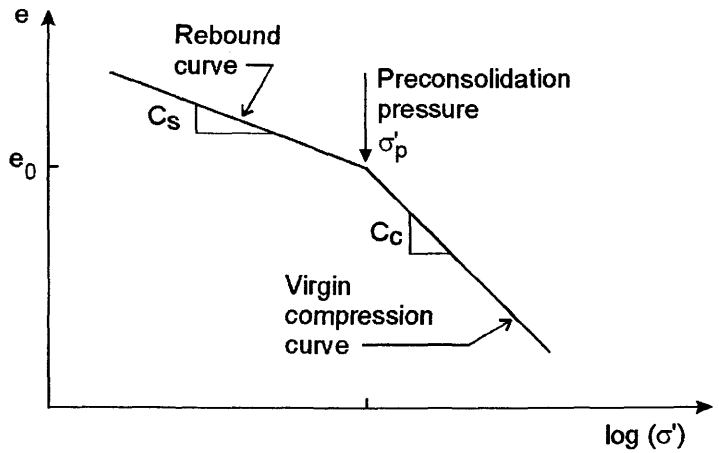

Figure 4.5 Relationship between void ratio and logarithm of effective stress

Fredlund (1979) suggested that the void ratio constitutive surface for an unsaturated soil could be linearized over a wide range of stress changes using the logarithm of the stress state variables. The void ratio under any set of stress conditions is written as follows:

$$e = e_0 - C_t \log\frac{(\sigma - u_a)}{(\sigma - u_a)_0} - C_m \log\frac{(u_a - u_w)}{(u_a - u_w)_0} \tag{4.16}$$

Similarly, the water content under any set of stress condition is written as follows:

$$w = w_0 - D_t \log\frac{(\sigma - u_a)}{(\sigma - u_a)_0} - D_m \log\frac{(u_a - u_w)}{(u_a - u_w)_0} \tag{4.17}$$

where:

e_0 = initial void ratio,

C_t = volume change index with respect to net normal stress,

C_m = volume change index with respect to matric suction,

$(\sigma - u_a)_0$ = initial net normal stress,

$(u_a - u_w)_0$ = initial matric suction,

w_0 = initial water content,

D_t = water content index with respect to net normal stress, and

D_m = water content index with respect to matric suction.

Equations (4.16) and (4.17) have the following form:

$$e = a + b\log(\sigma - u_a) + c\log(u_a - u_w) \tag{4.18}$$

where: a, b, and c are constants (i.e., fitting parameters).

An illustration of Eq. (4.18) is presented graphically in Fig. 4.6. This figure suggests that the void ratio surface is planar on a semi-logarithmic scale.

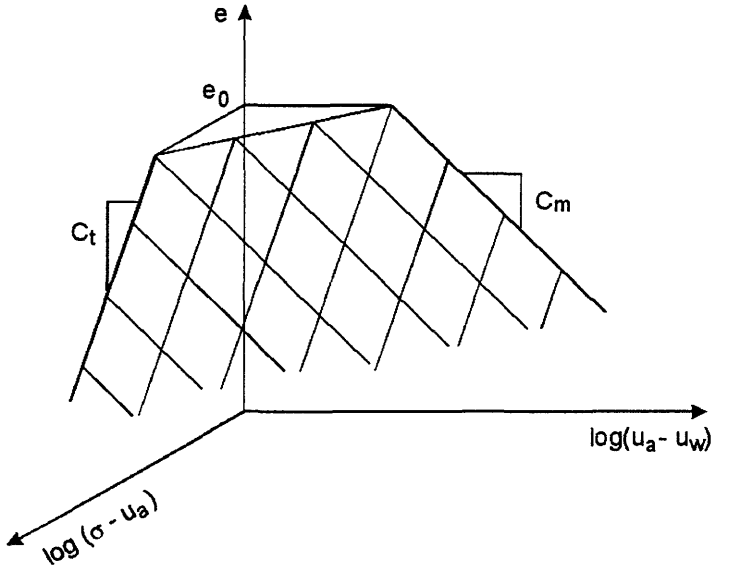

Figure 4.6 Schematic illustration of the void ratio surface proposed by Fredlund (1979)

Lloret and Alonso (1985) studied a number of mathematical equations (Table 4.1) for the description of the volume change constitutive surface of unsaturated soils subjected to confined or isotropic compression. The equations were used to best-fit experimental results on different soil types, and the optimum equations were selected on the basis of minimum fitting errors. The following conclusions were drawn for the void ratio and degree of saturation constitutive surfaces.

Table 4.1 Functions used for constitutive surface approximation (Lloret and Alonso, 1985)

Case	Function
1	$\begin{matrix} e \\ S_r \end{matrix} = a + b(\sigma - u_a) + c(u_a - u_w)$
2	$\begin{matrix} e \\ S_r \end{matrix} = a + b\log(\sigma - u_a) + c(u_a - u_w)$
3	$\begin{matrix} e \\ S_r \end{matrix} = a + b(\sigma - u_a) + c\log(u_a - u_w)$
4	$\begin{matrix} e \\ S_r \end{matrix} = a + b\log(\sigma - u_a) + c\log(u_a - u_w)$
5	$\begin{matrix} e \\ S_r \end{matrix} = a + b(\sigma - u_a) + c(u_a - u_w) + d(\sigma - u_a)(u_a - u_w)$
6	$\begin{matrix} e \\ S_r \end{matrix} = a + b\log(\sigma - u_a) + c(u_a - u_w) + d\log(\sigma - u_a)(u_a - u_w)$
7	$\begin{matrix} e \\ S_r \end{matrix} = a + b(\sigma - u_a) + c\log(u_a - u_w) + d(\sigma - u_a)\log(u_a - u_w)$
8	$\begin{matrix} e \\ S_r \end{matrix} = a + b\log(\sigma - u_a) + c\log(u_a - u_w) + d\log(\sigma - u_a)\log(u_a - u_w)$
9	$S_r = a - \left(\frac{e^{b(u_a - u_w)} - e^{-b(u_a - u_w)}}{e^{b(u_a - u_w)} + e^{-b(u_a - u_w)}} \right) \left(c + d(\sigma - u_a) \right)$
10	$S_r = a - \left\| 1 - \exp\left(-b(u_a - u_w) \right) \right\| c + d(\sigma - u_a) \|$

For a limited range in the total external stress, Lloret and Alonso (1985) suggested that a suitable analytical expression for the void ratio constitutive surface is:

$$e = a + b(\sigma - u_a) + c\log(u_a - u_w) + d(\sigma - u_a)\log(u_a - u_w) \tag{4.19}$$

If the range of significant stress variation is large, a more suitable equation for the void ratio surface is given by (Lloret and Alonso, 1985):

$$e = a + b\log(\sigma - u_a) + c\log(u_a - u_w) + d\log(\sigma - u_a)\log(u_a - u_w) \tag{4.20}$$

Either of the following two equations are suggested to describe the degree of saturation constitutive surface.

$$S = a - \left(\frac{e^{b(u_a-u_w)} - e^{-b(u_a-u_w)}}{e^{b(u_a-u_w)} + e^{-b(u_a-u_w)}}\right)(c + d(\sigma - u_a)) \tag{4.21}$$

$$S = a - \left(1 - e^{-b(u_a-u_w)}\right)(c + d(\sigma - u_a)) \tag{4.22}$$

where: *a, b, c,* and *d* are constants (i.e., fitting parameters).

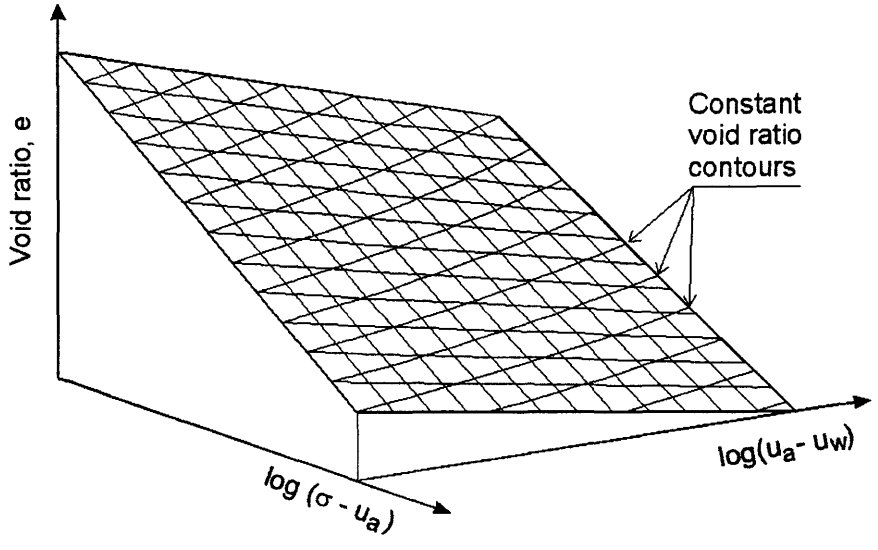

Figure 4.7 Schematic illustration of the void ratio surface proposed by Lloret and Alonso (1985)

The schematic illustrations of Eq. (4.20) and (4.21) are presented in Figs. 4.7 and 4.8, respectively. The constitutive curves on extreme planes are essentially linear on the semi-logarithmic scale (Ho and Fredlund, 1988). Figure 4.7 suggests that the void ratio surface on semi-logarithmic scale is curved; the surface appears to be a quarter section of the convex surface of a vertical cone. The degree of saturation surface on an arithmetic plot appears to be a continuous warping surface, with a linear curve on the net normal stress plane, and exponential curve on the matric suction plane.

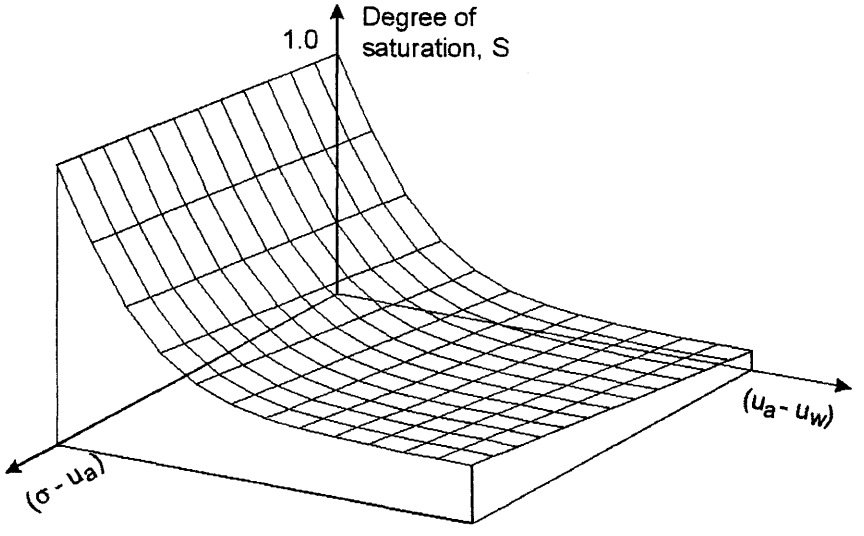

Figure 4.8 Schematic illustration of the degree of saturation surface proposed by Lloret and Alonso (1985)

Ho (1988) assumed a linear relation between net normal stress and matric suction at constant void ratio (i.e., the same assumption made in this study for the void ratio surface). The void ratio surface was approximated in semi-logarithmic plot by three planes, namely planes *I*, *II*, and *III*. The three planes converge at a void ratio ordinate corresponding to nominal values of the stress state variables (i.e., $\log(\sigma - u_a) = 0$ and $\log(u_a - u_w) = 0$). Plane *I* is perpendicular to the void ratio versus $\log(\sigma - u_a)$ plane. Plane *III* is perpendicular to the void ratio versus $\log(u_a - u_w)$ plane. Plane *II* represents a transition zone between planes *I* and *III*. Plane *II* intersects both the void ratio versus $\log(\sigma - u_a)$ plane and void ratio versus $\log(u_a - u_w)$ plane. The graphical

illustration of the approximated void ratio surface for swelling portion is presented in Fig. 4.9.

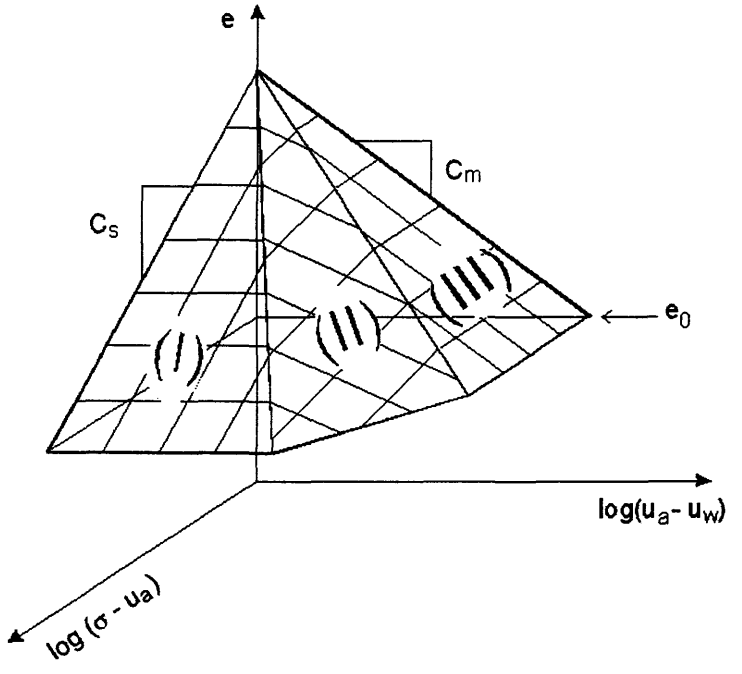

Figure 4.9 Void ratio surface proposed by Ho (1988) for unloading conditions

The equations describing planes *I*, *II*, and *III* can be written as follows:

$$e = \begin{cases} e_0 + C_s \log\left(\dfrac{(\sigma - u_a)_0}{(\sigma - u_a)}\right) & \text{for plane } I \\ e_0 + C_s' \log\left(\dfrac{(\sigma - u_a)_0}{(\sigma - u_a)}\right) + C_m' \log\left(\dfrac{(u_a - u_w)_0}{(u_a - u_w)}\right) & \text{for plane } II \\ e_0 + C_m \log\left(\dfrac{(u_a - u_w)_0}{(u_a - u_w)}\right) & \text{for plane } III \end{cases} \tag{4.23}$$

where:

e_0 = initial void ratio,

$(\sigma - u_a)_0$ = initial net normal stress,

$(u_a - u_w)_0$ = initial matric suction,

C_s = slope of the intersection line of plane *I* with the void ratio versus $log(\sigma\text{-}u_a)$ plane,

C_m = slope of the intersection line of plane *III* with the void ratio versus $log(u_a\text{-}u_w)$ plane,

$C_s^{'}$ = slope of the intersection line of plane *II* with the void ratio versus $log(\sigma\text{-}u_a)$ plane, and

$C_m^{'}$ = slope of the intersection line of plane *II* with the void ratio versus $log(u_a\text{-}u_w)$ plane.

Pereira (1996) used a five-parameter logistic function to fit the test results on a collapsing soil. The equation of void ratio versus matric suction was written as a five-parameter logistic function as follows:

$$e = e_u + \frac{e_f - e_u}{\left[1+\left(\frac{(u_a - u_w)}{c}\right)^b\right]^a} \tag{4.24}$$

where:

e_u = initial void ratio,

e_f = final void ratio,

a = the symmetry parameter which makes the logistic function asymmetric,

b = slope parameter, and

c = matric suction value at the inflection point.

Mathematical equations for void ratio should be developed for relationships between the parameters e_u, e_f, a, b, and c and net normal stress, $(\sigma - u_a)$.

M. Fredlund (2000) proposed a four-parameter equation that can be used to represent an overconsolidated soil that contains both a recompression curve and a virgin compression branch. The equation of void ratio as a function of stress was written as follow:

$$e = e_0 - \frac{C_r}{2}\ln\left[1+\left(\frac{\sigma}{P_s}\right)^2\right] - \frac{C_c - C_r}{2}\ln\left[1+\left(\frac{\sigma}{\sigma_p}\right)^2\right] \tag{4.25}$$

where:

e_0 = initial void ratio,

C_r = volume change index for the recompression curve,

C_c = volume change index for the virgin compression curve,

P_s = swelling pressure, and

σ_p = preconsolidation pressure.

Equation (4.25) has the following form for particular soil suction:

$$e = a + b\ln\left[1+\left(\frac{\sigma}{c}\right)^2\right] + d\ln\left[1+\left(\frac{\sigma}{f}\right)^2\right] \tag{4.26}$$

where: a, b, c, d, and f are constants (i.e., fitting parameters) at a constant suction.

M. Fredlund (2000) also suggested a three-parameter equation for the compression curve. It was noted that the shape of the compression curve is similar to the shape of the soil-water characteristic curve. The Fredlund and Xing (1994) equation for the soil-water characteristic curve was modified to provide mathematical representation for the compression curve. The original Fredlund and Xing (1994) equation for volumetric water content is written as follows:

$$\theta(\psi) = C(\psi)\frac{\theta_s}{\left\{\ln\left[\exp(1)+\left(\frac{\psi}{a}\right)^n\right]\right\}^m} \tag{4.27}$$

where:

θ_s = saturated volumetric water content,

a = fitting parameter closely related to the air entry value for the soil,

n = fitting parameter related to the maximum slope of the curve,

m = fitting parameter related to the curvature of the slope,

ψ_r = constant parameter used to adjust lower portion of curve, and

$C(\psi)$ = correcting function defined as

$$C(\psi) = \left[1 - \frac{\ln\left(1 + \frac{\psi}{\psi_r}\right)}{\ln\left(1 + \frac{10^6}{\psi_r}\right)}\right]$$

The Fredlund and Xing equation (1994) can be written for void ratio versus the applied total stress relationship with the correction function [i.e., $C(\psi)$] equal to 1.

$$e = \frac{e_0}{\left\{\ln\left[\exp(1) + \left(\frac{\sigma}{a}\right)^n\right]\right\}^m} \tag{4.28}$$

where:

e_0 = initial void ratio,

a = fitting parameter closely related to the preconsolidation pressure for the soil,

n = fitting parameter related to the maximum slope of the compression curve,

m = fitting parameter related to the shape of the curve.

Equation (4.28) takes the following form:

$$e = \frac{a}{\left\{\ln\left[\exp(1) + \left(\frac{\sigma}{b}\right)^c\right]\right\}^d} \tag{4.29}$$

where: a, b, c, and d are constants (i.e., fitting parameters) at a constant matric suction.

4.3.2 Low stress and zero suction problem

The low stress and zero suction problems occur when the elastic moduli are calculated from the swelling index, C_s, or other volume change indices. The problem is illustrated in Fig. 4.10. At extreme planes, the relationships between void ratio and the logarithm of net normal stress or matric suction are essentially linear (Fig. 4.10a). When the semi-log relationship is converted to an arithmetic plot (i.e., void ratio versus net normal stress or matric suction), void ratio tends to increase to infinity as the stress state variable approaches zero (Fig. 4.10b). Therefore, the calculated elastic modulus with respect to changes in net normal stress, E, becomes small (and approaches zero) at low net normal stresses [Fig. 4.10c and Eq. (2.29)]. The elastic modulus with respect to a change in matric suction, H, become small at low matric suction (or equal to zereo) when suction equals zero (Fig. 4.10.c and Eq. 2.30). These unrealistically small values of elastic moduli at low net normal stress and matric suction result in an unstable solution in numerical modelling. As well, the solutions produce unreasonably large deformations.

A part of this study is to find a procedure that can adequately describe the void ratio at low net normal stresses and matric suctions. The procedure should involve the use of a mathematical equation. This equation should be able to adequately describe the void ratio in the low net normal stress range and low matric suction range. In addition, this equation should be continuous, smooth, physically reasonable, and differentiable over the entire range of net normal stresses and matric suctions.

The equation can then be used to fit a set of measured data or data calculated from the swelling index or swelling indices. This approach is illustrated in Fig. 4.11. Figure 4.11 shows that unrealistically large values of void ratio at low net normal stresses and matric suctions need to be avoided.

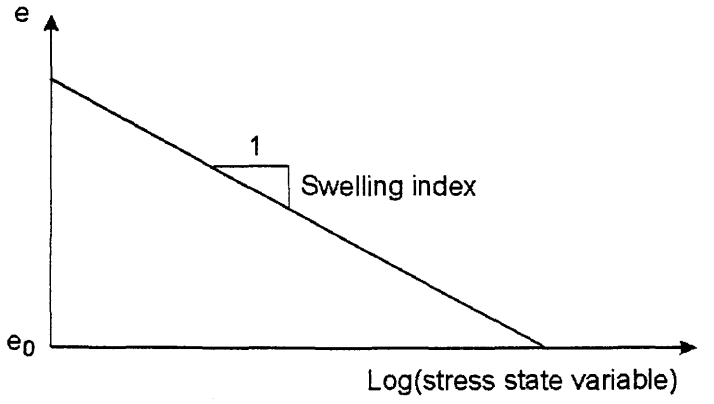

a) Semi-log plot of void ratio versus net normal stress or matric suction

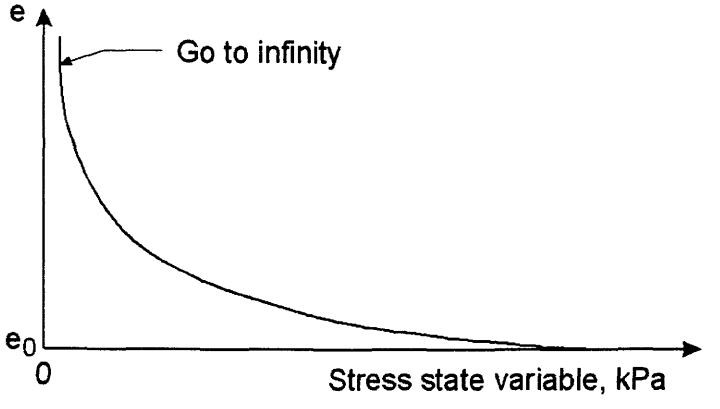

b) Converted arithmetic plot of void ratio versus net normal stress or matric suction

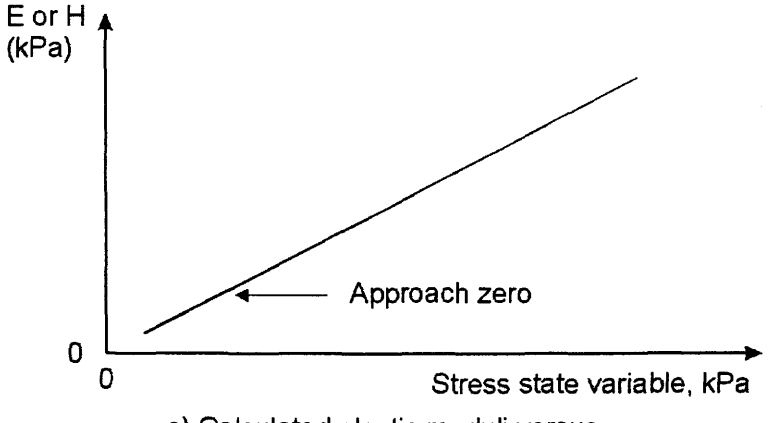

c) Calculated elastic moduli versus net normal stress or matric suction

Figure 4.10 Illustration of the problem associated with low net normal stress and zero suction

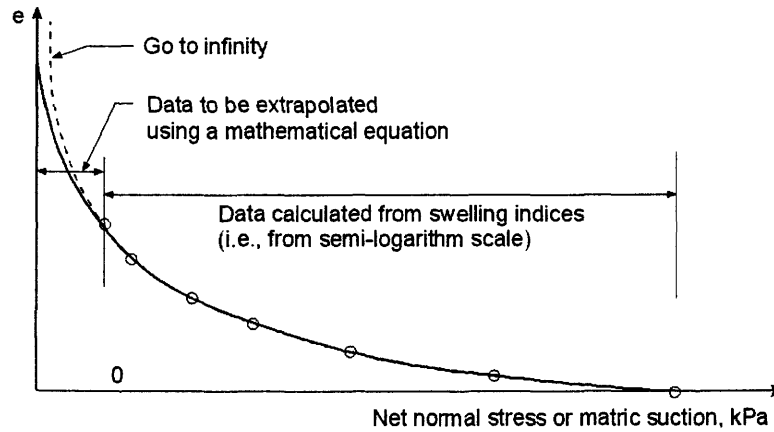

a) two-dimensional plot

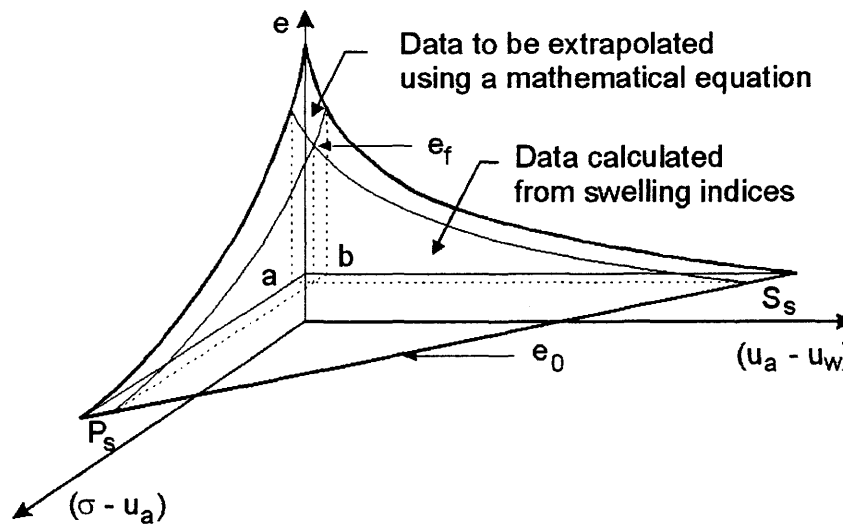

b) three-dimensional plot

Figure 4.11 Proposed procedure to solve the low net normal stress and suction problem

4.3.3 Proposed equation for void ratio constitutive relation

A mathematical equation is proposed to represent the void ratio constitutive surface. The equation is derived based on the method of heave prediction proposed by Fredlund et al. (1980) and the assumption of a linear relationship between net normal stress and matric suction on a constant void ratio plane.

The Fredlund et al. (1980) heave formulation was presented in Section 2.3.3. The method assumes a stress path that can be projected onto the net normal stress

plane (Fig. 4.12). The total heave stress path follows the rebound curve on the net normal stress plane from the initial stress state to the final stress state.

$$e_f = e_0 + C_s \log\left(\frac{P_f}{P_s}\right) \tag{4.30}$$

where:

P_f = final stress state, and

P_s = initial stress state (i.e., swelling pressure).

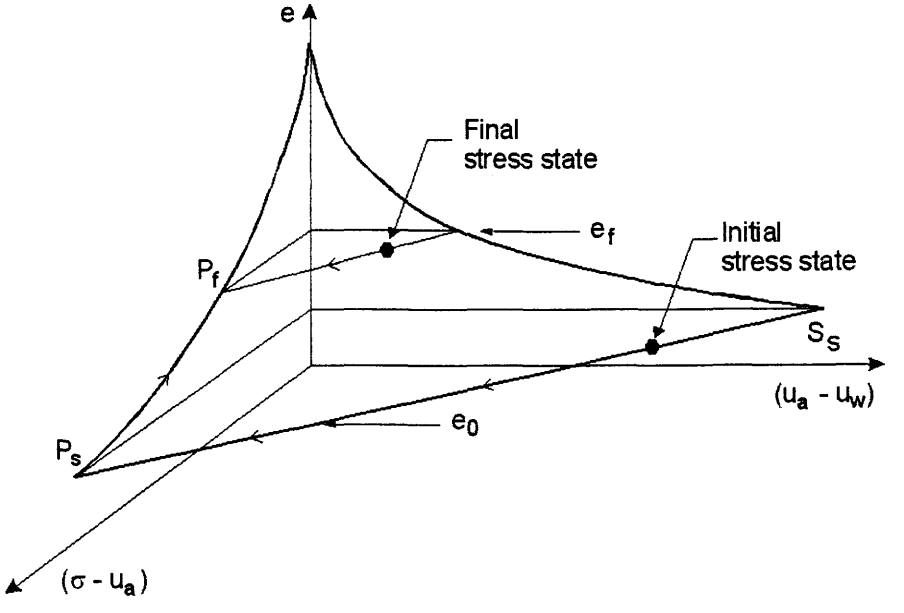

Figure 4.12 Stress paths followed in Fredlund et al. (1980) heave formulation during the wetting of a soil (modified from Fredlund et al., 1980)

The stress state in net normal stress plane, P_e, can be formulated as the sum of the net normal stress and the matric suction equivalent as follows (Fredlund et al., 1980):

$$P_e = (\sigma - u_a) + (u_a - u_w)_e \tag{4.31}$$

Lets ξ be the slope of the net normal stress versus matric suction line at constant void ratio. Equation (4.31) can then be visualised on Fig. 4.13 as follows:

$$P_e = (\sigma - u_a) + \xi(u_a - u_w) \tag{4.32}$$

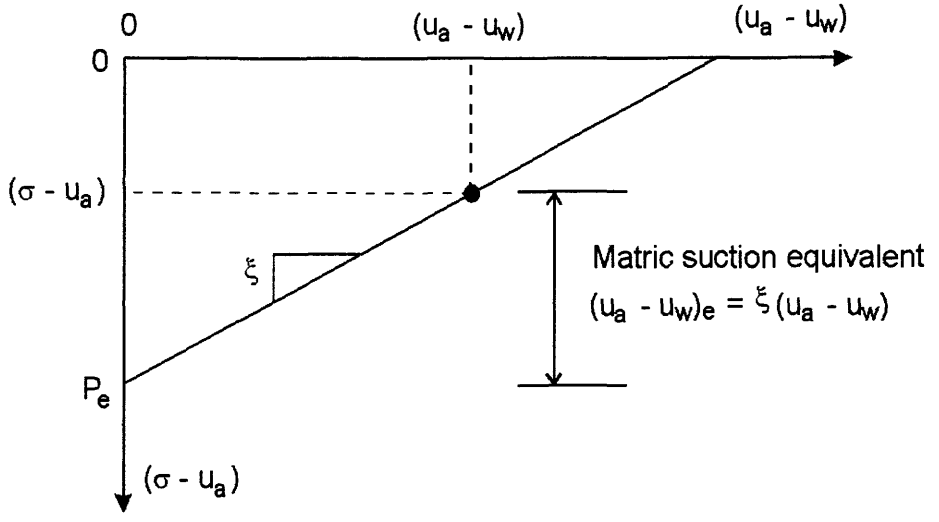

Figure 4.13 Illustration of the matric suction equivalent and determination of stress state, P_e

Substituting Eq. (4.32) into Eq. (4.30), the following equation can be written for any predetermined stress state:

$$e = e_0 + C_s \log\left(\frac{(\sigma - u_a) + \xi(u_a - u_w)}{P_s}\right) \tag{4.33}$$

Equation (4.33) can be rewritten as follows:

$$e = [e_0 - C_s \log(P_s)] + C_s \log[(\sigma - u_a) + \xi(u_a - u_w)] \tag{4.34}$$

Equation (4.34) suggests the following form for the void ratio function:

$$e = a + b \log[(\sigma - u_a) + c(u_a - u_w)] \tag{4.35}$$

where: a, b, and c are fitting parameters with $a > 0$; $b < 0$; and $c > 0$.

To allow the description of void ratio at zero net normal stress and matric suction [i.e., $(\sigma - u_a) = (u_a - u_w) = 0$], Eq. (4.35) can be modified as follows:

$$e = a + b\log[1 + (\sigma - u_a) + c(u_a - u_w)] \tag{4.36}$$

A number of functions of this type [i.e., having the form of Eqs. (4.30) and (4.36)] can be proposed to provide a better fit of void ratio constitutive surface. These functions are listed in Table 4.2. It can be noted that parameter *a* is the value of void ratio at zero net normal stress and matric suction. The parameters *c, d, f,* and *g* will take non-negative values to satisfy the logarithmic equation. A higher number of fitting parameters will increase the degree of approximation of the equation (i.e., better fit), but the physical interpretation of the parameters is rapidly lost (Lloret and Alonso, 1985). The proposed equations in Table 4.2 are evaluated to determine the optimal equation to be used for the swelling analysis in this study. The term *Unsat* is used to describe the functional relationship between void ratio (or water content) and the stress state.

Table 4.2 Proposed functions for void ratio surface approximation

ID	Function	Number of fitting parameters
Unsat-1	$e = a + b\log[1 + (\sigma - u_a) + c(u_a - u_w)]$	3
Unsat-2	$e = a + b\log[1 + c(\sigma - u_a) + (u_a - u_w)]$	3
Unsat-3	$e = a + b\log[1 + c(\sigma - u_a) + d(u_a - u_w)]$	4
Unsat-4	$e = a + b\log\left[\frac{1 + (\sigma - u_a) + c(u_a - u_w)}{1 + d(\sigma - u_a) + f(u_a - u_w)}\right]$	5
Unsat-5	$e = a + b\log\left[\frac{1 + c(\sigma - u_a) + (u_a - u_w)}{1 + d(\sigma - u_a) + f(u_a - u_w)}\right]$	5
Unsat-6	$e = a + b\log\left[\frac{1 + c(\sigma - u_a) + d(u_a - u_w)}{1 + f(\sigma - u_a) + g(u_a - u_w)}\right]$	6

4.3.4 Evaluation of equations for constitutive surfaces

A soil data for Regina clay (Shuai, 1996) was used to evaluate the proposed equations for void ratio surface. The experimental data are obtained under K_0-loading conditions. Two data sets can be presented for the void ratio constitutive surface. The first data set is generated from swelling indices of Regina clay by using the theory presented in Section 4.2. This data set is obtained under wetting, unloading test conditions. The second data set is the measured values, which are obtained under wetting, loading test conditions. More details of the test program and experimental data on Regina clay will be presented in Section 4.4.

The proposed equations for void ratio surface are also used to describe the water phase volume change of Regina clay.

Several software programs can be used for fitting of equations to data points. The programs used in this study are MathCAD, TableCurve, and SigmaPlot.

R^2 criterion and Akaike Information Criterion (AIC) are used to evaluate the mathematical equations. The AIC criterion takes into account the number of data points, the sum of the weighted squared residuals, and the number of fitting parameters. The value of R^2 closest to 1 and the lowest value of AIC indicate the best fit.

4.3.4.1 Void ratio data generated from swelling indices of Regina clay

A set of void ratio data can be generated from the swelling indices, initial void ratio, and swelling pressure for Regina clay using Eq. (4.13). The generated data are presented graphically in semi-logarithmic scale and arithmetic scale in Fig. 4.14. The following equations are considered: Fredlund (1979); Lloret and Alonso (1985); M. Fredlund (2000); and the equations suggested in this study (i.e., *Unsat* functions).

Table 4.3 Best-fit results of different void ratio equations to generated void ratio data of Regina clay

ID	Function	Fitting parameters	
Fredlund (1979)	$e = a + b\log(\sigma - u_a) + c\log(u_a - u_w)$	a = 1.071 b = -0.027	c = -0.024
Lloret & Alonso (1985)	$e = a + b\log(\sigma - u_a) + c\log(u_a - u_w) + d\log(\sigma - u_a)\log(u_a - u_w)$	a = 1.186 b = -0.091	c = -0.083 d = 0.034
M. Fredlund (2000)	$e = a + b\ln\left[1 + \left(\frac{\sigma}{c}\right)^2\right] + d\ln\left[1 + \left(\frac{\sigma}{f}\right)^2\right]$ where $a = a_1 + a_2(u_a - u_w)$ $b = b_1 + b_2\ln(u_a - u_w)$ $d = d_1 + d_2\ln(u_a - u_w)$	a1 = 1.205 a2 = -5.2E-5 b1 = -0.724 b2 = 0.292	c = 0.011 d1 = 0.705 d2 = -0.287 f = 0.010
Unsat-1	$e = a + b\log[1 + (\sigma - u_a) + c(u_a - u_w)]$	a = 1.186 b = -0.092	c = 0.610
Unsat-2	$e = a + b\log[1 + c(\sigma - u_a) + (u_a - u_w)]$	a = 1.203 b = -0.091	c = 1.666
Unsat-3	$e = a + b\log[1 + c(\sigma - u_a) + d(u_a - u_w)]$	a = 1.352 b = -0.089	c = 94.500 d = 56.617
Unsat-4	$e = a + b\log\left[\frac{1 + (\sigma - u_a) + c(u_a - u_w)}{1 + d(\sigma - u_a) + f(u_a - u_w)}\right]$	a = 1.205 b = -0.105 c = 0.711	d = 0.001 f = 0.001
Unsat-5	$e = a + b\log\left[\frac{1 + c(\sigma - u_a) + (u_a - u_w)}{1 + d(\sigma - u_a) + f(u_a - u_w)}\right]$	a = 1.217 b = -0.102 c = 1.466	d = 0.001 f = 0.001
Unsat-6	$e = a + b\log\left[\frac{1 + c(\sigma - u_a) + d(u_a - u_w)}{1 + f(\sigma - u_a) + g(u_a - u_w)}\right]$	a = 1.350 b = -0.095 c = 49.722	d = 34.571 f = 4.38e-4 g = 8.22e-4

The best-fit results of different void ratio equations to the generated void ratio data (Fig. 4.14) are presented in Table 4.3. It can be noted that M. Fredlund (2000) equation is modified to allow best-fit in three-dimensions.

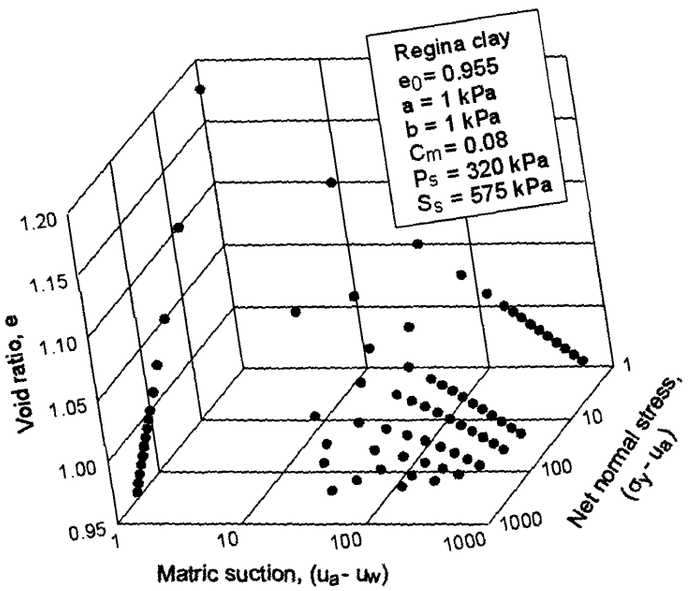

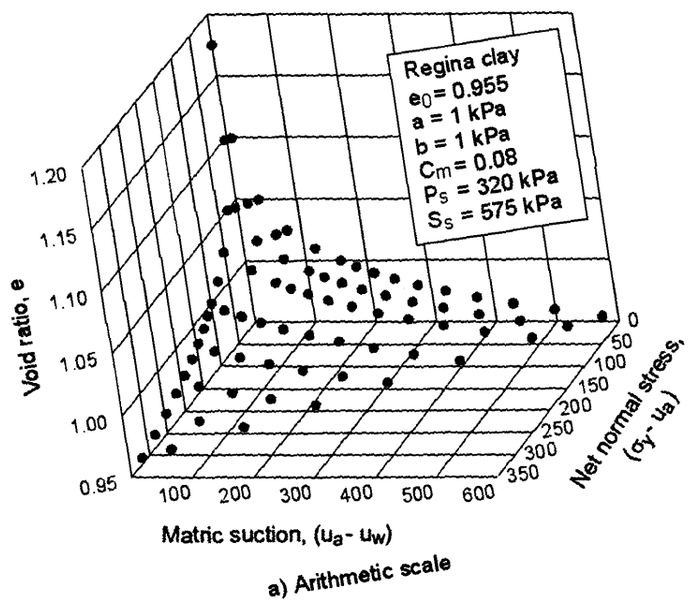

Figure 4.14 Generated data of void ratio surface for Regina clay

The correlation between the void ratio data and the predicted void ratio using Fredlund (1979) equation is presented in Fig. 4.15. The fitting results using Lloret and Alonso (1985) are shown in Figs. 4.16 and 4.17. Figure 4.18 presents correlation between the void ratio data and the predicted void ratio using M. Fredlund (2000) equation. The fitting results using *Unsat-1* function, the simplest form of its type, are shown in Figs. 4.19 and 4.20. The fitting results using *Unsat-6* function, the most general form of its type, are shown in Figs. 4.21 and 4.22.

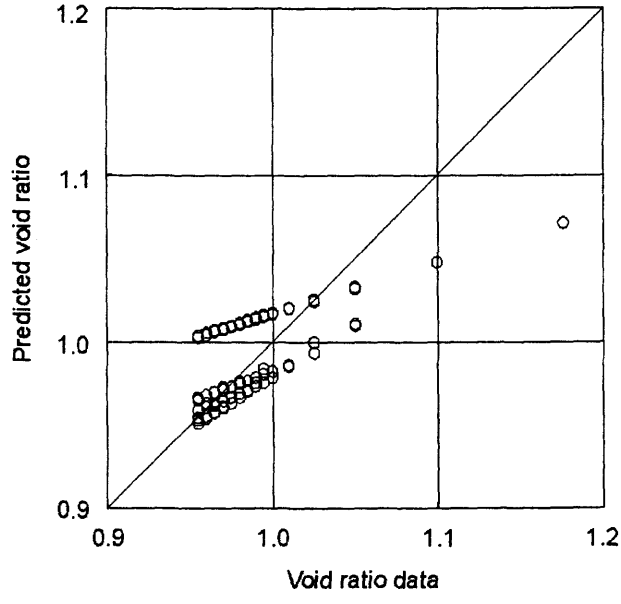

Figure 4.15 Correlation between void ratio data and predicted void ratio using Fredlund (1979) function for generated void ratio data of Regina clay

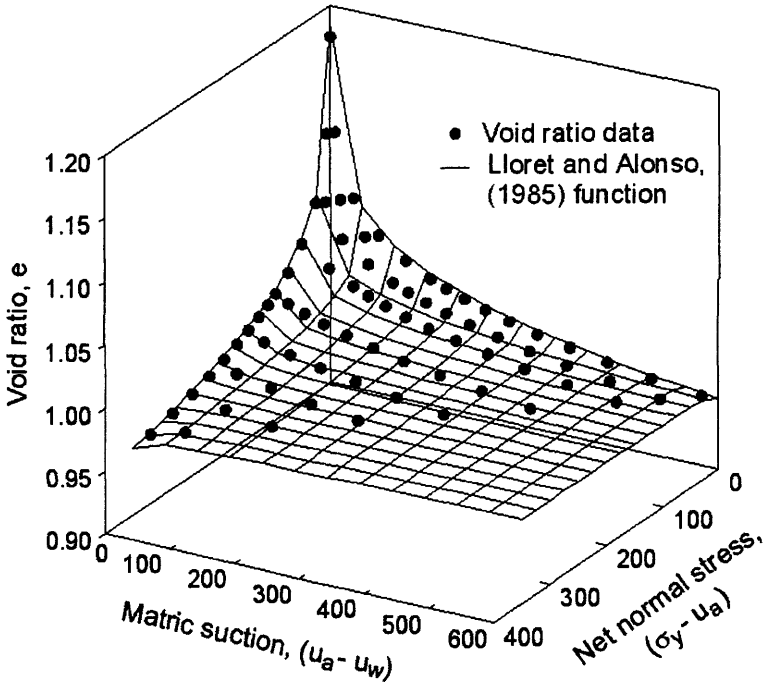

Figure 4.16 Best-fit void ratio surface using Lloret & Alonso (1985) function for generated void ratio data of Regina clay

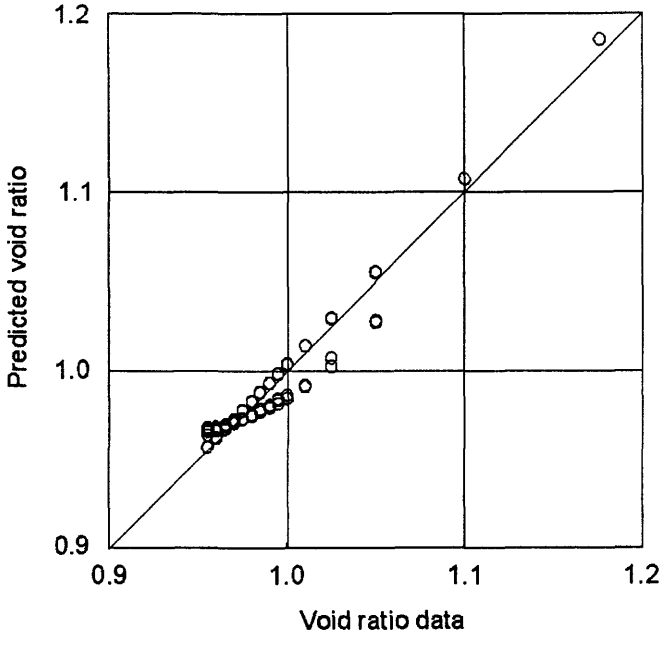

Figure 4.17 Correlation between void ratio data and predicted void ratio using Lloret & Alonso (1985) function for generated void ratio data of Regina clay

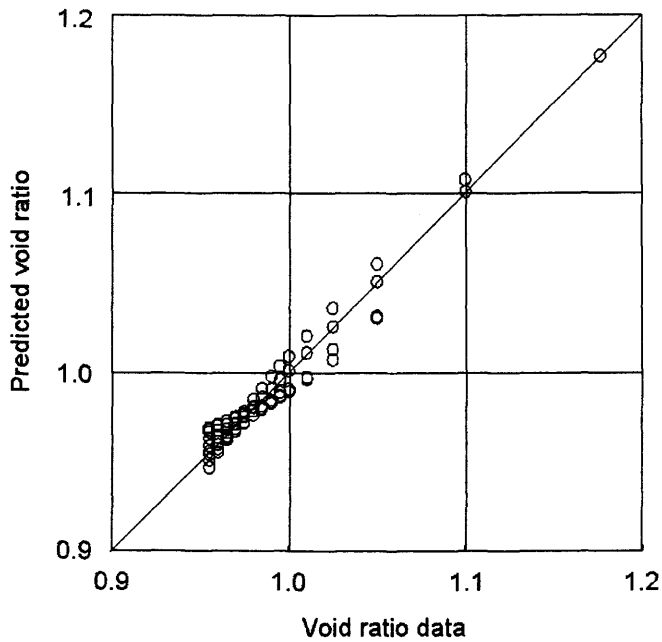

Figure 4.18 Correlation between void ratio data and predicted void ratio using M. Fredlund (2000) function for generated void ratio data of Regina clay

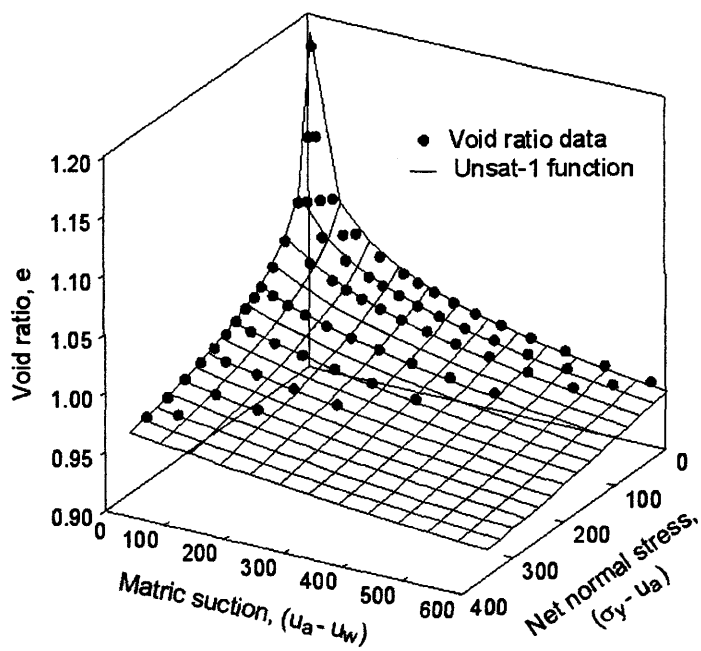

Figure 4.19 Best-fit void ratio surface using proposed Unsat-1 function for generated void ratio data of Regina clay

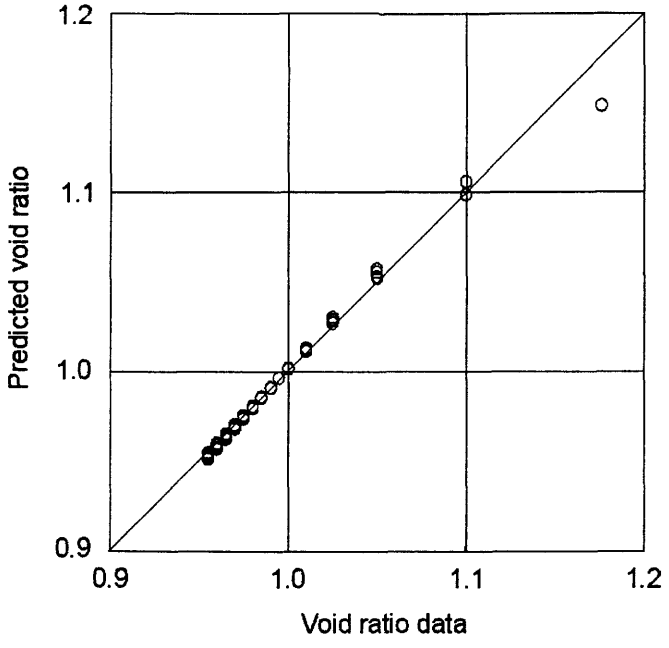

Figure 4.20 Correlation between void ratio data and predicted void ratio using proposed Unsat-1 function for generated void ratio data of Regina clay

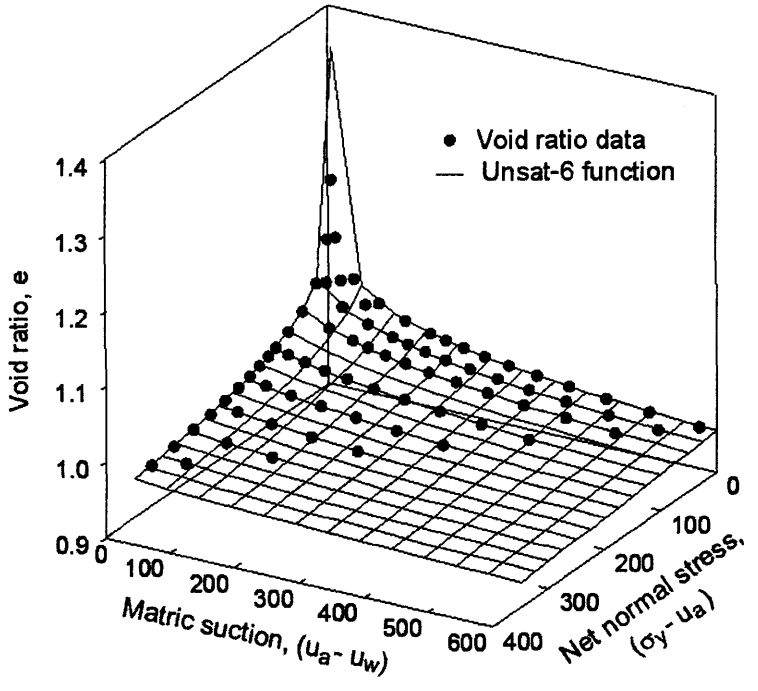

Figure 4.21 Best-fit void ratio surface using proposed Unsat-6 function for generated void ratio data of Regina clay

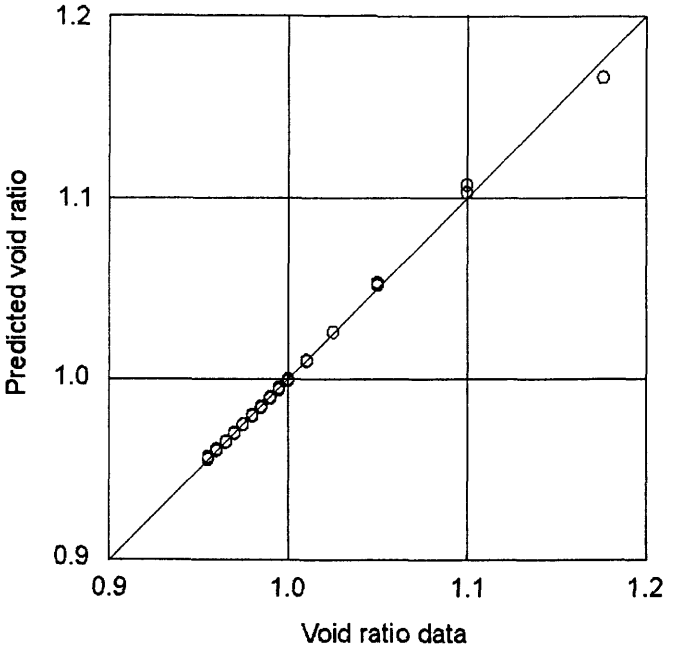

Figure 4.22 Correlation between void ratio data and predicted void ratio using proposed *Unsat-6* function for generated void ratio data of Regina clay

Statistical results of the proposed void ratio equations are presented in Table 4.4. Figure 4.23 presents comparison of different equations using the AIC criterion. The comparison using R^2 criterion is presented in Fig. 4.24. It can be seen that the *Unsat-6* function appears to provide a best fit to this set of data.

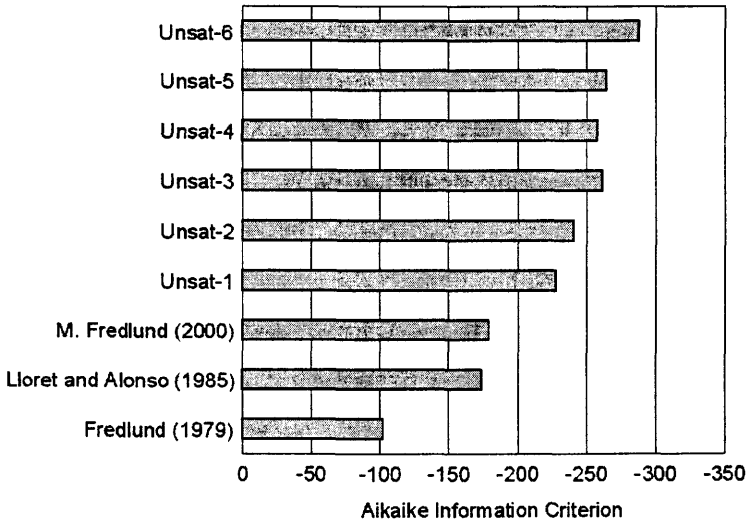

Figure 4.23 Aikaike Information Criterion for generated data of void ratio surface

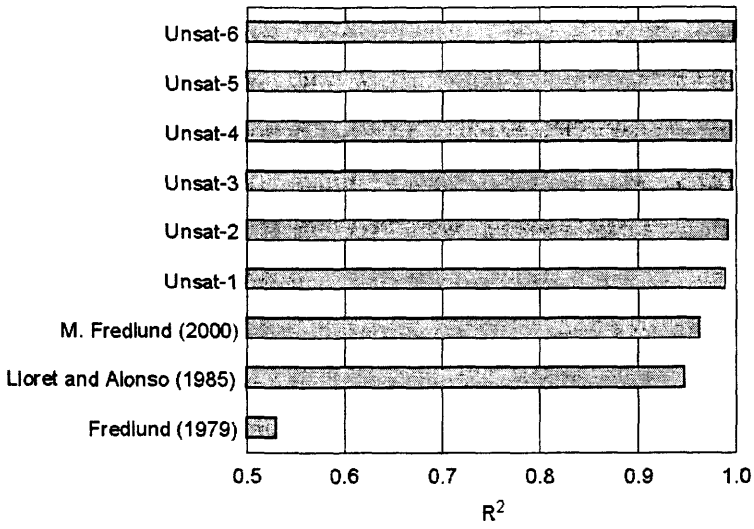

Figure 4.24 R^2 criterion for generated data of void ratio surface

Table 4.4 Statistical results of different void ratio equations for generated void ratio data of Regina clay

ID	Number of fitting parameters	R^2	AIC*
Fredlund (1979)	3	0.5299	-102
Lloret & Alonso (1985)	4	0.9469	-174
M. Fredlund (2000)	8	0.9622	-179
Unsat-1	3	0.9890	-228
Unsat-2	3	0.9916	-241
Unsat-3	4	0.9955	-262
Unsat-4	4	0.9949	-258
Unsat-5	4	0.9958	-265
Unsat-6	6	0.9979	-288

* Akaike Information Criterion

Figure 4.25 presents a semi-logarithmic plot of void ratio surface described by *Unsat-6* function. The shapes of void ratio versus logarithm of matric suction at constant net normal stress, and void ratio versus logarithm of net normal at constant stress matric suction can be visualised. The curves of net normal stress versus matric suction at constant void ratio in the logarithmic scale are also presented.

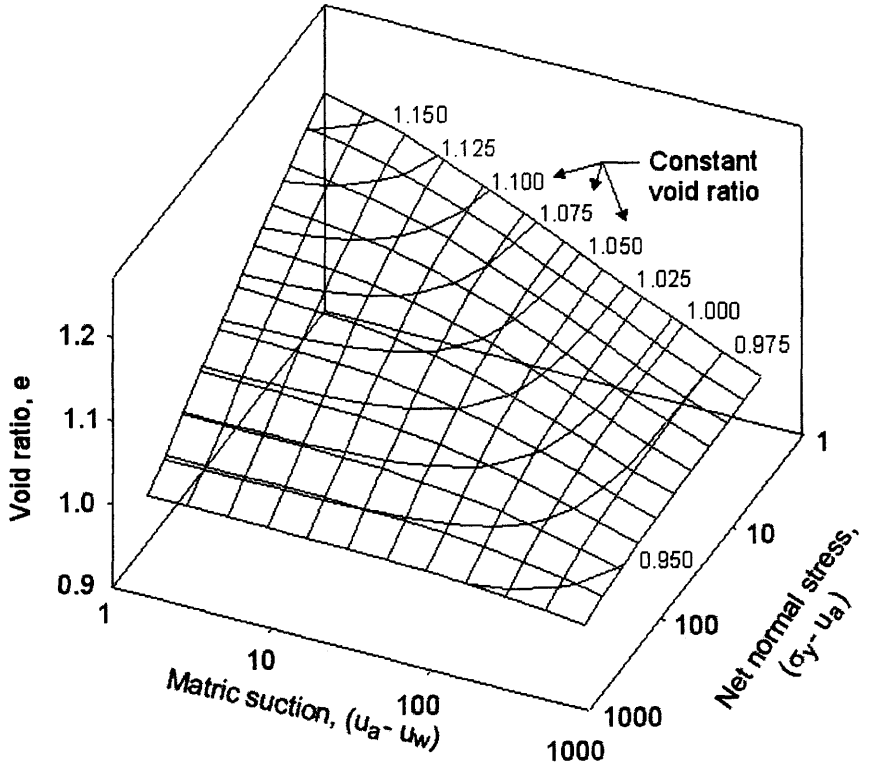

Figure 4.25 Illustration of generated void ratio surface
using *Unsat-6* function for Regina clay

4.3.4.2 Measured void ratio data of Regina clay

The measured data of void ratio constitutive surface obtained from Shuai (1996) are presented graphically on semi-logarithmic scale and an arithmetic scale in Figs. 4.26a and 4.26b, respectively. The data contain both the recompression portion and the virgin compression portion of the void ratio surface with respect to net normal stress.

The following functions are considered for analysis: Lloret and Alonso (1985); Fredlund and Xing (1994), Pereira and Fredlund (1996), M. Fredlund (2000) functions, and the *Unsat-6* function. Functions that originally presented the equations as functions of only one stress state variable have been extended to describe the function with respect to the second stress state variable.

Fitting results for different void ratio equations, for measured data on Regina clay are presented in Table 4.5.

Table 4.5 Fitting parameter results of different void ratio equations for measured void ratio data of Regina clay

ID	Function	Fitting parameters
Lloret & Alonso (1985)	$e = a + b\log(\sigma - u_a) + c\log(u_a - u_w) + d\log(\sigma - u_a)\log(u_a - u_w)$	a = 1.256 c = -0.109 b = -0.099 d = 0.036
Fredlund & Xing (1994)	$e = \frac{a}{\left\{\ln\left[\exp(1) + \left(\frac{\sigma}{b}\right)^c\right]\right\}^d}$ where: $a = a_1\ln[1 + (u_a - u_w)] + a_2$ $b = b_1[\exp(1)]^{b_2(u_a - u_w)}$ $c = \frac{c_1}{\left\{\ln\left[\exp(1) + \left(\frac{\sigma}{c_2}\right)^{c_3}\right]\right\}^{c_4}}$ $d = d_1(u_a - u_w)^2 + d_2(u_a - u_w) + d_3$	a_1 = -0.035 a_2 = 1.184 b_1 = 70.887 b_2 = 0.059 c_1 = 1.308 c_2 = 104.203 c_3 = 2.831 c_4 = 0.945 d_1 = 2.63E-3 d_2 = -0.113 d_3 = 0.277
Pereira & Fredlund (1996)	$e = e_u + \frac{e_f - e_u}{\left[1 + \left(\frac{(u_a - u_w)}{c}\right)^b\right]}$ where: $e_u = a_1 + a_2\ln(1+\sigma)$ $e_f = f_1 + f_2/(1+(\sigma/f_3)^{f_4})$ $b = b_1\sigma + b_2$ $c = c_1\sigma^2 + c_2\sigma + c_3$	a_1 = 0.901 b_1 = 4.94E-3 a_2 = 1.94E-3 b_2 = 0.727 f_1 = 1.180 c_1 = 1.36E-5 f_2 = -0.364 c_2 = 0.746 f_3 = 214.173 c_3 = 64.264 f_4 = -1.121
M. Fredlund (2000)	$e = a + b\ln\left[1 + \left(\frac{\sigma}{c}\right)^2\right] + d\ln\left[1 + \left(\frac{\sigma}{f}\right)^2\right]$ where: $a = a_1 + a_2(u_a - u_w)$ $b = b_1(u_a - u_w)^2 + b_2(u_a - u_w) + b_3$ $c = c_1(u_a - u_w)^3 + c_2(u_a - u_w)^2 + c_3(u_a - u_w) + c_4$ $d = d_1(u_a - u_w)^2 + d_2(u_a - u_w) + d_3$	a_1 = 1.176 c_1 = -4.24E-5 a_2 = -0.028 c_2 = 0.032 b_1 = -1.75E-5 c_3 = 0.540 b_2 = 1.17E-3 c_4 = 42.310 b_3 = -0.056 d_1 = 1.06E-8 d_2 = -7.47E-6 d_3 = -6.93E-5 f = -1.08E-8
Unsat-6	$e = a + b\log\left[\frac{1 + c(\sigma - u_a) + d(u_a - u_w)}{1 + f(\sigma - u_a) + g(u_a - u_w)}\right]$	a = 1.183 d = 0.045 b = -0.283 f = 0 c = 0.015 g = 5.34E-3

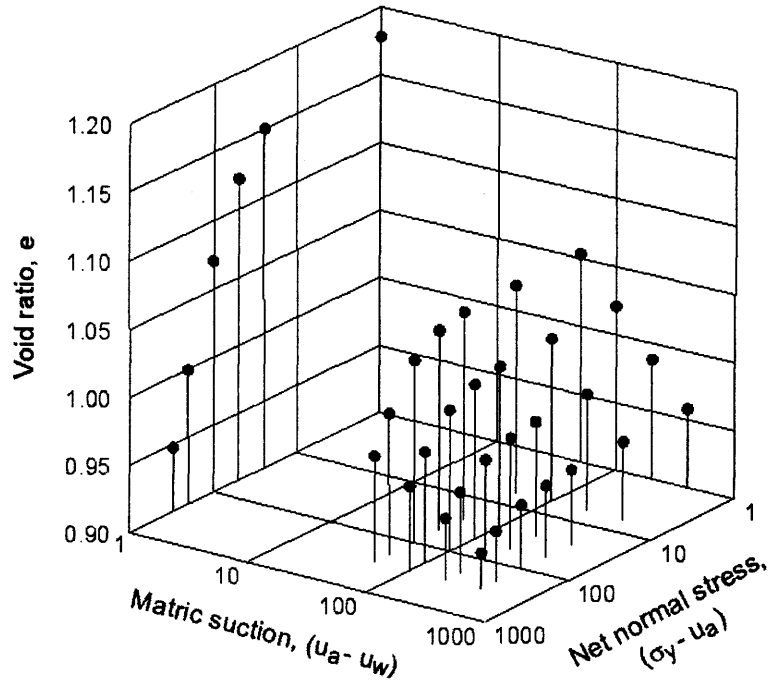

a) Semi-logarithmic scale

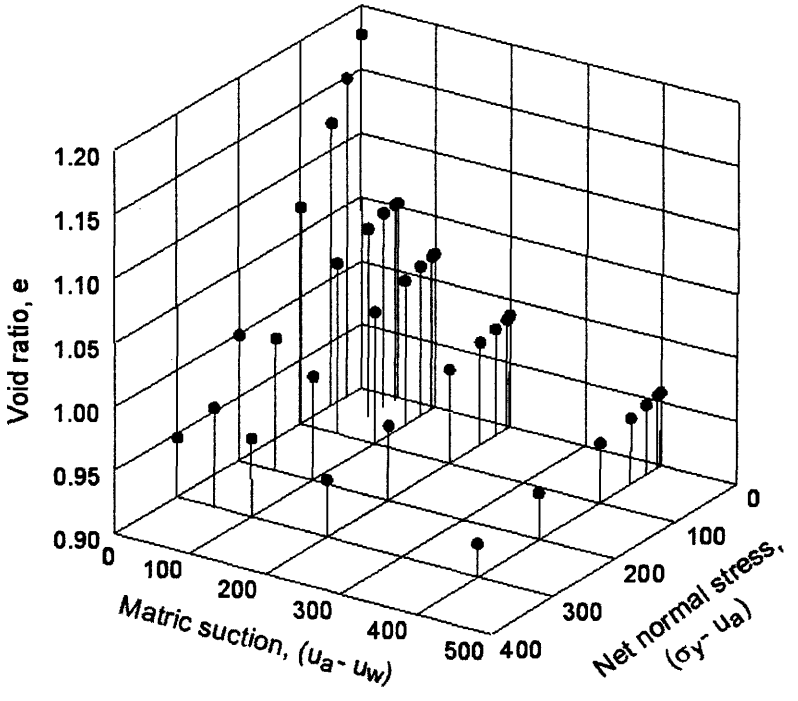

b) Arithmetic scale

Figure 4.26 Measured data of void ratio surface for Regina clay (from Shuai, 1996)

The best-fit results using the Lloret and Alonso (1985) function are presented in Figs. 4.27, 4.28, 4.29, and 4.30. The Lloret and Alonso (1985) function, with four fitting parameters, can not describe this set of experimental data adequately, especially at low range of matric suction and net normal stress.

The best-fit results using the Fredlund and Xing (1994) function are presented in Figs. 4.31, 4.32, 4.33, and 4.34. The Fredlund and Xing (1994) equation, with eleven fitting parameters, seems to be flexible, but it may need more experimental data points for the fitting. The void ratio constitutive surface described by this equation includes an unusual rise and drop of void ratio at about 10 kPa matric suction.

The best-fit results using the Pereira and Fredlund (1996) function are presented in Figs. 4.35, 4.36, 4.37, and 4.38. The Pereira and Fredlund (1996) function, with eleven fitting parameters, appears to describe this set of experimental data adequately.

The best-fit results using the M. Fredlund (2000) function are presented in Figs. 4.39, 4.40, 4.41, and 4.42. The M. Fredlund (2000) function, with thirteen fitting parameters, fits well to the experimental data, however, it does not describe the void ratio correctly at low suction range (i.e., under 50 kPa). More data points at low suction range may be needed for the use of this equation.

The best-fit results using the *Unsat-6* function are presented in Figs. 4.43, 4.44, 4.45, and 4.46. The *Unsat-6* function, with six fitting parameters, appears to perform well on this set of experimental data.

Statistical results on the proposed void ratio equations for measured data on Regina clay are presented in Table 4.6. Figure 4.47 presents comparison of different equations using the AIC criterion. The comparison using the R^2 criterion is presented in Fig. 4.48. The statistical results suggest that the Fredlund and Xing (1996) equation and the M. Fredlund (2000) equation provide best fit to the experimental data. However, by examining the entire constitutive surface described by these equations, it is noted that these equations can not be used in this study. It is suggested that the mathematical equation be evaluated not only by the statistical results of the fitting, but also by observation on the entire range of stress state. Both Pereira and Fredlund (1996) function and *Unsat-6* function could be used to describe the void ratio experimental data on Regina clay.

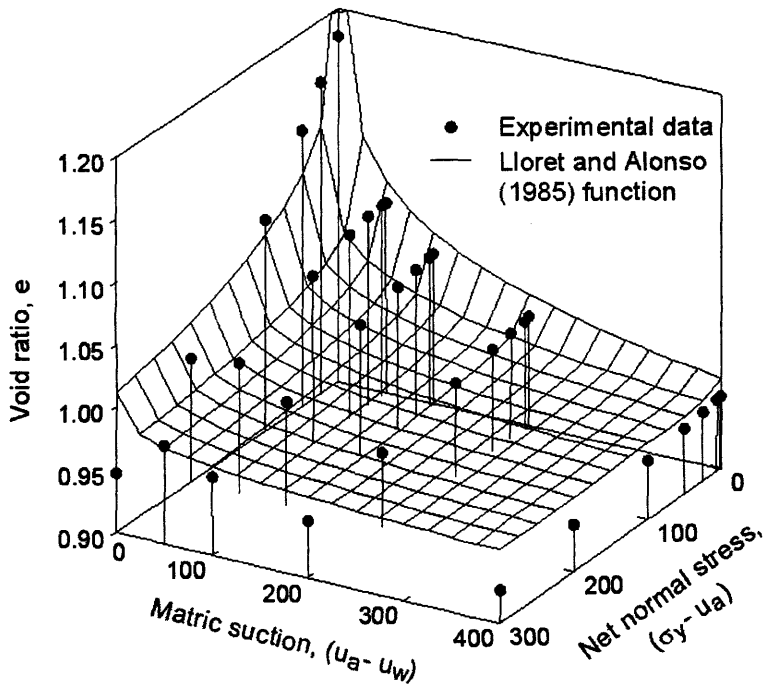

Figure 4.27 Best-fit void ratio surface using Lloret and Alonso (1985) function for measured void ratio data of Regina clay

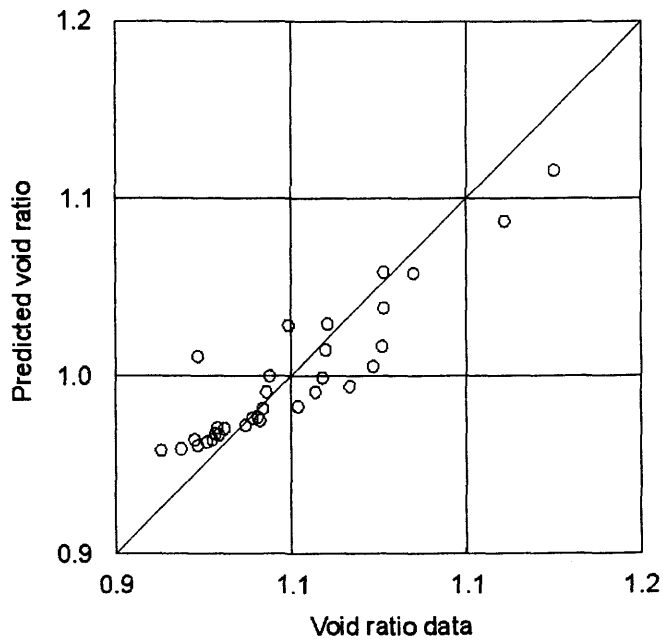

Figure 4.28 Correlation between measured and predicted void ratio using Lloret and Alonso (1985) function for Regina clay

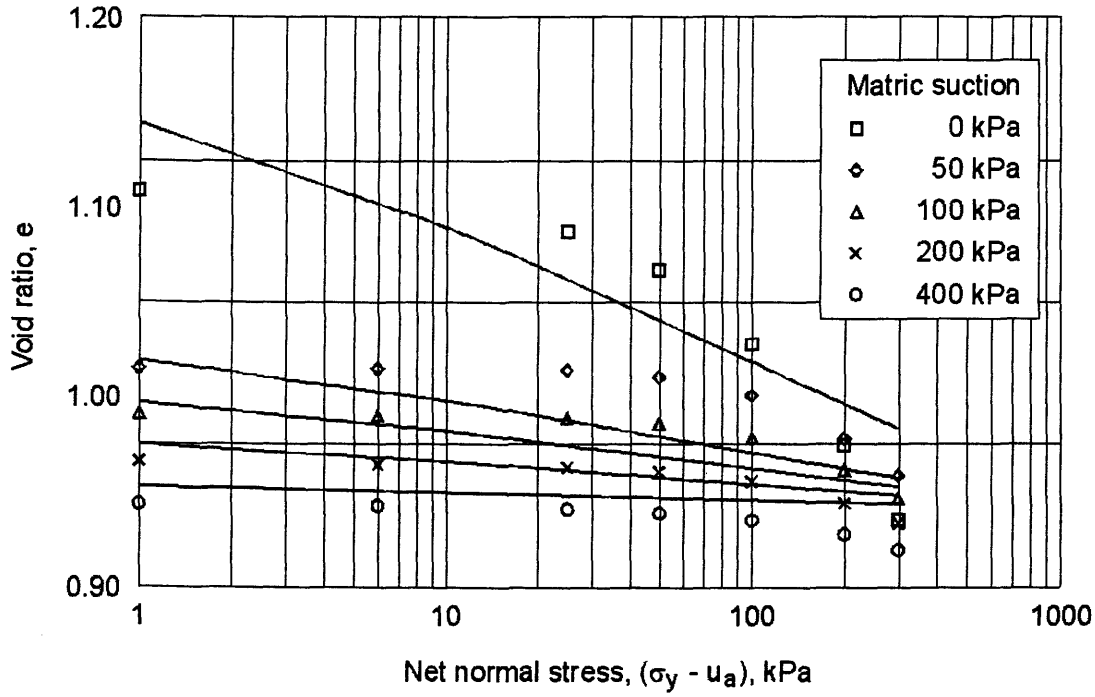

Figure 4.29 Void ratio versus net normal stress at various matric suctions using Lloret and Alonso (1985) function for Regina clay

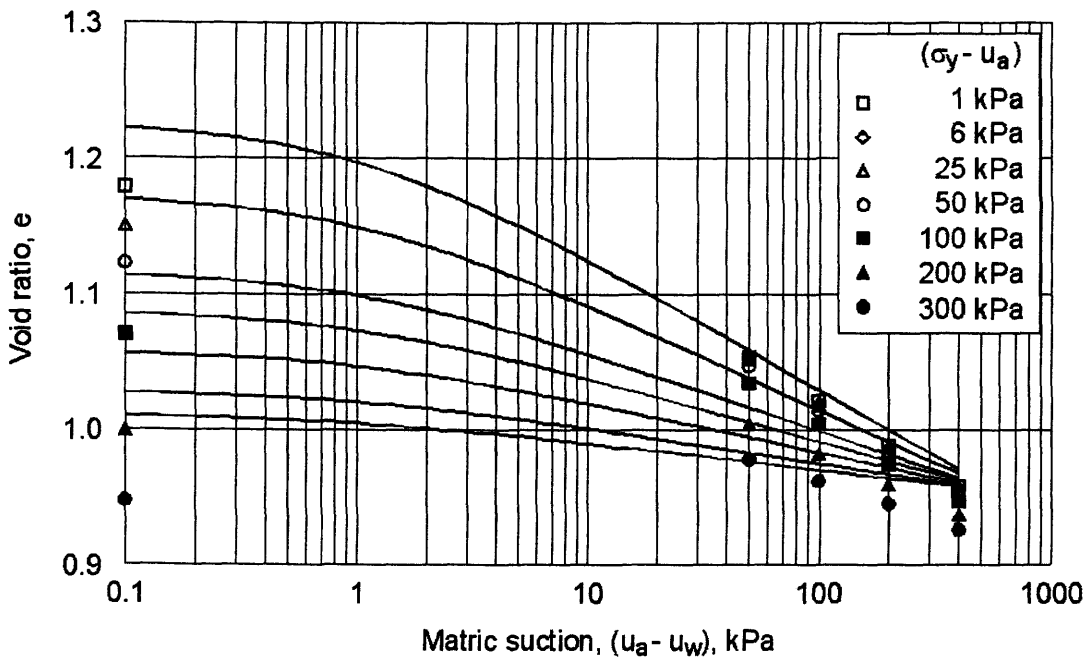

Figure 4.30 Void ratio versus matric suction at various net normal stresses using Lloret and Alonso (1985) function for Regina clay

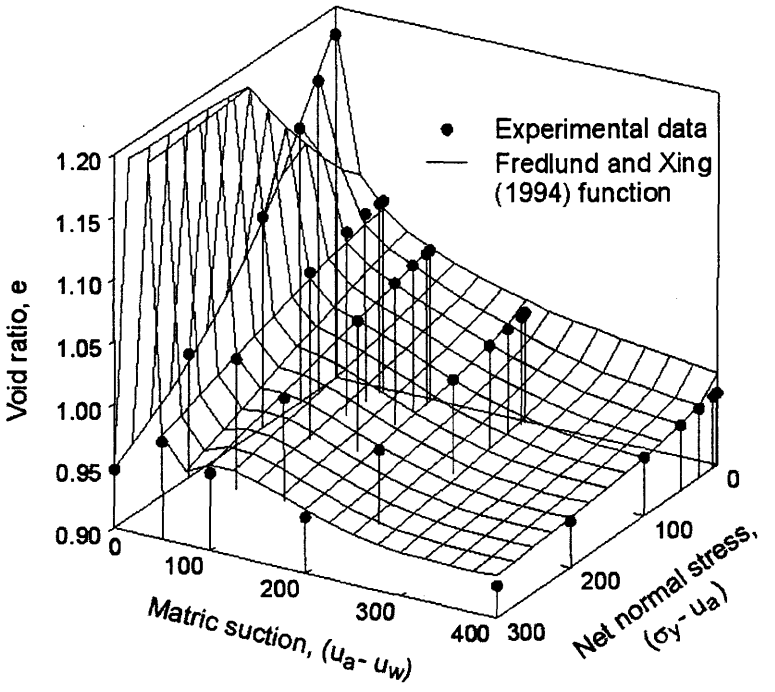

Figure 4.31 Best-fit void ratio surface using Fredlund and Xing (1994) function for measured void ratio data of Regina clay

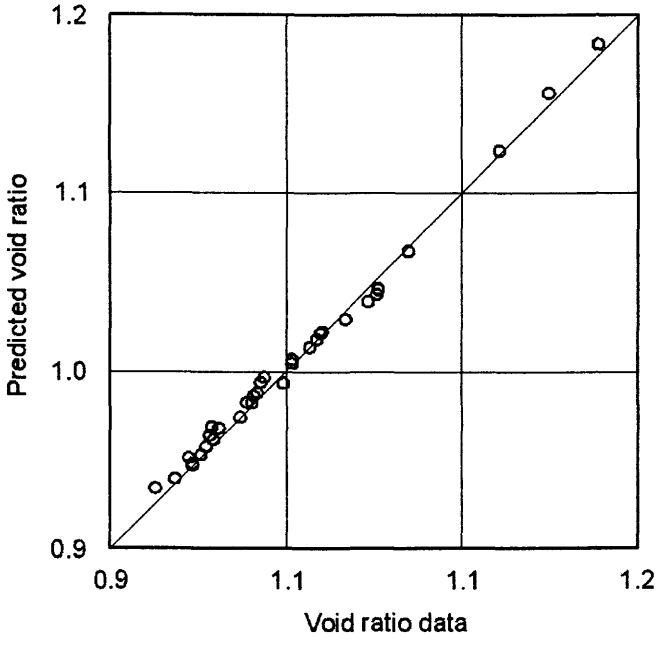

Figure 4.32 Correlation between measured and predicted void ratio using Fredlund and Xing (1994) function for Regina clay

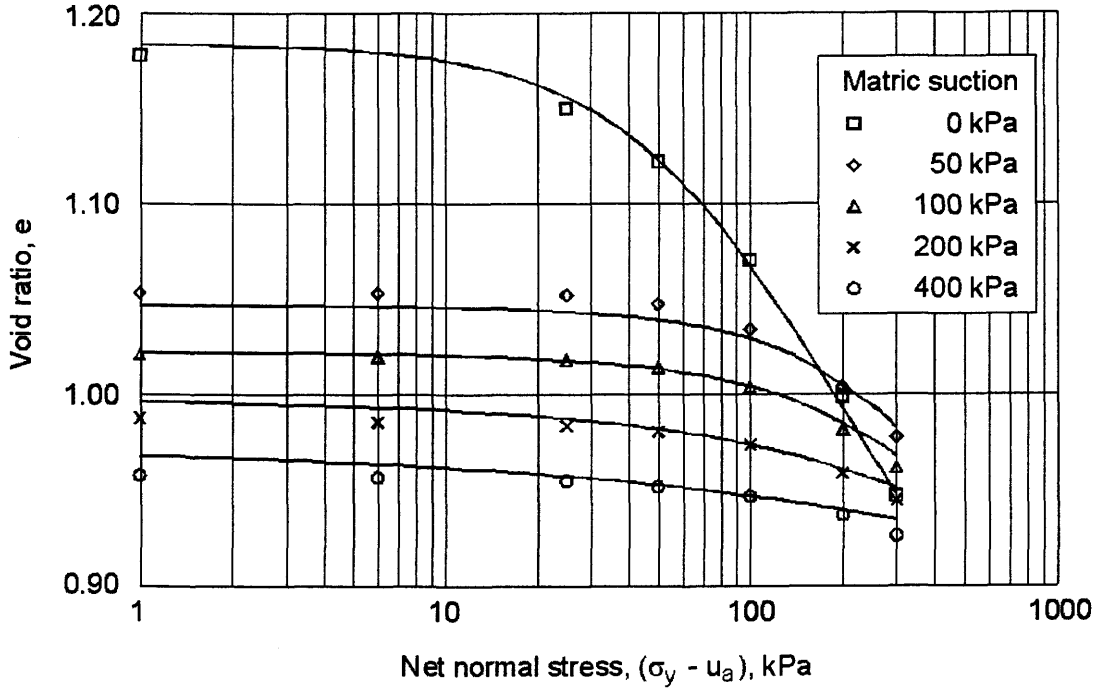

Figure 4.33 Void ratio versus net normal stress at various matric suctions using Fredlund and Xing (1994) function for Regina clay

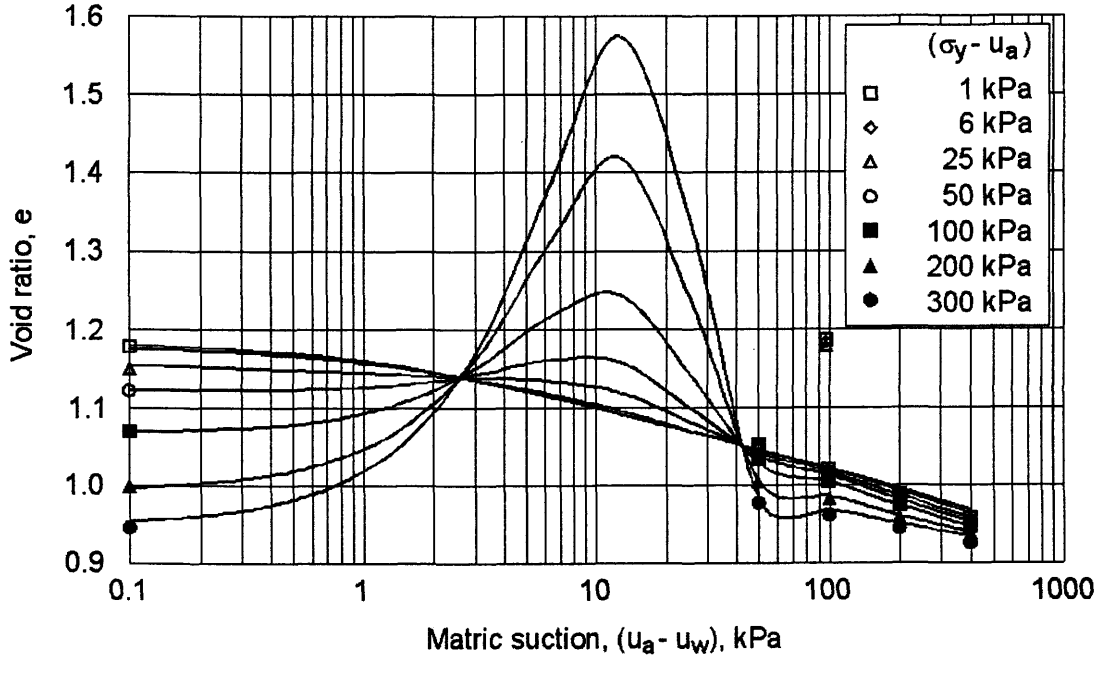

Figure 4.34 Void ratio versus matric suction at various net normal stresses using Fredlund and Xing (1994) function for Regina clay

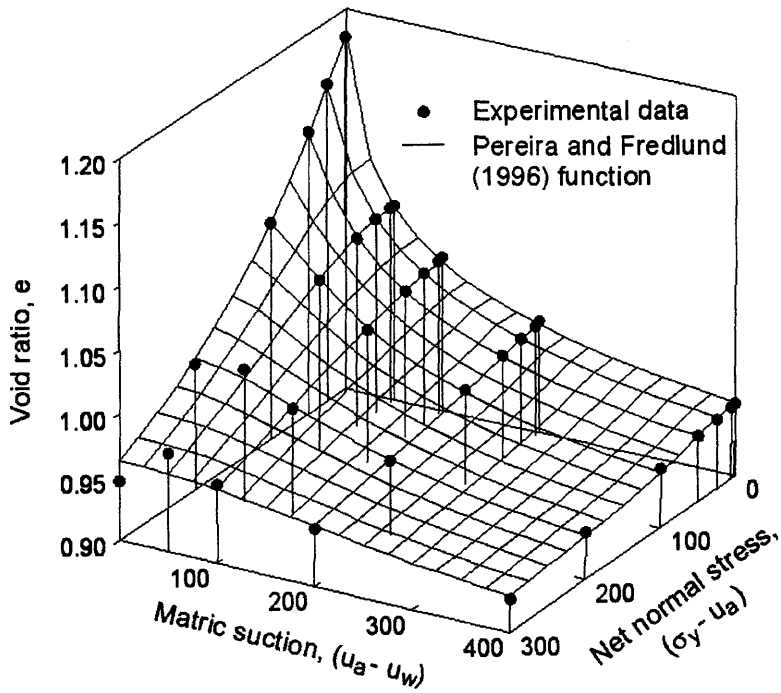

Figure 4.35 Best-fit void ratio surface using Pereira and Fredlund (1996) function for measured void ratio data of Regina clay

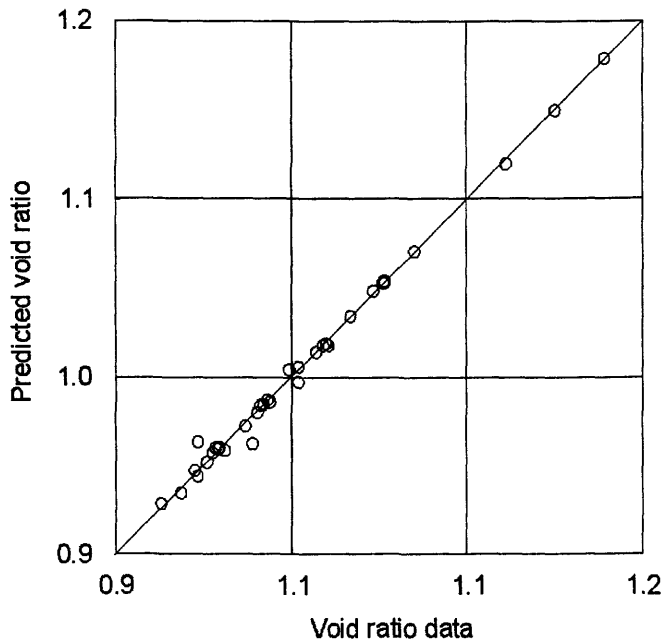

Figure 4.36 Correlation between measured and predicted void ratio using Pereira and Fredlund (1996) function for Regina clay

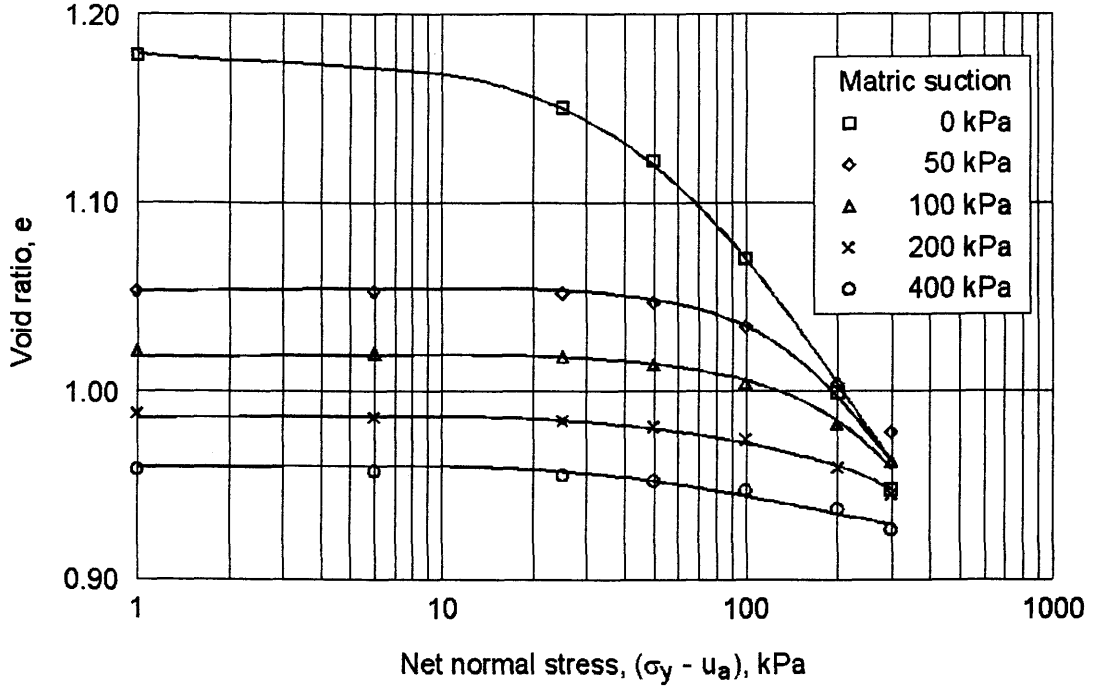

Figure 4.37 Void ratio versus net normal stress at various matric suctions using Pereira and Fredlund (1996) function for Regina clay

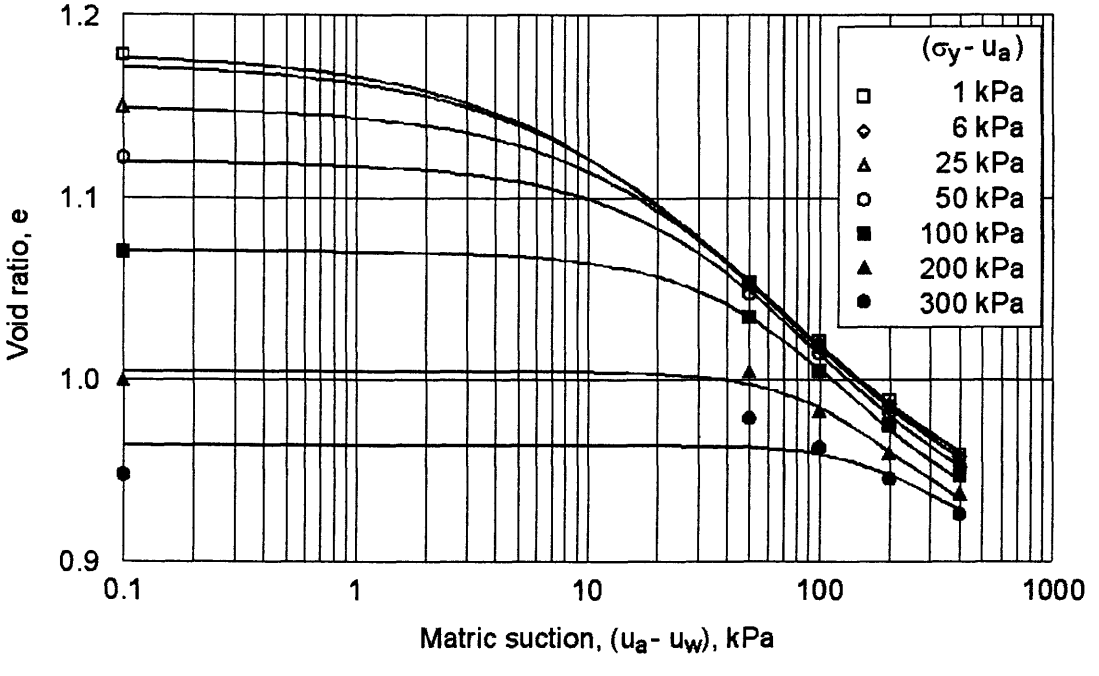

Figure 4.38 Void ratio versus matric suction at various net normal stresses using Pereira and Fredlund (1996) function for Regina clay

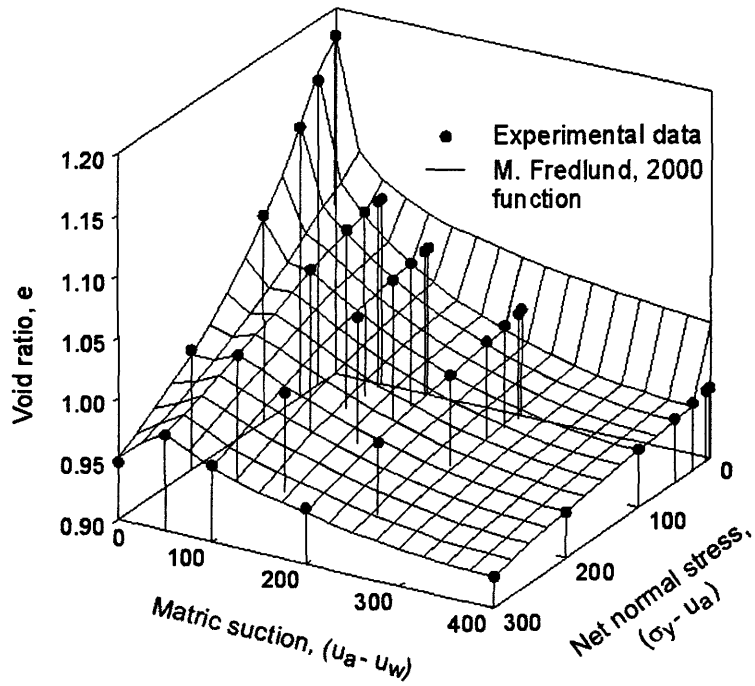

Figure 4.39 Best-fit void ratio surface using M. Fredlund (2000) function for measured void ratio data of Regina clay

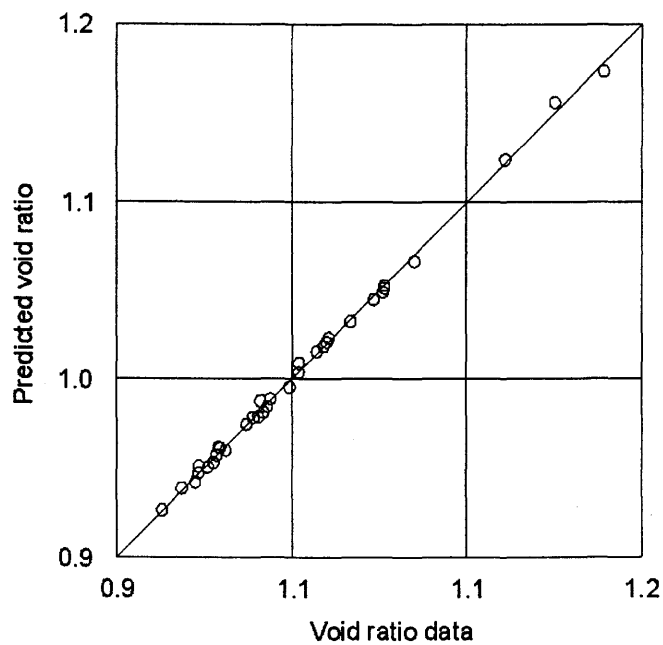

Figure 4.40 Correlation between measured and predicted void ratio using M. Fredlund (2000) function for Regina clay

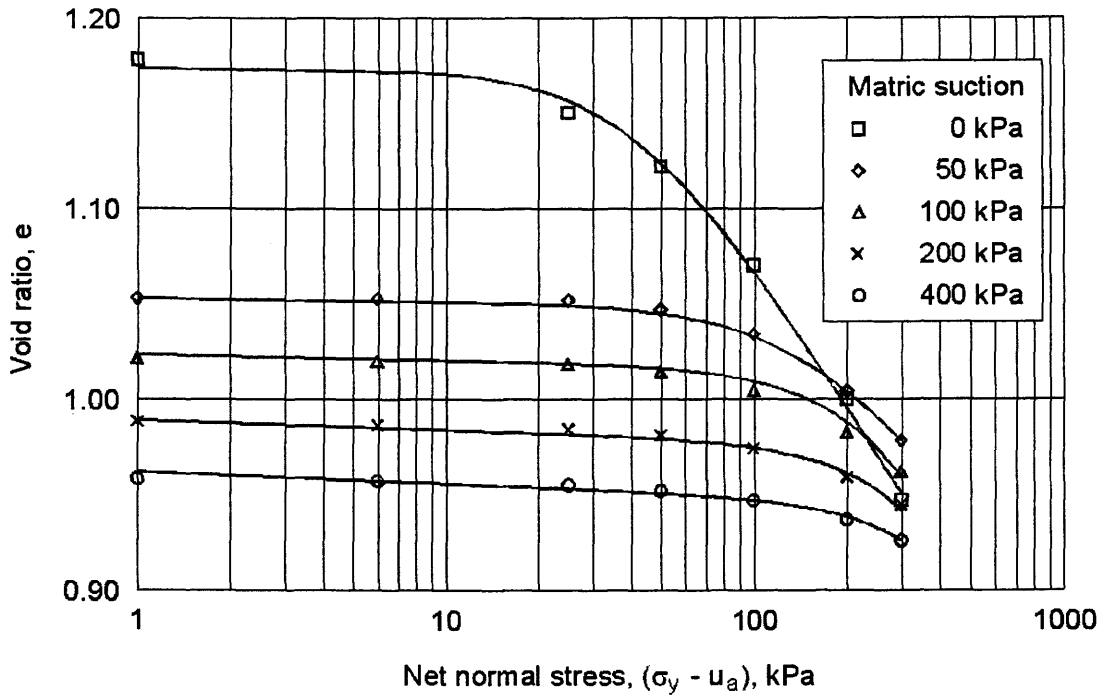

Figure 4.41 Void ratio versus net normal stress at various matric suctions using M. Fredlund (2000) function for Regina clay

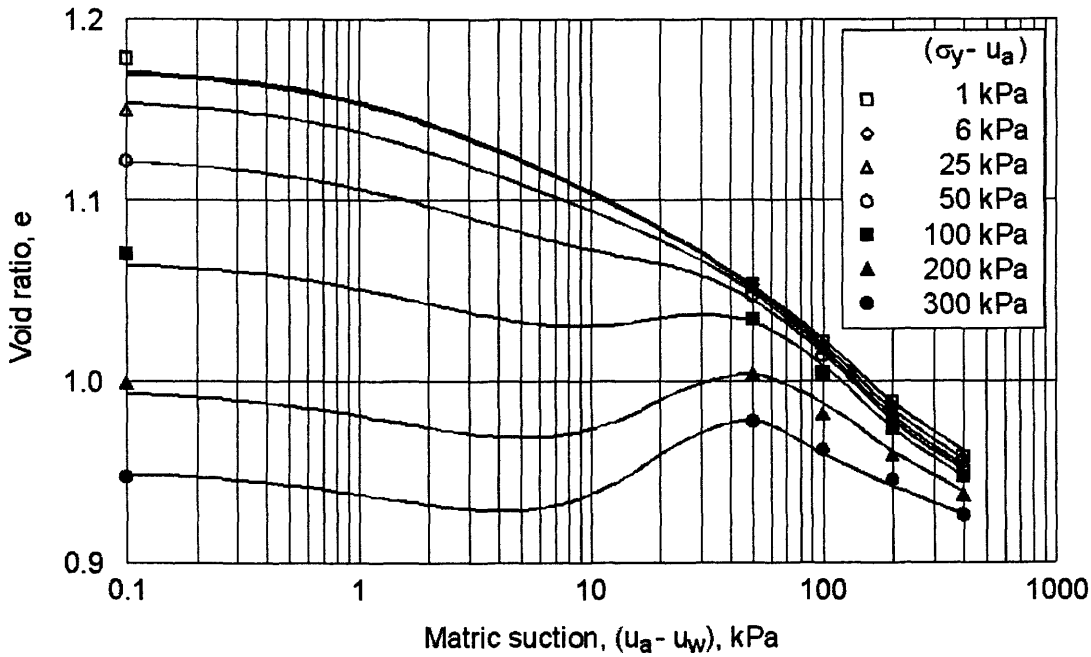

Figure 4.42 Void ratio versus matric suction at various net normal stresses using M. Fredlund (2000) function for Regina clay

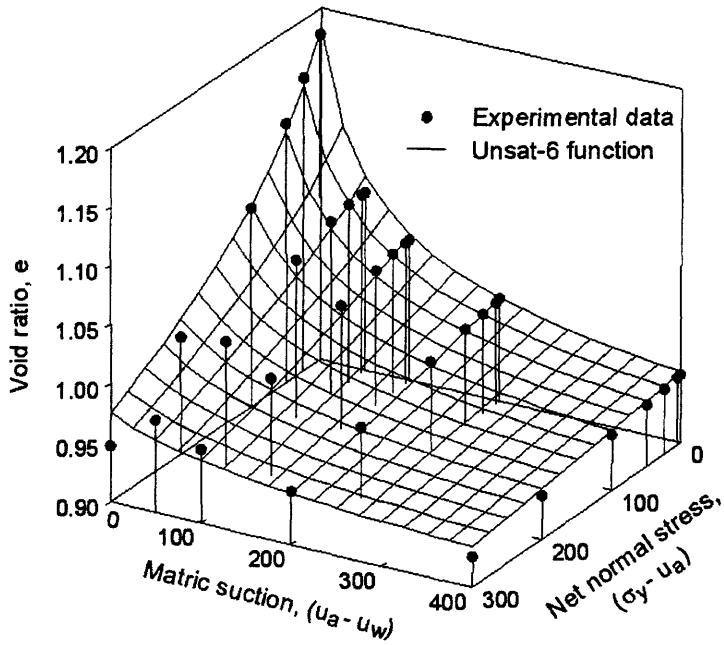

Figure 4.43 Best-fit void ratio surface using *Unsat-6* function for measured void ratio data of Regina clay

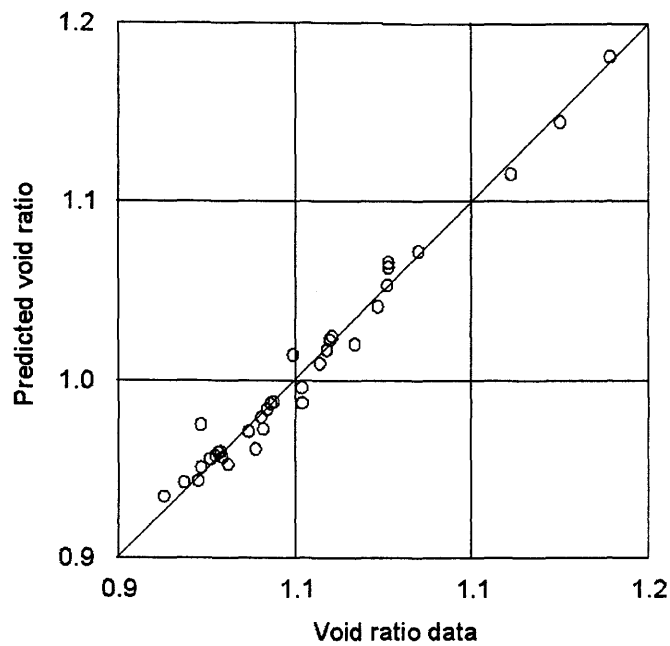

Figure 4.44 Correlation between measured and predicted void ratio using *Unsat-6* function for Regina clay

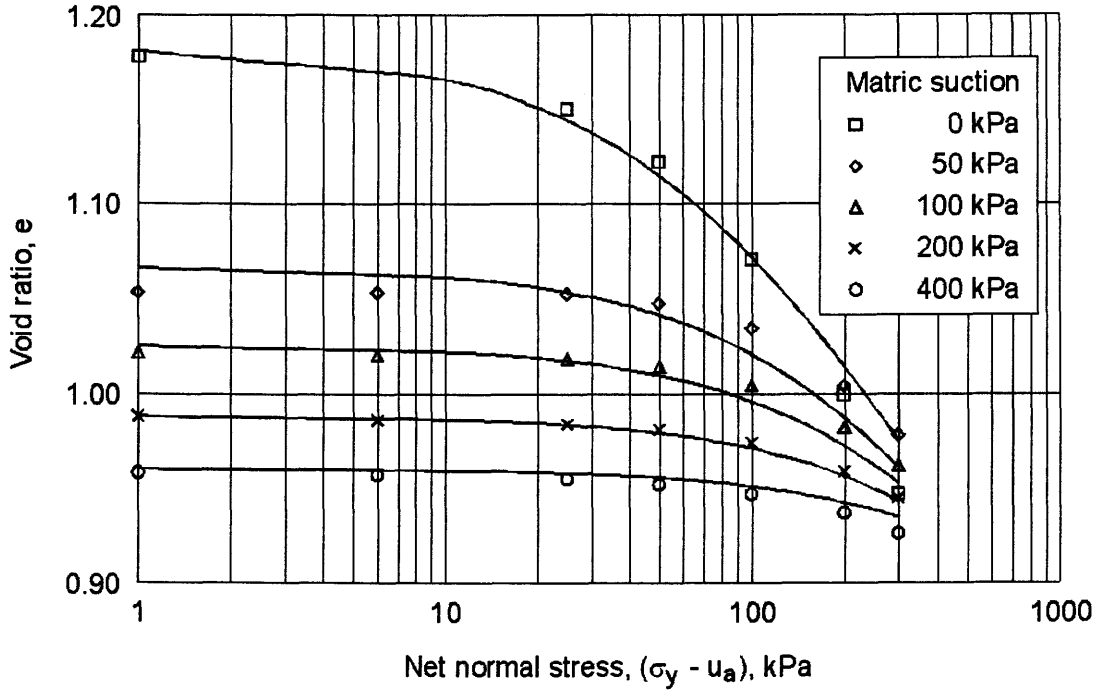

Figure 4.45 Void ratio versus net normal stress at various matric suctions using *Unsat-6* function for Regina clay

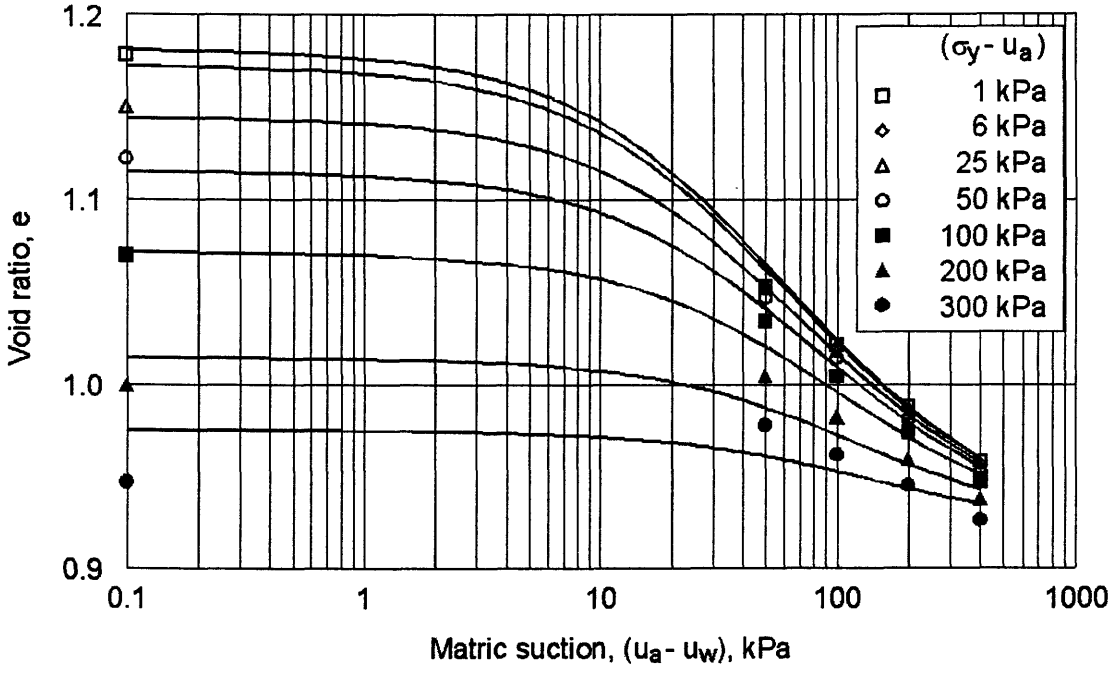

Figure 4.46 Void ratio versus matric suction at various net normal stresses using *Unsat-6* function for Regina clay

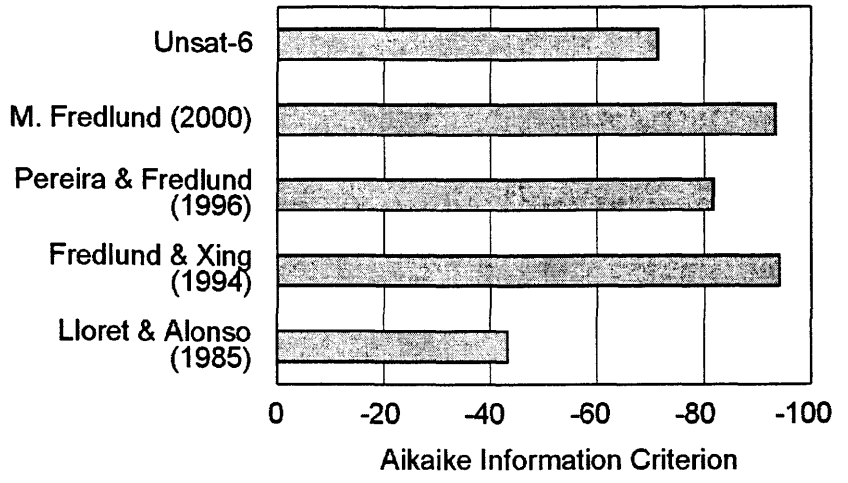

Figure 4.47 Aikaike Information Criterion for measured data of void ratio surface of Regina clay

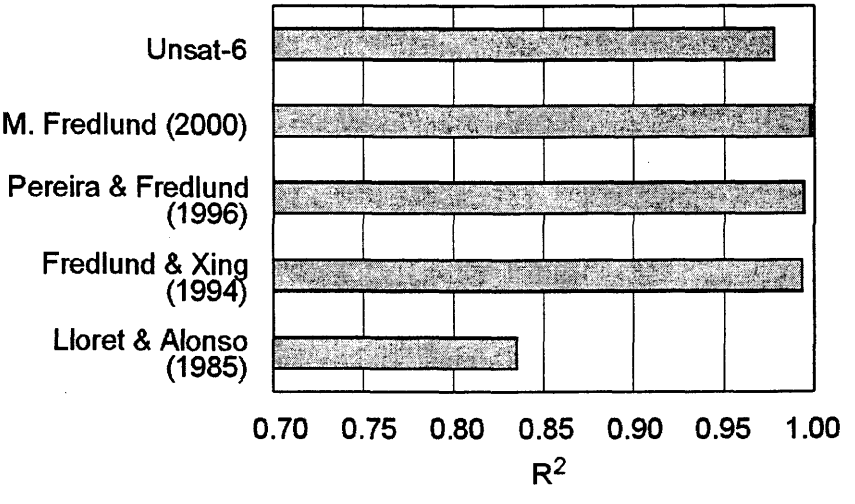

Figure 4.48 R^2 criterion for measured data of void ratio surface of Regina clay

Table 4.6 Statistical results of different void ratio equations for measured void ratio data of Regina clay

ID	Number of fitting parameters	R^2	AIC*
Lloret & Alonso (1985)	4	0.8355	-43
Fredlund & Xing (1994)	11	0.9932	-94
Pereira & Fredlund (1996)	11	0.9942	-82
M. Fredlund (2000)	13	0.9979	-93
Unsat-6	6	0.9779	-71

* Aikaike Information Criterion

4.3.4.3 Measured water content data of Regina clay

The measured data of water content constitutive surface obtained from Shuai (1996) are presented graphically on a semi-logarithmic scale and arithmetic scale in Figs. 4.49a and 4.49b, respectively.

The following functions are considered: Fredlund and Xing (1994), Pereira and Fredlund (1996) functions, and the *Unsat-6* function. The Fredlund and Xing (1994) and Pereira and Fredlund (1996) functions were originally presented as functions of only one stress state variable, but have now been extended as a function with fitting parameters for the second stress state variable.

Fitting parameter results for the different equations for measured water content data of Regina clay are presented in Table 4.7. The best-fit results using the Fredlund and Xing (1994) function are presented in Figs. 4.50 and 4.51. The best-fit results using the Pereira and Fredlund (1996) function are presented in Figs. 4.52 and 4.53. The best-fit results using the *Unsat-6* function are presented in Figs. 4.54 and 4.55. It can be seen that all of these function can be used to adequately describe the water content constitutive surface for Regina clay. However, the *Unsat-6* function has the least number of fitting parameters, i.e., six fitting parameters.

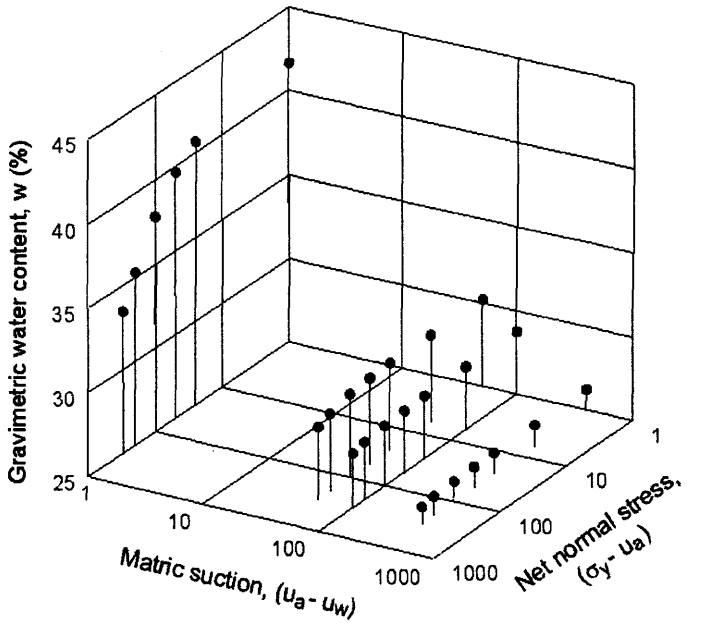

a) Semi-logarithmic scale

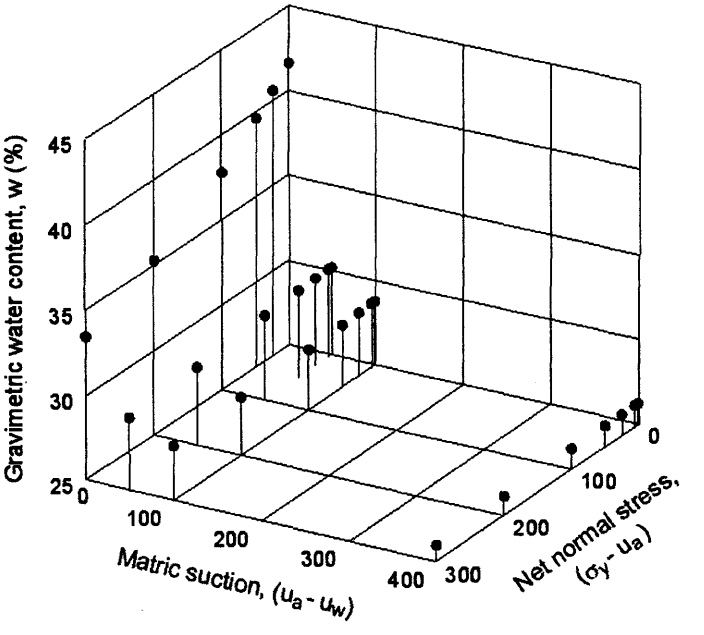

a) Arithmetic scale

Figure 4.49 Measured data of water content surface for Regina clay (from Shuai, 1996)

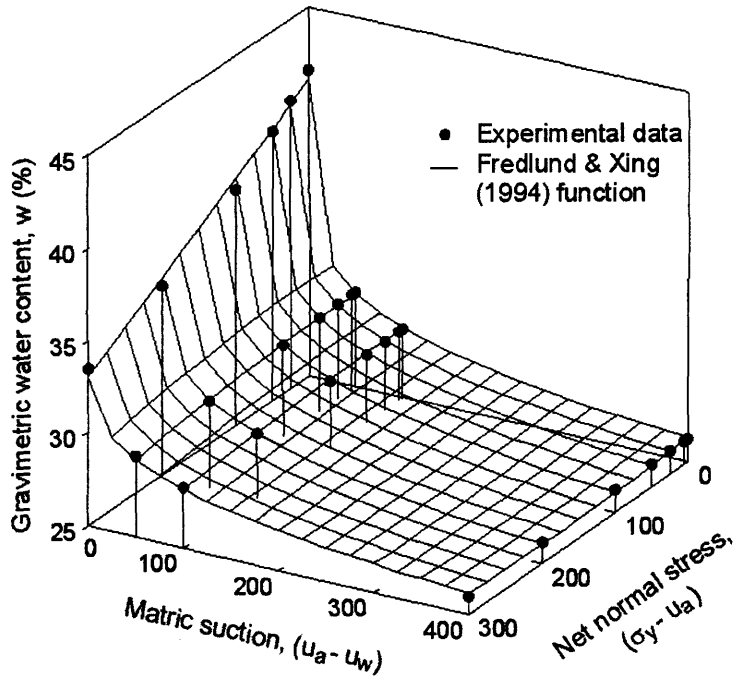

Figure 4.50 Best-fit water content surface using Fredlund and Xing (1994) function for Regina clay

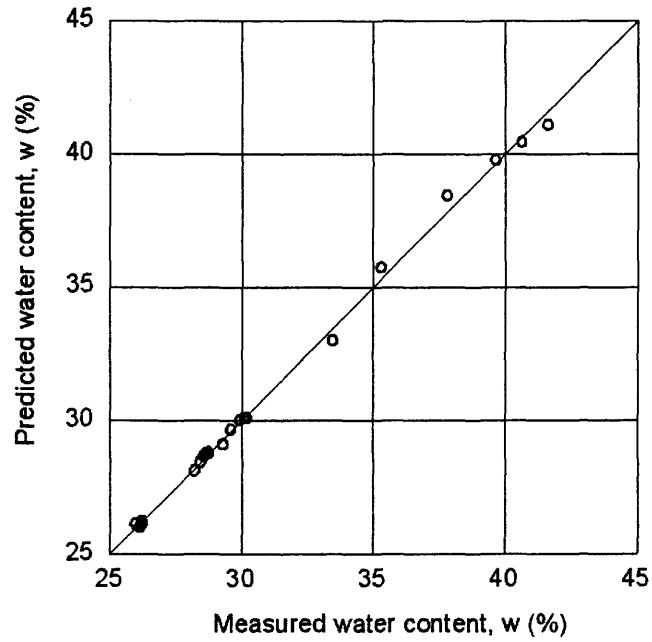

Figure 4.51 Correlation between measured and predicted water content using Fredlund and Xing (1994) function for Regina clay

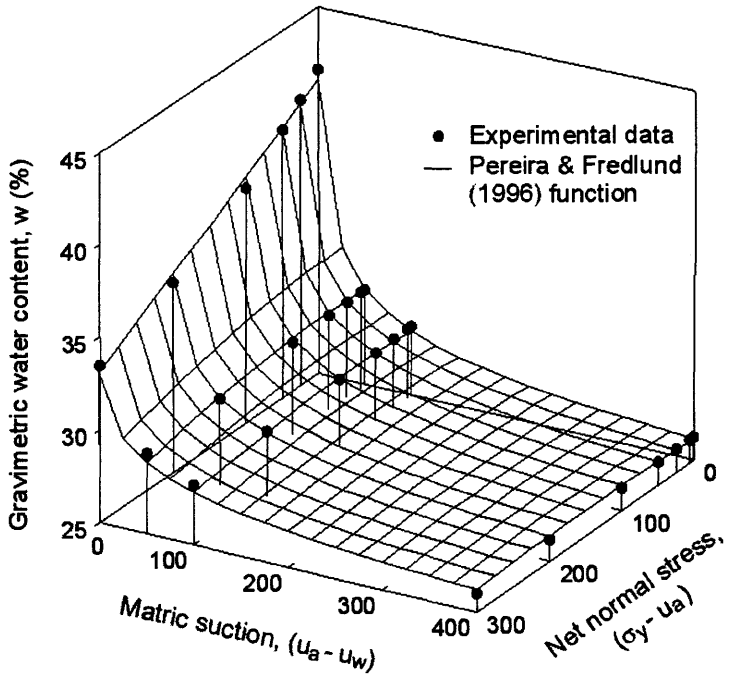

Figure 4.52 Best-fit water content surface using Pereira and Fredlund (1996) function for Regina clay

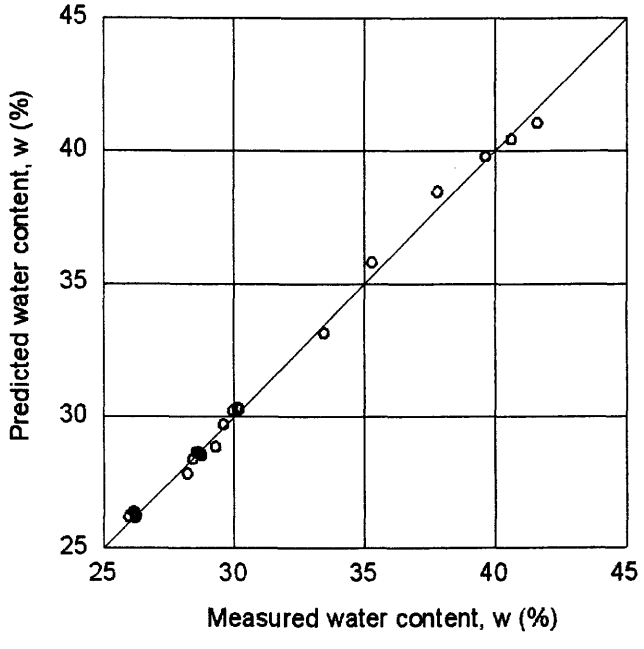

Figure 4.53 Correlation between measured and predicted water content using Pereira and Fredlund (1996) function for Regina clay

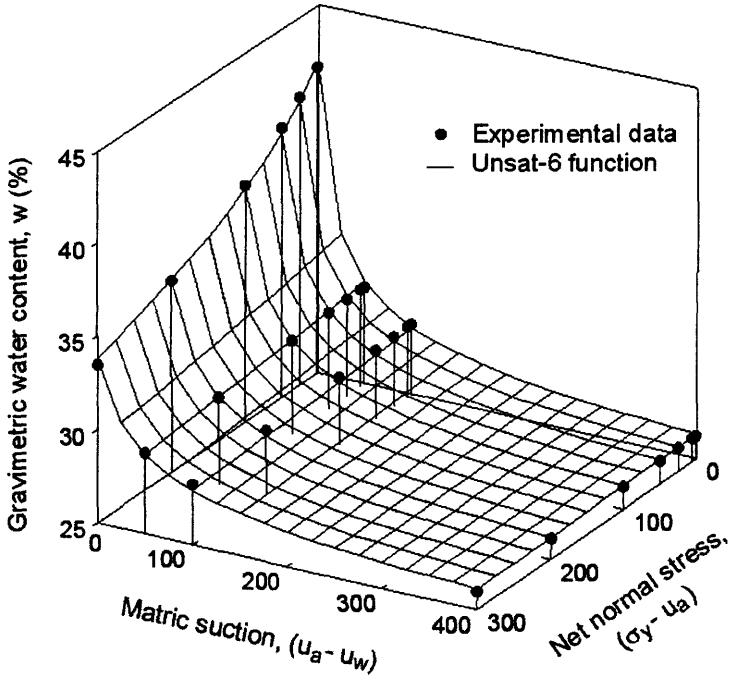

Figure 4.54 Best-fit water content surface using *Unsat-6* function for Regina clay

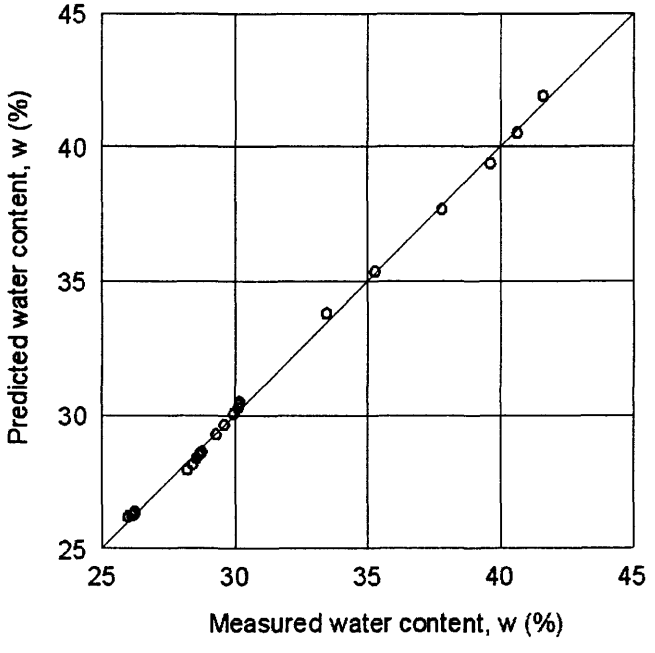

Figure 4.55 Correlation between measured and predicted water content using *Unsat-6* function for Regina clay

Statistical results of the proposed equations for measured water content data on Regina clay are presented in Table 4.8. The *Unsat-6* function is shown to provide the best fit to the experimental data of water content on Regina clay.

Table 4.7 Fitting parameter results of different SWCC equations for Regina clay (measured data)

ID	Function	Fitting parameters
Fredlund & Xing (1994)	$w = \frac{a}{\left\{\ln\left[\exp(1) + \left(\frac{(u_a - u_w)}{b}\right)^c\right]\right\}^d}$ where: $a = a_1\sigma + a_2$ $b = b_1\sigma + b_2$ $c = c_1\sigma + c_2$ $d = d_1\sigma + d_2$	a_1 = -2.70E-4 c_1 = 9.31E-4 a_2 = 0.411 c_2 = 0.337 b_1 = 0.035 d_1 = -1.22E-3 b_2 = 4.754 d_2 = 0.638
Pereira & Fredlund (1996)	$w = w_u + \frac{w_f - w_u}{\left[1 + \left(\frac{(u_a - u_w)}{c}\right)\right]^d}$ where: $w_u = a_1\sigma + a_2$ $w_f = f_1\sigma + f_2$ $c = c_1\sigma + c_2$	a_1 = 1.29E-5 c_1 = 0.094 a_2 = 0.242 c_2 = 21.735 f_1 = -2.65E-4 d = 0.697 f_2 = 0.411
Unsat-6	$w = a + b\log\left[\frac{1 + c(\sigma - u_a) + d(u_a - u_w)}{1 + f(\sigma - u_a) + g(u_a - u_w)}\right]$	a = 0.419 d = 0.250 b = -0.121 f = 6.83E-5 c = 0.013 g = 0.010

Table 4.8 Statistical results of different SWCC equations for Regina clay

ID	Number of fitting parameters	R^2	AIC*
Fredlund & Xing (1994)	8	0.9977	-83
Pereira & Fredlund (1996)	7	0.9967	-80
Unsat-6	6	0.9983	-90

* Aikaike Information Criterion

4.4 Soil property characterization for Regina clay

This section presents the soil property characterization for Regina clay. The experimental data, the mathematical description of the experimental data and the calculation of elasticity parameter functions are presented.

4.4.1 Experimental data for Regina clay

Regina clay is a highly swelling post-glacial lake deposit. The Unified Classification System places this soil in the class of inorganic clay of high plasticity. Soil properties and the volume change behaviour of Regina clay have been previously studied experimentally by numerous researchers. Significant contributions to understanding the volume change behaviour of Regina clay include research studies undertaken by Christiansen (1961), Gilchrist (1963), Fredlund (1964), Noble (1966), Lu (1969), Krahn and Fredlund (1972), Shuai (1996), Fredlund and Rahardjo (1993), and Feng et al. (1998).

Shuai (1996) performed a testing program on compacted Regina clay to study the volume change behaviour of swelling soils during oedometer tests. The tests were performed at the University of Saskatchewan, Saskatoon. These test results are used for the calculation of elastic moduli, as well as the coefficients of permeability required for the uncoupled and coupled analyses in this research study.

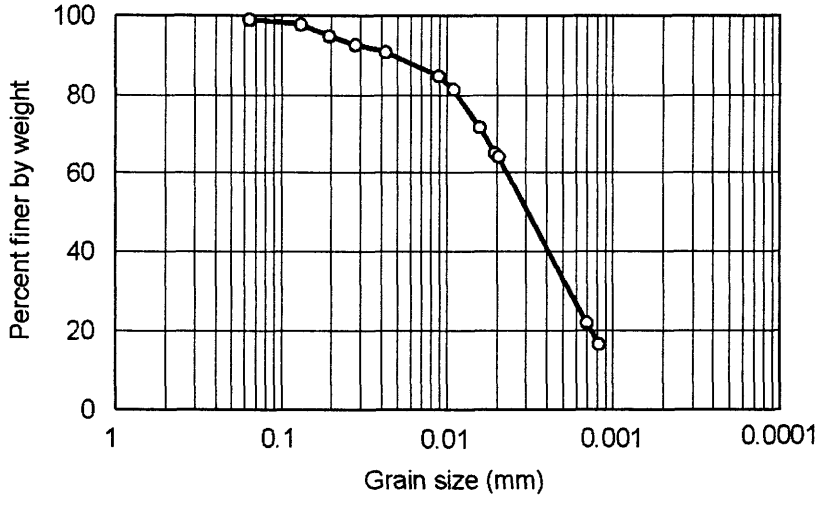

Figure 4.56 Particle size distribution curve for Regina clay (Shuai, 1996)

The particle size distribution curve for Regina clay is shown in Fig. 4.56. The index properties, mineral composition, and cations in the pore-water are presented in Table 4.9.

The test results include data for the soil structure constitutive surface, water phase constitutive surface and the coefficient of permeability function. The experimental results are presented in the following sections. More detail on the testing program, testing equipment, test procedures, and test results can be found in Shuai (1996).

Table 4.9 Index properties of the testing soil (Shuai, 1996)

Soil	Regina clay
Location	Regina, Sask., Canada
Atterberg limits	LL = 69.9% PL = 31.9% PI = 38.0%
Grain size distribution [a] (based on ASTM D422, 1988)	Sand: 2.2%, Silt: 32.9%, Clay: 64.9%
Unified Soil Classification System	CH, Inorganic clay of high plasticity
Standard compaction	Maximum dry density: 14.01 kN/m^3 Optimum water content: 28.5%
Mineralogical composition[b] (X-ray diffraction) (of minus 2 μ fraction)	Montmorillonite: 20%, Illite: 42%, Kaolinite: 14%, Mixed (12 Å) mineral layer: 24%
Cations in pore-water[b] (Saturation extract) (meq per 100g dry soil)	Sodium: 1.05 Calcium: 3.16 Magnesium: 1.66 Potassium: 0.33

[a] based on ASTM D422 (1988)
[b] from Fredlund (1964)

4.4.1.1 Experimental data for soil-water characteristic curve and swelling curve of Regina clay

The soil-water characteristic curve is required to define the coefficient of water volume change and to predict the unsaturated coefficient of permeability function. The soil-water characteristic curves were determined using a pressure plate apparatus. The results of tests that followed a wetting path are presented in Table 4.10 for both unconfined swelling conditions and K_0 confined swelling conditions.

Table 4.10 Experimental data for the soil-water characteristic curves

Matric suction (kPa)	Gravimetric water content, w (%)	
	Unconfined test (e_i = 0.949)	Confined test (e_i = 0.956)
575	26.12	26.20
485	26.56	26.35
415	26.75	26.48
350	27.06	26.70
280	27.52	27.00
210	28.33	27.42
140	29.19	27.97
65	30.64	29.18
30	32.90	30.48
12	-	32.09
0	38.45	37.35

The relationship between the void ratio and the water content at various matric suctions was determined using the shrinkage tests. Two specimens were tested under K_0 conditions, the tests followed a wetting path. The test results are presented in Table 4.11.

Table 4.11 Experimental data for the void ratio versus water content relationship

Test step	Shrinkage test 1		Shrinkage test 2	
	Water content (%)	Void ratio	Water content (%)	Void ratio
0	26.17	0.964	26.13	0.973
1	26.59	0.978	26.67	0.995
2	27.37	0.999	28.49	1.029
3	28.93	1.016	30.71	1.062
4	31.31	1.049	34.79	1.103
5	33.80	1.073	36.87	1.118
6	35.37	1.085	38.15	1.120
7	36.81	1.099		
8	38.06	1.102		

4.4.1.2 Experimental data for soil structure and water phase constitutive surfaces of Regina clay

The soil structure constitutive surface was determined from the measured values of void ratio at various matric suctions and applied loads. Likewise, the water phase constitutive surface was determined from the measured values of water content at various matric suctions and applied loads. These values were determined using a free swell oedometer test (ASTM Designation) and a series of constant suction consolidation tests. From an initial stress state, each specimen was allowed to swell and then it was consolidated under a constant matric suction. The void ratio and pore-water volume changes in the specimens were measured at various equilibrium states. The stress paths followed during the series of tests are illustrated in Fig. 4.57.

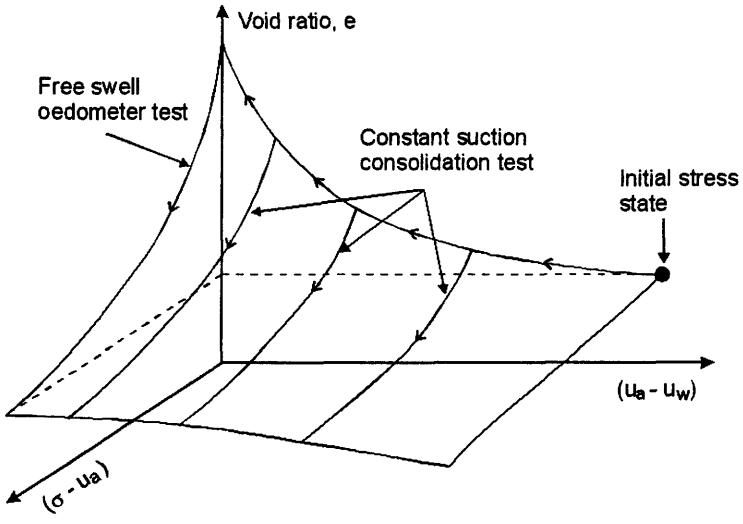

Figure 4.57 Stress path followed in the constant suction consolidation test

Table 4.12 Results of the constant suction consolidation tests

$(\sigma_y - u_a)$ (kPa)	$(u_a - u_w)$, (kPa)									
	0		50		100		200		400	
	e	S (%)	e	S (%)	e	S (%)	e	S (%)	e	S(%)
Initial	0.955	77.17	0.955	77.38	0.955	77.40	0.954	77.03	0.952	77.53
1	1.162	-	1.053	81.16	1.021	79.74	0.988	-	0.958	77.49
6	1.159	-	1.053	81.16	1.020	79.79	0.986	-	0.957	77.60
25	1.144	-	1.052	81.21	1.018	79.87	0.984	-	0.955	77.76
50	1.118	-	1.047	81.44	1.014	79.99	0.981	-	0.952	78.00
100	1.074	-	1.034	82.03	1.004	80.53	0.974	-	0.947	78.30
200	1.011	-	1.004	83.46	0.982	81.93	0.959	-	0.937	78.95
300	0.967	-	0.978	84.81	0.962	83.02	0.945	-	0.926	79.40

Note: Initial values correspond to the initial stress states (see Fig. 4.57)

4.4.1.3 Experimental data for the coefficient of permeability of Regina clay

The coefficient of permeability function for Regina clay was predicted from the saturated coefficient of permeability and the soil-water characteristic curve. The saturated coefficients of permeability were determined using the falling head permeability test (Shuai, 1996).

Two specimens were tested for the saturated coefficient of permeability at different applied loads. The relationship between the saturated coefficient of permeability and void ratio is presented in Fig. 4.58 for both specimens. The results show that there is essentially a unique relationship between the saturated coefficient of permeability and void ratio. The saturated coefficient of permeability is also essentially independent of the stress path.

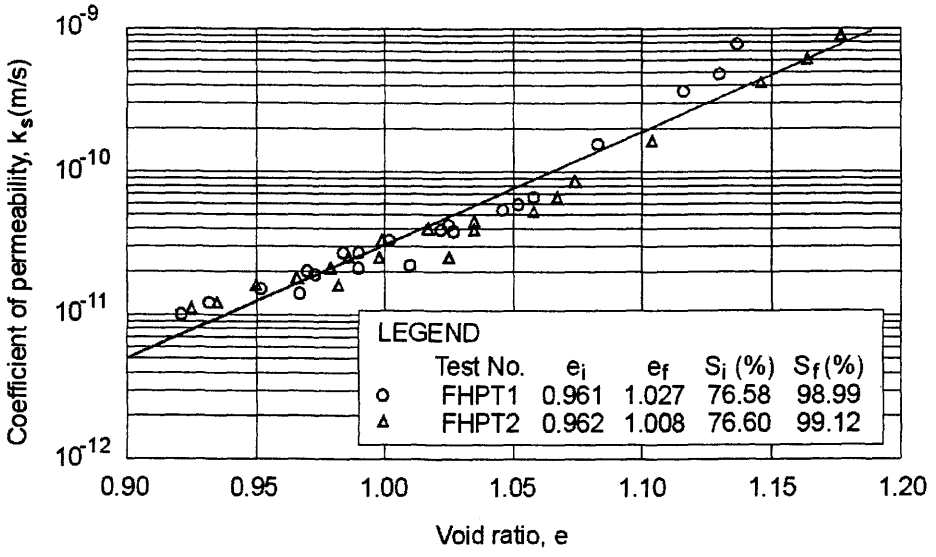

Figure 4.58 Saturated coefficient of permeability versus void ratio (Shuai, 1996)

4.4.2 Mathematical descriptions of the test data

The results of the evaluation of proposed functions presented in the previous section suggests that the *Unsat-6* function can be satisfactorily used to describe both soil structure and water phase constitutive surface. The *Unsat-6* function can be rewritten as follows:

$$f(x,y) = a + b\log\left(\frac{1+cx+dy}{1+fx+gy}\right) \tag{4.37}$$

where $f(x,y)$ can be void ratio, gravimetric water content, volumetric water content or degree of saturation, and x, y are net normal stress and matric suction, respectively.

Parameter a represents a value of the function at x and y equal to zero. Parameters c, d, f and g are non-negative constants.

The calculation of coefficients of volume change and the elasticity parameters requires the derivatives of the constitutive equations for soil structure and water phase. The derivatives of Eq. (4.37) are as follows:

$$\frac{\partial}{\partial x} f(x,y) = \frac{b[c(1+fx+gy) - f(1+cx+dy)]}{(1+fx+gy)(1+cx+dy)\ln(10)} \tag{4.38}$$

$$\frac{\partial}{\partial y} f(x,y) = \frac{b[d(1+fx+gy) - g(1+cx+dy)]}{(1+fx+gy)(1+cx+dy)\ln(10)} \tag{4.39}$$

The *Unsat-6* function can be written for two-dimensional fitting (i.e., function of only one stress state variable) as follows:

$$f(x) = a + b\log\left(\frac{1+cx}{1+dx}\right) \tag{4.40}$$

where $f(x)$ can be void ratio, gravimetric water content, volumetric water content or degree of saturation, and x can be net normal stress or matric suction. Parameter a represents a value of the function at x equals to zero. Parameters c and d are non-negative constants.

Equation (4.37) is used to describe the void ratio and water content constitutive surfaces. Equation (4.40) can be used to describe most of the constitutive relations in two-dimensions for measured data on Regina clay.

Figure 4.59 presents the best-fit gravimetric water content versus matric suction curve to measured data under both confined and unconfined tests followed a wetting path.

The best-fit curve to the shrinkage test results under confined, wetting condition is presented in Fig. 4.60. The following equation is used for void ratio versus gravimetric water content:

$$e = a + b\ln(w) + \frac{c}{\ln(w)} \tag{4.41}$$

where:

a = 2.808

b = 0.948

c = 0.756

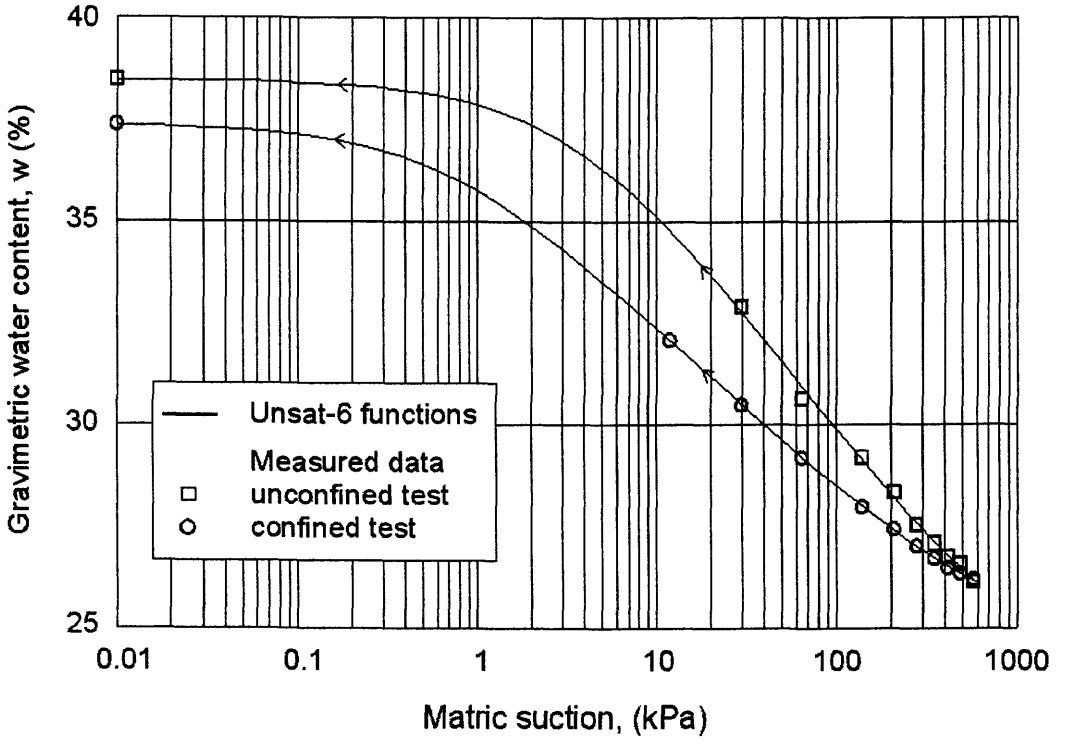

Figure 4.59 Best-fit gravimetric water content versus matric suction curve to measured data (Shuai, 1996) under wetting conditions for Regina clay using *Unsat-6* function

The volumetric water content and void ratio can be calculated from the test results presented in Figs. 4.59 and 4.60 for confined, wetting condition. Figure 4.61 presents the best-fit curve to measured volumetric water content versus matric suction. Figure 4.62 presents the best-fit curve to void ratio versus matric suction. It can be seen that the linear relationship between void ratio and logarithmic of matric suction is not valid at low soil suctions.

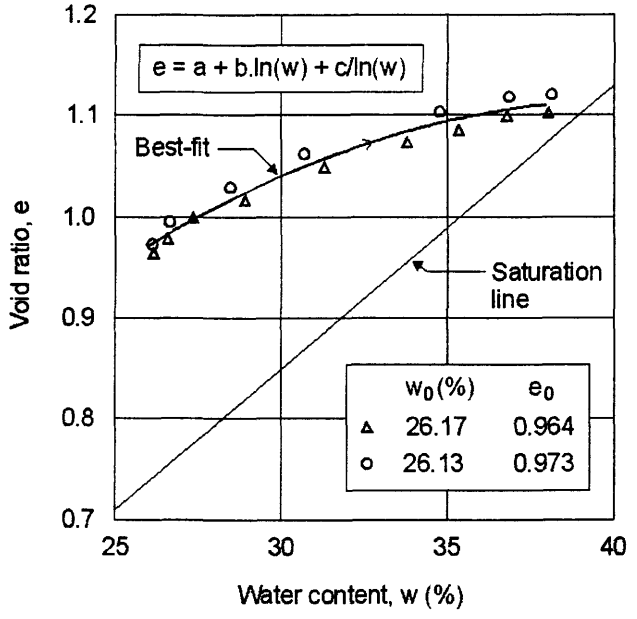

Figure 4.60 Best-fit void ratio versus water content curve to measured data (Shuai, 1996) under confined, wetting condition for Regina clay

Best-fit results of water content and void ratio versus matric suction for the measured data for Regina clay using *Unsat-6* function are presented in Table 4.13.

Table 4.13 Fitting parameter results of water content and void ratio versus matric suction for Regina clay

Soil property	Fitting parameters				Figure
	a	b	c	d	
SWCC, w, unconfined condition	0.3845	-0.0627	0.2446	9.76E-04	4.59
SWCC, w, confined condition	0.3735	-0.0425	1.3954	1.54E-03	4.59
SWCC, θ_w, confined condition	0.5015	-0.047	1.7146	1.78E-03	4.61
Void ratio versus matric suction	1.1078	-0.0624	0.2936	4.80E-04	4.62

The best-fit equation to the oedometer test results (i.e., tests OT1 and OT2) are presented for all the loading, unloading, and reloading curves in Figs. 4.63 and 4.64. The compressibility of soils can be obtained by differentiating of these curves. Figure 4.65 present the best-fit of Eq. (4.40) to measured data from constant suction consolidation tests at various matric suctions. The fitting results for these curves are presented in Table 4.14.

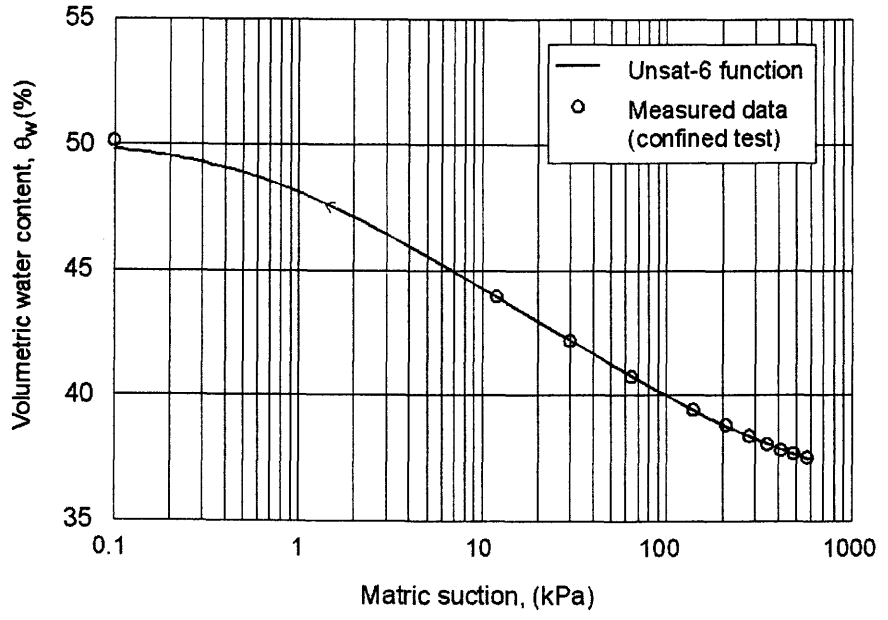

Figure 4.61 Best-fit volumetric water content versus matric suction curve to measured data (Shuai, 1996) under confined, wetting condition for Regina clay using *Unsat-6* function

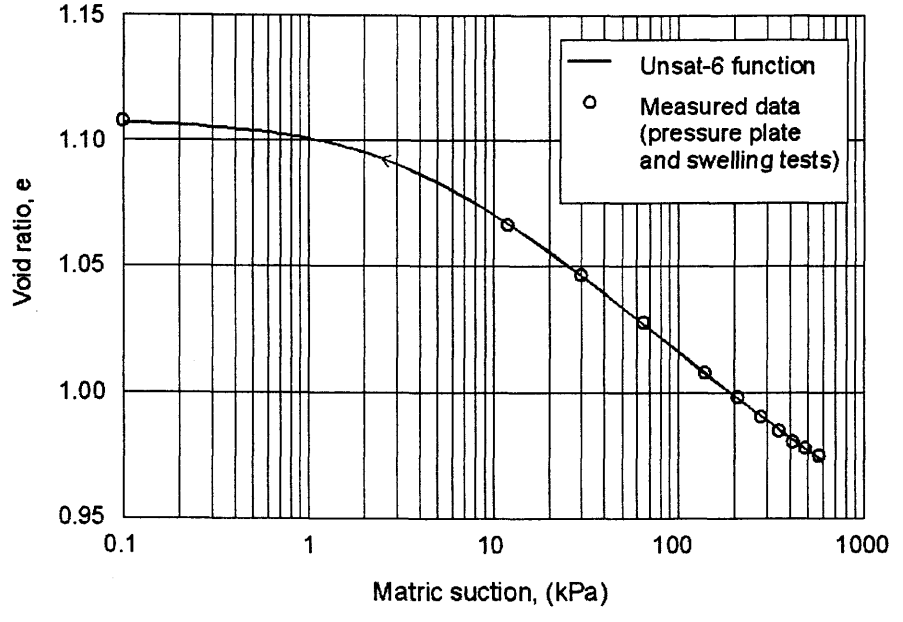

Figure 4.62 Best-fit void ratio versus matric suction curve to measured data (Shuai, 1996) under confined, wetting condition for Regina clay using *Unsat-6* function

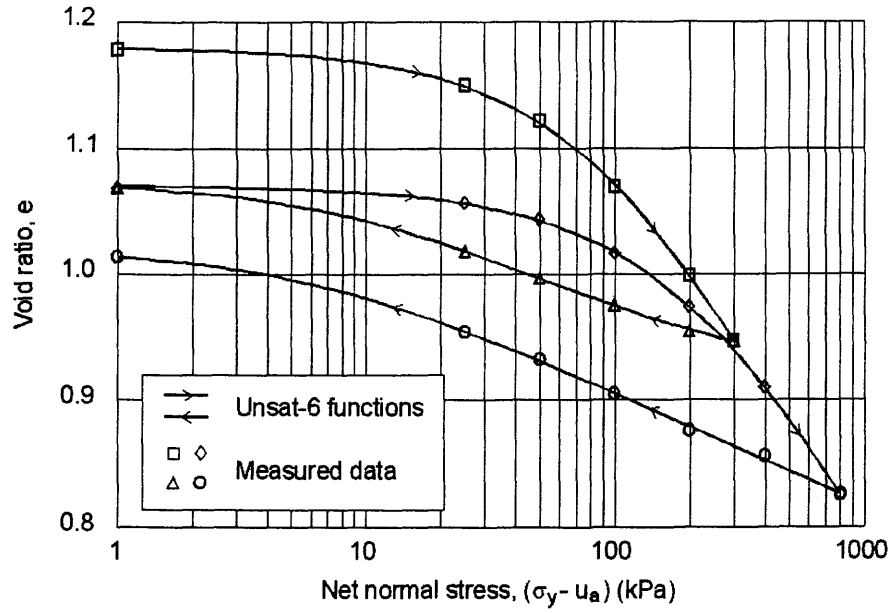

Figure 4.63 Best-fit to oedometer test results (test OT1, Shuai, 1996) or Regina clay using *Unsat-6* function

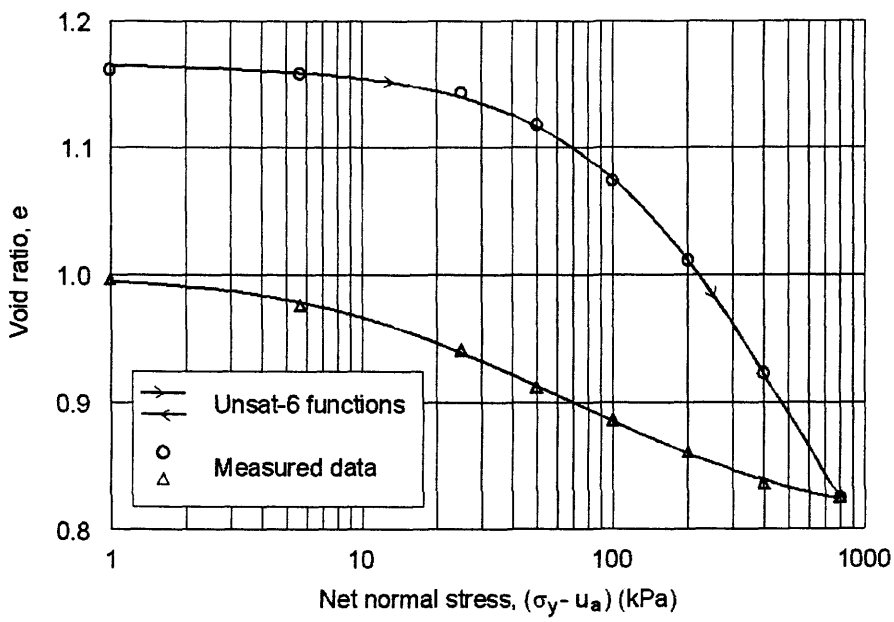

Figure 4.64 Best-fit to oedometer test results (test OT2, Shuai, 1996) for Regina clay using *Unsat-6* function

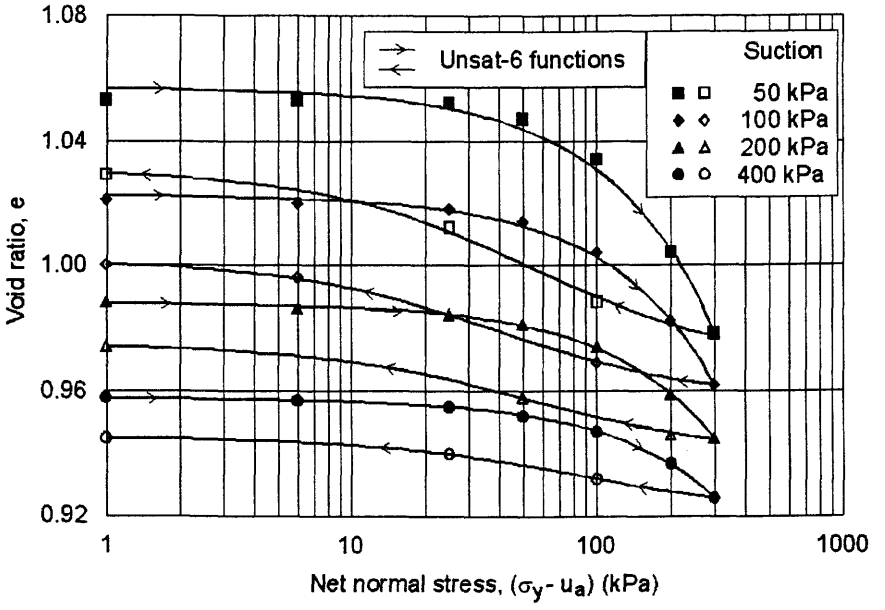

Figure 4.65 Best-fit to constant suction consolidation test results (Shuai, 1996) for Regina clay using *Unsat-6* function

4.4.3 Calculation of elasticity parameters from measured void ratio and water content surfaces under K_0-loading conditions

The best-fit surface for measured void ratio data is presented graphically in Fig. 4.66. Figures 4.67, 4.68, and 4.69 show the gravimetric water content, volumetric water content, and degree of saturation surfaces for one-dimensional swelling conditions. Soil properties are plotted with respect to the net vertical stress and matric suction associated with one-dimensional wetting. The fitting results associated with these constitutive surfaces are summarised in Table 4.15.

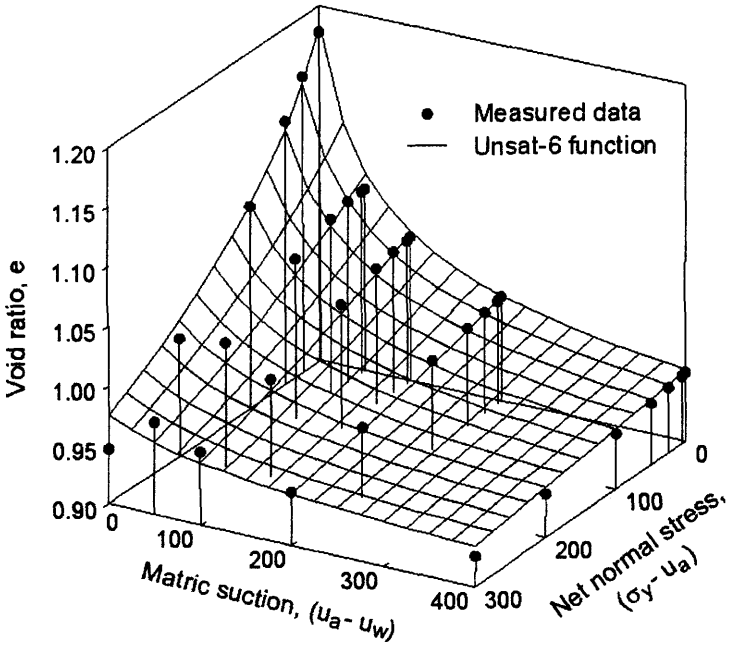

Figure 4.66 Best-fit to measured void ratio surface (Shuai, 1996) for Regina clay using *Unsat-6* function

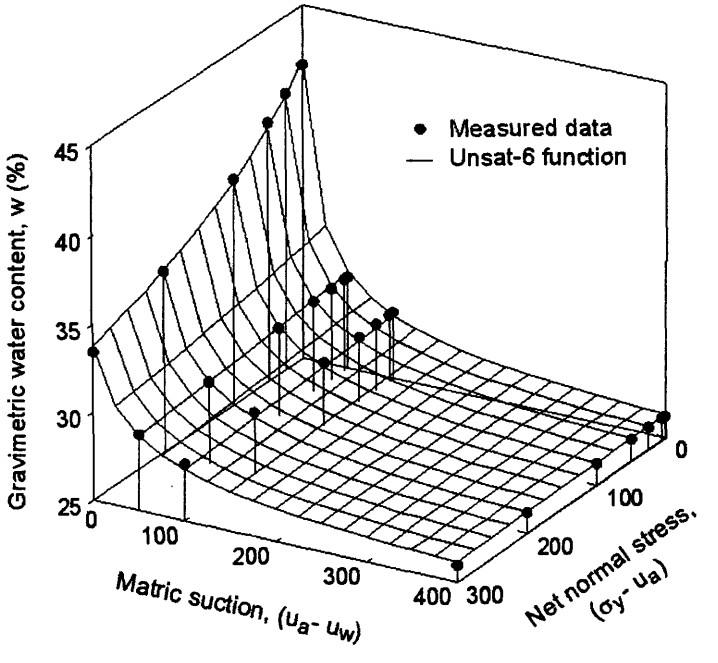

Figure 4.67 Best-fit to measured gravimetric water content surface (Shuai, 1996) for Regina clay using *Unsat-6* function

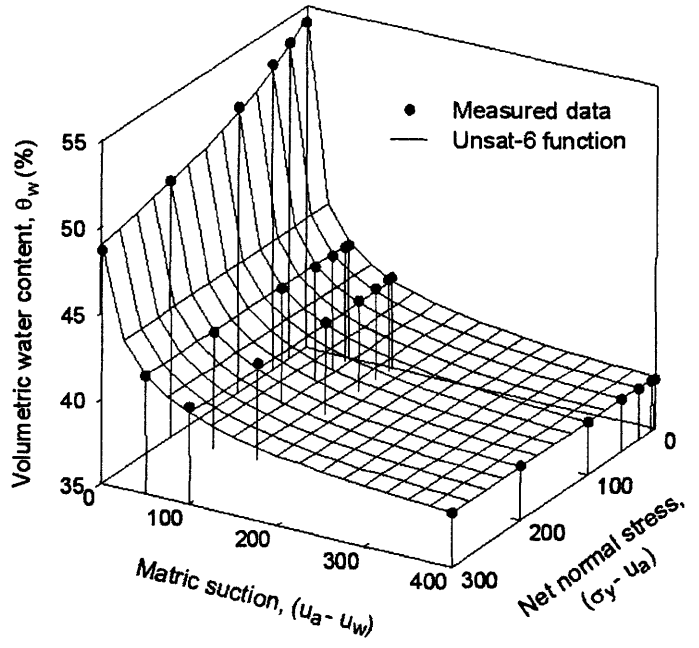

Figure 4.68 Best-fit to measured volumetric water content surface (Shuai, 1996) for Regina clay using *Unsat-6* function

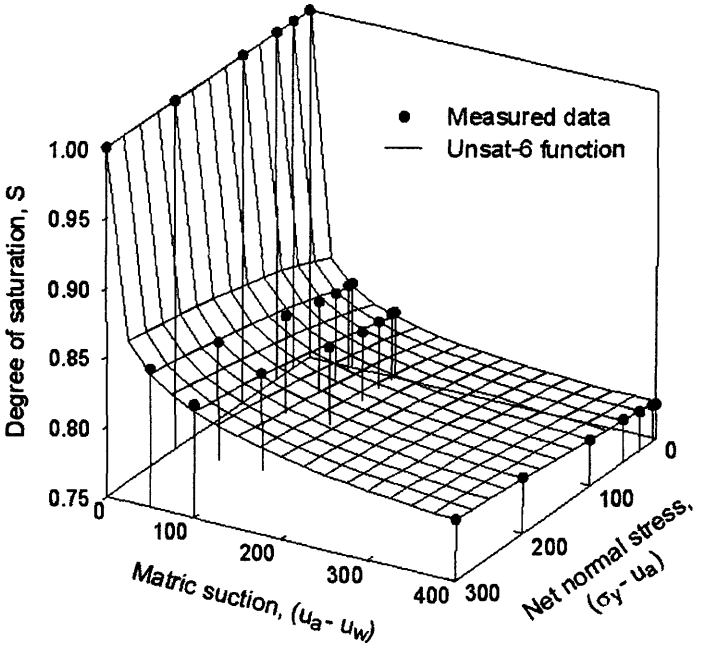

Figure 4.69 Best-fit to measured degree of saturation surface (Shuai, 1996) for Regina clay using *Unsat-6* function

Table 4.14 Fitting parameter results of oedometer and constant suction consolidation test results for Regina clay

Test	Suction (kPa)	Curves	Parameters				Figure
			a	b	c	d	
OT-1	0	Load	1.1808	-1.6128	4.52E-03	1.57E-03	4.63
		Rebound	1.0732	-0.1148	0.0924	4.18E-03	
		Load	1.0708	-1.0867	1.88E-03	6.16E-04	
		Rebound	1.0203	-0.0922	0.1686	1.06E-04	
OT-2	0	Load	0.96	0.9521	0.945	0	4.64
		Rebound	0.9991	-0.1336	0.08	2.70E-03	
CSCT-1	50	Load	1.0569	-16.3199	4.68E-05	0	4.65
		Rebound	1.0306	-4.5774	0.0188	0.0181	
CSCT-2	100	Load	1.0225	-19.7065	2.35E-05	0	
		Rebound	1.0014	-2.9187	0.0256	0.0247	
CSCT-3	200	Load	0.9877	-16.2418	2.02E-05	0	
		Rebound	0.9747	-2.3071	0.018	0.0174	
CSCT-4	400	Load	0.9577	-14.6335	1.83E-05	1.72E-06	
		Rebound	0.9453	-1.6035	0.0112	0.0108	

Table 4.15 Fitting parameter results of constitutive surfaces for Regina clay

Surfaces	Fitting parameters						Figure
	a	b	c	d	f	g	
Void ratio, e	1.1828	-0.2832	0.0147	0.0454	0	5.34E-03	4.66
Water content, w	0.4195	-0.1205	0.0129	0.2495	6.83E-05	0.0102	4.67
Water content, θ_w	0.5443	-0.0844	0.0142	0.8321	7.05E-04	7.10E-03	4.68
Degree of saturation, S	1	-0.0725	9.71E-03	11.7122	9.71E-03	7.07E-03	4.69

The coefficient of volume change associated with the soil structure and water phase can be calculated by differentiating the constitutive surfaces (Table 2.2) assuming that strains are small.

$$m_{1\text{-}1D}^{s} = \frac{1}{1+e_0}\frac{de}{d(\sigma_y - u_a)} \tag{4.42}$$

$$m_{2\text{-}1D}^{s} = \frac{1}{1+e_0}\frac{de}{d(u_a - u_w)} \tag{4.43}$$

$$m_{1\text{-}1D}^{w} = \frac{d\theta_w}{d(\sigma_y - u_a)} \tag{4.44}$$

$$m_{2\text{-}1D}^{w} = \frac{d\theta_w}{d(u_a - u_w)} \tag{4.45}$$

where:

e = void ratio,

e_0 = initial void ratio, and

θ_w = volumetric water content.

The coefficients of pore-water volume change can also be calculated from void ratio surface and degree of saturation surface.

$$m_{1\text{-}1D}^{w} = \frac{S}{1+e_0}\frac{de}{d(\sigma_y - u_a)} + \frac{e}{1+e_0}\frac{dS}{d(\sigma_y - u_a)} \tag{4.46}$$

$$m_{2\text{-}1D}^{w} = \frac{S}{1+e_0}\frac{de}{d(u_a - u_w)} + \frac{e}{1+e_0}\frac{dS}{d(u_a - u_w)} \tag{4.47}$$

where:

S = degree of saturation.

Figures 4.70 and 4.71 graphically present the coefficients of volume change of soil structure with respect to changes in net normal vertical stress and matric suction, respectively, for one-dimensional swelling conditions. Figures 4.72 and 4.73 present graphically the coefficients of water volume change with respect to changes in net normal vertical stress and matric suction, respectively, for one-dimensional swelling conditions.

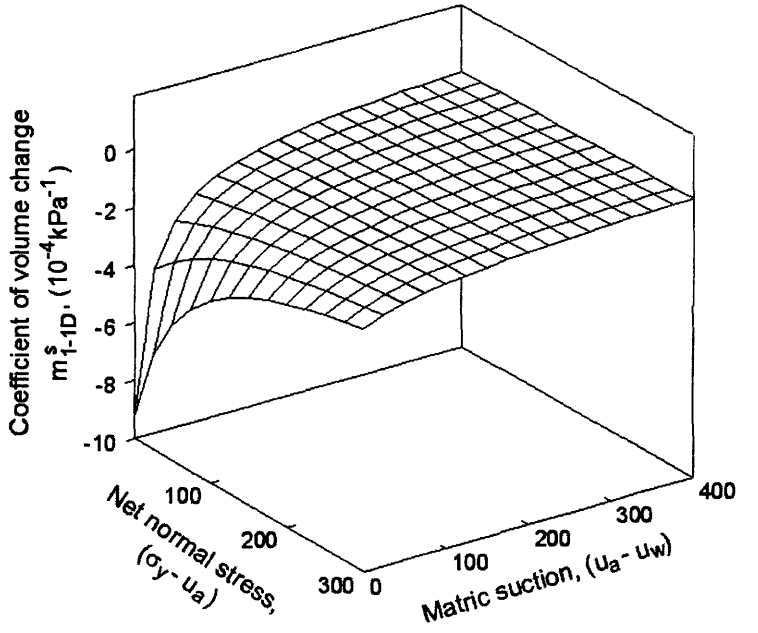

Figure 4.70 Coefficient of volume change, m^s_{1-1D}, with respect to changes in net normal stress under K_0-loading condition for Regina clay

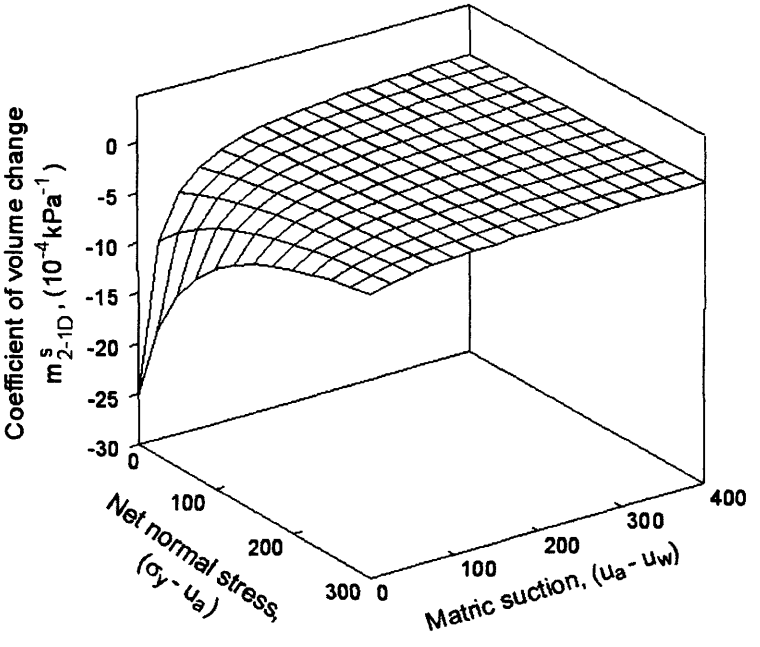

Figure 4.71 Coefficient of volume change, m^s_{2-1D}, with respect to changes in matric suction under K_0-loading condition for Regina clay

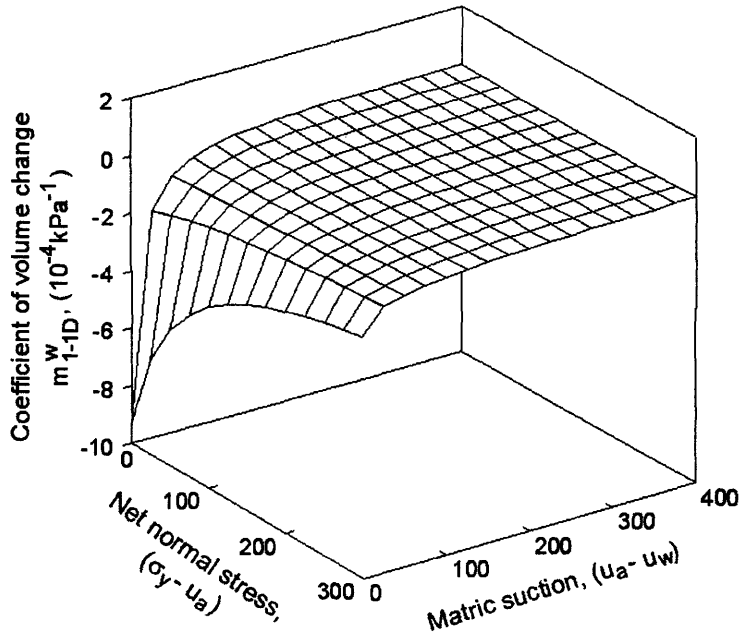

Figure 4.72 Coefficient of water volume change, m^w_{1-1D}, with respect to changes in net normal stress under K_0-loading condition for Regina clay

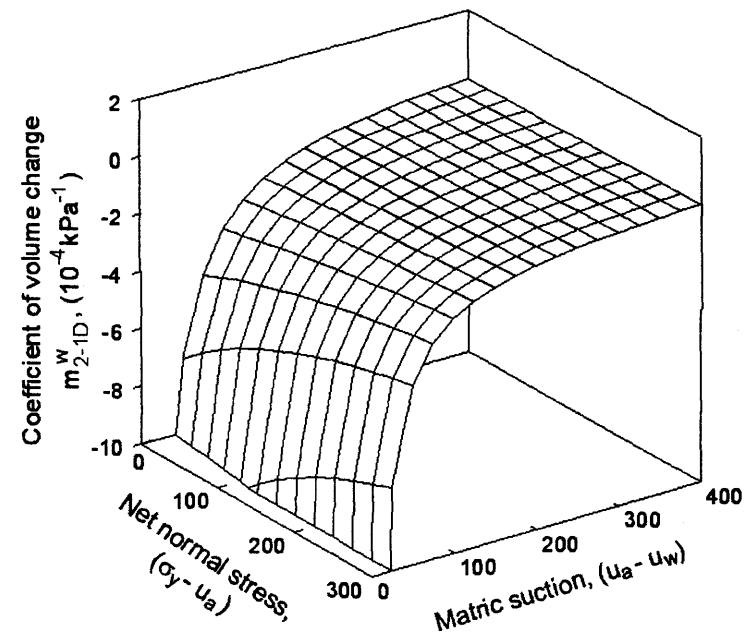

Figure 4.73 Coefficient of water volume change, m^w_{2-1D}, with respect to changes in matric suction under K_0-loading condition for Regina clay

The coefficients of volume change, with an assumed value of Poisson's ratio, can be used to calculate the elasticity parameters (Table 2.4).

$$E = \frac{(1+\mu)(1-2\mu)}{(1-\mu)m^{s}_{1\text{-}1D}} \tag{4.48}$$

$$H = \frac{(1+\mu)}{(1-\mu)m^{s}_{2\text{-}1D}} \tag{4.49}$$

$$E_{w} = \frac{(1+\mu)}{(1-\mu)m^{w}_{1\text{-}1D}} \tag{4.50}$$

$$H_{w} = \left(m^{w}_{2\text{-}1D} + \frac{2}{3}\frac{(1-2\mu)}{(1-\mu)}\frac{m^{s}_{2}}{m^{s}_{1}} m^{w}_{1} \right)^{-1} \tag{4.51}$$

The elasticity parameter functions associated with soil structure, E and H, are presented graphically in Figs. 4.74 and 4.75, respectively. Figures 4.76 and 4.77 present the elasticity parameter functions associated with water phase, E_w and H_w, respectively. Poisson's ratio was assumed to be a constant and equal to 0.4.

4.4.4 Calculation of elasticity parameters from measured void ratio and water content surfaces under general three-dimensional loading conditions

Void ratio data associated with general three-dimensional swelling can be generated from swelling indices for Regina clay [see section 4.2 and Eq. (4.13)]. Figure 4.78 presents a set of generated void ratios with an assumed Poisson's ratio equal to 0.4. The best-fit surface to the void ratio data set is presented in Fig. 4.79. The degree of saturation surface can be assumed for general three-dimensional swelling as showed in Fig. 4.80.

The fitting results for the generated void ratio and degree of saturation constitutive surfaces are shown in Table 4.16.

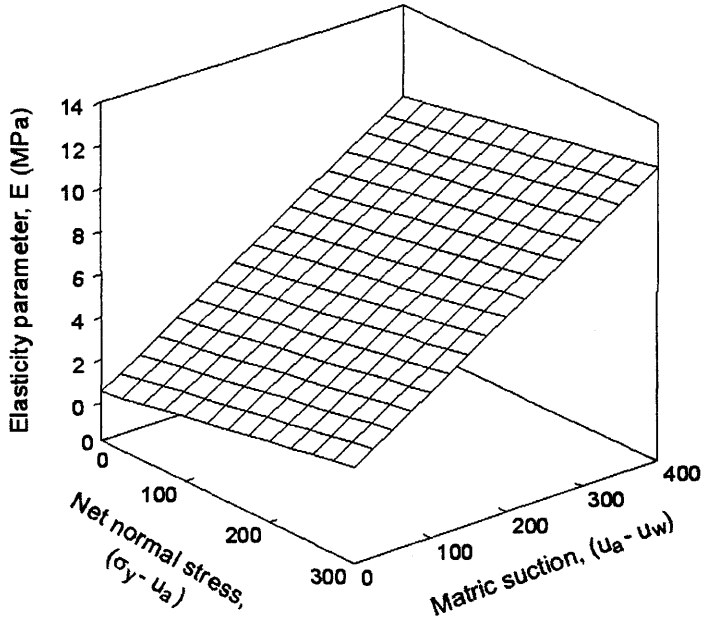

Figure 4.74 Elasticity parameter for soil structure, *E*, with respect to changes in net normal stress under K_0-loading condition for Regina clay

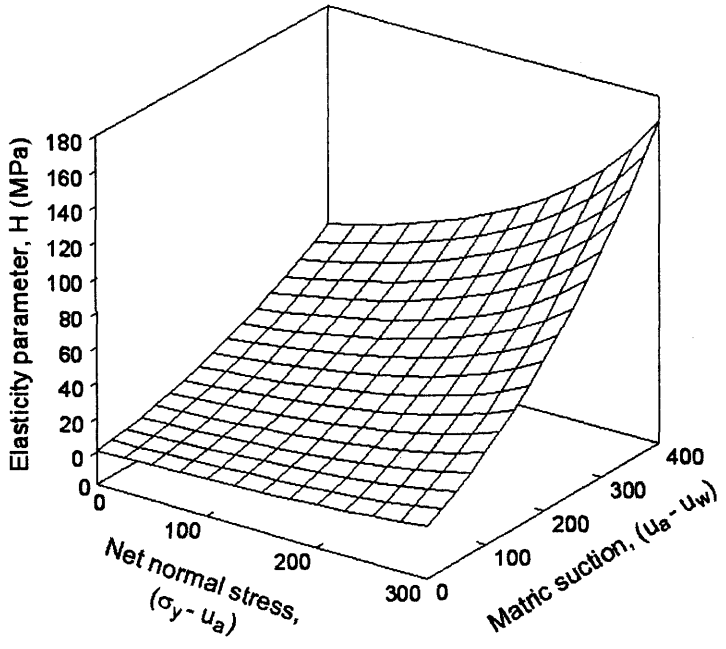

Figure 4.75 Elasticity parameter for soil structure, *H*, with respect to changes in matric suction under K_0-loading condition for Regina clay

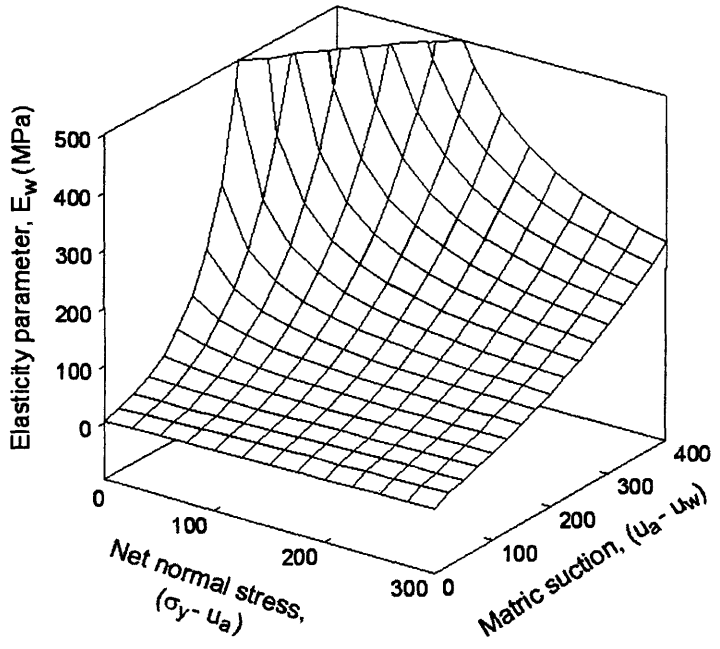

Figure 4.76 Elasticity parameter for water phase, E_w, with respect to changes in net normal stress under K_0-loading condition for Regina clay

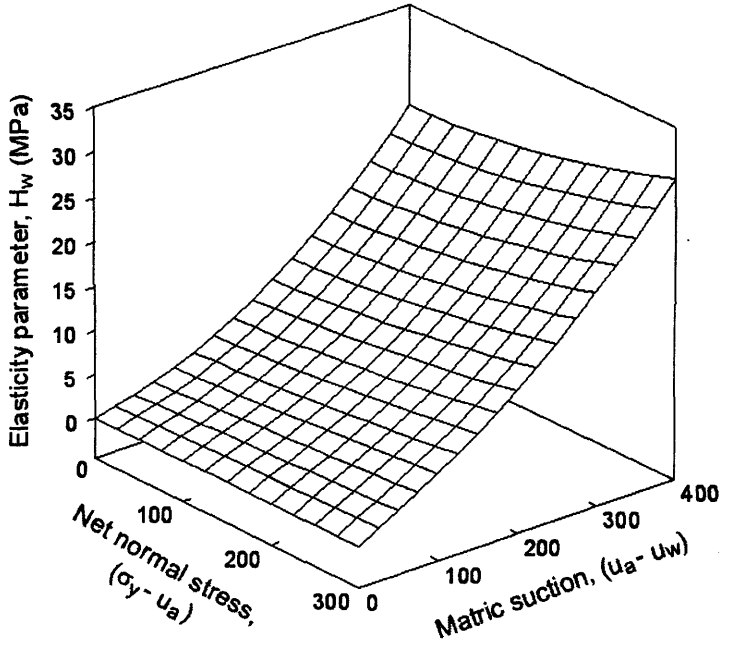

Figure 4.77 Elasticity parameter for water phase, H_w, with respect to changes in matric suction under K_0-loading condition for Regina clay

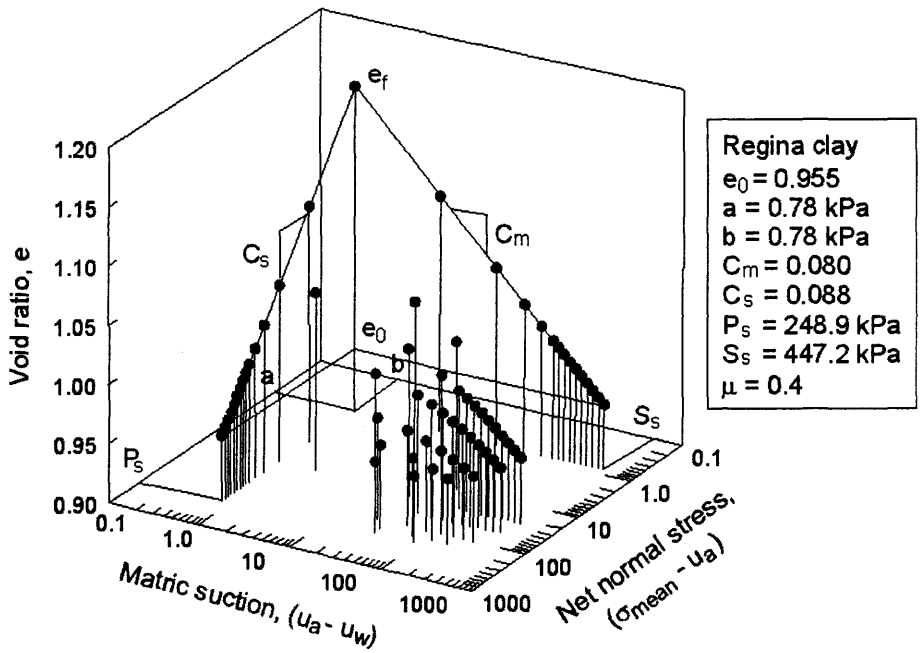

Figure 4.78 Generated void ratio data for three-dimensional unloading condition for Regina clay

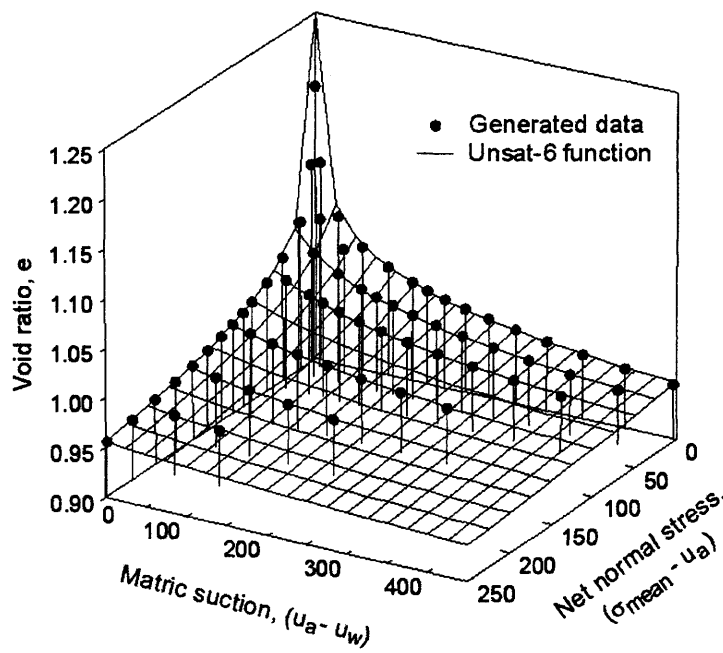

Figure 4.79 Best-fit to generated void ratio data for three-dimensional unloading condition for Regina clay

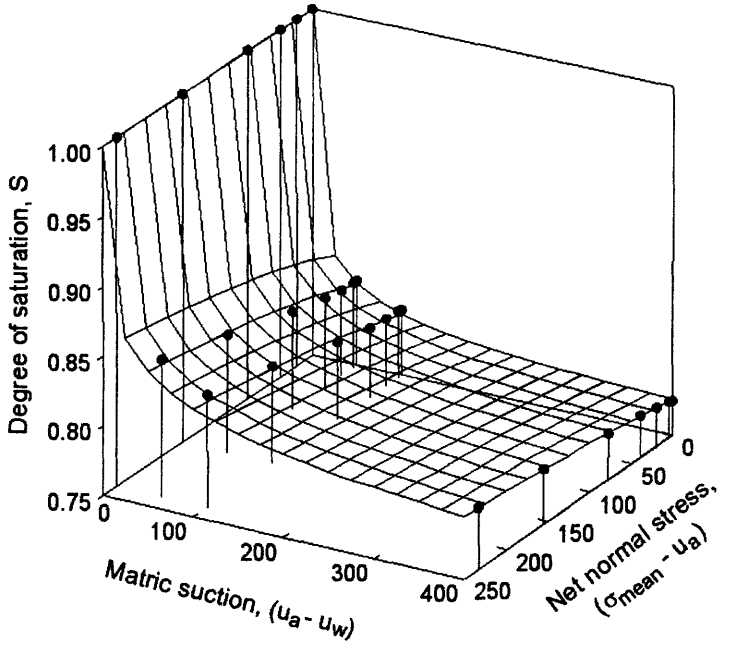

Figure 4.80 Best-fit to assumed degree of saturation data for three-dimensional unloading condition for Regina clay

Table 4.16 Fitting parameter results of general three-dimensional constitutive surfaces for Regina clay

Constitutive surface	Fitting parameters						Figure
	a	b	c	d	f	g	
Void ratio, e	1.2492	-0.0979	4.8240	4.3330	0.0009	0.0012	4.79
Degree of saturation, S	1.0000	-0.0725	0.0125	11.7265	0.0125	0.0071	4.80

The coefficient of volume change associated with soil structure and water phase can be calculated for general three-dimensional swelling (Table 2.2) by differentiating the constitutive surfaces assuming that strains are small.

$$m_1^s = \frac{1}{1+e_0}\frac{de}{d(\sigma_{mean} - u_a)} \tag{4.52}$$

$$m_2^s = \frac{1}{1+e_0}\frac{de}{d(u_a - u_w)} \tag{4.53}$$

$$m_1^w = \frac{S}{1+e_0}\frac{de}{d(\sigma_{mean}-u_a)} + \frac{e}{1+e_0}\frac{dS}{d(\sigma_{mean}-u_a)} \tag{4.54}$$

$$m_2^w = \frac{S}{1+e_0}\frac{de}{d(u_a-u_w)} + \frac{e}{1+e_0}\frac{dS}{d(u_a-u_w)} \tag{4.55}$$

The coefficients of volume change associated with the generated void ratio data (Fig. 4.79) and assumed degree of saturation surface (Fig. 4.80) are presented in Figs. 4.81, 4.82, 4.83, and 4.84.

The elasticity parameters can be calculated for general three-dimensional swelling as follows (Table 2.4):

$$E = 3\frac{(1-2\mu)}{m_1^s} \tag{4.56}$$

$$H = \frac{3}{m_2^s} \tag{4.57}$$

$$E_w = \frac{3}{m_1^w} \tag{4.58}$$

$$H_w = \frac{1}{m_2^w} \tag{4.59}$$

The elasticity parameter functions are presented graphically in Fig. 4.85, 4.86, 4.87, and 4.88.

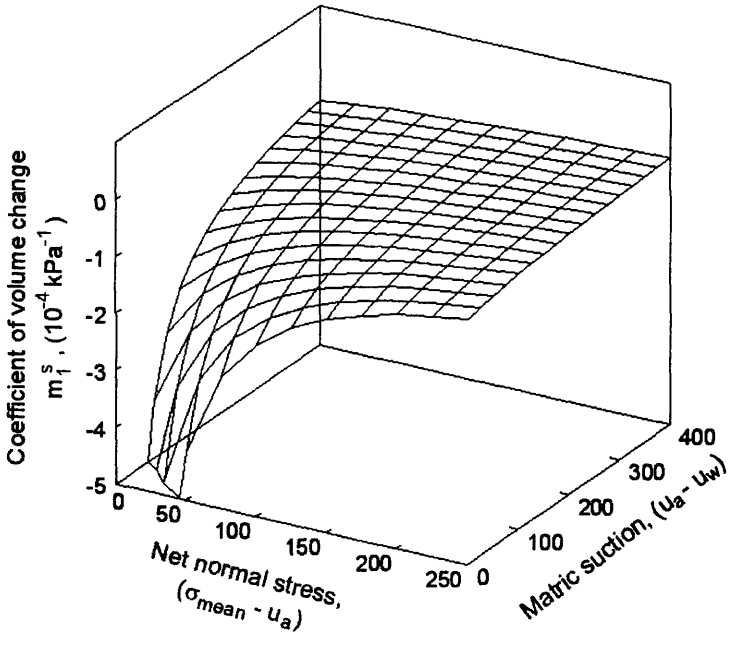

Figure 4.81 Coefficient of volume change, m_1^s, with respect to changes in net normal stress under three-dimensional unloading condition for Regina clay

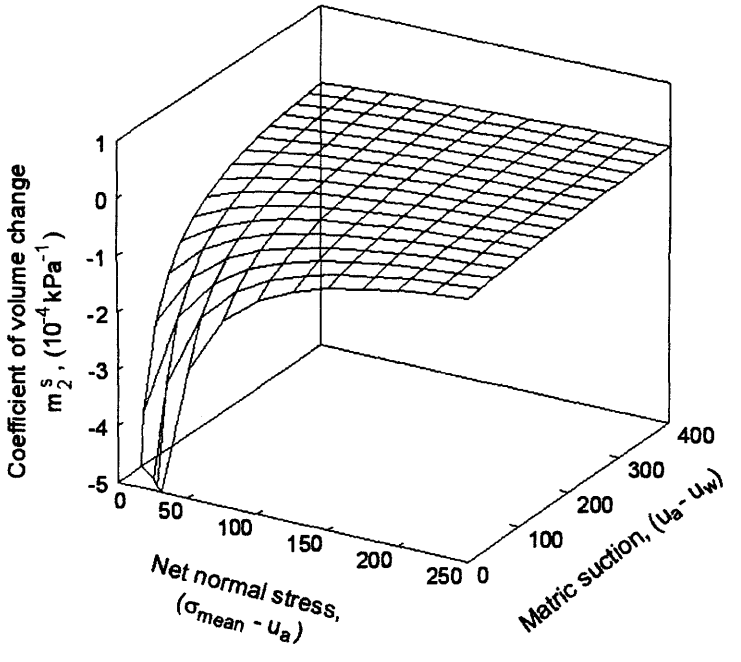

Figure 4.82 Coefficient of volume change, m_2^s, with respect to changes in matric suction under three-dimensional unloading condition for Regina clay

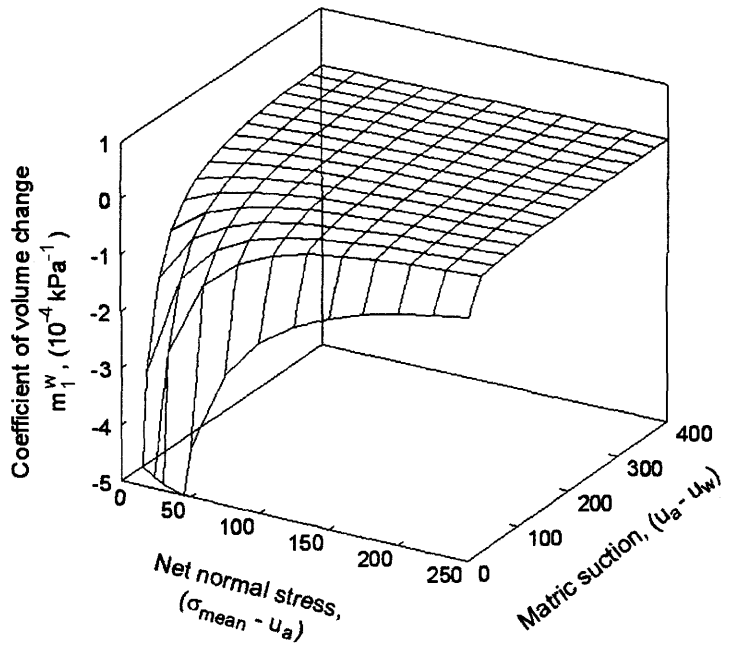

Figure 4.83 Coefficient of water volume change, m_1^w, with respect to changes in net normal stress under three-dimensional unloading condition for Regina clay

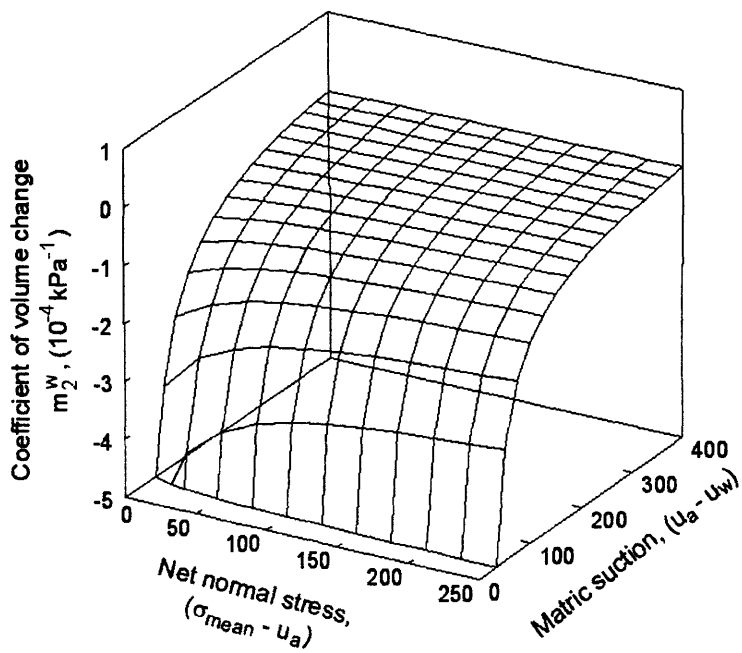

Figure 4.84 Coefficient of water volume change, m_2^w, with respect to changes in matric suction under three-dimensional unloading condition for Regina clay

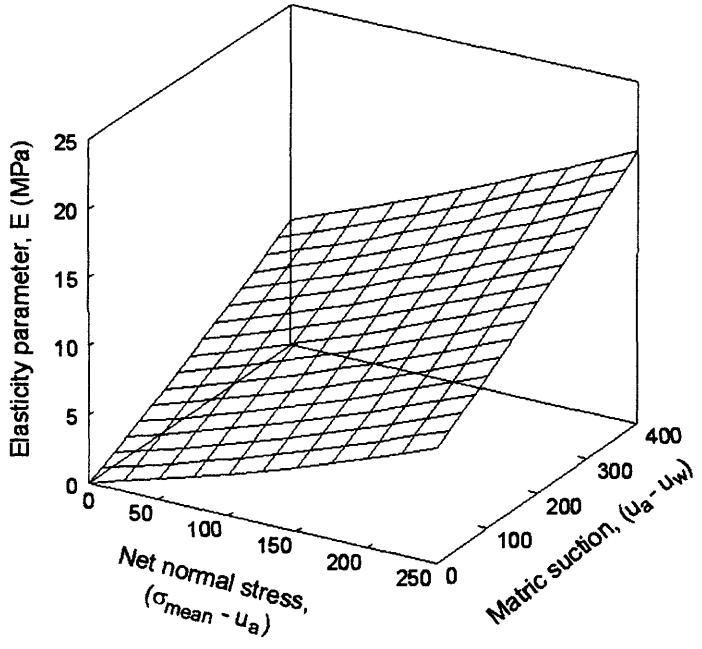

Figure 4.85 Elasticity parameter for soil structure, *E*, with respect to changes in net normal stress under three-dimensional unloading condition for Regina clay

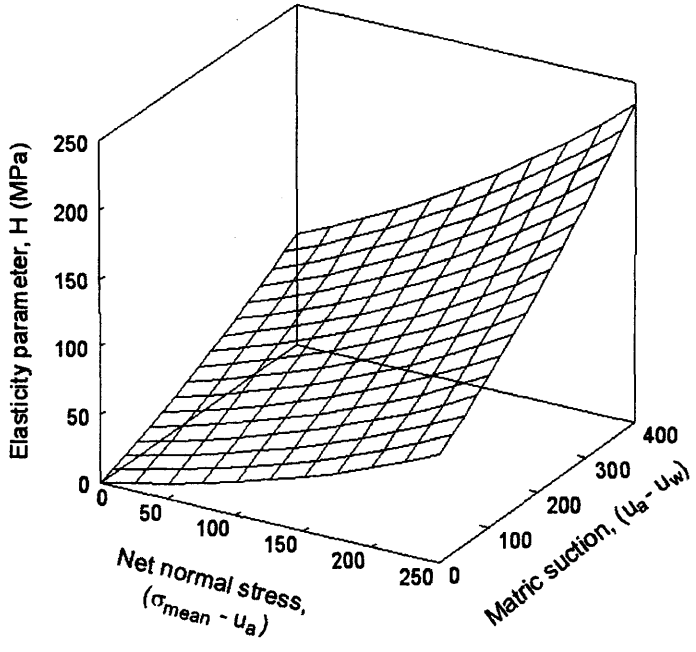

Figure 4.86 Elasticity parameter for soil structure, *H*, with respect to changes in matric suction under three-dimensional unloading condition for Regina clay

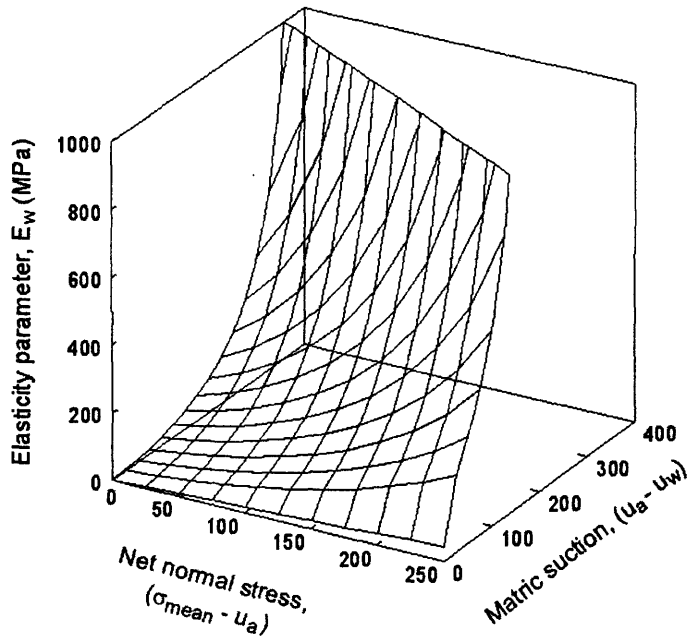

Figure 4.87 Elasticity parameter for water phase, E_w, with respect to changes in net normal stress under three-dimensional unloading condition for Regina clay

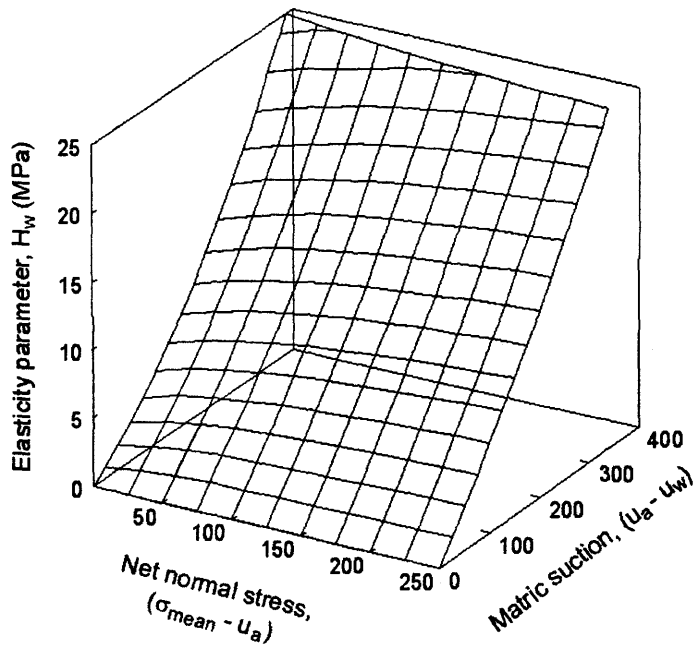

Figure 4.88 Elasticity parameter for water phase, H_w, with respect to changes in matric suction under three-dimensional unloading condition for Regina clay

4.4.5 Coefficient of permeability function

The coefficient of permeability function is predicted from the saturated coefficient of permeability and the soil-water characteristic curve. Shuai (1996) presented the coefficient of permeability function for Regina clay using Gardner (1958) equation as follows:

$$k_w = \frac{k_{w0} e^b}{1 + a\left(\frac{(u_a - u_w)}{\rho_w g}\right)^n} \tag{4.60}$$

where:

k_{w0} = 0.4×10^{-8} *m/s*,

e = void ratio,

b = 18.5,

a = 0.01, and

n = 1.1

The coefficient of permeability constitutive surface is presented graphically in Fig. 4.89 for the void ratio surface shown in Fig. 4.79.

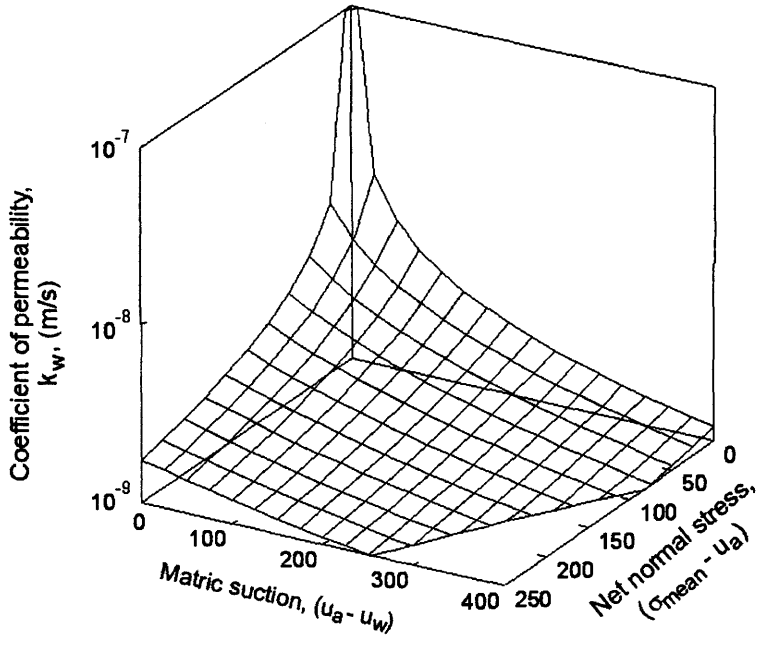

Figure 4.89 Coefficient of permeability constitutive surface for Regina clay

4.5 Summary of the theory of constitutive surfaces

Void ratio constitutive surface can be estimated from the swelling indices C_s and C_m, initial void ratio; and swelling pressure. The following assumptions are made regarding the void ratio constitutive surface: i) there is a linear relationship on the void ratio versus logarithm of net normal stress plot at an extreme net normal stress plane; ii) there is a linear relationship on void ratio versus logarithm of matric suction plot at an extreme matric suction plane; iii) the void ratio constitutive surface converges to a single point on the void ratio axis; and iv) constant void ratio plane intersects the void ratio constitutive surface at a straight line.

The problem associated with void ratio in the range of low net normal stress and low matric suction range can be solved. The solutions are obtained through the use of a mathematical equation that is continuous, smooth, physically reasonable and differentiable over the entire range of net normal stresses and matric suctions.

Mathematical equations that were originally presented as functions of only one stress state variable have been extended to describe the function with respect to second stress state variable. These equations appear to be adequate to describe the void ratio constitutive surface; however, a large number of data points are required because of the large number of the fitting parameters present in the modified equation (i.e., 11 to 15 fitting parameters). Large number of fitting parameters also presents difficulty in the fitting of the equation to the data points.

A mathematical equation is proposed in this study for the description of the entire void ratio constitutive surface. The proposed equation can also be used to describe the constitutive surface for water phase. The equation has been used successfully to characterise the soil properties of Regina clay (i.e., void ratio constitutive surface, water content constitutive surface, degree of saturation constitutive surface, SWCC, compression and rebound curves of oedometer test results).

The elasticity parameters associated with unsaturated, expansive soils can be calculated from the constitutive surfaces for the soil structure and for water phase with assumed value of Poisson's ratio. Using the equation proposed in this study, the elasticity parameters can also be calculated for the low range of net normal stress and matric suction.

CHAPTER 5

Research Program

5.1 General

Hung (2000) presented and verified an uncoupled method for one- and two-dimensional volume change analysis of unsaturated, expansive soils. Figure 5.1 shows the example problems and case histories that were analysed and discussed. This study is a continuance and extension of the previous research presented by Hung (2000).

This chapter presents the computer programs used for numerical analyses and outlines the research program of this study. The research program is required for the implementation of the swelling soil formulations presented in Chapter 3 and the theory of constitutive surface presented in Chapter 4. The layout of the research program is illustrated in Figure 5. 2. The research program involves three parts. Part 1 is a study of the effects of water uptake by trees to surrounding soils and to the footings of a house using an uncoupled approach. Part 2 includes the uncoupled and coupled solutions of two typical swelling problems (i.e., the leakage of water below floor slab and the infiltration of water from ground surface). Part 3 studies the effect of assumed Poisson's ratio on the coupled solutions.

The results of the research program, as well as the discussion of the results, are presented in subsequent chapters.

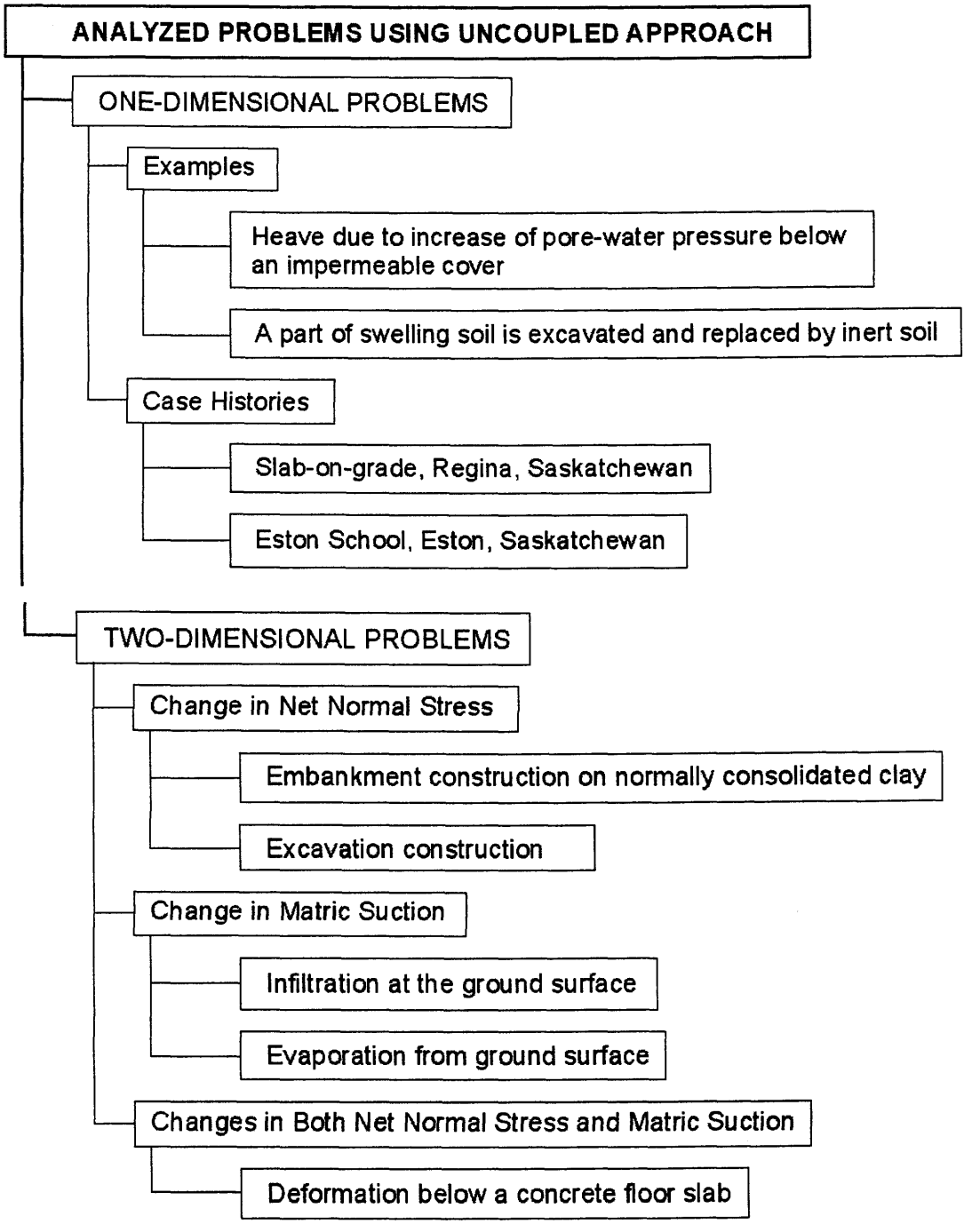

Figure 5.1 Problems analysed using the uncoupled approach by Hung, 2000

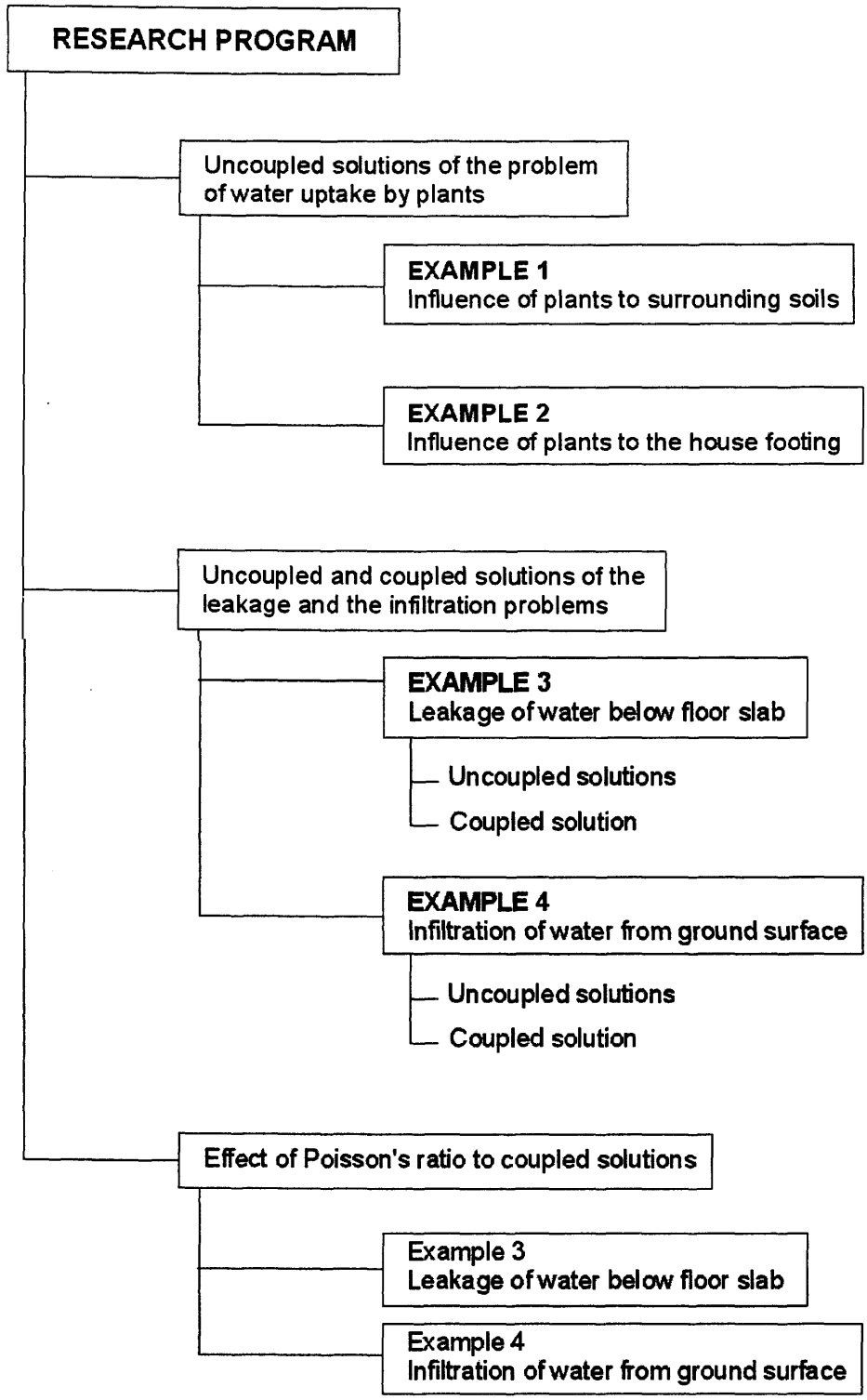

Figure 5.2 Present research program outline for this thesis

5.2 Computer programs

Several partial differential equation solvers have recently become available for solving systems of non-linear partial differential equations using the finite element method. These include FEMLAB, marketed by Comsol Inc., PDEase2D, marketed by Macsyma Inc., and FlexPDE, marketed by PDE Solutions Inc. PDEase2D and FlexPDE have been recently used at the University of Saskatchewan, Saskatoon. The use of these programs is applied to the study of behaviour of unsaturated soils. Thieu (1999) used PDEase2D to analyse saturated-unsaturated seepage problems. Hung (2000) and Hung and Fredlund (2002) solved uncoupled heave problems using PDEase2D and FlexPDE. Pentland (2000) used FlexPDE to solve problems of heat transfer in unsaturated soils. Pham (2002) used FlexPDE for the study of the slope stability problem. Verifications of the programs were presented in the research studies mentioned above.

A general-purpose partial differential equation solver, FlexPDE, is used herein for obtaining uncoupled solutions. A finite element computer program called COUPSO, is used for obtaining coupled solutions of two-dimensional volume change problems associated with unsaturated, expansive soils.

Attempts were made to use FlexPDE for coupled solutions. However, the attempts were not successful because the elastic parameter functions with respect to net normal stress cannot be handled automatically and the cross derivatives in coupled equations cannot be defined.

A brief description of FlexPDE and COUPSO programs is presented in the following sections.

5.2.1 Partial differential equation solver, FlexPDE

FlexPDE is a general-purpose computer program that can be used to solve systems of first or second order partial differential equations in Cartesian or axi-symmetric two-dimensional geometry, or in three-dimensional Cartesian geometry. The system can be steady-state or time-dependent. The equations can be linear or non-linear. Non-linear equations are solved by applying a modified Newton-Raphson iteration

process. Boundary conditions can be specified as a dependent variable type or as the derivative of a dependent variable type.

FlexPDE combines several modules to provide a problem solving system. A script-editing module provides a text editing facility and a graphical domain preview. A symbolic equation analyzer expands defined parameters and relations, performs spatial differentiation, and symbolically applies integration by parts to reduce second order terms to create Galerkin equations. These equations are then differentiated to form the Jacobian matrix. A mesh generation module constructs a triangular finite element mesh over a two-dimensional problem domain. A finite element numerical analysis module selects an appropriate solution scheme for steady-state, time-dependent or eigenvalue problems, with separate procedures for linear and nonlinear systems. The finite elements may be either quadratic or cubic. An error estimation procedure measures the adequacy of the mesh and refines the mesh wherever the error is large. The system iterates the mesh refinement for the solution until a user-defined error tolerance is achieved. A graphical output module accepts arbitrary algebraic functions of the solution and plots contours, surface, vector or elevation plots. A data export module writes text reports in several formats, including simple tables and full finite element mesh data.

This software package has several special features that are of interest to geotechnical engineers. Major features of the FlexPDE program include:

- AutoCAD style CAD input,
- automatic mesh generation and refinement,
- adaptive time step design and refinement,
- ensuring convergence when solving non-linear equations,
- allowing material properties to be input in a variety of forms, and
- input three-dimensional problems as surfaces and layers using survey data.

More details on the FlexPDE program are presented in the FlexPDE reference manual.

5.2.2 Computer program, COUPSO

COUPSO program was developed by Pereira (1996) to solve a coupled problem of a small earth dam associated with unsaturated, collapsing soils. The program implements coupled equations presented in Section 3.6, which couples stress equilibrium and water flow in unsaturated soils (Fredlund and Rahardjo, 1993). The saturated condition of the soil is a special case of the general theory of unsaturated soil. COUPSO uses the concept of incremental loading in order to simulate changes that occur in the soils.

The COUPSO program uses two-dimensional nine-node finite elements. Interpolation is performed by using Lagrange's polynomials. Integration is performed by using Gauss-Legendre quadrature. The program has been changed to accommodate a coupled analysis for volume change problems associated with unsaturated, expansive soils in this study. A detailed description of the program and its verification were presented in Pereira (1996).

5.3 Uncoupled solutions to the problem of water uptake by trees

The effects of water uptake by tree roots on lightly loaded structures are studied using the uncoupled approach. A series of factors that influence the magnitude of damage to engineering structures are analysed. These factors are water uptake rate, root zone (e.g., the roots of trees), soil and groundwater conditions, foundation depth and the distance from trees.

Two typical two-dimensional examples are analysed and discussed. The first example, called Example 1, is associated with deformations in a soil profile due to water being extracted from the root zone within a soil mass. The root zone is simulated as a flux applied to the soil mass. The second example, called Example 2, is associated with the settlement of a house caused by a line of trees growing close to the house. Computer program FlexPDE is used for both the unsaturated seepage and stress-deformation analyses associated with the uncoupled approach.

Soil properties are assumed as follows. The coefficient of permeability of the soil is described using Gardner's (1958) equation with a saturated coefficient of permeability equal to 5.79×10^{-8} m/s (i.e., 5 mm/day), and parameters a and n equal to

0.001 and 2, respectively. The initial void ratio of the soil is equal to 1.0, the volume change index with respect to matric suction, C_m, is equal to 0.2 and Poisson's ratio is assumed to be 0.3.

The elastic modulus function, H, with respect to changes in suction for the soil can be calculated from Eq. (2.30) for plane strain conditions.

$$H = 59.9\ (u_a - u_w) \tag{5.1}$$

The coefficient of permeability function and the elastic modulus function are shown graphically in Fig. 5.3.

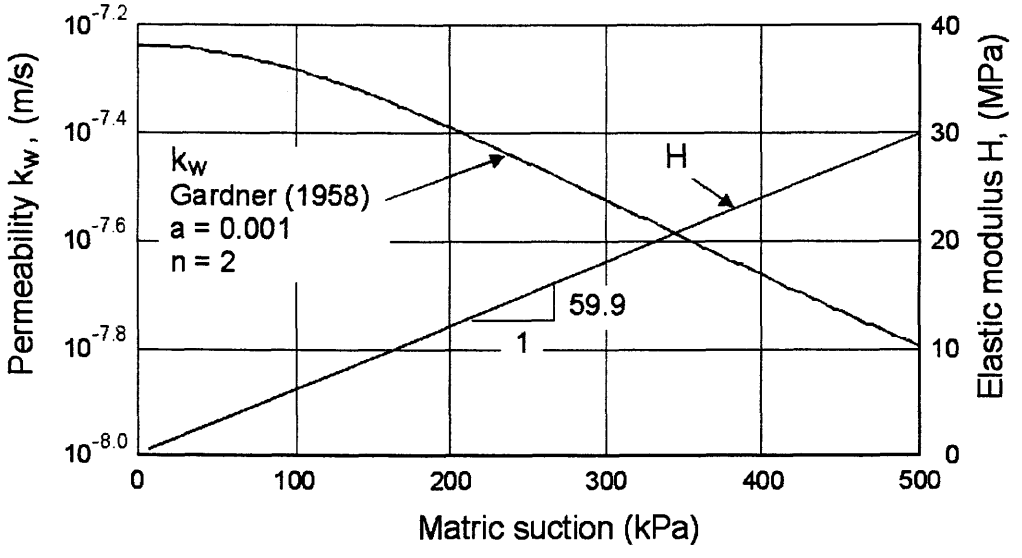

Figure 5.3 Permeability function, k_w and elastic modulus function, H, used for Example No. 1 and Example No. 2

5.3.1 Example 1: Influence of plants on surrounding soils

The first example problem is associated with the deformation that can be caused by a line of trees. It is assumed that the trees are planted in a line at 5 m intervals. The example considers a 10 m thick layer of clay soil (Fig. 5.4). The geometry of the problem is symmetrical, and therefore, only half of the geometry needs to be considered in the analysis.

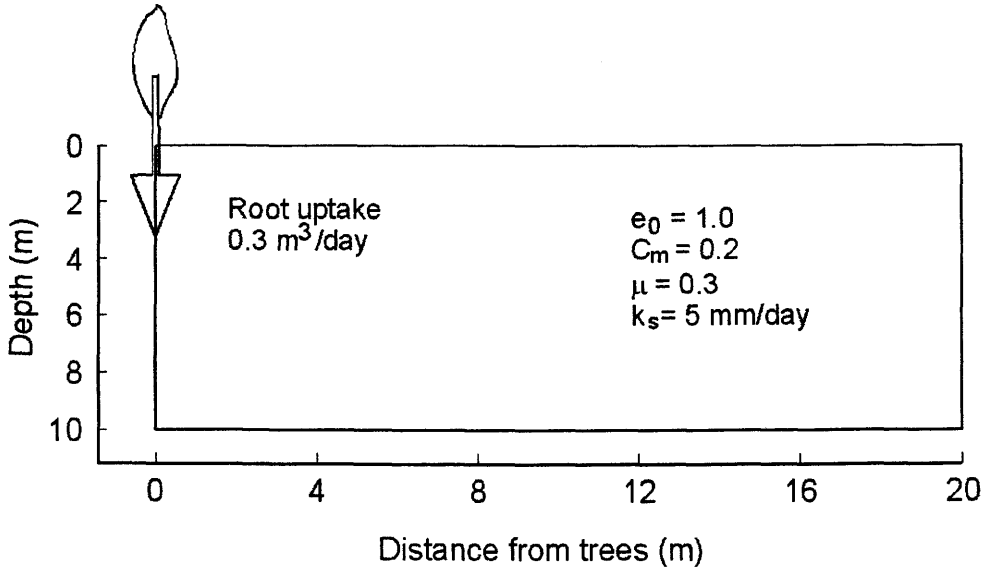

Figure 5.4 Illustration of the geometry and key variables for Example 1

The coefficient of permeability function and the elastic modulus function with respect to changes in matric suction shown in Fig. 5.3 are used for analysis. These functions are assumed to be independent of net normal stress in the soil profile for Examples No. 1 and No. 2.

The initial matric suction is computed based on a hydrostatic condition with an unchanged ground water table at the 15 m depth. This represents the water content conditions in the soil during the winter when water uptake by the trees is low. It is then assumed that one tree will extract 0.3 m^3 of water per day in summer and eventually steady state conditions are attained. A value for water uptake of 0.25 to 0.5 m^3/day was suggested by Perpich et. al. (1965). The water uptake zone for the trees is from the 1 m to 3 m depth, with the uptake rate decreasing linearly with depth. This pattern of water uptake from the tree root zone was suggested by de Jong (2000). Deformations in the soil profile due to water uptake by trees (i.e., from initial to final matric suction states) are predicted. The example is also analysed for various values of volume change indices and water uptake rates.

5.3.2 Example 2: Influence of plants on the footings of the houses

Example 2 simulates the settlement of a house caused by a row of trees growing close to the house. This example is illustrated in Fig. 5.5. The house foundation is placed at a 2 m depth in a clay soil layer that is 10 m thick. The line of trees is 4 m from the house. The water uptake rate for the trees is 0.5 m^3/day per tree and the water uptake zone is from 1 m to 3 m depth. It is assumed that the groundwater table is unchanged at 15 m below ground surface. A layer of 0.3 m thick of concrete with an elastic modulus of 100,000 kPa is used to describe the foundation and basement walls of the house. The soil properties are the same as those used in Example 1 (Fig. 5.3). Detailed boundary conditions are presented in the next chapter.

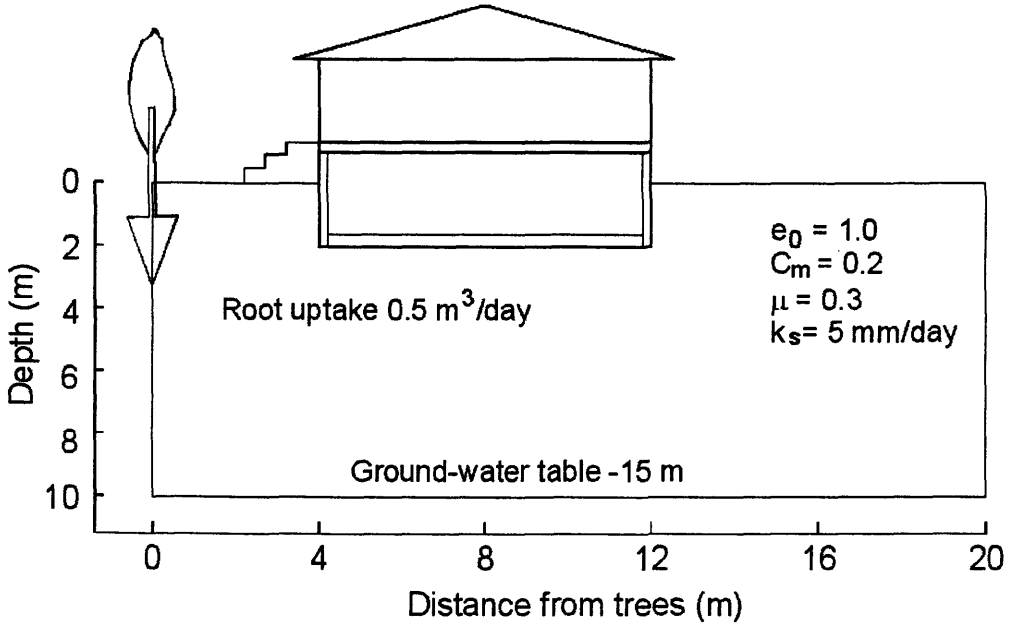

Figure 5.5 Illustration of the geometry and key variables for Example 2

A parametric analysis is also performed to study the influence of the depth of the root zone, distance from the trees to the house, thickness of the expansive soil layer and the rate of water uptake by tree to the house footing. The variables used in this study are illustrated in Fig. 5.6. The root zone equal to 2 m (i.e., Z = 2 m) was assumed for all analyses. Various combinations of the parameters are presented in

Table 5.1. Settlements at points A, B, and C for each combination of the parameters are predicted. The variables shown in Fig. 5.6 are as follows:

D = distance from tree row to the house,

H = thickness of the swelling soil profile,

R = soil depth of water uptake,

F = depth of foundation,

Distance between trees in a row = 5 m,

Width of the house = 8 m, and

Swelling index with respect to matric suction, $C_m = 0.07$.

Table 5.1 Various combinations of parameters for the analysis of Example 2

Case	D (m)	H (m)	F (m)	R (m)	Water uptake m^3/day
1	4	10	0.3	2	0.5
2	4	10	0.3	2	0.3
3	4	10	0.3	2	0.1
4	4	10	0.3	1	0.5
5	4	10	0.3	1	0.3
6	4	10	0.3	1	0.1
7	6	10	0.3	2	0.5
8	6	10	0.3	2	0.3
9	6	10	0.3	2	0.1
10	6	10	0.3	1	0.5
11	6	10	0.3	1	0.3
12	6	10	0.3	1	0.1
13	4	6	0.3	1	0.5
14	4	8	0.3	1	0.5
15	4	12	0.3	1	0.5
16	4	10	0.3	3	0.5
17	10	10	0.3	1	0.5
18	4	10	0.6	1	0.5
19	4	10	1.0	1	0.5
20	4	10	2.0	1	0.5

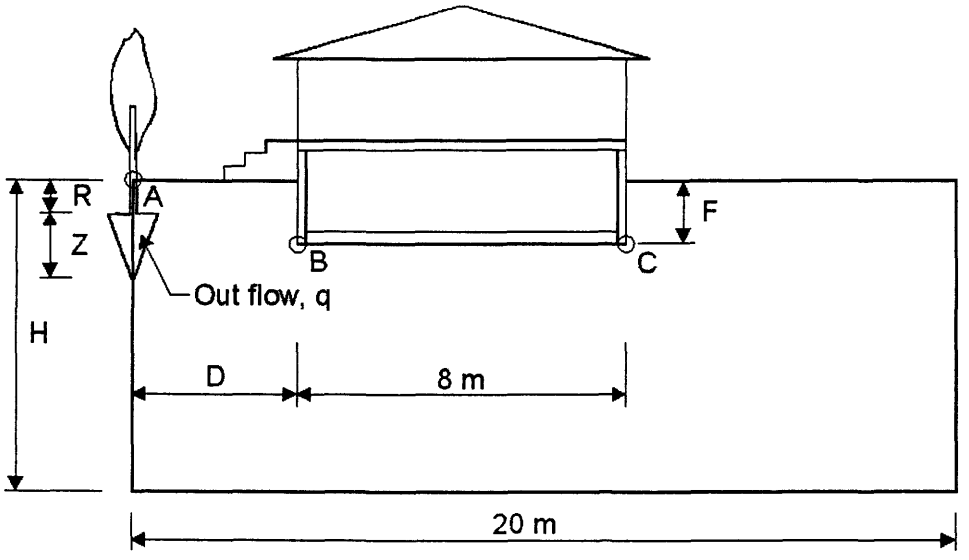

Figure 5.6 Illustrations of parameters for sensitivity study, Example 2

5.4 Uncoupled and coupled solutions of the leakage and the infiltration problems

The objective of this part of the research program is to analyse volume change problems associated with an unsaturated, swelling soil using two different approaches (i.e., uncoupled and coupled approaches). This section presents another two problems, one associated with the leakage of water under a flexible cover (i.e., Example 3), and the other problem is associated with water infiltration into a soil mass (i.e., Example 4). These two example problems are analysed using both an uncoupled and a coupled approach. The uncoupled solutions and coupled solutions are then compared. Experimental data obtained from tests on compacted Regina clay specimens are used for these examples.

Uncoupled solutions are obtained using the FlexPDE program, and coupled solutions are obtained using the COUPSO program.

The soil properties used for the uncoupled and coupled analyses in this section were shown in Chapter 4 for Regina clay. Fig. 4.79 presented the void ratio constitutive surface, Fig. 4.80 presented the degree of saturation constitutive surface and Fig. 4.89 showed the coefficient of permeability function. The void ratio

constitutive surface was estimated from swelling indices and swelling pressures for Regina clay. The void ratio constitutive surface and degree of saturation constitutive surface were described using the mathematical equation suggested in this study [i.e., Eq. (4.37)]. A Poisson's ratio equal to 0.4 was assumed. It was observed that the assumed value of Poisson's ratio affects the results of two- and three-dimensional volume change problems. However, the most realistic function for Poisson's ratio was not a subject of this study. The elastic parameter functions, E, H, E_w, *and* H_w were calculated from the constitutive surfaces and presented graphically in Figs. 4.85, 4.86, 4.87, and 4.88, respectively.

There are several approaches used in the uncoupled analysis. The differences arise from the stress state used for the seepage and stress-deformation analyses. Four types of uncoupled analysis were used in this research study. The uncoupled solutions obtained from these analyses are named as UCS1, UCS2, UCS3, and UCS4. The solution obtained using a coupled approach is named as CS. The stress path followed in each type of analysis is shown in Figs. 5.7 and 5.8 for the seepage and stress-deformation analyses, respectively. It should be noted that initial stress state may vary from one type of uncoupled analysis to another, while boundary conditions remain the same.

In the UCS1 uncoupled analysis, soil properties obtained for the extreme plane are used for the entire constitutive surface. Therefore, net normal stress is not considered for both the seepage and stress-deformation analysis. No volume change and no changes in stress were assumed in the seepage analysis. A net mean stress of 0.78 kPa (at which the volume change index, C_m, was obtained) was used for the UCS1 uncoupled analysis in this study.

In the UCS2 uncoupled analysis, the variation in the stress state in the soil profile under initial stress state conditions was considered. Zero volume change and no changes in net normal stress were assumed in the seepage analysis. No change in net normal stress was considered in the stress-deformation analysis.

In the UCS3 uncoupled analysis, the assumptions related to the seepage analysis are the same as those used in the UCS2 analysis; however, changes in net normal stress are considered in the stress-deformation analysis.

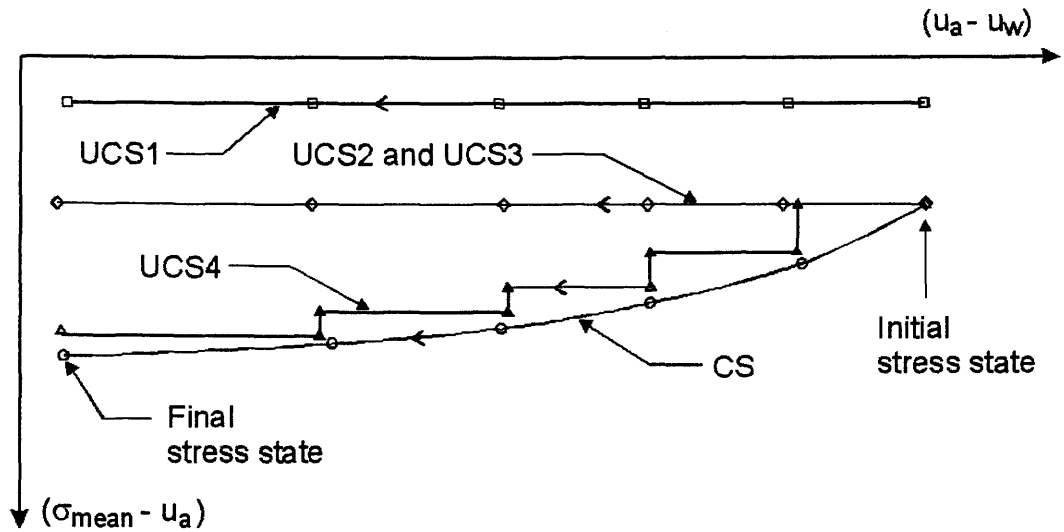

Figure 5.7 Stress path followed by various types of seepage analysis

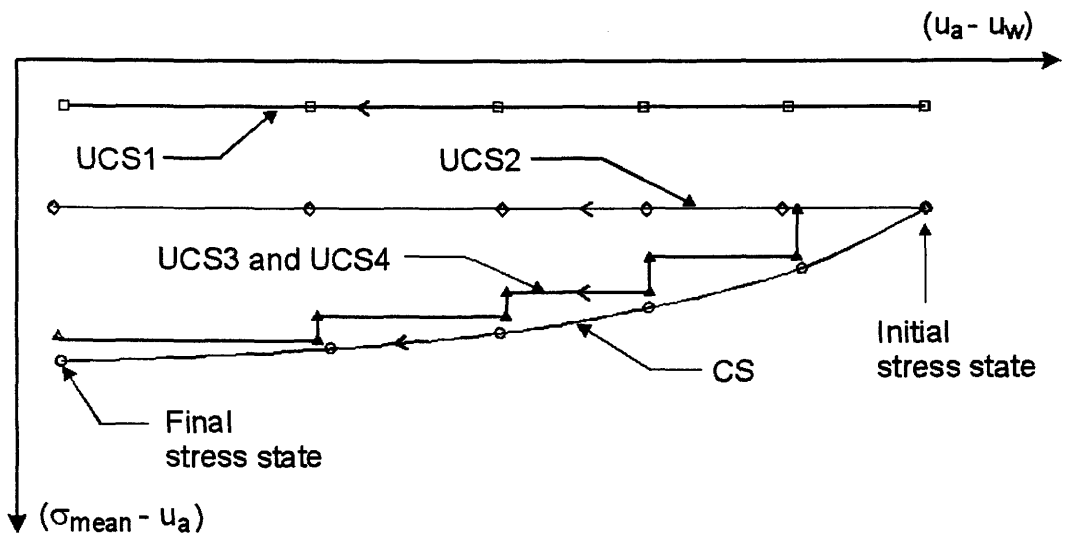

Figure 5.8 Stress path followed by various types of stress-deformation analysis

In the UCS4 uncoupled analysis, the changes in volume and changes in net normal stress are considered in both the seepage and stress-deformation analysis. Variations in the stress state in the soil better reflect the stress state conditions in the real problem (i.e., in coupled analysis).

The examples presented in this section are analysed using various types of uncoupled analysis and the results are then compared with the coupled solutions.

5.4.1 Example 3: Leakage of water from below a floor slab

Example 3 considers the hypothetical case of a 5 m layer of swelling clay below a flexible cover (Fig. 5.9). The initial matric suction is taken to be constant throughout the depth and equal to 400 kPa. The initial stress conditions can be calculated using the total stress theory assuming that the coefficient of earth pressure at-rest, K_0, is equal to 0.67. It is assumed that a leaking water line produced zero pore-water pressure under the cover. Deformation and matric suction profiles versus time were computed.

Experimental data obtained from tests on compacted specimen of Regina clay are used for the analysis.

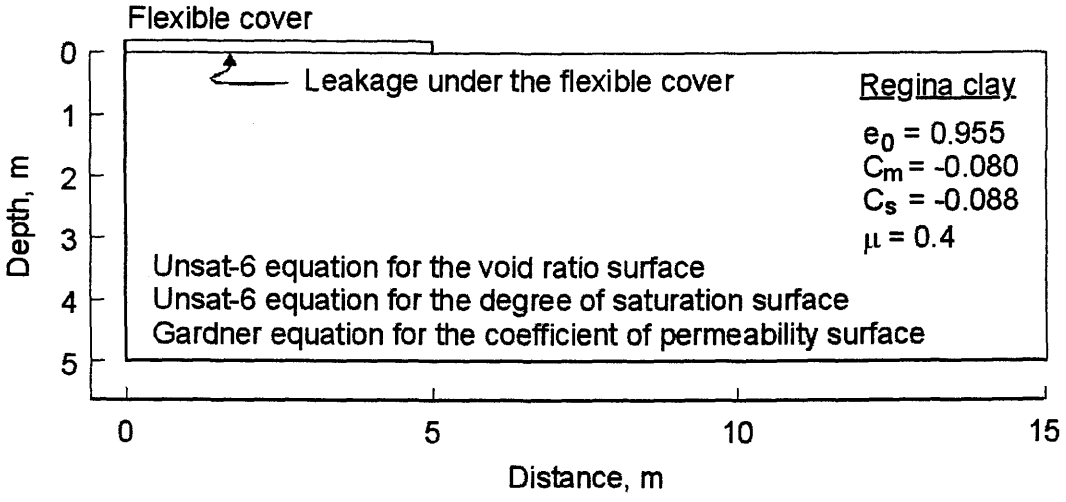

Figure 5.9 Illustration of the geometry and key variables for Example 3

5.4.2 Example 4: Infiltration of water from ground surface

This example considers the hypothetical case of a 5 m deep deposit of swelling clay. The surface is partially covered with a flexible cover (Fig. 5.10). The initial matric suction in the soil mass is assumed to be constant and equal to 400 kPa. The coefficient of earth pressure at-rest, K_0, is equal to 0.67 for the calculation of initial

stress condition. The transient wetting process is introduced by imposing a water infiltration rate equal to $2x10^{-8}$ m/s at the uncovered portion of the ground surface. Such a wetting condition simulates the water infiltration into the soil mass due to the watering of a lawn or a light rain. The analysis is performed to track both the swelling soil behaviour and matric suction changes as the transient wetting front advances into the soil mass.

Experimental data obtained from tests on compacted specimens of Regina clay are used for the analysis.

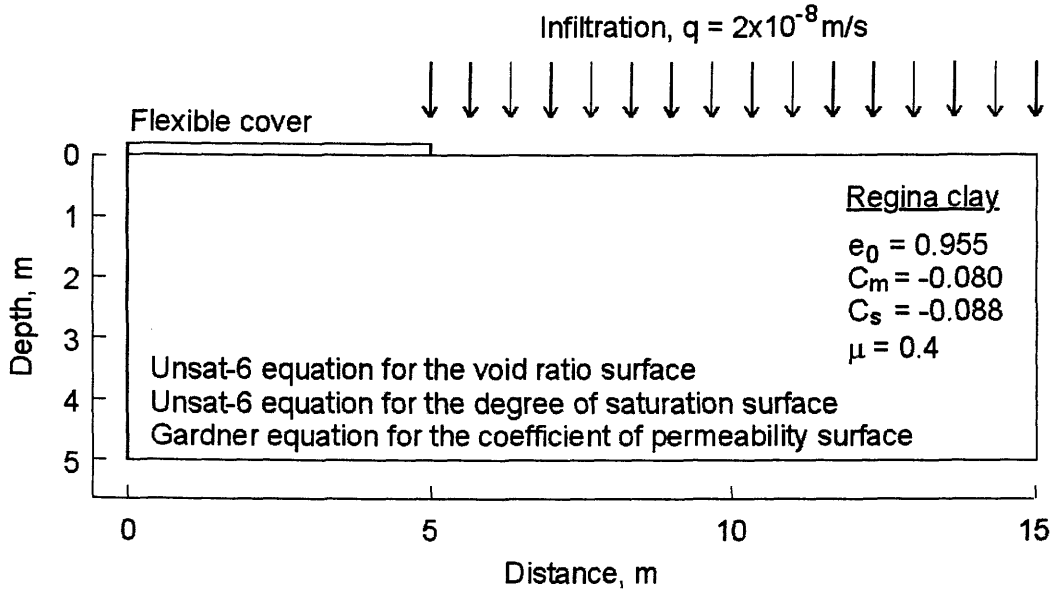

Figure 5.10 Illustration of the geometry and key variables for Example 4

5.5 Parametric study with respect to the assumed value of Poisson's ratio for coupled solutions

As presented in Sections 2.2.2.3 and 4.4, the elasticity parameters are calculated from the constitutive surfaces for the soil structure and water phase assuming a fixed value of Posson's ratio. This section is designed to study the effect of the assumed value of Poisson's ratio on coupled solutions. Two example problems (i.e., Example 3 and

Example 4) are analysed using a coupled approach for various values of Poisson's ratio.

5.6 Summary of the research program

Two computer programs are used to analyse volume change associated with an unsaturated, expansive soil. The FlexPDE program was used for both unsaturated seepage and stress-deformation analyses as part of the uncoupled approach. The COUPSO program was used for the coupled seepage and stress-deformation analysis.

The influence of water uptake by tree root system on surrounding soils and the footings of the house was analysed using an uncoupled approach through Example 1 and Example 2. The coefficient of permeability and the elastic parameter with respect to changes in matric suction were assumed to be function of matric suction (i.e., independent with net normal stress).

Example 3 and Example 4 were analysed by using both uncoupled and coupled approaches. There are several types of uncoupled analyses. The differences arise from the assumptions related to the stress path followed in the seepage analysis and stress-deformation analysis in the uncoupled solutions. Soil properties presented in Chapter 4 for Regina clay, with an assumed value for Poisson's ratio were used for both examples.

The effect of the assumed value of Poisson's ratio was studied for coupled solutions associated with Example 3 and Example 4.

The results of the analyses are presented in Chapter 6 and the discussion of the results is presented in Chapter 7.

CHAPTER 6

Presentation of Results

6.1 General

This chapter presents the results of the research program outlined in chapter 5. The research program of this study involves three parts. Part 1 study the effects of water uptake by trees to surrounding soils and to the footings of the house using an uncoupled approach. Part 2 includes the uncoupled and coupled solutions of two typical swelling problems, i.e., the leakage of water below floor slab and the infiltration of water from ground surface. Part 3 studies the effect of assumed Poisson's ratio to coupled solutions.

Uncoupled solutions are obtained using FlexPDE program, and Coupled solutions are obtained using COUPSO program. The errors associated with numerical analyses and the validation of the results are presented in Appendix D.

The discussions and comparisons of the results are presented in the next chapter.

6.2 Uncoupled solutions of the problem of water uptake by trees

The results of two example problems associated with water uptake by trees are presented. The first example is associated with deformations in a soil profile due to water being extracted from the root zone within a soil mass. The second example is associated with the settlement of a house footing caused by a line of trees growing close to the house. A series of factors that influence the magnitude of deformations are analysed. The results of analyses presented in this section were obtained using FlexPDE with an uncoupled approach.

6.2.1 Example 1: Influence of plants to surrounding soils

This example was illustrated in Fig. 5.4. The permeability function, k_w, and the elastic parameter function, H, with respect to changes in matric suction were shown in Fig. 5.3.

Figure 6.1 shows boundary conditions for seepage analysis. For initial suction conditions, a –15 m total head was specified at the lower boundary and zero flux was applied at the other boundaries. For final matric suction conditions, a –15 m total head was specified at the lower boundary. A boundary outflow value was specified along the left side of the soil domain at a depth from 1 m to 3 m and zero flux was specified at other boundaries. The outflow value decreased linearly from 15 mm/day at the 1 m depth to zero mm/day at the 3 m depth. This boundary condition represents 0.3 m^3/day of water being extracted by one tree from the soil (i.e., 2 sides x 2 m depth x 5 m wide x 15 mm/day = 0.3 m^3/day).

The matric suction distributions in the soil at equilibrium are shown in Figs. 6.2 and 6.3 for initial and final conditions, respectively. The initial matric suction varied from 147 kPa at ground surface to 49 kPa at the 10 m depth. The final matric suction varied from 260 kPa at tree root depth to 49 kPa at the 10 m depth.

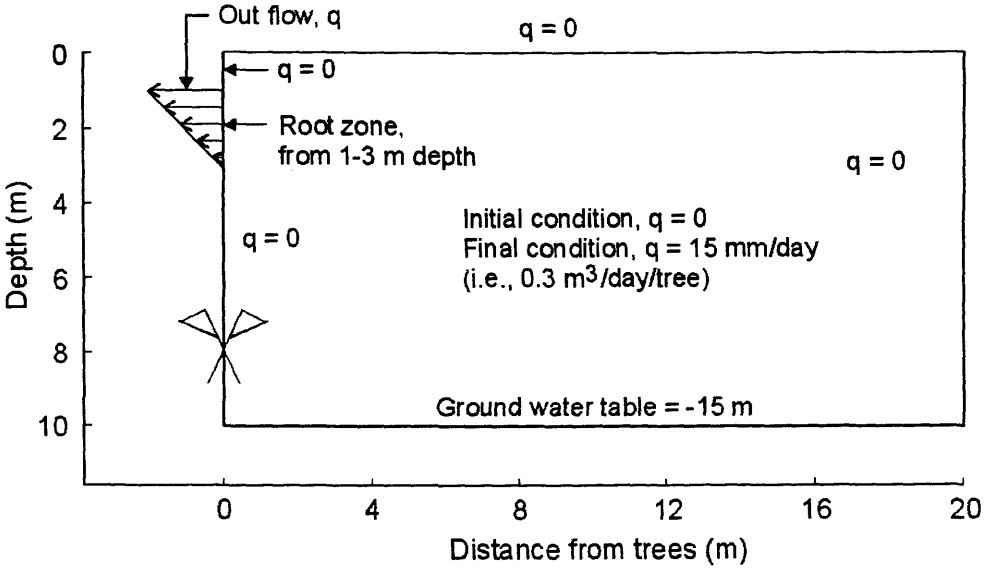

Figure 6.1 Boundary conditions for seepage analysis, Example 1

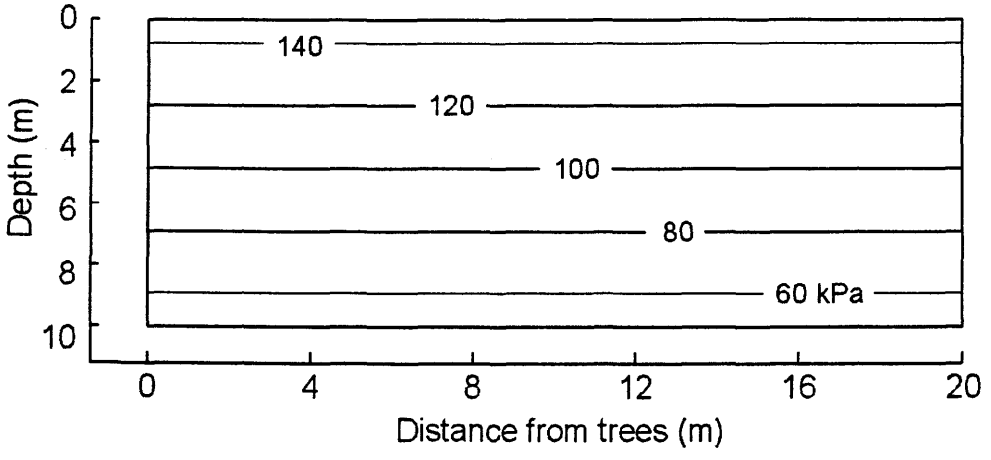

Figure 6.2 Distribution of initial matric suction (kPa), Examples 1 and 2

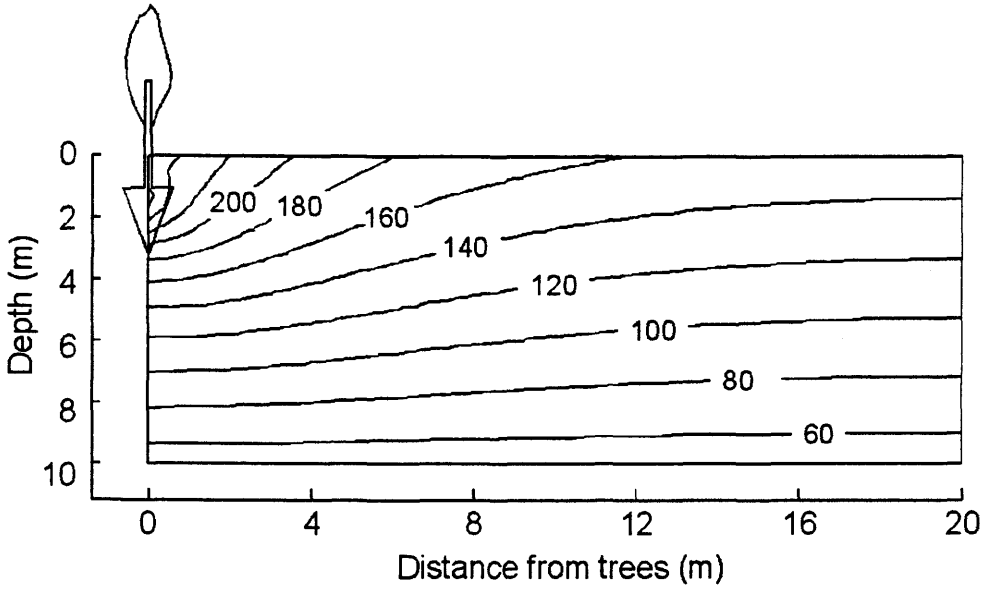

Figure 6.3 Distribution of final matric suction (kPa), Example 1

The deformations in the soil profile due to water uptake by tree roots was then predicted using the stress-deformation analysis. The boundary condition for the stress-deformation analysis is shown in Fig. 6.4. The soil was free to move in the vertical direction and fixed in horizontal direction at the left and right sides of the domain. The lower boundary was fixed in both directions.

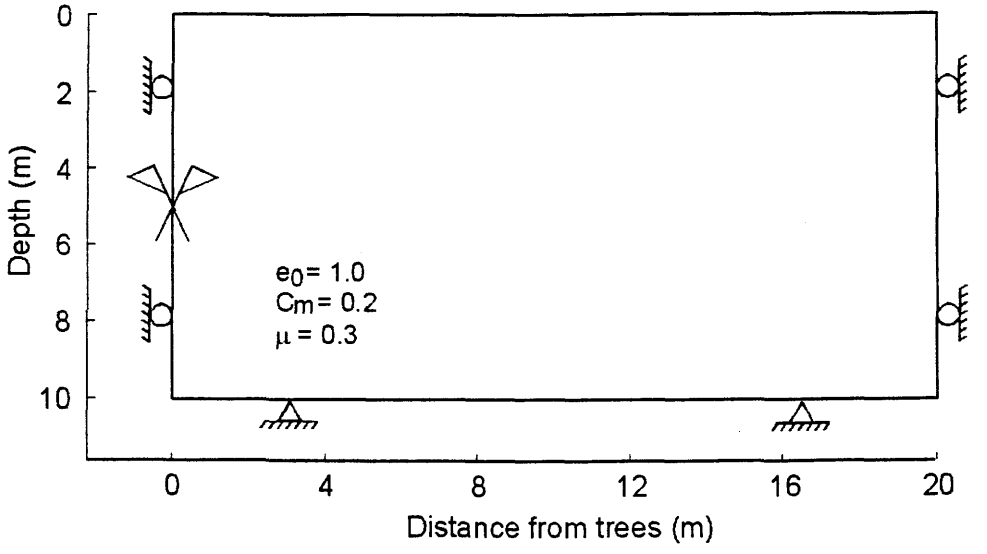

Figure 6.4 Boundary conditions for stress-deformation analysis, Example 1

Figure 6.5 presents contours of vertical displacement in the soil for this example, with the volume change index with respect to matric suction, C_m, equal to 0.2 and the tree-root uptake rate equal to 0.3 m^3/day per tree. The ground movements at various depths are shown in Fig. 6.6.

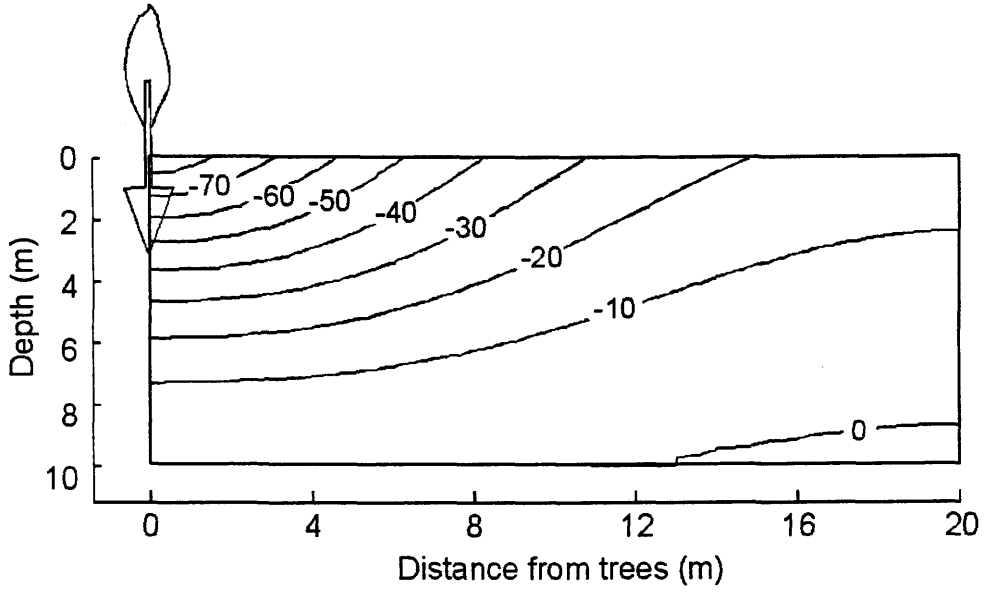

Figure 6.5 Contours of vertical displacement (mm), Example 1

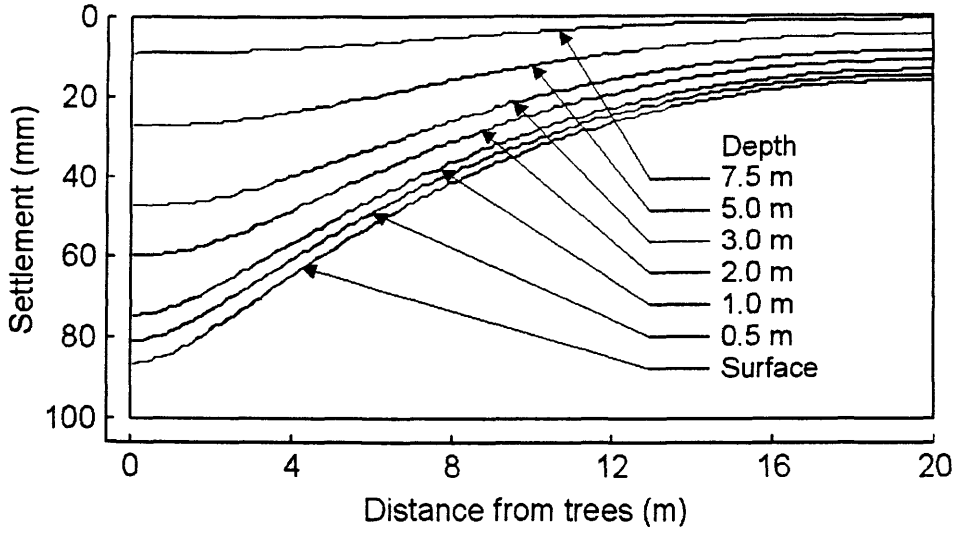

Figure 6.6 Variation with depth of vertical displacement near a tree, Example 1

The example was also analysed for the case where the water uptake rate was 0.3 m^3/day and the volume change index varied with overburden pressure in soils (i.e., volume change index decreases linearly from 0.2 at ground surface to 0.05 at the 10 m depth). Contours of vertical displacement are presented in Fig. 6.7 for this case.

Figure 6.8 presents contours of settlement for the case of a volume change index, C_m equal to 0.2 and a water uptake rate equal to 0.5 m^3/day.

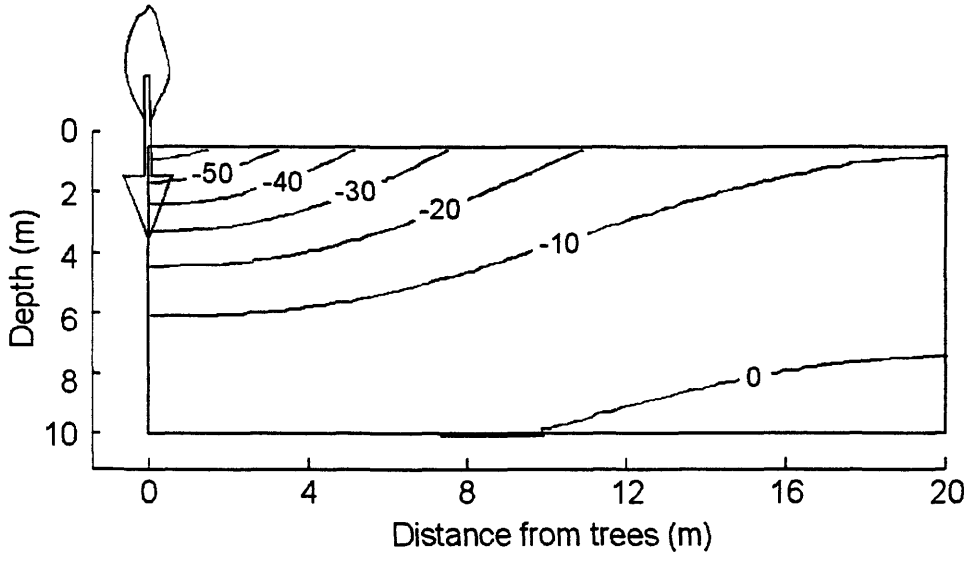

Figure 6.7 Contours of vertical displacement (mm), Example 1. Volume change index varies from 0.05 at 10 m depth to 0.2 at surface

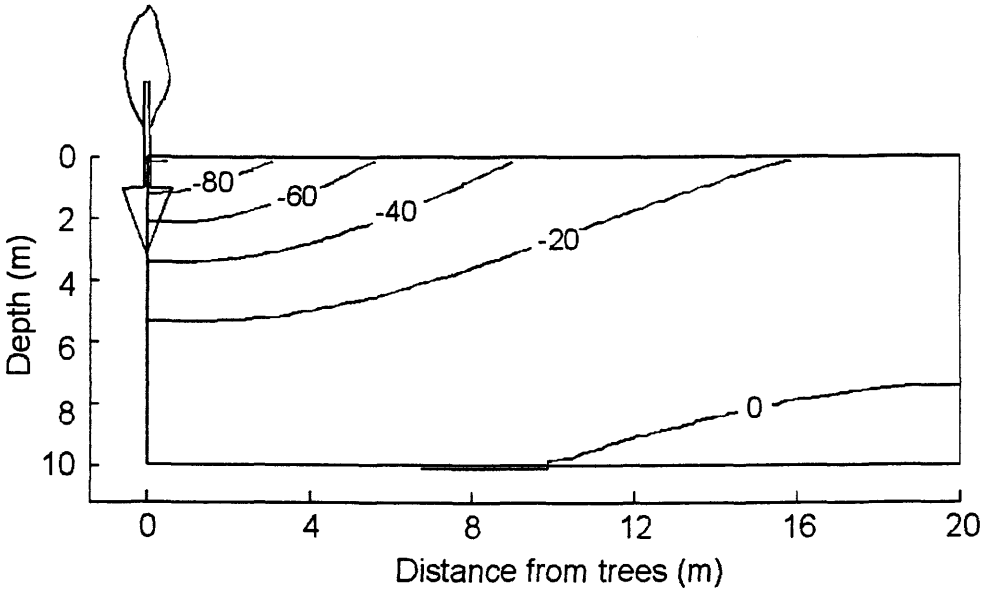

Figure 6.8 Contours of vertical displacement (mm), Example 1. Water uptake is 0.5 m^3/day

6.2.2 Example 2: Influence of plants on the house footing

This example is illustrated in Fig. 5.5. Soil properties are the same as those used in Example 1 (Fig. 5.3). Matric suction conditions in the soil profile were obtained through steady state unsaturated seepage analyses. Boundary conditions specified for this example are shown in Fig. 6.9. The initial matric suction profile is the same as that shown in Fig. 6.2. The final matric suction profile is shown in Fig. 6.10. Final matric suctions varied from 409 kPa at tree root level to 49 kPa at the lower boundary of the soil domain. The contours of changes in matric suction are presented in Fig. 6.11.

Figure 6.12 presents the boundary conditions for the stress-deformation analysis associated with this example. A 0.3 m thick layer of concrete with an elastic modulus of 100,000 kPa is used to describe the foundation and basement walls of the house. The results of the stress-deformation analysis are shown in Figs. 6.13 and 6.14 as contours of horizontal displacement and contours of vertical displacement, respectively.

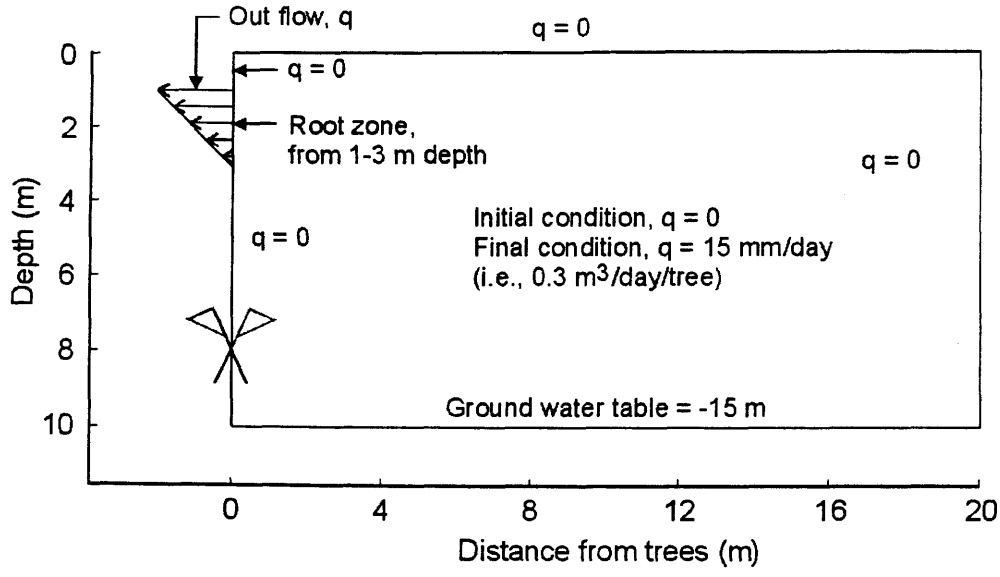

Figure 6.9 Boundary conditions for seepage analysis, Example 2

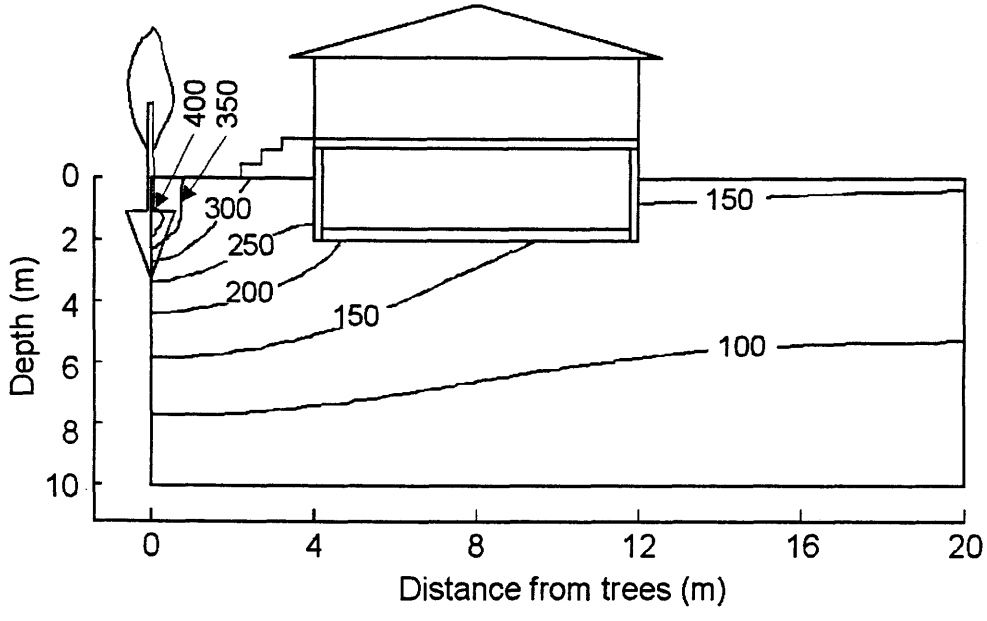

Figure 6.10 Distribution of final matric suction (kPa), Example 2

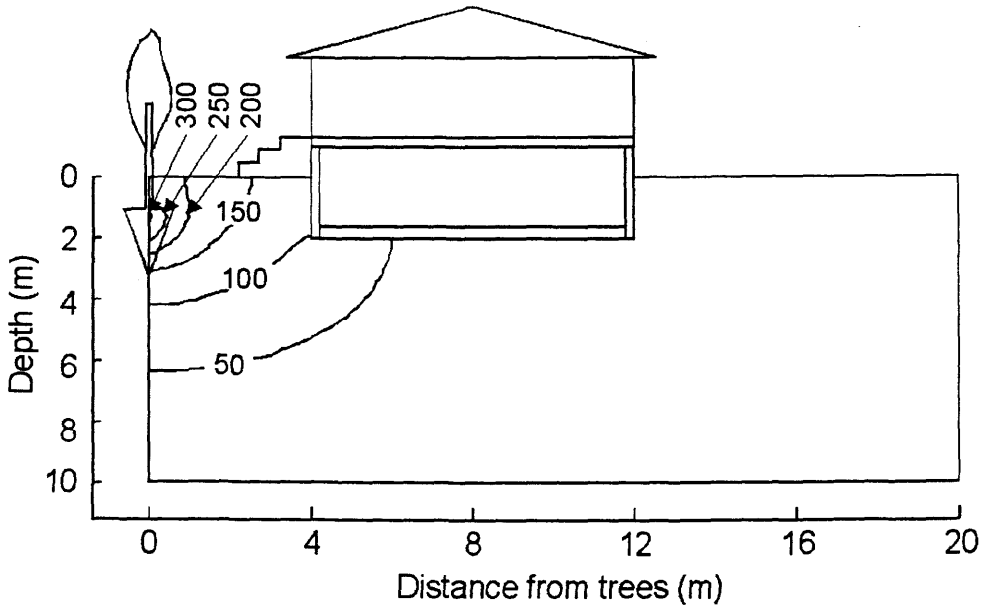

Figure 6.11 Contours of changes in matric suction (kPa), Example 2

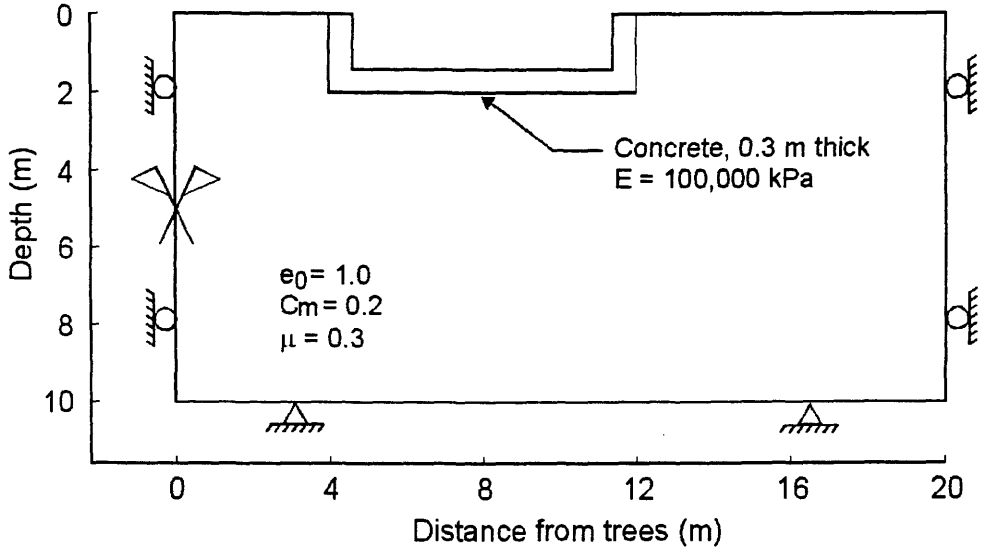

Figure 6.12 Boundary conditions for stress-deformation analysis, Example 2

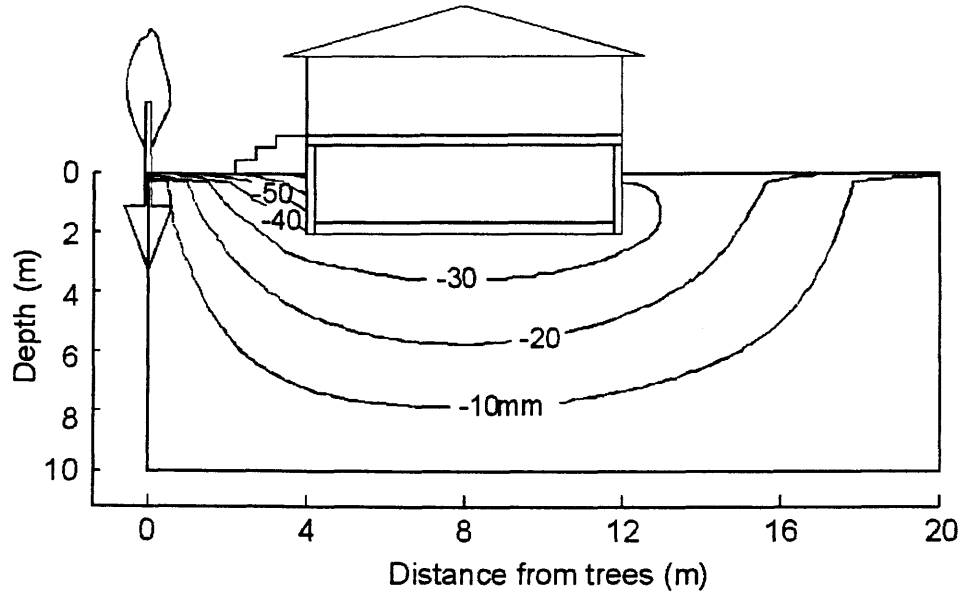

Figure 6.13 Contours of horizontal displacement (mm), Example 2

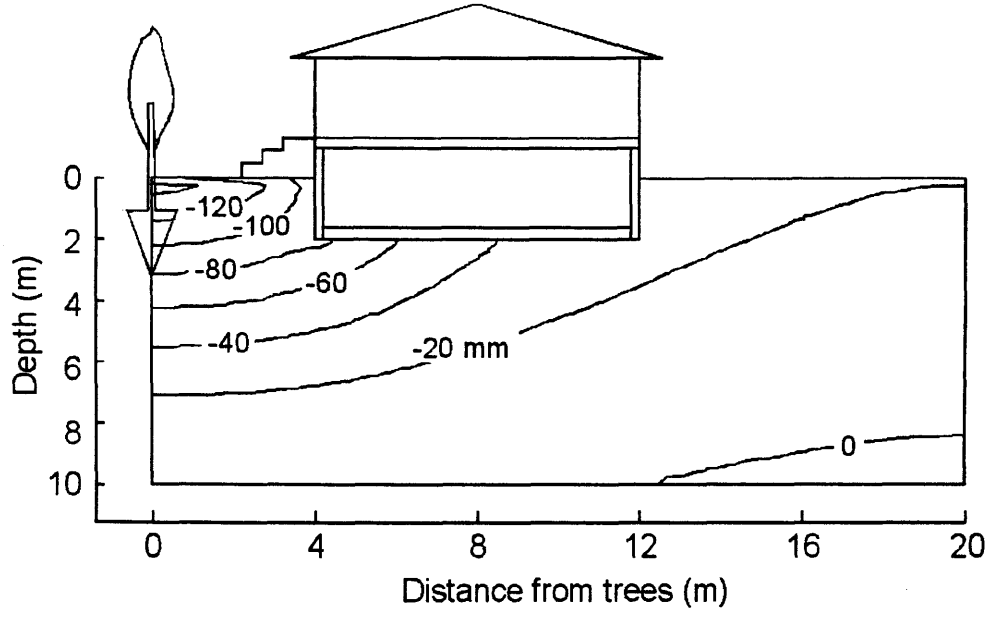

Figure 6.14 Contours of vertical displacement (mm), Example 2

A parametric analysis was performed to study the influence of the depth of root zone, distance from tree to the house, thickness of the expansive soil layer and the rate of water uptake by tree to the house footing. The variables used in this study are illustrated in Fig. 5.6. The root zone equal to 2 m (i.e., Z = 2 m) was assumed for all analyses. Predicted settlements at points A, B, and C for various combinations of the parameters are presented in Table 6.1.

Table 6.1 Predicted settlements at points A, B, and C for various boundary conditions, Example 2

Case	D (m)	H (m)	F (m)	R (m)	Water uptake m^3/day	Settlement (mm)		
						A	B	C
1	4	10	0.3	2	0.5	44	32	13
2	4	10	0.3	2	0.3	28	21	8
3	4	10	0.3	2	0.1	10	7	3
4	4	10	0.3	1	0.5	48	34	14
5	4	10	0.3	1	0.3	30	21	8
6	4	10	0.3	1	0.1	11	7	3
7	6	10	0.3	2	0.5	44	27	10
8	6	10	0.3	2	0.3	28	17	6
9	6	10	0.3	2	0.1	10	6	2
10	6	10	0.3	1	0.5	48	27	11
11	6	10	0.3	1	0.3	30	17	7
12	6	10	0.3	1	0.1	11	6	2
13	4	6	0.3	1	0.5	24	13	2
14	4	8	0.3	1	0.5	35	22	6
15	4	12	0.3	1	0.5	63	48	25
16	4	10	0.3	3	0.5	41	31	13
17	10	10	0.3	1	0.5	48	18	12
18	4	10	0.6	1	0.5	48	32	12
19	4	10	1.0	1	0.5	48	31	12
20	4	10	2.0	1	0.5	51	27	9

6.3 Uncoupled and coupled solutions of leakage and infiltration problems

This section presents the uncoupled and coupled solutions of Example 3, (i.e., the leakage problem) and Example 4 (i.e., the infiltration problem).

The soil properties used for the uncoupled and coupled analyses in this section are shown in Fig. 4.79 for the void ratio constitutive surface, Fig. 4.80 for the degree of saturation constitutive surface and Fig. 4.89 for the coefficient of permeability function. The void ratio constitutive surface was estimated from swelling indices and swelling pressures for Regina clay. A Poisson's ratio equal to 0.4 was assumed. The elastic parameter functions, E, H, E_w, *and* H_w are presented graphically in Figs. 4.85, 4.86, 4.87, and 4.88, respectively. The initial stress state in the soil profile is shown in Fig. 6.15 for both Example 3 and Example 4.

The examples presented in this section are analysed using various types of uncoupled analysis and the results are then compared with the coupled solutions.

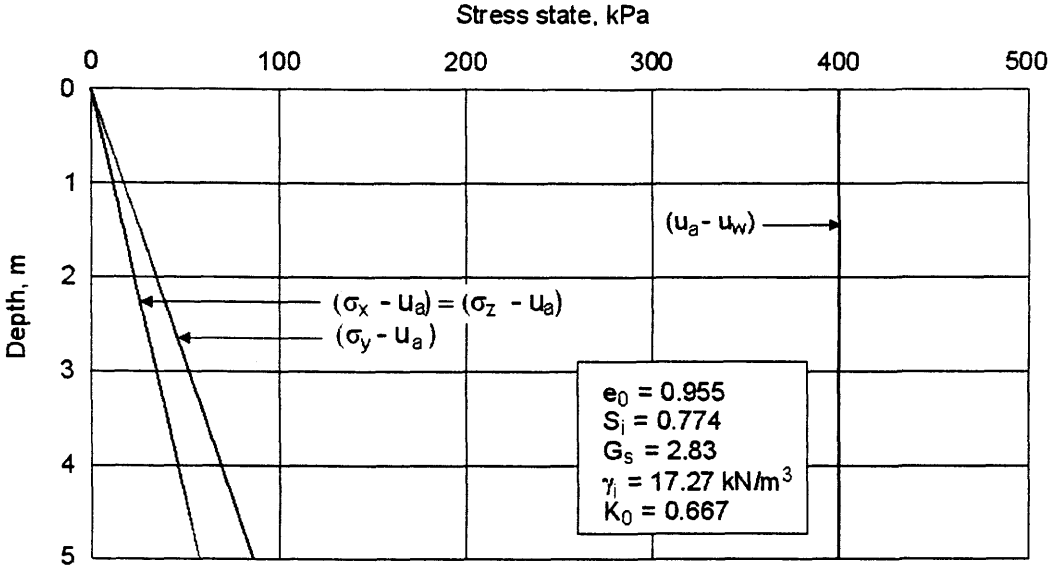

Figure 6.15 Initial net normal stress state, matric suction state, and key variables, Examples 3 and 4

6.3.1 Example 3: Leakage of water below floor slab

The illustration of this problem is presented in Fig. 5.9. Four types of analysis were used for this example, consisting of three uncoupled analyses, UCS2, UCS3, UCS4, and one coupled analysis, CS. The results obtained from the uncoupled analysis, UCS4 and the coupled analysis, CS are presented below. The results obtained from uncoupled analyses, UCS2 and UCS3 are presented in Appendix B.

6.3.1.1 Uncoupled analysis, UCS4 for Example 3, leakage problem

In this analysis, volume change and induced net normal stress are considered in both the seepage analysis and stress-deformation analysis. The rate of change in volumetric strain and net normal stress is updated at the following elapsed times: 0.2 days, 0.5 days, 1 day, 2 days, 5 days, 9 days, 16 days, 25 days, 36 days, 56 days, 100 days and after that at each 50 day period.

Figure 6.16 shows boundary conditions for seepage analysis for this example. The transient wetting process is induced by imposing a total head equal to zero under the flexible cover, at the ground surface of the soil deposit. Flux equal to zero is specified elsewhere on the boundary. The analysis is conducted to predict matric suction changes with time as wetting front advances into the soil mass.

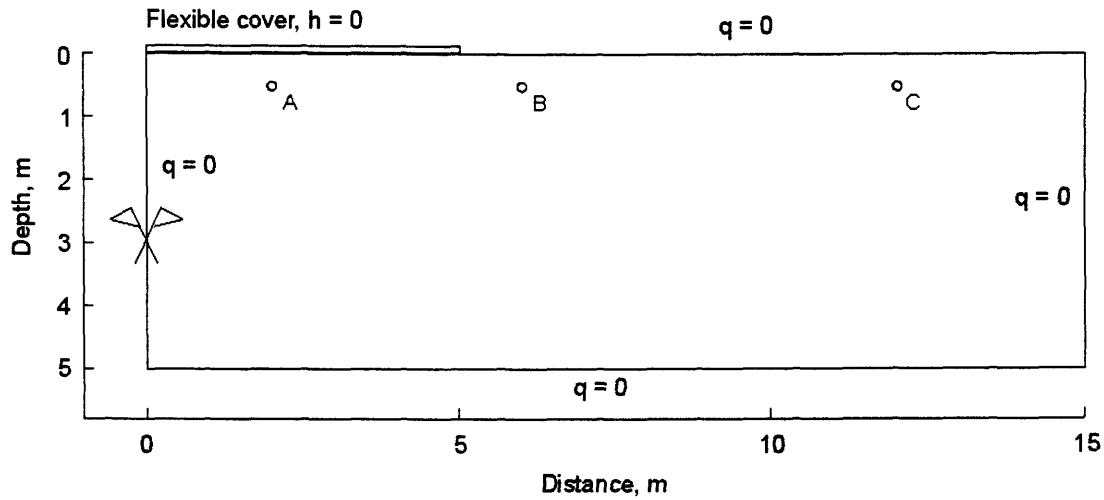

Figure 6.16 Boundary conditions for seepage analysis, Example 3, uncoupled solution

Boundary conditions for stress-deformation analysis of this example are presented in Fig. 6.17. The soil was free to move in the vertical direction and fixed in horizontal direction at the left and right sides of the domain. The lower boundary was fixed in both directions.

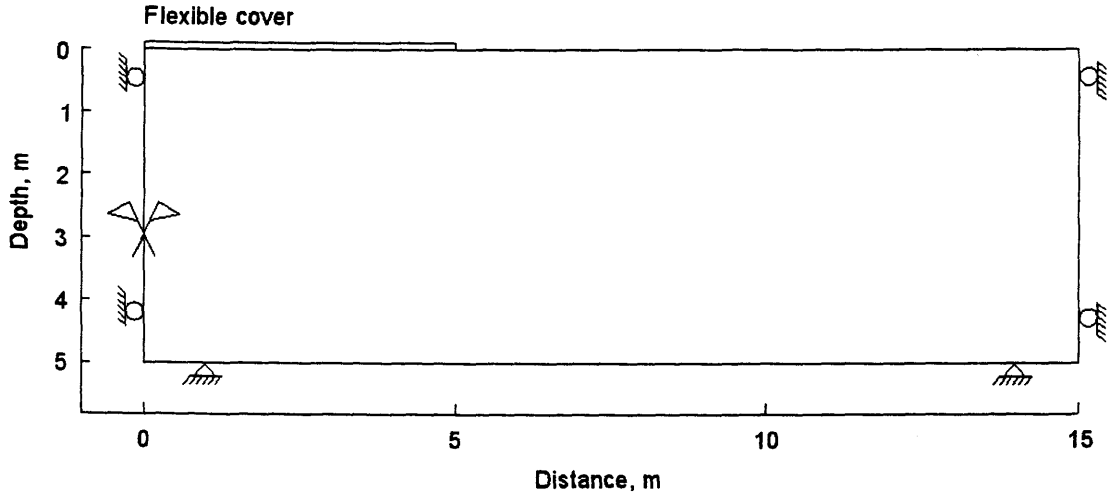

Figure 6.17 Boundary conditions for stress-deformation analysis, Examples 3 and 4, uncoupled solution

Figures 6.18 to 6.22 present the results obtained at day 56 after the wetting commenced. The distribution of matric suction is presented in Fig. 6.18. Distributions of horizontal and vertical displacement are presented in Figs. 6.19 and 6.20, respectively. Distributions of horizontal and vertical strains are presented in Figs. 6.21 and 6.22, respectively.

Figures 6.23 to 6.27 present the results obtained at day 150 after the wetting commenced. The distribution of matric suction is presented in Figs. 6.23. Distributions of horizontal and vertical displacement at day 150 are presented in Figs. 6.24 and 6.25, respectively. Distributions of horizontal and vertical strains at day 150 are presented in Figs. 6.26 and 6.27, respectively.

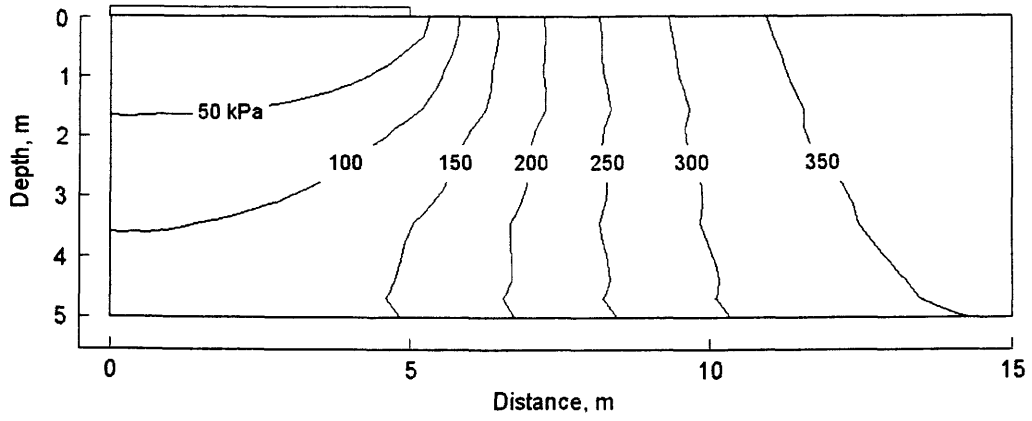

Figure 6.18 Distribution of matric suction at day 56, Example 3, uncoupled analysis UCS4

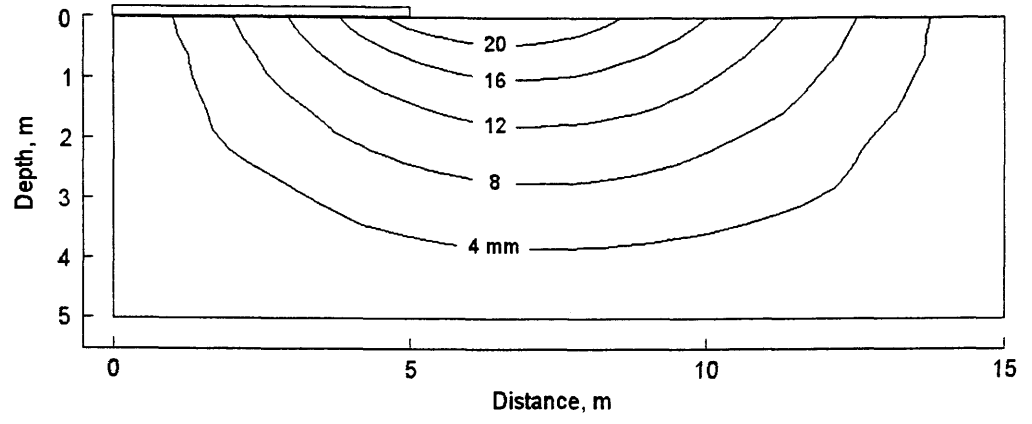

Figure 6.19 Distribution of horizontal displacement at day 56, Example 3, uncoupled analysis UCS4

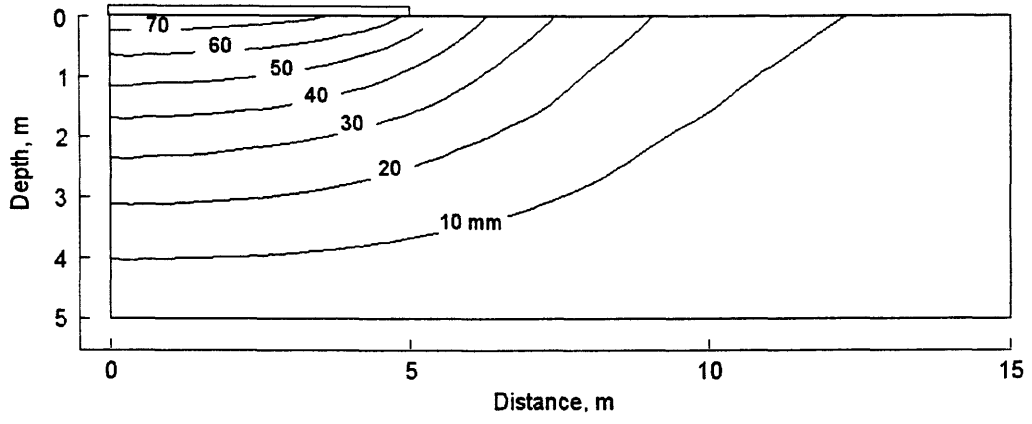

Figure 6.20 Distribution of vertical displacement at day 56, Example 3, uncoupled analysis UCS4

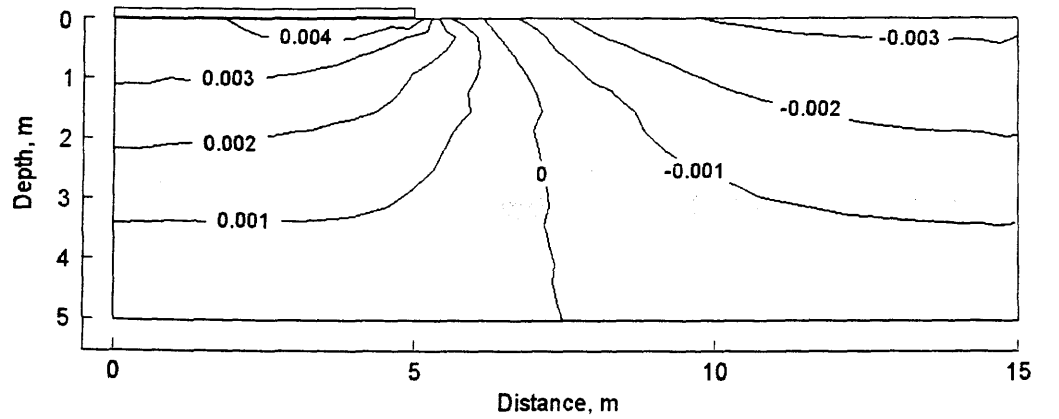

Figure 6.21 Distribution of horizontal strain at day 56, Example 3, uncoupled analysis UCS4

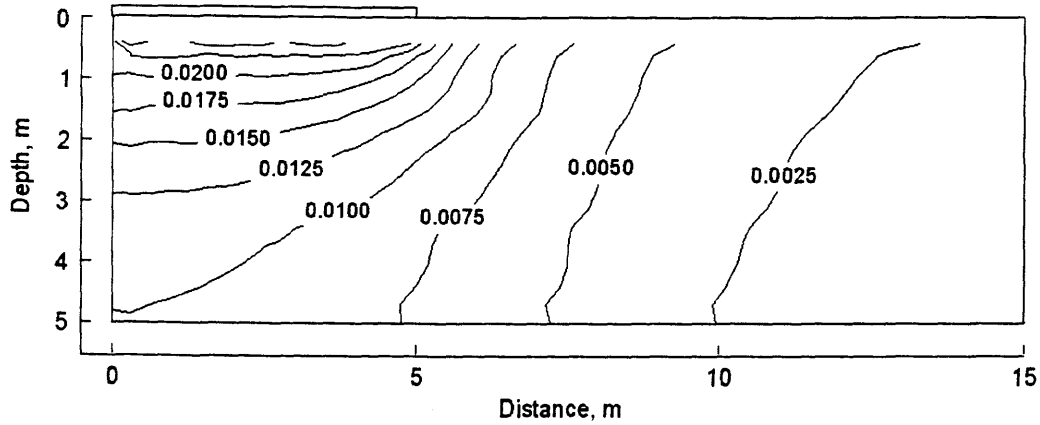

Figure 6.22 Distribution of vertical strain at day 56, Example 3, uncoupled analysis UCS4

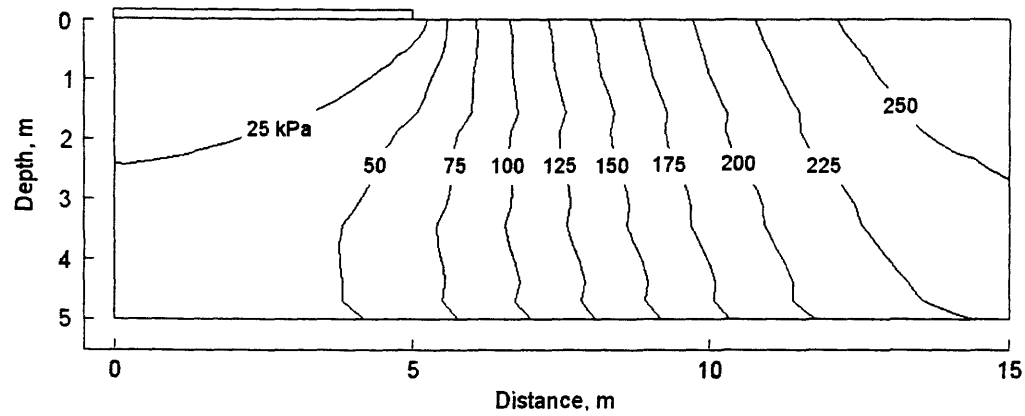

Figure 6.23 Distribution of matric suction at day 150, Example 3, uncoupled analysis UCS4

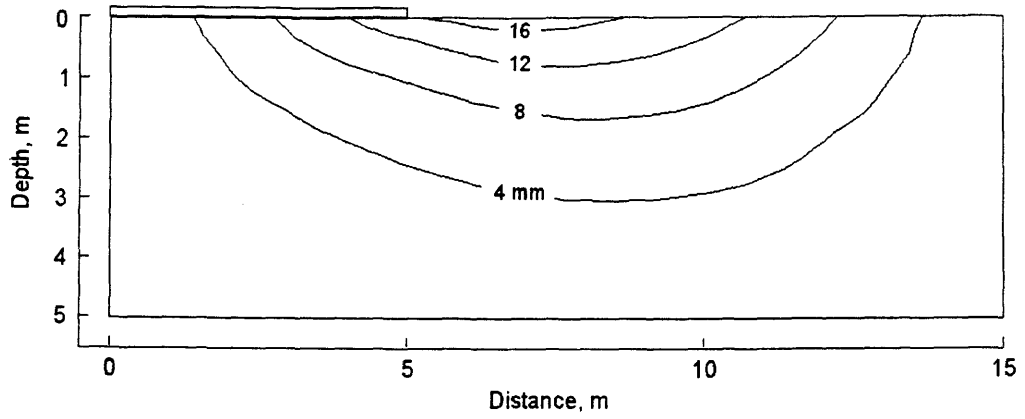

Figure 6.24 Distribution of horizontal displacement at day 150, Example 3, uncoupled analysis UCS4

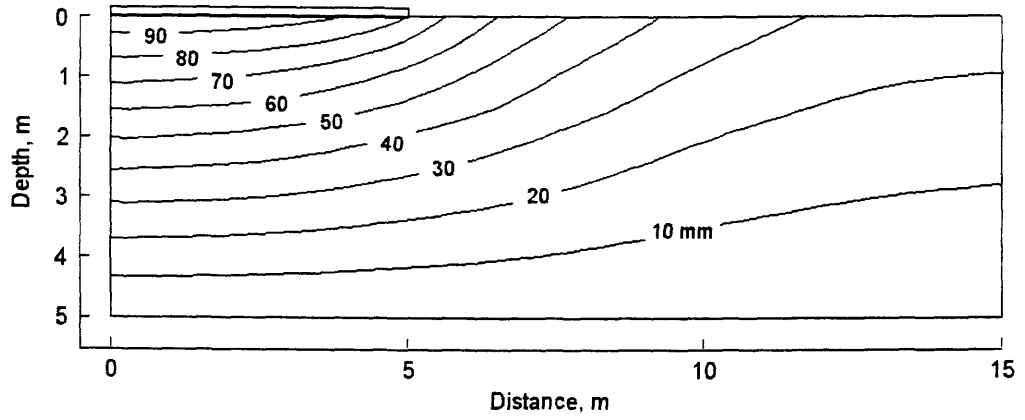

Figure 6.25 Distribution of vertical displacement at day 150, Example 3, uncoupled analysis UCS4

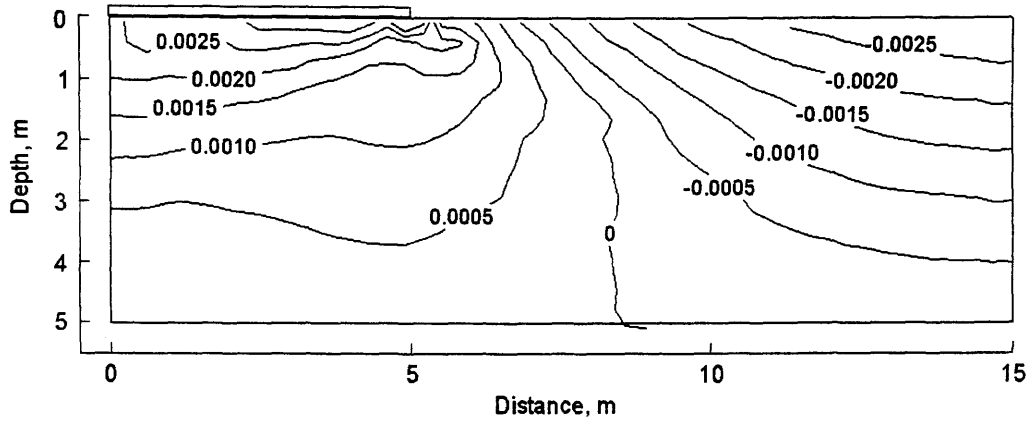

Figure 6.26 Distribution of horizontal strain at day 150, Example 3, uncoupled analysis UCS4

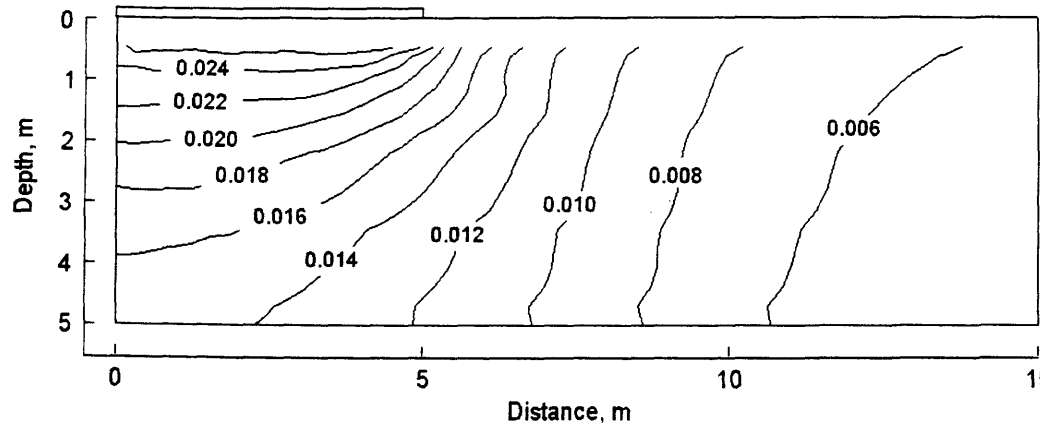

Figure 6.27 Distribution of vertical strain at day 150, Example 3, uncoupled analysis UCS4

Change of matric suction with time for points A, B, and C in the soil mass is presented in Fig. 6.28. Change of matric suction versus depth below the cover is presented for various elapsed times in Fig. 6.29.

Figures 6.30 and 6.31 show the change of horizontal and vertical displacement with time at points A, B, and C in the soil mass. Figure 6.32 shows the change of heave at ground surface with time. Figure 6.33 presents the change of heave below the cover versus depth with time.

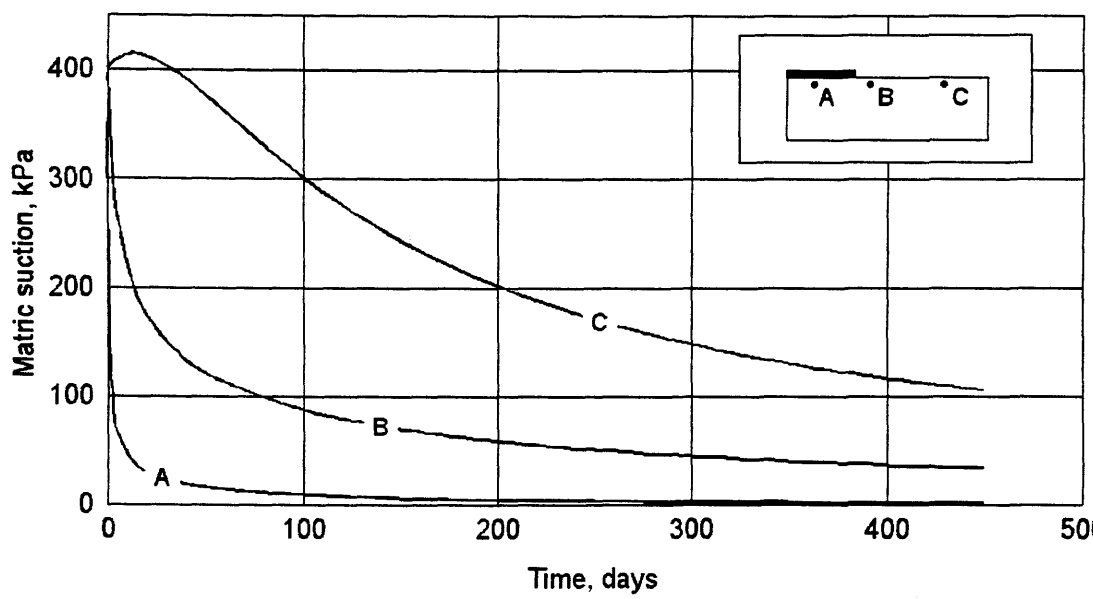

Figure 6.28 Change of matric suction with time for points A, B, and C, Example 3, uncoupled analysis UCS4

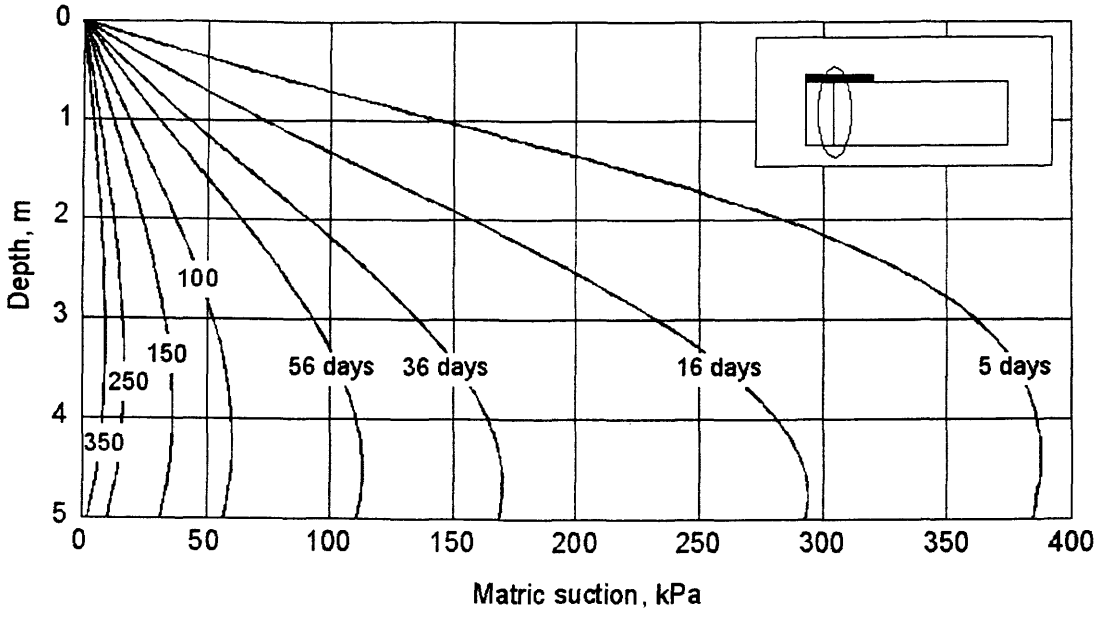

Figure 6.29 Change of matric suction versus depth with time, Example 3, uncoupled analysis UCS4

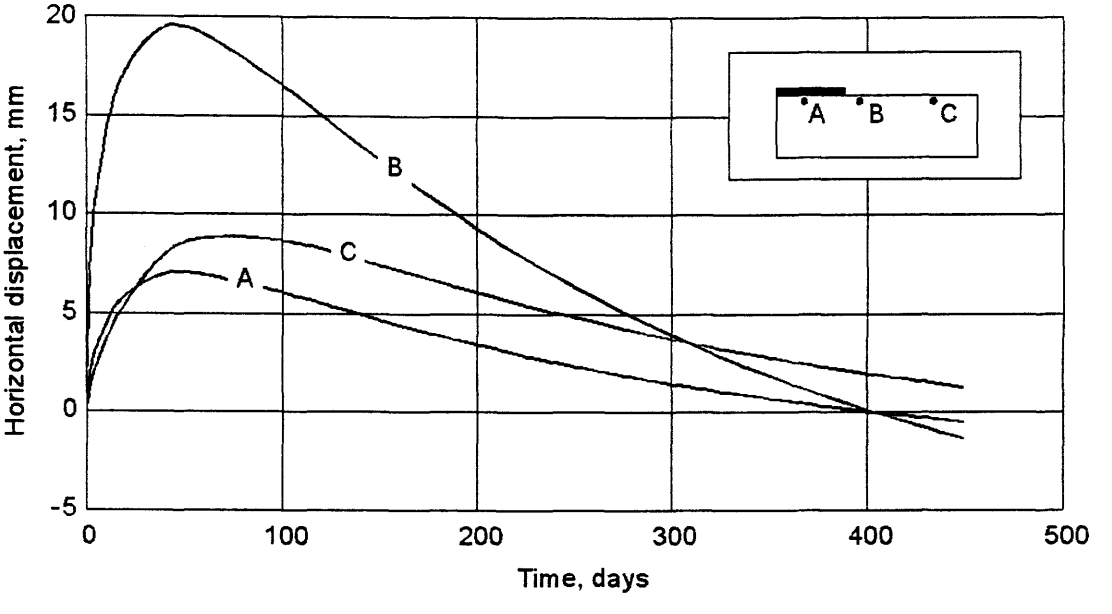

Figure 6.30 Change of horizontal displacement with time for points A, B, and C, Example 3, uncoupled analysis UCS4

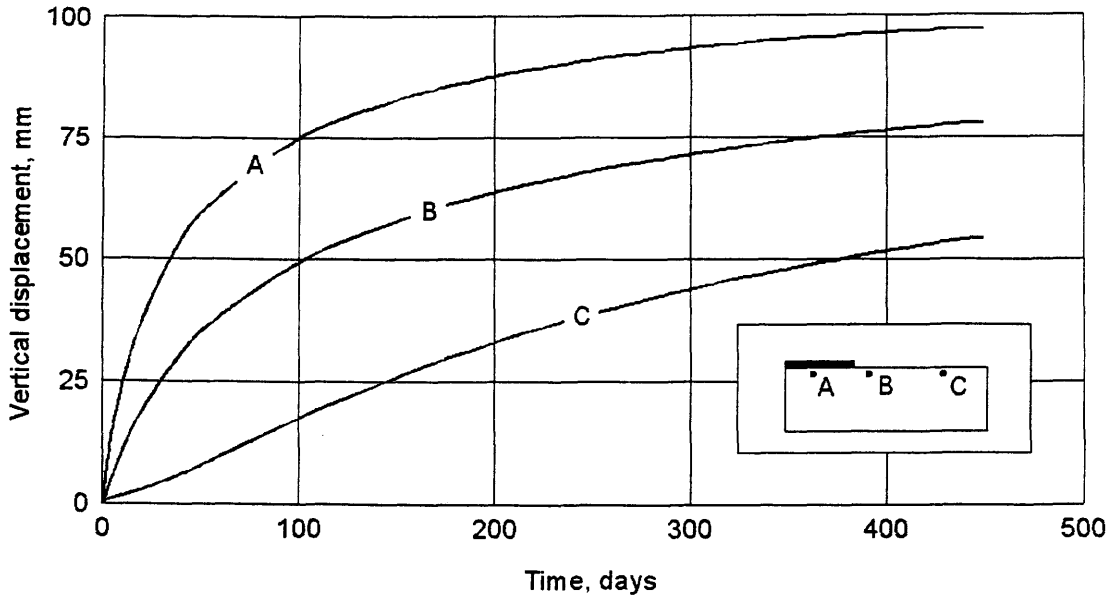

Figure 6.31 Change of vertical displacement with time for points A, B, and C, Example 3, uncoupled analysis UCS4

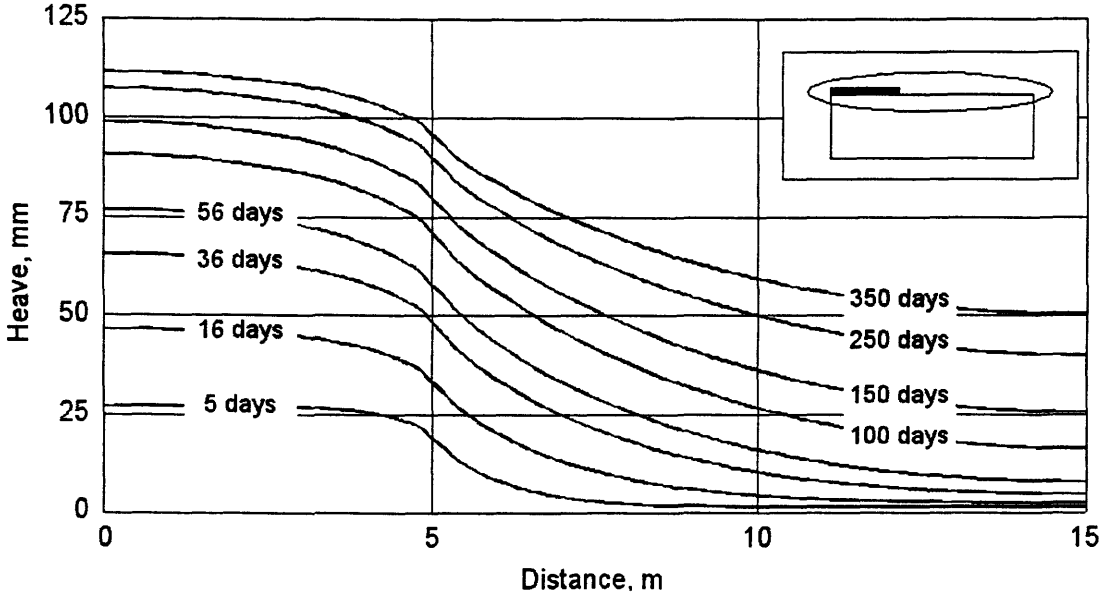

Figure 6.32 Change of heave at ground surface with time, Example 3, uncoupled analysis UCS4

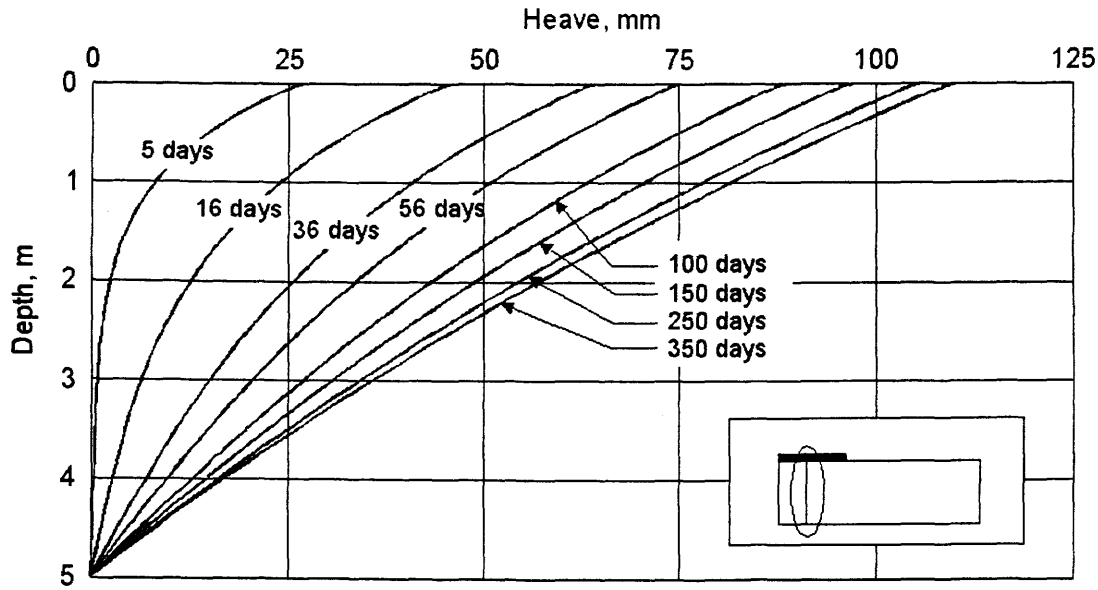

Figure 6.33 Change of heave below the cover versus depth with time, Example 3, uncoupled analysis UCS4

6.3.1.2 Coupled analysis, CS for Example 3, leakage problem

The boundary conditions for coupled analysis of this example are presented in Fig. 6.34. The transient wetting process is induced by imposing a total head equal to zero at the ground surface of the soil deposit, under the flexible cover. Flux equal to zero is specified elsewhere on the boundary. The soil was free to move in the vertical direction and fixed in horizontal direction at the left and right sides of the domain. The lower boundary was fixed in both directions.

The analysis is first performed for various finite element meshes. It is noted that unchanged solutions can be obtained with the mesh of 75 nine-node quadrilateral elements and 341 nodes. Comparisons of the results for days 100 and 200 obtained from mesh 1 (60 elements), mesh 2 (75 elements) and mesh 3 (90 elements) are presented in Appendix A for distributions of matric suction, horizontal displacement, and vertical displacement, respectively. The comparisons of these results are also presented numerically. A finite element mesh of 75 elements and 341 nodes was used for the coupled analysis of this example. The finite element mesh is shown in Fig. 6.34.

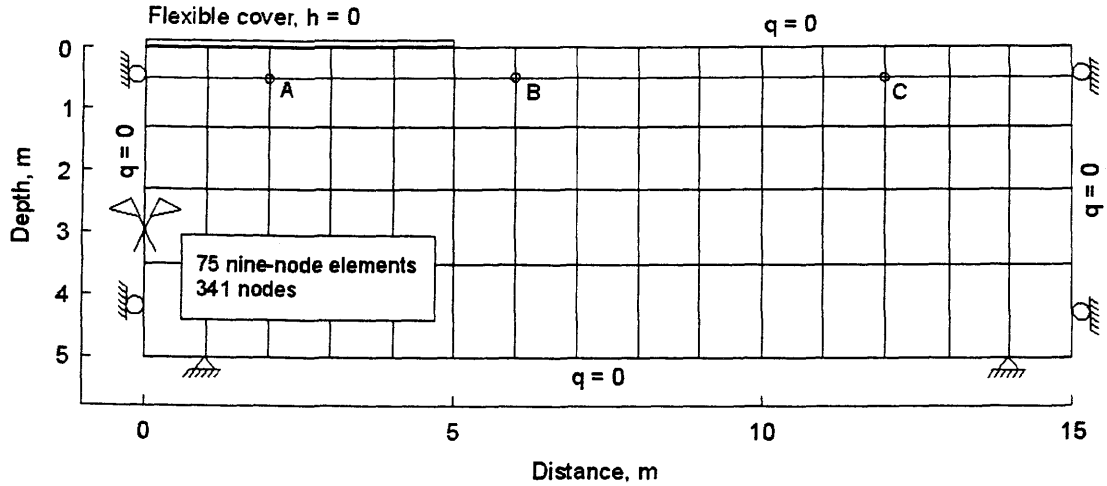

Figure 6.34 Finite element mesh and boundary conditions, Example 3, coupled analysis

The analysis is conducted by tracking both the displacements and matric suction changes as a function of time as the wetting front advances into the soil mass.

Figures 6.35 to 6.43 present the results obtained at day 56 after the wetting commenced. Distribution of matric suction is presented in Fig. 6.35. Distributions of horizontal and vertical stress are presented in Figs. 6.36 and 6.37, respectively. Figures 6.38 and 6.39 present the distributions of void ratio and degree of saturation. Distributions of horizontal and vertical displacement are presented in Figs. 6.40 and 6.41, respectively. Distributions of horizontal and vertical strains are presented in Figs. 6.42 and 6.43, respectively.

Figures 6.44 to 6.52 present the results obtained at day 150 after the wetting commenced. Distribution of matric suction is presented in Fig. 6.44. Distributions of horizontal and vertical stress are presented in Figs. 6.45 and 6.46, respectively. Figures 6.47 and 6.48 present the distributions of void ratio and degree of saturation. Distributions of horizontal and vertical displacement are presented in Figs. 6.49 and 6.50, respectively. Distributions of horizontal and vertical strains are presented in Figs. 6.51 and 6.52, respectively.

Figure 6.53 shows the change of matric suction with time for points A, B, and C. The change of horizontal stress with time for points A, B, and C is presented in Fig. 6.54. Figures 6.55 and 6.56 show the change of horizontal and vertical

displacement with time at points A, B, and C in the soil mass. Figure 6.57 shows the change of heave at ground surface with time. Figure 6.58 presents the change of heave below the cover versus depth with time.

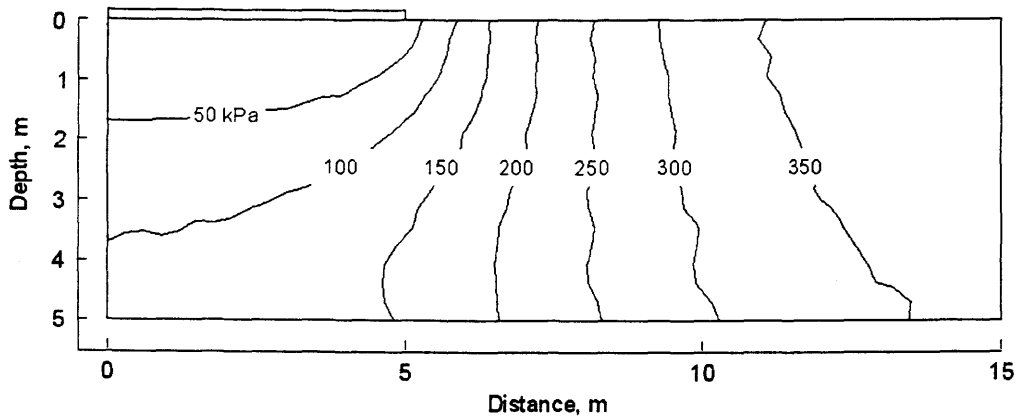

Figure 6.35 Distribution of matric suction at day 56, Example 3, coupled solution

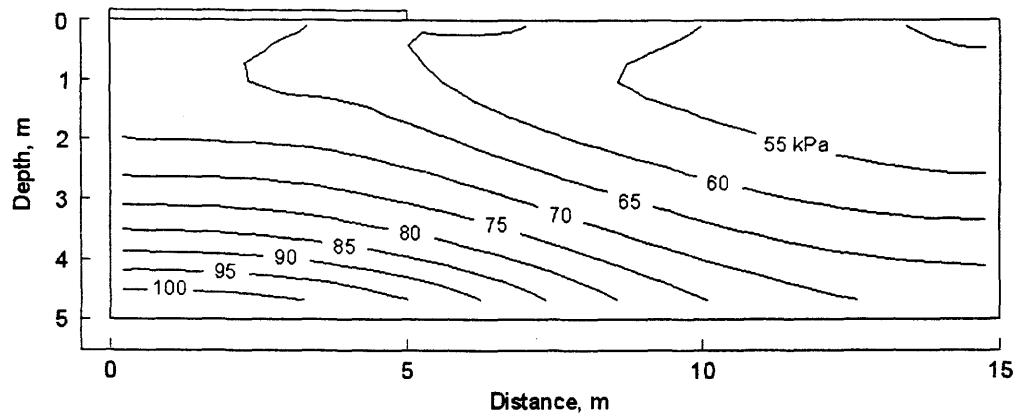

Figure 6.36 Distribution of horizontal stress at day 56, Example 3, coupled solution

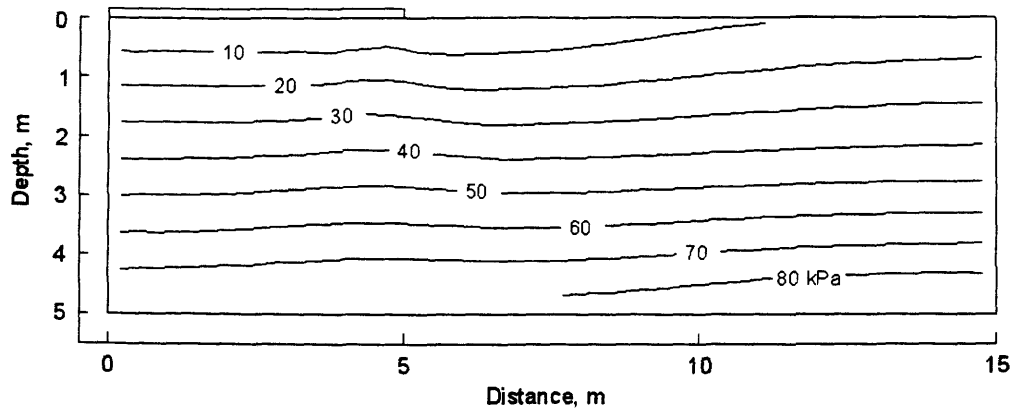

Figure 6.37 Distribution of vertical stress at day 56, Example 3, coupled solution

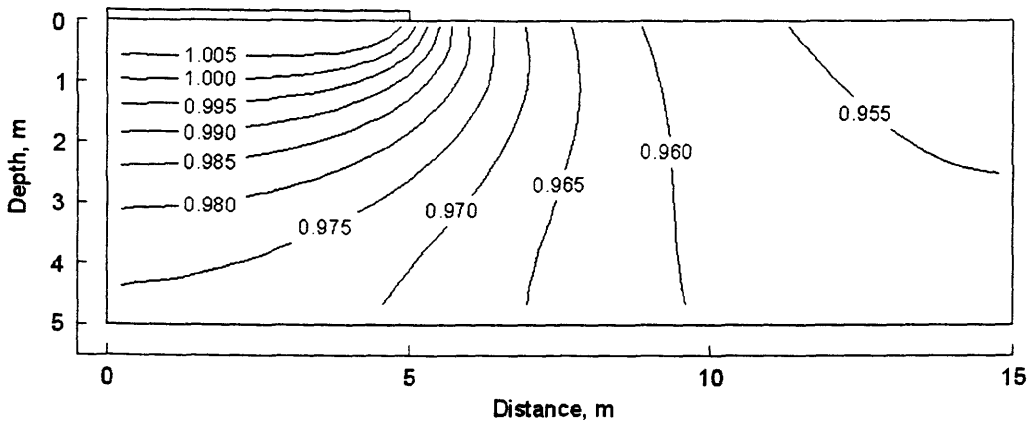

Figure 6.38 Distribution of void ratio at day 56, Example 3, coupled solution

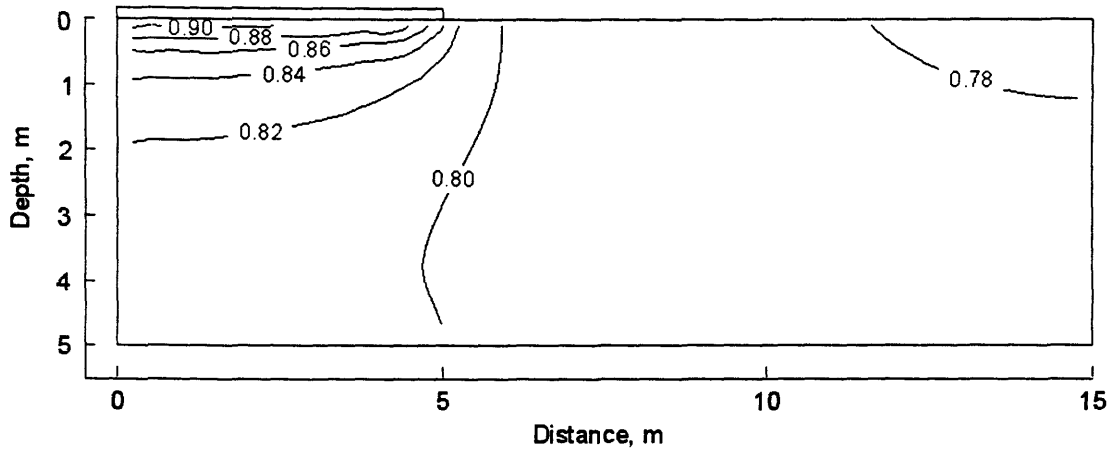

Figure 6.39 Distribution of degree of saturation at day 56, Example 3, coupled solution

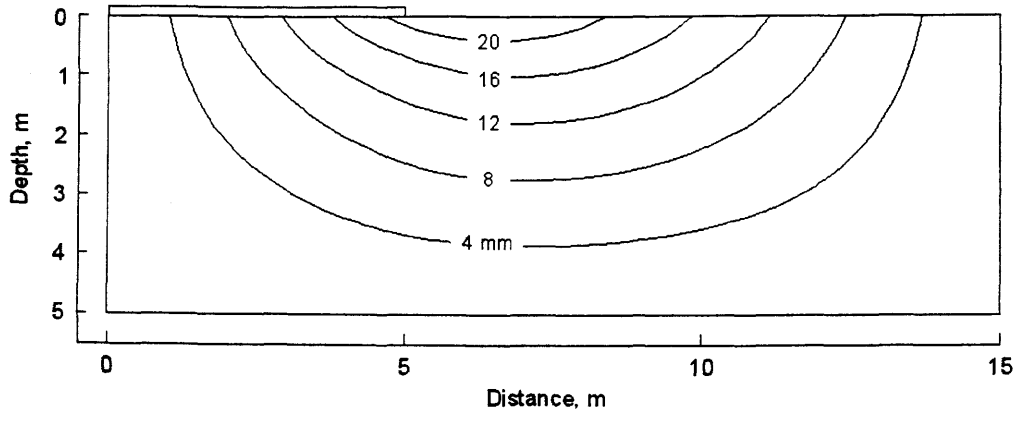

Figure 6.40 Distribution of horizontal displacement at day 56, Example 3, coupled solution

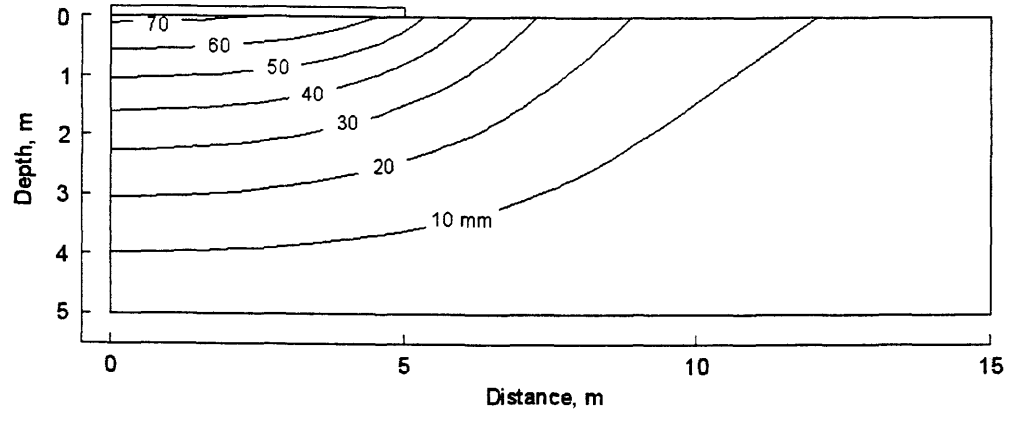

Figure 6.41 Distribution of vertical displacement at day 56, Example 3, coupled solution

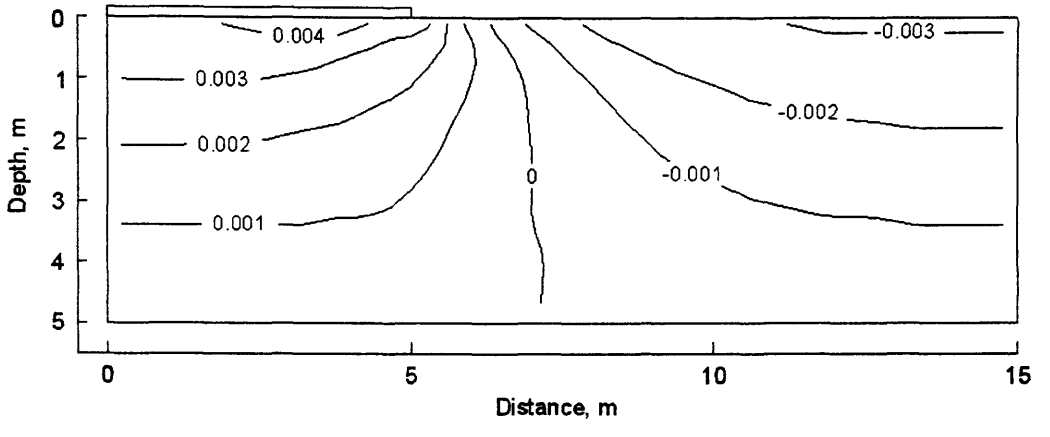

Figure 6.42 Distribution of horizontal strain at day 56, Example 3, coupled solution

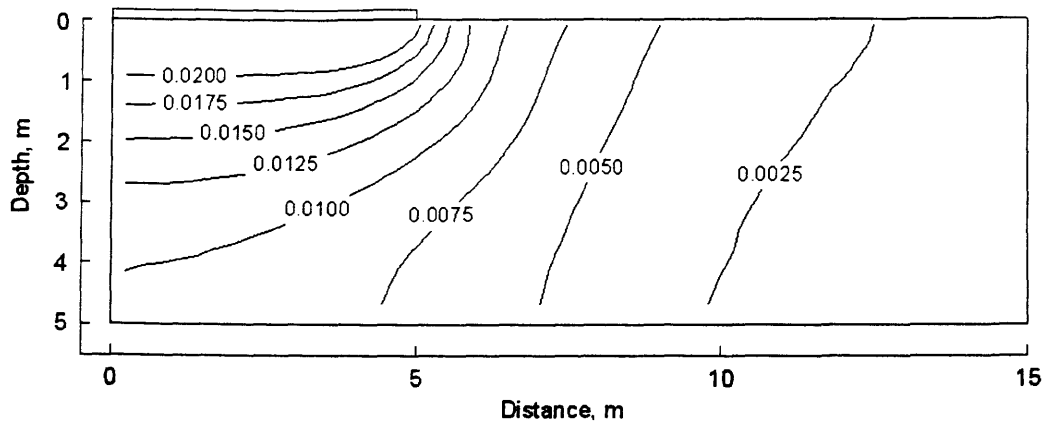

Figure 6.43 Distribution of vertical strain at day 56, Example 3, coupled solution

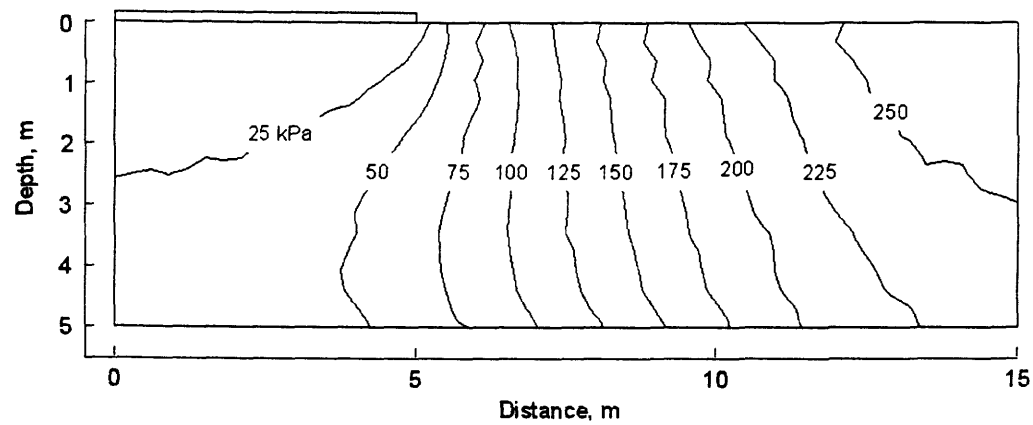

Figure 6.44 Distribution of matric suction at day 150, Example 3, coupled solution

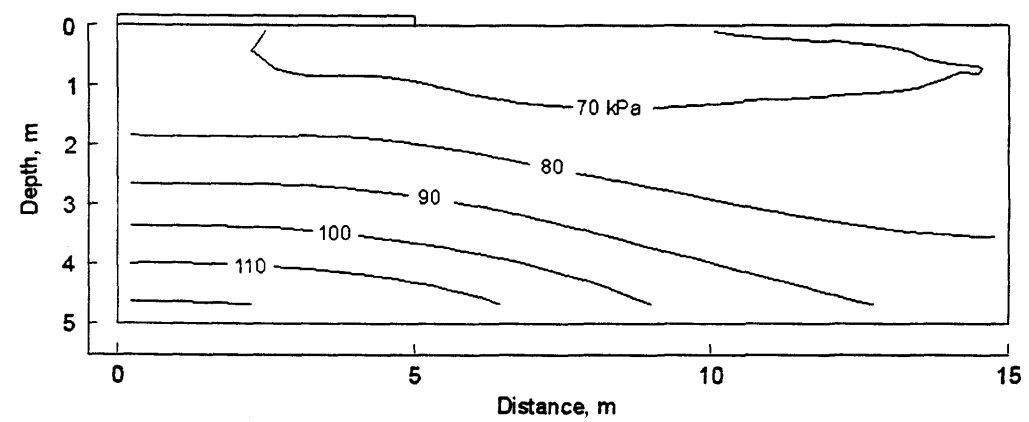

Figure 6.45 Distribution of horizontal stress at day 150, Example 3, coupled solution

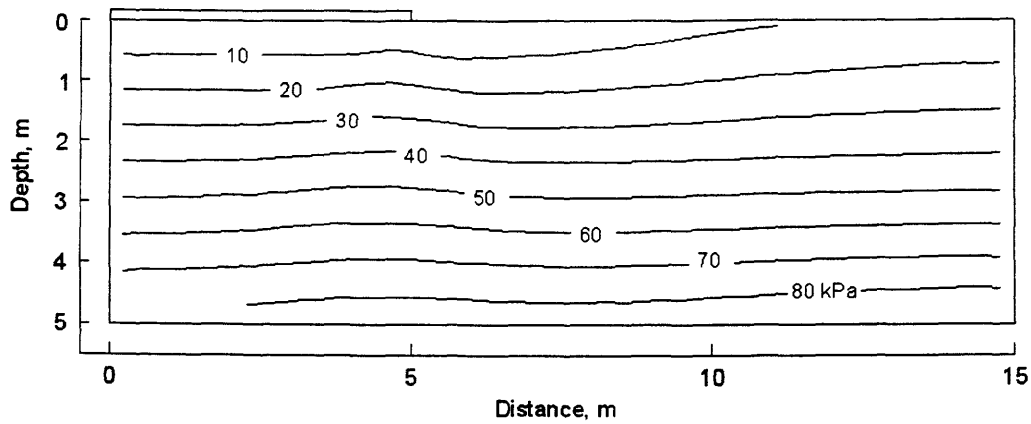

Figure 6.46 Distribution of vertical stress at day 150, Example 3, coupled solution

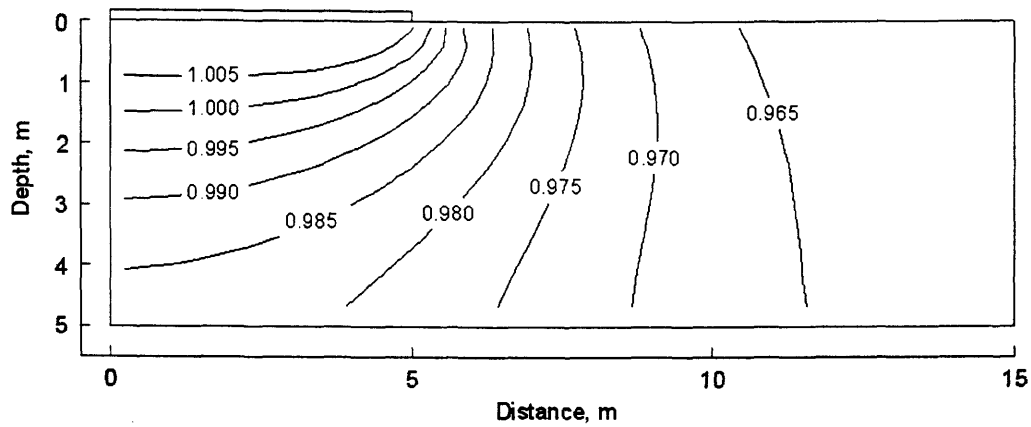

Figure 6.47 Distribution of void ratio at day 150, Example 3, coupled solution

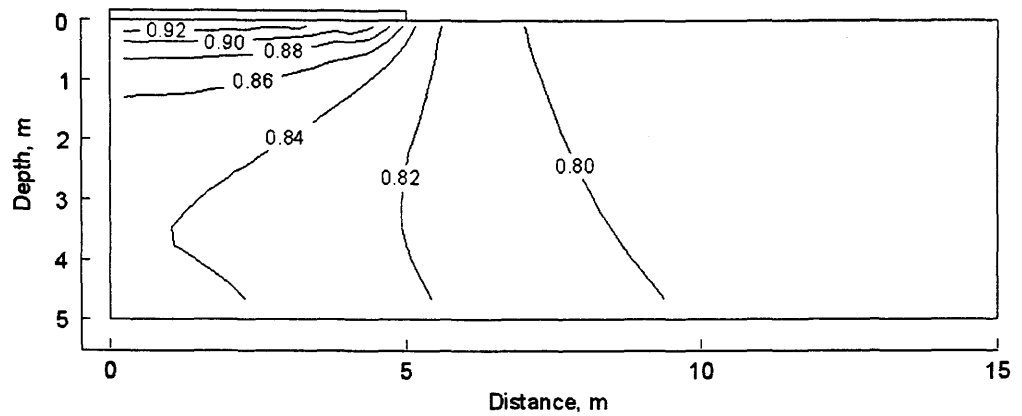

Figure 6.48 Distribution of degree of saturation at day 150, Example 3, coupled solution

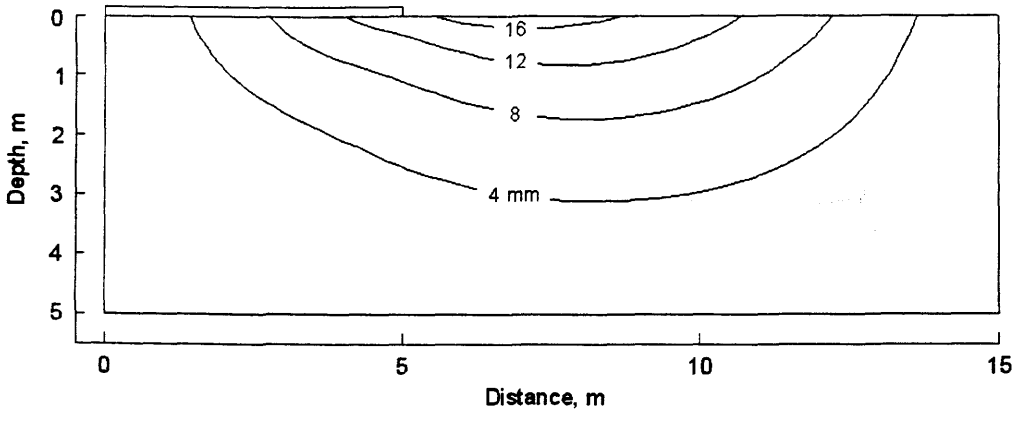

Figure 6.49 Distribution of horizontal displacement at day 150, Example 3, coupled solution

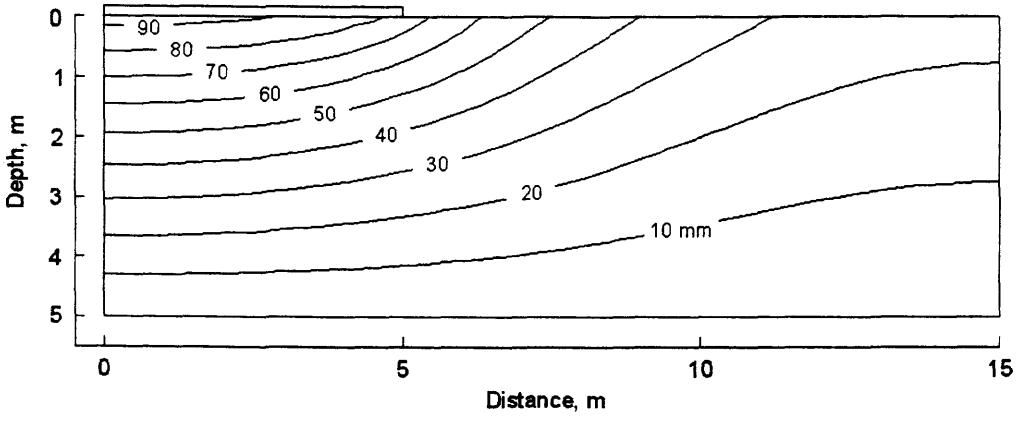

Figure 6.50 Distribution of vertical displacement at day 150, Example 3, coupled solution

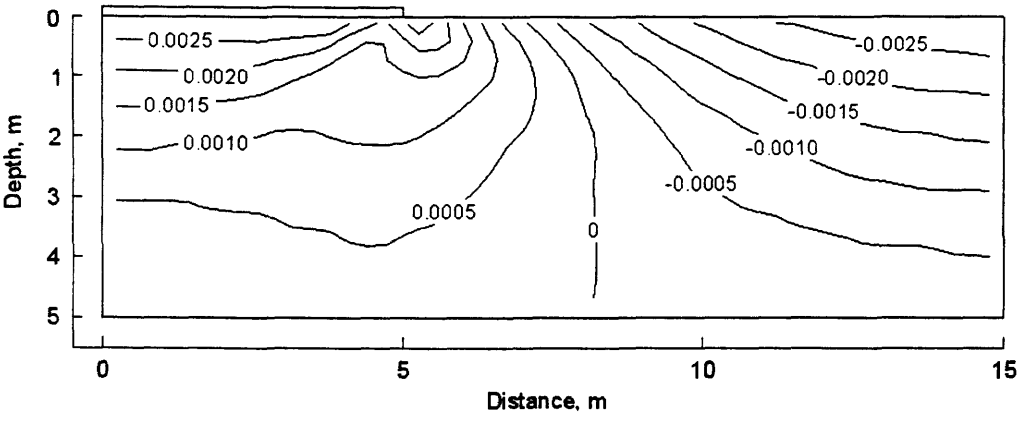

Figure 6.51 Distribution of horizontal strain at day 150, Example 3, coupled solution

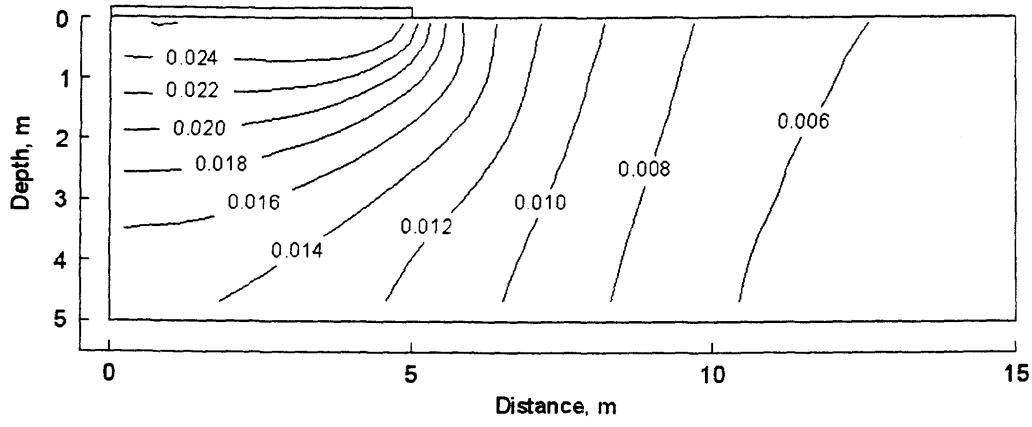

Figure 6.52 Distribution of vertical strain at day 150, Example 3, coupled solution

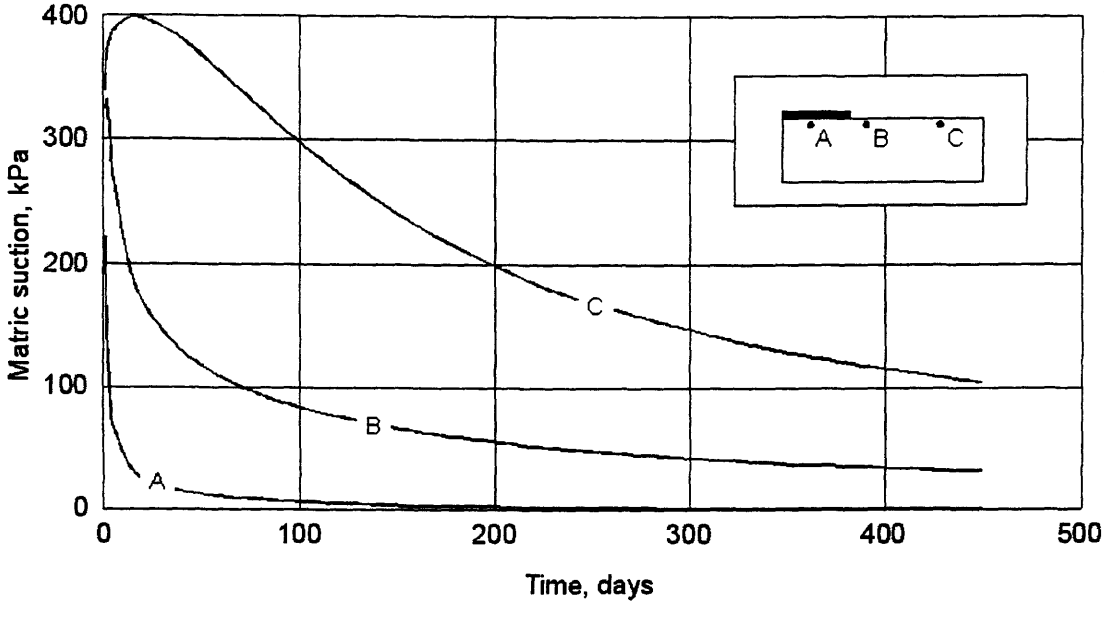

Figure 6.53 Change of matric suction with time for points A, B, and C, Example 3, coupled solution

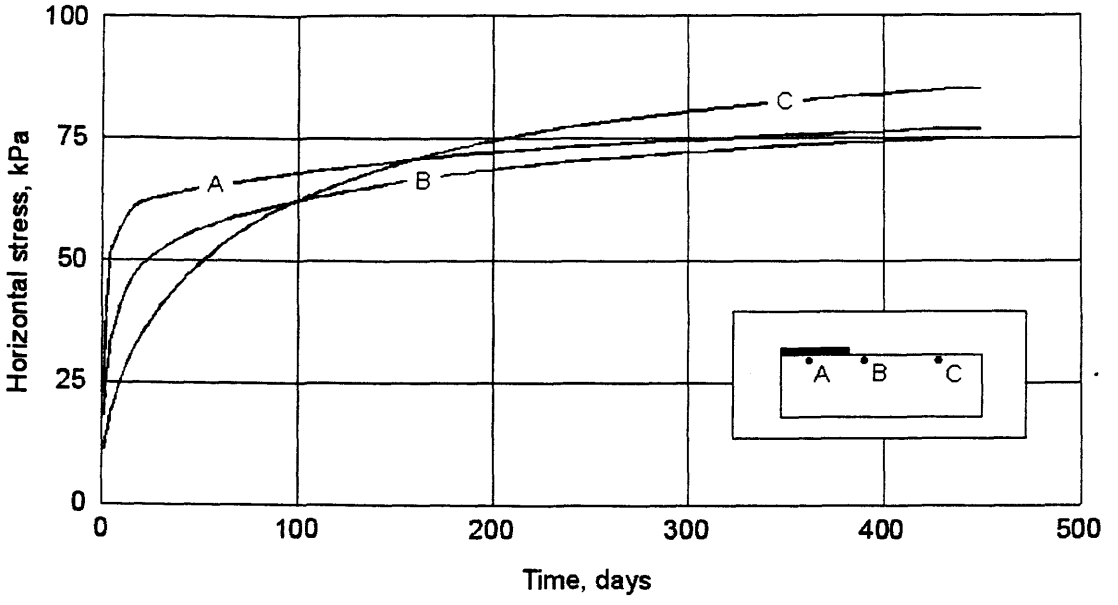

Figure 6.54 Change of horizontal stress with time for points A, B, and C, Example 3, coupled solution

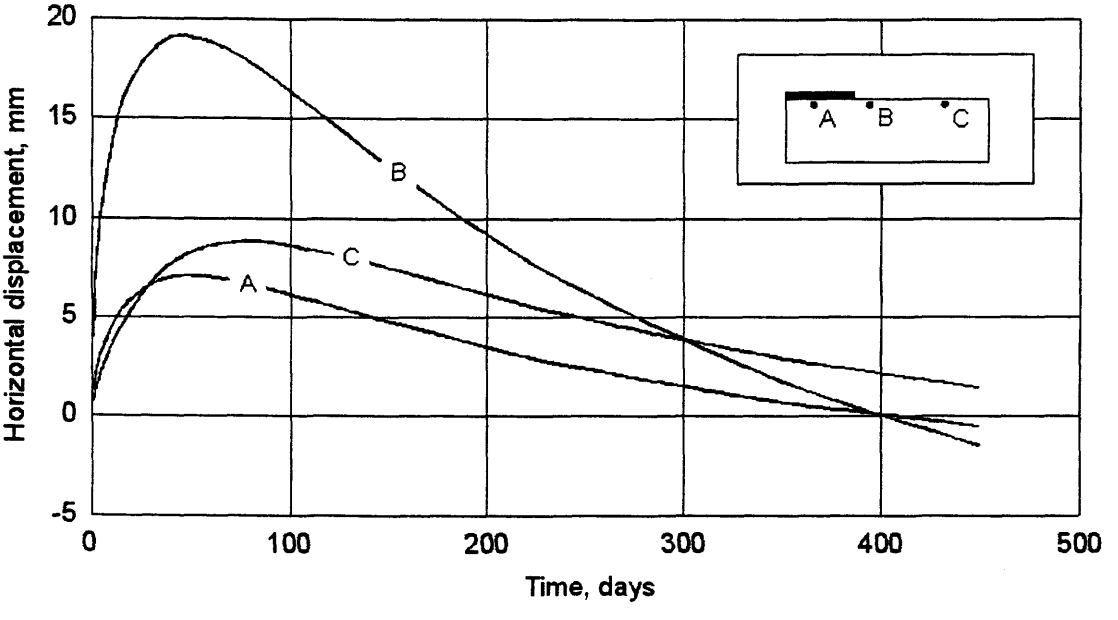

Figure 6.55 Change of horizontal displacement with time for points A, B, and C, Example 3, coupled solution

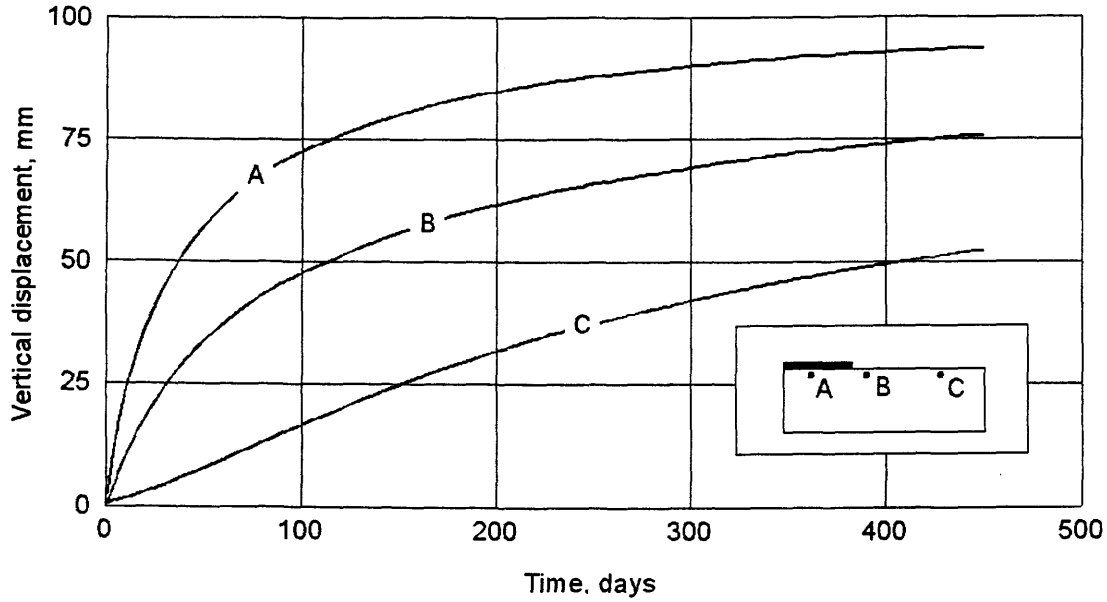

Figure 6.56 Change of vertical displacement with time for points A, B, and C, Example 3, coupled solution

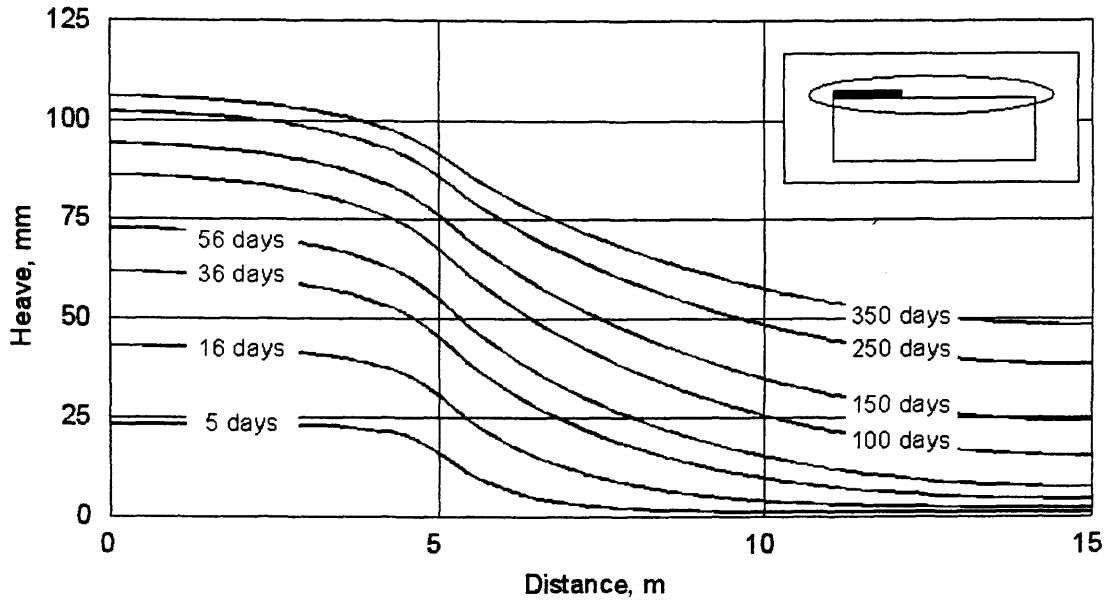

Figure 6.57 Change of heave at ground surface with time, Example 3 coupled solution

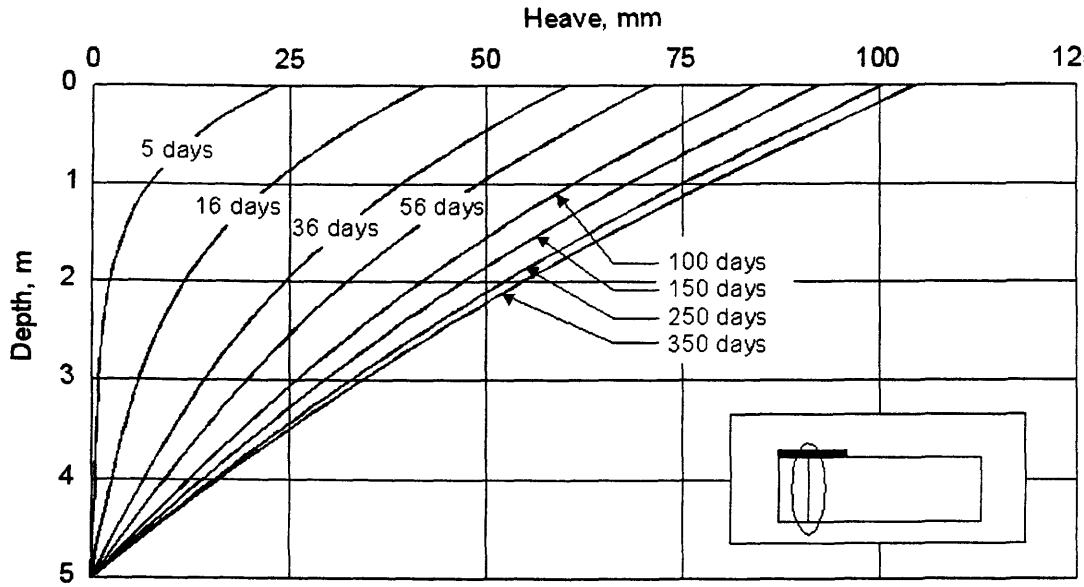

Figure 6.58 Change of heave below the cover versus depth with time, Example 3, coupled solution

6.3.2 Infiltration of water from ground surface

The illustration of this problem is presented in Fig. 5.10. The initial stress state in the soil profile is shown in Fig. 6.15. Four types of analysis were used for this example, consisting of three uncoupled analyses, UCS1, UCS2, UCS4, and one coupled analysis, CS. The results obtained from the uncoupled analysis, UCS4 and coupled analysis, CS are presented below. The results obtained from uncoupled analyses, UCS1 and UCS2 are presented in Appendix C.

6.3.2.1 Uncoupled analysis, UCS4 for Example 4, infiltration problem

In this analysis, volume change and induced net normal stress are considered in both seepage analysis and stress-deformation analysis. The rate of change in volumetric strain and net normal stress is updated at the following elapsed times: 13 days, 33 days, 53 days, 93 days, 133 days, 175 days, and after that at each 100 day period.

Figure 6.59 shows boundary conditions for the seepage analysis for this example. The transient wetting process is induced by imposing a water infiltration rate equal to 2.0×10^{-8} m/s at the uncovered portion of the ground surface. A value of

matric suction equal to 400 kPa is specified at lower boundary, zero flux is specified on the other parts of the boundary.

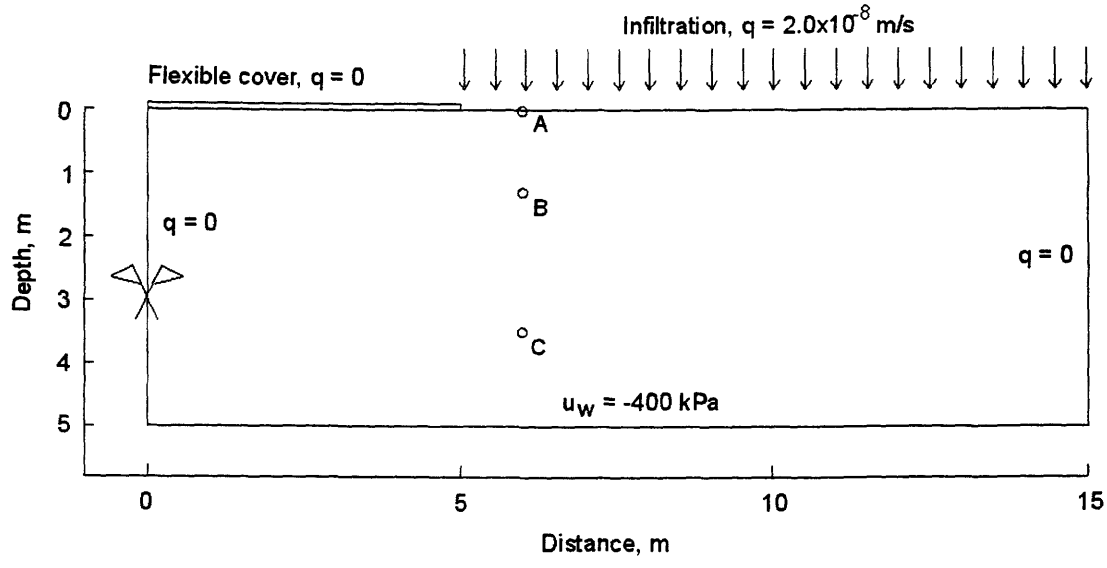

Figure 6.59 Boundary conditions for seepage analysis, Example 4, uncoupled solution

Boundary conditions for the stress-deformation analysis of this example are the same of those for Example 3 (i.e., Fig. 6.17). The soil is free to move in the vertical direction and fixed in horizontal direction at the left and right sides of the domain. The lower boundary is fixed in both directions.

Figures 6.60 to 6.64 present the results obtained at day 53 after the wetting commenced. The distribution of matric suction is presented in Fig. 6.60. Distributions of horizontal and vertical displacement are presented in Figs. 6.61 and 6.62, respectively. Distributions of horizontal and vertical strains are presented in Figs. 6.63 and 6.64, respectively.

Figures 6.65 to 6.69 present the results obtained at day 175 after the wetting commenced. The distribution of matric suction is presented in Fig. 6.65. Distributions of horizontal and vertical displacement at day 150 are presented in Figs. 6.66 and 6.67, respectively. Distributions of horizontal and vertical strains at day 150 are presented in Figs. 6.68 and 6.69, respectively.

Change of matric suction with time for points A, B, and C in the soil mass is presented in Fig. 6.70. Figures 6.71 shows the change of horizontal and vertical displacement with time at points A, B, and C in the soil mass. Figure 6.72 shows the change of heave at ground surface with time. Figure 6.73 presents the change of heave below the cover versus depth with time. The zigzags appeared near the left and right boundaries should be ignored because of the errors in the graphical processing of results.

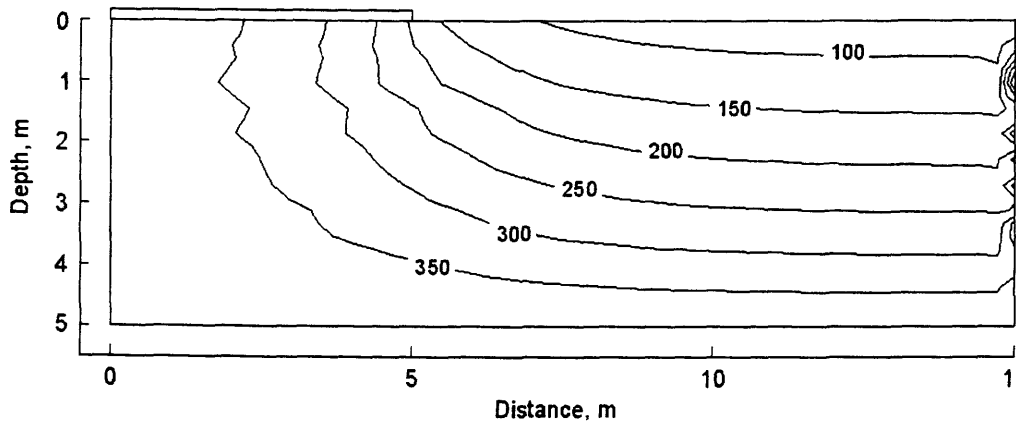

Figure 6.60 Distribution of matric suction at day 53, Example 4, uncoupled solution UCS4

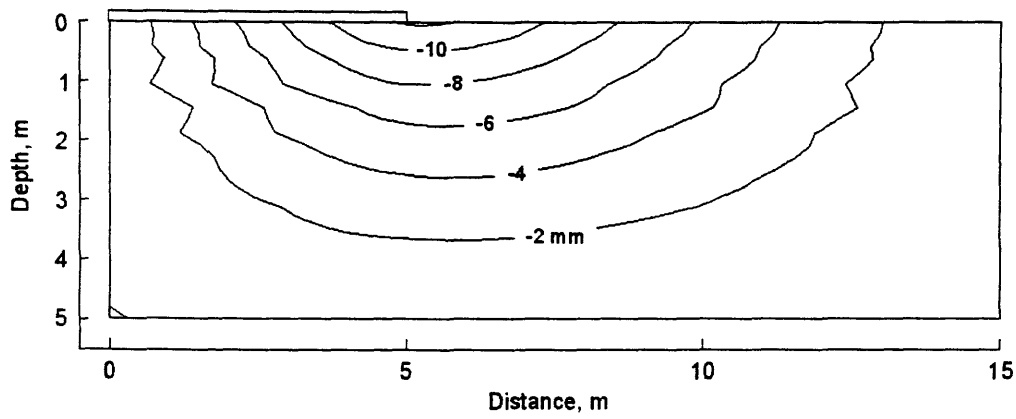

Figure 6.61 Distribution of horizontal displacement at day 53, Example 4, uncoupled solution UCS4

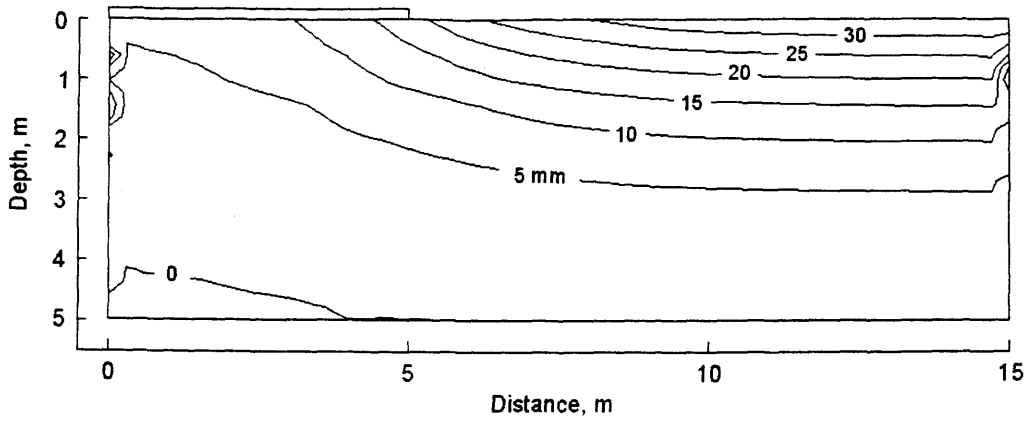

Figure 6.62 Distribution of vertical displacement at day 53, Example 4, uncoupled solution UCS4

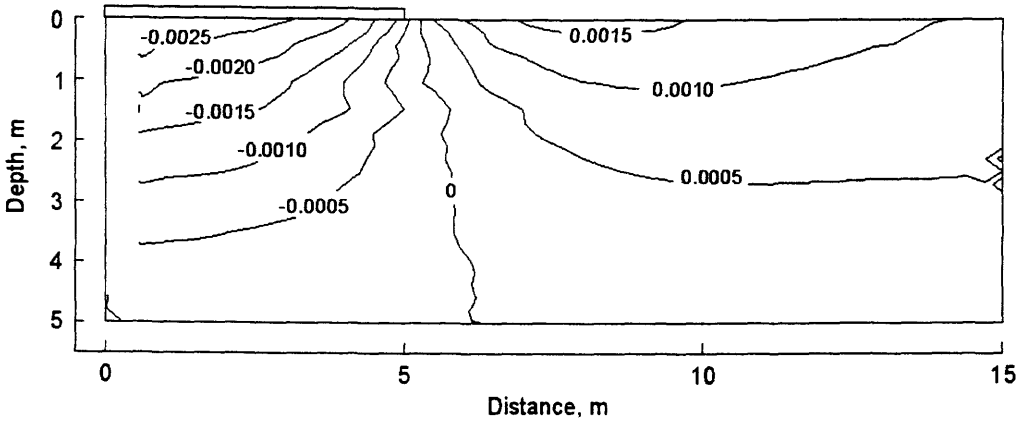

Figure 6.63 Distribution of horizontal strain at day 53, Example 4, uncoupled solution UCS4

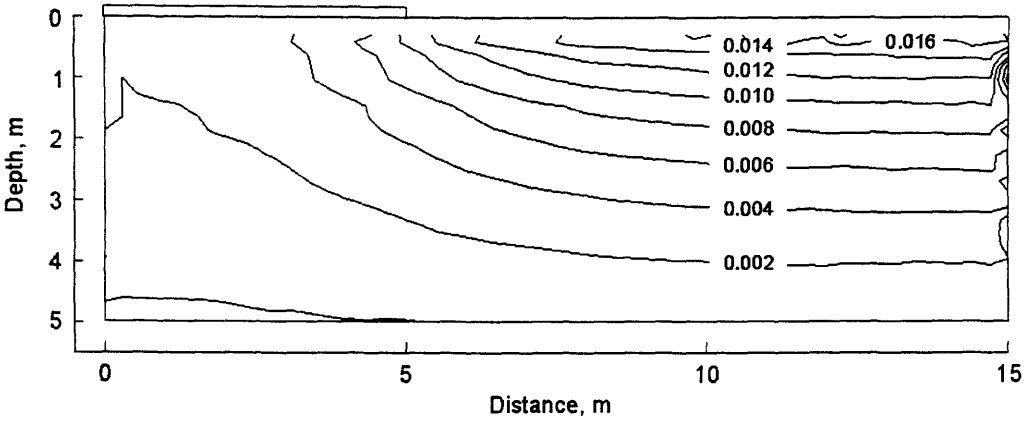

Figure 6.64 Distribution of vertical strain at day 53, Example 4, uncoupled solution UCS4

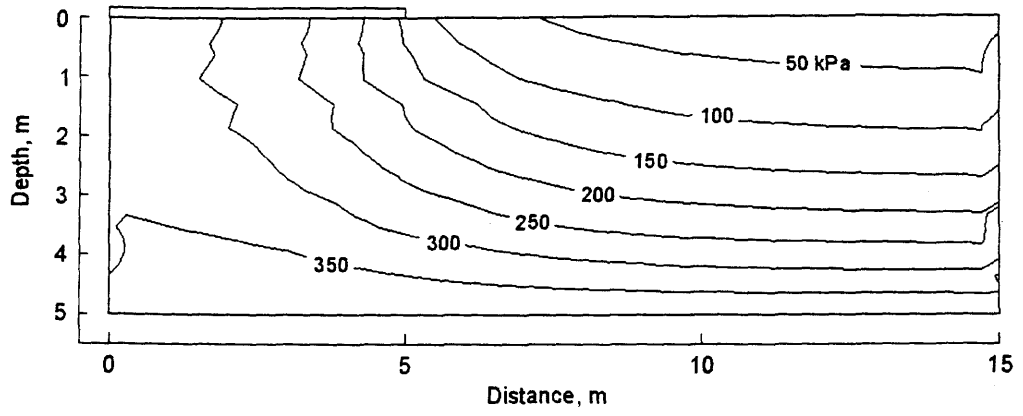

Figure 6.65 Distribution of matric suction at day 175, Example 4, uncoupled solution UCS4

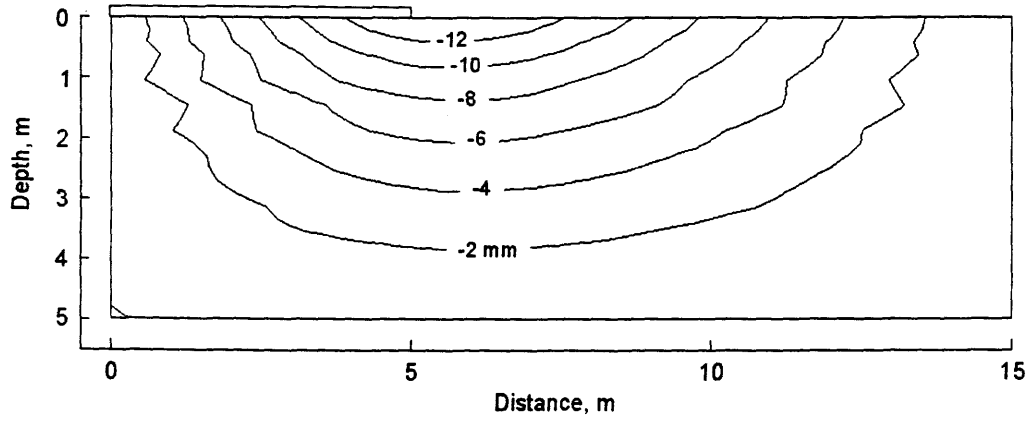

Figure 6.66 Distribution of horizontal displacement at day 175, Example 4, uncoupled solution UCS4

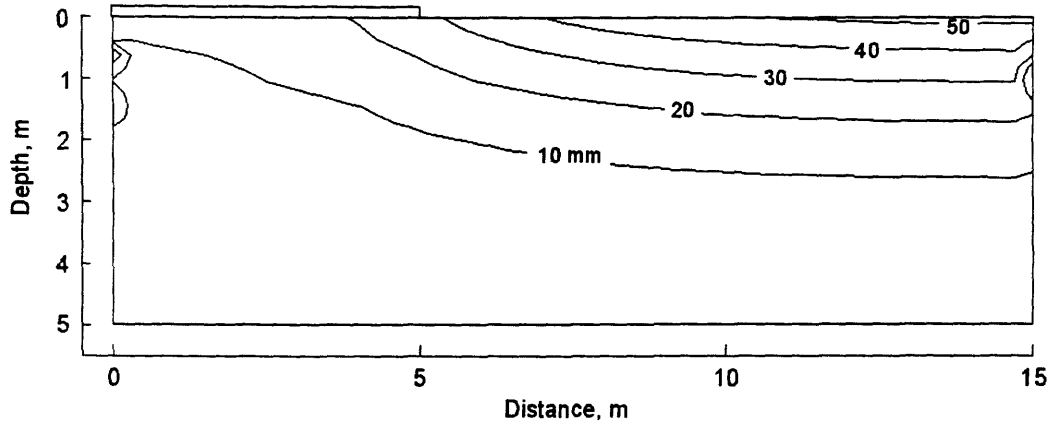

Figure 6.67 Distribution of vertical displacement at day 175, Example 4, uncoupled solution UCS4

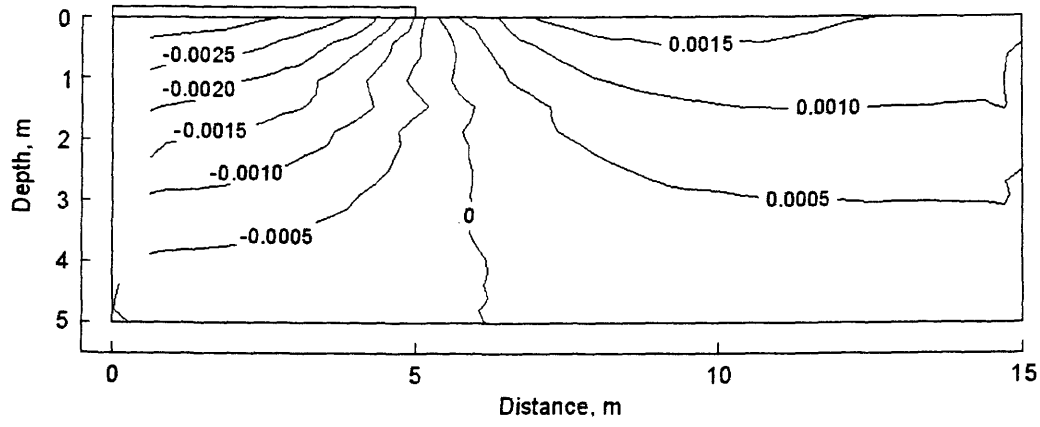

Figure 6.68 Distribution of horizontal strain at day 175, Example 4, uncoupled solution UCS4

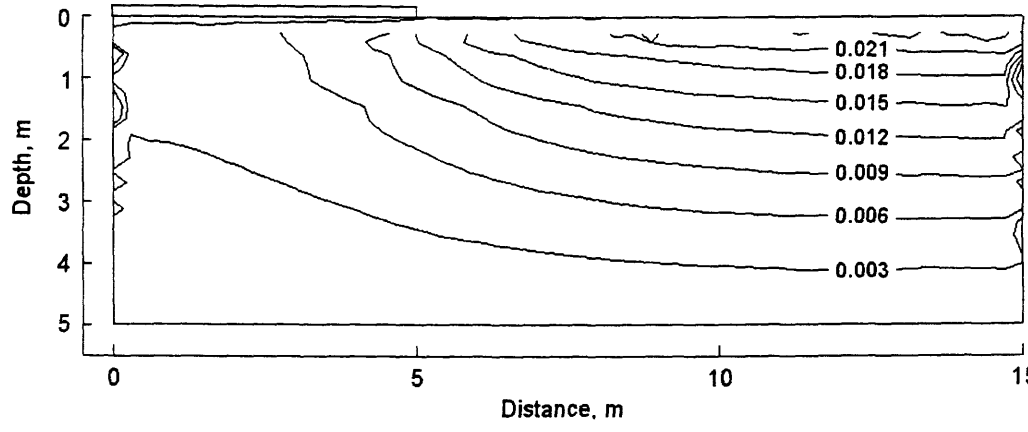

Figure 6.69 Distribution of vertical strain at day 175, Example 4, uncoupled solution UCS4

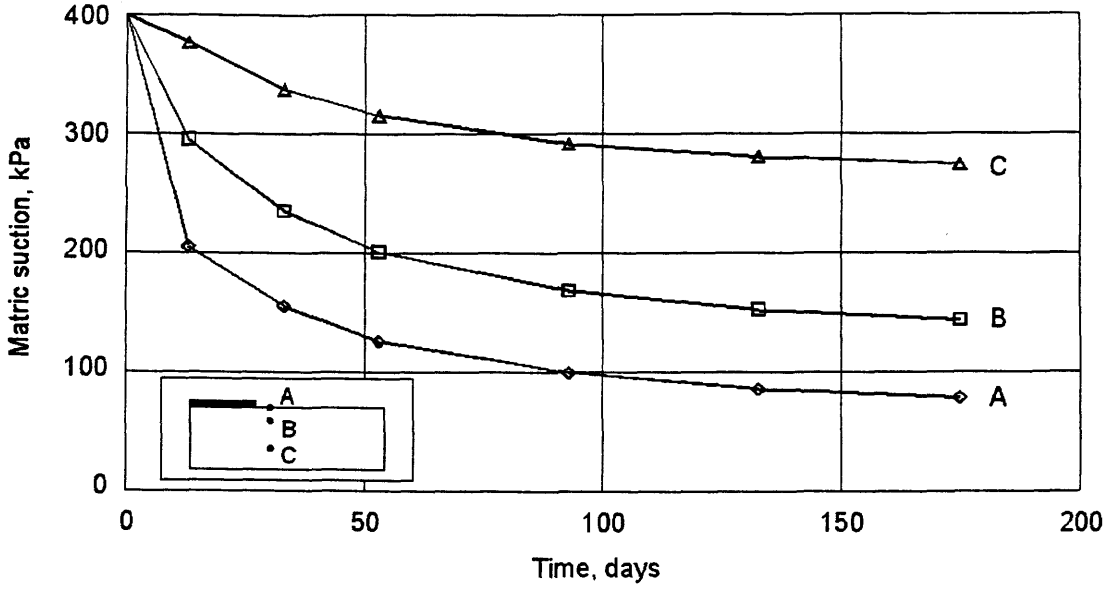

Figure 6.70 Change of matric suction with time for points A, B, and C, Example 4, uncoupled solution UCS4

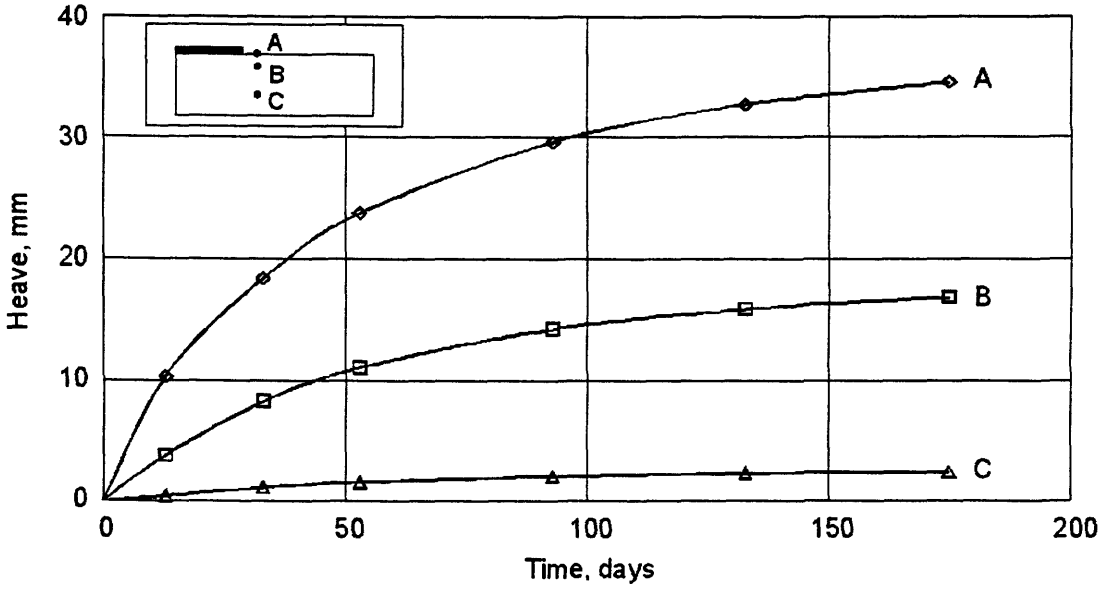

Figure 6.71 Change of vertical displacement with time for points A, B, and C, Example 4, uncoupled solution UCS4

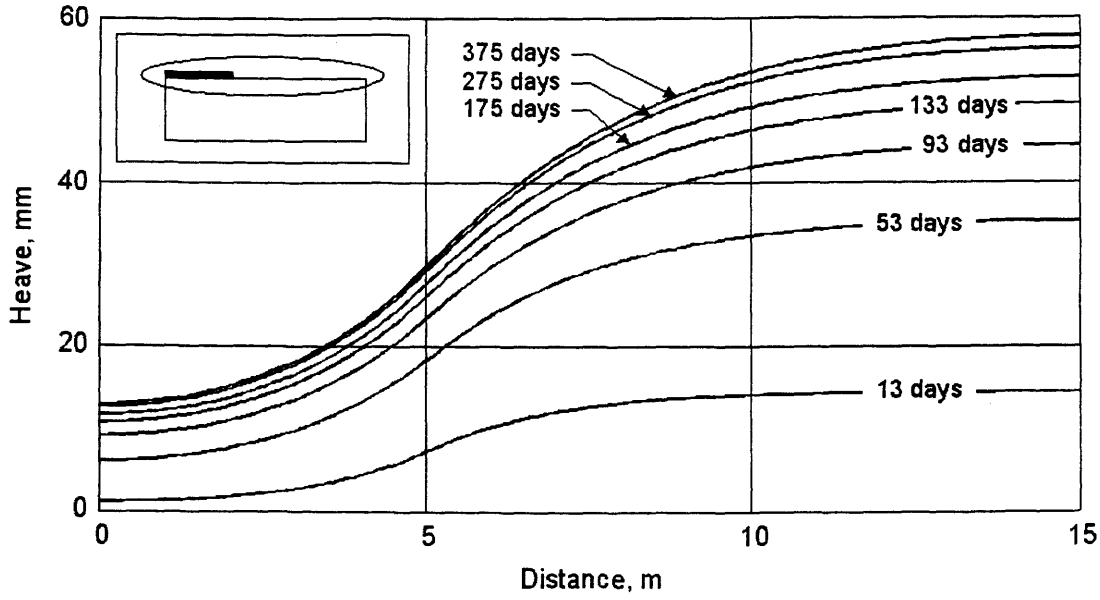

Figure 6.72 Change of heave at ground surface with time, Example 4, uncoupled solution UCS4

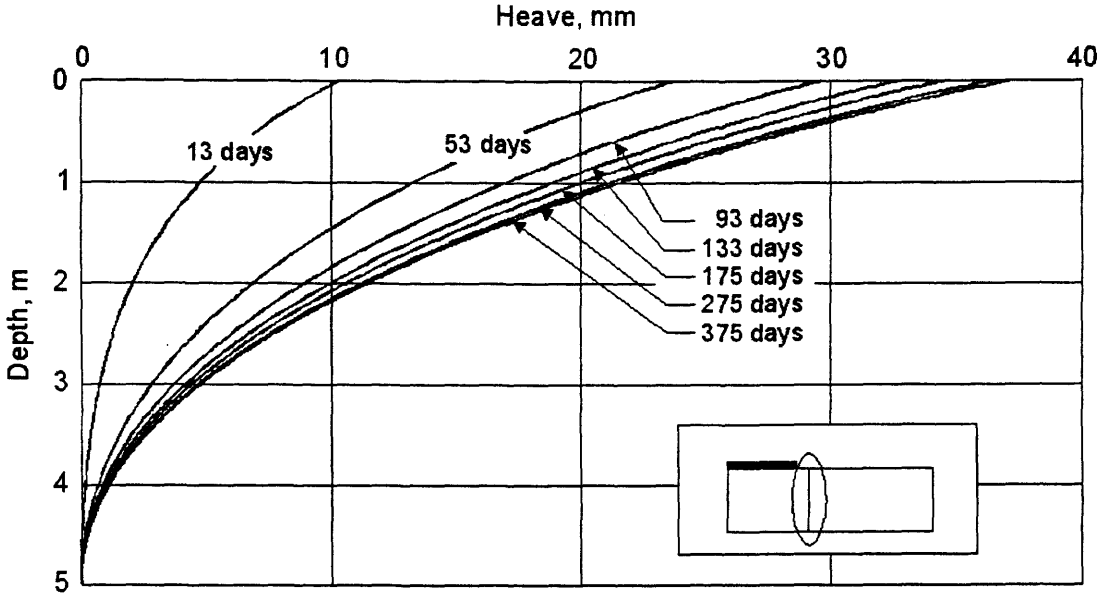

Figure 6.73 Change of heave below the cover versus depth with time, Example 4, uncoupled solution UCS4

6.3.2.2 Coupled analysis, CS for Example 4, infiltration problem

The boundary conditions for the coupled analysis of this example are presented in Fig. 6.74. The transient wetting process is induced by imposing a water infiltration rate equal to 2.0×10^{-8} m/s at the uncovered portion of the ground surface. A value of matric suction equal to 400 kPa is specified at lower boundary, zero flux is specified on the other parts of the boundary. The soil is free to move in the vertical direction and fixed in the horizontal direction at the left and right sides of the domain. The lower boundary is fixed in both directions.

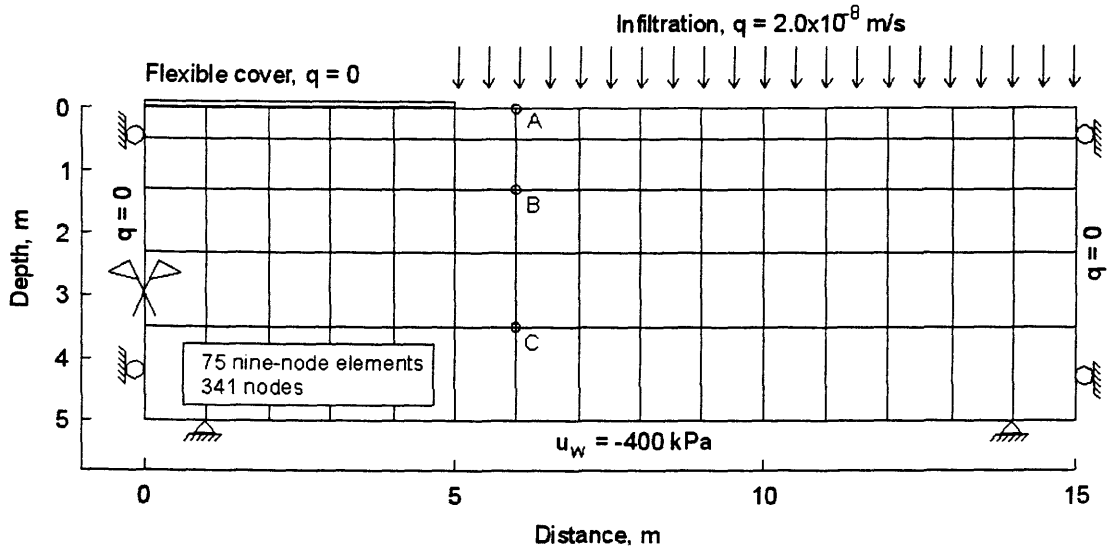

Figure 6.74 Finite element mesh and boundary conditions, Example 4, coupled analysis

The analysis is first performed for various finite element meshes. It is noted that unchaged solutions can be obtained with the mesh of 75 nine-node quadrilateral elements and 341 nodes. Comparisons of the results at days 53 and 355 obtained from mesh 1 (60 elements), mesh 2 (75 elements) and mesh 3 (90 elements) are presented in Appendix A for distributions of matric suction, horizontal displacement, and vertical displacement, respectively. The comparisons of these results are also presented numerically. The finite element mesh of 75 elements and 341 nodes is used for the coupled analysis of this example. The finite element mesh is shown in Fig. 6.74.

The analysis is conducted by tracking both the displacements and matric suction changes as a function of time as the wetting front advances into the soil mass.

Figures 6.75 to 6.83 present the results obtained at day 53 after the wetting commenced. The distribution of matric suction is presented in Fig. 6.75. Distributions of horizontal and vertical stress are presented in Figs. 6.76 and 6.77, respectively. Figures 6.78 and 6.79 present the distributions of void ratio and degree of saturation. Distributions of horizontal and vertical displacement are presented in Figs. 6.80 and 6.81, respectively. Distributions of horizontal and vertical strains are presented in Figs. 6.82 and 6.83, respectively.

Figures 6.84 to 6.92 present the results obtained at day 150 after the wetting commenced. The distribution of matric suction is presented in Fig. 6.84. Distributions of horizontal and vertical stress are presented in Figs. 6.85 and 6.86, respectively. Figures 6.87 and 6.88 present the distributions of void ratio and degree of saturation. Distributions of horizontal and vertical displacement are presented in Figs. 6.89 and 6.90, respectively. Distributions of horizontal and vertical strains are presented in Figs. 6.91 and 6.92, respectively.

Figure 6.93 shows the change of matric suction with time for points A, B, and C. The change of horizontal stress with time for points A, B, and C is presented in Fig. 6.94. Figures 6.95 shows the change of vertical displacement with time at points A, B, and C in the soil mass. Figure 6.96 shows the change of heave at ground surface with time. Figure 6.97 presents the change of heave below the cover versus depth with time.

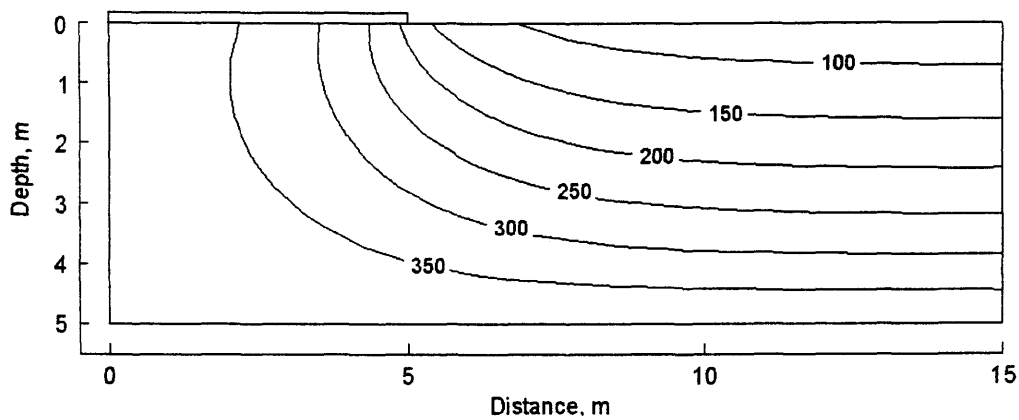

Figure 6.75 Distribution of matric suction at day 53, Example 4, coupled solution

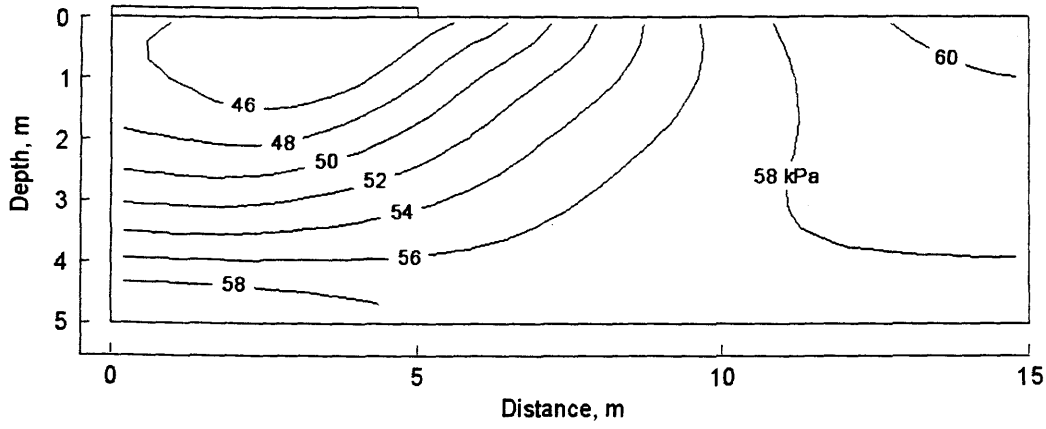

Figure 6.76 Distribution of horizontal stress at day 53, Example 4, coupled solution

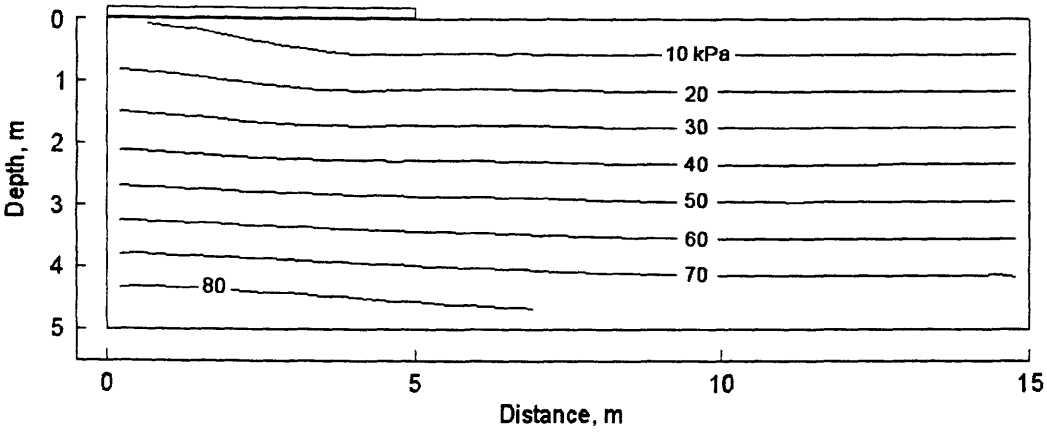

Figure 6.77 Distribution of vertical stress at day 53, Example 4, coupled solution

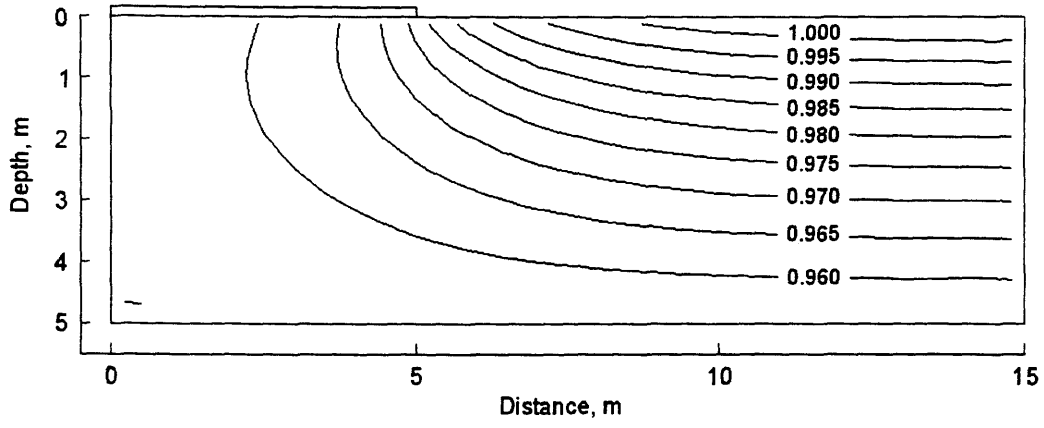

Figure 6.78 Distribution of void ratio at day 53, Example 4, coupled solution

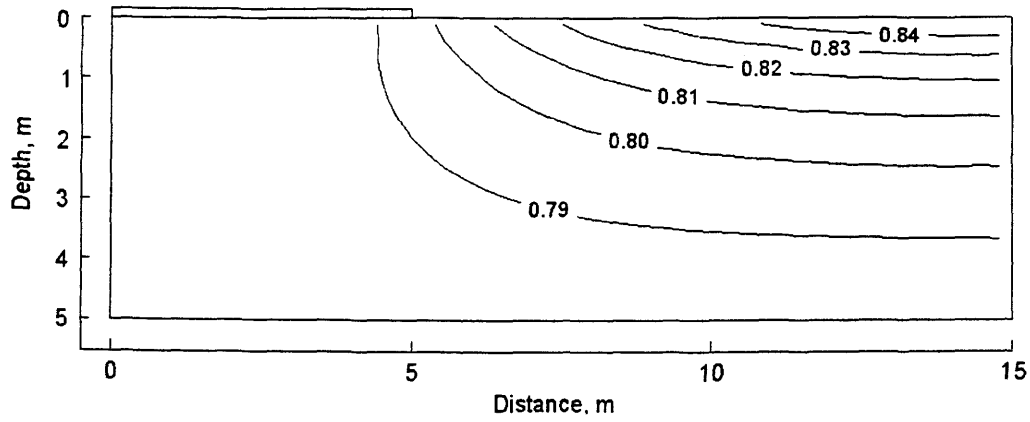

Figure 6.79 Distribution of degree of saturation at day 53, Example 4, coupled solution

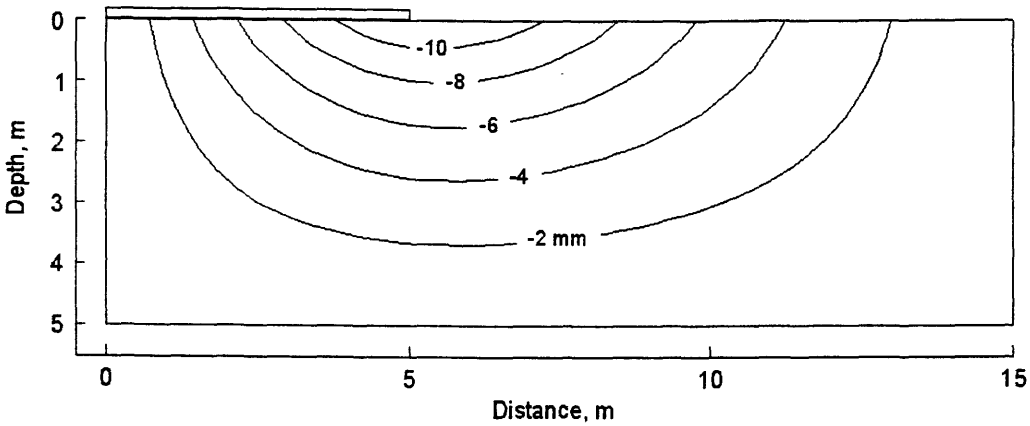

Figure 6.80 Distribution of horizontal displacement at day 53, Example 4, coupled solution

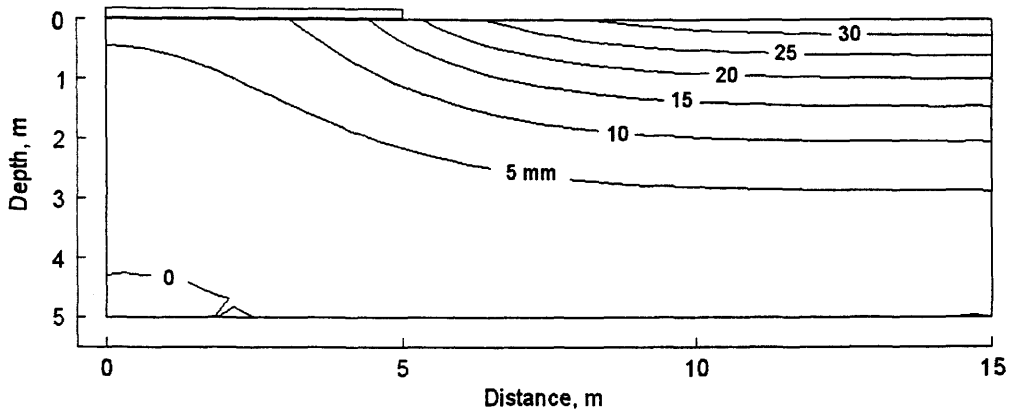

Figure 6.81 Distribution of vertical displacement at day 53, Example 4, coupled solution

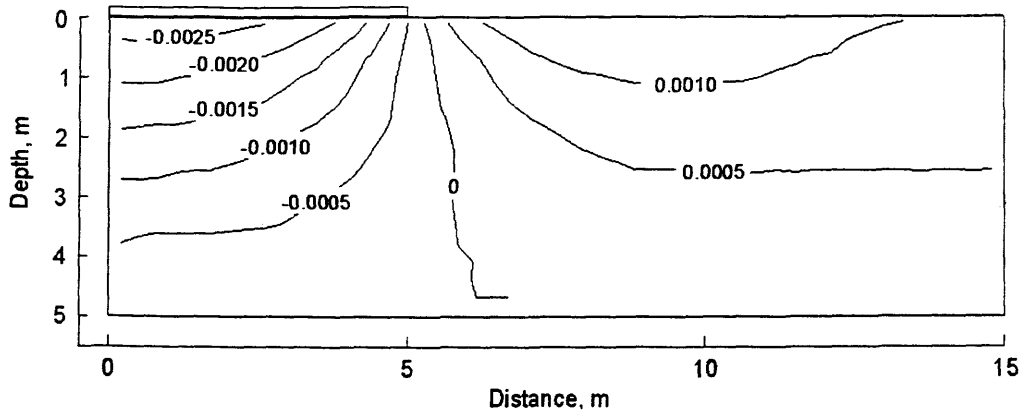

Figure 6.82 Distribution of horizontal strain at day 53, Example 4, coupled solution

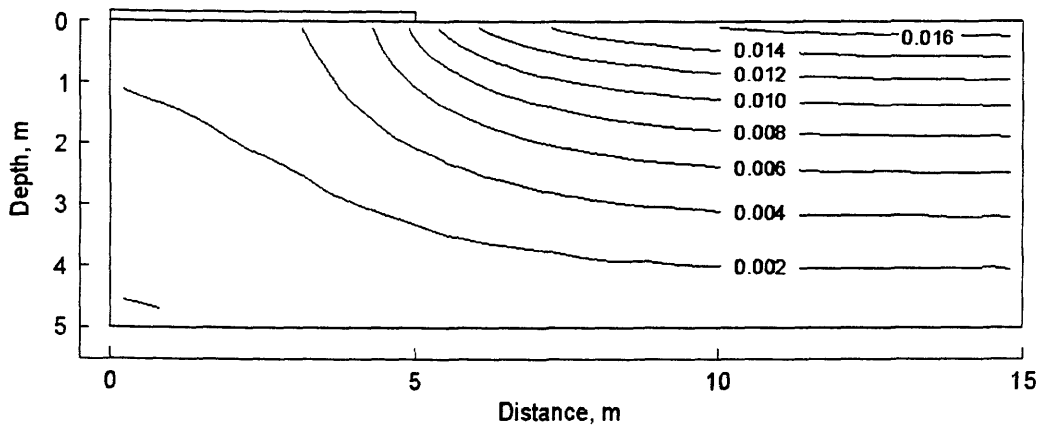

Figure 6.83 Distribution of vertical strain at day 53, Example 4, coupled solution

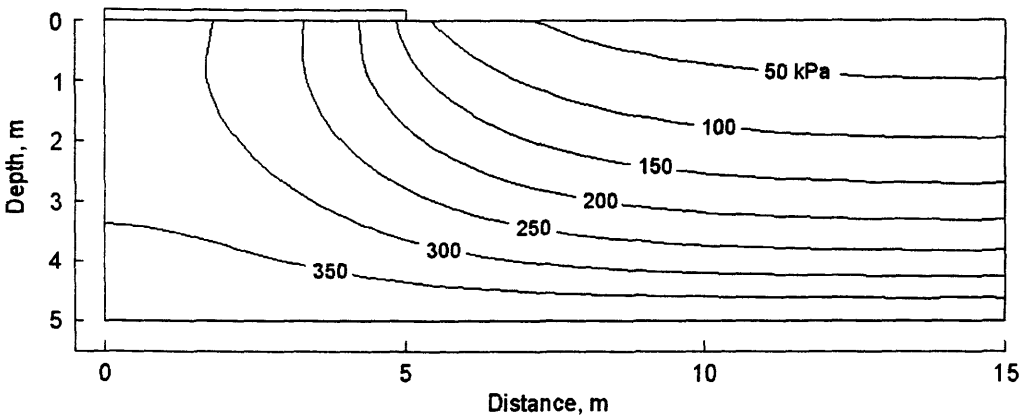

Figure 6.84 Distribution of matric suction at day 175, Example 4, coupled solution

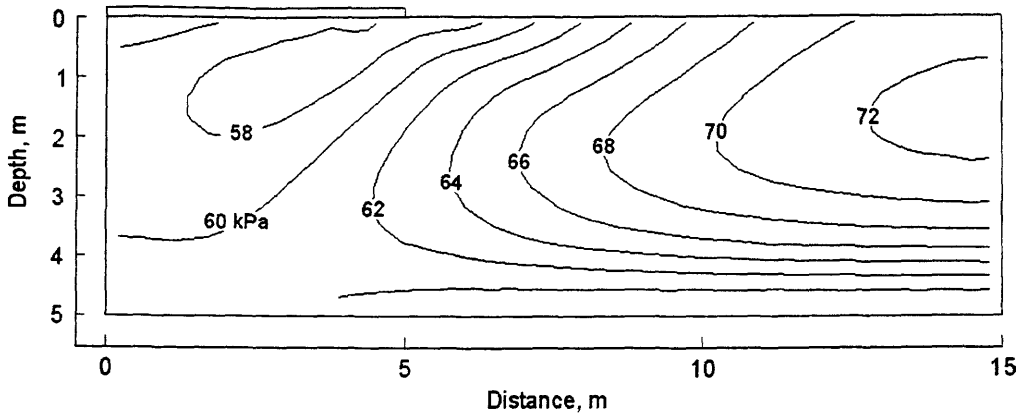

Figure 6.85 Distribution of horizontal stress at day 175, Example 4, coupled solution

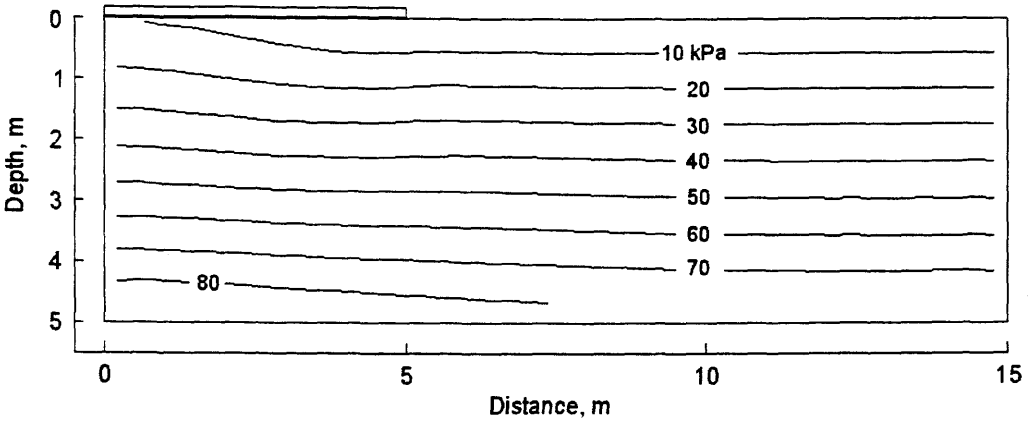

Figure 6.86 Distribution of vertical stress at day 175, Example 4, coupled solution

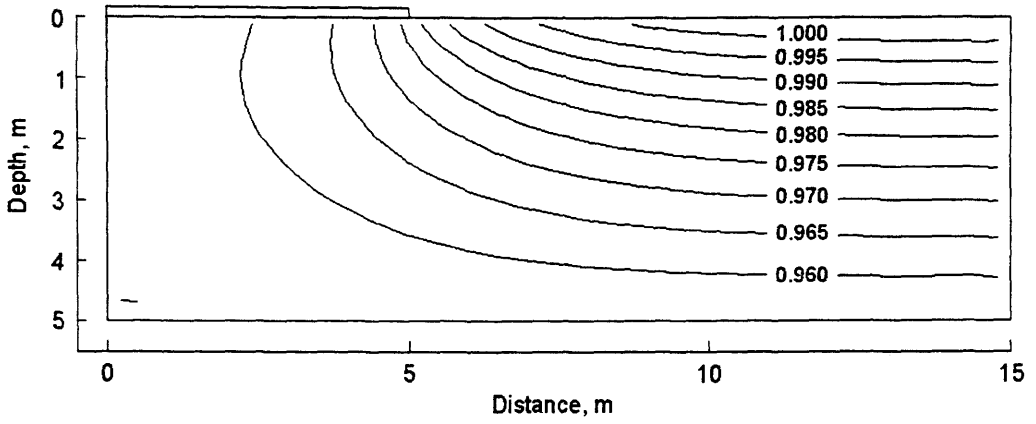

Figure 6.87 Distribution of void ratio at day 175, Example 4, coupled solution

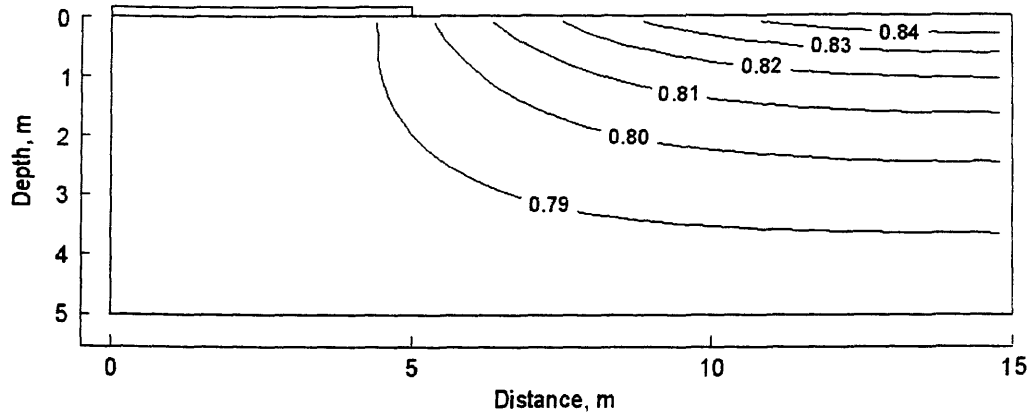

Figure 6.88 Distribution of degree of saturation at day 175, Example 4, coupled solution

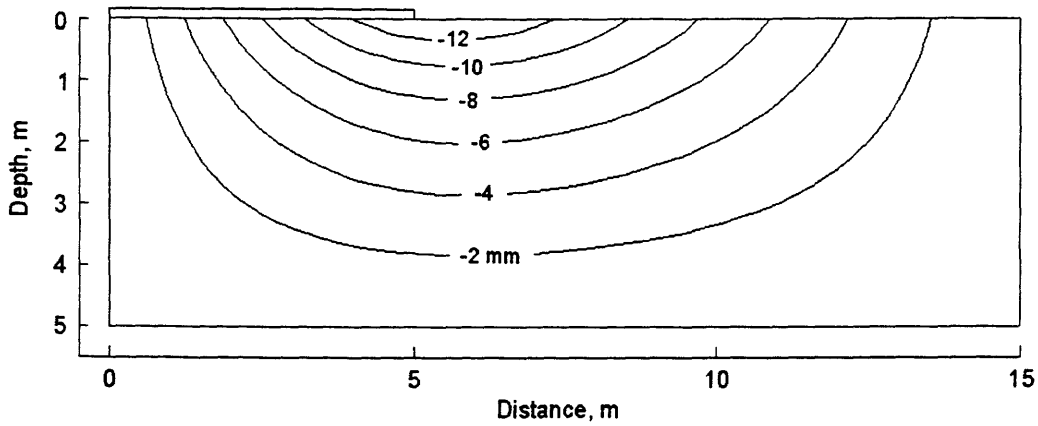

Figure 6.89 Distribution of horizontal displacement at day 175, Example 4, coupled solution

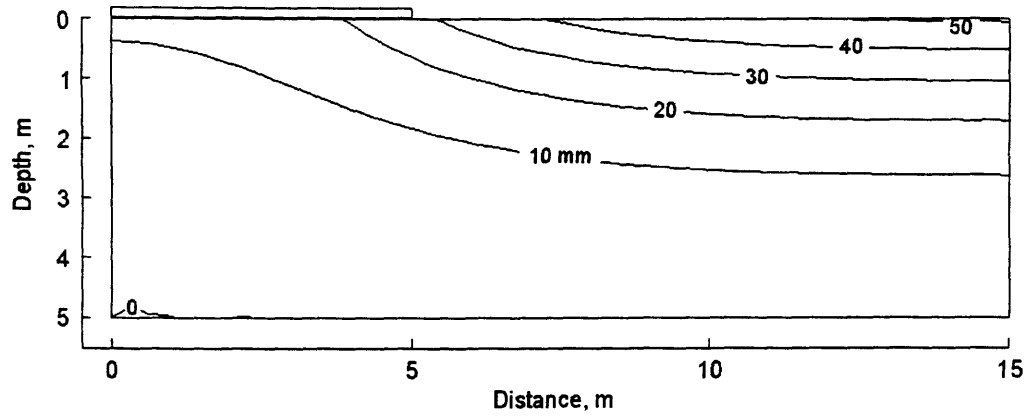

Figure 6.90 Distribution of vertical displacement at day 175, Example 4, coupled solution

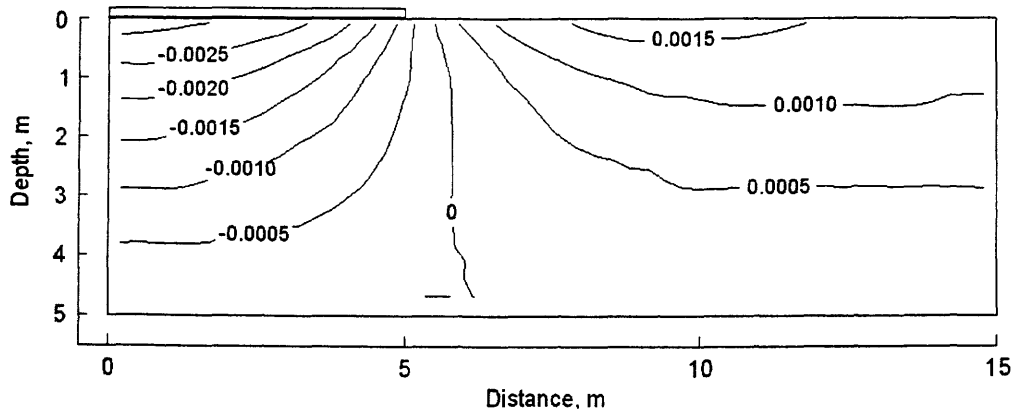

Figure 6.91 Distribution of horizontal strain at day 175, Example 4, coupled solution

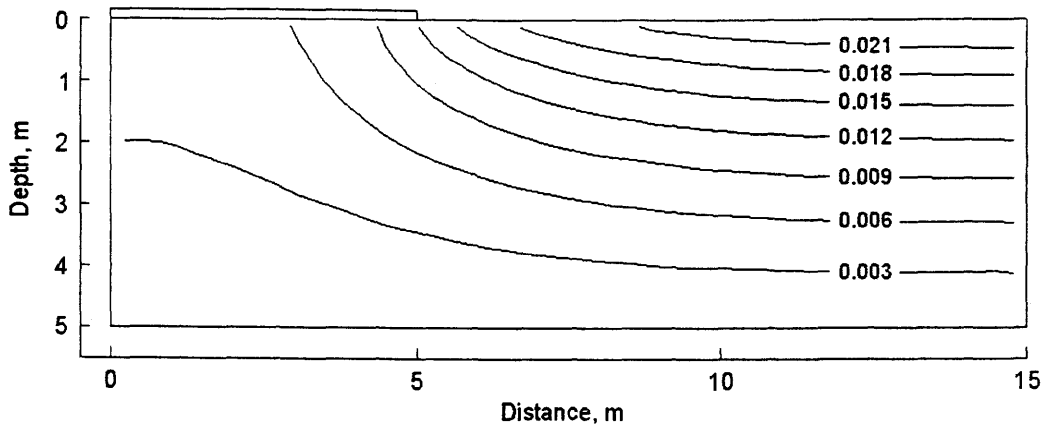

Figure 6.92 Distribution of vertical strain at day 175, Example 4, coupled solution

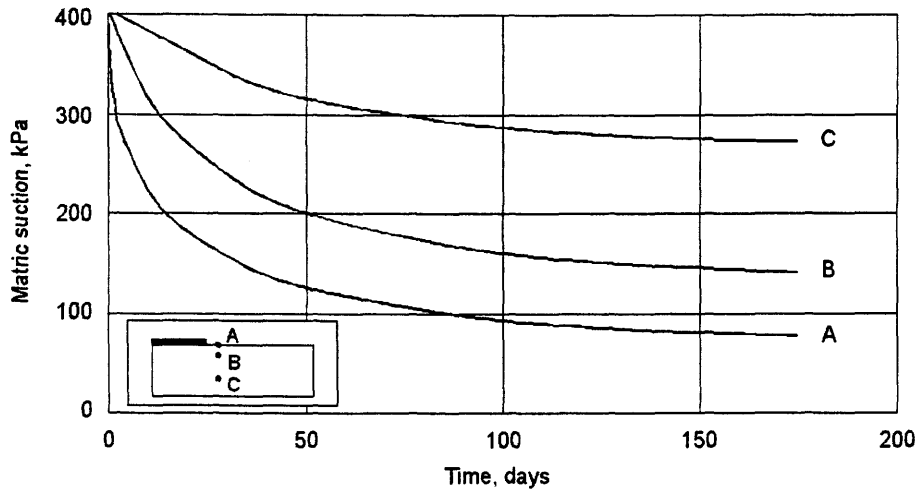

Figure 6.93 Change of matric suction with time for points A, B, and C, Example 4, coupled solution

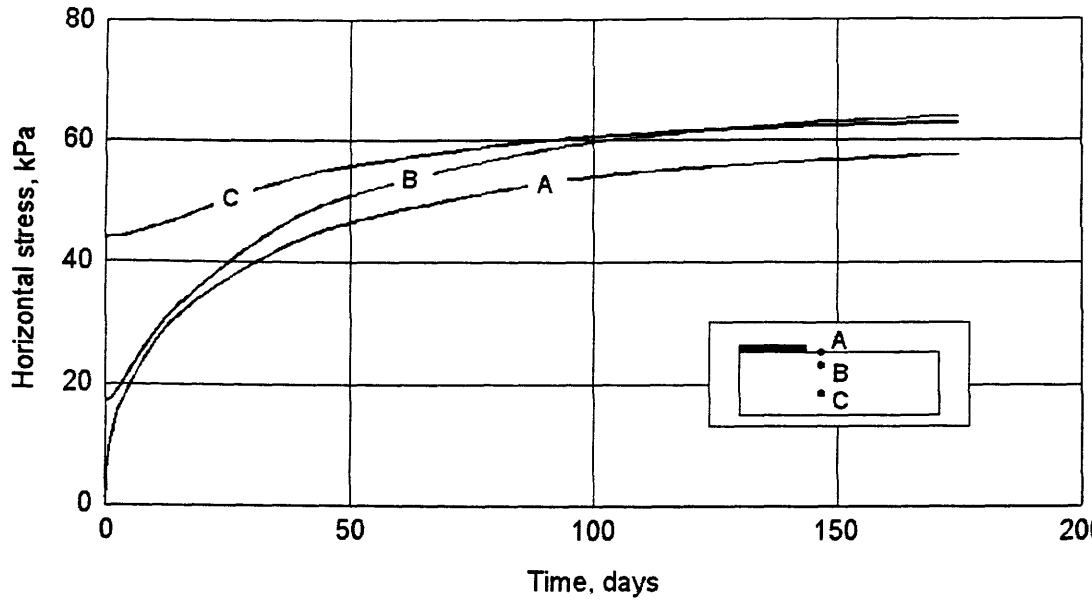

Figure 6.94 Change of horizontal stress with time for points A, B, and C, Example 4, coupled solution

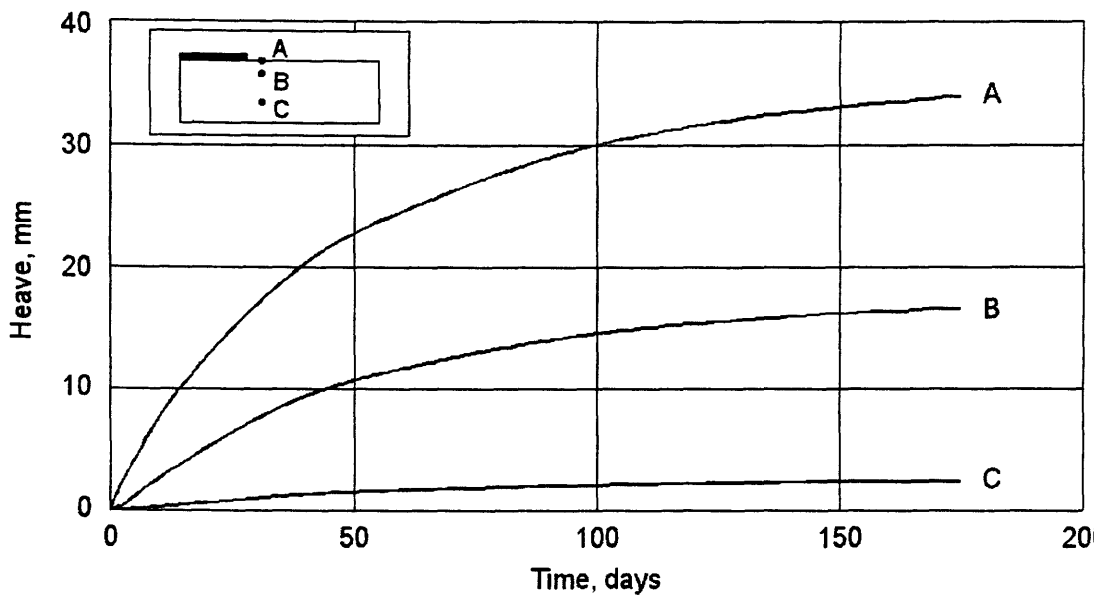

Figure 6.95 Change of vertical displacement with time for points A, B, and C, Example 4, coupled solution

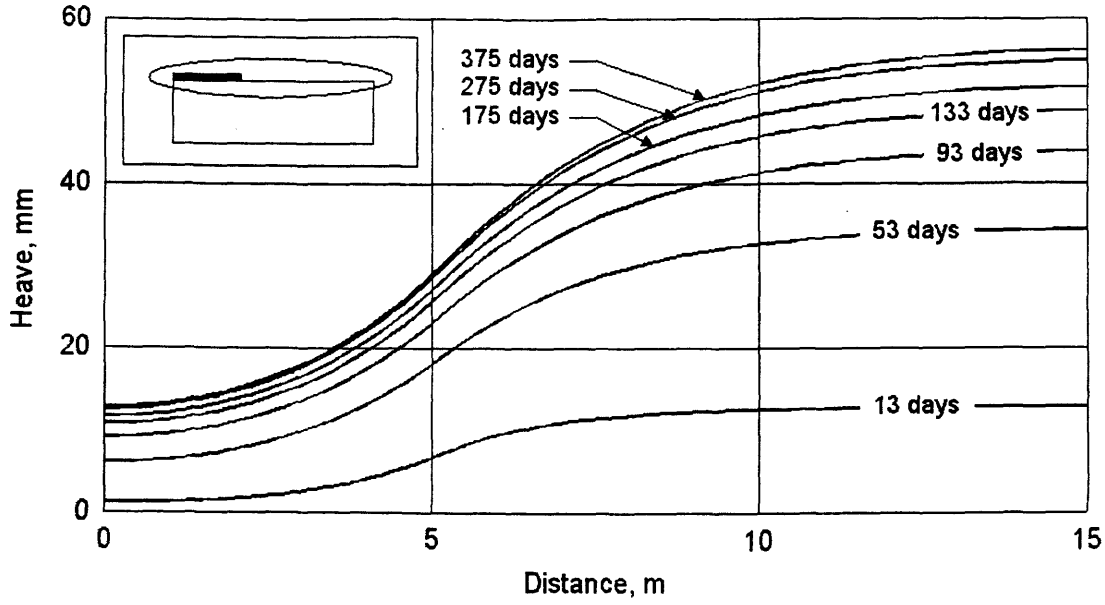

Figure 6.96 Change of heave at ground surface with time, Example 4 coupled solution

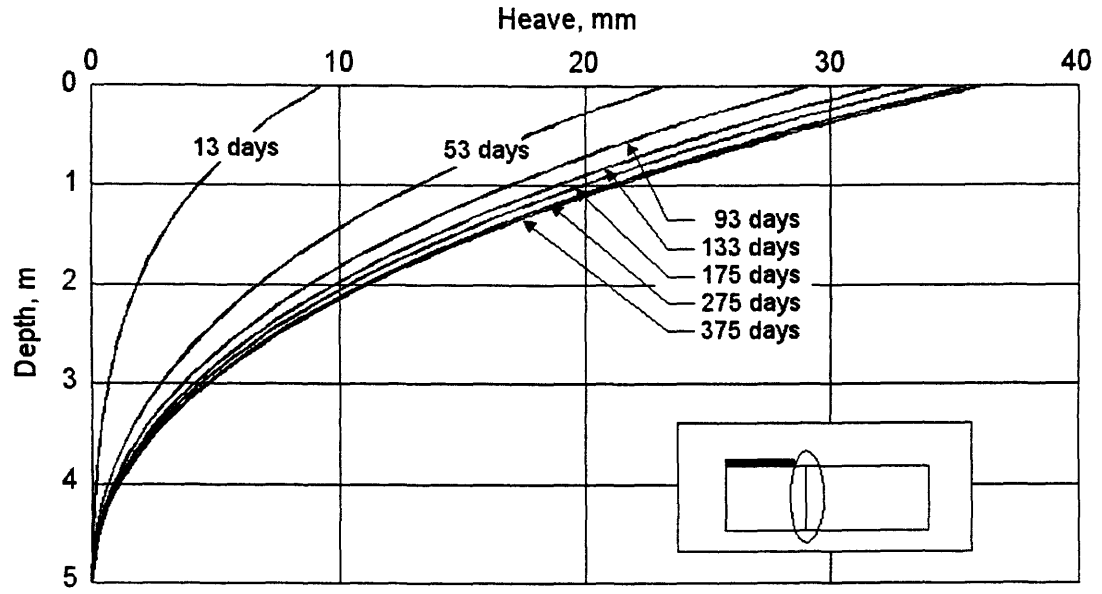

Figure 6.97 Change of heave below the cover versus depth with time, Example 4, coupled solution

6.4 Parametric study with respect to the assumed value of Poisson's ratio for coupled solutions

This section presents the effect of the assumed value of Poisson's ratio on coupled solutions. Two example problems (i.e., Example 3 and Example 4) are analysed using a coupled approach for various values of Poisson's ratio.

6.4.1 Parametric study with respect to the assumed value of Poisson's ratio, Example 3

Figure 6.98 presents the change of matric suction at point B for various values of Poisson's ratio. Figure 6.99 presents the matric suction versus Poisson's ratio relationship for various times. Figure 6.100 presents the change of horizontal displacement at point B for various values of Poisson's ratio. Figure 6.101 presents the horizontal displacement versus Poisson's ratio relationship for various times. Figure 6.102 presents the change of vertical displacement at point B for various values of Poisson's ratio. Figure 6.103 presents the vertical displacement versus Poisson's ratio relationship for various times.

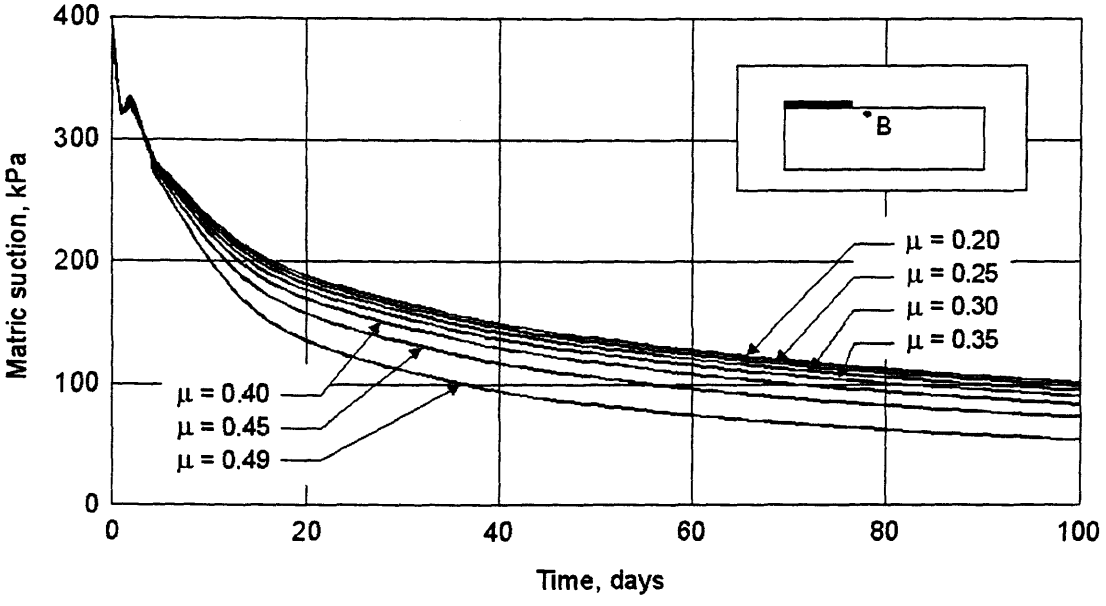

Figure 6.98 Change of matric suction at point B for various values of Poisson's ratio, Example 3, coupled solution

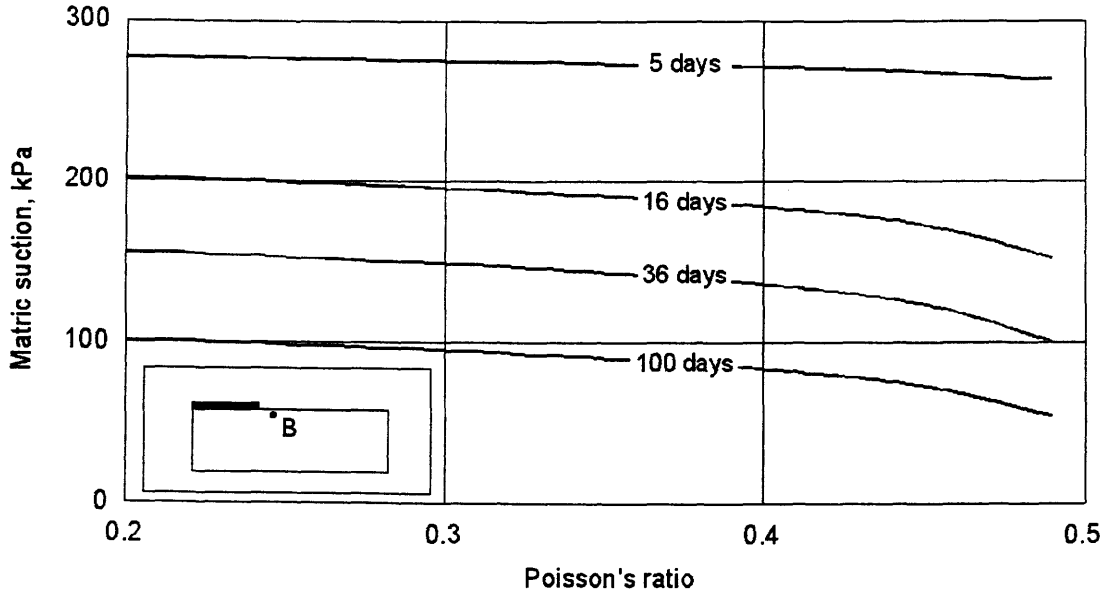

Figure 6.99 Matric suction at point B versus Poisson's ratio for various elapsed times, Example 3, coupled solution

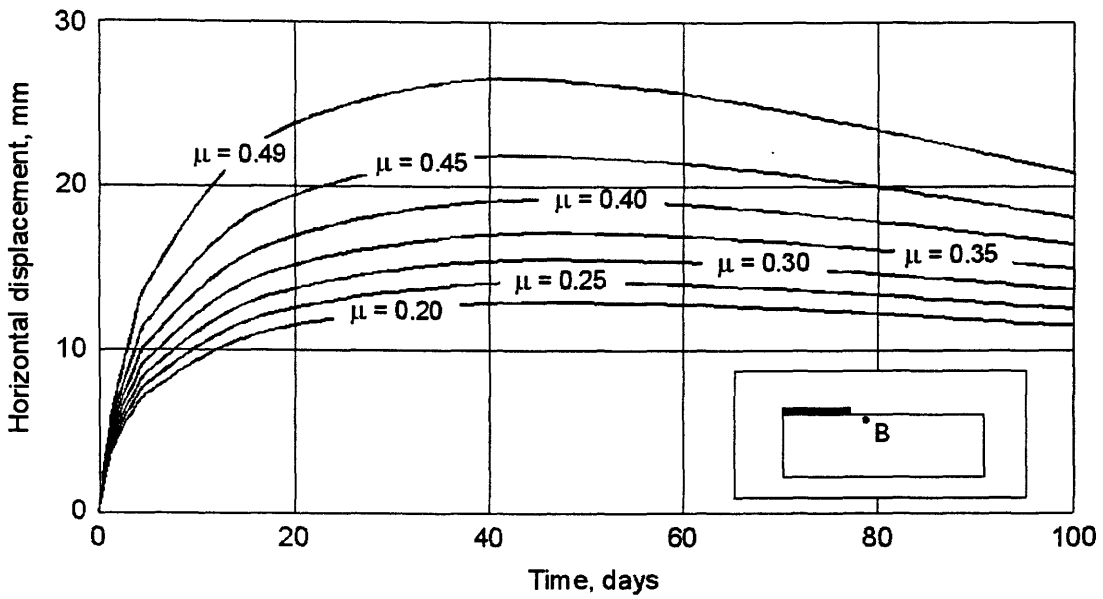

Figure 6.100 Change of horizontal displacement at point B for various values of Poisson's ratio, Example 3, coupled solution

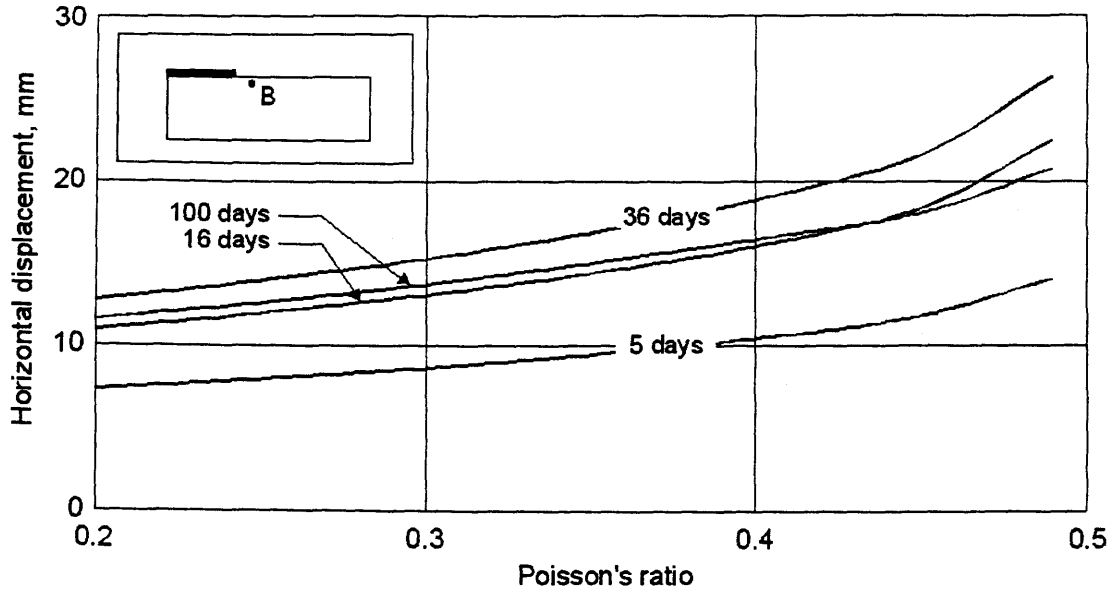

Figure 6.101 Horizontal displacement at point B versus Poisson's ratio for various elapsed time, Example 3, coupled solution

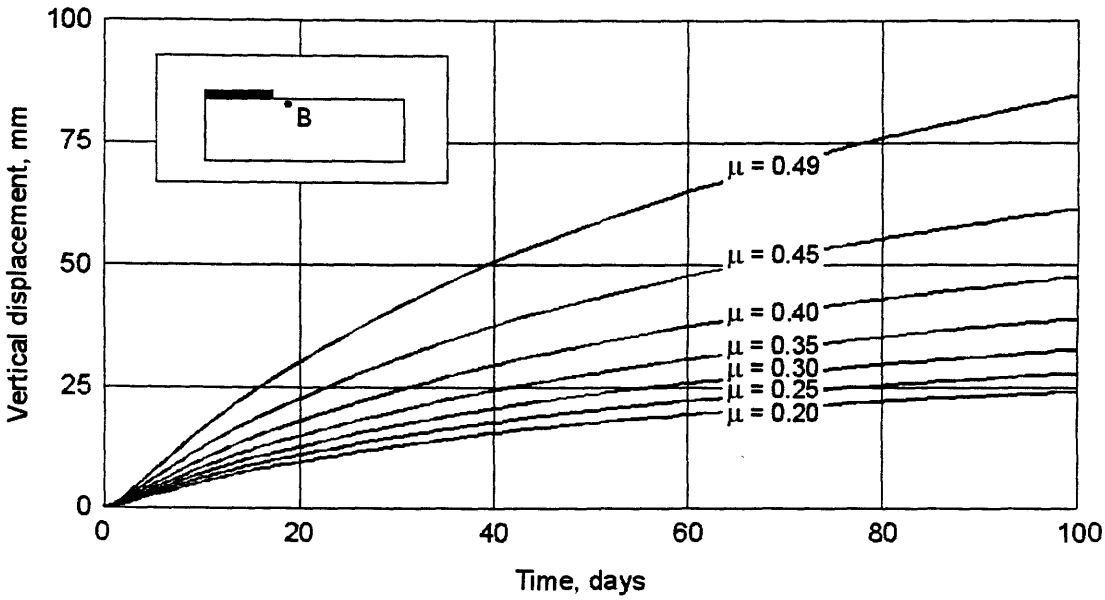

Figure 6.102 Change of vertical displacement at point B for various values of Poisson's ratio, Example 3, coupled solution

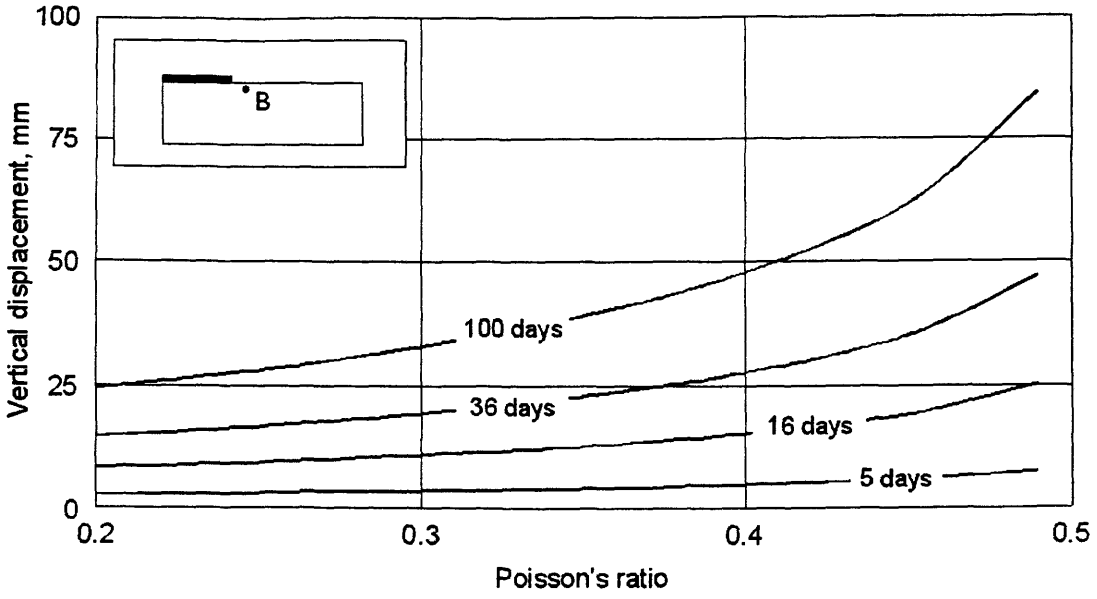

Figure 6.103 Vertical displacement at point B versus Poisson's ratio for various elapsed time, Example 3, coupled solution

6.4.2 Parametric study with respect to the assumed value of Poisson's ratio, Example 4

Figure 6.104 presents the change of matric suction at point B for various values of Poisson's ratio. Figure 6.105 presents the matric suction versus Poisson's ratio relationship for various times. Figures 6.106 presents the relationship between horizontal stress and Poisson's ratio obtained at day 175. Figures 6.107 presents the relationship between vertical stress and Poisson's ratio obtained at day 175. Figure 6.108 presents the change of horizontal displacement at point B for various values of Poisson's ratio. Figure 6.109 presents the horizontal displacement versus Poisson's ratio relationship for various times. Figure 6.110 presents the change of vertical displacement at point B for various values of Poisson's ratio. Figure 6.111 presents the vertical displacement versus Poisson's ratio relationship for various times.

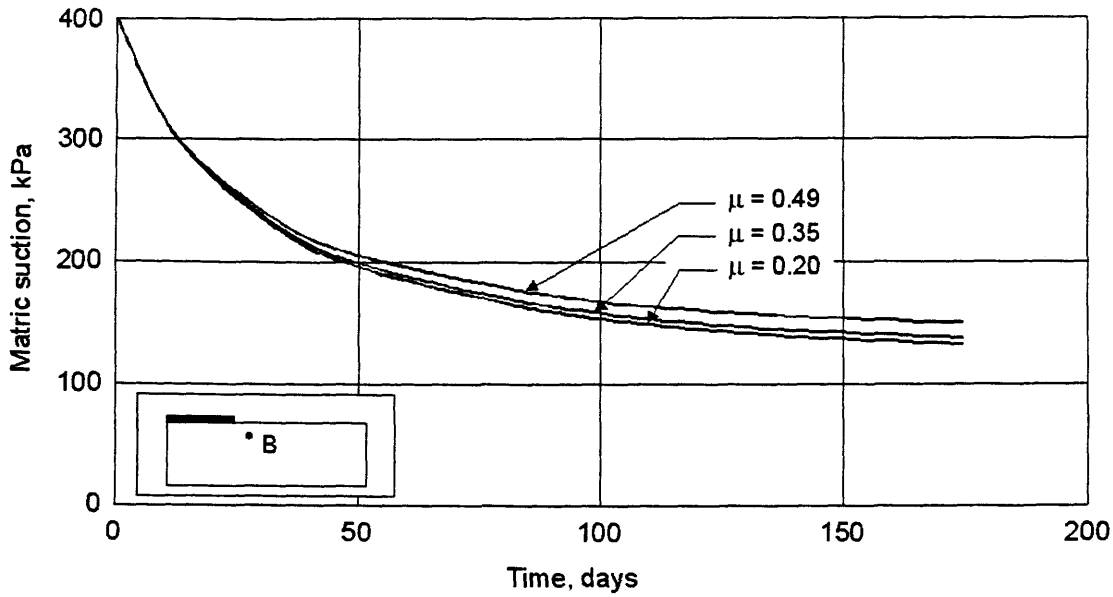

Figure 6.104 Change of matric suction at point B for various values of Poisson's ratio, Example 4, coupled solution

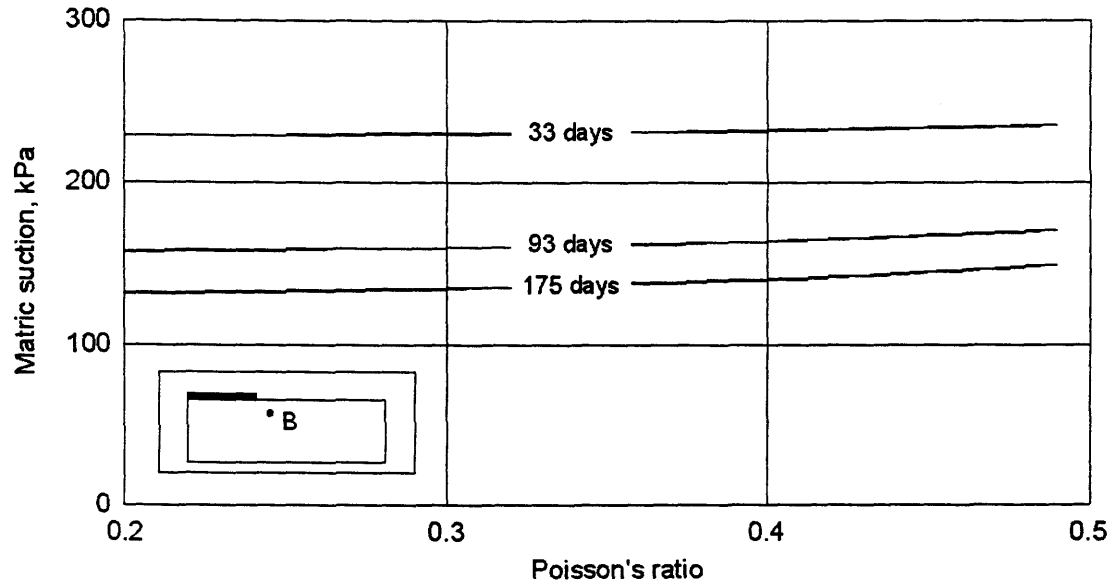

Figure 6.105 Matric suction at point B versus Poisson's ratio for various elapsed times, Example 4, coupled solution

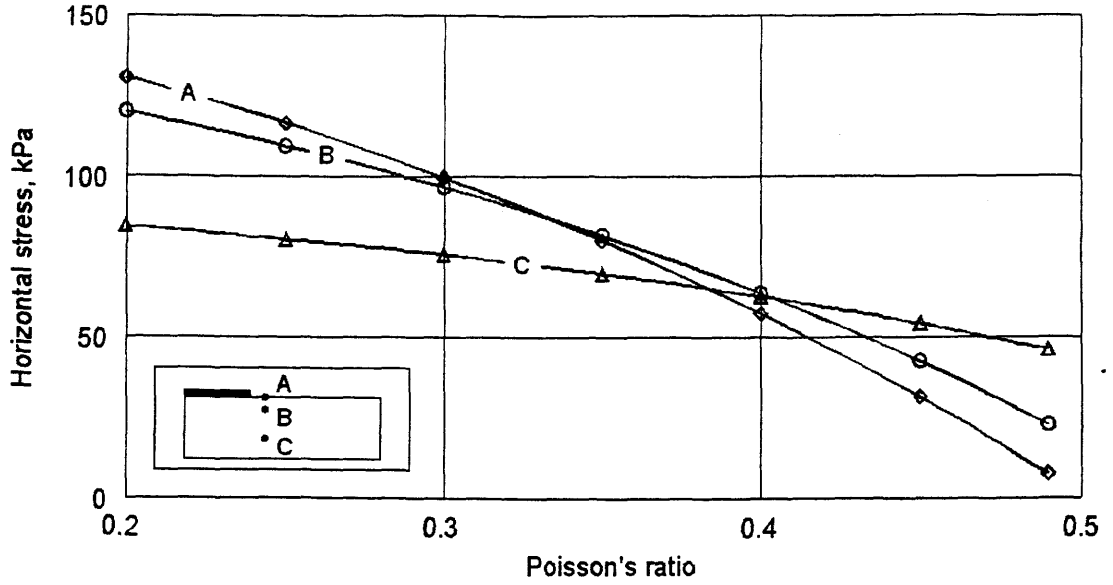

Figure 6.106 Horizontal stress versus Poisson's ratio for points A, B, and C at day 175, Example 4, coupled solution

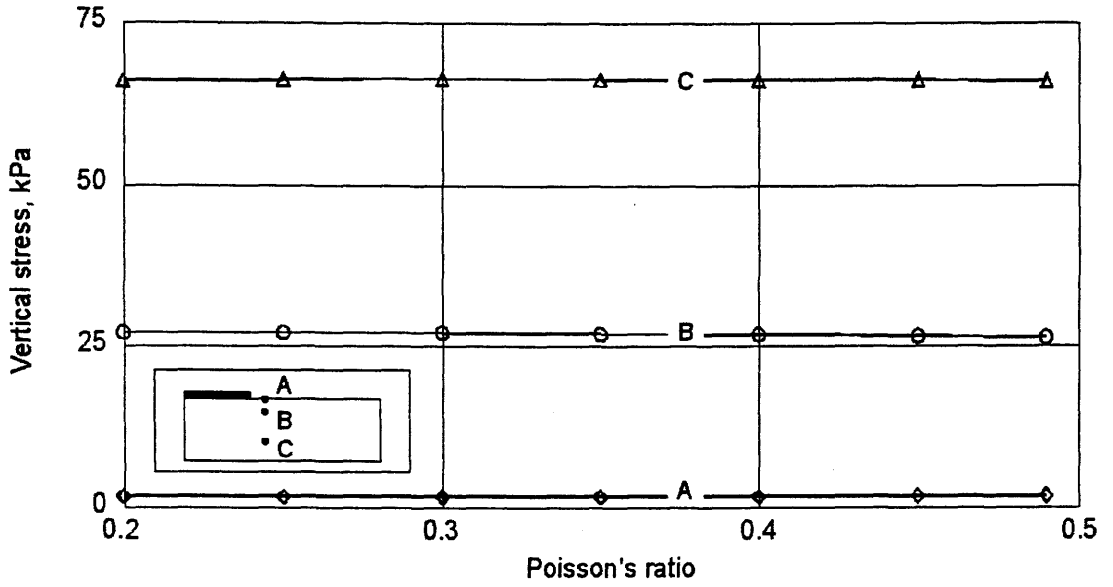

Figure 6.107 Vertical stress versus Poisson's ratio for points A, B, and C at day 175, Example 4, coupled solution

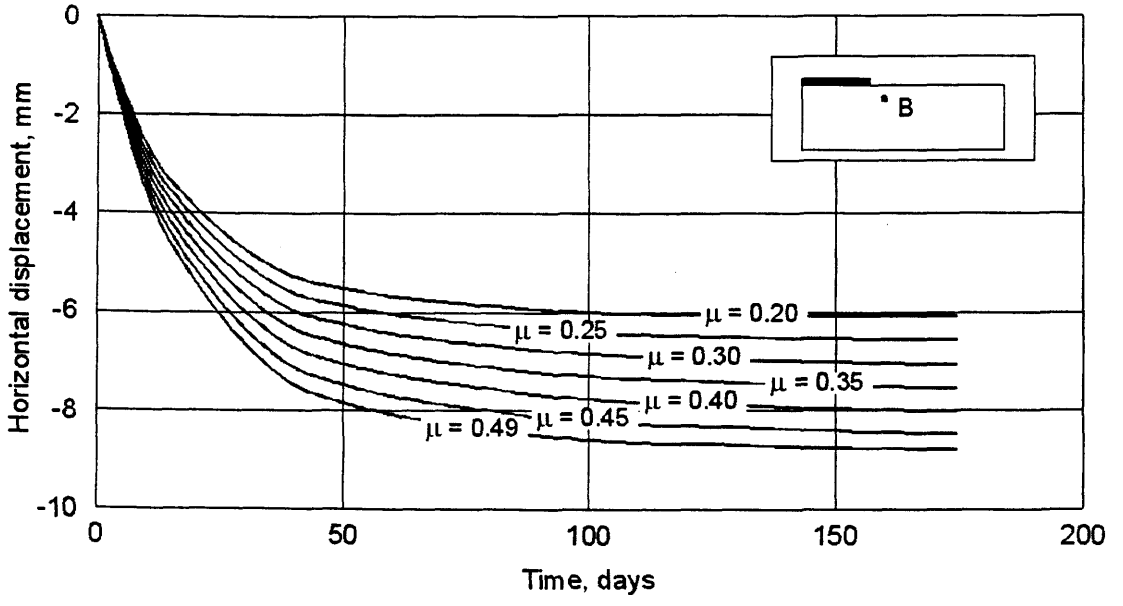

Figure 6.108 Change of horizontal displacement at point B for various values of Poisson's ratio, Example 4, coupled solution

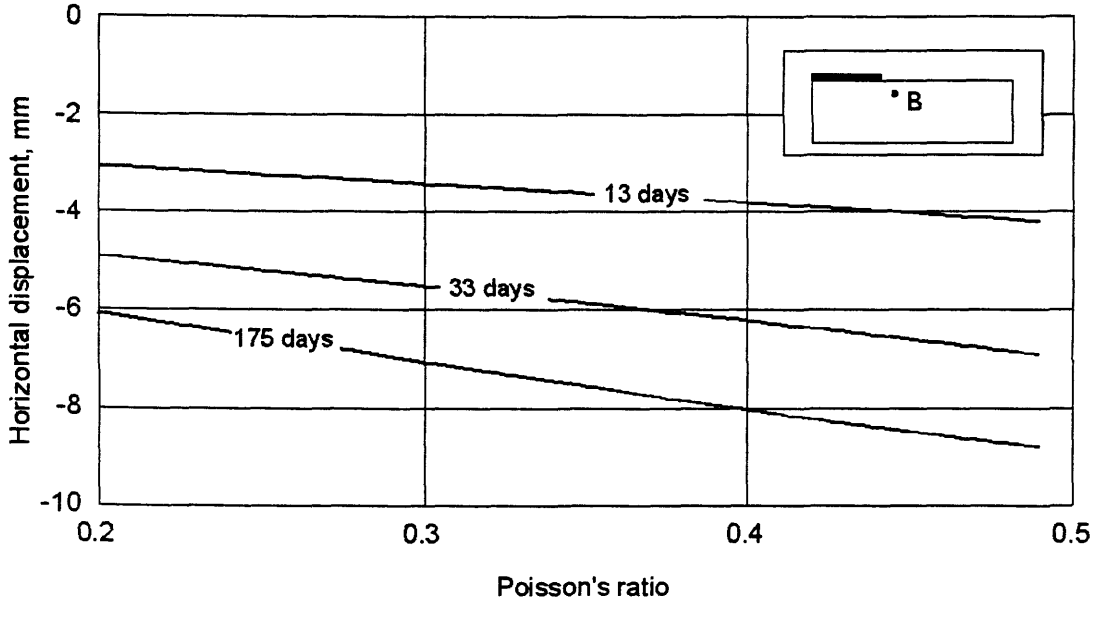

Figure 6.109 Horizontal displacement at point B versus Poisson's ratio for various elapsed times, Example 4, coupled solution

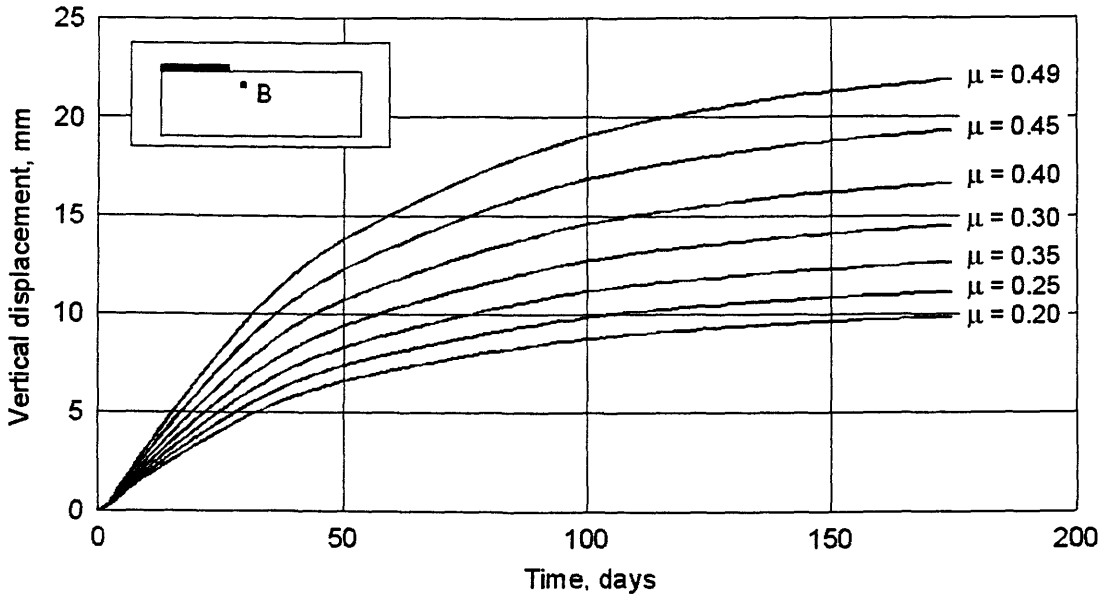

Figure 6.110 Change of vertical displacement at point B for various values of Poisson's ratio, Example 4, coupled solution

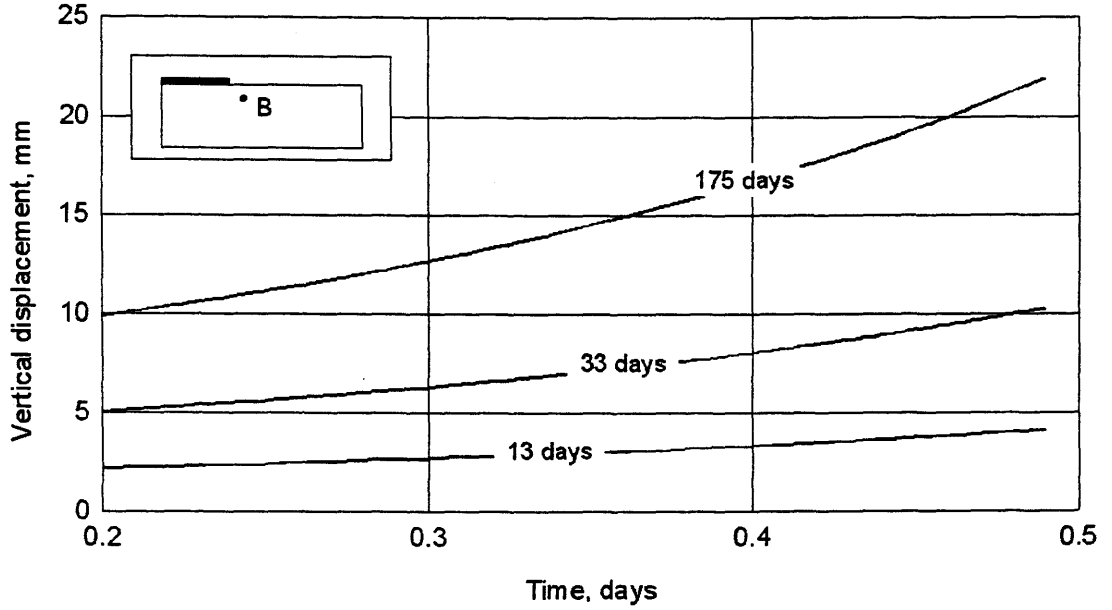

Figure 6.111 Vertical displacement at point B versus Poisson's ratio for various elapsed times, Example 4, coupled solution

6.5 Summary of the presentation of results

Volume change problems associated with unsaturated, expansive soils can be analysed using both uncoupled and coupled approaches. The analysis results of four example problems are presented. The discussion of the results will be presented in the next chapter.

CHAPTER 7

Discussions of the Results

7.1 General

This chapter presents a discussion of the results of analyses presented in Chapter 6. The problem of water uptake by trees is discussed with respect to the uncoupled solutions of two examples (i.e., Example 1 and Example 2) in section 7.2. The problems associated with water leakage under a flexible cover (i.e., Example 3) and water infiltration from ground surface (i.e., Example 4) are discussed for both uncoupled solutions and coupled solutions in sections 7.3. Various types of uncoupled analyses have been carried out for Examples 3 and 4. Section 7.3 also presents the discussion on the agreement between uncoupled and coupled solutions associated with each example. Section 7.4 discusses the effect of Poisson's ratio on the coupled solutions for Examples 3 and 4. Section 7.5 summarizes the discussion of the results of the analysis.

7.2 Uncoupled solutions to the problem of water uptake by trees

Jones and Holtz (1973) reported that a high cost of damage in the US was caused by expansive soils. The loss figure was about $6000 million annually. About 20% of this damage could be contributed to desiccation effects due to vegetation (Holtz, 1983). Williams and Pidgeon (1983) reported that the removal of vegetation causes the most significant change in the stress state of the soil, which exceeds any changes that may be caused by building load or excavation for small structures. Ward (1953) suggested that trees, which transpired large quantities of moisture, could damage building at distances up to the height of the tree. The smallest tree at which a problem was noted

was 250 mm in diameter. This indicated that only mature trees caused serious problems. It was suggested that a deepening of the foundation from a traditional depth of 1 to 1.5 m would considerably reduce the change of damage.

In Chicago, trees were found to be the predominant reason for desiccation and shrinkage. Individual trees may lose from 0.25 to 0.50 m^3 of water on a sunny day (Perpich et al., 1965). In general, when the soil suction approaches 1500 kPa, the wilting point of the tree is attained and leaf growth stops (Kramer & Kozlowski, 1960). However, the value of soil suction imposed by trees has been measured experimentally in the field and found to be up to 3000 kPa.

Ground movements due to trees, in excess of 150 mm were recorded in expansive clays in Adelaide, Australia (Richards et al., 1983). The ground movements of about 150 mm associated with the removal of vegetation on expansive clays in South Africa were recorded in many areas, and the most extensive heave recorded was 374 mm in Kimberley (Williams and Pidgeon, 1983). In the UK, vertical movements due to large trees are often on the order of 100 mm and can cause serious damage to structures.

Root depth varies linearly with potential evapotranspiration for each type of tree. The depth of root zone depends largely upon the soil type. The depth of root zone was assumed in this study because the analysis was performed for a hypothetical case, while no specific type of tree or soil type was assumed.

In this study, a linear variation in the extraction rate with depth was assumed. This assumption was justified by Prasad (1988).

The magnitude of water uptake rate is not a constant, but varies throughout the year as a function of environmental and plant factors (Kramer & Kozlowski, 1960). Environmental factors include the pressures in the water vapour of the surrounding air, humidity of the surrounding air, temperature, light, wind, and supply of water in the soil. This study assumed that water uptake rate was a constant to illustrate methods of volume change analysis.

7.2.1 Example 1: Influence of trees on surrounding soils

The matric suction distributions in the soil at equilibrium are presented in Figs. 6.2 and 6.3 for initial and final conditions, respectively. The initial matric suction varied from 147 kPa at ground surface to 49 kPa at the 10 m depth. The final matric suction varied from 260 kPa at tree root to 49 kPa at the 10 m depth. A maximum change in matric suction was observed at the tree root level and the change in matric suction decreased with distance from the tree.

Figure 6.5 presents contours of vertical displacement in the soil for this example, with the volume change index with respect to matric suction equal to 0.2 and the tree-root uptake rate equal to 0.3 m^3/day per tree. The ground movements at various depths are shown in Fig. 6.6. It can be seen that the movements near the ground surface were quite large within a horizontal distance of about 4 m from the trees. The movements decreased rapidly with distance until a distance of 12 m. The displacements also decreased rapidly with depth. The predicted displacements shown in Fig. 6.6 have the same pattern of displacements as those monitored by Bozozuk and Burn (1960). At ground surface, a value of settlement of 85 mm at the tree location decreased to 40 mm at 8 m from the trees. At 4 m from the trees, a settlement of 65 mm at ground surface decreased to 40 mm at the 3 m depth, and about 20 mm at the 5 m depth.

Figure 6.7 presents the contours of vertical displacement for the case where the water uptake rate was 0.3 m^3/day and the volume change index varied with overburden pressure in the soil (i.e., volume change index decreases linearly from 0.2 at ground surface to 0.05 at the 10 m depth). Most of the displacements take place near ground surface. It can be seen that about 70% of total settlement occurred in the top 4 m of the soil.

Figure 6.8 presents contours of settlement for the case with a volume change index equal to 0.2 and a water uptake rate equal to 0.5 m^3/day. About 12% more settlement was obtained at tree location in comparison to the case when the water uptake rate was 0.3 m^3/day (i.e., (102 – 85)/85 = 12%).

7.2.2 Example 2: Influence of plants on the house footing

The distribution of final matric suction is presented in Fig. 6.10. Final matric suction varied from 409 kPa at tree root to 49 kPa at lower boundary of the soil domain. The contours of changes in matric suction are presented in Fig. 6.11. Most of suction change took place in the soil portion close to the trees. The closer to the trees, the larger the magnitude in the change in suction. Figure 6.11 also showed a similar pattern of moisture deficit near the trees to that presented by Biddle (1983).

The results of stress-deformation analysis are presented in Figs. 6.13 and 6.14 as contours of horizontal displacement and contours of vertical displacement, respectively. A maximum foundation settlement of 80 mm and a minimum settlement of 25 mm was observed. A maximum settlement in the soil profile took place at tree location and decreased with horizontal distance and depth.

Table 6.1 presents the results of the parametric study for this example. A parametric study was performed with respect to the rate of water uptake, the distance from tree row to the house, the thickness of the swelling soil profile, the soil depth of water uptake, and the depth of foundation. Cases 1, 2, and 3 indicated that the magnitude of settlement depended significantly upon the rate of water uptake. Cases 1, 7, 17 showed the dependence of the settlement of footings upon the distance from trees. The effect of thickness of the swelling soil profile to magnitude of settlements was shown in cases 13, 14, 15, and 16. Cases 1, 4 and 16 shows that settlements at the monitoring points (i.e., points A, B, and C) decrease as the depth of water uptake increases. Cases 18, 19, and 20 showed that the magnitude of settlement decreases with increases in the depth of foundation.

The results of the analysis show that it is possible to combine an unsaturated seepage analysis and a stress-deformation analysis to study the influence of vegetation on light engineering structures. The magnitude of movements appears to be reasonable when using the swelling index as input data.

7.3 Uncoupled and coupled solutions of leakage and infiltration problems

Figure 6.15 presents the initial stress state and matric suction conditions in the soil profile for both Examples 3 and 4. The value of the coefficient of earth pressure at

rest, K_0, was assumed to be 0.667. Initial matric suction of 400 kPa was assumed. The initial stress state and initial values of the key variables presented in Fig. 6.15 are used for all uncoupled and coupled analyses, for both Example 3 and Example 4 in this study.

7.3.1 Example 3: Leakage of water below floor slab

The discussions are first presented for uncoupled solutions, followed by coupled solutions and then there is a comparison of the uncoupled and coupled solutions.

7.3.1.1 Uncoupled solutions for Example 3, leakage problem

Uncoupled solutions, UCS2 and UCS3 are presented in Appendix C. Results of the uncoupled solution, UCS4 are discussed in this suction.

The results of the uncoupled analysis, UCS4, are first discussed for two elapsed times, at the 56^{th} day and 150^{th} day after the commencement of wetting. Discussions are then presented for the change of matric suction, horizontal and vertical displacement with time.

Figures 6.18 to 6.22 present the distribution of matric suction, horizontal displacement, vertical displacement, horizontal strain, and vertical strain in the soil profile at day 56. Immediately after wetting was introduced below the flexible cover, water flowed downward and to the right of the soil domain. Matric suctions under the cover reduced from 400 kPa to 50 kPa to a depth of 2 m, and less than 150 kPa to a depth of 5 m. Soil displaced horizontally and vertically because of the decrease in matric suction. Horizontal displacement decreased with depth, with a maximum value of 24 mm at ground surface near to the cover. Horizontal displacements vanished at the left and right boundaries because of the specified boundary conditions. About 70 mm of heave took place at the cover location. The horizontal strain pattern shown in Fig. 6.21 indicated that at this moment, soil strained to the right in the left half of the soil mass, and strained to the left in the other half of the soil mass. Most of the vertical strain took place under the cover. The magnitude of vertical strain decreased with depth and distance from the cover.

Figures 6.23 to 6.27 present the distribution of matric suction, horizontal displacement, vertical displacement, horizontal strain, and vertical strain in the soil profile at day 150. At this time, matric suction below the cover reduced to less than 50 kPa. The wetting front reached the right end of the soil mass. Matric suction varied from 0 to 300 kPa in the soil mass at this time. Cumulative horizontal and vertical displacements had the same patterns as those at day 56; however, soil in the right portion of the soil mass was pushed to the left as matric suction reduced significantly in this portion. Maximum cumulative heave of 105 mm took place at the centre of the cover. About 25 mm of heave could be observed at the far side of the soil mass.

Figure 6.28 shows the change of matric suction with time for three monitoring points (i.e., A, B, and C). It can be seen that point C might experience a temporary increase in initial matric suction. Figure 6.29 presents the change of matric suction versus depth with time. Matric suction below the cover reduced rapidly in the first 50 days. The soil under the cover reached complete saturation in about 350 days. The rate of change in matric suction in the soil mass reduced with time. It should be noted that a layer of soil immediately under the cover reached saturation right after the wetting was introduced.

Figure 6.30 presents the change of horizontal displacement with time for the monitoring points. It can be observed that the largest horizontal displacement took place at the surface in the middle of the soil profile. The soil was pushed to the right in the first 50 days, then gradually pushed back to the left. Maximum horizontal displacement of about 20 mm was computed at point B. The horizontal displacement reduced to less than 2 mm in the soil mass after 400 days of wetting.

Figure 6.31 presents the change of vertical displacement with time for the monitoring points. Figure 6.32 shows the change of heave at ground surface with time. Figure 6.33 presents the change of heave versus depth with time. The heave pattern shown in these figures indicates that most of the heave below the cover occurred in the first 100 days after wetting commenced. Most of the difference in heave (about 65 mm) took place in the first 56 days. In the period from day 56 to day 150, heave increased gradually, with the same rate in the entire soil mass. After this

period, heave developed faster in the right side of the soil mass. A maximum heave of 112 mm was predicted at day 350.

7.3.1.2 Coupled solutions for Example 3, leakage problem

The results of coupled analysis, CS, are first discussed for two elapsed times, at 56th day and 150th day after the commencement of wetting. The discussions are then presented for the change of matric suction, horizontal and vertical displacement with times.

Figures 6.35 to 6.43 present the distributions of matric suction, horizontal stress, vertical stress, void ratio, degree of saturation, horizontal displacement, vertical displacement, horizontal strain, and vertical strain in the soil profile at day 56, respectively. Immediately after wetting was introduced below the flexible cover, water flowed downward and to the right of the soil domain. Matric suction under the cover reduced from 400 kPa to 50 kPa to the depth of 2 m. Matric suction below the cover reduced to less than 150 kPa. There was a significant increase in horizontal stress that could be observed near ground surface, especially under the cover. An increase of about 60 kPa in the horizontal stress was predicted for the soil near ground surface, where the soil had a high potential to swell. There were increases in vertical stress because of the increase of the soil self-weight due to saturation, but these changes were insignificant in comparison with the change in horizontal stress.

Most of the increases in void ratio and degree of saturation took place under the cover, near ground surface. Corresponding to the changes in matric suction, soil displaced horizontally and vertically. Horizontal displacement decreased with depth, with maximum value of 24 mm at ground surface near to the cover. About 70 mm of heave took place at the cover location. The horizontal strain pattern shown in Fig. 6.42 indicated that at this moment, soil strained to the right in the left half of the soil mass, and strained to the left in the other half of the soil mass. Most of the vertical strain took place under the cover and the magnitude of vertical strain decreased with depth and distance from the cover.

Figures 6.44 to 6.52 present the distribution of matric suction, horizontal stress, vertical stress, void ratio, degree of saturation, horizontal displacement,

vertical displacement, horizontal strain, and vertical strain in the soil profile at day 150, respectively. At this time, matric suction below the cover reduced to less than 50 kPa. The wetting front reached the extreme ends of the soil mass. Matric suctions varied from 0 to 300 kPa in the soil mass at this time. About 20 kPa of increase in horizontal stress could be observed near ground surface from day 56 to day 150. The horizontal stress varied from 65 to 125 kPa in the soil mass. Again, there were small increases in vertical stress because of the increase of the soil self-weight due to saturation, but these changes were insignificant in comparison with the change in horizontal stress. The changes in vertical stress were small since the soil was free to move in the vertical direction. Cumulative horizontal and vertical displacements had the same patterns as those at day 56; however, soil in the right portion of the soil mass was pushed to the left as matric suction reduced significantly in this portion. Maximum cumulative heave of 105 mm took place at the centre of the cover. About 25 mm of heave could be observed at the far side of the soil mass.

Figure 6.53 shows the change of matric suction with time for three monitoring points (i.e., A, B, and C). Matric suctions below the cover reduced rapidly in the first 50 days. The soil directly below the cover reached complete saturation in about 300 days. The rate of change in matric suction in the soil mass reduced with time.

Figure 6.54 presents the change of horizontal stress with time for the monitoring points. The horizontal stress increased rapidly in the first 50 days, corresponding to the change in suction. The increase in horizontal stress was more gradual in the right side of the soil mass. A total increase of about 80 kPa in the horizontal stress was predicted.

Figure 6.55 presents the change of horizontal displacement with time for the monitoring points. It can be observed that the largest horizontal displacement took place at the surface in the middle of the soil profile. The soil was pushed to the right in the first 50 days, then gradually pushed back to the left. Maximum horizontal displacement of about 20 mm was computed at point B. The horizontal displacement reduced to less than 2 mm in the soil mass after 400 days of wetting.

Figure 6.56 presents the change of vertical displacement with time for the monitoring points. Figure 6.57 shows the change of heave at ground surface with

time. Figure 6.58 presents the change of heave versus depth with time. The heave pattern shown in these figures indicates that most of the heave below the cover occurred in the first 100 days after wetting commenced. Most of the difference in heave (about 65 mm) took place in the first 56 days. In the period from day 56 to day 150, heave increased gradually, at the same rate in the entire soil mass. After this period, heave developed faster along the right side of the soil mass. A maximum heave of 112 mm was predicted at day 350.

7.3.1.3 Comparison of the results for various types of analyses for Example 3, leakage problem

Figures 7.1 to 7.10 compare the results of the uncoupled solution, UCS4, and the coupled solution, CS for two elapsed times (i.e., day 56 and day 150). The comparisons are presented for the distribution of matric suction, horizontal displacement, vertical displacement, horizontal strain, and vertical strain. Matric suctions obtained from uncoupled analysis, UCS4, are higher than those obtained from the coupled analysis, CS, below the cover, but the matric suctions are lower in the right half of the soil mass (Figs. 7.1 and 7.6). The solutions compared well in terms of horizontal displacement and horizontal strains. Vertical displacements appear to be higher for the uncoupled solution and the differences decrease with depth.

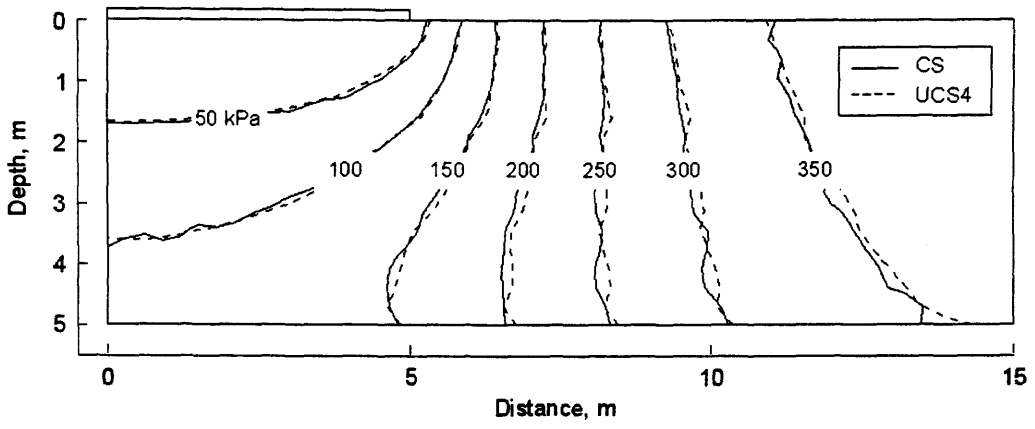

Figure 7.1 Comparison of matric suction distribution at day 56, Example 3

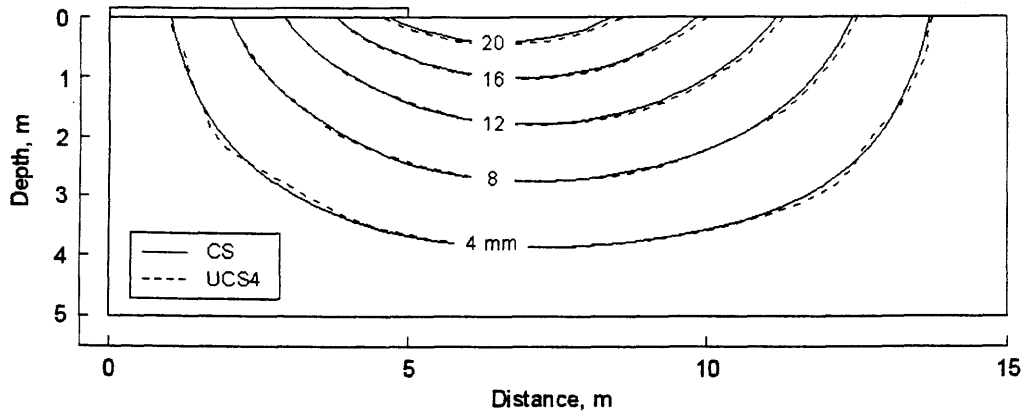

Figure 7.2 Comparison of horizontal displacement distribution at day 56, Example 3

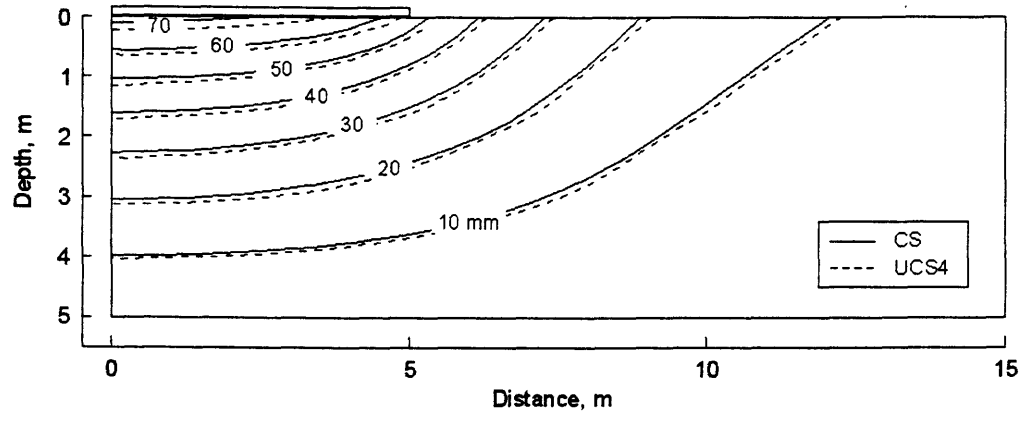

Figure 7.3 Comparison of vertical displacement distribution at day 56, Example 3

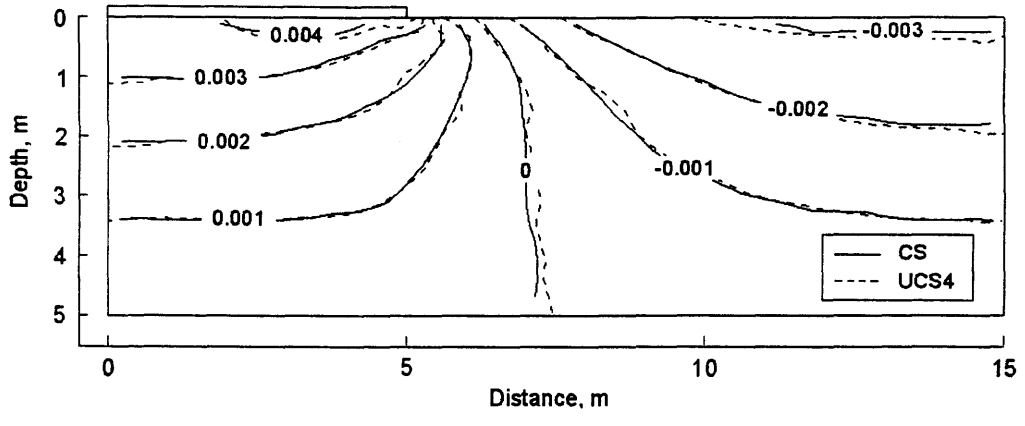

Figure 7.4 Comparison of horizontal strain distribution at day 56, Example 3

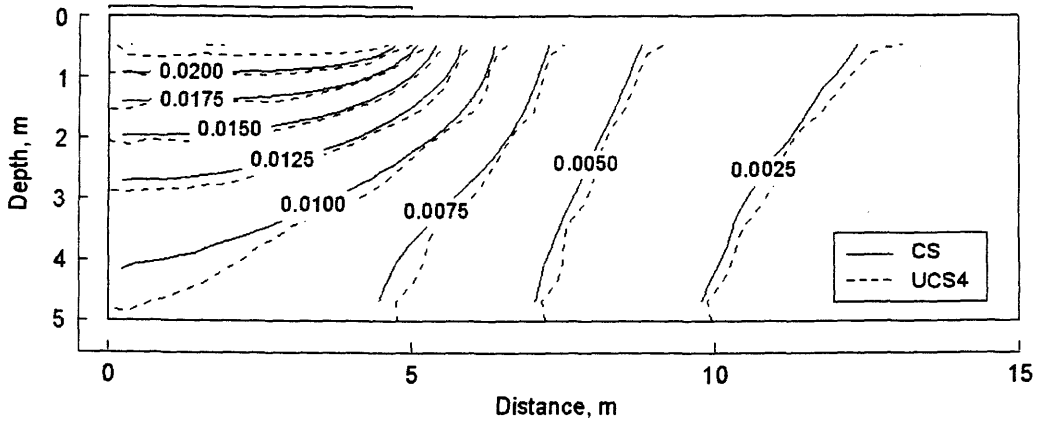

Figure 7.5 Comparison of vertical strain distribution at day 56, Example 3

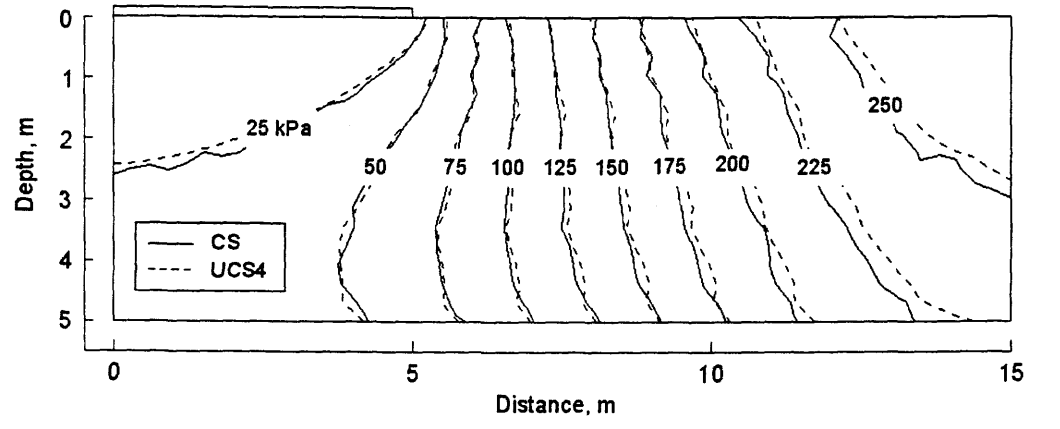

Figure 7.6 Comparison of matric suction distribution at day 150, Example 3

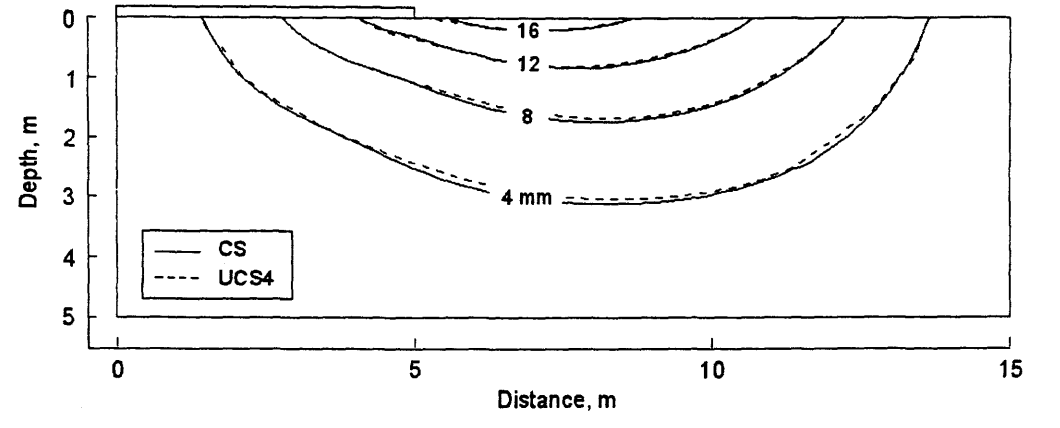

Figure 7.7 Comparison of horizontal displacement distribution at day 150, Example 3

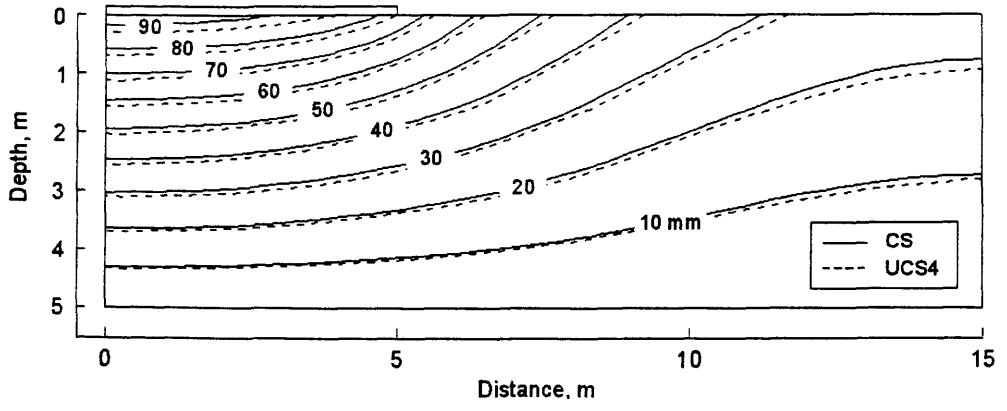

Figure 7.8 Comparison of vertical displacement distribution at day 150, Example 3

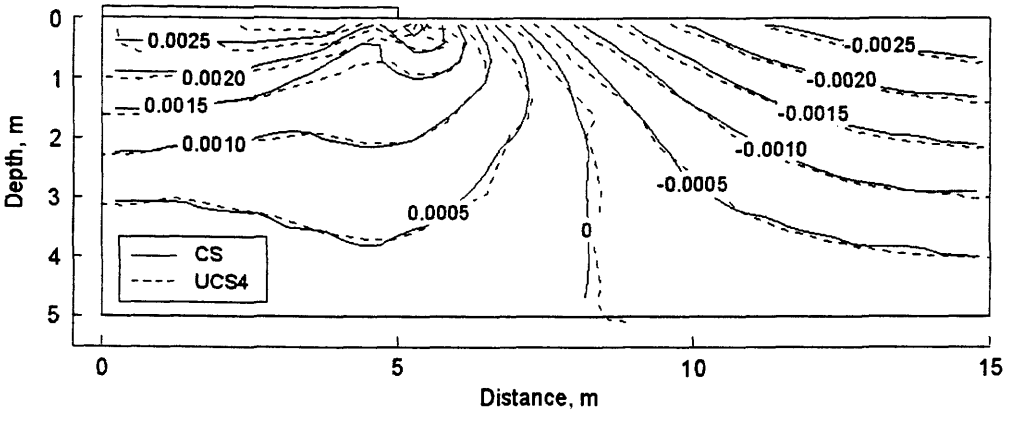

Figure 7.9 Comparison of horizontal strain distribution at day 150, Example 3

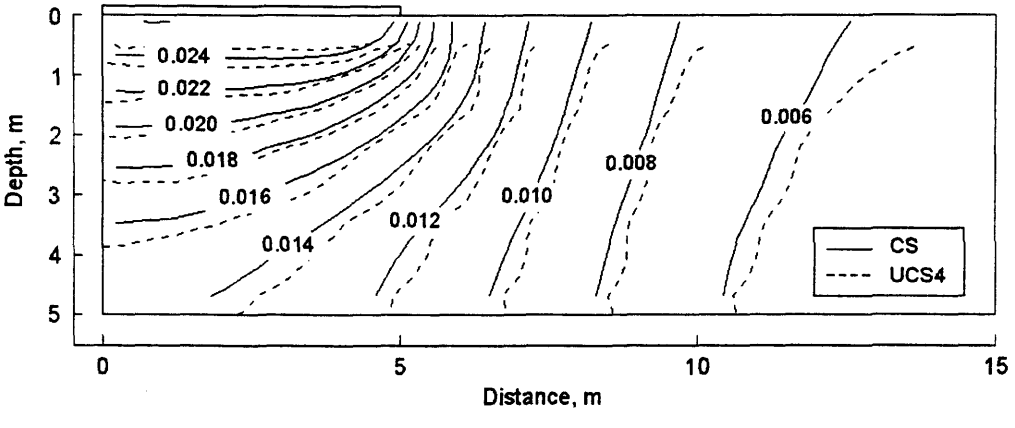

Figure 7.10 Comparison of vertical strain distribution at day 150, Example 3

Figures 7.11 to 7.13 compare the changes of matric suction, horizontal displacement, and vertical displacement at a point in the soil mass for various types of analyses. Figure 7.11 shows that water flowed faster in the uncoupled analyses, when changes in stress and deformation were not considered in the seepage equation (i.e., UCS2 and UCS3). The changes in matric suction at any elapsed time were over predicted in these analyses, resulting in differences in horizontal and vertical displacements. It should be noted that changes in stress were not considered in solution UCS2, but were considered in solutions UCS3 and UCS4. Uncoupled analyses in this study used the elastic parameters at a net normal stress that is lower than the actual net normal stresses. The stiffness of an unsaturated, expansive soil decreases with a decrease in net normal stress, resulting in the prediction of a larger heave in the uncoupled analysis. The magnitude of the differences between uncoupled and coupled solutions therefore depends on the differences in stress paths followed in the uncoupled solutions. The uncoupled solution, UCS4 compares well with the coupled solution, CS.

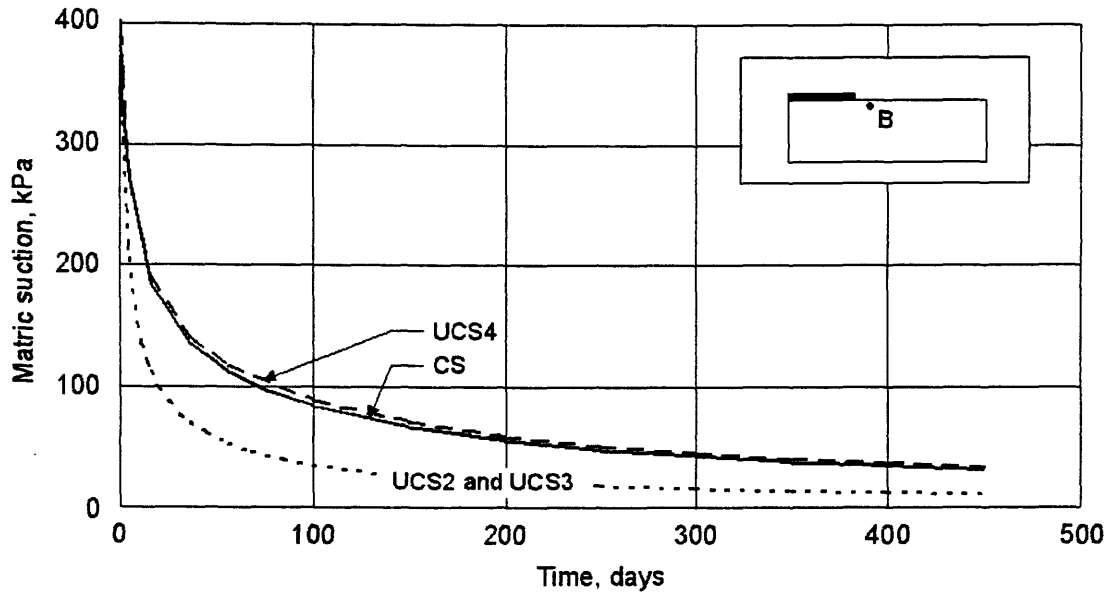

Figure 7.11 Comparison of matric suction change with time for point B, Example 3

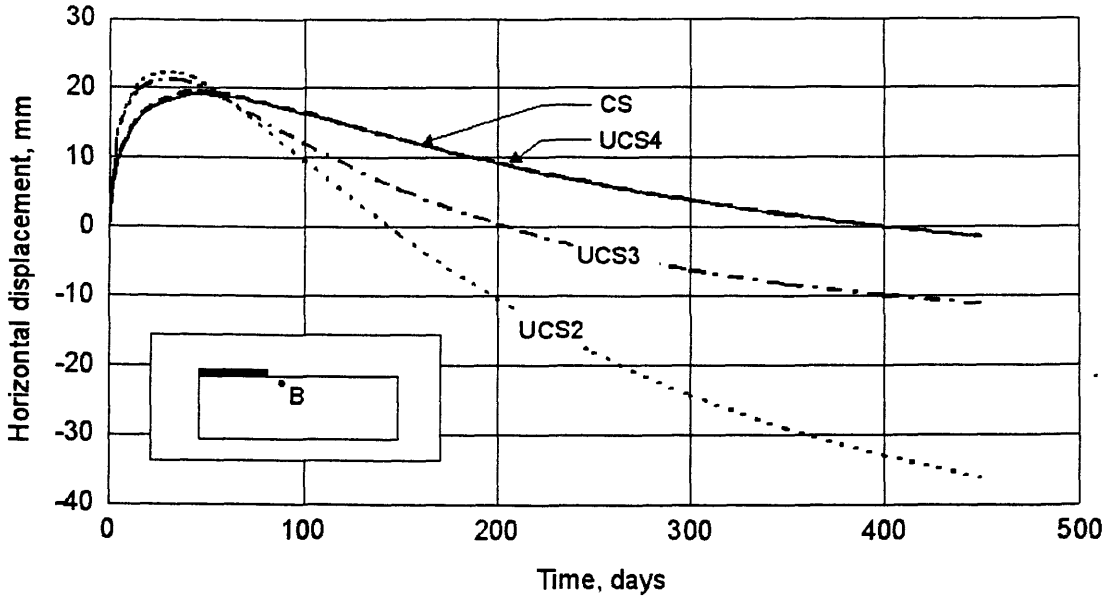

Figure 7.12 Comparison of horizontal displacement change with time for points B, Example 3

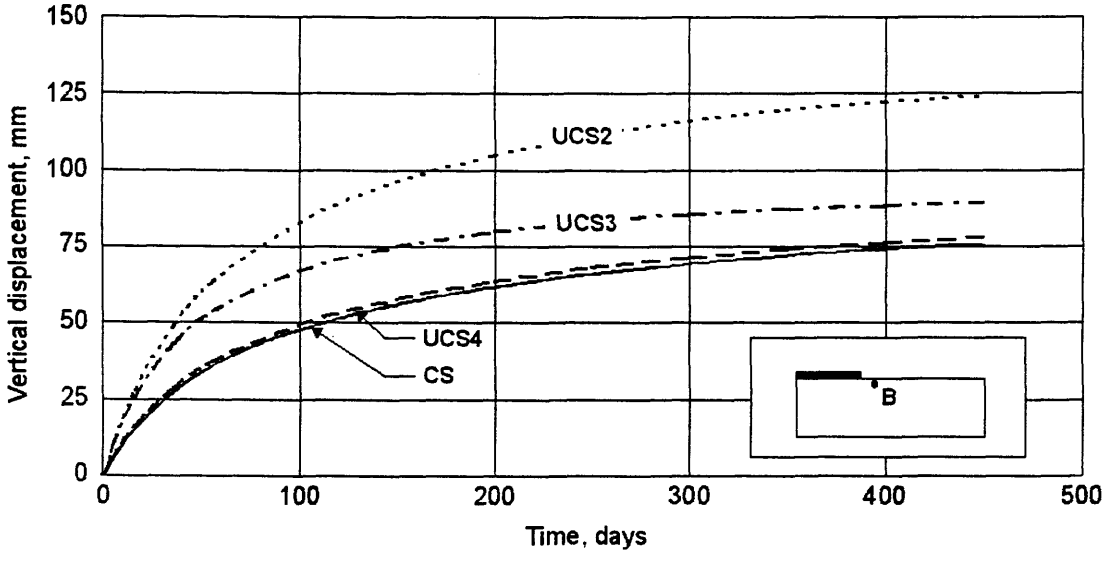

Figure 7.13 Comparison of vertical displacement change with time for point B, Example 3

7.3.2 Example 4: Infiltration of water from ground surface

The discussions are first presented for uncoupled solutions, followed by coupled solutions and then the comparison of uncoupled and coupled solutions.

7.3.2.1 Uncoupled solutions for Example 4, infiltration problem

Uncoupled solutions, UCS1 and UCS2 are presented in Appendix D. Results of the uncoupled solution, UCS4 are discussed in this suction.

The results of the uncoupled analysis, UCS4 are first discussed for two elapsed times, at the 53^{th} day and 175^{th} day after the commencement of wetting. The discussions are then presented for the change of matric suction, horizontal and vertical displacement with times.

Figures 6.60 to 6.64 present the distribution of matric suction, horizontal displacement, vertical displacement, horizontal strain, and vertical strain in the soil profile at day 53. Immediately after wetting was introduced into the soil from the uncovered surface, water flowed downward and to the left of the soil domain. Matric suction reduced to less than 100 kPa near ground surface. Most of the soil suction changes occurred below the uncovered portion, where infiltration took place. The soil was displaced horizontally and vertically because of the decrease in matric suction. Horizontal displacements decreased with depth, with a maximum value of 13 mm at ground surface near to the cover. About 34 mm of heave took place at the uncovered location. The horizontal strain pattern shown in Fig. 6.63 indicated that at this moment, soil strained to the left in the left half of the soil mass, and strained to the right in the other half of the soil mass. Most of the vertical strain took place in the uncovered portion of the soil mass, the magnitude of vertical strain decreased with depth.

Figures 6.65 to 6.69 present the distribution of matric suction, horizontal displacement, vertical displacement, horizontal strain, and vertical strain in the soil profile at day 175. At this time, matric suction below the uncovered surface reduced to less than 50 kPa. The wetting front reached the right end of the soil mass. Cumulative horizontal and vertical displacements had the same patterns as those at day 53. A maximum cumulative heave of 52 mm took place at the upper-right corner

of the soil domain. About 12 mm of heave could be observed at the centre of the cover.

Figure 6.70 shows the change of matric suction with time for three monitoring points (i.e., A, B, and C). Matric suction below the cover reduced rapidly in the first 50 days. It can be noted that the matric suction in the soil mass has not stabilised in the first 175 days; however, the rate of change in matric suction in the soil mass reduced rapidly with time.

Figure 6.71 presents the change of vertical displacement with time for the monitoring points. Most of the heave at the monitoring points occurred in the first 100 days after wetting commenced. Figure 6.72 shows the change of heave at ground surface with time. Figure 6.73 presents the change of heave versus depth with time. A maximum differential heave of about 30 mm might occur between the cover location and the far point of the uncovered portion. A maximum heave of about 58 mm could take place at the surface and heave would stop after about 400 days of infiltration.

7.3.2.2 Coupled solutions for Example 4, infiltration problem

The results of the coupled analysis, CS, are first discussed for two elapsed times, at 53^{th} day and 175^{th} day after the commencement of wetting. The discussions are then presented for the change of matric suction, horizontal and vertical displacement with times.

Figures 6.75 to 6.83 present the distributions of matric suction, horizontal stress, vertical stress, void ratio, degree of saturation, horizontal displacement, vertical displacement, horizontal strain, and vertical strain in the soil profile at day 53, respectively. Immediately after wetting was introduced below the uncovered surface, water flowed downward and to the left of the soil domain. Matric suction near the uncovered surface reduced to less than 100 kPa. There was a significant increase in horizontal stress that could be observed near ground surface, especially within the uncovered portion. An increase of about 60 kPa of horizontal stress was predicted for the soil near ground surface, where the soil had a high potential to swell. There were increases in vertical stress because of the increase of the soil self-weight due to saturation, but these changes were insignificant in comparison with the change

in horizontal stress. Most of the increases in void ratio and degree of saturation took place within the uncovered portion, near to the ground surface, where infiltration took place. Horizontal displacements decreased with depth, with a maximum value of 11 mm at ground surface near to the cover. About 33 mm of heave took place at the uncovered location. The horizontal strain pattern shown in Fig. 6.82 indicated that at this moment, soil strained to the left in the left half of the soil mass, and strained to the right in the another half of the soil mass. Most of the vertical strain took place under the uncovered portion and the magnitude of vertical strain decreased with depth.

Figures 6.84 to 6.92 present the distribution of matric suction, horizontal stress, vertical stress, void ratio, degree of saturation, horizontal displacement, vertical displacement, horizontal strain, and vertical strain in the soil profile at day 175, respectively. At this time, matric suction near the uncovered surface reduced to less than 50 kPa. The wetting front reached the left end of the soil mass. About 10 kPa of increase in horizontal stress could be observed near ground surface from day 53 to day 175. The horizontal stress varied from 55 to 74 kPa in the soil mass. Again, there were small increases in vertical stress because of the increase of the soil self-weight due to saturation, but these changes were insignificant in comparison with the change in horizontal stress. The changes in vertical stress were small since the soil was free to move in the vertical direction. Cumulative horizontal and vertical displacements had the same patterns as those at day 53. A maximum cumulative heave of 52 mm took place at the uncovered surface. About 12 mm of heave could be observed at the centre of the cover.

Figure 6.93 shows the change of matric suction with time for three monitoring points (i.e., A, B, and C). Matric suction below the cover reduced rapidly in the first 50 days. The rate of change in matric suction in the soil mass reduced rapidly with time.

Figure 6.94 presents the change of horizontal stress with time for the monitoring points. Corresponding to the change in suction, the horizontal stress increased rapidly in the first 50 days. Horizontal stress increased more near ground surface, where the soil had higher swelling potential. A total increase of about 58 kPa

in horizontal stress was predicted for point A. A total increase of about 20 kPa in horizontal stress was observed for point C.

Figure 6.95 presents the change of vertical displacement with time for the monitoring points. Figure 6.96 shows the change of heave at ground surface with time. Figure 6.97 presents the change of heave versus depth with time. A maximum differential heave of about 30 mm can occur between the cover location and the far point of the uncovered portion. A maximum heave of about 58 mm could take place at the surface and heave would stop after about 400 days of infiltration.

7.3.2.3 Comparison of the results for various type of analysis for Example 4, infiltration problem

Figures 7.14 to 7.23 compare the results of the uncoupled solutions, UCS1, UCS2, UCS4 and coupled solution, CS for two elapsed times, day 53 and day 175. The comparisons are presented for the distribution of matric suction, horizontal displacement, vertical displacement, horizontal strain, and vertical strain.

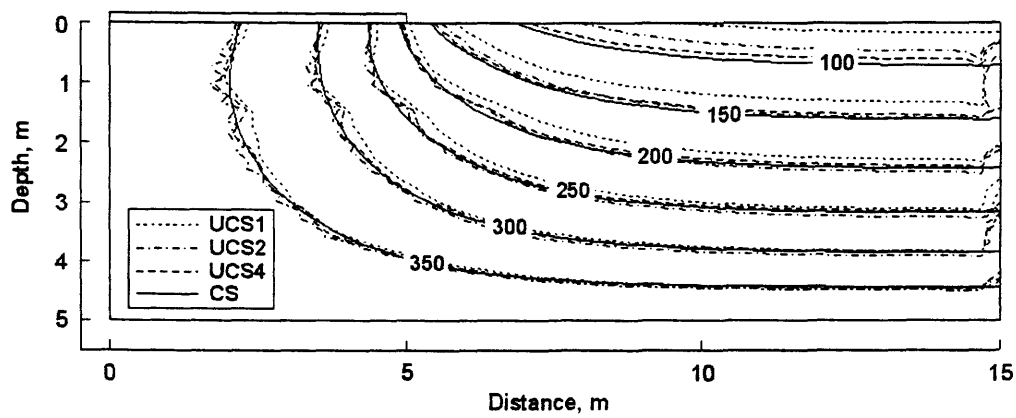

Figure 7.14 Comparison of matric suction distribution at day 53, Example 4

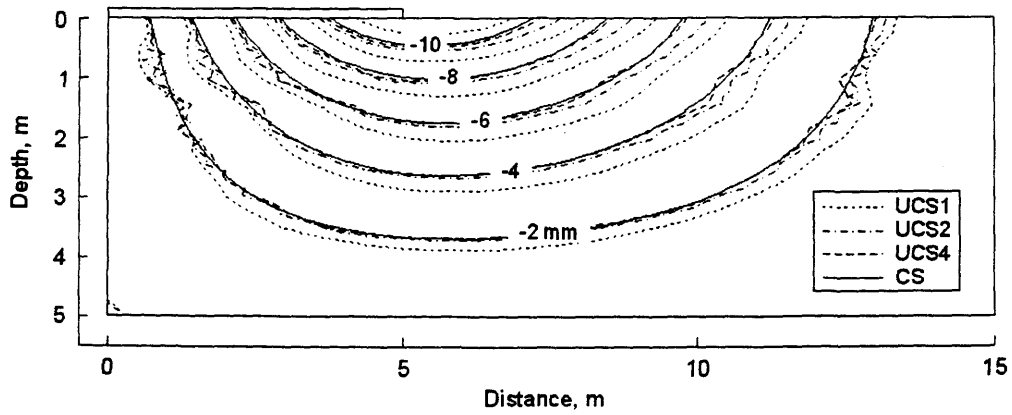

Figure 7.15 Comparison of horizontal displacement distribution at day 53, Example 4

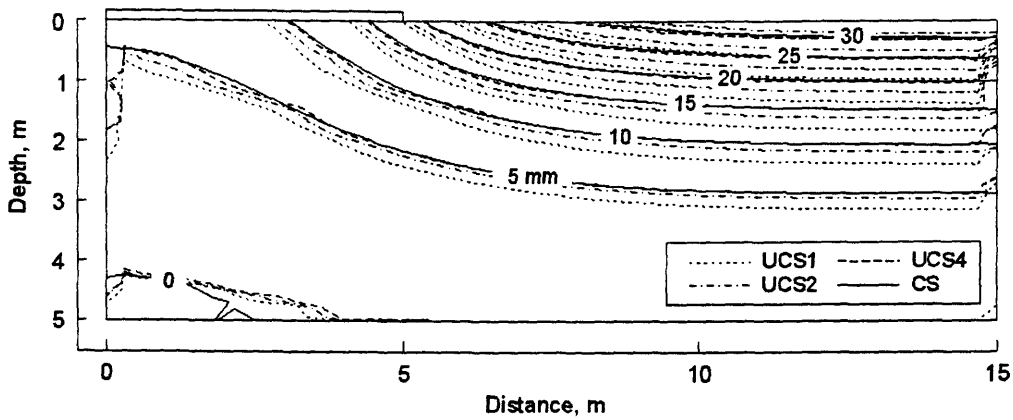

Figure 7.16 Comparison of vertical displacement distribution at day 53, Example 4

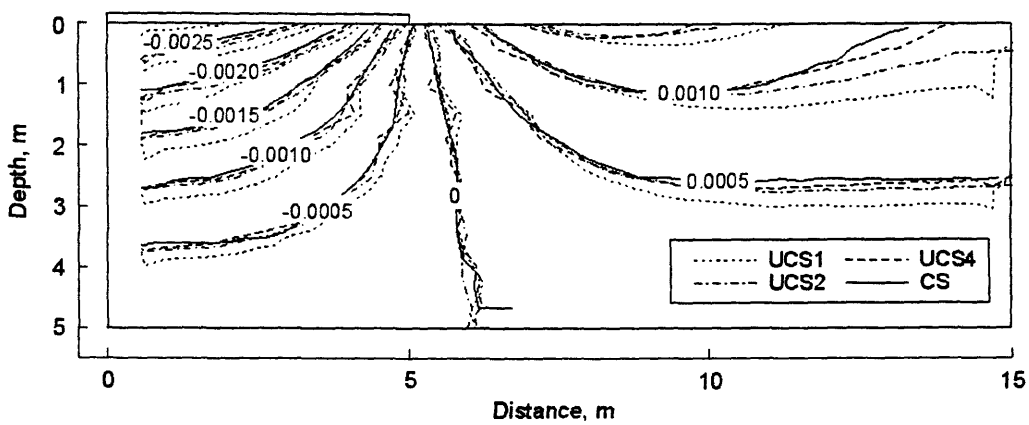

Figure 7.17 Comparison of horizontal strain distribution at day 53, Example 4

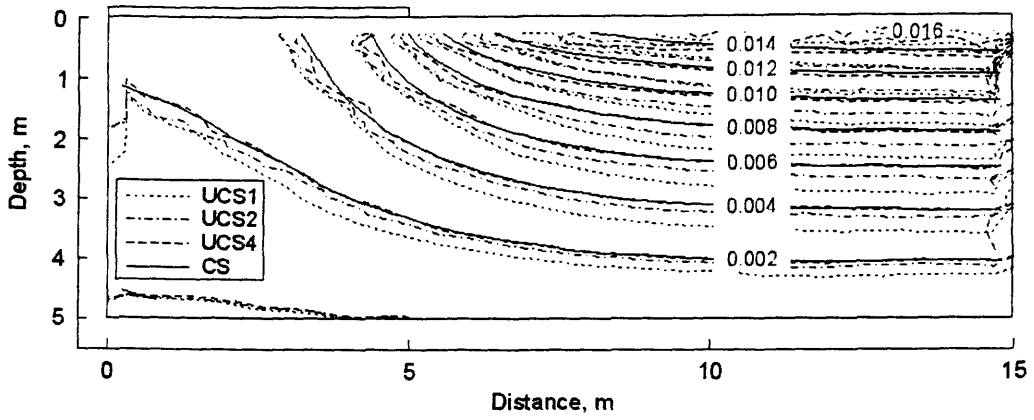

Figure 7.18 Comparison of vertical strain distribution at day 53, Example 4

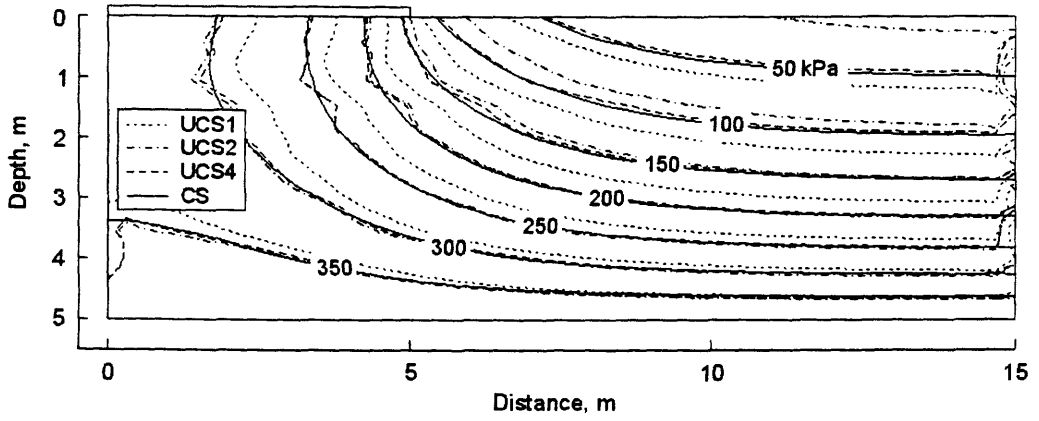

Figure 7.19 Comparison of matric suction distribution at day 175, Example 4

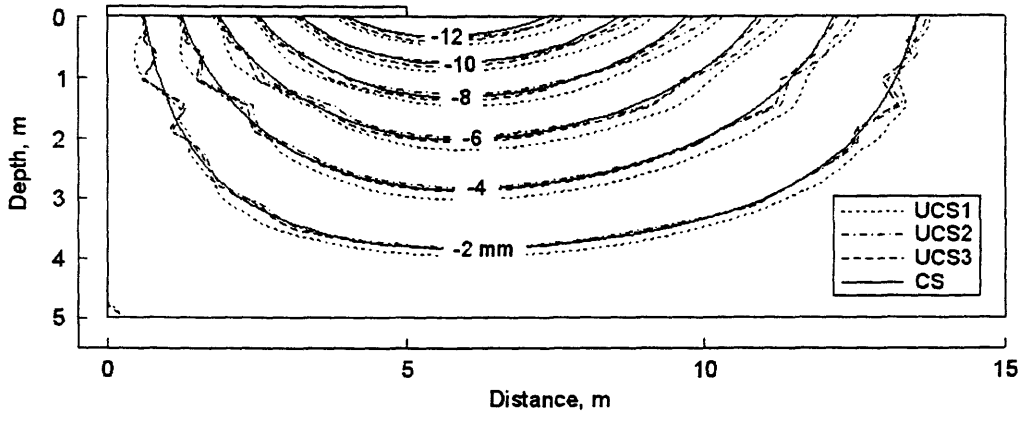

Figure 7.20 Comparison of horizontal displacement distribution at day 175, Example 4

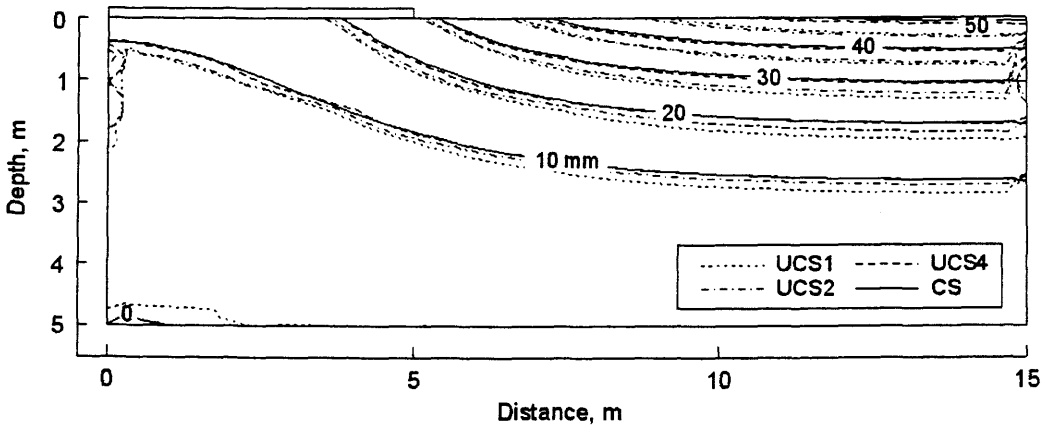

Figure 7.21 Comparison of vertical displacement distribution at day 175, Example 4

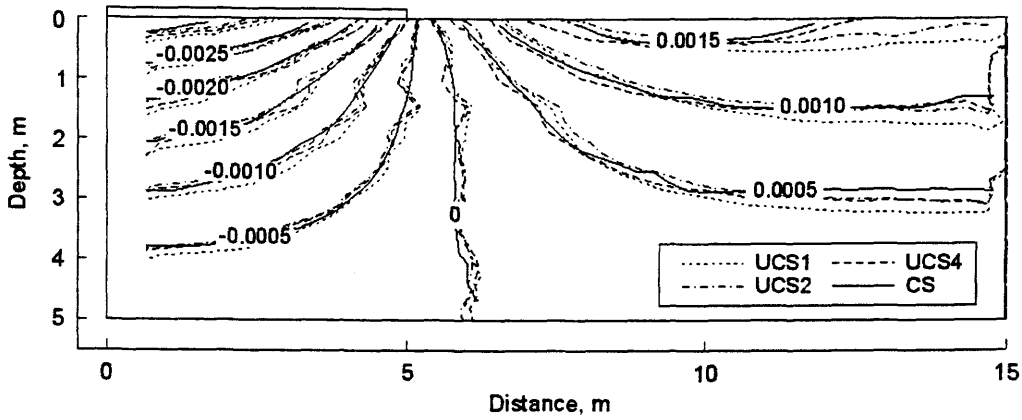

Figure 7.22 Comparison of horizontal strain distribution at day 175, Example 4

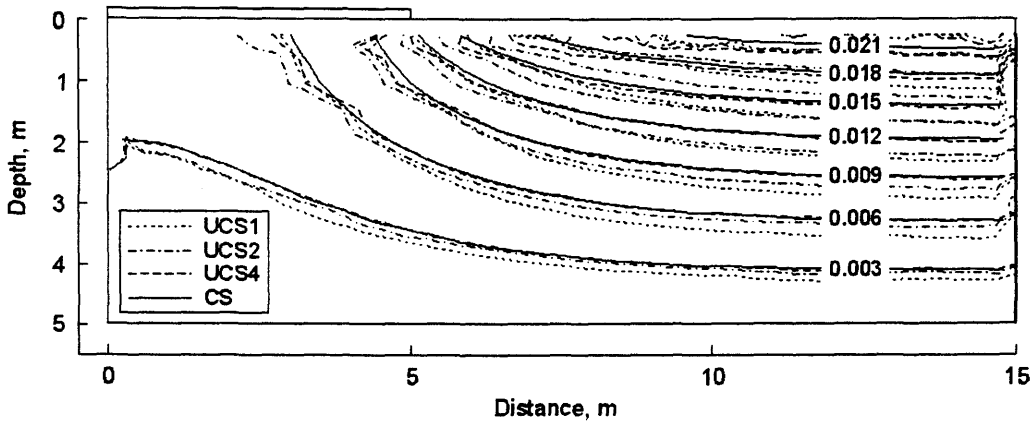

Figure 7.23 Comparison of vertical strain distribution at day 175, Example 4

Figures 7.24 and 7.25 compare the changes of matric suction and vertical displacement at the monitoring points in the soil mass for various types of analysis. The changes in matric suction at any elapsed time were over-predicted in the uncoupled analyses, resulting in the differences in horizontal and vertical displacements. Uncoupled analyses in this study used the elastic parameters at net normal stress that are lower than the actual net normal stresses. The stiffness of an unsaturated, expansive soil decreases with the decrease in net normal stress, resulting in a larger amount of heave in uncoupled analyses. The magnitude of the differences between uncoupled and coupled solutions, therefore, depends on the differences in stress paths followed in the uncoupled solutions. The uncoupled solution, UCS4 appear to be the same as those of the coupled solution, CS.

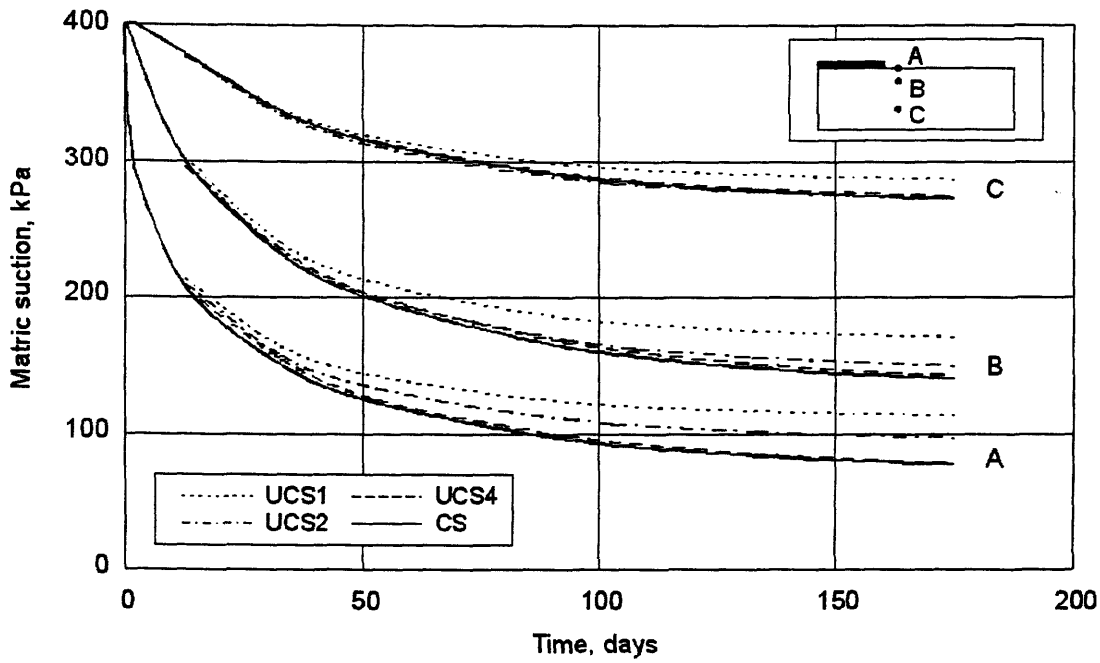

Figure 7.24 Comparison of matric suction change with time for points A, B, and C, Example 4

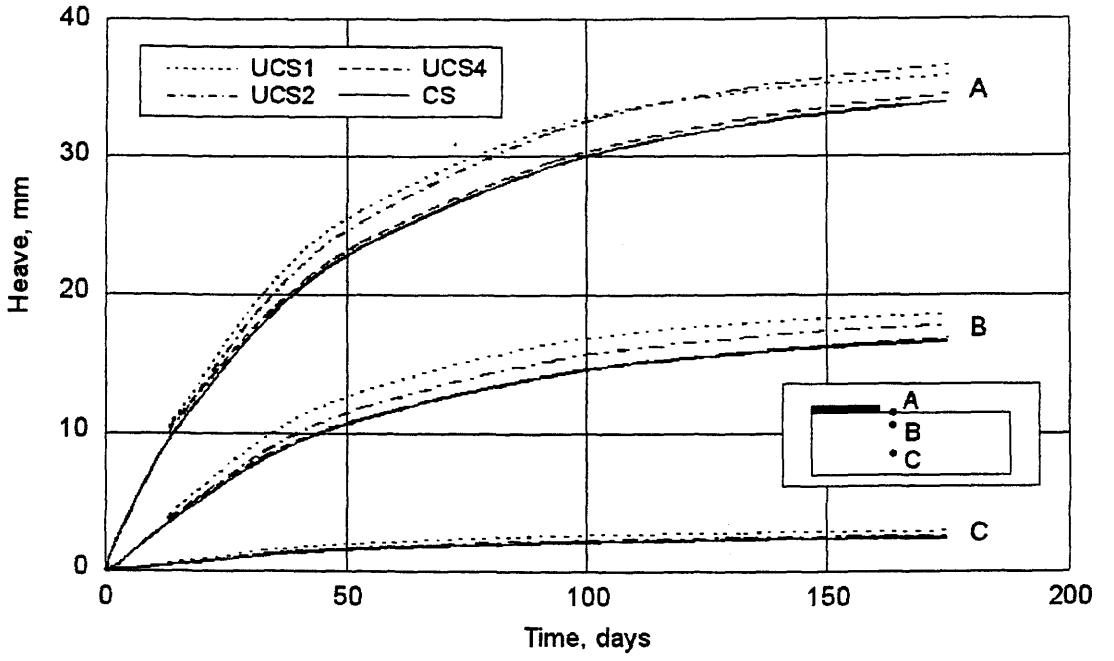

Figure 7.25 Comparison of vertical displacement change with time for points A, B, and C, Example 4

7.4 Parametric study with respect to the assumed value of Poisson's ratio (for coupled solutions)

Poisson's ratio plays an important role in the volume change analysis in this study. It must be noted that Poisson's ratio is not a constant for an unsaturated soil. Rather, it is a function of the stress state in the soil (i.e., net normal stress and matric suction). This study assumes a constant value of Poisson's ratio for the calculation of the other elastic parameters (i.e., E, H, E_w, and H_w). The assumed value of Poisson's ratio is also used to convert the elasticity parameters from one loading condition to another. Since the assumed value of Poisson's ratio affects the magnitudes of the elastic parameters, it affects the amount of predicted matric suction, induced stresses and predicted deformations. If Poisson's ratio is used to define the initial stress state in soils, it will affect the results of the analysis because the initial conditions provide the location of the starting point along the stress-strain curve in the non-linear problem.

A Poisson's ratio of 0.3 has been often used in numerical simulations of the behaviour of unsaturated, collapsing soils (Miranda, 1988; Alonso et al., 1988; Lloret

et al., 1993). It was suggested that a Poisson's ratio equal to 0.3 might reflect the as-compacted condition of a loosely compacted embankment.

Pereira (1996) evaluated the value of Poisson's ratio for saturated, collapsing soils by using triaxial test results and oedometer test results. It was shown that Poisson's ratio increased with increasing net mean stress. It was also assumed that Poisson's ratio increased with decreasing in matric suction.

Schiffman et al. (1969) studied the Mandel-Cryer effect (Mandel, 1950, 1953; Cryer, 1963) for two-dimensional consolidation of a saturated soil. The Mandel-Cryer effect is characterised by an increase in the excess pore pressure at early times over the initial excess pore pressure. It was noted that there was a significant variation in the excess pore pressure behaviour with changes in Poisson's ratio. The magnitude of the Mandel-Cryer effect is reduced with an increasing value of Poisson's ratio. The Mandel-Cryer effect disappeared as Poisson's ratio approached 0.5. The lateral distribution of excess pore pressure in a normally loaded half-plane was shown to be more uniform as Poisson's ratio became larger. The higher the values of Poisson's ratio, the more pronounced the effect of pore pressure spreading.

Hwang et al. (1970) presented solutions to two-dimensional consolidation problems by finite element methods. The effect of Poisson's ratio on time-settlement was shown to be significant. Calculated settlement increased for decreased Poisson's ratio. The calculated settlement was almost doubled when Poisson's ratio varied from 0.4 to 0. The calculated settlements agreed well with those presented by Gibson et al. (1970).

Lewis et al. (1991) analysed a coupled problem of a single aquifer pumped from a fully penetrating well. Different sets of Young modulus, E, and Poisson's ratio, μ, for the same coefficient of compressibility were used. The value of Poisson's ratio varied from 0 to 0.4 for the analysis. It was noted that settlements increased significantly for decreased Poisson's ratios. Excess pore-water pressure increased for increased Poisson's ratio.

Bowles (1996) stated that Poisson's ratio has little effect on the predicted settlement, showing that the extreme range from 0 to 0.5 only produced a maximum difference of 25 percent.

This research study presents the effect of Poisson's ratio on coupled solutions of the volume change problems (i.e., Examples 3 and 4).

7.4.1 Parametric study with respect to the assumed value of Poisson's ratio for Example 3, leakage problem

Figure 6.98 presents the change of matric suction at point B with time for various values of Poisson's ratio. The higher the value for Poisson's ratio, the lower the matric suctions that were predicted and the larger the changes in matric suction, resulting in larger volume change. The rate of change of matric suction for various Poisson's ratio is almost uniform after 20 days of wetting. Figure 6.99 shows the relationship between matric suction and Poisson's ratio for various elapsed times. Matric suction started to deviate with increases in Poisson's ratio after 5 days after the wetting commenced. Matric suctions decreased more rapidly when Poisson's ratio were larger than 0.45.

Figure 6.100 presents the change of horizontal displacement at point B with time for various values of Poisson's ratio. Figure 6.101 shows the relationship between horizontal displacement and Poisson's ratio for various elapsed times. It can be seen that the magnitude of horizontal displacement increased for increases in Poisson's ratio. Maximum changes in the predicted horizontal displacement took place at 40 days after the wetting commenced. Horizontal displacement increased more rapidly when Poisson's ratio was larger than 0.45.

Figure 6.102 presents the change of vertical displacement at point B with time for various values of Poisson's ratio. Figure 6.103 shows the relationship between vertical displacement and Poisson's ratio for various elapsed times. It can be seen that the magnitude of vertical displacement increased for increased Poisson's ratio. Vertical displacement increased more rapidly when Poisson's ratio was larger than 0.35.

7.4.2 Parametric study with respect to the assumed value of Poisson's ratio for Example 4, infiltration problem

Figure 6.104 presents the change of matric suction at point B with time for various values of Poisson's ratio. Figure 6.105 shows the relationship between matric suction and Poisson's ratio for various elapsed times. The higher the value for Poisson's ratio, the lower the matric suctions that were predicted. Therefore, there was a larger change in matric suction from the initial matric suction. Larger volume change can therefore be expected. However, only small variations of the predicted matric suctions with changes in Poisson's ratio were observed.

Figure 6.106 presents the relationship between the magnitude of horizontal stress and Poisson's ratio for monitoring points A, B, and C. The horizontal stress decreased for an increase in Poisson's ratio. Figure 6.107 presents the relationship between the magnitude of vertical stress and Poisson's ratio for monitoring points A, B, and C. It can be observed that vertical stress remained essential the same for changes in Poisson's ratio.

Figure 6.108 presents the change of horizontal displacement at point B with time for various values of Poisson's ratio. Figure 6.109 shows the relationship between horizontal displacement and Poisson's ratio for various elapsed times. It can be seen that the magnitude of horizontal displacement increased for an increase in Poisson's ratio.

Figure 6.110 presents the change of vertical displacement at point B with time for various values of Poisson's ratio. Figure 6.111 shows the relationship between vertical displacement and Poisson's ratio for various elapsed times. It can be seen that the magnitude of vertical displacement increased for an increase in Poisson's ratio. Vertical displacements increased more rapidly when Poisson's ratio was larger than 0.4.

7.5 Summary of the discussion of the results

The analysis of the results suggests that it is possible to combine unsaturated seepage and stress-deformation analyses to study the volume change behaviour of an unsaturated, swelling soil. The examples presented in this study represent typical

volume change problems that are often encountered in engineering practice (i.e., influence of vegetation on light engineering structures, water leakage under floor slab, infiltration of water from ground surface.)

Solutions to the volume change problems associated with unsaturated, expansive soils can be obtained from either an uncoupled or a coupled analysis. There are several types of uncoupled analyses. The differences are related to the assumptions made regarding the stress path followed in the seepage analysis and the stress-deformation analysis in the uncoupled solutions. Coupled analyses produced generally smaller displacements when compared to uncoupled analyses. The uncoupled solutions appeared to be identical with coupled solutions when changes in stress and deformations were considered in both water flow analysis and stress-deformation analysis.

Taking into account the changes in stress and deformation in the water flow analysis is a necessity in swelling soils when the soil is close to saturation (i.e., at low matric suction, Example 3, solutions UCS2 and UCS3). The effect of the changes in stress and deformation appeared to be minimal when the soil is at higher matric suction (i.e., Example 4, solutions UCS1 and UCS2).

Analyses carried out with different values of Poisson's ratio can lead to significant differences in terms of the distributions of matric suction, stress, and displacements.

The analyses presented in this study produced results that are physically reasonable from a quantitative standpoint and in accordance with anticipated behaviour.

CHAPTER 8

Conclusions and Recommendations

8.1 Conclusions

The conclusions associated with this study are summarized under the following headings: conclusions associated with the theory of constitutive surfaces, conclusions associated with uncoupled and coupled solutions, conclusions associated with the computer programs used in this study (i.e., FlexPDE and COUPSO), and general conclusions.

8.1.1 Theory of constitutive surfaces

1. Void ratio constitutive surface can be estimated from the following soil data: i) swelling index with respect to net normal stress, C_s; ii) swelling index with respect to matric suction, C_m; iii) initial void ratio; and iv) swelling pressure. The following assumptions are made for the void ratio constitutive surface: i) there is a linear relationship between void ratio and the logarithm of net normal stress at an extreme net normal stress plane; ii) there is a linear relationship between void ratio and the logarithm of matric suction at the extreme matric suction plane; iii) the void ratio constitutive surface converges to a single point on the void ratio axis; and iv) the constant void ratio plane intersects the void ratio constitutive surface at a straight line.
2. The problem associated with the estimation of void ratio in the range of low net normal stress and low matric suction range has been solved. The solutions are obtained through the use of a mathematical equation that is continuous,

smooth, physically reasonable and differentiable over the entire range of net normal stresses and matric suctions.

3. Mathematical equations that were originally presented as functions of only one stress state variable have been extended to form functions of both stress state variables. These include: Fredlund and Xing (1994) equation, Pereira and Fredlund (1996) equation, and M. Fredlund (2000) equation. These equations appear to adequately describe the void ratio constitutive surface; however, a large number of data points are required because of the large number of the fitting parameters present in the modified equation (i.e., 11 to 15 fitting parameters). The large number of fitting parameters also presents a difficulty in the fitting of the equation to the data points.
4. New mathematical equations have been proposed in this study for the description of the entire void ratio constitutive surface. The proposed equation can also be used to describe the constitutive surface for water phase. The equations have been used successfully to characterise the soil properties of Regina clay (i.e., void ratio constitutive surface, water content constitutive surface, degree of saturation constitutive surface, SWCC, compression and rebound curves of oedometer test results).
5. The elasticity parameters associated with unsaturated, expansive soils can be calculated from the constitutive surfaces for the soil structure and water phase with an assumed value of Poisson's ratio. Using the proposed equations in this study, the elasticity parameters can also be calculated for the low range of net normal stress and matric suction.
6. The use of the equations that suggested in this study has improved convergence problems.

8.1.2 Uncoupled and coupled solutions

1. The analytical study showed that it is possible to combine unsaturated seepage and stress-deformation analyses to study the volume change behaviour of an unsaturated, swelling soil. The examples presented in this study represents typical volume change problems that are often encountered in engineering

practice (i.e., influence of vegetation on light engineering structures, water leakage under floor slab, infiltration of water from ground surface).

2. Solutions to the volume change problems associated with unsaturated, expansive soils can be obtained through either an uncoupled or a coupled analysis. There are several types of uncoupled analyses. The differences arise from the assumptions related to the stress path followed in the water flow analysis and stress-deformation analysis in the uncoupled solutions. The coupled analysis generally produces slightly smaller displacements when compared to the uncoupled analyses.
3. It is necessary to take into account the changes in stress and deformation in the water flow analysis in swelling soils when the soil is close to saturation, (i.e., at low matric suction) (Example 3, solutions UCS2 and UCS3). The effect of the changes in stress and deformation appeared to be minimal when the soil is at higher matric suctions (Example 4, solutions UCS1 and UCS2).
4. Analyses carried out with different values of Poisson's ratio can lead to significantly different answers in terms of the distributions of matric suction, stress, and displacements.
5. The analyses presented in this study produced results that are qualitatively reasonable and in accordance with anticipated behaviour.
6. The coupled seepage-deformation model provides a more rigorous understanding of the swelling behavior of expansive soils.

8.1.3 Computer programs

1. FlexPDE solver forms a powerful computing tool for solving volume change problems associated with an unsaturated, expansive soil. Special features of FlexPDE, such as fully automated adaptive grid refinement, fully automated time step refinement and automatic convergence control to satisfy maximum required error, appear to be particularly valuable for solving highly non-linear unsaturated soil problems.

2. FlexPDE solver provides flexibility for the description of soil property functions. Soil properties can be described as mathematical expressions of the dependent variables and their derivatives.
3. Current version of FlexPDE cannot be used for coupled seepage and stress-deformation analysis. The elastic parameter functions with respect to net normal stress cannot be handled automatically. The cross derivatives in coupled equations cannot be defined.
4. The computer program, COUPSO is a potential tool that can be used to perform fully coupled analyses associated with expansive soil behaviour.

8.1.4 General conclusions

1. The general theory of consolidation and swelling for unsaturated soils can be applied to the analysis of volume change associated with unsaturated, expansive soils.
2. Soil properties required to predict two- or three-dimensional behaviour of an unsaturated, expansive soil under transient wetting include: i) the elasticity parameter of the soil structure with respect to net normal stress, E; ii) the elasticity parameter of the soil structure with respect to matric suction, H; iii) the elasticity parameter of the water phase with respect to net normal stress, E_w; iv) the elasticity parameter of the water phase with respect to matric suction, H_w; v) the Poisson's ratio, μ; and vi) the coefficient of permeability, k. The soil properties are functions of both net normal stress and matric suction. Numerical analysis conducted in this study assumed a constant value of Poisson's ratio.
3. Swelling problems associated with unsaturated, expansive soils can be analysed using either an uncoupled approach or a coupled approach. Coupled solutions appear to be difficult to obtain, in part, because of the non-linear soil property functions. Uncoupled solutions can be more easily obtained than coupled solutions because the soil property functions involved in each process (i.e., water flow or stress-deformation process) are considered separately.

4. The uncoupled and coupled solutions compared well for the example problems presented in this research study.
5. The general-purpose partial differential equation solver, FlexPDE can be used to analyse a wide range of volume change problems associated with an unsaturated, expansive soil using an uncoupled approach.
6. The numerical computer program, COUPSO is a potential computing tool that can be used to perform coupled analysis associated with expansive soil behaviour.

8.2 Recommendations for future studies

Several recommendations for future studies can be made based on the results of this study. The recommendations are made with respect to the equations for constitutive relationships and with respect to the uncoupled and coupled solutions of volume change problems associated with an unsaturated, expansive soil.

8.2.1 Equations for constitutive relationships

1. It is suggested that the constitutive relationships for both unsaturated and saturated soils be described using a mathematical equation (as suggested in this study). The use of mathematical equations appears to be superior to the use of volume change indices. Using this approach, the experimental data for both recompression and compression can be described in one equation, and it is not necessary to assume a lower limit for each stress state variable. Soil parameters such as volume change indices, coefficients of volume change, and elasticity parameters can be obtained by differentiating the proposed equation. These parameters can then be expressed as mathematical functions of net normal stress and/or matric suction.
2. The equations suggested in this study for the constitutive surfaces have been evaluated and verified for Regina clay. Evaluation of the proposed equations on different soil types should be carried out.

3. Uncoupled and coupled analyses should be carried out when using various equations describing the constitutive surfaces. These analyses could determine the sensitivity of different mathematical equations to the solutions obtained.

8.2.2 Uncoupled and coupled solutions

1. It is suggested that uncoupled solutions are adequate for the analysis of most volume change problems involving unsaturated, expansive soils.
2. The uncoupled and coupled techniques presented in this study can be used to study the cyclic heave-settlement problems. Realistic boundary conditions associated with water flow equations must be described.
3. Three-dimensional volume change problems can be analyzed with FlexPDE when using the uncoupled approach.
4. The effect of each soil property function on the solutions of water flow and stress-deformation problems should be studied. The results of such analyses may assist in the simplification of the soil property functions used in the analyses.
5. It is suggested that FlexPDE be extended to accommodate coupled seepage, stress-deformation analyses.
6. Coupled analyses can be performed to study the swelling pressures applied on engineering structures such as retaining wall problems and foundations associated with unsaturated, expansive soils. It is recommended that the technique presented in this study be used for design and construction of light structures constructed on expansive soils. Uplift pressure can also be estimated.
7. This research study assumed an initial stress state for the soil. Solutions of non-linear problems depend on the initial stress state. It is suggested that further research should be carried out to study the coefficient of earth pressure at-rest associated with an unsaturated, expansive soil.
8. The assessment of initial stresses in a swelling soil mass must be properly defined to determine the initial position where each point will start its stress path on the constitutive surfaces.

9. There is need for additional research on the possible value of the Poisson's ratio for an unsaturated, expansive soil. It is anticipated that Poisson's ratio is also a function of net normal stress and matric suction.
10. The computer program, COUPSO, has been used to simulate volume change problems associated with collapsing soils and expansive soils. A study should be carried out to assess both heave and collapse behaviour of an unsaturated soil.
11. The suggested uncoupled and coupled models in this study assumed that the soil is isotropic, elastic and non-linear. The model should be extended to cover an anisotropic and elasto-plastic behaviour of soils.
12. The uncoupled and coupled models should be verified against measured data and field case histories.

REFERENCES

Abduljauwad S.N., Al-Sulaimani G.J., Basunbul I.A., and Al-Buraim I. 1998. Laboratory and Field Studies of Response of Structures to Heave of Expansive Clay. Geotechnique, 48(1):103-121.

Aitchison G.D. 1961. Relationship of Moisture and Effective Stress Functions in Unsaturated Soils. Pore Pressure and Suction in Soils Conf., London, England, pp. 47-52.

Aitchison G.D. 1973. The Quantitative Description of the Stress-Deformation of Expansive Soils – Preface to Set of Papers. Proc. 3rd Int. Conf. Expansive Soils, Haifa, Israel, vol. 2, pp. 79-82.

Aitchison G.D., Peter P. and Martin R. 1973. The Instability Indices I_{pm} and I_{ps} in Expansive Soils. Proc. 3rd Int. Conf. Expansive Soils, Haifa, Israel, vol. 2, pp. 101-104.

Aitchison G.D. and Martin R. 1973. A Membrane Oedometer for Complex Stress-Path Studies in Expansive Clays. Proc. 3rd Int. Conf. Expansive Soils, Haifa, Israel, vol. 2, pp. 83-88.

Aitchison G.D. and Woodburn J.A. 1969. Soil Suction in Foundation Design. Proc. 7th Int. Conf. Soil Mech. Found. Eng., Mexico, pp. 1-8.

Akaike, H. 1974. A New Look at the Statistical Model Identification. IEEE Transactions on Automatic Control, AC. 19(6): 716-723.

Alonso E.E. 1993. Constitutive Modelling of Unsaturated Soils. Unsaturated soils: Recent Developments and Applications, Civil Engineering European Courses, 86 p.

Alonso E.E. and Lloret A. 1995. Settlement of a 12 Storey Building due to Dessication Induced by Trees: A Case Study. Proc. 1st Int. Conf. Unsaturated Soils, pp. 935-943.

Alonso E.E., Batlle F., Gens A., and Lloret A. 1988. Consolidation Analysis of Partially Saturated Soils. Application to Earthdam Construction. Proc. 6th Int. Conf. Num. Meth. Geomech., Insbruck, pp. 1303-1308.

Alonso E.E., Gens A., and Hight D.W. 1987. Special Problem Soils. General Report. Proc. of the 9th European Conf. on Soil Mech. Found. Eng., Dublin, vol. 3, pp. 1087-1146.

Alonso E.E., Gens A., Josa A. 1990. A Constitutive Model for Partially Saturated Soils. Geotechnique, 40(3): 405-430.

Alonso E.E., Lloret A., Gens A., and Yang D.Q. 1995. Experimental Behaviour of Highly Expansive Double-structure Clay. Proc. 1st Int. Conf. Unsaturated Soils, Paris, pp. 11-16.

Alonso E.E., Vaunat J. and Gens A. 1999. Modelling the Mechanical Behaviour of Expansive Clays. J. Eng. Geo., vol. 54, pp.173-183.

Al-Shamrani M.A. and Al-Mhaidib A.I. 1999. Prediction of Potential Vertical Swell of Expansive Soils Using a Triaxial Stress Path Cell. Q. J. Eng. Geo., vol. 32, pp. 45-54.

Al-Shamrani M.A. and Al-Mhaidib A.I. 2000. Swelling Behaviour Under Oedometric and Triaxial Loading Conditions. GeoDenver 2000: Advances in Unsaturated Geotechnics, ASCE, pp. 344-360.

Baguley D., and Hose D.R. 1994. How to – Understand Finite Element Jargon. Bell and Bain Ltd., Glasgow, 66p.

Baguley D., and Hose D.R. 1997. How to – Interpret Finite Element Results. Bell and Bain Ltd., Glasgow, 66p.

Barbour S.L., Fredlund D.G., Gan J. K-M., and Wilson G. W. 1992. Prediction of Moisture Movement in Highway Subgrade Soils. Proc. 45th Can. Geotech. Conf., pp. 41A1-41A13.

Barden L. 1965. Consolidation of Compacted and Unsaturated Clays. Geotechnique, 15(3): 267-286.

Barden L. 1974. Consolidation of Clays Compacted 'Dry' and 'Wet' of Optimum Water Content. Geotechnique, 24(4): 605-625.

Barden L., Madedor A.O., and Sides G.R. 1969. Volume Change Characteristics of Unsaturated Clay. J. Soil Mech. Found. Div., ASCE, 95(SM1): 33-51.

Barden L. and Pavlakis G. 1971. Air and Water Permeability of Compacted Unsaturated Cohesive Soil. J. Soil. Sci, 22(3): 302-317.

Barden L., and Sides G.R. 1970. Engineering Behavior and Structure of Compacted Clay. J. Soil Mech. Found. Div., ASCE, 96(SM4): 1171-1200.

Barden L., Madellor, A.D., and Sides, G.R. 1969. Volume Change Characteristics of Unsaturated Clay. J. Soil Mech. and Found. Eng. Division, ASCE, vol. 95, pp. 33-51.

Basma A.A., Al-Homoud A.S., Malkawi A.I.H., and Al-Bashabsheh M.A. 1996. Swelling-Shrinkage Behavior of Natural Expansive Clays. Applied Clay Science, vol. 11, pp. 211-227.

Bear J. 1972. Dynamics of Fluid Flow in Porous Media. Amsterdam Elsevier.

Biddle P.G. 1983. Patterns of Soil Drying and Moisture Deficit in the Vicinity of Trees on Clay Soils. Geotechnique, 18(2): 107-126.

Biddle P.G. 1998. The Root Damage to Buildings, Volume 1: Causes, Diagnosis and Remedy. Willowmead Publishing Ltd., Swindon, 376 p.

Biddle P.G. 1998. The Root Damage to Buildings, Volume 2: Patterns of Soil Drying in Proximity to Trees on Clay Soils. Willowmead Publishing Ltd., Swindon, 299 p.

Biot, M.A., 1941. General Theory of Three-Dimensional Consolidation. J. Appl. Phys., Vol..12, pp. 155-164.

Biot M.A. 1955. Theory of Elasticity and Consolidation for a Porous Anisotropic Solid. J. Appl. Phys., 26(2): 182-185.

Bishop A.W. 1959. The Principle of Effective Stress, Lecture Delivered in Oslo, Norway. Teknisk Ukeblad, 106(39): 859-863.

Bishop A.W. 1960. The Measurement of Pore Pressure in Triaxial Test. Proc. Conf. Pore Pressure and Suction in Soils, London, Butterworths, pp. 63-66.

Bishop A.W. and Blight G.E. 1963. Some Aspects of Effective Stress in Saturated and Partly Saturated Soils. Geotechnique, 13(3): 177-197.

Bishop A.W. and Eldin A.K.G. 1950. Undrained Triaxial Tests on Saturated Sands and their Significance in the General Theory of Shear Strength. Geotechnique, vol. 2, pp. 13-32.

Blight G.E. 1965. The Time-rate of Heave of Structures on Expansive Clays. Symposium on Moisture Equilibria and Moisture Change in Soils beneath Covered Area, Australia, pp. 78-88.

Blight G.E. 1965. A Study of Effective Stresses for Volume Change. Symposium on Moisture Equilibria and Moisture Change in Soil Beneath Covered Area, Australia, pp. 259-269.

Bozozuk M. and Burn K.N. 1960. Vertical Ground Movement near Elm Trees. Geotechnique, vol. 10, pp. 19-32.

Bowles J.E. 1996. Foundation Analysis and Design. McGraw Hill Companies, Inc., 1175 p.

Brackley I.J.A. 1971. Partial Collapse in Unsaturated Expansive Clay. Proc. 5th Reg. Conf. Soil Mech. Found. Eng., South Africa, pp. 23-30.

Brackley I.J.A. 1973. Swell Pressure and Free Swell in a Compacted Clay. Proc. 3rd Int. Conf. Expansive Soils, Haifa, Israel, vol. 1, pp.169-176.

Brackley I.J.A. and Sanders P.J. 1992. In-situ Measurement of Total Natural Horizontal Stresses in an Expansive Clay. Geotechnique, 42(2): 443-451.

Buckingham E. 1907. Studies of the Movement of Soil Moisture. U.S.D.A. Bur. of Soils, Bulletin No. 38.

Burland J.B. 1965. Some Aspects of the Mechanical Behaviour of Partly Saturated Soils. Symposium on Moisture Equilibria and Moisture Change in Soil beneath Covered Area, Australia, pp. 270-278.

Casagrande A. 1936. The Determination of the Preconsolidation Load and Its Practical Significance. Discussion D-34, Proc. 1st Int. Conf. Soil Mech. Found. Eng., Cambridge, MA, vol. 3, pp. 60-64.

Chandrasekharaiah D.S. and Debnath L. 1994. Continuum Mechanics. Academic Press Ltd., 595 p.

Chang C.S. and Duncan J.M. 1983. Consolidation Analysis for Partly Saturated Clay by using an Elastic-plastic Effective Stress-strain Model. Int. J. Numer. and Anal. Methods in Geomechanics, vol. 7, pp. 39-55.

Chen F.H. 1973. The Basic Physical Property of Expansive Soils. Proc. 3rd Int. Conf. Expansive Soils, Haifa, Israel, vol. 1, pp. 17-25.

Chen F.H. 1988. Foundations on Expansive Soil. Elsevier, Amsterdam, 463 p.

Chen Z-H., Fredlund D.G., and Gan J.K-M. 1999. Overall Volume Change, Water Volume Change, and Yield associated with an Unsaturated Compacted Loess. Can. Geotech. J., vol. 36, pp. 321-329.

Chen Z-H., Zhou H., Fredlund D.G., and Gan J.K-M. 1998. A Non-linear Model for Unsaturated Soils. Proc. 2nd Int. Conf. Unsaturated Soils, Beijng, China, pp. 461-466.

Cheng Y., and Pettry D.E. 1993. Horizontal and Vertical Movements of Two Expansive Soils in Mississippi. Soil Sci. Soc. A. J., vol. 57, pp. 1542-1547.

Childs E.C. and Collis-GeorgeN. 1950. The Permeability of Porous Materials. Proc. Royal. Soc., vol. 210A, pp. 392-405.

Chu T.Y. and Mou C.H. 1973. Volume Change Characteristics of Expansive Soils Determined by Controlled Suction Tests. Proc. 3rd Int. Conf. Expansive Soils, Haifa, Israel, vol. 1, pp. 177-185.

Cokca E. and Birand A. 2000. Suction-Swelling Relations. GeoDenver 2000: Advances in Unsaturated Geotechnics, ASCE, pp. 379-392.

Coleman J.D. 1962. Stress/Strain Relation for Partly Saturated Soils. Geotechnique (Correspondence), 12(4): 348-350.

Corapcioglu M.Y. 1984. Land subsidence - A State of the Art Review. Fundamentals of Transport Phenomena in Porous Media, Nijhoff, Dordrecht, pp. 371-444.

Cryer C.W. 1963. A Comparison of the Three-dimensional Consolidation Theories of Biot and Terzaghi. Quart. Journ. Mech. and Appl. Math., 16(4): 401-412.

Dakshanamurthy V. 1979. A Stress-controlled Study of Swelling Characteristics of Compacted Expansive Clays. Geotech. Test. J., ASTM, 2(1): 57-60.

Dakshanamurthy V., Fredlund D.G., and Rahardjo H. 1984. Coupled Three-dimensional Consolidation Theory of Unsaturated Porous Media. Proc. 5th Int. Conf. on Expansive Soils, Adelaide, South Australia, pp. 99-103.

Darcy H. 1856. Histoire des Foundataines Publique de Dijon. Dalmont, Paris, pp. 590-594.

Day R.W. 1994. Performance of Slab-on-grade Foundations on Expansive Soil. J. of Perform. of Cons. Facility., ASCE, 8(2): 129-138.

de Jong E. 2000. Personal communication. College of Agriculture, University of Saskatchewan, Saskatoon.

Delage P. and Graham J. 1995. Mechanical Behaviour of Unsaturated Soils: Understanding the behaviour of unsaturated soils requires reliable conceptual models. Proc. 1st Int. Conf. Unsaturated Soils, Paris, France, pp. 1223-1256.

Desai C.S. and Siriwardane H.J. 1984. Constitutive Laws for Engineering Materials with Emphasis on Geologic Materials. Prentice-Hall, Inc., Englewoood Cliffs, New Jersey, 468 p.

Desai C.S., Vulliet L., Laloui L., and Geiser F. 1996. Disturbed State Concept for Constitutive Modelling of Partially Saturated Porous Media. Institute des Sols, Roches et Fondations, 27 p.

Dhowian A.W. 1990. Simplified Heave Prediction Model for Expansive Shale. Geotech. Test. J., ASTM, 13(4): 323-333.

Dif A.E. and Bluemel W.F. 1991. Expansive Soils under Cyclic Drying and Wetting. Geotech. Test. J., Amer. Soc. of Civil Eng., 14(1): 96-102.

Dinh T.T. 1996. Plane Strain Modelling of Volume Change in Expansive Soil. M.Sc. thesis, Faculty of Engineering and Surveying, University of Southern Queensland, Australia.

Donaldson G.W. 1973. The Prediction of Differential Movement on Expansive Soils. Proc. 3rd Int. Conf. Expansive Soils, Haifa, Israel, vol. 1, pp. 289-293.

Dow J.O. 1999. A Unified Approach to the Finite Element Method and Error Analysis Procedures. Academic Press, 533 p.

Dow J.O., Harwood, S.A., Jones, M.S., and Stevenson I. 1991. Validation of a Finite Element Error Estimator. AIAA Journal, Vol 29 (10): pp. 1736-1742.

Driscoll R. 1983. The Influence of Vegetation on the Swelling and Shrinking of Clay Soils in Britain. Geotechnique, 18(2): 93-105.

Driscoll R. 1984. A Review of British Experience of Expansive Clay Problems. Proc. 5th Int. Conf. Expansive Soils, Adelaide Australia, pp. 192-196.

Desai C.S., and Christian, J.T. 1977. Numerical Methods in Geotechnical Engineering. McGraw-Hill, New York, 783 p.

Ducan J.M., and Chang, C.Y. 1970. Nonlinear Analysis of Stress and Strain in Soils. J. Soil Mech. Found. Div., pp. 1629-1653.

Erol A.O., Dhowian A., and Youssef A. 1987. Assessment of Eodometer Methods for Heave Prediction. Proc. 6th Int. Conf. Expansive Soils. New Delhi, India, pp. 99-103.

Escario V. 1969. Swelling of Soils in Contact with Water at a Negative Pressure. Proc. 2nd Int. Conf. Expansive Soils, Texas, pp. 207-217.

Escario V. 1969. Determination of the Geotechnical Characteristics of Expansive Soils. Proc. 2nd Int. Conf. Expansive Soils, Texas, pp. 114-120.

Escario V., Juca J.F.T., and Coppe M.S. 1989. Strength and Deformation of Partly Saturated Soils. Proc. 12nd Int. Conf. Soil Mech. Found. Eng., 1:43-46.

Escario V., Saez J., and Fisicas C. L. 1973. Measurement of the Properties of Swelling and Collapsing Soils under Controlled Suction. Proc. 3rd Int. Conf. Expansive Soils, pp. 195-200.

Fargher P.J. and Stevens R.L. 1973. Notes on the Design Assumptions and Methods for Grillage Raft Footings. Hosking, Fargher and Oborn Pty, Ltd., Adelaide.

FlexPDE Manual, Version 3.00. 2001. PDE Solution Inc. Fremont, CA, USA.

Fredlund D.G. 1964. Comparison of Soil Suction and One-dimensional Consolidation Characteristics of a Highly Plastic Clay. M.Sc. thesis, University of Alberta, Edmonton.

Fredlund D.G. 1969. Consolidometer Test Procedural Factors Affecting Swell Properties. Proc. 2nd Int. Conf. on Expansive Soils, Texas A & M, College Station, Texas, pp. 435-456.

Fredlund D.G. 1973. Volume Change Behaviour of Unsaturated Soils. Ph.D. dissertation, University of Alberta, Edmonton, 490 p.

Fredlund D.G. 1979. Second Canadian Geotechnical Colloquium: Appropriate Concepts and Technology for Unsaturated Soils. Can. Geotech. J., 16(1): 121-139.

Fredlund D.G. 1981. Discussion: "Consolidation of Unsaturated Soils including Swelling and Collapse Behaviour" by Lloret and Alonso, 1981, Geotechnique, 30(4): 449-477. Discussion in Geotechnique.

Fredlund D.G. 1985. Soil Mechanics Principles that Embrace Unsaturated Soils. Proc., 11th Int. Conf. Soil Mech. and Found. Eng., San Francisco, USA., vol. 2, pp. 465-473.

Fredlund D.G. 1987. The Stress State for Expansive Soils. Proc., 6th Int. Conf. on Expansive Soils, New Delhi, India, pp. 1-9.

Fredlund D.G. 1987. The Prediction and Performance of Structures on Expansive Soils. Proc., Int. Symposium on Prediction and Performance in Geotechnical Engineering, Calgary, Canada, pp. 51-60.

Fredlund D.G. 1995. The Scope of Unsaturated Soils Mechanics: An Overview. Proc., 1st Int. Conf. on Unsaturated Soils, Paris, France, vol. 3, pp. 1155-1177.

Fredlund D.G. 1997. From Theory to the Practice of Unsaturated Soil Mechanics. Proc. 3rd Brazilian Symposium on Unsaturated soils, Rio de Janeiro, Brazil, vol.2.

Fredlund D.G. 1999. The Implementation of Unsaturated Soil Mechanics into Geotechnical Engineering. R.M. Hardy Address, 52nd Can. Geotech. Conf., Regina.

Fredlund D.G. 2000. Historical Developments and Milestones in Unsaturated Soil Mechanics. Proc. of the Asian Conf. on Unsaturated Soils, Singapore, pp. 53-68.

Fredlund D.G., and Morgenstern N.R. 1976. Constitutive Relations for Volume Change in Unsaturated Soils. Can. Geotech. J., 13(3): 261-276.

Fredlund D.G., and Morgenstern N.R. 1977. Stress State Variables for Unsaturated Soils. J. Geotech. Eng. Div., ASCE (GT5), 103: 447-466.

Fredlund D.G., and Hasan J. 1979. One-dimensional Consolidation Theory: Unsaturated Soils. Can. Geotech. J., 16(2): 521-531.

Fredlund D.G., Hasan J.U., and Filson H. 1980. The Prediction of Total Heave. Proc., Fourth Int. Conf. on Expansive Soils, Denver, CO., June 16-18, Vol. 1, pp. 1-17.

Fredlund D.G., and Rahardjo, H. 1985. Theoretical Context for Understanding Unsaturated Residual Soil Behavior. Proc. 1st Int. Conf. Geomechanics in Tropical Lateritic and Saprolitic Soils, Brazilia, Brazil, pp. 295-306.

Fredlund D.G., and Rahardjo, H. 1993. Soil Mechanics for Unsaturated Soil. John Wiley & Sons, New York, 560 p.

Fredlund D.G., and Xing, A. 1994. Equations for the Soil-Water Characteristic Curve. Can. Geotech. J., 31(3): 521-532.

Fredlund D.G., and Rahardjo H. 1985. Unsaturated Soil Consolidation Theory and Laboratory Experimental Data. In Consolidation of Soils: Testing and Evaluation, ASTM STP 892.

Fredlund G.G., Hung V.Q., and Thieu N.T.M. 2000. A Component System Approach to Solving Saturated/Unsaturated Soils Problems. Proc. Annual Conf. of the Can. Soc. Civil Eng., London, Ontario, pp. 448-455.

Fredlund D.G. and Hung V.Q. 2001. Prediction of Volume Change in an Expansive Soil as a Result of Vegetation and Environmental Changes. Geotechnical Special Publication No. 115, Expansive Clay Soils and Vegetative Influence on Shallow Foundations, Vipulanandan C., Addison M.B., Hasen M. ed., ASCE, Houston, Texas, vol. 115, pp. 24-43.

Fredlund M.D. 2000. The Role of Unsaturated Soil Property Functions in the Practice of Unsaturated Soil Mechanics. Ph.D. dissertation, University of Saskatchewan, Saskatoon, 292 p.

Freeze R.A. and Cherry J.A, 1979. Groundwater. Englewood Cliffs, Prentice-Hall, New York, 604 p.

Fung Y.C. 1994. A First Course in Continuum Mechanics, 3rd Edition. Prentice-Hall, Englewood Cliffs, New Jersey.

Gardner W.R. 1958. Some Steady State Solutions of the Unsaturated Moisture Flow Equation with Application to Evaporation from a Water-Table. Soil Sci., 85(4): 228-232.

Gehling W.Y.Y., Alonso E.E., and Gens A. 1995. Stress-path Testing of Expansive Compacted Soils. Proc. 1st Int. Conf. Unsaturated Soils, Paris, pp. 77-82.

Gens A., and Alonso E.E. 1992. A Framework for the Behaviour of Unsaturated Expansive Clays. Can. Geotech. J., vol. 29, pp. 1013-1032.

Gibson R.E., England G.L., and Hussey M.J.L. 1967. The Theory of One-dimensional Consolidation of Saturated Clays. Geotechnique, vol. 17, pp. 261-273.

Gibson R.E., Schiffman R.L. and Pu S.L. 1970. Plane Strain and Axially Symmetric Consolidation of a Clay Layer on a Smooth Impervious Base. Q. J. Mech. Appl. Maths.

Gilchrist H.G. 1963. A Study of Volume Change of a Highly Plastic Clay. M.Sc. thesis, University of Saskatchewan, Saskatoon, 141 p.

Goode J.C. 1982. Heave Prediction and Moisture Migration beneath Slabs on Expansive Soils. M.Sc. thesis, Colorado State University, Fort Collins, Colorado, 241 p.

Goode J.C., Hamberg D.J. and Nelson J.D. 1984. Moisture Content and Heave beneath Slabs on Grade. Proc. 5th Int. Conf. Expansive Soils, Adelaide Australia, pp. 212-217.

Graham J. 1997. Elastic-Plastic Soil Mechanics for Geotechnical Engineer. Short Course held under the Auspices of the Department of Civil Engineering, University of Saskatchewan, Saskatoon.

Habib S.A., Kato T., and Karube D. 1995. Suction Controlled One-dimensional Swelling and Consolidation Behaviour of Expansive Soil. Proc. 1st Int. Conf. Unsaturated Soils, Paris, pp. 101-107.

Habib S.A. 1995. Lateral Pressure of Unsaturated Expansive Clay in Looped Stress Path. Proc. 1st Int. Conf. Unsaturated Soils, Paris, pp. 95-100.

Hamberg D.J. and Nelson J.D. 1984. Prediction of Floor Slab Heave. Proc. 5th Int. Conf. Expansive Soils, Adelaide, Australia, pp. 137-140.

Hamilton J.J. 1963. Volume Changes in Undisturbed Clay Profiles in Western Canada. Can. Geotech. J., 1(1): 27-42.

Hamilton J.J, 1977. Foundations on Swelling or Shrinking Sub-soils. Can. Building Digest, CBD 184, Div. of Building Research, Nat. Res. Council, Ottawa, 4 p.

Hamouche K.K., Leroueil S., Roy M., and Lutenegger A.J. 1995. In-situ Evaluation of K_0 in Eastern Canada Clays. Can. Geotech. J., vol. 32, pp. 677-688.

Hanafy E.A.D.E. 1991. Swelling/Shrinkage Characteristic Curve of Desiccated Expansive Clays. Geotech. Test. J., ASCE, 14(2): 206-211.

Hardy R.M. 1965. Identification and Performance of Swelling Soil Types. Can. Geotech. J., 2(2): 141-153.

Ho D.Y.F. 1988. The Relationships between the Volumetric Deformation Moduli of Unsaturated Soils. Ph.D. dissertation, University of Saskatchewan, Saskatoon, 379 p.

Ho D.Y.F., Fredlund, D.G., and Rahardjo, H. 1992. Volume Change Indices During Loading and Unloading of an Unsaturated Soil. Can. Geotech. J., 29(2): 195-207.

Holtz R.D., and Kovacs, W.D. 1981. An Introduction to Geotechnical Engineering. Prentice-Hall, Englewood Cliffs, New Jersey, 733 p.

Holtz W.G. 1983. The Influence of Vegetation on the Swelling and Shrinking of Clays in the United State of America. Geotechnique, 18(2): 159-163.

Holtz W.G. and Gibbs H.J. 1956. Engineering Properties of Expansive Clays. Trans. ASCE, vol. 121, pp. 641-663.

Hoyos Jr. L.R. and Macari E.J. 2000. Nature of Principal Strain Response of Unsaturated Soils under Multi-axial Stress State. GeoDenver 2000: Advances in Unsaturated Geotechnics, ASCE, pp. 333-343.

Hu Y. and Randolph M.F. 1998. A Practical Numerical Approach for Large Deformation Problems in Soil. Int. J. Numer. Anal. Meth. Geomech, vol. 22, pp. 327-350.

Hung V.Q. 2000. Finite Element Method for the Prediction of Volume Change in Expansive Soils. M.Sc. thesis, University of Saskatchewan, Saskatoon, 314 p.

Hung V.Q. and Fredlund D.G. 2000. Volume Change Predictions in Expansive Soils using a Two-dimensional Finite Element Method. Proc. of the Asian Conf. on Unsaturated Soils, Singapore, pp. 231-235.

Hung V.Q. and Fredlund D.G. 2001. Prediction of Heave using a General Partial Differential Equation Solver. Proc. Conf. Comp. Meth. and Adv. in Geotech., Tuson, Arizona, pp. 813-818.

Hung V.Q., Fredlund D.G., and Pereira J.H.F. 2001. Analysis of Swelling Behaviour of Soils by a Coupled Solution. Proc. Int. Conf. on Management of the Land and Water Resources, Hanoi, Vietnam, pp. 94-103.

Hung V.Q. and Fredlund D.G. 2002. Using Volume Change Indices for Two-dimensional Swelling Analysis. Proc. 55th Can Geotech Conf., Ontario.

Hung V.Q., Fredlund D.G., and Pereira J.H.F. 2002. Coupled Solution for the Prediction of Volume Change in Expansive Soils. Proc. 3rd Int. Conf. Unsaturated Soils, Recife, Brazil, pp. 181-186.

Hwang C.T., Morgenstern N.R., and Murray D.W. 1971. On Solutions of Plane Strain Consolidation Problems by Finite Element Methods. Can. Geotech. J., Vol. 8, pp. 109-118.

Jennings J.E. 1961. A Revised Effective Stress Law for Use in the Prediction of the Behaviour of Unsaturated Soils. Pore Pressure and Suction in Soils Conf., London, England, pp. 26-30.

Jennings J.E.B. and Burland J.B. 1962. Limitations to the use of Effective Stresses in Partly Saturated Soils. Geotechnique, 12(2): 125-144.

Jennings J.E. and Knight K. 1957. The Prediction of Total Heave from the Double Oedometer Test. Proc. Symp. Expansive Clays, South African Inst. of Civil Engineers, Johanesberg, 7(9): 13-19.

Jimenez-Salas J.A. 1995. Foundation and Pavements on Unsaturated Soils - Part two: exppansive clays. Proc. 1st Int. Conf. Unsaturated Soils, Paris, France, pp. 1441-1464.

Johnson L.D. 1977. Evaluation of Laboratory Suction Tests for Prediction of Heave in Foundation Soils. Tech. Reports S-77-7, U.S. Army Engineer Waterways Experiment Station, Vicksburg, 118 p.

Jones D.E. and Holtz W.G. 1973. Expansive Soils – The Hidden Disaster. Civil Eng., New York, pp. 87-89.

Juca J.F.T., Ferreira R.N. and Bastos E.G. 1998. Volume Change and Shear Strength of an Unsaturated Expansive Clay. Proc. 2nd Int. Conf. Unsaturated Soils, Beijng, China, pp. 72-77.

Justo J.L., Delgado A., and Ruiz J. 1984. The Influence of Stress-path in the Collapse-Swelling of Soils at the Laboratory. Proc. 5th Int. Conf. Expansive Soils, Adelaide Australia, pp. 67-71.

Kassiff G., Baker R. and Ovadia Y. 1973. Swell-pressure Relationships at Constant Suction Changes. Proc. 3rd Int. Conf. Expansive Soils, Haifa, Israel, vol. 1, pp. 201-208.

Khalili N. and Khabbaz M.H. 1995. On the Theory of Three-dimensional Consolidation in Unsaturated Soils. Proc. 1st Int. Conf. Unsaturated Soils, Paris, France, pp. 745-750.

Klausner Y. 1991. Fudamentals of Continuum Mechanics of Soils. Springer-Verlag, London, 607 p.

Kohgo Y. 1995. A Consolidation Analysis Method for Unsaturated Soils Coupled with an Elastoplastic Model. Proc. 1st Int. Conf. Unsaturated Soils, Paris, France, pp. 1085-1092.

Komornik A., Wiseman G., and Ben-Yaacob Y. 1969. Studies of In-situ Moisture and Swelling Potential Profiles. Proc. 2nd Int. Conf. Expansive Soils, Texas, pp. 348-361.

Kramer P.J. and Kozlowski T.T. 1960. Physiology of Trees. McGraw-Hill, New York.

Krohn J.P. and Slosson J.E. 1980. Assessment of Expansive Soils in the United States. Proc. 4th Conf. Expansive Soils, Denver, vol. 1, pp. 596-608.

Lambe T.W., and Whitman R.V. 1969. Soil Mechanics. John Wiley & Sons, 553 p.

Laughton A.S. 1955. The Compaction of Ocean Sediments. Ph.D. dissertation, University of Cambridge, England.

Leong E.C., and Rahardjo H. 1997. Review of Soil-Water Characteristic Curve Equations. J. of Geotech. and Geoenviron. Eng., pp. 1106-1117.

Leong E.C., and Rahardjo H. 1997. Permeability Functions for Unsaturated Soils. J. of Geotech. and Geoenviron., pp. 1118-1126.

Lewis R.W., Bettesss P., and Hinton E. (eds). 1984. Numerical Methods in Coupled Systems. Wiley, Chichester.

Lewis R.W., Hinton E., and Bettesss P. (eds). 1987. Numerical Methods in Transient and Coupled Systems. Wiley, Chichester.

Lewis R.W., Roberts G.K., and Zienkiewicz O.C. 1976. A Non-linear Flow and Deformation Analysis of Consolidated Problems. Proc. 2nd Inter. Conf. Numer. Meth. in Geomech., pp. 1106-1118.

Lewis R.W., Schrefler B.A., and Simoni L. 1991. Coupling versus Uncoupling in Soil Consolidation. Inter. J. Numer. Anal. Meth. Geomech., vol. 15, pp. 533-548.

Lloret A. and Ledesma. 1993. Finite Element Analysis of Deformations of Unsaturated Soils. Unsaturated soils: Recent developments and applications, Civil engineering European Courses.

Lloret A., and Alonso E.E. 1980. Consolidation of Unsaturated Soils including Swelling and Collapse Behaviour. Geotechnique, 18(4): 449-477.

Lloret A., and Alonso E.E. 1985. State Surfaces for Partially Saturated Soils. Proc. 11th Int. Conf. Soil Mech. Found. Eng. San Francisco, pp. 557-562.

Lu Y. 1969. Swell Properties of Desiccated Regina Clay. M.Sc. Thesis. University of Saskatchewan, Saskatoon, 135 p.

Lytton R. L. 1977. Foundation on Expansive Soils. Numerical Methods in Geotechnical Engineering, edited by Desai, McGraw-Hill, London, pp. 427-457.

Lytton R.L. 1985. Notes on Volume Change and Flow Calculations in Expansive Soils. University of Houston.

Lytton R.L. 1995. Foundations and Pavements on Unsaturated Soils. Proc. 1st Int. Conf. Unsaturated Soils, Paris, France, 1201-1206.

Lytton R.L. 1994. Prediction of Movement in Expansive Clay. Vertical and Horizontal Deformations of Foundations and Embankments, Geotechnical Special Publication No. 40, Yeung A.T. and Felio G.Y. ed., ASCE, New York, New York, Vol. 2, pp. 1827-1845.

Madedor A.O. 1967. Consolidation Characteristics of Compacted Clay. M.Sc. thesis, University of Witwatersrand, South Africa.

Mandel J. 1953. Consolidation des Sols (Etude Methematique). Geotechnique, vol. 3, pp. 287-299.

Matsuoka H., Sun D., Kogane A., Fukuzawa N., and Ichihara W. 2002. Stress-strain Behaviour of Unsaturated Soil in True Triaxial Tests. Can. Geotech. J., vol. 39, pp. 608-619.

Matyas E.L. 1969. Some Properties of Two Expansive Clays from Western Canada. Proc. 2nd Int. Conf. Expansive Soils. Texas A&M Univ., College Station, pp. 263-278.

Matyas E.L., and Radhakrishna, H.S. 1968. Volume Change Characteristics of Partially Saturated Soils. Geotechnique, 18(4): 432-448.

McKeen R.G. 1976. Design and Construction of Airport Pavements on Expansive Soils. FAA-RD-76-66, Federal Aviation Administration, Washington.

McKeen R.G. 1992. A Model for Predicting Expansive Soil Behaviour. Proc. 7th Int. Conf. Expansive Soils, pp. 1-6.

McNamee J., and Gibson R.E. 1960. Plane Strain and Axially Symmetric Problems of the Consolidation of a Semi-infinite Clay Stratum. Q. J. Mech. and Appl. Math., 13(2): 210-227.

McOmber R.M. and Thompson R.W. 2000. Verification of Depth of Wetting for Potential Heave Calculations. GeoDenver 2000: Advances in Unsaturated Geotechnics, ASCE, pp. 409-422.

Miller D.J., Durkee D.B., Chao K.C., and Nelson J.D. 1995. Simplified Heave Prediction for Expansive Soils. Proc. 1st Int. Conf. Unsaturated Soils, Paris, France, pp. 891-897.

Milovic D. 1992. Stresses and Displacements for Shallow Foundations. Elsevier, 620 p.

Miranda A.N. 1988. Behaviour of Small Earth Dams during Initial Filling. Ph.D. dissertation, Colorado State University, Colorado, 223 p.

Mitchell P.W. 1980. The Structural Analysis of Footings on Expansive Soil. Webb & Son, Adelaide, Australia, 152 p.

Mitchell J.K. 1993. Fundamentals of Soil Behavior. John Wiley & sons, New York, 422 p.

Mitchell J.K. 1991. Conduction Phenomena: from Theory to Geotechnical Practice. Geotechnique, vol. 41, pp. 299-340.

Mitchell P.W. and Avalle D.L. 1984. A Technique to Predict Expansive Soil Movements. Proc. 5th Int. Conf. Expansive Soils, Adelaide Australia, pp. 124-130.

Modaressi A. and Abou-Bekr N. 1994. Constitutive Model for Unsaturated Soils: Validation on a Silty Material. Proc. 3rd Europian Conf. Numer. Meth. Geotech. Eng., Manchester, pp. 91-96.

Mohan D., and Rao B.G. 1965. Moisture Variation and Performance of Foundations in Black Cotton Soils in India. Symp. on Moisture Equilibria and Moisture Change in Soil Beneath Covered Area, Australia, pp. 175-183.

Morgenstern N.R.. 1979. Properties of Compacted Soils. Contribution to Panel Discussion, Proc. 6th Panamerican Conf. Soil Mech. Found. Eng., Lima, Peru, vol. 3, pp. 349-354.

Morgenstern N.R., and Eisenstein Z. 1970. Methods of Estimating Lateral Loads and Deformations. Proc. of Specialty Conf. Lateral Stresses in the Ground and Design of Earth Retaining Structures, New York, pp. 51-102.

Nanda A., Delage P., and Gatmiri B. 1995. Comparison of Two Finite Element Models for Unsaturated Consolidation. Proc. 1st Int. Conf. Unsaturated Soils, Paris, France, pp. 1129-1134.

Navarro V., and Alonso E.E. 2000. Modelling Swelling Soils for Disposal Barries. Computer and Geotechnics, vol. 27, pp. 19-43.

NAVFAC. 1971. Soil Mechanics Foundation and Earth Structures, Design Manual. NAVFACDM-7, Naval Facilities Engineering Command, Bureau of Yards and Docks, Washington.

Noble C.A. 1966. Swelling Measurements and Prediction of Heave for Lacustrine Clay. Can. Geotech. J., 3(1): 32-41.

PDEase2D 3.0 Reference Manual, 3rd Edition. 1996. Macsyma Inc. Arlington, MA, 02174 USA.

Pentland J.S. 2000. Use of a General Partial Differential Equation Solver for Solution of Heat and Mass Transfer Problems in Soils. M.Sc. thesis, University of Saskatchewan, Saskatoon. 175 p.

Perko H.A., Thompson R.W., and Nelson J.D. 2000. Suction Compression Index based on CLOD Test Results. GeoDenver 2000: Advances in Unsaturated Geotechnics, ASCE, pp. 393-408.

Pereira J.H.F. 1996. Numerical Analysis of the Mechanical Behavior of Collapsing Earth Dams during First Reservoir Filling. Ph.D. dissertation, University of Saskatchewan, Saskatoon, 449 p.

Pereira J.H.F., and Fredlund, D.G. 1997. Constitutive Modelling of a Metastable-structured Compacted Soil. Proc., Int. Symposium on Recent Developments in Soil and Pavement Mechanics, Rio de Janeiro, Brazil, pp. 317-326.

Perpich W.M., Lukas R.G., and Baker, Jr.C.N. 1965. Dessiccation of Soil by Trees related to Foundation Settlement. Can. Geotech. J., 2(1):23-39.

Pham H.T.V. 2002. Slope Stability Analysis using Dynamic Programming Method Combined with a Finite Element Stress Analysis. M.Sc. thesis, University of Saskatchewan, Saskatoon, 200 p.

Phillip J.R. 1986. Linearized Unsteady Multidimensional Infiltration. Water Resour. Res., vol. 22, pp. 1717-1727.

Picornell M., and Lytton R.L. 1984. Modelling the Heave of a Heavily Loaded Foundation. Proc., 5th Int. Conf. on Expansive Soils, Australia, pp. 104-108.

Pidgeon J.T. 1987. The Prediction of Differential Heave for Design of Foundation in Expansive Soil Areas. Proc. 9th African Reg. Conf. Soil Mech. Found. Eng., Lagos, pp. 117-128.

Pile K.C. and McInnes D.B. 1984. Laboratory Technology for Measuring Properties of Expansive Soils. Proc. 5th Int. Conf. Expansive Soils. Adelaide, South Australia, pp. 85-93.

Prasad R. 1988. A Linear Root Water Uptake Model. J. Hydrol., vol. 99, pp. 297-306.

Pufahl D.E., Fredlund D.G., and Rahardjo H. 1983. Lateral Earth Pressures in Expansive Clay Soils. Can. Geotech. J., 20(2): 228-241.

Rahardjo H. 1990. The Study of Undrained and Drained Behaviour of Unsaturated Soils. Ph.D. dissertation, University of Saskatchewan, Saskatoon, 385 p.

Rahardjo H., and Fredlund D.G. 1995. Experimental Verification of the Theory of Consolidation for Unsaturated Soils. Can. Geotech. J., 32(5): 749-766.

Rao R.R., Rahardjo H., and Fredlund D.G. 1988. Closed-form Heave Solutions for Expansive Soils. J. of Geotech. Eng., ASCE, 114(5): 573-588.

Ravina I. 1983. The Influence of Vegetation on Moisture and Volume Changes. Geotechnique, 18(2): 151-157.

Reddy J.N. 1984. An Introduction to the Finite Element Method. McGraw-Hill, Inc., 495 p.

Rees S.W. and Thomas H.R. 1993. Simulating Seasonal Ground Movement in Unsaturated Clay. Journal of Geotechnical Engineering, ASCE, 119(7): 1127-1143.

Rendulic L. 1936. Relation between Void Ratio and Effective Principal Stress for a Remolded Silty Clay. Proc. 1st Int. Conf. Soil Mech. Found. Eng., vol. 3, pp. 48-51.

Richards L. A. 1931. Capillary Conduction of Liquids Through Porous Medium. J. Physics, vol. 1, pp. 318-333.

Richards B.G. 1967. Moisture Flow and Equilibria in Unsaturated Soils for Shallow Foundation. Symp. on Permeability and Capillary in Soils, ASTM Spec. Tech. Pub., 47(7): 185-191.

Richards B.G. 1984. Finite Element Analysis of Volume Change in Expansive Clays. Proc., 5th Int. Conf. on Expansive Soils, Autralia, pp. 141-148.

Richards B.G. 1995. Numerical Analyses and Coupling. Proc. 1st Int. Conf. Unsaturated Soils, Paris, France, pp. 1381-1389.

Richards B.G., Horn R., Baumgartl T., and Graesle. 1995. The Role of Stress on the Behaviour of Unsaturated Soils. Proc. 1st Int. Conf. Unsaturated Soils, Paris, France, pp. 785-790.

Richards B.G., Peter P., and Emerson W.W. 1983. The Effect of Vegetation on the Swelling and Shrinking of Soils in Australia, Geotechnique, 18(2): 127-139.

Richards B.G., Peter P. and Martin R. 1984. The Determination of Volume Change Properties in Expansive Soils. Proc. 5th Int. Conf. Expansive Soils, Adelaide Australia, pp. 179-186.

Sabbagh. 1995. Prediction of Volume Change in Unsaturated Clays. Proc. 1st Int. Conf. Unsaturated Soils, Paris, France, pp. 791-796.

Sampson E., Schuster R.L. and Budge W.D. 1965. A Method of Determining Swell Potential of an Expansive Clay. Proc. 1st Int. Conf. Expansive Soils, Texas, pp. 255-275.

Sattler P.J., Fredlund, D.G. 1990. Numerical Modelling of Vertical Ground Movements in Expansive Soils. Can. Geotech. J., 28(2): 189-199.

Sattler P.J. 1989. Numerical Modelling of Vertical Ground Movements. M.Sc. thesis, University of Saskatchewan, Saskatoon, 425 p.

Schiffman R.L., Chen A.T-F., and Jordan J.C. 1969. An Analysis of Consolidation Theories. J. of the Soil Mech. and Found. Div., ASCE, 95(SM1): 285-312.

Shanker N.B., Ratnam M.V., and Rao A.S. 1987. Multi-dimensional swell behaviour of expansive clays. Proc. 6th Int. Conf. Expansive Soils, New Dehli, India, pp. 143-147.

Shuai F., 1996. Simulation of Swelling Pressure Measurements on Expansive Soils. Ph.D. dissertation, University of Saskatchewan, Saskatoon, 228 p.

Shuai F. and Fredlund D.G. 1997. Measured and Simulated Behaviour of an Expansive Soil. Proc. 3rd Brazilian Symp. Unsaturated Soils, Rio de Janeiro, Brazil, vol. 1, pp. 253-260.

Skempton A.W. 1961. Effective Stress in Soils, Concrete and Rocks. Proc. Conf. Pore Pressure, London, pp. 4-16.

Smith A.W. 1973. Method for Determining the Potential Vertical Rise, PVR. Proc. Workshop Expansive Clays and Shales in Highway Design and Construction, University of Wyoming, Laramie, vol. 1, pp. 189-205.

Snethen D.R. 1980. Characterization of Expansive Soils using Soil Suction Data. Proc. 4th Int. Conf. Expansive Soils, Colorado, pp. 54-75.

Snethen D.R. 1986. Expansive Soils: Where Are We?. Nat. Res. Council Comm. on Ground Failure Hazards, vol. 3, pp. 12-16.

Sorochan E.A. 1991. Construction of building on expansive soils. Balkema A.A, 298 p.

Surkirman Y., and Lewis R.W. 1993. A Finite Element Solution of a Fully Coupled Implicit Formulation for Reservoir Simulation. Inter. J. Numer. Anal. Meth. Geomech., vol.17, pp. 677-698.

Sullivan R.A. and Mc.Clelland B. 1969. Predicting Heave of Buildings on Unsaturated Clay. Proc. 2nd Conf. Expansive and Collapsing Soils, Texas, pp. 404-420.

Surkirman Y., and Lewis R.W. 1993. A Finite Element Solution of a Fully Coupled Implicit Formulation for Reservoir Simulation. Inter. J. Numer. Anal. Meth. Geomech., vol. 17, pp. 677-698.

Thieu N.T.M. 1999. Solution of Saturated/Unsaturated Seepage Problems Using a General Partial Differential Equation Solver. M.Sc. thesis, University of Saskatchewan, Saskatoon, 193 p.

Thieu N.T.M., Fredlund D.G., and Hung V.Q. 2000. General Partial Differential Equation Solvers for Saturated-Unsaturated Seepage. Proc. of the Asian Conf. on Unsaturated Soils, Singapore, pp. 201-206.

Thieu N.T.M., Fredlund M.D., Fredlund D.G., and Hung V.Q. 2001. Seepage Modelling in a Saturated/Unsaturated Soil System. Proc. Int. Conf. on Management of the Land and Water Resources, Hanoi, Vietnam, pp. 49-56.

Terzaghi K. 1925. Erdbaumechanik. FranzDeuticke, Vienna.

Terzaghi K. 1936. The Shearing Resistance of Saturated Soils and the Angle between the Planes of Shear. Proc. 1st Int. Conf. Soil Mech., vol. 1, pp. 54-56.

Terzaghi K. 1943. Theoretical Soil Mechanics. Wiley, New York, 510 p.

Terzaghi K. and Peck R.B. 1967. Soil Mechanics in Engineering Practice. John Wiley & Sons, Inc., New York. 549 p.

Thomas H.R. 1992. On the Development of a Model of Coupled Heat and Moisture Transfer in Unsaturated Soil. Can. Geotech. J., vol. 29, pp. 1107-1112.

Thomas H.R. and Cleall. 1999. Inclusion of Expansive Clay Behaviour in Coupled Thermo Hydraulic Mechanical Models. Engineering Geology, vol. 54, pp. 93-108.

Thomas P.J., Baker J.C., and Zelazny L.W. 2000. An Expansive Soil Index for Predicting Shrink-Swell Potential. Soil Sci. Soc. Am. J., vol. 64, pp. 268-274.

Toll D.G. 1990. A Framework for Unsaturated Soil Behaviour. Geotechnique, 40(1): 34-44.

Tratch D.J., Fredlund D.G., and Wilson G.W. 1995. An Introduction to Analytical Modeling of Plant Transpiration for Geotechnical Engineers. Proc. 48th Canadian Geotech. Conf., pp. 771-780.

van Genuchten M.T. 1980. A Close Form Equation for Predicting the Hydraulic Conductivity of Unsaturated Soils. Soil Sci. Soc. Amer. J., vol. 44, pp. 892-898.

Vulliet L. and Laloui L. 2001. Unsaturated Soil Mechanics: Constitutive Modelling and Coupling Effects. Proc. 10th Int. Conf. Comp. Meth. Adv. Geomech., Tucson, pp. 765-774.

Wallace K.B. and Sapkota B.K. 1994. Modelling the Response of Pavements to Subgrade Volume Change. Proc. of the 17th ARRB Conf., part 2, Australian Road Research, pp. 199-210.

Ward W.H. 1953. Soil Movement and Weather. Proc. 3rd Int. Conf. Soil Mech., vol. 1, pp. 277-288.

Wheeler S.J. and Karube D. 1995. Constitutive Modelling. Proc. 1st Int. Conf. Unsaturated Soils, Paris, France, pp. 1323-1356.

Williams A.A.B. 1965. The Deformation of Roads Resulting From Moisture Change in Expansive Soils in South Africa. Symposium on Moisture Equilibria and Moisture Change in Soil Beneath Covered Area, Australia, pp. 143-155.

Williams A.A.B. and Pidgeon J.T. 1983. Evapo-transpiration and Heaving Clays in South Africa. Geotechnique, 18(2):141-150.

Wong H.Y. and Yong R.M. 1973. A Study of Swelling and Swelling Force during Unsaturated Flow in Expansive Soils. Proc. 3rd Int. Conf. Expansive Soils, Haifa, Israel, vol. 1, pp. 143-151.

Wong T.T., Fredlund D.G., and Krahn J. 1998. A Numerical Study of Coupled Consolidation in Unsaturated Soils. Can. Geotech. J., vol. 35, pp. 926-937.

Yoshida R.T., Fredlund D.G., and Hamilton J.J. 1983. The Prediction of Total Heave of a Slab-on-grade Floor on Regina Clay. Can. Geotech. J., 20(1): 69-81.

Zienkiewicz O.C. and Taylor R.L. 1989. The Finite Element Method, Volume 1, fourth edition. McGRAW-HILL Inc., 648 p.

Zienkiewicz O.C. and Taylor R.L. 1991. The Finite Element Method, Volume 2, fourth edition. McGRAW-HILL Inc., 807 p.

Zienkiewicz O.C., and Zhu J.Z. 1987. A Simple Error Estimator and Adaptive Procedure for Practical Engineering Analysis. International Journal for Numerical Methods in Engineering, Vol. 24, pp. 337-357.

APPENDIX A

Comparison of the Coupled Solutions Obtained by Various Finite Element Meshes for Examples 3 and 4

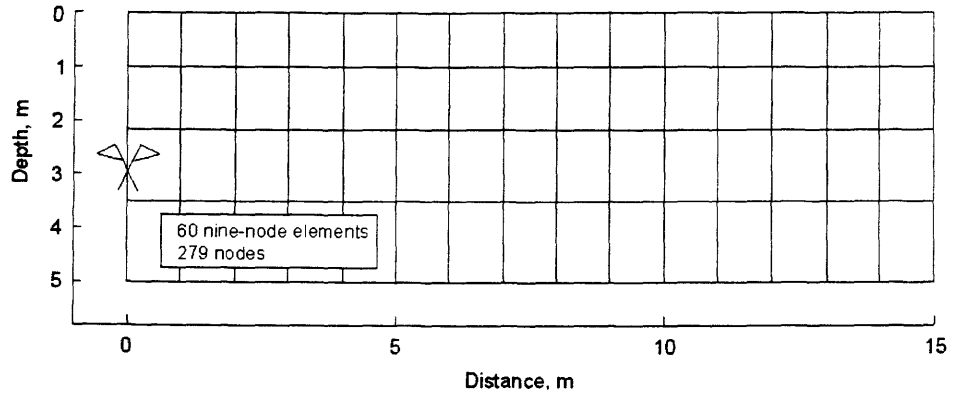

Figure A.1 60-element finite element mesh (i.e., mesh 1) for coupled analysis, Examples 3 and 4

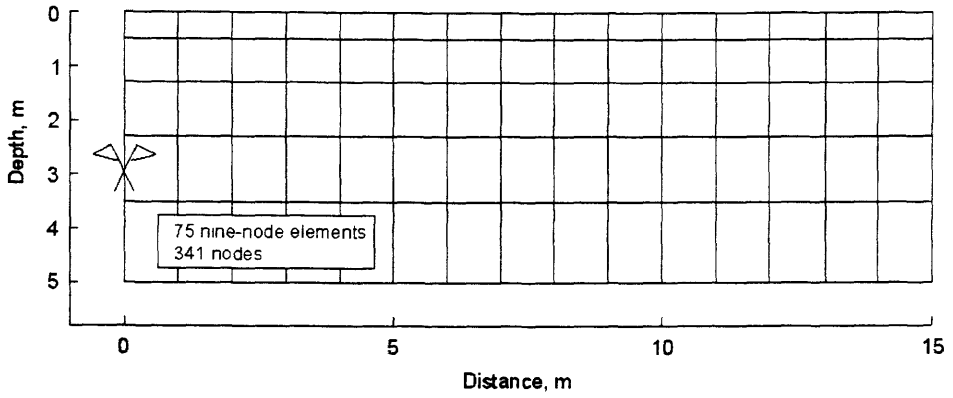

Figure A.2 75-element finite element mesh (i.e., mesh 2)for coupled analysis, Examples 3 and 4

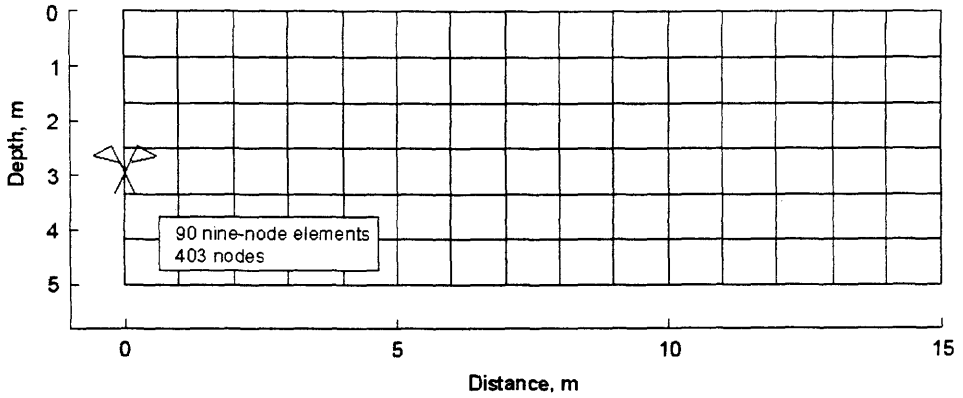

Figure A.3 90-element finite element mesh (i.e., mesh 3) for coupled analysis, Examples 3 and 4

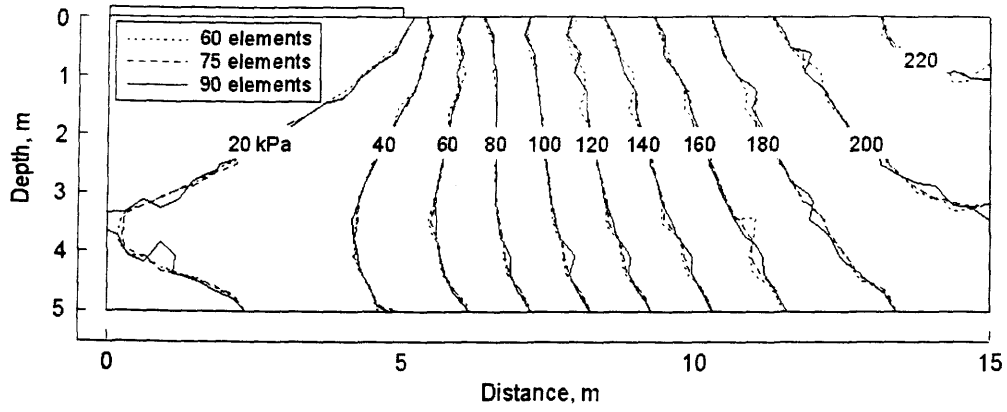

Figure A.4 Comparison of matric suction distribution at day 200 for various finite element meshes, Example 3, leakage problem

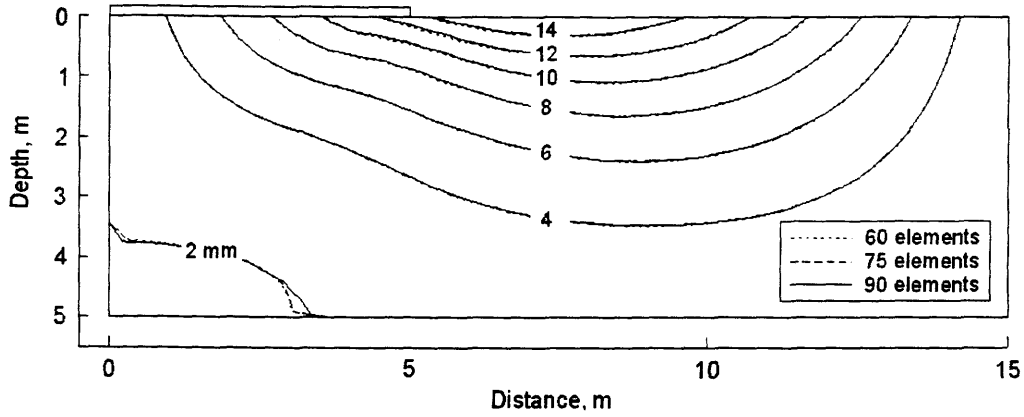

Figure A.5 Comparison of horizontal displacement distribution at day 200 for various finite element meshes, Example 3, leakage problem

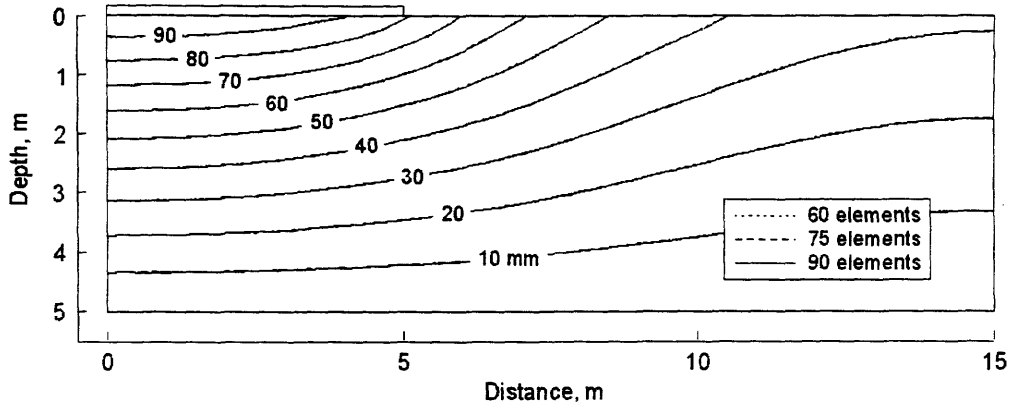

Figure A.6 Comparison of vertical displacement distribution at day 200 for various finite element meshes, Example 3, leakage problem

Table A.1 Comparison of predicted results at ground surface at day 100 for different finite element meshes, Example 3, coupled solution

Distance (m)	Matric suction (kPa)			Horizontal displacements (mm)			Vertical displacements (mm)		
	Mesh 1	Mesh 2	Mesh 3	Mesh 1	Mesh 2	Mesh 3	Mesh 1	Mesh 2	Mesh 3
0.0	0	0	0	0	0	0	86.36	86.16	86.19
2.5	0	0	0	9.07	9.01	9.01	83.49	83.37	83.40
5.0	0	0	0	18.78	18.69	18.70	67.53	67.81	67.78
7.5	174.79	172.37	172.43	20.79	20.77	20.77	40.29	40.45	40.43
10.0	250.14	253.17	253.49	15.65	15.66	15.65	25.46	25.59	25.58
12.5	325.03	322.45	322.32	8.19	8.20	8.20	17.73	17.82	17.81
15.0	326.87	330.31	330.78	0	0	0	15.34	15.42	15.41

Table A.2 Comparison of predicted results at ground surface at day 200 for different finite element meshes, Example 3, coupled solution

Distance (m)	Matric suction (kPa)			Horizontal displacements (mm)			Vertical displacements (mm)		
	Mesh 1	Mesh 2	Mesh 3	Mesh 1	Mesh 2	Mesh 3	Mesh 1	Mesh 2	Mesh 3
0.0	0	0	0	0	0	0	99.05	98.83	98.86
2.5	0	0	0	5.57	5.52	5.52	96.47	96.33	96.36
5.0	0	0	0	11.16	11.08	11.09	81.86	82.08	82.06
7.5	117.82	116.31	116.31	14.12	14.08	14.09	56.70	56.84	56.82
10.0	167.48	169.45	169.70	11.40	11.38	11.38	42.17	42.29	42.28
12.5	220.52	218.73	218.63	6.19	6.18	6.18	34.23	34.33	34.31
15.0	222.22	224.35	224.71	0	0	0	31.70	31.80	31.79

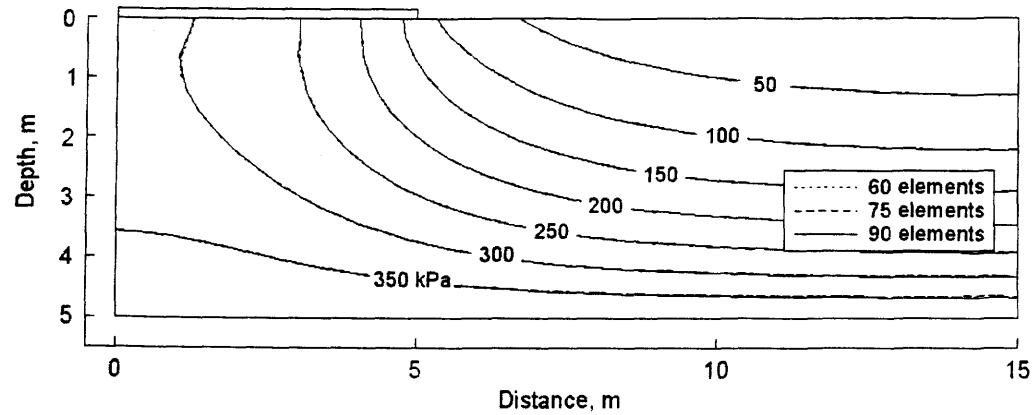

Figure A.7 Comparison of matric suction distribution at day 355 for various finite element meshes, Example 4, infiltration problem

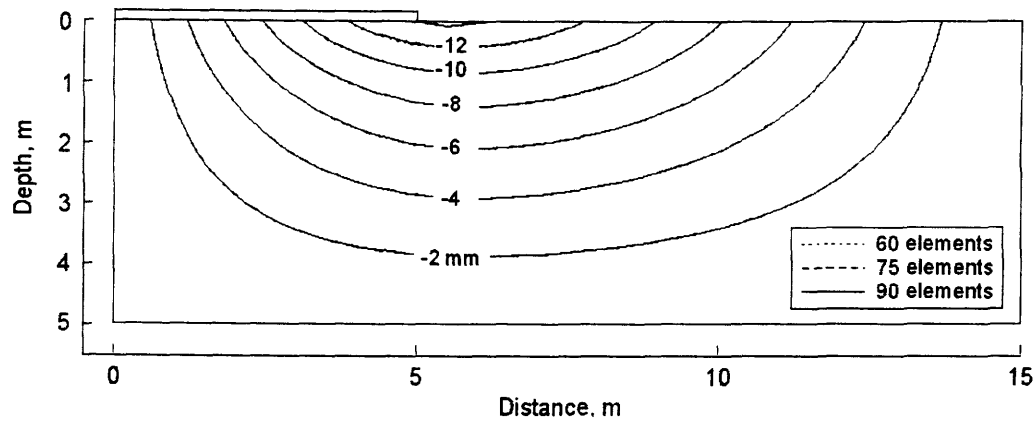

Figure A.8 Comparison of horizontal displacement distribution at day 355 for various finite element meshes, Example 4, infiltration problem

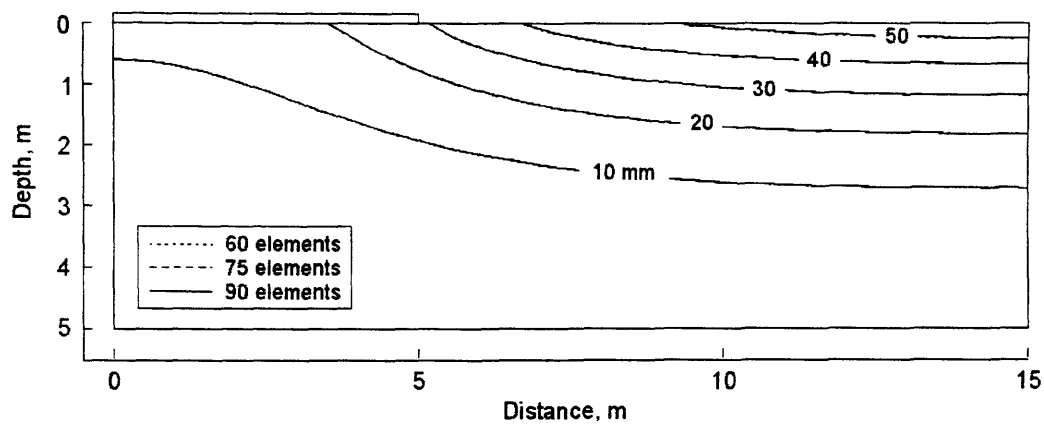

Figure A.9 Comparison of vertical displacement distribution at day 355 for various finite element meshes, Example 4, infiltration problem

Table A.3 Comparison of predicted results at ground surface at day 53 for different finite element meshes, Example 4, coupled solution

Distance (m)	Matric suction (kPa)			Horizontal displacements (mm)			Vertical displacements (mm)		
	Mesh 1	Mesh 2	Mesh 3	Mesh 1	Mesh 2	Mesh 3	Mesh 1	Mesh 2	Mesh 3
0	377.96	377.60	377.49	0	0	0	6.02	6.02	6.02
2.5	342.51	342.63	342.68	-6.96	-6.96	-6.96	8.55	8.55	8.55
5.0	186.57	186.32	186.32	-12.02	-12.02	-12.02	18.01	18.02	18.02
7.5	88.32	88.47	88.45	-9.58	-9.58	-9.58	28.49	28.51	28.51
10.0	71.37	71.49	71.55	-5.64	-5.64	-5.64	32.62	32.64	32.64
12.5	66.26	66.29	66.26	-2.50	-2.50	-2.50	33.98	34.00	34.00
15.0	65.48	65.68	65.75	0	0	0	34.29	34.31	34.31

Table A.4 Comparison of predicted results at ground surface at day 355 for different finite element meshes, Example 4, coupled solution

Distance (m)	Matric suction (kPa)			Horizontal displacements (mm)			Vertical displacements (mm)		
	Mesh 1	Mesh 2	Mesh 3	Mesh 1	Mesh 2	Mesh 3	Mesh 1	Mesh 2	Mesh 3
0.0	310.08	309.80	309.71	0	0	0	12.71	12.71	12.71
2.5	271.79	271.88	271.92	-8.24	-8.24	-8.24	16.24	16.25	16.25
5.0	125.48	125.29	125.29	-14.25	-14.25	-14.25	28.99	29.00	29.00
7.5	35.00	35.17	35.15	-12.51	-12.51	-12.51	44.23	44.26	44.26
10.0	13.97	14.08	14.12	-8.14	-8.14	-8.14	51.78	51.81	51.81
12.5	5.72	5.82	5.78	-3.87	-3.86	-3.86	54.95	54.98	54.98
15.0	3.86	4.08	4.13	0	0	0	55.80	55.83	55.83

APPENDIX B

More Results on Uncoupled Analyses of Example 3, Leakage Problem

B.1 Uncoupled solution, UCS2 for Example 3, leakage problem

B.2 Uncoupled solution, UCS3 for Example 3, leakage problem

B.1 Uncoupled analysis, UCS2 for Example 3, leakage problem

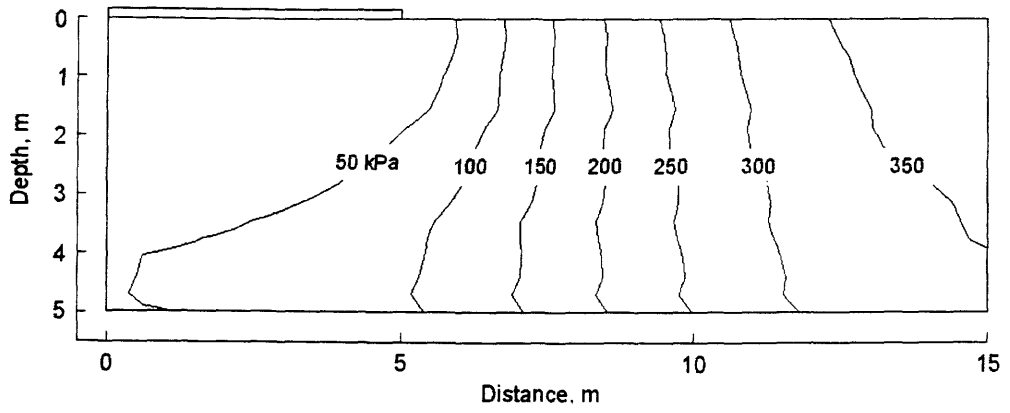

Figure B.1 Distribution of matric suction at day 56,
Example 3, uncoupled analysis UCS2

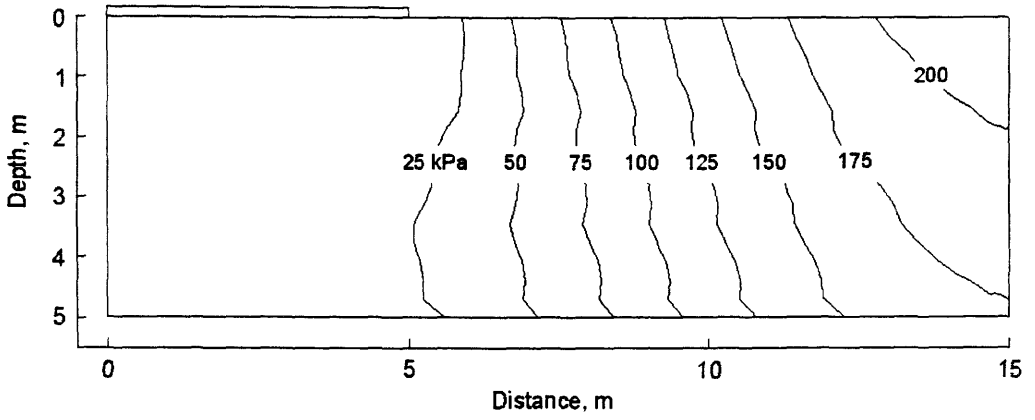

Figure B.2 Distribution of matric suction at day 150,
Example 3, uncoupled analysis UCS2

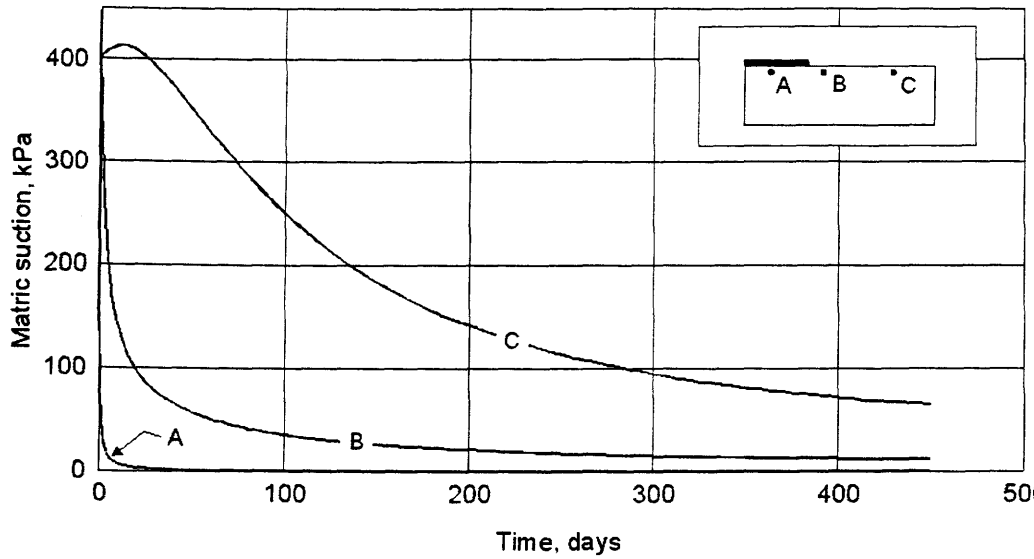

Figure B.3 Development of matric suction with time for points A, B, and C, Example 3, uncoupled analysis UCS2

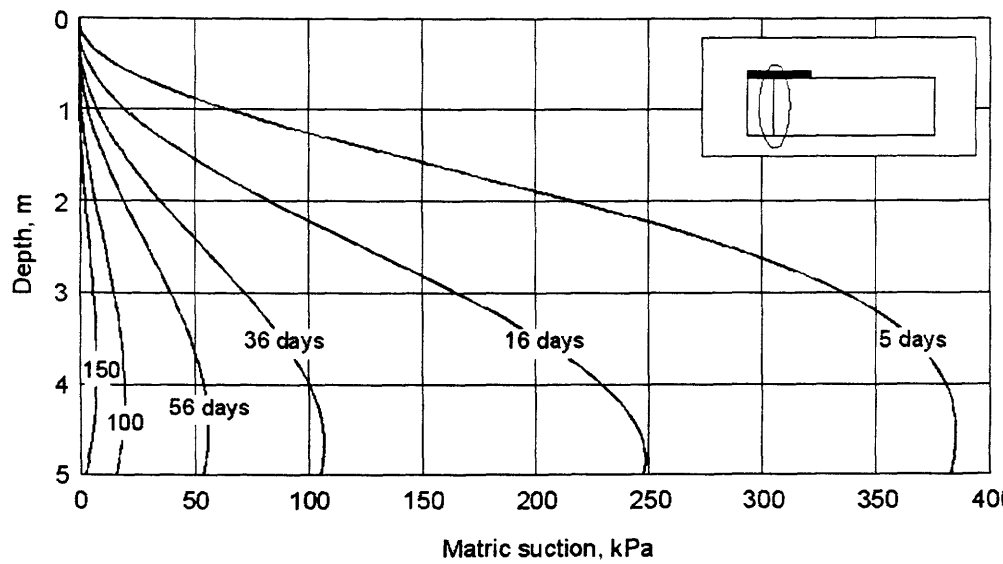

Figure B.4 Development of matric suction versus depth with time, Example 3, uncoupled analysis UCS2

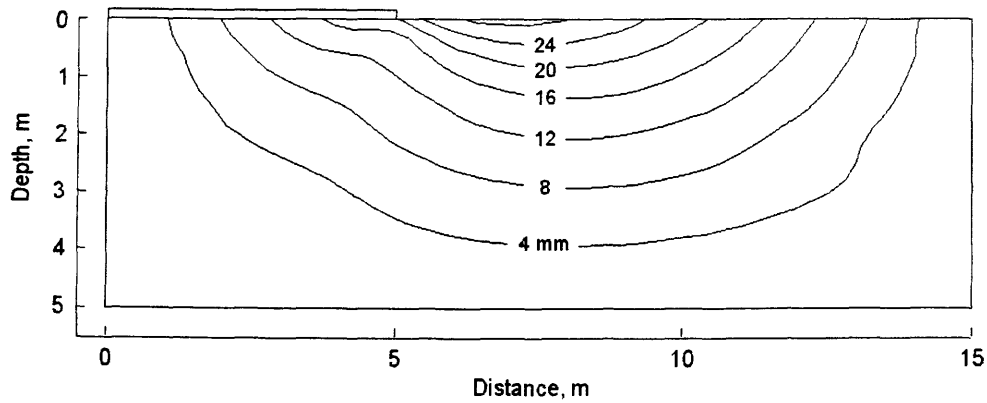

Figure B.5 Distribution of horizontal displacement at day 56,
Example 3, uncoupled analysis UCS2

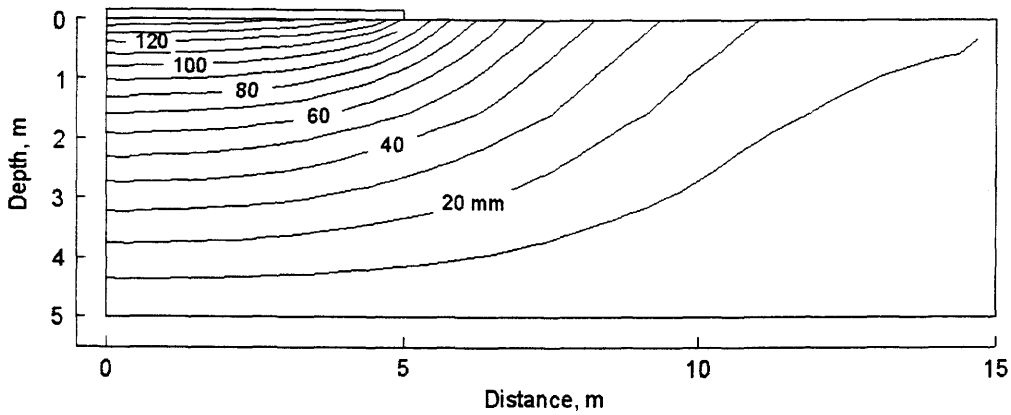

Figure B.6 Distribution of vertical displacement at day 56,
Example 3, uncoupled analysis UCS2

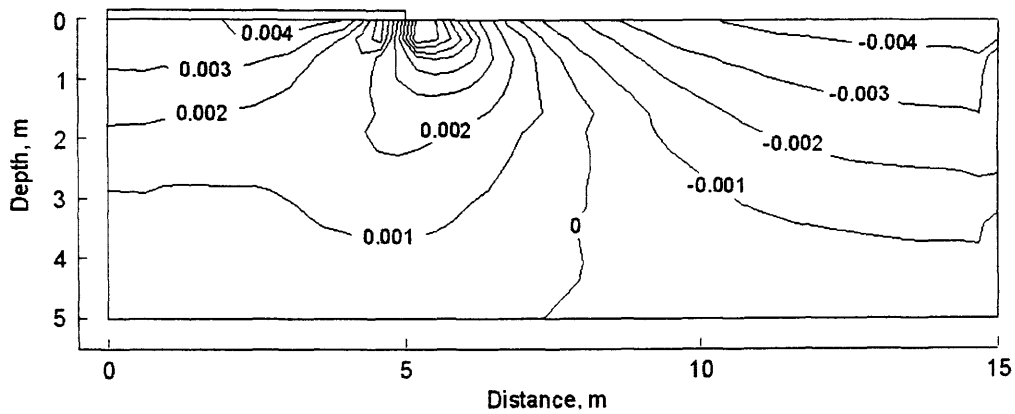

Figure B.7 Distribution of horizontal strain at day 56,
Example 3, uncoupled analysis UCS2

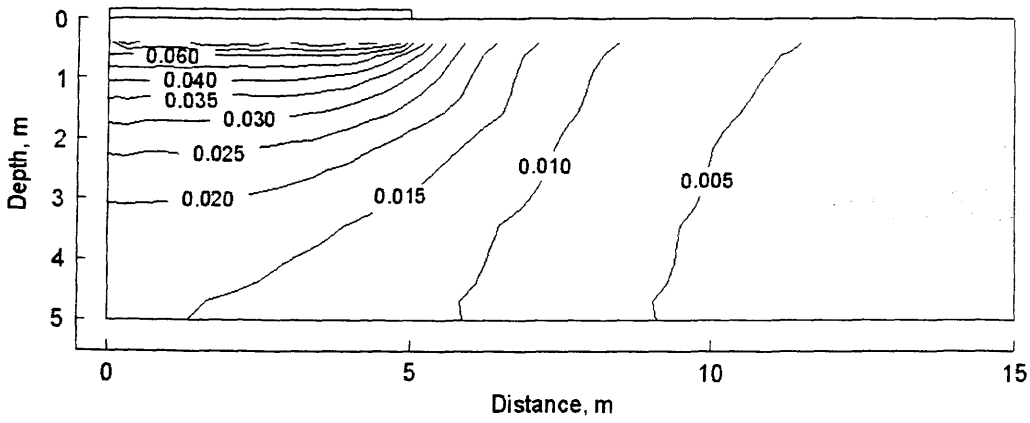

Figure B.8 Distribution of vertical strain at day 56,
Example 3, uncoupled analysis UCS2

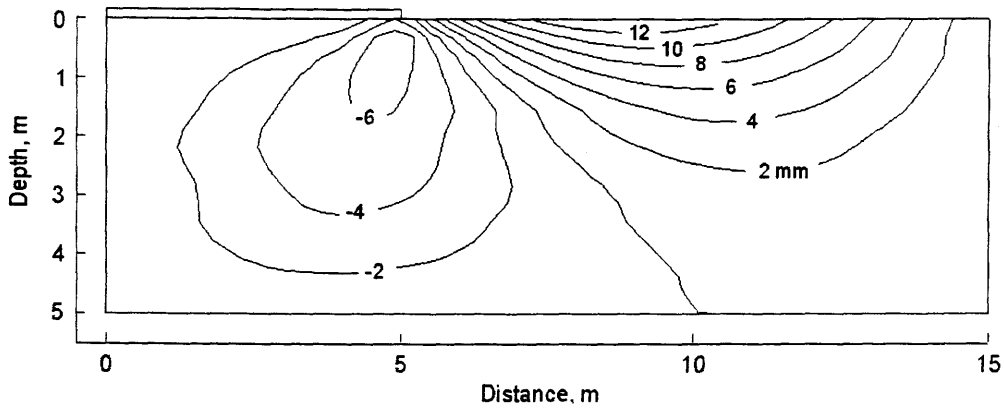

Figure B.9 Distribution of horizontal displacement at day 150,
Example 3, uncoupled analysis UCS2

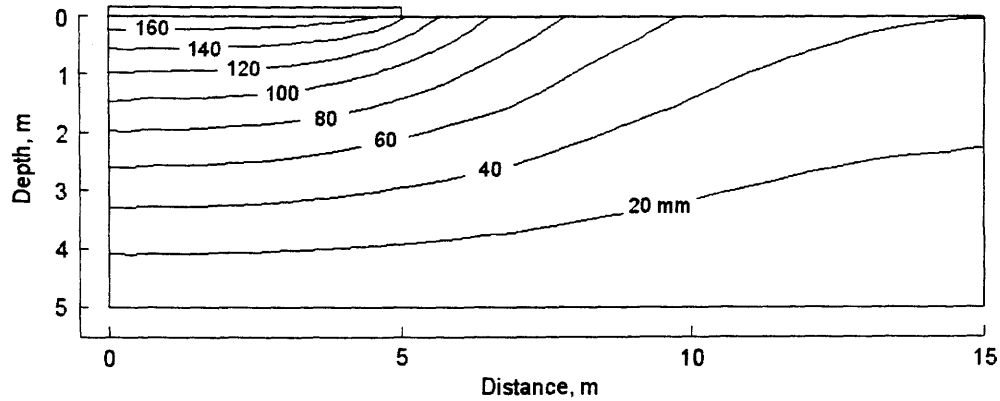

Figure B.10 Distribution of vertical displacement at day 150,
Example 3, uncoupled analysis UCS2

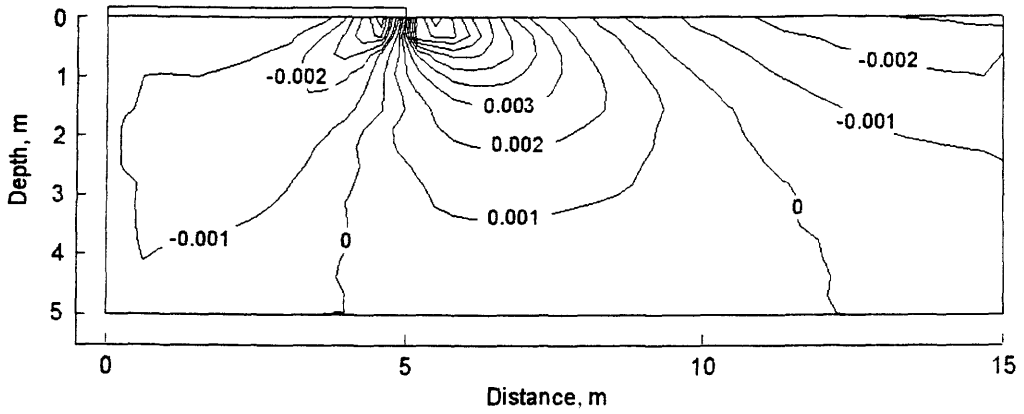

Figure B.11 Distribution of horizontal strain at day 150,
Example 3, uncoupled analysis UCS2

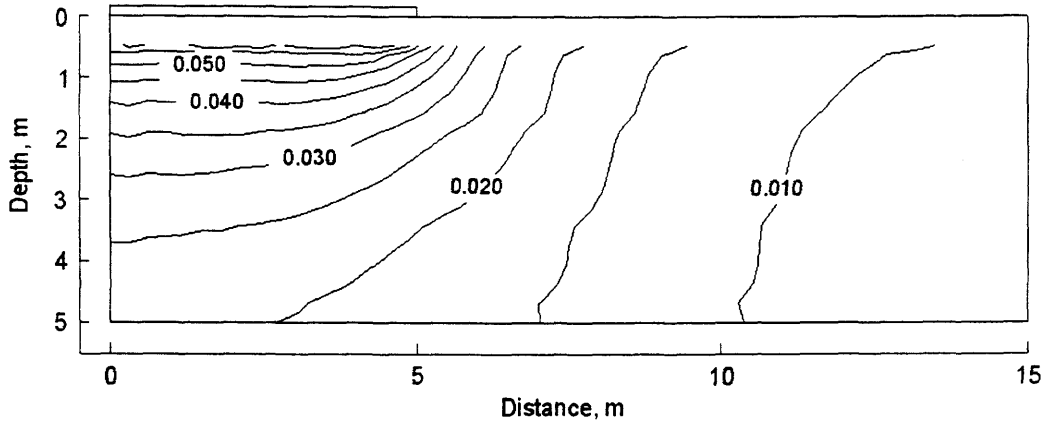

Figure B.12 Distribution of vertical strain at day 150,
Example 3, uncoupled analysis UCS2

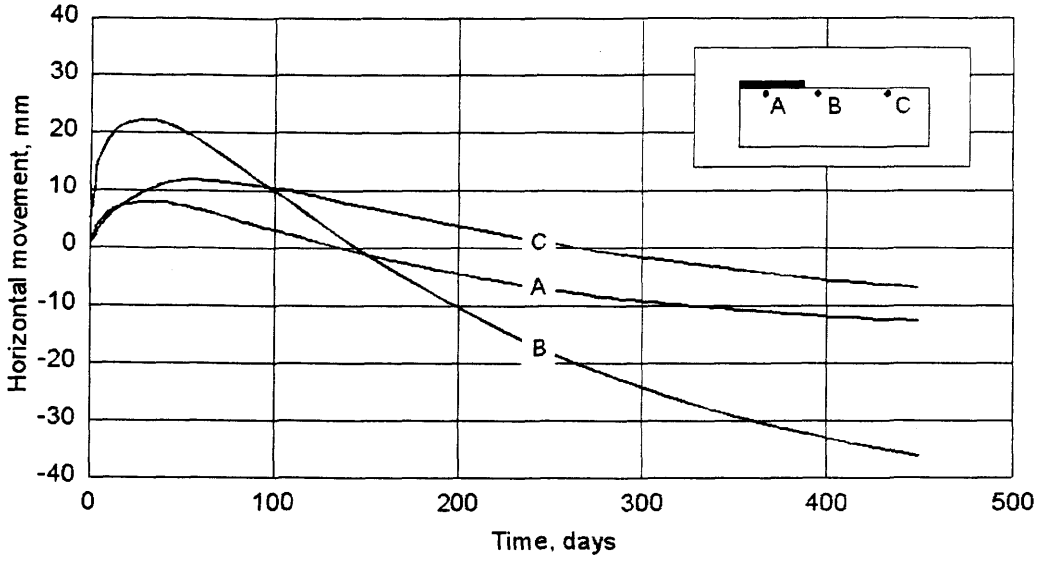

Figure B.13 Development of horizontal displacement with time for points A, B, and C, Example 3, uncoupled analysis UCS2

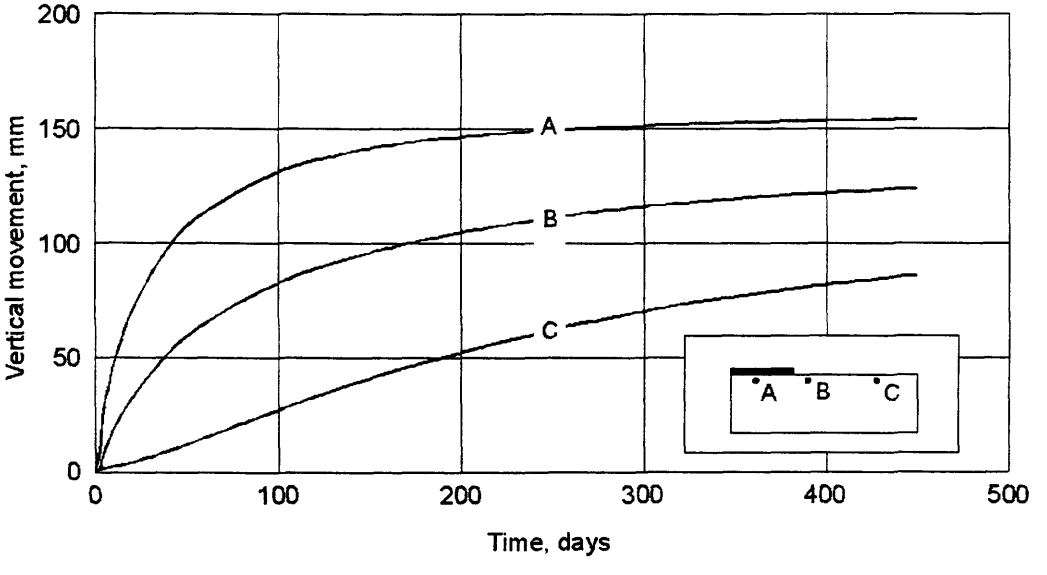

Figure B.14 Development of vertical displacement with time for points A, B, and C, Example 3, uncoupled analysis UCS2

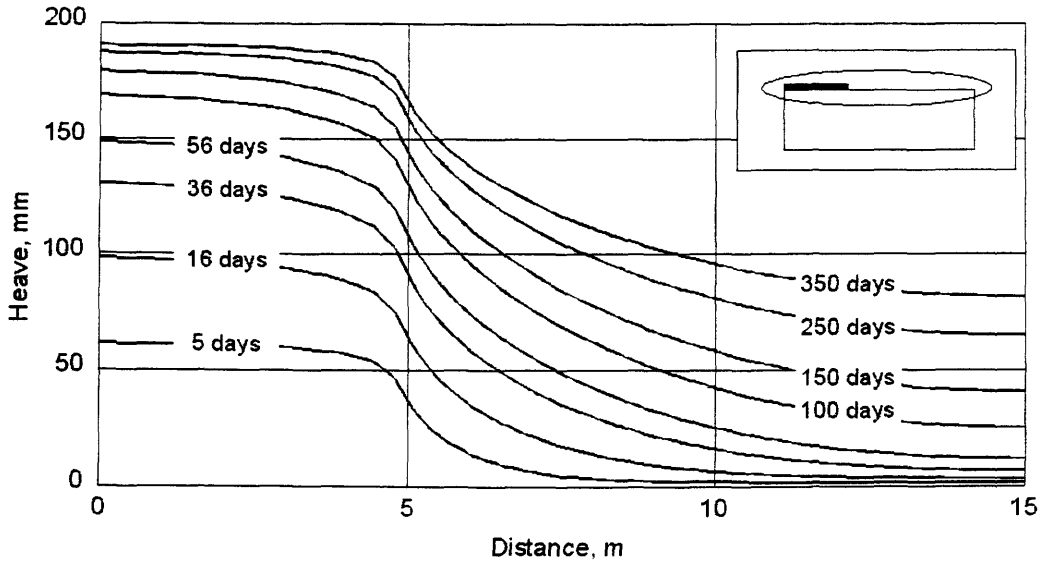

Figure B.15 Development of heave at ground surface with time, Example 3, uncoupled analysis UCS2

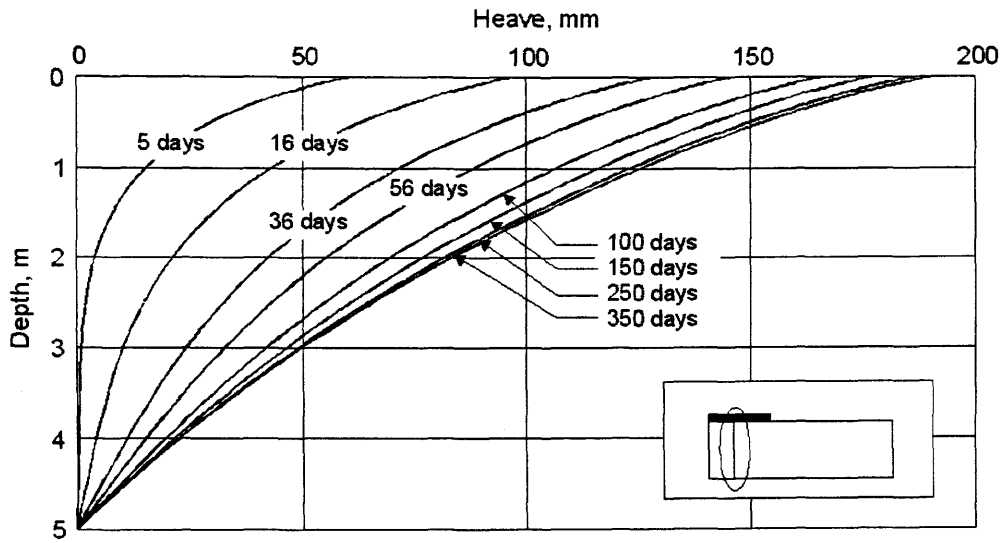

Figure B.16 Development of heave below the cover versus depth with time, Example 3, uncoupled analysis UCS2

B.2 Uncoupled analysis, UCS3 for Example 3, leakage problem

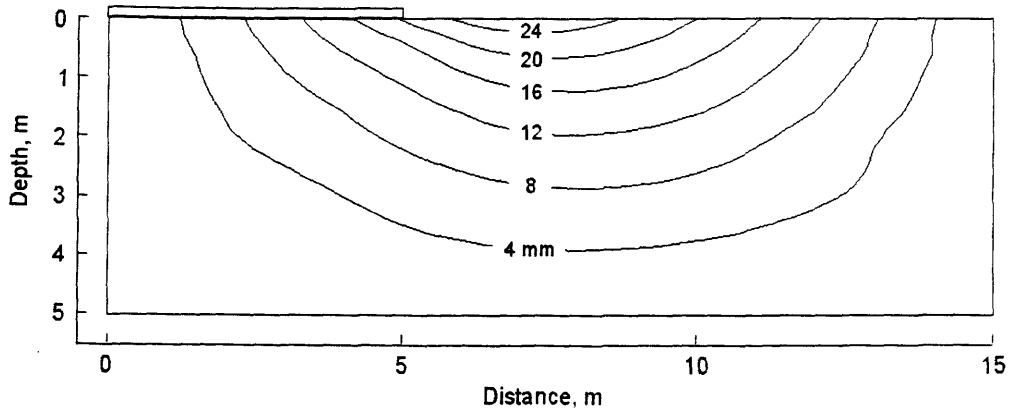

Figure B.17 Distribution of horizontal displacement at day 56,
Example 3, uncoupled analysis UCS3

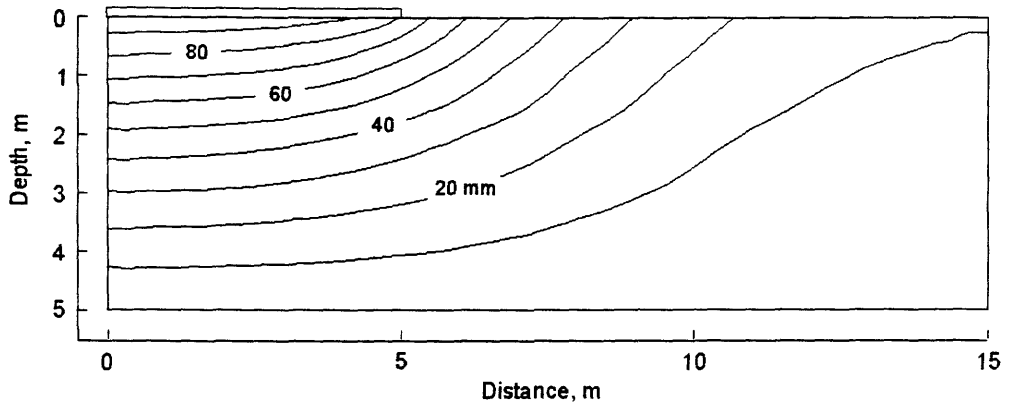

Figure B.18 Distribution of vertical displacement at day 56,
Example 3, uncoupled analysis UCS3

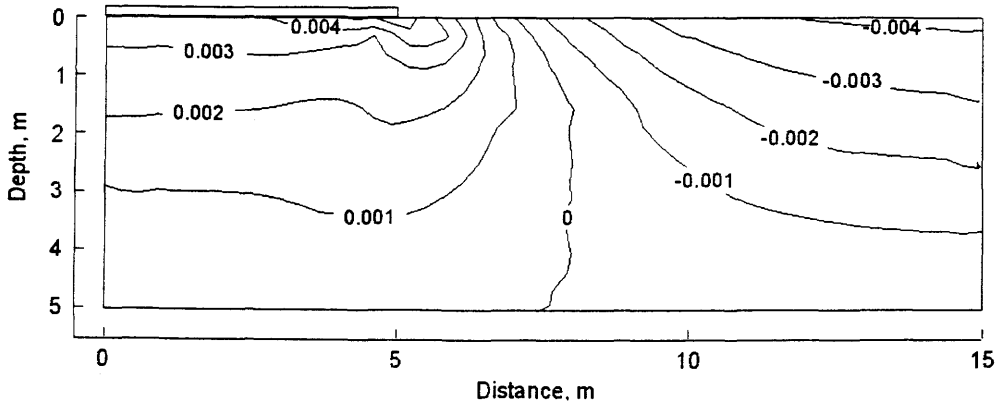

Figure B.19 Distribution of horizontal strain at day 56,
Example 3, uncoupled analysis UCS3

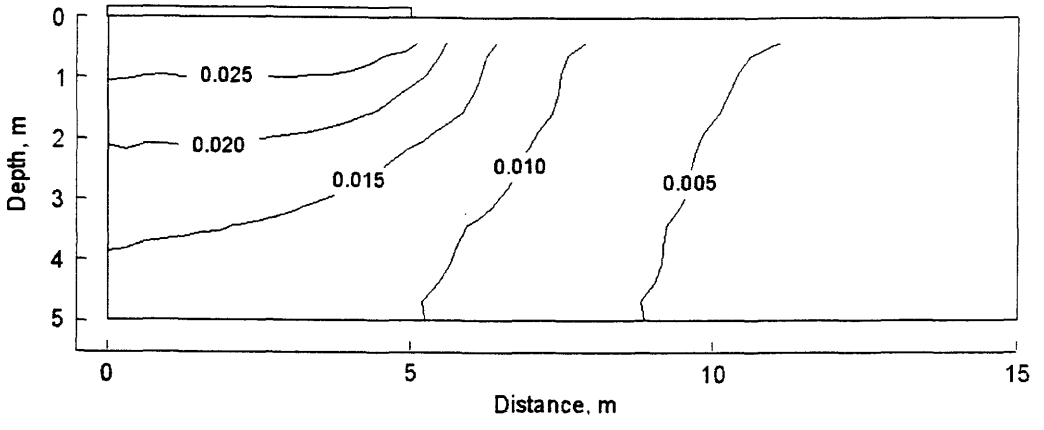

Figure B.20 Distribution of vertical strain at day 56,
Example 3, uncoupled analysis UCS3

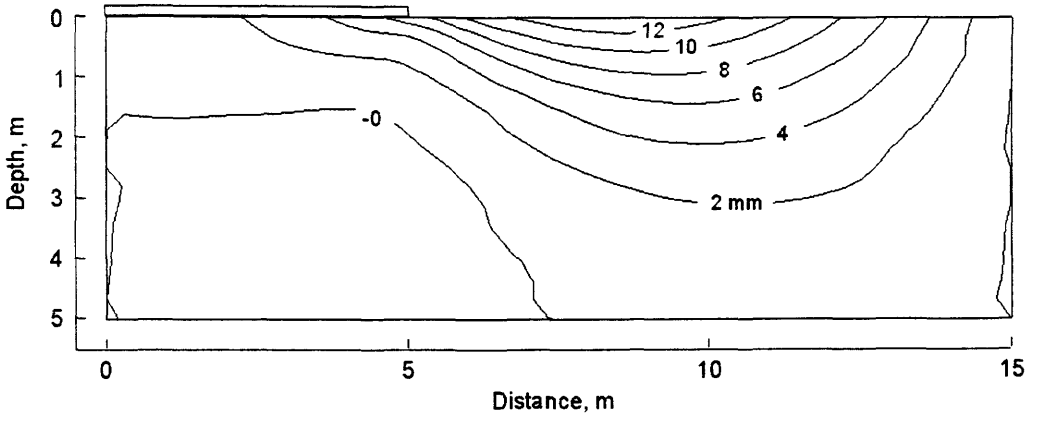

Figure B.21 Distribution of horizontal displacement at day 150,
Example 3, uncoupled analysis UCS3

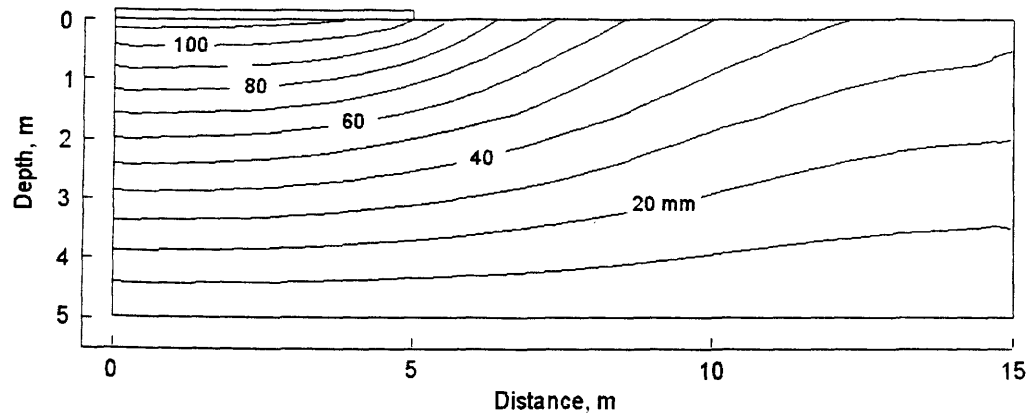

Figure B.22 Distribution of vertical displacement at day 150,
Example 3, uncoupled analysis UCS3

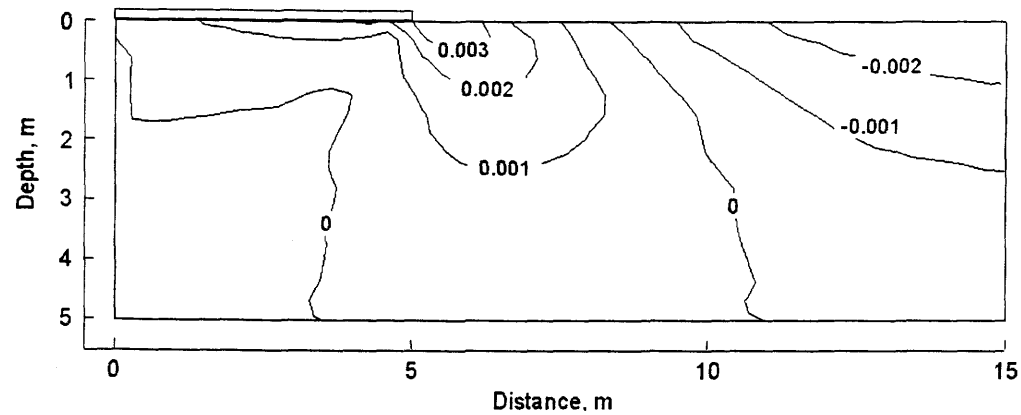

Figure B.23 Distribution of horizontal strain at day 150,
Example 3, uncoupled analysis UCS3

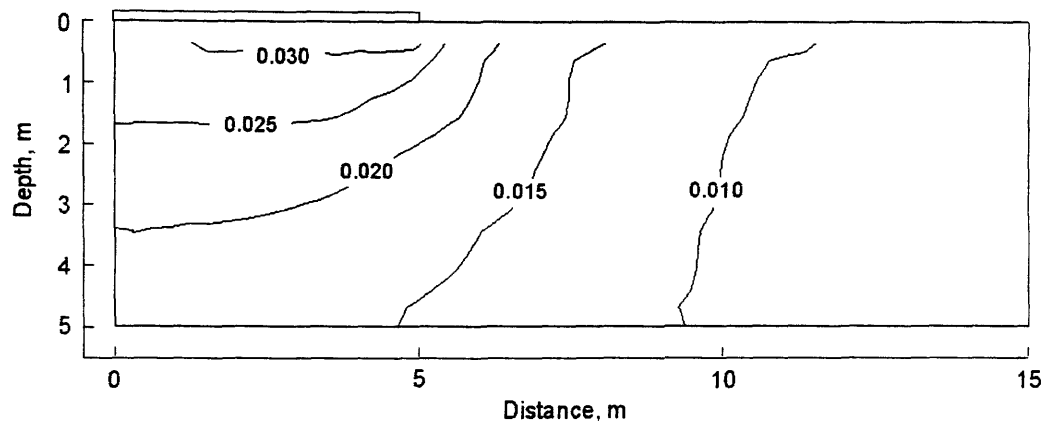

Figure B.24 Distribution of vertical strain at day 150,
Example 3, uncoupled analysis UCS3

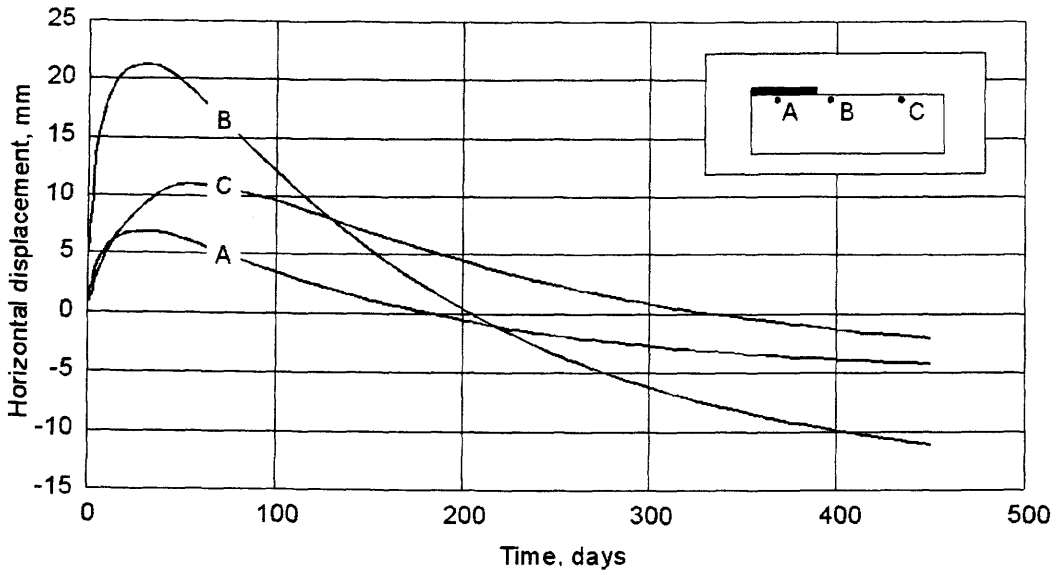

Figure B.25 Development of horizontal displacement with time for points A, B, and C, Example 3, uncoupled analysis UCS3

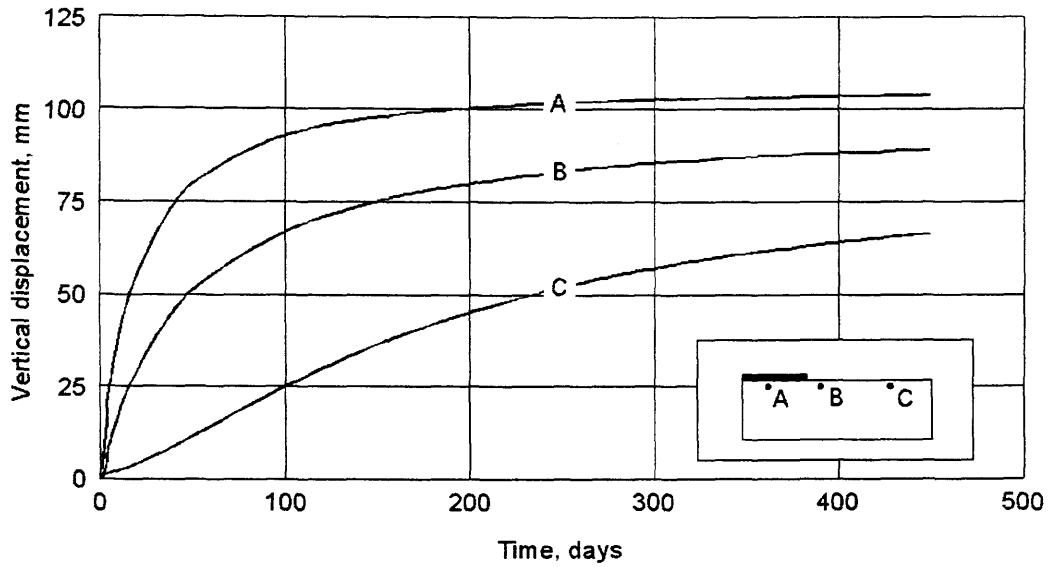

Figure B.26 Development of vertical displacement with time for points A, B, and C, Example 3, uncoupled analysis UCS3

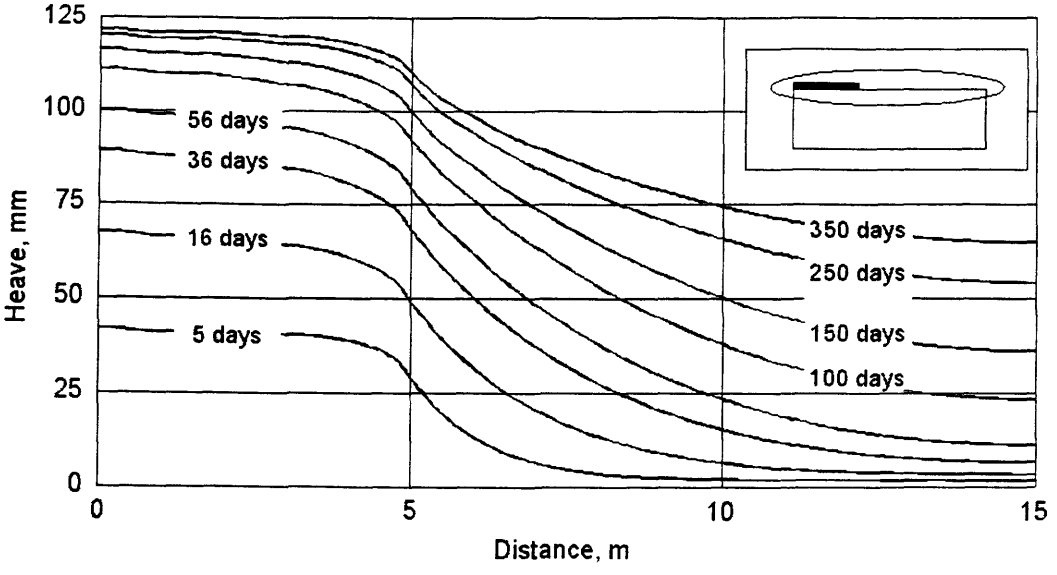

Figure B.27 Development of heave at ground surface with time, Example 3, uncoupled analysis UCS3

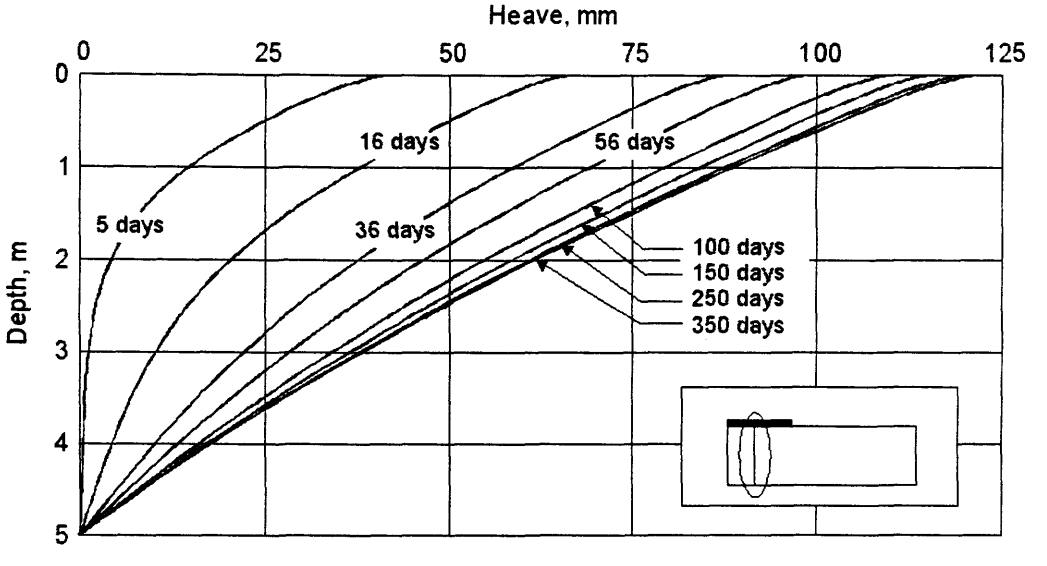

Figure B.28 Development of heave below the cover versus depth with time, Example 3, uncoupled analysis UCS3

APPENDIX C

More Results on Uncoupled Analyses of Example 4, Infiltration Problem

C.1 Uncoupled solution, UCS1 for Example 4, infiltration problem

C.1 Uncoupled solution, UCS2 for Example 4, infiltration problem

C.1 Uncoupled analysis, UCS1 for Example 4, infiltration problem

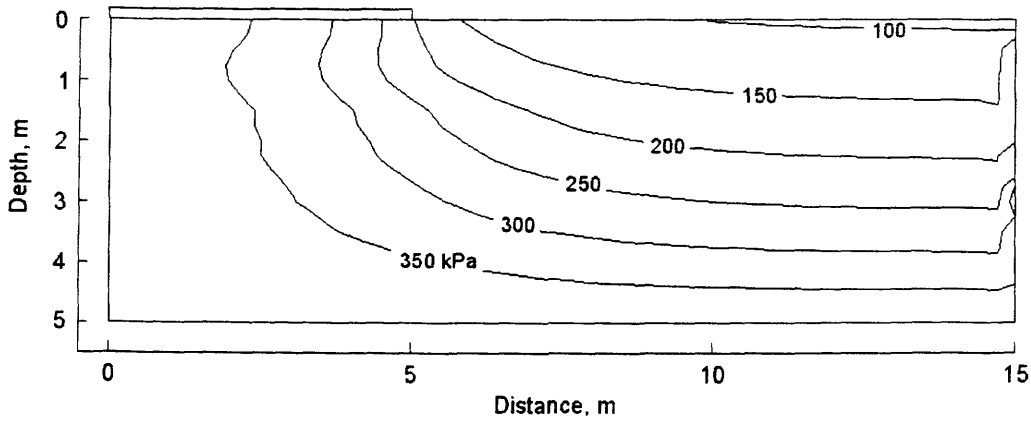

Figure C.1 Distribution of matric suction at day 53,
Example 4, uncoupled solution UCS1

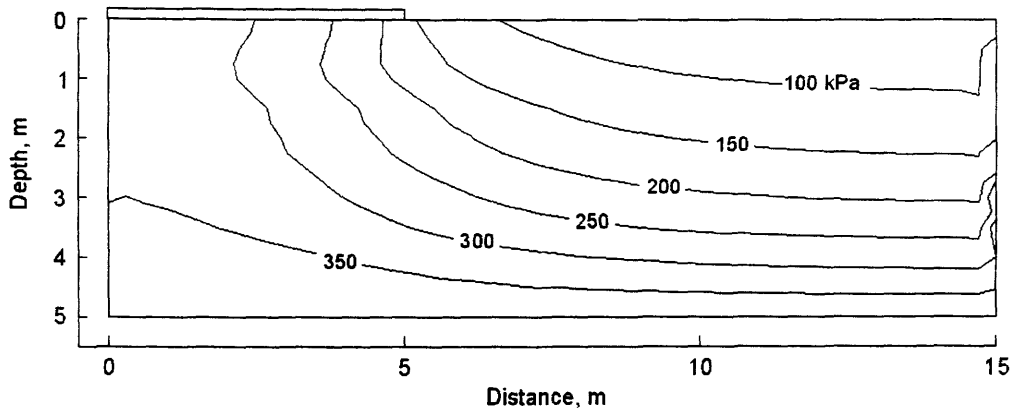

Figure C.2 Distribution of matric suction at day 175,
Example 4, uncoupled solution UCS1

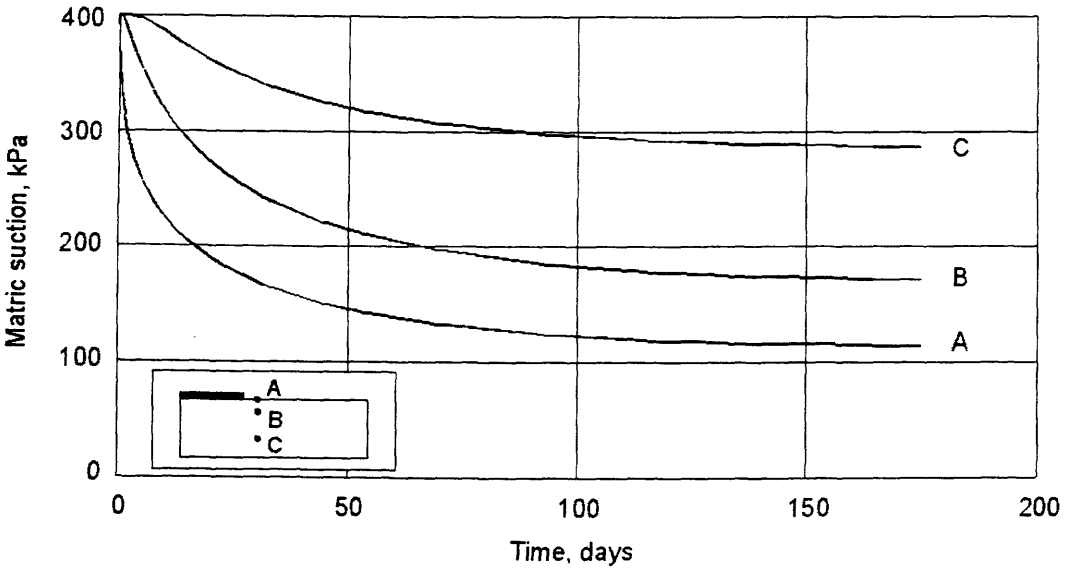

Figure C.3 Development of matric suction with time for points A, B, and C, Example 4, uncoupled solution UCS1

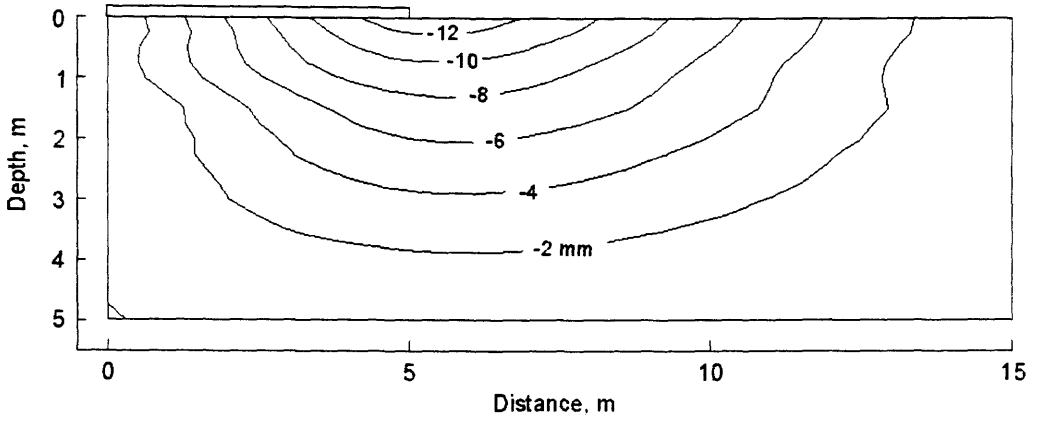

Figure C.4 Distribution of horizontal displacement at day 53, Example 4, uncoupled solution UCS1

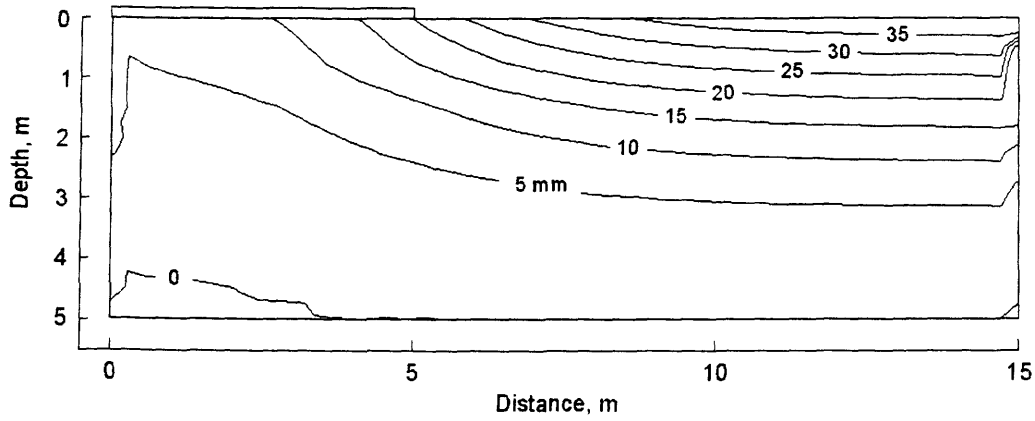

Figure C.5 Distribution of vertical displacement at day 53,
Example 4, uncoupled solution UCS1

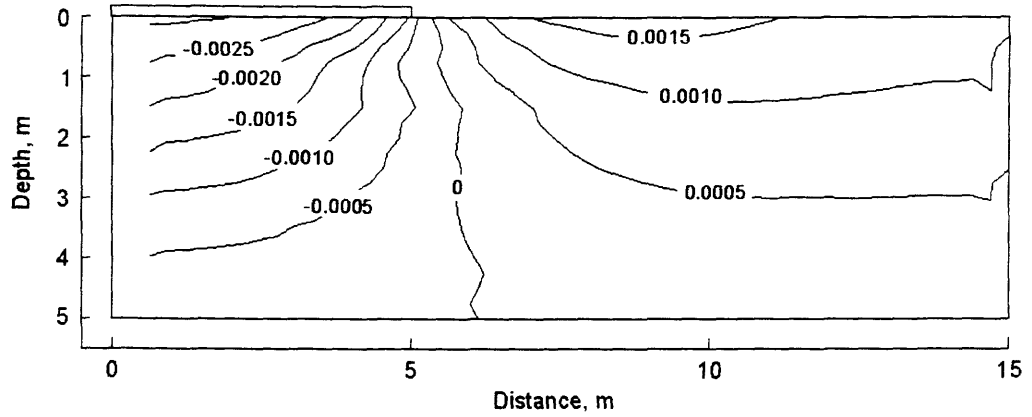

Figure C.6 Distribution of horizontal strain at day 53,
Example 4, uncoupled solution UCS1

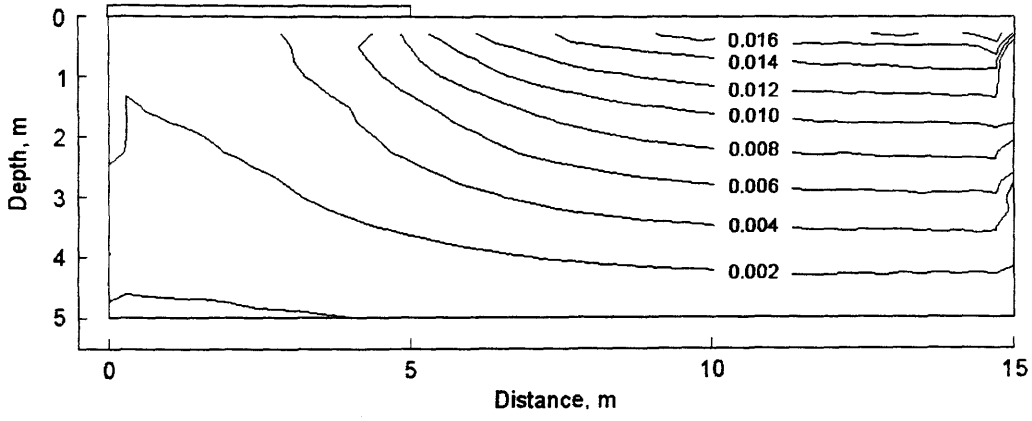

Figure C.7 Distribution of vertical strain at day 53,
Example 4, uncoupled solution UCS1

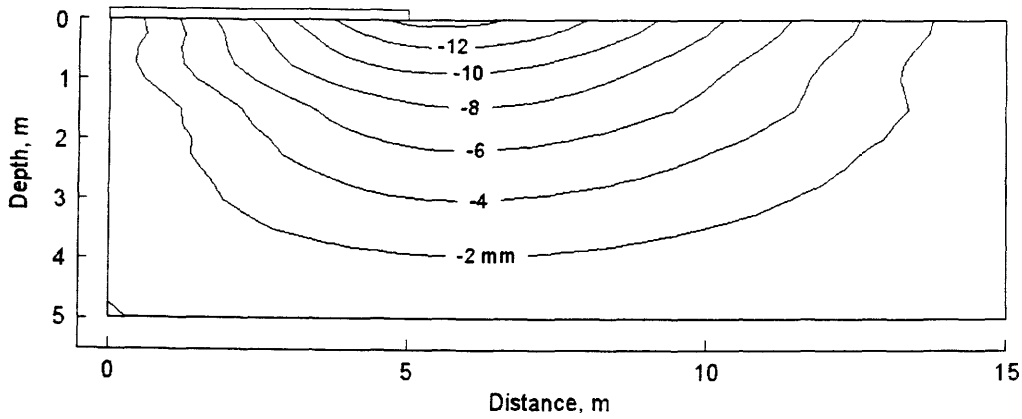

Figure C.8 Distribution of horizontal displacement at day 175,
Example 4, uncoupled solution UCS1

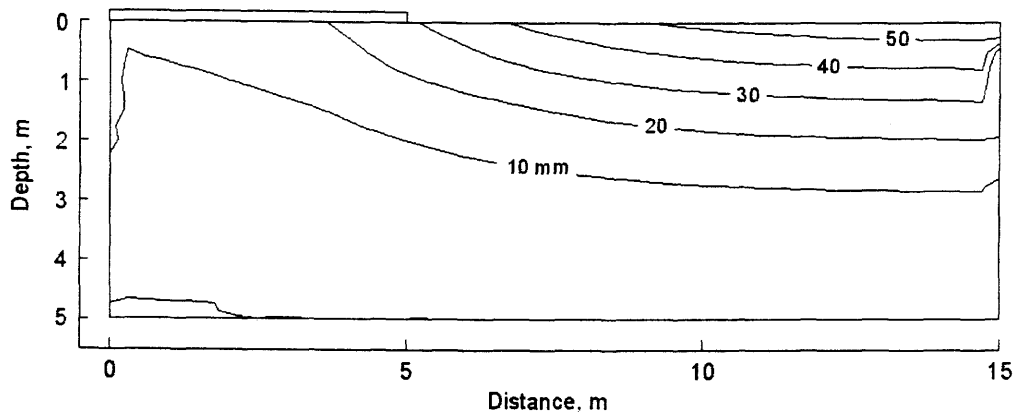

Figure C.9 Distribution of vertical displacement at day 175,
Example 4, uncoupled solution UCS1

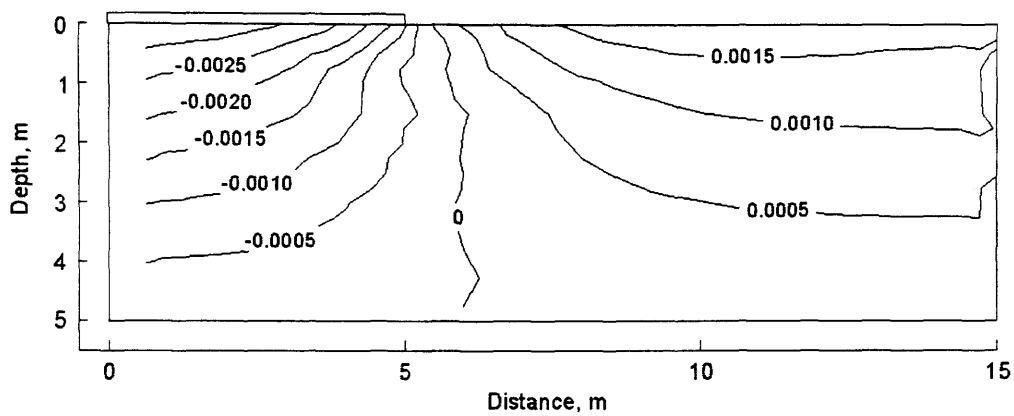

Figure C.10 Distribution of horizontal strain at day 175,
Example 4, uncoupled solution UCS1

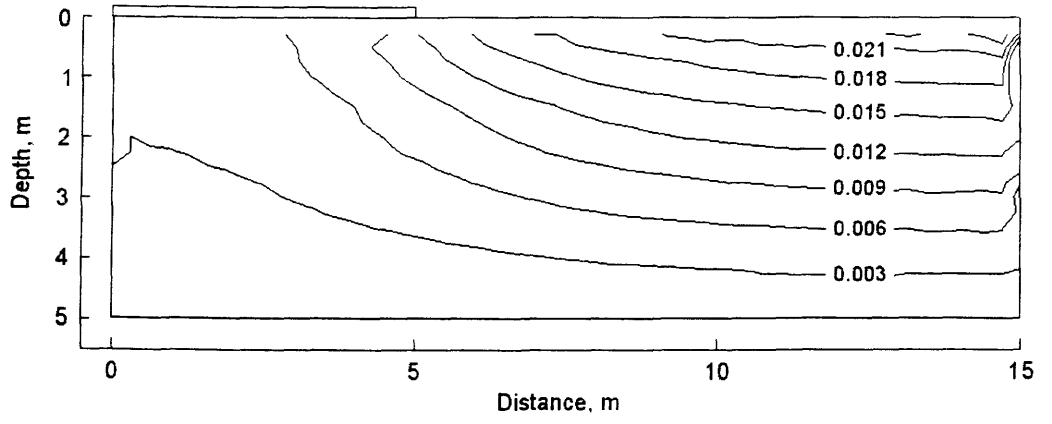

Figure C.11 Distribution of vertical strain at day 175,
Example 4, uncoupled solution UCS1

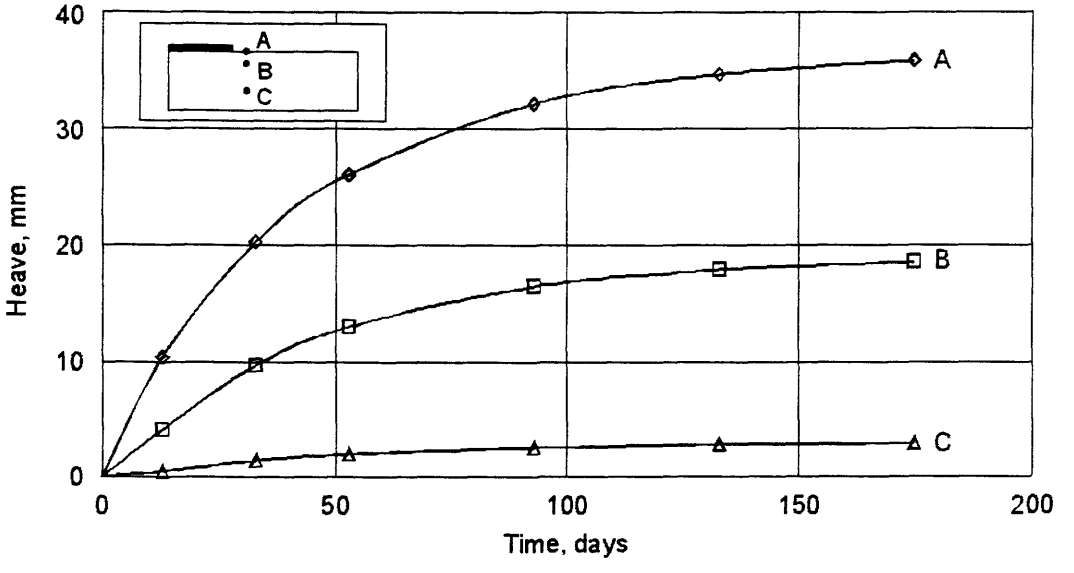

Figure C.12 Development of vertical displacement with time for points A, B, and C,
Example 4, uncoupled solution UCS1

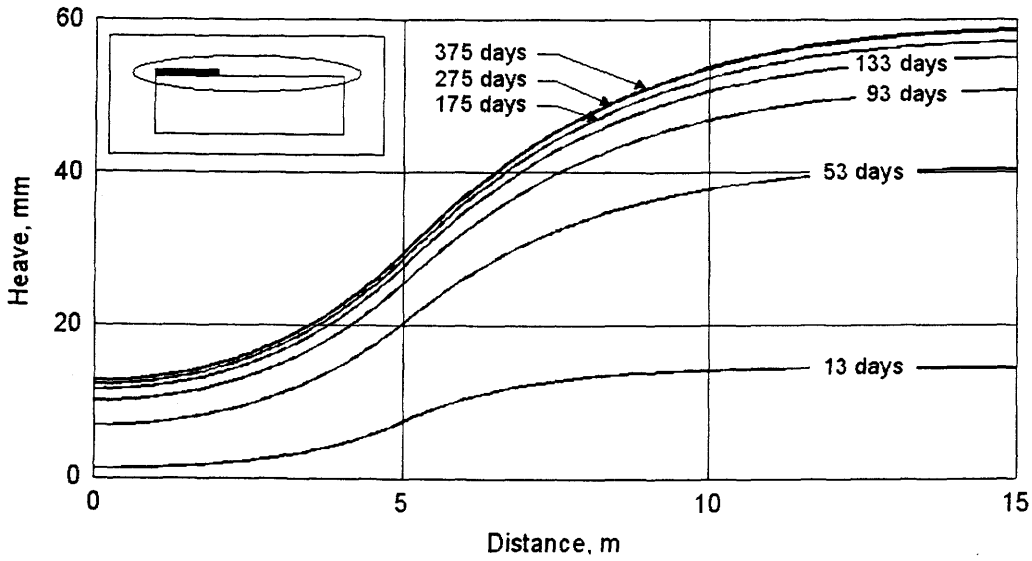

Figure C.13 Development of heave at ground surface with time, Example 4, uncoupled solution UCS1

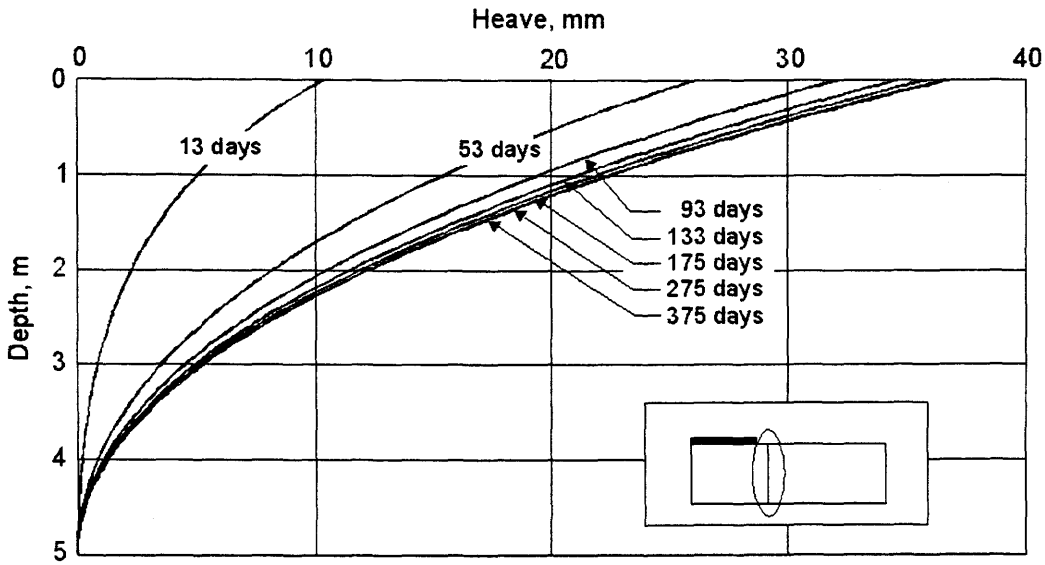

Figure C.14 Development of heave below the cover versus depth with time, Example 4, uncoupled solution UCS1

C.2 Uncoupled analysis, UCS2 for Example 4, infiltration problem

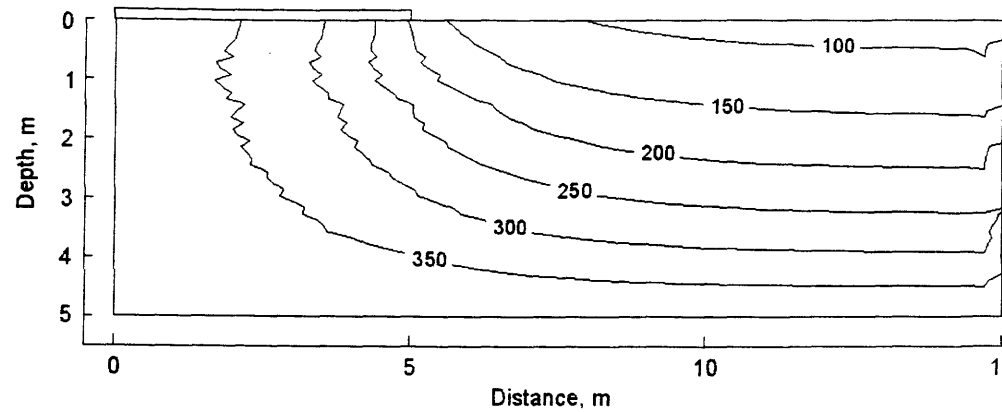

Figure C.15 Distribution of matric suction at day 53,
Example 4, uncoupled solution UCS2

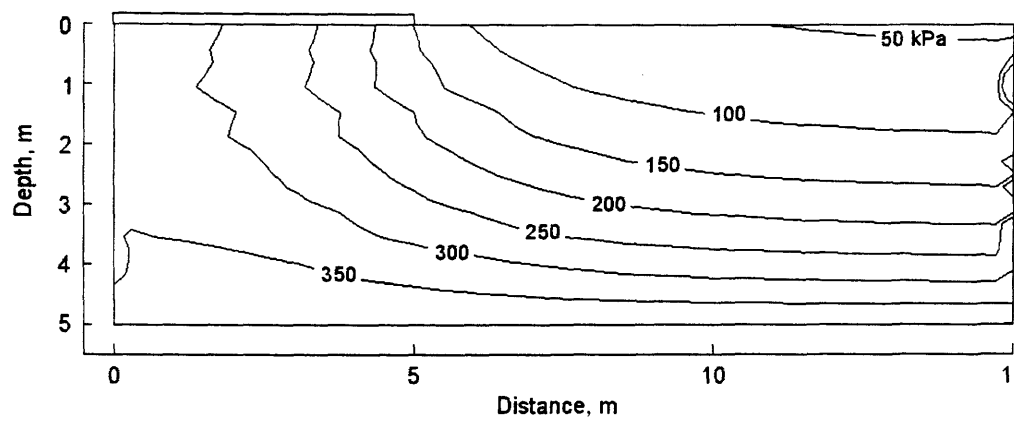

Figure C.16 Distribution of matric suction at day 175,
Example 4, uncoupled solution UCS2

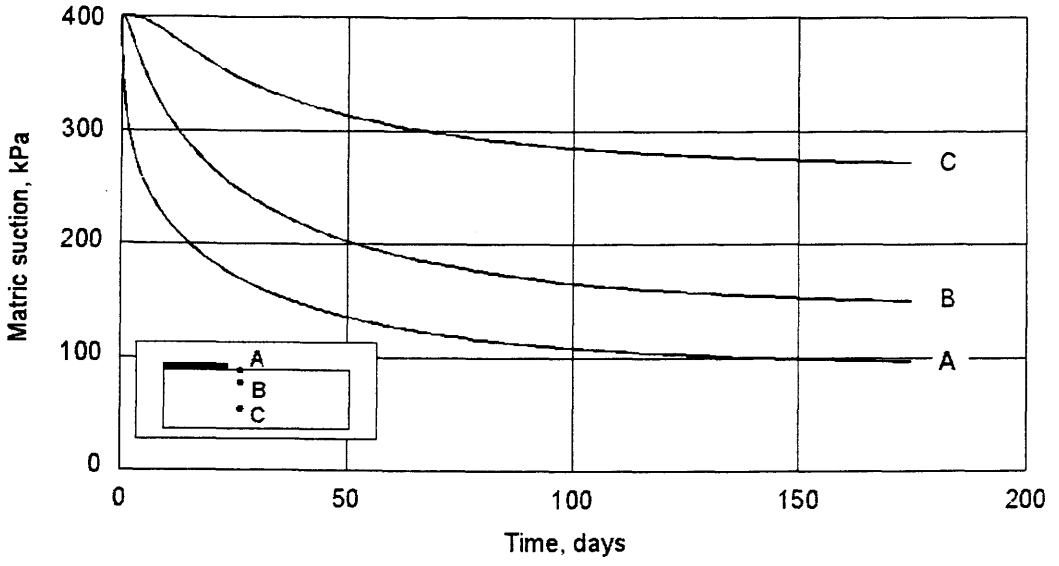

Figure C.17 Development of matric suction with time for points A, B, and C, Example 4, uncoupled solution UCS2

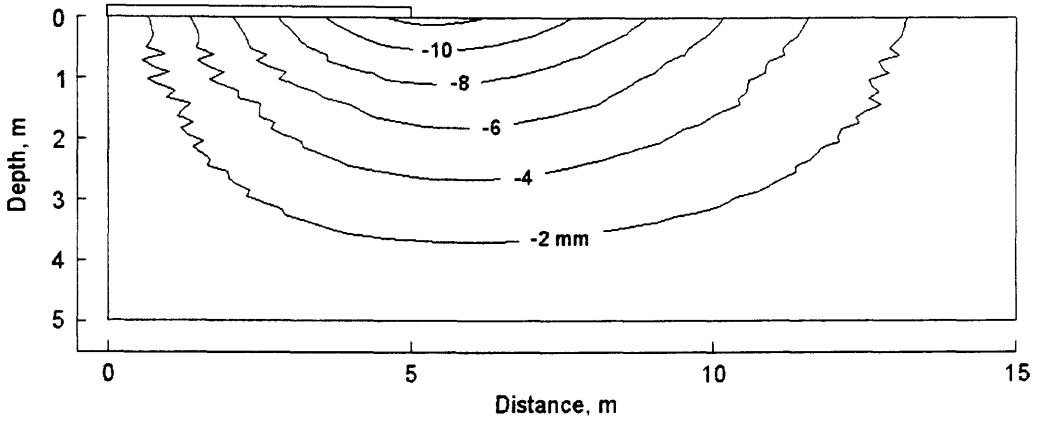

Figure C.18 Distribution of horizontal displacement at day 53, Example 4, uncoupled solution UCS2

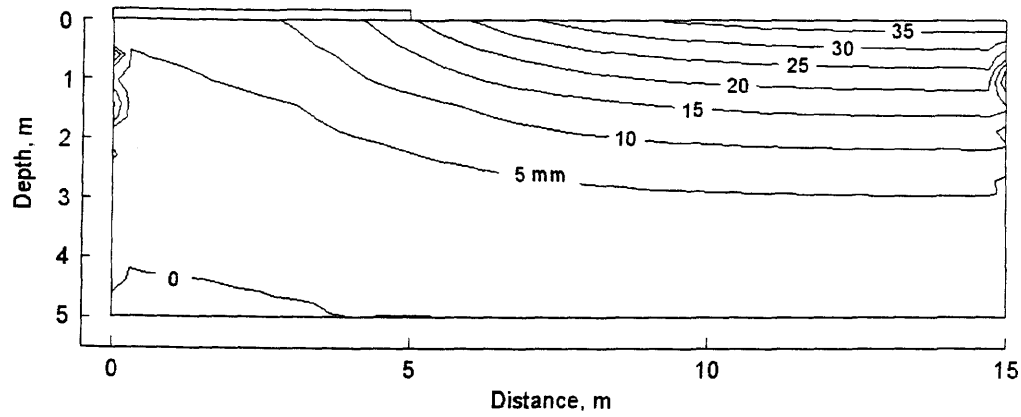

Figure C.19 Distribution of vertical displacement at day 53,
Example 4, uncoupled solution UCS2

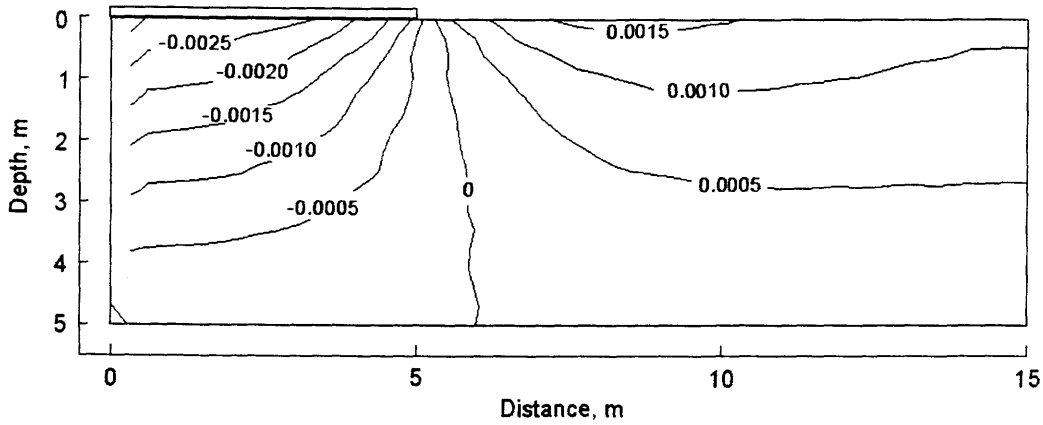

Figure C.20 Distribution of horizontal strain at day 53,
Example 4, uncoupled solution UCS2

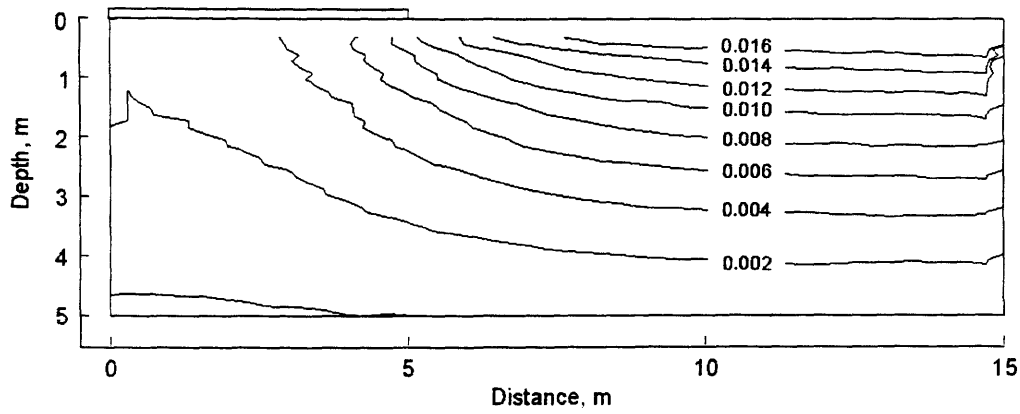

Figure C.21 Distribution of vertical strain at day 53,
Example 4, uncoupled solution UCS2

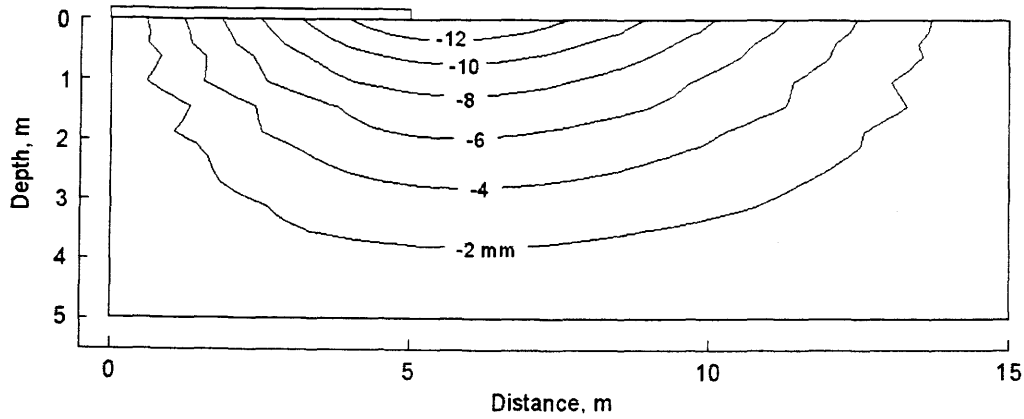

Figure C.22 Distribution of horizontal displacement at day 175,
Example 4, uncoupled solution UCS2

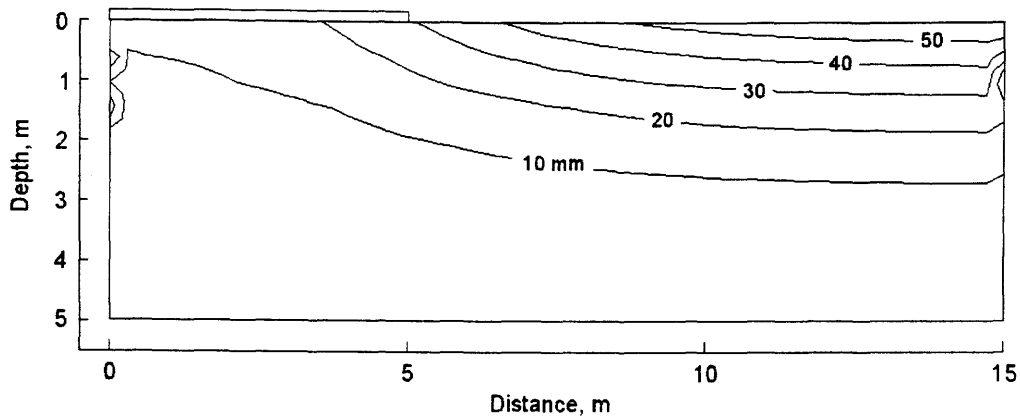

Figure C.23 Distribution of vertical displacement at day 175,
Example 4, uncoupled solution UCS2

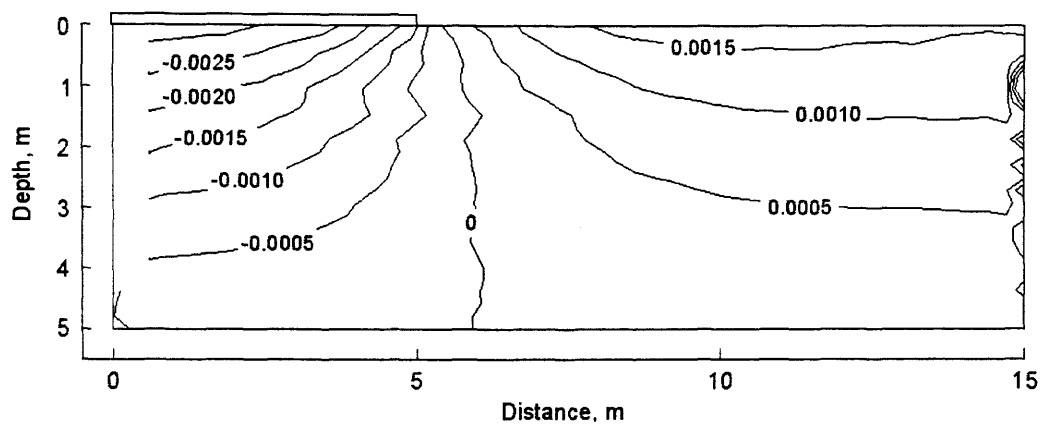

Figure C.24 Distribution of horizontal strain at day 175,
Example 4, uncoupled solution UCS2

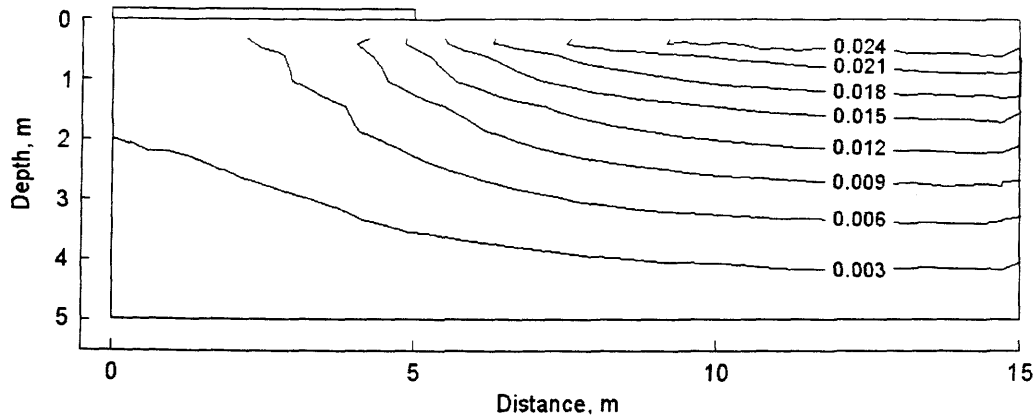

Figure C.25 Distribution of vertical strain at day 175,
Example 4, uncoupled solution UCS2

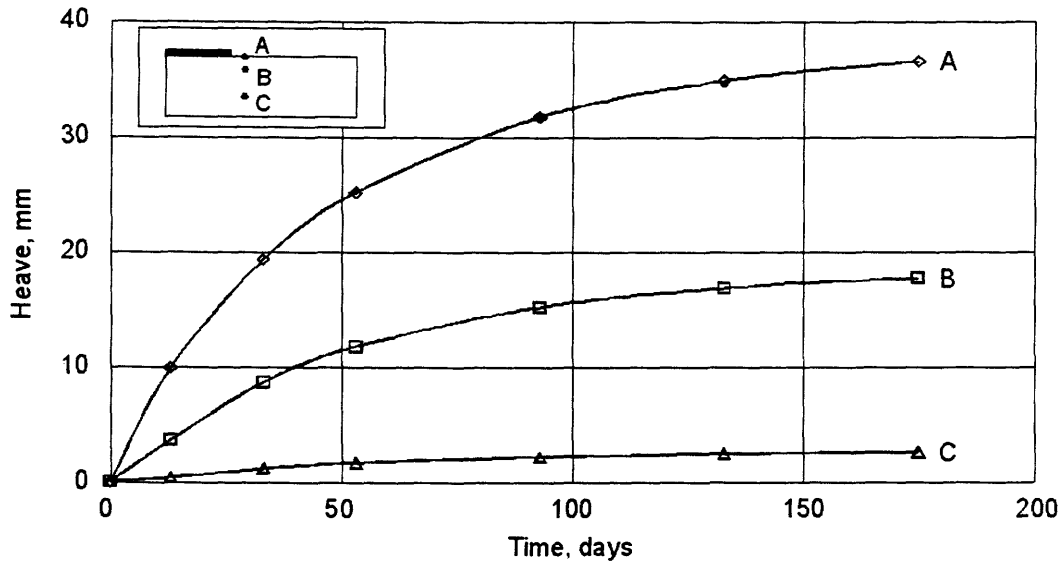

Figure C.26 Development of vertical displacement with time for points A, B, and C,
Example 4, uncoupled solution UCS2

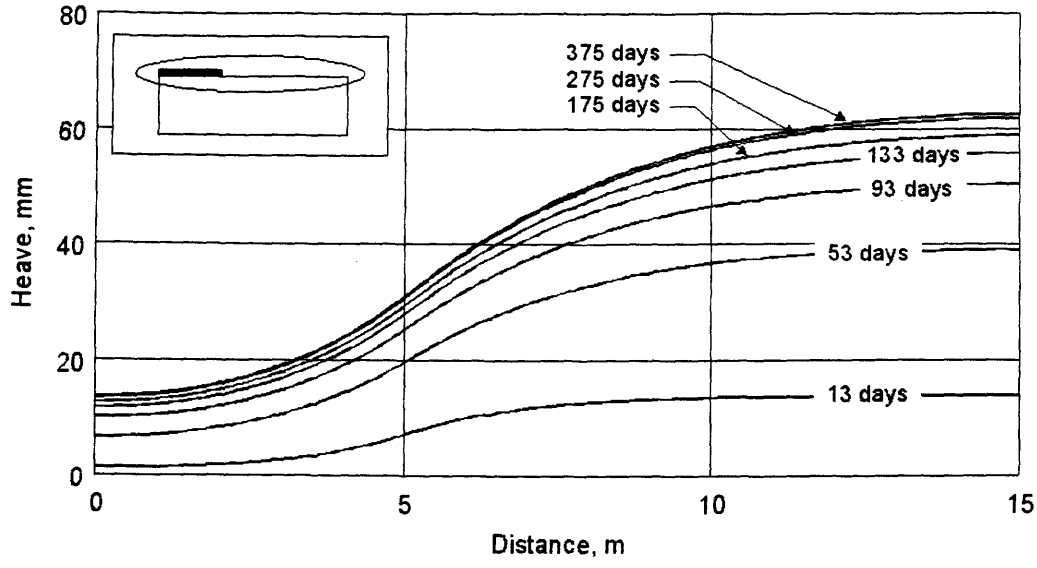

Figure C.27 Development of heave at ground surface with time, Example 4, uncoupled solution UCS2

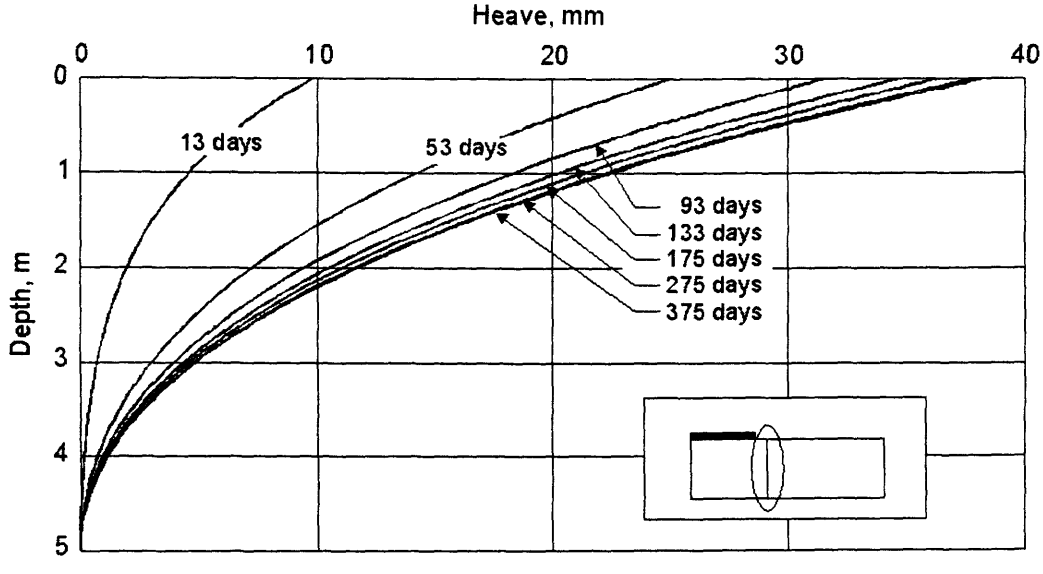

Figure C.28 Development of heave below the cover versus depth with time, Example 4, uncoupled solution UCS2

APPENDIX D

Accuracy of the Numerical Solutions

D.1 General

The finite element analysis of soil consolidation/swelling approximates pore-water pressure and displacements in soils in time. The closeness between of the approximation and the real behaviour of soils depends on the assumptions that forms the basic of the mathematical model, the data set available and the numerical errors in the solution of the mathematical model. The soil properties and their spatial distributions (i.e., elasticity parameters including Poisson's ratio, the coefficient of permeability, the soil-water characteristic curve,) are seldom known accurately and completely. The stress state conditions (i.e., the value and distribution of net vertical stress, the coefficient of earth pressure at rest, and pore-water pressure) are stress history dependent and they are difficult to be quantified accurately. There are limitations in the assessment of boundary conditions in space and time. The numerical errors are due to the spatial and temporal discretization of the domain, the round-off and truncation errors when system of equations is solved in computer, the convergence criteria used and the description of boundary conditions.

This Appendix discusses the issues associated with the numerical errors of a finite element solution and presents how some of the numerical results presented in this study have been validated. In other words, the difficulties associated with obtaining an accurate assessment of the soil properties and the boundary conditions (i.e., the value of infiltration at ground surface) will not be presented.

D.2 The issues related to the accuracy of a finite element solution

"*Accuracy* of a numerical solution is a measure of the closeness between the approximate solution and the exact solution" (Reddy, 1993). The following issues related to the accuracy of a finite element solution are presented: mesh generation and refinement, convergence, precision, round-off and truncation errors, boundary conditions, automatic mesh refinement, incremental procedure, time steps and the description of nonlinear functions. The computer programs (i.e., FlexPDE and Coupso) are also mentioned in the discussion.

D.2.1 Mesh generation and refinement

The number, shape (i.e., triangular or rectangular), type (i.e., linear, quadratic or cubic), and density (i.e., mesh refinement) of elements used in a given problem effects computational cost and accuracy of the solution.

Certain geometric shapes of elements may cause numerical ill-conditioning of element matrices. Aspect ratio is also an important factor. Generally, bodies with high aspect ratios are more ill-conditioned for numerical solution than bodies with an aspect ratio of one. FlexPDE uses quadratic (six-node) and cubic (9-node) triangular elements. The program tends to produce elements with aspect ratio of 1 in relatively open area. Elements with large aspect ratio may appear in regions where closed spaced boundaries exist (not in my problems), however, the maximum aspect ratio of the element can be specified. The maximum aspect ratio of element used in the analyses presented in this study is a default value (i.e., equal 4). COUPSO uses quadratic (nine-node) quadrilateral elements. The maximum aspect ratio of two was used in the coupled analysis.

The accuracy of the finite element solution depends on the choice of the finite element mesh. For example, if the selected mesh violates the symmetry of the problem, the resulting solution will be less accurate than one obtained using a mesh that agrees with the physical symmetry of the problem. A mesh is generated and refined with consideration of the symmetries available in the problem and the evaluation of the results obtained. The accuracy of a finite element solution increases as the size of the finite elements get smaller or the order of the polynomial in the approximation function increases (Zienkiewicz and Taylor, 1988). Fine mesh should be generated in regions with high gradient of solution. The mesh can be refined by making the mesh finer over parts or all of the body (i.e., h-refinement), making the element order higher (i.e., p-refinement), or making the mesh finer with higher order element (i.e., hp-refinement). Mesh density requirements should be determined by testing the solution for convergence. The refinement process is repeated globally or locally in regions of steep gradients, until differences in solutions become small.

D.2.2 Automatic mesh refinement

Automatic mesh refinement processes allow that specified accuracy can be achieved. FlexPDE refines its mesh automatically based on an estimate of the errors in the solution obtained using the current mesh. At the end of each solution phase, FlexPDE measures the accuracy by comparing its calculated RMS error measured across all elements with the specified error limit and the individual element errors with a multiple of the specified error limit (default value is 10 times specified error limit). If either the test of the RMS error or the test of the individual element errors fail, FlexPDE subdivides all elements which error is greater than the specified error limit and then repeat the solution phase. The accuracy of the solution can be checked by plotting the derivative of dependent variable. The fluctuation appear in this plot is minimized by using a smaller specified error limit. The specified error limit of 0.001 is adequate for the solution of both seepage and stress-deformation of the problems presented in this study.

D.2.3 Convergence

"*Convergence* means the tendency of a numerical solution to a particular result as the numerical error is reduced" (Baguley and Hose, 1994). The general solution has converged when a subsequent run with a finer mesh does not alter the results. For each time step in a transient analysis, the iteration process continues until the specified tolerance is achieved (i.e., convergence for each time step).

The convergence of uncoupled solutions with a specified error limit (i.e., seepage and stress-deformation) was checked automatically by FlexPDE (see section D.2.8).

In COUPSO program, tolerances are the allowable maximum percentage difference between two consecutive values (at nodes) for displacements "TOLD" and pore-water pressure "TOLP". A small tolerance may result in excessive number of iterations required to reach a solution, a big tolerance may result in false convergence, thereby making the solution unrealistic. The coupled solutions of the problems presented in this study were obtained with TOLD and TOLP vary from 0.01 to 0.05. The convergence process in each time step can be watched while the program

running. The errors of solution reported on screen were small and decreased monotonically. The solutions were checked again by examining the displacement and pore-water pressure profiles, the converged solution would be smooth and logical while the non-converged solution would show a 'jerky' profile. The convergence of coupled solutions was finally checked by comparing the solutions obtained from three different meshes (i.e., with 60, 75 and 90 nine-node elements, respectively).

D.2.4 Precision

The value of predicted or measured variables (i.e., pore-water pressures and displacements) can be precise without being accurate, and an accurate data may be imprecise. The precision of the computer calculations has been greatly improved in recent computers since many decimal digits of a number can be considered. The reporting of predicted or measured displacements can be to the nearest one-thousandth of a centimetre, pore-water pressures to the nearest of one hundredth of kPa. In many cases, the displacements are only known within a centimetre. For example, a small change in Poisson's ratio will change the displacements by much more than the precision of the predicted results indicates. The predicted displacements were reported to one-thousandth of a centimetre in this study because of the purpose of checking convergence of the solution and comparison between the solutions.

D.2.5 Round-off errors and truncation error

When large systems of equations are being solved repeatedly, round-off error due to numbers rounded-off to a finite number of digits can become a problem. Large value of co-ordinates x, y (i.e., big numbers) can lead to round-off error, the co-ordinates should be used as close to zero as possible. Differences in elastic parameters and differences in element size will also lead to round-off error. Round-off error will also affect the convergence of the problem due to repeated additions and subtractions of nodal co-ordinates. The numbering of nodes and elements affects the size of semi-bandwidth of the stiffness matrix therefore effects the time taken for solution and the round-off errors.

The volume change problems of an unsaturated, expansive soil involve highly nonlinear properties, which results in a great number of computations. This tends to make the solutions prone to error due to the accumulation of round-off errors in finite precision calculations. However, these errors are small in this study since the computer can carry an adequate number of significant digits.

D.2.6 Boundary conditions

The example problems presented in this study were assumed geometrically symmetric and therefore only one half of the soil profile was analyzed. In geotechnical practice, not many problems are completely geometrically symmetric, but this assumption is acceptable in many cases. The horizontal and vertical extension of the soil profile and boundary conditions to be specified must be evaluated properly for a real problem. The lower limit must cover the entire of active zone.

In most cases, there are singular points on the boundary. These are points of the mesh where both natural boundary conditions and essential boundary conditions can be specified, or two different values of a primary variable.

The variation of boundary flux in time and space may require the refinement of the finite element mesh where the flux is specified and the time steps for an accurate solution. For example, in the problem of water uptake by trees, very fine mesh is required at water uptake zone.

D.2.7 Incremental approach for stress-deformation analysis in uncoupled solution using FlexPDE

An incremental procedure was used in FlexPDE for the calculation of displacement. This procedure underestimates the displacements. The error associated with the incremental procedure depends on the size of stress step used. Figure D.1 shows the typical relationship between errors and size of stress step (for suction change from 150 kPa to 50 kPa in Example 4, Infiltration). In all of the example problems, size of stress step less than 2 kPa was used, the relative error produced from this approach was less than 0.1%.

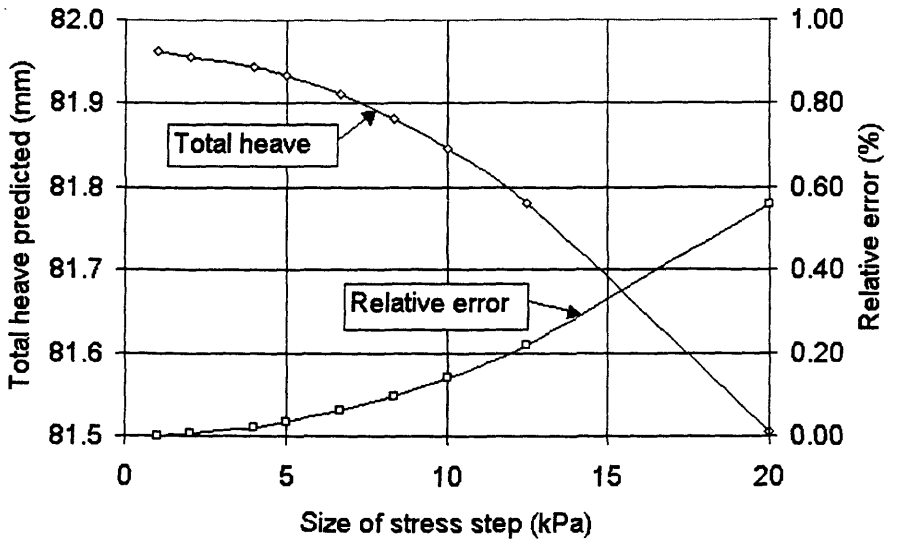

Figure D.1. Total heave and corresponding relative error versus size of stress step

D.2.8 Time steps

The solution accuracy is sensitive to the magnitude of the time step. If an analysis is performed with a time step exceeding the critical time step (for a stable solution), the errors resulting from numerical integration and from round-off can be large.

FlexPDE solves transient problems by a three-step approach. First, a half-step solution estimates the values at the mid-step. Then a full-step estimates the values at step end. Finally, a half-step advances from mid-step to end-step. The two independent estimates of the end-step values allow the determination of the solution error in time. The time step is controlled so that the RMS error is less than the specified error limit. Default time scheme in FlexPDE (i.e., Crank-Nicolson, $\theta = 0.5$) is used in this study. For seepage analysis of Example 4, infiltration problem, with specified error limit of 0.001 (about 0.1 kPa of pore-water pressure), the first time step (also is the smallest) was 216 seconds (i.e., 0.0025 day), the last time step (the biggest) was 86.09 days. Total number of time step was 31 for the duration of 375 days. The final mesh had 386 elements with 839 nodes. The RMS error was 4.482E-5, Max error was 1.961 E-4. The same solution was obtained when the specified error limit was 0.00001, the first time step (the smallest) was 88 seconds (i.e., 0.001 day), the last time step (the biggest) was 94.02 days. Total number of time step was 42 for

the duration of 375 days. The final mesh has 386 elements with 839 nodes. The RMS error was 4.470E-5, the max error was 1.954E-4.

When solving coupled problems using COUPSO, the same approach as suggested in FlexPDE for choosing time steps was used. However, comparisons were made for the vertical displacement at only one monitoring node (the maximum value) and the resulting horizontal stress at one monitoring Gauss point. The actual time step is selected if the two independent values of vertical displacement varied less than 3% and values of resulting horizontal stress varied 5%. For example 4, infiltration problem, with the mesh of 75 elements and 341 nodes, the first (also is the smallest) time step was 0.02 day, the largest time step was 5 days.

D.2.9 Description of nonlinear functions

The description of nonlinear soil properties functions is extremely important for the convergence and the accuracy of solution. There are five soil property functions in the coupled analysis of a volume change problem associated with an unsaturated, expansive soil. They are functions of both stress state variables. The functions are elasticity parameter functions, E, H, E_w, and H_w, and the coefficient of permeability function, k_w. The mathematical equations proposed in this study provide best fit to the experimental data; therefore, improve the accuracy of the solution. The use of these equations for the description of unsaturated soil property functions improved the convergence of solution significantly.

D.3 Validation techniques

D.3.1 Uncoupled solutions using FlexPDE program

FlexPDE computer program was used for both unsaturated seepage and stress-deformation analyses in the uncoupled approach. The program was validated by comparing its solutions to the solutions of the other well-accepted geotechnical software (i.e., Geoslope/W) and analytical solutions from literature. The validations for two-dimensional seepage were presented in Thieu (1999) and Hung (2000), the validations for stress-deformation were presented in Hung (2000).

The uncoupled results obtained using the method of heave analysis suggested in this study were compared to analytical solutions and the measured data for two case histories and two example problems. The comparisons were made only for one-dimensional problems and were presented in Hung (2000).

Three important checks were conducted for the uncoupled results. They are the check for input data (i.e., the geometry data, the soil property functions, and the boundary conditions), the adequacy of stress step (in incremental procedure), and the adequacy of the specified error limit (for the mesh refinement and time step refinement). The graphical output capability of FlexPDE allows these checks to be performed visually by examining the plots of dependent variables, their derivatives and the differences in the form of contours, elevation, and surface. The uncoupled solutions obtained using FlexPDE compared well with the coupled solutions obtained using the COUPSO program.

D.3.2 Coupled solutions using the COUPSO program

The Coupso computer program was validated by comparing its results with analytical and numerical solutions from literature. The results were compared for consolidation problems on saturated soils and presented in Pereira (1996). The problems for the validation of the COUPSO program include one-dimensional problems and two-dimensional problems. One-dimensional problems include consolidation of a homogeneous and saturated soil layer, consolidation of contiguous layers, consolidation of a soil profile due to a time-varying load applied to the soil surface. Two-dimensional problem was the analysis of a time versus settlement relationship for a strip footing on a layer of finite thickness. Close agreements between the COUPSO's solutions and closed form solutions (and/or numerical solution from literature) were observed.

The coupled results were checked in several solution steps. It was checked for the input data (i.e., the geometry data, the soil property functions, the boundary conditions) and the adequacy of the convergence criteria (tolerance for displacements and pore-water pressure), time steps, and finite element mesh. The graphical results were carefully examined and judged for the reasonableness. The validity of the

idealization of boundary conditions was not validated because hypothetical problems were analyzed.

The close agreement between uncoupled and coupled solutions, which were obtained by using two different computer programs, suggested that both solutions converged to the correct solution.

D.4 Concluding remarks

The hypothetical examples developed in this research study are for the purpose of the illustration of the analysis procedures and the comparisons of the results for uncoupled and coupled approaches. The solutions are empirically verified by comparison of a series of results when the finite element mesh, time step and stress step (in FlexPDE, using incremental procedure) are refined. The solutions of uncoupled and coupled solutions are also verified by comparing to each other. For problems encounters in geotechnical engineering practice, the numerical errors are often small in comparison with the errors introduced from the assessment of soil properties and boundary conditions.